Catalogue of Analytical Solutions for Consolidation of Unsaturated Soils Subjected to Various Initial Conditions and Time-Dependent Loadings

A thesis in fulfilment of the requirement
for the award of the degree

Doctor of Philosophy

from

University of Technology Sydney (UTS)

by

LIEM HUU HO, BEng (1st class Hons, UTS)

School of Civil and Environmental Engineering,
Faculty of Engineering and Information Technology

2016

CERTIFICATE OF ORIGINAL AUTHORSHIP

I certify that the work in this thesis has not previously been submitted for a degree nor has it been submitted as part of requirements for a degree except as fully acknowledge within the text.

I also certify that the thesis has been written by me. Any help that I have received in my research work and the preparation of the thesis itself has been acknowledged. In addition, I certify that all information sources and literature used are indicated in the thesis.

Liem Ho
February 2016

ABSTRACT

Soil consolidation has been a primary geotechnical interest for decades. Such phenomenon involves the gradual dissipation of excess pore pressures from the soil deposit subjected to an external applied load, resulting in a considerable reduction of soil volume. Majority of industrial and residential areas have been vigorously developed in arid and semi-arid climatic regions, where the underground water table is relatively deep. In these regions, construction activities can significantly influence the upper unsaturated zone. In particular, the earthworks, such as excavation and compaction, and changes in the climate and surface vegetation may result in further creation of unsaturated soils, whose properties are much more complicated than those of saturated soils. Past decades have witnessed the significant growth of engineering interests in unsaturated soils and that has motivated researchers to conduct more insightful research. A great attention has been given to the unsaturated consolidation theory due to many foundation-related problems particularly relate to time-dependent soil volume change and settlement. However, a typical unsaturated soil usually has nonlinear properties and intricate phase relationships, which result in theoretical difficulties in formulating a reliable model for the consolidation prediction.

This thesis presents a systematic catalogue of analytical solutions for the consolidation of unsaturated soils subjected to various loading and initial conditions. Particularly, eigenfunction expansions and standard Laplace transformation techniques are used to solve the consolidation equations. This research provides rigorous solutions to estimate the rates of excess pore-air and pore-water pressure dissipation and consolidation settlement under the one-dimensional (1D), two-dimensional (2D) plane strain and axisymmetric consolidation conditions. For the mathematical derivation, uniform and linearly depth-dependent initial conditions are adopted along with homogeneous boundary conditions, including one-way and two-way drainage boundary conditions. In addition, effects of time-dependent loadings are also captured in this study. Four primary types of external loads, namely ramping, asymptotic, sinusoid and damped sine wave, are simulated and then incorporated in the proposed solutions. On the other hand, the 1D consolidation of unsaturated soils under non-isothermal conditions is sufficiently discussed. This study also demonstrates that the proposed

analytical solutions can change back to the traditional equations for saturated soils. Most results are graphically presented in the semi-logarithmic plots. Changes in excess pore pressures and settlement are investigated against the air to water permeability ratio (k_a/k_w). Moreover, pore pressure isochrones along the flow domains are also highlighted in each consolidation field. Verification exercises are conducted by comparing the predicted results with other solutions obtained from existing literature. The proposed equations can be used by practicing engineers. Programmable methods such as Microsoft Excel or MATLAB can be simply adopted to generate results from proposed equations to predict the time-dependent settlement of unsaturated soils.

For all consolidation cases, it is predicted that variations in the permeability ratio k_a/k_w result in double inverse S curves for the excess pore-water pressure and settlement, while forming a single S curve for the excess pore-air pressure. The study shows that the 1D consolidation process in the two-way drainage soil stratum tends to proceed more quickly than that in the one-way drainage system. However, the consolidation rates under these boundary conditions are almost comparable when drain wells (for the 2D plane strain and axisymmetric cases) are installed in the soil profile. In the 2D plane strain consolidation system, if the horizontal permeability is greater than the vertical permeability (i.e. $k_x/k_z > 1$), the horizontal flow will govern the dissipation rate and the effects of vertical flow is much attenuated. This point is also supported in the axisymmetric analysis.

Additionally, the time-dependent loadings and temperature variations have significant impacts on changes in excess pore pressures and settlement. For the loading effects, it can be predicted that excess pore-water pressures and settlement are considerably influenced by the loading patterns irrespective of k_a/k_w values. However, in most loading cases, effects of the applied loads on the excess pore-air pressure are less pronounced as k_a/k_w increases. On the other hand, variations in soil temperature are substantially attributed to the air temperature and the heat from solar radiation. It is predicted that, for time-dependent linear temperature variations, the excess pore-air pressure initially increases dramatically and then attains a constant value, while the excess pore-water pressure diminishes a very long time after the heat begins to increase. Besides, excess pore-air and pore-water pressures near the ground surface increase faster than those at lower depths when the temperature increases exponentially. Both

pressures then are fully dissipated as the temperature approaches the maximum value. For the case of diurnal temperature wave, the excess pore pressure curves would oscillate capturing damping and retarding effects. Development of analytical solutions for the unsaturated consolidation incorporating the above influencing factors would provide fundamental understandings of deformation of unsaturated soils.

To my father, *Tuan Huu Ho*, my mother, *Thu Thi Le*, my brothers, *Hieu Huu Ho* and *Tai Huu Ho*, and my sister, *Vy Khanh Ho*, who shared love and strength with me throughout this marvellous journey.

ACKNOWLEDGEMENT

Studying a doctoral course at University of Technology Sydney (UTS) has offered me profound experiences in my academic life. During the PhD program, I have developed a genuine passion for academic research through rigorous assessments. However, this marvellous achievement would not have been possible without immense supports from my supervisors, family members and research colleagues.

First of all, I would like to express the deepest gratitude to my principal supervisor, Dr Behzad Fatahi, and my co-supervisor, A/Prof Hadi Khabbaz, for their immeasurable kindness, exhaustive guidance and encouragements. They have provided me sufficient supports and opportunities to overcome challenging tasks successfully. My PhD project could not have been achievable without their constructive feedbacks and worthy recommendations.

Secondly, I also gratefully thank all geotechnical research fellows who have been directly or indirectly involved in my doctoral study. More specifically, I am very grateful to Thu Minh Le who efficiently assisted me to develop numerical codes for data generation, to Antonio Reyno and Lam Nguyen for the laboratory assistance, and to Ali Parsa-Pajouh, Aslan Sadeghi Hokmabadi, Harry Nguyen, Balaka Ghosh and many others for their restless supports during the academic program.

In addition, I would like to sincerely acknowledge UTS Faculty of Engineering and Information Technology, and Centre of Built Infrastructure Research (CBIR) for encouraging awards and scholarships which enable me to complete the PhD research. I also appreciate Van Le and Phyllis Agius for their kind assistance.

Last but not least, I would like to express the immeasurable appreciation to my parents who have always been watching over my progress from overseas. Their consistent encouragement and love give me strength to strive against many difficulties in life. I also specially thank my younger brothers and sister who always bring joys and happiness to the family. They are motivation for me to work hard and attain my goals successfully. I am very fortunate to have such lovely family.

LIST OF PUBLICATIONS

❖ Published Journal Articles

Ho, **L**, Fatahi, B & Khabbaz, H 2014, 'Analytical solution for one-dimensional consolidation of unsaturated soils using eigenfunction expansion method', *International Journal for Numerical and Analytical Methods in Geomechanics*, vol. 38, no. 10, pp. 1058-1077.

Ho, **L**, & Fatahi, B 2015, 'Analytical solution for the two-dimensional plane strain consolidation of an unsaturated soil stratum subjected to time-dependent loading', *Computers and Geotechnics*, vol. 67, pp. 1-16.

Ho, **L**, Fatahi, B & Khabbaz, H 2015, 'A closed form analytical solution for two-dimensional plane strain consolidation of unsaturated soil stratum', *International Journal for Numerical and Analytical Methods in Geomechanics*, vol. 39, no. 15, pp. 1665-1692.

Ho, **L**, & Fatahi, B 2015, 'One-dimensional consolidation analysis of unsaturated soils subjected to time-dependent loading', *International Journal for Geomechanics*, vol. 16, no. 2, pp. 1-19.

Ho, **L**, Fatahi, B & Khabbaz, H 2015, 'Analytical solution to axisymmetric consolidation in unsaturated soils with linearly depth-dependent initial conditions', *Computers and Geotechnics*, vol. 74, pp. 102-121.

Ho, **L**, & Fatahi, B 2015, 'Axisymmetric consolidation in unsaturated soil deposit subjected to time-dependent loadings', *International Journal for Geomechanics*, doi: 10.1061/(ASCE)GM.1943-5622.0000686.

❖ Published Conference Papers

Ho, **L**, Fatahi, B & Khabbaz, H 2013, 'Exact solution to predict excess pore pressures and settlement of unsaturated soil deposit due to uniform loading', *GEO Montreal 2013*, Canadian Geotechnical Society, Montreal, pp. 1-6.

Ho, **L**, Fatahi, B & Khabbaz, H 2014, 'One-dimensional consolidation of unsaturated soil deposit with various initial conditions', *Geo-Shanghai 2014*, American Society of Civil Engineers (ASCE), pp. 145-155.

Ho, **L**, Fatahi, B & Khabbaz, H 2014, 'Analytical solution for one-dimensional consolidation of unsaturated soil deposit subjected to step loading', *Proceedings of the 6th International Conference on Unsaturated Soils – UNSAT 2014*, Taylor & Francis Group, Sydney, pp. 1763-1769.

Ho, **L**, Fatahi, B & Khabbaz, H 2015, 'Exact analytical solution for one-dimensional consolidation of unsaturated soil stratum subjected to damped sine wave loading', *Proceedings of the 12th Australia New Zealand Conference on Geomechanics*, New Zealand Geotechnical Society and the Australian Geomechanics Society, Wellington, pp. 1115-1122.

TABLE OF CONTENTS

LIST OF FIGURES

LIST OF TABLES

LIST OF NOTATIONS

English letters

C_a	interactive constant associated with the air phase;
C_w	interactive constant associated with the water phase;
$c_{v_r}^a$	coefficient of consolidation with respect to the air phase in the radial domain;
$c_{v_z}^a$	coefficient of consolidation with respect to the air phase in the vertical domain;
$c_{v_x}^a$	coefficient of volume change with respect to the air phase in x-direction;
c_σ^a	coefficient of consolidation due to total stress with respect to the air phase;
$c_{v_r}^w$	coefficient of consolidation with respect to the water phase in the radial domain;
$c_{v_z}^w$	coefficient of consolidation with respect to the water phase in the vertical domain;
$c_{v_x}^w$	coefficient of volume change with respect to the water phase in x-direction;
c_σ^w	coefficient of consolidation due to total stress with respect to the water phase;
g	gravitational constant;
H	thickness of the soil stratum;
i	integer for the Fourier sine series (for 2D plane strain consolidation) Fourier Bessel series (for axisymmetric consolidation);
j	integer for the Fourier sine series (for both plane strain and axisymmetric conditions);
K	eigenvalue for vertical boundary condition (for 1D consolidation);
K	ratio of the changes in horizontal (or radial) and vertical stresses at a point;
k	integer for the Fourier sine series (for 1D consolidation);
k_{a_r}	coefficient of permeability for the air phase in the radial domain;

k_{a_x} coefficient of permeability for air in x-direction;

k_{a_z} coefficient of permeability for the air phase in the vertical domain;

k_{w_r} coefficient of permeability for the water phase in the radial domain;

k_{w_x} coefficient of permeability for water in x-direction;

k_{w_z} coefficient of permeability for the water phase in the vertical domain;

L width of soil layer;

M molecular mass of the air phase;

m_v coefficient of volume change in saturated soils;

m_1^a coefficient of volume change of the air phase with respect to the change of net stress;

m_2^a coefficient of volume change of the air phase with respect to the change of suction;

m_1^s coefficient of volume change of the soil with respect to the change of net stress;

m_2^s coefficient of volume change of the soil with respect to the change of suction;

m_1^w coefficient of volume change of the water phase with respect to the change of net stress;

m_2^w coefficient of volume change of the water phase with respect to the change of suction;

n porosity;

q_z external loading;

R universal air constant;

$R_a(r)$ eigenfunction with respect to the excess pore-air pressure for domain r;

$R_w(r)$ eigenfunction with respect to the excess pore-water pressure for domain r;

r investigated radius;

r_e radius of zone of influence;

r_p pore radius;

r_w radius of the drain well;

S matric suction;

S^* normalized settlement;

$S(t)$	consolidation settlement;
S_{max}	maximum settlement;
S_r	degree of saturation;
S_∞	final ground surface settlement;
s_f	final matric suction;
s_0	initial matric suction;
T	time factor;
$T_a(t)$	generalized Fourier coefficients varying with time with respect to the air phase;
$T_w(t)$	generalized Fourier coefficients varying with time with respect to the water phase;
t	elapsed time;
U	degree of consolidation;
$\overline{U}$	average degree of consolidation;
U_r	degree of consolidation under axisymmetric conditions;
u	displacement in x-domain;
u_a	excess pore-air pressure;
$u_{a,t}$	first order of partial differential equation (PDE) of air with respect to time;
$u_{a,r}$	first order of partial differential equation (PDE) of air with respect to radius;
$u_{a,rr}$	second order of partial differential equation (PDE) of air with respect to radius;
$u_{a,xx}$	second order of partial differential equation (PDE) of air with respect to width;
$u_{a,zz}$	second order of partial differential equation (PDE) of air with respect to depth;
u_{atm}	atmospheric pressure;
u_a^0	maximum initial excess pore-air pressure;
u_w	pore-water pressure;
$u_{w,t}$	first order of partial differential equation (PDE) of water with respect to time;

$u_{w,r}$ first order of partial differential equation (PDE) of water with respect to radius;

$u_{w,rr}$ second order of partial differential equation (PDE) of water with respect to radius;

$u_{w,xx}$ second order of partial differential equation (PDE) of water with respect to width;

$u_{w,zz}$ second order of partial differential equation (PDE) of water with respect to depth;

u_w^0 maximum initial excess pore-water pressure;

V_0 initial volume of the soil element;

V_a volume of air within soil element;

V_w volume of water within soil element;

v displacement in y-domain;

$v(r_p, s)$ predicted volume fraction of pores at suction s;

w displacement in z-domain;

$X_a(x)$ eigenfunction with respect to pore-air pressure for domain x;

$X_w(x)$ eigenfunction with respect to pore-water pressure for domain x;

x investigated width;

$Z_a(z)$ eigenfunction with respect to the excess pore-air pressure for domain z;

$Z_w(z)$ eigenfunction with respect to the excess pore-water pressure for domain z; and

z investigated depth;

Greek letters

γ_w water unit weight;

Δs suction change;

$\Delta\overline{\sigma}$ change in net stress;

ε_v total volumetric strain;

Θ absolute temperature in Kelvin;

θ angular coordinate;

θ° temperature in degree Celsius;

λ_a^{ij} separation constant with respect to the air phase;

λ_w^{ij} separation constant with respect to the water phase;

μ^j eigenvalue for vertical boundary condition (i.e., PTIB and PTPB);

ξ^i eigenvalue for radial boundary condition;

σ_r total stress in r-domain;

σ_x total stress in x-direction;

σ_z total stress in z-domain;

σ_θ total stress in θ-domain; and

$\overline{\sigma}$ net stress.

CHAPTER 1

INTRODUCTION

1.1. General

Under an undrained condition, the application of external loads, mainly induced by the self-weight of engineered structures, may generate excess pore pressures in a soil stratum. After a certain period of time, these excess pore pressures gradually dissipate towards the permeable boundaries and subsequently lead to a noticeable reduction of soil volume at a variable rate. Such phenomenon is defined as *consolidation*. As a common issue in many engineering applications and designs, consolidation in a particular soil stratum has been a major interest in the geotechnical field for decades. An original consolidation theory was studied by Terzaghi (1925), who employed the effective stress principle and constituted a solid framework to predict the rates of excess pore pressure dissipation and settlement, in a limit of saturated soil mechanics. This pioneered work has formed a solid background for many later studies.

Through vigorous developments in geotechnical engineering, it has come to realisation that characteristics of natural soils in the subterranean zone have no longer been consistent to the traditional soil mechanics studies (Terzaghi 1925, 1943). Environmental changes, long-term climatic conditions (i.e. arid and semi-arid climates) and human-induced activities (i.e. compaction, excavation) may account for such inconsistencies (Fredlund et al. 2012). Likewise, the emergence of flux boundary problems due to the imbalance between evaporation and precipitation of groundwater has lowered the phreatic level in the soil profile and subsequently altered the saturated nature of soil beneath the ground to an unsaturated manner (Thornthwaite 1948; Fredlund 1996; Cameron 2001; Cameron & Mills 2009; Fredlund et al. 2012). Figure 1.1 visualises the flux surface boundary problem occurring at about the surface of the hill slope. Most light-engineered and residential structures have been constructed in a

direct contact with the upper unsaturated ground, also known as upper *vadose zone* (Bouwer 1978), and induce significant compression on the ground surface. Due to the complex nature of unsaturated soils, the consolidation-related problems in arid and semi-arid regions have not yet been comprehensively understood.

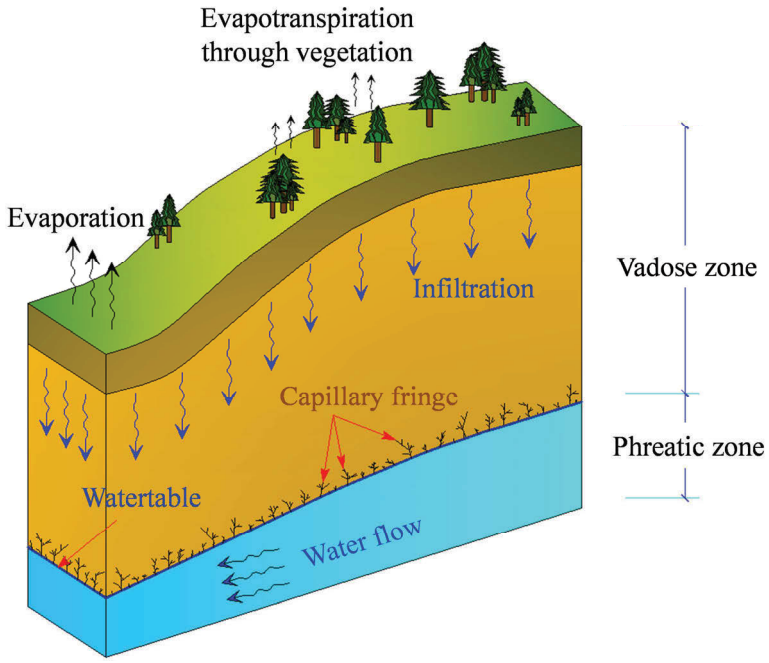

Figure 1.1. Schematic of flux surface boundary occurring at the surface of unsaturated soil system

Existing literature (e.g. Ng & Menzies 2007; Lambe & Whitman 2008; Fredlund et al. 2012) refer to a typical unsaturated soil as a three-phase composition consisting of solid particles, water and air. The inclusion of air phase within the soil element has brought about a great challenge in obtaining a generalised constitutive model that is able to capture various soil state conditions. The properties of unsaturated soil, likewise, are much more sophisticated than those of fully saturated soil, resulting in highly nonlinear consolidation problems. These aforementioned shortcomings may hinder the computational capabilities in the consolidation field of unsaturated soils.

The escalating awareness of changes in soil properties caused by environmental impacts emphasises the importance of unsaturated soil mechanics studies, particularly

consolidation theory, for the sake of proper structural development. However, a considerable number of past studies have not yet provided satisfactory understandings about the mechanical behaviour of consolidation and likewise profound knowledge of the field have been left undiscovered for years due to complex problems. Nevertheless, a vigorous improvement in computational tools has recently enabled numerous in-depth research investigations regarding deformation of unsaturated soils to be established, thus enhancing prediction accuracy. This has also allowed extensive capabilities of analytical and numerical approaches to evaluate the consolidation in an unsaturated porous medium. A following section in this chapter explains statement of problem and the concept of consolidation of unsaturated soils, in terms of changes in excess pore-air and pore-water pressures and consolidation settlement. This chapter also discusses the research objectives and scopes, and later provides an outline of content for this thesis.

1.2. Statement of problem

Settlement of a natural soil induced by external applied loads can be categorised into three stages including instantaneous (immediate), primary (consolidation) and secondary (creep) settlements, as shown in Figure 1.2. Immediately after loading, instantaneous settlement occurs as a soil only experiences shear deformation, which subsequently leads to changes in shape while maintaining constant volume of soil. It is worth mentioning that no dissipation of excess pore pressures occurs during the instantaneous settlement. Primary settlement, on the other hand, manifests a notable change in the soil volume characterised through dissipation process of both excess pore-air and pore-water pressures. When time elapses, such excess pore pressures gradually dissipate towards permeable boundaries and correspondingly the soil volume would reduce due to air and water being squeezed out of pores. Primary settlement is therefore considered to be a time-dependent process and may take years to complete. Theoretically, the consolidation settlement ends when both excess pore-air and pore-water pressures approach zero. Once excess pore pressures diminish, the soil continues to settle as a result of rearrangement of soil skeleton under loading. This phenomenon is known as secondary settlement and it is also considered as a time-dependent process. However, the secondary settlement may proceed at a slower rate compared to the primary settlement and the amount of secondary settlement may not be very significant

(Coduto & Huitric 1990; Coduto et al. 2011). The main highlight in this thesis is the primary consolidation settlement of unsaturated soils.

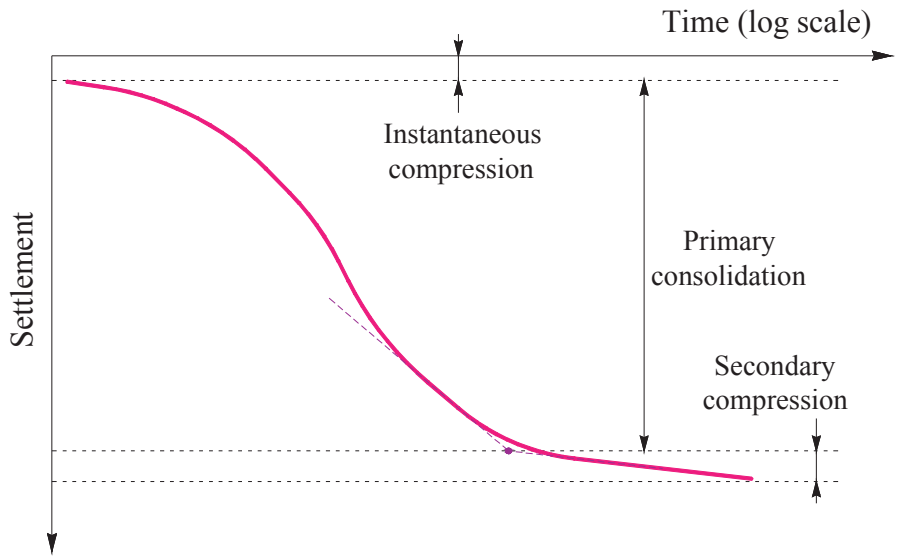

Figure 1.2. A typical settlement curve obtained from oedometer test

Although geotechnical studies have witnessed a number of investigations on the consolidation theory for unsaturated soils since the mid of 1960s, its true mechanism still has been far unfathomable to certainty. Consolidation-related problems in regards to the field of interest have not been comprehensively understood for decades. There was a realisation that the study of unsaturated soil mechanics was much more sophisticated than that of fully saturated soil mechanics (Fredlund et al. 2012). The constitutive model of unsaturated soils was likewise developed adopting complex stress state variables to accommodate pore-air pressure, resulting in a highly nonlinear consolidation problem that requires a cumbersome evaluation for predicting purposes. In the early 1960s, the original yet well-known studies of this field were conducted by Blight (1961), who introduced a consolidation equation for the dry, rigid and unsaturated soils; Scott (1963), who estimated the consolidation of unsaturated soil with occluded air bubbles; and Barden (1965, 1974) who analysed the consolidation of compacted and unsaturated clays.

Consolidation studies for unsaturated soils have progressed rigorously since the inception of one-dimensional (1D) consolidation theory proposed by Fredlund & Hasan

(1979). This theory introduces the nonlinear governing equations describing independent flows of air and water in unsaturated deposits. Later, Dakshanamurthy & Fredlund (1980), and Dakshanamurthy et al. (1984) accomplished the consolidation theories by expanding the existing equations to two-dimensional (2D) and three-dimensional (3D) models, respectively. This set of theories has inspired a large number of recent studies on analytical and numerical models for estimating the consolidation settlement in unsaturated soils. Several prominent research accentuated the general problems such as 1D consolidation settlement of a single-layer unsaturated soil (e.g. Qin et al. 2008; Qin et al. 2010a, 2010b; Shan et al. 2012, 2013; Zhou & Zhao 2014; Zhou et al. 2014), consolidation of multi-layered soil (e.g. Shan et al. 2014), consolidation for viscoelastic soil (e.g. Qin et al. 2014), 2D plane strain consolidation (e.g. Conte 2004), and axisymmetric consolidation problems (e.g. Conte 2006; Qin et al. 2010c; Zhou & Tu 2012; Zhou 2013). Results given by the aforementioned models generally emphasised effects of air to water permeability ratio on excess pore-air and pore-water dissipation rates, and consolidation settlement. In addition, pore pressure isochrones along dissipation domains were investigated.

Among the mentioned models, a very modest number of analytical approaches have been proposed. Most studies preferred different numerical methods to deal with the complexity of governing equations of flow, particularly those derived from 2D plane strain and axisymmetric conditions. An initial analytical study about consolidation of unsaturated soils was developed by Qin et al. (2008), who introduced the velocity of water (v_w) and mass rate of air (J_a) to the mathematical process. Assuming all the consolidation parameters remain constant during the loading process, Qin et al. (2008) employed Cayley-Hamilton and Laplace transformation techniques to obtain the final solution. Moreover, Qin et al. (2010b) further estimated the dissipation rate of excess pore pressures and consolidation settlement of unsaturated soil deposits subjected to an exponentially time-dependent loading. Although the results gave good agreement with the numerical predictions, the analytical solution is relatively impractical for use because of the complexity of the obtained equations. Shan et al. (2012) and Zhou et al. (2014) derived an existing set of inhomogeneous governing flow equations given by Fredlund & Hasan (1979) to a homogeneous equations prior to delivering the mathematical procedure. Separation of variables was directly applied to the newly

proposed governing equations and alternative solutions would be subsequently obtained. These indirect methods (Shan et al. 2012; Zhou et al. 2014) require several intermediate steps, which are usually cumbersome, to obtain actual solutions. On the other hand, there has been a very limited analytical research about the consolidation settlement of unsaturated soils under the plane strain and axisymmetric conditions. Numerical approaches for both plane strain and axisymmetric cases were provided by Conte (2004, 2006), and for axisymmetric case only presented by Qin et al. (2010c) using Fourier series approximation and by Zhou & Tu (2012) and Zhou (2013) using the differential quadrature method (DQM). Besides analytical and numerical predictions, many experimental research (Fredlund & Rahardjo 1986; Rahardjo & Fredlund 1995; Wong et al. 1998) have also been conducted to investigate properties of unsaturated soil such as permeability and volume change coefficients to name a few.

Apart from the consistent growth in numerical models for estimating the consolidation of unsaturated soils, analytical studies have recently become more accessible due to the vast improvements in computational capabilities. This has enabled geotechnical researchers to analytically predict characteristics of unsaturated consolidation. Besides numerical approaches, it should be noted that analytical approaches are widely applicable for homogeneous and nonhomogeneous partial differential equations (PDEs) under complex boundary and initial conditions, thus providing a decent approximation to consolidation theory. Development of analytical methods would also provide comprehensive understandings of time-dependent deformation of unsaturated soils. Furthermore, proposed analytical solutions can be used to validate the existing numerical models and experimental results. Having realised many undiscovered potentials in the analytical field, it is necessary to invest more on analytical frameworks for the sake of proper prediction.

1.3. Objectives and scope of research

The main objective of this study is to develop a systematic catalogue of analytical models to predict the dissipation of excess pore-air and pore-water pressures and consolidation settlement of unsaturated soils under three categories: (1) 1D consolidation, (2) 2D plane strain consolidation, and (3) axisymmetric consolidation. In addition, effects of time-dependent loadings applied on the ground surface and non-

isothermal conditions are addressed and incorporated in the proposed solutions. Graphical presentations will mainly highlight effects of the air to water permeability ratio on the consolidation process, particularly time-dependent changes in excess pore pressures and settlement. Parametric studies associated with environmental variables, such as external loads and temperature, are presented against the dissipation rates and settlement of unsaturated soil. This study also demonstrates pore pressure isochrones along the dissipation domains. Moreover, effects of a vertical sand drain, which is installed in the unsaturated soil profile, under the axisymmetric conditions are addressed. The specific objectives of this research are:

- Providing a simple yet novel analytical method for predicting the consolidation of unsaturated soil deposits under 1D, 2D plane strain and axisymmetric conditions;
- Estimating the dissipation rates of excess pore-air and pore-water pressures and settlement induced by constant and time-dependent loadings;
- Investigating the 1D consolidation of unsaturated soil deposits induced by time-dependent temperature variations; and
- Evaluating the efficiency of the proposed analytical models and providing guidelines as well as step-by-step development of the model for practicing geotechnical engineers.

For the analytical procedure, Fourier Bessel and sine series, and standard Laplace transformation are employed to yield final solutions. In particular, these solutions are derived from governing equations of flow adopted from existing consolidation theories (Fredlund & Hasan 1979; Dakshanamurthy & Fredlund 1980, 1981; Darkshanamurthy et al. 1984). A set of governing equations is presented under PDEs with variables of time and flow domains. Fourier Bessel and sine series can be applied to PDEs to present the eigenfunctions (flow function) whereas Laplace transformation and Laplace inverse can be employed to derive the generalised Fourier coefficients (time function) and subsequently obtain the solutions. Generally, this research includes the following parts:

- Developing analytical solutions to predict the 1D, 2D plane strain and axisymmetric consolidation of unsaturated soil deposits subjected to a constant loading, while capturing both uniform and linear initial conditions;

- Developing analytical solutions for the 1D, 2D plane strain and axisymmetric consolidation incorporating the simulated time-dependent loadings, such as ramping, asymptotic, sinusoidal and damp sine wave;
- Developing an analytical solution to predict the 1D consolidation of unsaturated soil deposits, while considering non-isothermal conditions; and
- Verifying the proposed models for 1D, 2D plane strain consolidation with existing data previously published in the literature.

In addition, it is necessary to address some limitations of the research as follows:

- Coefficients of consolidation, volume change coefficients and consolidation-related properties are assumed constant under a transient process at a particular loading increment;
- Model verifications are not sufficiently provided in Chapters 5, 6, 8 and 9 due to the shortage of experimental results;
- Consolidation model does not capture the hysteresis effect;
- Unsaturated soil stratum is subjected to an isotropic loading;
- Flows of air and water phases are considered on a basis of fluid flow and are assumed to be continuous and independent; and
- Vagaries of environmental factors (e.g., wind, rain, snow) and climatic irregularities are neglected.

1.4. Organisation of thesis

Ten major chapters are presented in this thesis, including:

- Chapter 1 promptly presents an overall view as well as an importance of unsaturated soil mechanics in consolidation theory. Additionally, the scope and objectives are clearly highlighted in this chapter.
- Chapter 2 delivers a comprehensive literature review of unsaturated soil mechanics studies associated with consolidation problems. This chapter also introduces the stress state variables, namely suction and net stress, and volume-mass constitutive models for unsaturated soils. Development of governing equations is also highlighted. Moreover, existing analytical and numerical models for saturated and unsaturated soils are sufficiently reviewed in this chapter.

- Chapter 3 presents the detailed development of analytical model to predict the 1D consolidation of unsaturated soil stratum subjected to a constant loading while capturing both uniformly and linearly distributed initial excess pore pressures. Homogeneous boundary conditions (e.g., one-way and two-way drainage systems) are introduced to the mathematical derivation. Changes in excess pore-air and pore-water dissipation and settlement are discussed and graphically demonstrated against time, under semi-logarithmic plots. Pore pressure isochrones along with the vertical domain (z-direction) is also investigated. Besides, to check for the validity of the proposed solution, a verification exercise against other existing consolidation solutions is presented.
- Chapter 4 presents the rigorous development of an analytical model to predict the 1D consolidation of unsaturated soil stratum subjected to different time-dependent loadings. Four loading functions, namely ramping, asymptotic, sinusoid and damp sine wave, are mathematically simulated and incorporated in the procedure to yield solutions. The mathematical procedure employs homogenous boundary conditions and a uniform initial condition. For the graphical demonstration, dissipation rates of excess pore-air and pore-water pressures as well as the consolidation settlement are investigated against time. Furthermore, parametric studies in regards to effects of loading parameters on the consolidation patterns are conducted for each loading case. A verification exercise against existing models is carried out to check for the validity of the proposed solutions.
- Chapter 5 introduces an analytical model to predict the 1D consolidation of unsaturated soil stratum mainly induced by effects of temperature change with time and depth. Governing flow equations are first modified incorporating temperature variations. Thermal equations are simulated under forms of linear, exponential and diurnal sin wave, and are subsequently incorporated in the proposed solutions. Dissipation rates of excess pore pressures at various depths are examined against time. This chapter also conducts parametric studies by investigating effects of thermal parameters on the 1D consolidation of unsaturated soil deposit.
- Chapters 6 and 7 are to provide an analytical approach that predicts the 2D plane strain consolidation behaviour of unsaturated soil stratum. In Chapter 6, the mathematical procedure captures both uniform and linearly depth-dependent initial conditions along with the constant loading condition to obtain final solutions. Fourier

sine series are adopted as eigenfunctions for x- and z-domains whereas Laplace transformation is applied to yield the function of time. Chapter 7, on the other hand, presents the analytical solution for the 2D plane strain system, while incorporating time-dependent loadings in the obtained equations.

- Chapters 8 and 9 present an analytical approach to evaluate the axisymmetric consolidation of unsaturated soil stratum considering both radial and vertical flows. Governing equations are first transformed into a set of polar equations. Chapter 8 adopts the constant loading applied to the soil foundation. Separation of variables and Laplace transformation techniques are employed to yield final solutions. Chapter 9 presents the analytical prediction for axisymmetric consolidation of unsaturated soils subjected to different time-dependent loadings.
- Finally, Chapter 10 briefly provides the summary of the thesis and then presents the conclusions and recommendations for forthcoming studies. This chapter is followed by references and appendices.

CHAPTER 2

LITERATURE REVIEW

2.1. General

2.1.1. Phases in unsaturated soil

Referring to Dregne (2011), the long-term climatic conditions have resulted in fully dry or unsaturated (partially dry) soils in the proximity of the ground surface, accounting for approximately a third of the earth's surface. These soils are located well above the groundwater table and are frequently unsaturated due to the excessive evaporation and evapotranspiration through vegetation, and insufficient water precipitation (Fredlund et al. 2012) (see Figure 1.1).

A typical unsaturated soil is commonly known as a three-phase geomaterial consisting of soil particles, water and air (Ng & Menzies 2007; Lambe & Whitman 2008; Fredlund et al. 2012). Existence of even the tiniest amount of air in a soil element, for instance air bubbles, renders a soil unsaturated. Soil particles form an irregular framework called *soil skeleton*, and spaces between solid particles are called *voids* which can be occupied by only water or air or combination of both. In practice, the soil portion immediately above the phreatic line can be referred as the *capillary zone*, where pore-water pressures are reported to be negative (Fredlund & Rahardjo 1993; Fredlund et al. 2012). Soils in the capillary zone are usually considered as unsaturated soils with the presence of negative pore-water pressures.

In unsaturated soils, concepts and principles required to establish the volume-mass constitutive models are usually complex due to the intricate phase relationships and soil properties. It is also worth mentioning that the unsaturated soil studies, particularly the consolidation theory, have been no longer consistent to the traditional framework

proposed by Terzaghi (1925, 1943). In some prevalent consolidation research, the soil particles are assumed to be incompressible and changes in the soil volume are therefore mainly governed by flows of pore-air and pore-water. Barden (1965) reported that the air and water flow in accordance with the continuity of fluid phases. Thus, in an attempt to evaluate the soil deformation, flows of air and water phases are usually assumed to be independent and continuous.

Later studies (e.g. Fredlund & Morgenstern 1977; Ng & Menzies 2007; Fredlund et al. 2012) claimed the air-water interface within a soil element to be a fourth phase which is known as *contractile skin*. This phase can be described as a thin yet elastic membrane formed throughout the voids of soil, separating the pore-air and pore-water. Stress state changes in contractile skin may noticeably influence the physical properties such as water content, soil volume, and shear strength. According to Fredlund et al. (2012), physical properties and mechanical interactions of contractile skin are different from the contiguous air and water phases, and as a result the contractile skin should be considered as an independent phase when analysing the stress state and physical interactions in unsaturated soils. Figure 2.1 demonstrates an unsaturated soil element consisting of soil solids, air, water and contractile skin.

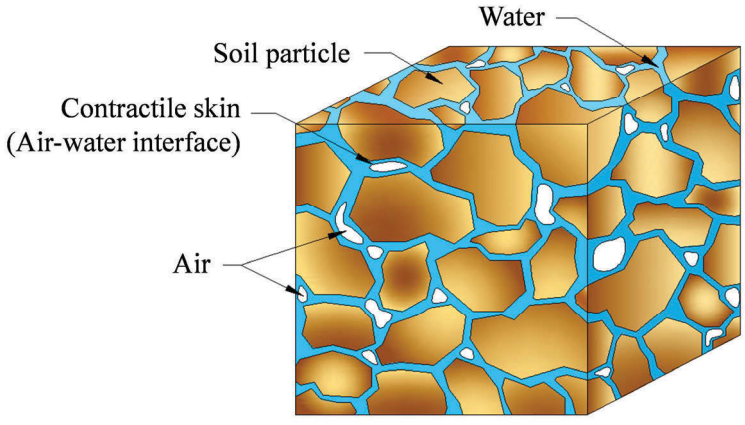

Figure 2.1. An unsaturated soil element with air, water and contractile

However, the contractile skin is composed of only a few thin molecular layers, its physical subdivision may not be essential for constituting volume-mass models for unsaturated soils. Thus, the contractile skin can be practically considered as part of

water phase (Fredlund & Rahardjo 1993; Fredlund et al. 2012). Current studies have employed the simplified three-phase composition for practical investigation. Figure 2.2(a) demonstrates the mass and volume quantities in the four-phase diagram whereas Figure 2.2(b) schematically shows a simplified phase diagram of unsaturated soil.

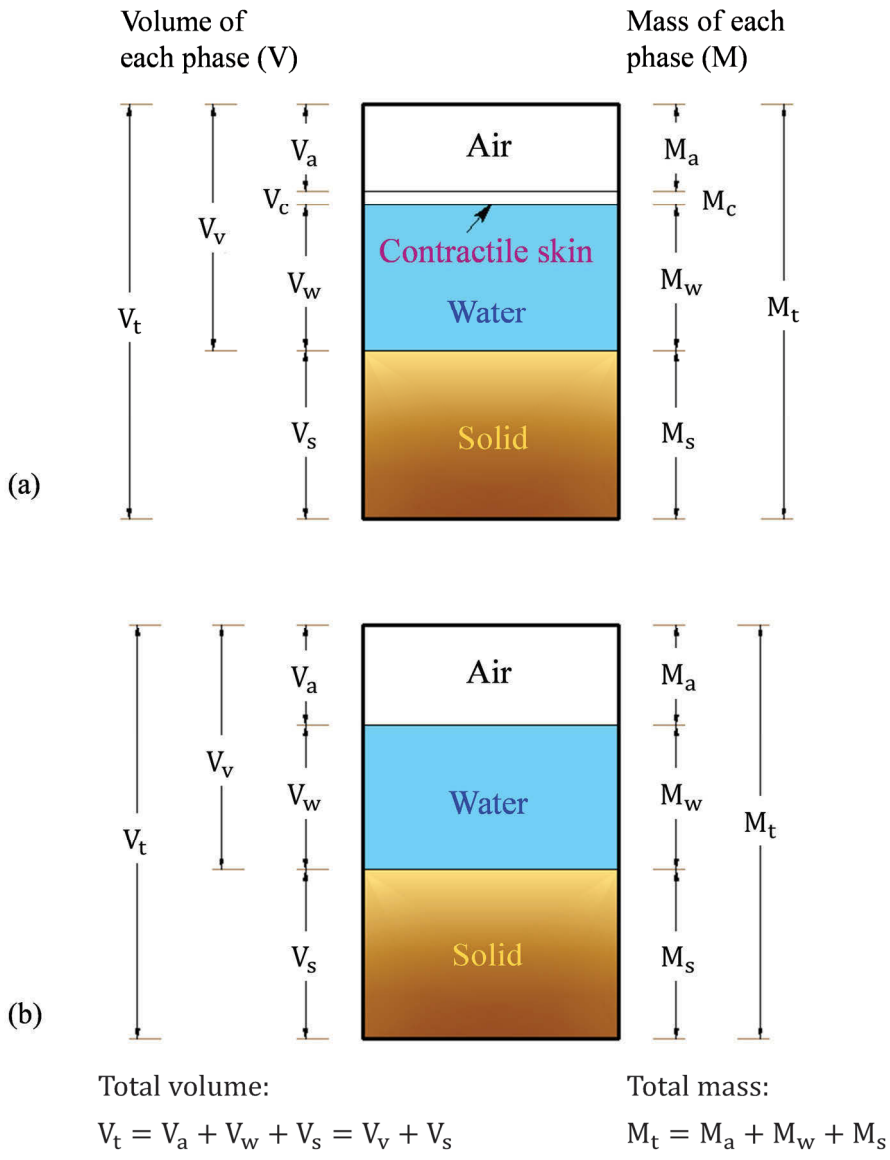

Figure 2.2. Schematic phase diagram of unsaturated soil: (a) four-phase soil system and (b) simplified three-phase soil system (modified after Fredlund & Rahardjo 1993)

2.1.2. Surface tension on the contractile skin

Surface tension, denoted as T_s, occurs when intermolecular forces are exerted on molecules of contractile skin. As mentioned by Fredlund et al. (2012), the molecules within water are surrounded by equally intermolecular forces whereas the molecules within the contractile skin (i.e. the air-water interface) are subjected to unbalanced forces, as shown in Figure 2.3(a). Due to the unbalanced force condition, the contractile skin acts like a flexible membrane that exhibits a concave segment towards the larger pressure and induces surface tension for the sake of pressure equilibrium. This tension phenomenon can be depicted in Figure 2.3(b). As observed, pressures exerted on each side of the contractile skin are u and $(u + \Delta u)$. Additionally, the radius of concave curvature is called *meniscus* and is denoted as R_s. It is worth mentioning that the surface tension decreases with increasing temperature (Kaye & Laby 1921). Table 2.1 presents decreasing magnitudes of surface traction as temperature increases.

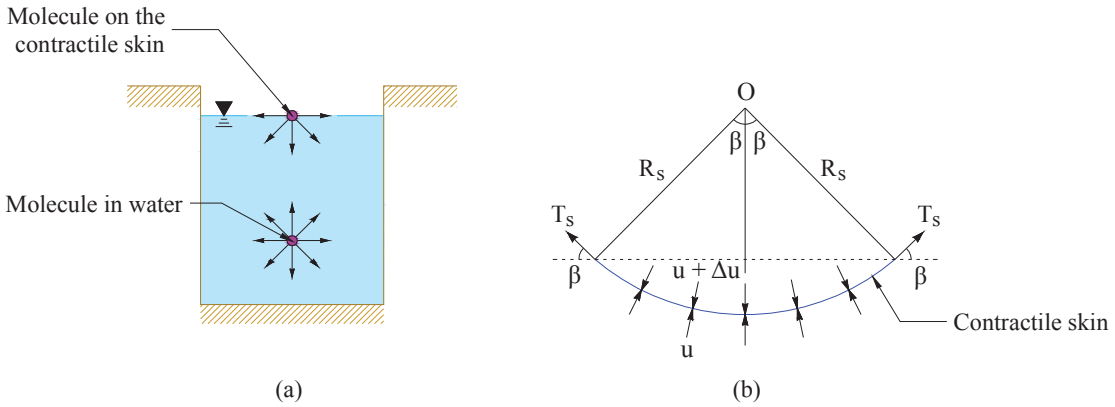

Figure 2.3. Surface tension effect in the contractile skin: (a) intermolecular forces acting on a molecule in the contractile skin and on a molecule in water; (b) a concave segment and surface tension in the contractile skin (after Fredlund et al. 2012)

Based on Figure 2.3(b), Ng & Menzies (2007), and Fredlund et al. (2012) suggested the force equilibrium in the vertical direction as follows:

$$2\, T_s \sin\beta = 2\, \Delta u\, R_s \sin\beta \qquad [2\text{-}1]$$

Table 2.1. Relation between surface tension and temperature (after Kaye & Laby 1921)

Temperature (℃)	**Surface tension T_s (mN/m)**
0	75.7
10	74.2
20	72.75
30	71.2
40	69.6
50	67.9
60	66.2
70	64.4
80	62.6
100	58.8

Note that the parameter Δu presented in Equation [2-1] would be determined by taking a difference between the pore-air pressure (u_a) and pore-water pressure (u_w), and that is defined as the *matric suction*. Thus, Equation [2-1] can be further simplified as shown below:

$$u_a - u_w = \frac{T_s}{R_s} \qquad [2\text{-}2]$$

When the three-dimensional (3D) membrane is considered (Figure 2.4), Equation [2-2] becomes:

$$u_a - u_w = T_s\left(\frac{1}{R_1} + \frac{1}{R_2}\right) \qquad [2\text{-}3]$$

where R_1 and R_2 are radii of curvature of 3D membrane in two orthogonal planes.

Assuming that radii of curvature are similar in all directions, Equation [2-3] then can be rewritten as:

$$u_a - u_w = \frac{2T_s}{R_s} \qquad [2\text{-}4]$$

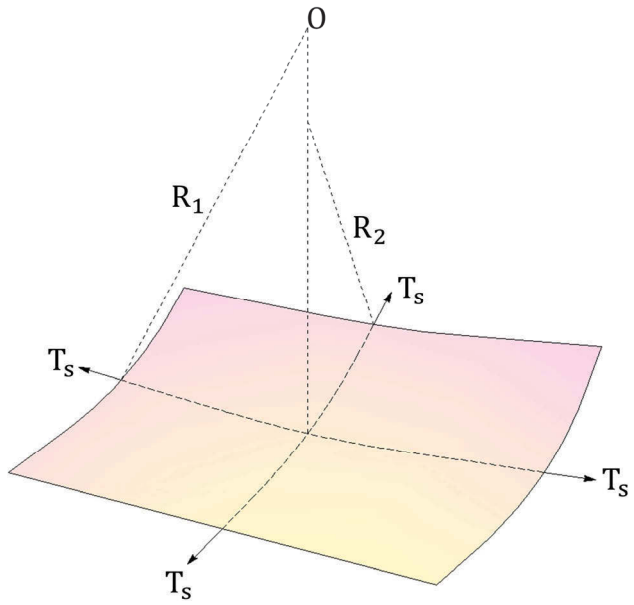

Figure 2.4. The 3D membrane with radii of curvature (modified after Fredlund et al. 2012)

Equation [2-4] is provided by Fredlund et al. (2012), demonstrating a clear correlation between the matric suction ($u_a - u_w$) and the meniscus (R_s). In particular, the meniscus is inversely proportional to the matric suction, implying that the decreases in matric suction leads to the increases in radius of curved air-water interface. In a case when the meniscus approaches infinity, the matric suction would be equal to zero and the air-water interface would become flat.

2.1.3. Soil suction

The total suction, symbolised as ψ, is considered to be a free energy of soil water and consists of two major components, namely the matric suction ($u_a - u_w$) and osmotic suction (π) (Edlefsen & Anderson 1943). The total suction can be formulated in a simple equation as shown below:

$$\psi = (u_a - u_w) + \pi \qquad [2\text{-}5]$$

On the other hand, Richards (1966) and Sposito (1981) also introduced a qualitative equation that describes the soil suction in terms of the partial vapour pressure of soil water as follows:

$$\psi = -\frac{R\Theta}{\upsilon_{w_0}\omega_v}\ln\left(\frac{\bar{u}_v}{\bar{u}_{v_0}}\right) \qquad [2\text{-}6]$$

where R is the universal gas constant (i.e., $8.31\,\mathrm{J/(mol.K)}$); $\Theta = (\theta^{\circ} + 273)$ is the absolute temperature (K); θ° is the temperature (°C); υ_{w_0} is the specific volume of water ($\mathrm{m^3/kg}$); ω_v is the molecular mass of water vapour (i.e., $8.31\,\mathrm{kg/kmol}$); $\bar{u}_v$ is the partial pressure of pore-water vapour (kPa); and $\bar{u}_{v_0}$ is the saturation pressure of water vapour over a flat surface of pure water at the same temperature (kPa). It is also worth mentioning that the fraction $\bar{u}_v/\bar{u}_{v_0}$ is defined as the *relative humidity* (R_h).

As stated by Fredlund et al. (2012), both matric suction ($u_a - u_w$) and osmotic suction (π) contribute to a reduction of the relative humidity (R_h). The osmotic suction can be applicable to both saturated and unsaturated soil mechanics. It is a result of retention energy due to the amount of dissolved salts in the pore fluid and is expressed in terms of pressure (Murray & Sivakumar 2010). Therefore, changes in osmotic suction are most likely due to changes in the salt content within the soil. The mechanical properties of the soil, such as total volume and shear strength, are significantly susceptible to effects of osmotic suction when the dissolved salts are contaminated. The matric suction, on the other hand, mainly associates with the capillary phenomenon and contractile skin. The relationship between the matric suction and contractile skin is mathematically presented in Equation [2-4]. Changes in matric suction are mainly due to the environmental variables, climatic vagaries and earthworks (e.g., compaction, excavation) (Fredlund et al. 2012). Most unsaturated soil problems are related to the environmental changes (e.g. excessive rainfall, drought etc.), which significantly influence the matric suction component but results in minor changes in the osmotic suction component. In other words, the strength of unsaturated soils is fundamentally governed by the matric suction despite a considerable amount of salts within the soil water (Alonso et al. 1987).

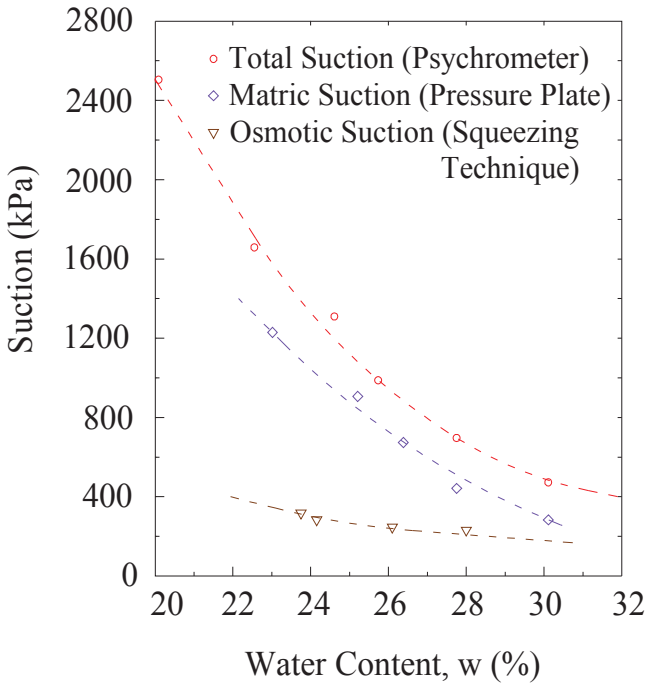

Figure 2.5. Total, matric and osmotic suctions obtained using compacted Regina clay (modified after Krahn & Fredlund 1972)

Figure 2.5 demonstrates the total, matric and osmotic suction measurements based on the compacted Regina clay using different experiments (e.g., transistor psychrometer, pressure plate, squeezing technique). It can be observed that the matric suction change is very much congruent to the total suction change, particularly at higher water content values (w). These results obtained by Krahn & Fredlund (1972) indicate that the total suction changes are equivalent to the matric suction changes. The matric suction therefore may essentially represent the total suction when dealing with unsaturated soil settlement problems (Fredlund et al. 2012). Tang et al. (2002) also reported that an increase in matric suction would result in a pronounced increase in soil strength. However, it is noteworthy that marine soils near coastal areas or particular soils composed of low porosities and high cation exchange capacity usually exhibit a high osmotic suction, which significantly affects the volumetric behaviour of soils (Fritz & Marine 1983; Graham et al. 1992; Feng et al. 2003; Sreedeep & Singh 2006). Referring to existing soil deformation analyses (Alonso et al. 1990; Loret & Khalili 2002; Sheng et al. 2008; Fredlund et al. 2012), this thesis only highlights effects of matric suction for the constitutive formulation in unsaturated soils.

2.1.4. Fabric modifications induced by soil suction

Soil deformation associated with microstructural changes is of great interest in unsaturated soil mechanics. According to Romero & Simms (2008), many macroscopic soil properties such as water content, hydraulic conductivity, and volume changes may be characterised by the microstructural behaviour. Compacted soils are mainly composed of two structure levels, namely *macrostructure* and *microstructure* (Koliji et al. 2006). The soil macrostructure is related to the structural assemblage of soil aggregates and spaces between these aggregates are termed *macropores*, also known as *inter-aggregate*. On the other hand, the microstructure associates with the elementary arrangement within individual aggregates. Spaces within these individual aggregates can be defined as *micropores* or *intra-aggregates*. In some existing literature (Cuisinier & Laloui 2004; Koliji et al. 2006), the pore classes are usually bordered at about 1μm. It is also worth mentioning that, in fissured porous media, Valliappan & Khalili-Naghadeh (1990) consider the macropores as fissures and the micropores as spaces in porous blocks. Such distinctive division of pore classes yields the double porosity concept of soils.

The compacted soil fabric can be determined using two prominent techniques: (1) mercury intrusion porosimetry (MIP) for interpreting the soil porosity and pore-size distribution (PSD) (Delage et al. 1996; Romero & Simms 2008); and (2) scanning electron microscopy (SEM) for investigating the spatial arrangement and structure of micropores and small particles (Delage et al. 1996; Cuisinier & Laloui 2004; Koliji et al. 2010). As reported by Delage & Lefebvre (1984), both techniques show that the macropores would first retract notably during the consolidation process and the micropores are eventually subjected to compression when larger pores completely collapse. Of two techniques, the MIP is more suitable to investigate the double porosity theory and structural evolution as it successfully measures a large pore range, in which pore classes (i.e., microporosity and macroporosity) are clearly identified (Cuisinier & Laloui 2004). The MIP also provides qualitative interpretations on soil fabric modifications induced by suction increase (i.e., Δs or $\Delta(u_a - u_w)$). This point was evidenced from experimental investigations on a compacted glacial till conducted by Simms & Yanful (2001, 2002). These studies demonstrated that increases in matric suction (i.e., from about $0 - 2500\text{kPa}$) would lead to the bimodal PSD curve in a way

that the microporosity rises considerably companied with a pronounced decrease in the macroporosity. Figure 2.6 illustrates PSD curves induced by matric suction variations. It is observed that the suction increase has little effects on the volume fraction of pores when the pore-size is approximately smaller than 0.2μm (Zone 1) or greater than 20μm (Zone 4). The PSD curves in Zone 2 correspond to the micropore volume, which increases significantly during the drying process (i.e., suction increase). It is also observed that the reduction of total porosity of soil is ascribed by the notable shrinkage of the macropore volume (Zone 3). From the MIP test results, Cuisinier & Laloui (2004) elucidated that soil samples might undergo significant fabric modifications without changing the total porosity and void ratio. Koliji et al. (2006) further formulated the double-structure model based on the PSD curves as follows:

$$v(r_p, s) = \begin{cases} v(r_p, s_0); & (\text{Zone 1: } r < R_1) \\ v(r_p, s_0) + \left(\frac{V_{2e}}{V_2}\right)\left[v(r_p, s_f) - v(r_p, s_0)\right]; & (\text{Zone 2: } R_1 < r < R_2) \\ v(r_p, s_0); & (\text{Zone 3a: } R_2 < r < R(s)) \\ v(r_p, s_0) - \left(\frac{V_s}{V_3}\right)^2\left[v(r_p, s_0) - v(r_p, s_f)\right]; & (\text{Zone 3b: } R_2 < R(s) < R_3) \\ v(r_p, s_0); & (\text{Zone 4: } r > R_3) \end{cases} \quad [2\text{-}7]$$

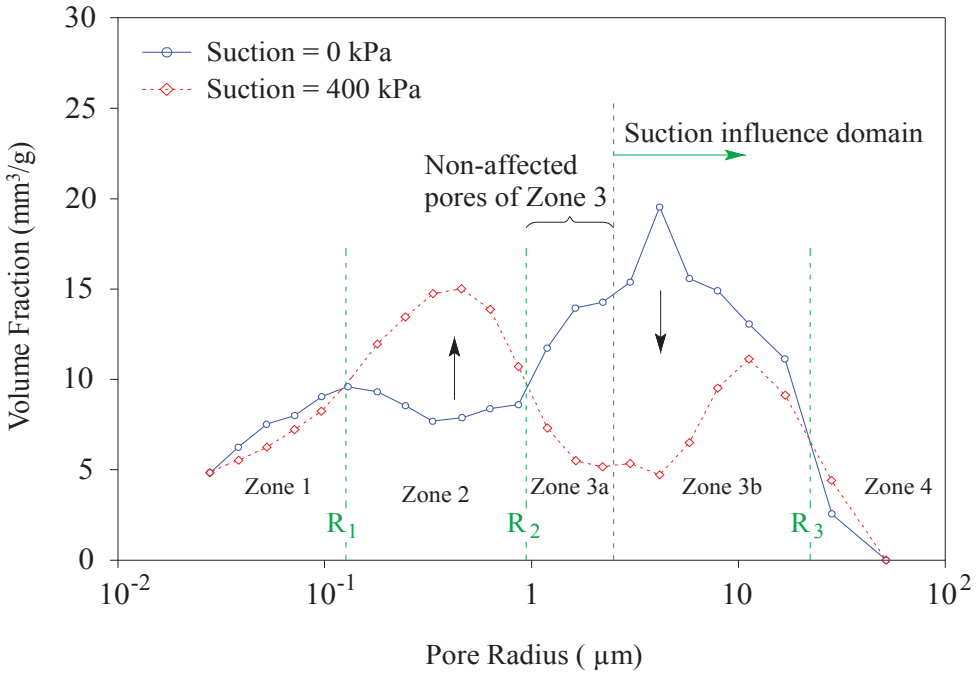

Figure 2.6. Soil fabric modification due to varying suctions (after Koliji et al. 2006)

where $v(r_p, s)$ is the predicted volume fraction of pores at suction s; r_p is the pore radius; R is the pore radius at particular zone; s_0 and s_f are the initial and final matric suctions; and V_2, V_{2e} and V_3 are volume fraction of pores at particular zone.

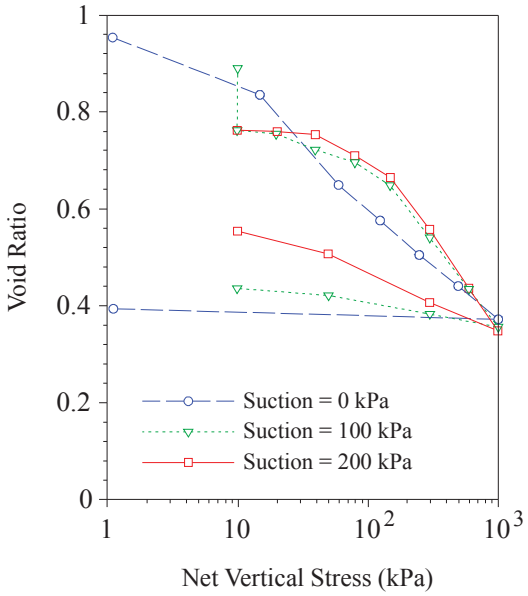

Figure 2.7. Compression indices influenced by suction increase (after Cuisinier & Laloui 2004)

Experimental studies conducted by Cuisinier & Laloui (2004) also show that a pre-consolidation stress (i.e., $p_0(s)$) obtained in an unsaturated soil sample is significantly higher than that in a fully saturated soil at a particular stress increment ($10 - 10^3$kPa) (Figure 2.7). In other words, the pre-consolidation stress $p_0(s)$ is prone to increase as the matric suction increases. It is also reported that the compression indices κ and $\lambda(s)$ associated with settlement analyses would increase with increasing suction (Cuisinier & Laloui 2004). However, at a very high applied stress (e.g., 10^3kPa), compression curves of unsaturated soil samples would relatively converge to those of saturated samples (Figure 2.7). This phenomenon implies that the matric suction has insignificant effects on the volume change of the tested samples when the vertical applied stress increases. A plausible explanation for this observation associates with the change in degree of saturation (S_r) (Cuisinier & Laloui 2004). The void ratio of the unsaturated soil sample reduces during the compression process and consequently the degree of saturation approaches close to 100 per cent at the later stages of compression. This condition leads

to a pronounced increase in the meniscus, which in turn causes the matric suction to diminish as the loading progresses. Thus, compression curves of both saturated and unsaturated soils would approach a similar value when the loading increases.

2.2. Wetting-induced volume change issues

2.2.1. Problematic soils in response to saturation

Volume change prediction of soils has been a major interest in geotechnical engineering since the robust growth of classic soil mechanics introduced by Terzaghi (1925). In the mid 1960's, it was however realised that mechanical behaviours of a large portion of earth deposits in arid and semi-arid regions appeared to be inconsistent to the traditional saturated soil studies. A notable attention was given to a number of problematic soils associated with wetting-induced volume change in such areas. In particular, the naturally occurring deposits as well as compacted fills may be usually wetted as the results of excessive rainfalls or human-induced changes in groundwater regime. The wetting may lead to decreases or increases in a volume depending on the type and structure of soil, initial density, and the stress states to name a few (Ng & Menzies 2007). According to Houston (1996), soils exhibiting considerable deformation due to changes in moisture content can be regarded as *moisture-sensitive soils*.

Most soils under the arid climates appear to be problematic as they expand, collapse, or disperse and subsequently experience a significant ground deformation (Rezaei et al. 2012). Particularly, two common problems in response to the effect of wetting that geotechnical and foundation engineers have frequently encountered in real practice are related to collapsible soils and expansive soils (Houston et al. 1988; Bell & Maud 1995; Bell & Culshaw 2001; Tripathy et al. 2002; Fredlund 2014). When moisture content increases, collapsible soils are usually subjected to pronounced reduction of volume or collapse whereas expansive soils are prone to heave. Both problematic soils are moisture-sensitive and would lead to foundation distress and differential movements, which consequently result in severe damages to the structural components (Ng & Menzies 2007; Sheng 2011). It is worth mentioning that such soils are relevant to unsaturated soil mechanics, which contradicts to the saturated soil theories due to their different natures and properties.

2.2.2. Collapsible soils

Arid and semi-arid climates have been immensely attributable to the formation of problematic collapsible soils (Houston et al. 2001). Furthermore, over the past decades, urbanisation in such climatic areas has significantly disturbed the groundwater level and increased the moisture content within the foundation region. Thus, the soil volume would eventually suffer from a dramatic reduction upon wetting. Particles of collapsible soils are originally comprised of loosely packed grains, ranging from gravels and cobbles to fine sands and silts with coatings of small amounts of clay (Fookes & Parry 1994). Clevenger (1956) also reports that the silt and sand contents in the collapsible soils (e.g. loess, colluvium, alluvium, brickearth etc.) may be up to 90 per cent of the soil weight. Ng & Menzies (2007) further explained that such naturally occurring soils possess a metastable structure with typically low density, and may be cemented by various salts, oxides and dried clays. It should be noted that the matric suction has substantial impacts on properties of those soils, particularly the void ratio. As explained by Fredlund (2014), the reduction in matric suction due to wetting would lead to a notable decrease in void ratio of the metastable-structured soils, and an increase in void ratio of the stable-structured soils. When wetted, the soil tends to move downwards rapidly as particles slip past each other to become more tightly compacted. Significant amount of clay contained in soils, however, would hinder the collapse rate (Bell & Culshaw 2001).

During the vigorous urbanisation, engineering activities such as alterations and modifications of natural flow patterns have been responsible for the collapse of soil (Ng & Menzies 2007). Several methods have been proposed to predict the collapse issue upon wetting. Clevenger (1956) developed a dry density based criteria to determine if a soil is liable to the collapse when the moisture content increases. Specifically, the soil may be predicted to experience a significant collapse for the dry density smaller than about $1.3\ \mathrm{t/m^3}$, and the soil may undergo a less pronounced collapse for the dry density greater than $1.44\ \mathrm{t/m^3}$ (Clevenger 1956). Gibbs & Bara (1962) recommended criteria for detecting the collapsibility based on the dry unit weight when the liquid limit is greater than 20 per cent. Handy (1973), on the other hand, suggested much simpler method to estimate the probability of collapse by investigating the quantity of clay.

Detailed criteria indicating the probability of soil collapse due to saturation are provided in Table 2.2.

Table 2.2. Criteria for determining collapsibility based on clay content (modified after Handy 1973)

Clay Content (%)	**Probability of Collapse upon Wetting**
Below 16	High probability for collapse
16 – 25	Probably collapsible
25 – 32	Less than 50%
Above 32	Non-collapsible

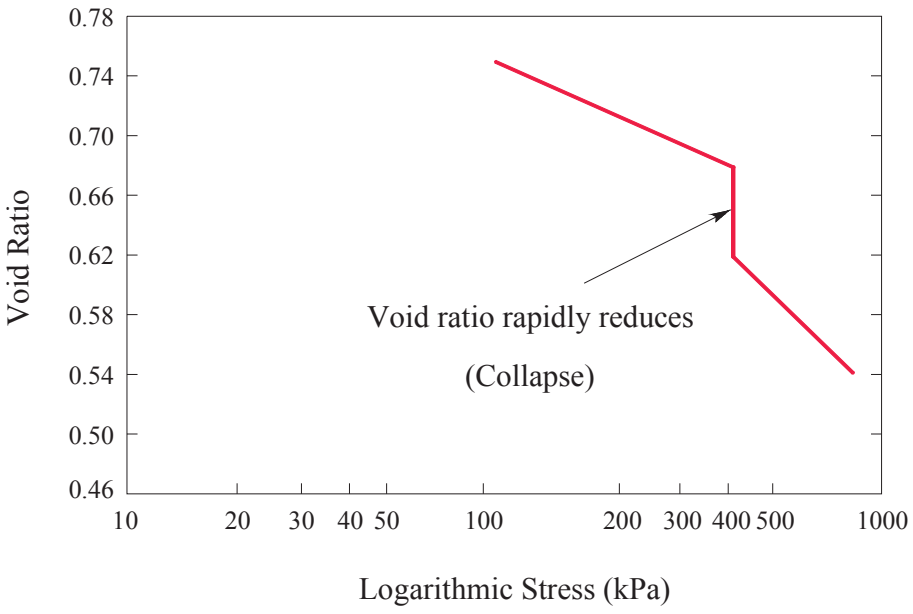

Figure 2.8. Result generated by oedometer test indicating collapse of metastable-structured brickearth (modified after Northmore et al. 1996)

Pells et al. (1975) conducted oedometer tests to investigate the effect of wetting on identical metastable-structured soils. In particular, specimens were prepared in the way that they could maintain natural moisture content, and then they were subjected to the same loading sequences. After the loading reached a given target, the unsaturated specimens were inundated with water for over 24 hours while maintaining the loading condition. Reduction of volume of the specimen eventually occurred and the collapse strain was recorded. Then, the specimens experienced further applied load. Figure 2.8 presents a typical collapse evidence of metastable-structured brickearth (taken from the south Essex) under the oedometer test condition carried out by Northmore et al. (1996). Based on experimental results, Pells et al. (1975) further summarised the potential severity of collapse by measuring the collapse percentage (i.e., $\Delta e/(1+e)$, in which 'e' is the void ratio) (Table 2.3).

Table 2.3. Criteria indicating severity of collapse based on percentage of collapse (modified after Pells et al. 1975)

Collapse Percentage (%)	**Severity of Problem**
0 – 1	No problem
1 – 5	Moderate problem
5 – 10	Problem
10 – 20	Severe problem
Above 20	Very severe problem

Identifying collapse potential deposits prior to construction and proposing proper solutions to alleviate collapse problems have always been great challenges for geotechnical engineers. The lack of thorough understanding of the wetting-induced volume change leads to unsatisfactory remedy for the problem. Practically, light-weight

to moderate-weight structures and many other cost-competitive construction projects may be susceptible to critical damages because the financial investments spent on the site investigation and mitigation alternatives are usually limited (Ng & Menzies 2007). Some available solutions have been proposed to deal with the collapse phenomenon such as removal of moisture-sensitive soils (Anayev & Volyanick 1986), chemical stabilisation (Sokolovich & Semkin 1984), dynamic compaction (Lutenegger 1986), pile foundations (Gao et al. 2007), and differential settlement resistance foundations (Souza et al. 1995) to name a few. The soil collapsibility is not comprehensively understood and, in most practical cases, it is only discovered after the structure is completely constructed. To overcome such problem, great cares should be given to the site investigation and pre-construction mitigation plan prior to construction.

2.2.3. Expansive soils

Essentially expansive soils account for many critical failures of foundation in response to wetting. This geotechnical problem has been frequently reported in several parts of the world, but is found to be the most critical in arid and semi-arid climatic areas, where urbanisation takes place (Jones & Jefferson 2012). Due to an increase in water content within foundation, moisture-sensitive soils may be subjected to substantial volume changes characterised by swell-shrink processes. According to Jones & Jefferson (2012), foundation beneath infrastructures and buildings primarily consists of clay-rich deposits, such as smectite and montmorillonite, with high swelling potential. It should be noted that if a soil contains larger amounts of clay, its welling potential will become very high and the soil is able to absorb more water. In this case, the soil volume would subsequently swell or expand due to the water absorption. It is common for most expansive clays to experience volume changes of more than 10 per cent (Nelson & Miller 1997; Chen 2012). In contrast, clays with shrinkage potential may be exposed to a dry condition during a long-term drought and therefore become more susceptible to the shrinkage and cracking phenomena. Holtz & Kovacs (1981) report that the swell-shrink behaviours of clays are irreversible processes. However, latest results from cyclic swell-shrink tests have demonstrated that compacted clays subjected to numerous wetting and drying cycles would almost recover to the original soil thickness (Subba Rao & Satyadas 1987; Day 1994; Al-Homoud et al. 1995; Songyu et al. 1998; Tripathy et al. 2002; Ng & Menzies 2007).

Soils with high swelling potential would be liable to volume expansions when wetted, lifting up and damaging engineered structures, particularly the low-rise or light-weight structures. Contrariwise, soils with shrinkage potential would become rigid under the dry condition, inducing shrinkage and cracking of the ground. Referring to Bell & Culshaw (2001), the swell-shrink response of clays substantially depends on seasonal variations (e.g. rainfall, drought), precipitation and evapotranspiration of vegetation. More importantly, a decent portion of clay contained in soils would be a crucial factor that contributes immensely to swelling (Tripathy et al. 2002). Reportedly, kaolinite is usually categorised into a clay group that has the least swelling capacity; illite can expand up to 15 per cent and would further expand to 60 per cent or more when it is mixed with montmorillonite; calcium montmorillonite has the swelling range from about 50 to 100 per cent; and sodium montmorillonite exhibits very high expansion with up to 2000 per cent of the initial volume and is likely to appear in a gel form when wetted (Bell & Culshaw 2001). The wetting-induced volume change is also characterised by the initial density and the soil structure. Expansion of a densely packed soil tends to proceed more quickly compared to that of a loosely packed soil. It is worth noting that undisturbed expansive clays support the soil structure against swelling pressures and therefore become less susceptible to vertical deformations (Ng & Menzies 2007).

Table 2.4. Potential swell-shrink of clayey soils based on various categories of PI (modified after BRE 1993)

PI (%)	**Potential Swell-Shrink**
Below 18	Low
12 – 32	Medium
22 – 48	High
Above 35	Very high

According to Bell & Maud (1995), volume change detection methods available in engineering practice include empirical, soil suction and oedometer methods. The empirical method usually involves determining various properties such as Liquid Limit (LL), Plastic Limit (PL), natural moisture content, and void ratio to name a few. The Building Research Establishment (BRE) (1993) shows the degree of swelling and shrinkage potentials of clayey soils by referring to the Plasticity Index (PI) (see Table 2.4). Note that overlapping categories of PI presented in Table 2.4 are due to the fact that data was collected from various sources (Jones & Jefferson 2012). Nevertheless, the prediction criteria based on PI is found to be rather simple yet impractical as it does not capture effects of moisture content, soil suction and structure which principally control the swell-shrink behaviour (Bell & Culshaw 2001).

Soil suction is considered to be a substantial factor influencing the degree of volume change. Particularly, matric suction reduces in response to an increase in moisture content, resulting in a swelling behaviour of soils. When a soil achieves the maximum expansion, the value of matric suction would reach zero (Ng & Menzies 2007). For the volume change detection method related to suction, O'Neil & Poormoayed (1980) adopted the United States Army Engineers Waterways Experimental Station (USAEWES) to present swelling potentials and their classifications corresponding to various groups of in situ suction, LL and PL, as shown in Table 2.5.

Table 2.5. Potential swell and classifications based on USAEWES (modified after O'Neil & Poormoayed 1980)

In situ Suction (kPa)	**LL (%)**	**PL (%)**	**Potential Swell (%)**	**Classifications**
Below 145	Below 50	Below 25	Below 0.5	Low
145 – 385	50 – 60	25 – 35	0.5 – 1.5	Marginal
Above 385	Above 60	Above 35	Above 1.5	High

Alternatively, the potential swell of a soil can be determined by adopting oedometer tests. Undisturbed clayey specimens can be prepared and placed firmly in the oedometer and then subjected to different stress paths. Subsequently, data related to vertical strain of soil specimen is collected and analysed. As reported by Bell & Culshaw (2001), both lateral and vertical strains develop locally within the ground, inducing visible cracking in soils. Furthermore, oedometer test results revealed that the swelling and shrinkage deformations do not happen one-dimensionally. Thus, an exclusion of lateral strain in the study may overestimate the extent of the problems (Bell & Culshaw 2001).

Expansive soils may cause a long-term heave beneath structures due to wetting and induce a differential settlement as well as cracking in response to drying. To deal with these expansive problems, some solutions have been used in engineering practice such as ground substitution (Katti & Katti 1994), ground stabilisation (Nelson & Miller 1997), stabilisation of moisture content, flexible structure design, rigid structure design (Rosenhaupt & Mueller 1963), and deep foundations (Blight 1984). Also, careful site investigations and explorations should be carried out prior to construction to avoid potentially expansive problems.

2.3. Stress State Variables in Unsaturated Soils

2.3.1. Single-valued effective stress equations

Volume change characteristics and shear strength are generally regarded as mechanical properties which can be described in terms of stress state in a soil. The term "*stress state variables*" refers to combinations of stress variables in the soil that characterise physical deformations. According to Ng & Menzies (2007), typical stress state variables of an elastic body describe the strain and stress fields and the geometry of the body. In addition, stress state variables can be used to establish a constitutive model predicting soil behaviours associated with the volume change and shear strength. It should be also noted that these stress variables are independent of physical properties of soil and can be therefore applicable to a wide range of soil particles such as sands, silts and clays (Fung 1965; Ng & Menzies 2007).

Table 2.6. Single-valued effective stress equations for unsaturated soils (modified after Fredlund 1987)

Equations	**Authors**
$\sigma' = \sigma - \beta' u_w$ where β' is the bonding factor which is measure of number of bonds under tension, effective in contributing to soil strength.	Croney et al. (1958)
$\sigma' = (\sigma - u_a) + \chi(u_a - u_w)$ where u_a is the pore-air pressure; and χ is the parameter related to the degree of saturation.	Bishop (1959)
$\sigma' = \sigma - \beta p''$ where β is the statistical factor of same type as contact area; and p'' is the pore-water pressure deficiency.	Jennings (1960)
$\sigma' = \sigma - \psi p''$ where ψ is the parameter with values ranging from zero to one.	Aitchison (1961)
$\sigma' = (\sigma - u_a) + \chi_m(h_m + u_a) + \chi_s(h_s + u_a)$ where χ_m is the effective stress parameter for matric suction; χ_s is the effective stress parameter for solute suction; h_m is the matric suction; and h_s is the solute suction.	Richards (1966)

In saturated soil studies, the effective stress principle and one-dimensional (1D) consolidation theory were initiated by Terzaghi (1925), who claimed that the stiffness and shear strength are principally controlled by an effective stress. This 1D consolidation theory was later expanded to the three-dimensional (3D) consolidation field by Biot (1941). The effective stress in saturated soil mechanics can be considered as a single stress state variable and is expressed as follows:

$$\sigma' = \sigma - u_w \qquad [2\text{-}8]$$

where σ' is the effective normal stress; σ is the total normal stress; and u_w is the pore-water pressure. The single-valued effective stress equation for fully saturated soils has been proven to be valid through numerous experiments conducted by Rendulic (1936), Bishop & Eldin (1950), and Skempton (1984). The validity of effective stress theory in saturated soil mechanics has motivated further developments of single-valued effective stress equations for unsaturated soils. In late 1950s and early 1960s, many progressions were made to adopt the effective stress concept by Croney et al. (1958), Bishop (1959), Jennings (1960), Aitchison (1961), and Richards (1966). Table 2.6 summarises various single-valued effective stress equations proposed for unsaturated soils.

Later studies (e.g. Brackley 1971; Morgenstern 1979; Wheeler & Karube 1996) however revealed that unsaturated soil frameworks adopting the single effective stress might lead to many practical difficulties. Morgenstern (1979) found that the volumetric behaviour and shear strength might not be practically governed by the same effective stress parameters. Wheeler & Karube (1996), on the other hand, reported that expansive and collapsible soil effects could not be captured in the proposed effective stress equations. Experimental results also showed little support on the use of a single-valued effective stress (Wheeler & Karube 1996). According to Morgenstern (1979), soil parameters used in the proposed equations, particularly χ, may not be comprehensively understood. Moreover, the soil property (i.e., degree of saturation) incorporated in effective stress make the proposed equations no longer single-valued (Fredlund et al. 2012). Many studies (Coleman 1962; Jennings & Burland 1962; Bishop & Blight 1963; Burland 1964; Blight 1965) demonstrate that the soil property associated with effective stress would rather vary depending on different physical problems such as volume change and shear strength, different stress paths, and different types of soil. In

concerning several limitations when adopting the single-valued effective stress for unsaturated soils, Matyas & Radhakrishna (1968), Barden et al. (1969), and Fredlund & Morgenstern (1977) recommended separate stress state components for further formulation of constitutive models. The concept of independent stress state variables has been used in many theoretical formulations for fluid flows (e.g. Fredlund & Hasan 1979; Dakshanamurthy & Fredlund 1980, 1981; Darkshanamurthy et al. 1984) and elastoplastic (EP) frameworks for volume change prediction (e.g. Alonso et al. 1990; Cui & Delage 1996; Chiu & Ng 2003; Georgiadis et al. 2005; Thu et al. 2007).

It is however worth mentioning that the effective stress equation for unsaturated soils have been recently modified and incorporated in many well-recognised EP models (e.g. Kohgo et al. 1993; Loret & Khalili 2000, 2002; Sheng et al. 2004; Pereira et al. 2005; Sun et al. 2007; Nuth & Laloui 2008). These EP models were constituted on the basis of Bishop's effective stress theory to predict the volume change of soils while capturing the plastic collapse phenomenon. Likewise, the effective parameter χ, as introduced by Bishop (1959), was qualitatively defined with decent accuracy. Based on experimental results extracted from past literature studies, Khalili & Khabbaz (1998) expressed the parameter χ as a function of matric suction as follows:

$$\chi = \begin{cases} 1 & s \leq s_{ae} \\ \left(\frac{s}{s_{ae}}\right)^{-\gamma} = \left[\frac{(u_a - u_w)}{(u_a - u_w)_b}\right]^{-0.55} & s > s_{ae} \end{cases} \qquad [2\text{-}9]$$

where s or $(u_a - u_w)$ is the matric suction; s_{ae} or $(u_a - u_w)_b$ is the air entry suction; and γ is constant parameter obtained from the best-fit data and usually has a value of 0.55. Note that the value of γ varies depending on different soil particles. Particularly, the parameter γ may be higher than 0.55 for the coarser soils and smaller than 0.55 for the finer soils (Khalili & Khabbaz 1998). On the other hand, as observed in Equation [2-9], the effective parameter χ decreases as the matric suction increases. It should be noted that the parameter χ is imperative for the development of single-valued effective stress equation. A recent study conducted by Alonso et al. (2010) shows that χ can also be expressed in terms of effective degree of saturation (i.e. S_r^e). The EP models adopting the effective stress principle to predict the volume change of unsaturated soils are discussed in Section 2.5.

2.3.2. Equilibrium analyses and newly proposed stress state variables

There was a realisation that the proposed single-valued effective stress variables, shown in Section 2.3.1, contributed very little practicality to the definition of stress state in unsaturated soils (Brackley 1971; Morgenstern 1979). According to Wheeler & Karube (1996), the qualitative difference in action modes of matric suction and external applied stress within the soil skeleton may account for this unsatisfactory stress state description. More specifically, the suction only provides the normal bonding forces (i.e., N_s) at contacts of adjacent particles while external stress applied to a soil element induces the normal and tangential forces (i.e., N_σ and T_σ, respectively) at particle contacts (Wheeler & Karube 1996). Therefore, combining these stresses to produce a single effective stress parameter would result in failure to describe unsaturated soil problems associated with volume change and shear strength. Figure 2.9 illustrates inter-particle forces generated by the external stress and matric suction. Many constitutive models predicting volume change of unsaturated soils have instead adopted independent stress state variables (Alonso et al. 1990; Cui & Delage 1996; Chiu & Ng 2003; Georgiadis et al. 2005; Thu et al. 2007; Fredlund et al. 2012).

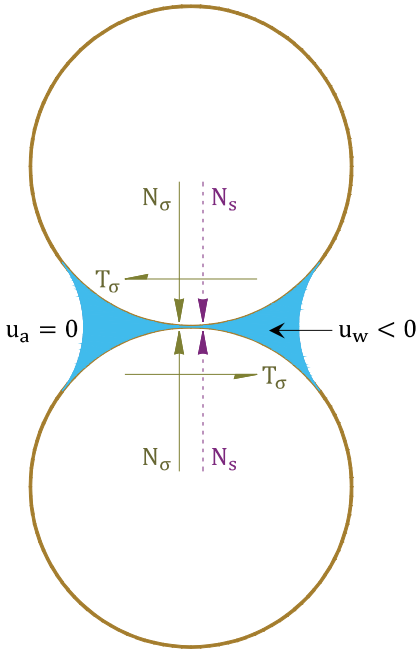

Figure 2.9. Effects of external total stress and matric suction on inter-particle forces at contact of adjacent particles (after Wheeler & Karube 1996)

In an attempt to formulate constitutive models that capture both volumetric and shear behaviours of unsaturated soils, contemporary studies conducted by Matyas & Radhakrishna (1968), Barden et al. (1969), Fredlund & Morgenstern (1977) and numerous others have recommended the use of combination of independent stress state variables. Considering the unsaturated soil as a four-phase composition, it is essential to separate stress variables in an independent manner. Fredlund & Morgenstern (1977) suggested that any two of three stress variables $(\sigma - u_a)$, $(\sigma - u_w)$ and $(u_a - u_w)$ can be selected to define the stress state and can therefore be used to establish constitutive equations for unsaturated soils. It is worth mentioning that the constitutive behaviour described from deformation analyses normally associates with overall equilibrium (Morgenstern 1979). Thus, the proposed stress state variables can be extracted from the equilibrium equations.

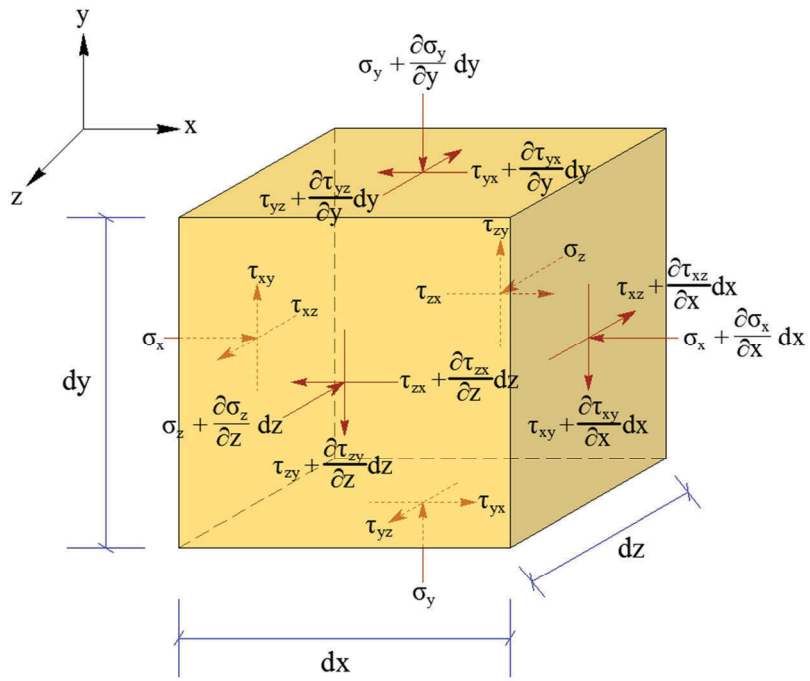

Figure 2.10. Normal and shear stresses acting on a cuboidal soil element (after Fredlund et al. 2012)

According to Fredlund et al. (2012), stress state variables control behaviour of unsaturated soils, in terms of volume change and shear strength, and can be used to describe the equilibrium of soil structure. Fredlund & Rahardjo (1993) also recommended that measurable stresses such as the total normal stress (σ), pore-air (u_a)

and pore-water (u_w) pressures are potential parameters to present stress state variables. A cuboidal element of unsaturated soil is commonly used when analysing the stress equilibrium at a point. Figure 2.10 presents the cuboidal soil element with the infinitesimal dimensions dx: dy: dz subjected to external stresses.

As observed in Figure 2.10, two primary types of stress acting on a plane of soil mass, such as total normal stresses (i.e., σ_x, σ_y and σ_z) and shear stresses (i.e., τ_{xz}, τ_{xy} and τ_{zy}), mainly contribute to the overall equilibrium of soil structure. The normal stress is perpendicular to the plane of unsaturated soil element while the shear stress is transverse to the element plane. For the sign convention, all compressive normal stresses presented in Figure 2.10 are suggested to be positive whereas tensile normal stresses are negative (Holtz & Kovacs 1981). Shear stresses, on the other hand, can be arbitrarily selected to be positive in a particular direction and negative in an opposite direction, as suggested by Sowers & Sowers (1951), or counter-clockwise shear stresses are positive and clockwise shear stresses are negative, as recommended by Taylor (1948), Dunn et al. (1980), Holtz & Kovacs (1981), and Das (1998). As supported by Fredlund & Rahardjo (1993), the force equilibrium is analysed capturing the concept of conservation of linear momentum. Assuming the y-direction is the vertical direction, equilibrium equations of an unsaturated soil structure can be algebraically determined by computing the resultant forces in the multiphase system (Fredlund & Morgenstern 1977), as follows:

$$\frac{\partial \tau_{xy}}{\partial x} + \frac{\partial (\sigma_y - u_a)}{\partial y} + (n_w + n_c f^*) \frac{\partial (u_a - u_w)}{\partial y} + \frac{\partial \tau_{zy}}{\partial z} + (n_c + n_s) \frac{\partial u_a}{\partial y} + n_s \rho_s g - F_{sy}^a - F_{sy}^w + n_c (u_a - u_w) \frac{\partial f^*}{\partial y} = 0 \quad [2\text{-}10]$$

where n_c is the porosity related to the contractile skin; n_s is the porosity related to the soil particles; n_w is the porosity related to the water phase; f^* is the interaction between the contractile skin and the soil structure equilibriums; F_{sy}^a is the interaction force between the air phase and soil particles in the y-direction; F_{sy}^w is the interaction force between the water phase and soil particles in the y-direction; ρ_s is the density of soil particles; and g is the gravitational constant.

It should be noted that Fredlund & Rahardjo (1993) derived Equation [2-10] while taking the pore-air pressure (u_a) as a reference pressure. Thus, the porosity with respect to the air phase can be expressed in terms of other porosity components, giving:

$$n_a \frac{\partial u_a}{\partial y} = (1 - n_w - n_c - n_s) \frac{\partial u_a}{\partial y} \quad [2\text{-}11]$$

where n_a is the porosity related to the air phase. Equation [2-11] is used to derive Equation [2-10]. Detailed force components for multiphase equilibrium (i.e., soil solids, air, water and contractile) can be depicted in Figure 2.11. For the equilibrium analysis, the soil element is subjected to the gravitational force (i.e., ρg) and interaction forces (i.e., F^a_{sy}, F^a_{cy}, F^w_{sy} and F^w_{cy}) in the vertical direction (i.e., y-direction) only. These forces, known as *body forces*, act through the centroid of soil mass. Contractile skin, on the other hand, induces surface tractions in the unsaturated soil element, as discussed in Section 2.1.2, and significantly influences the equilibrium conditions. It is worth noting that the matric suction ($u_a - u_w$) in both compressible and incompressible soils has notable impacts on the contractile skin equilibrium whereas the total stress affects the contractile skin equilibrium for only a case of compressible soils. Therefore, changes in degree of saturation (S_r) or water content of the soil are more likely attributed to the change in matric suction (Fredlund & Rahardjo 1993).

Three stress variables, namely $(\sigma_y - u_a)$, $(u_a - u_w)$ and (u_a), can be extracted from the equilibrium equation for the unsaturated soil structure (i.e., Equation [2-10]). These stress variables are referred as stress state variables characterising the mechanical behaviour of soils. It should be noted that the stress variable (u_a) can be omitted when the incompressible soils are considered in the analysis (Fredlund & Rahardjo 1993). Thus, possible stress state variables for further constitutive formulations are $(\sigma_y - u_a)$ and $(u_a - u_w)$.

Alternatively, the equilibrium equation of soil structure can be obtained by using the pore-water pressure (u_w) as a reference pressure. Hence, the relationship of porosities of individual phases is:

$$n_w \frac{\partial u_w}{\partial y} = (1 - n_a - n_c - n_s) \frac{\partial u_w}{\partial y} \quad [2\text{-}12]$$

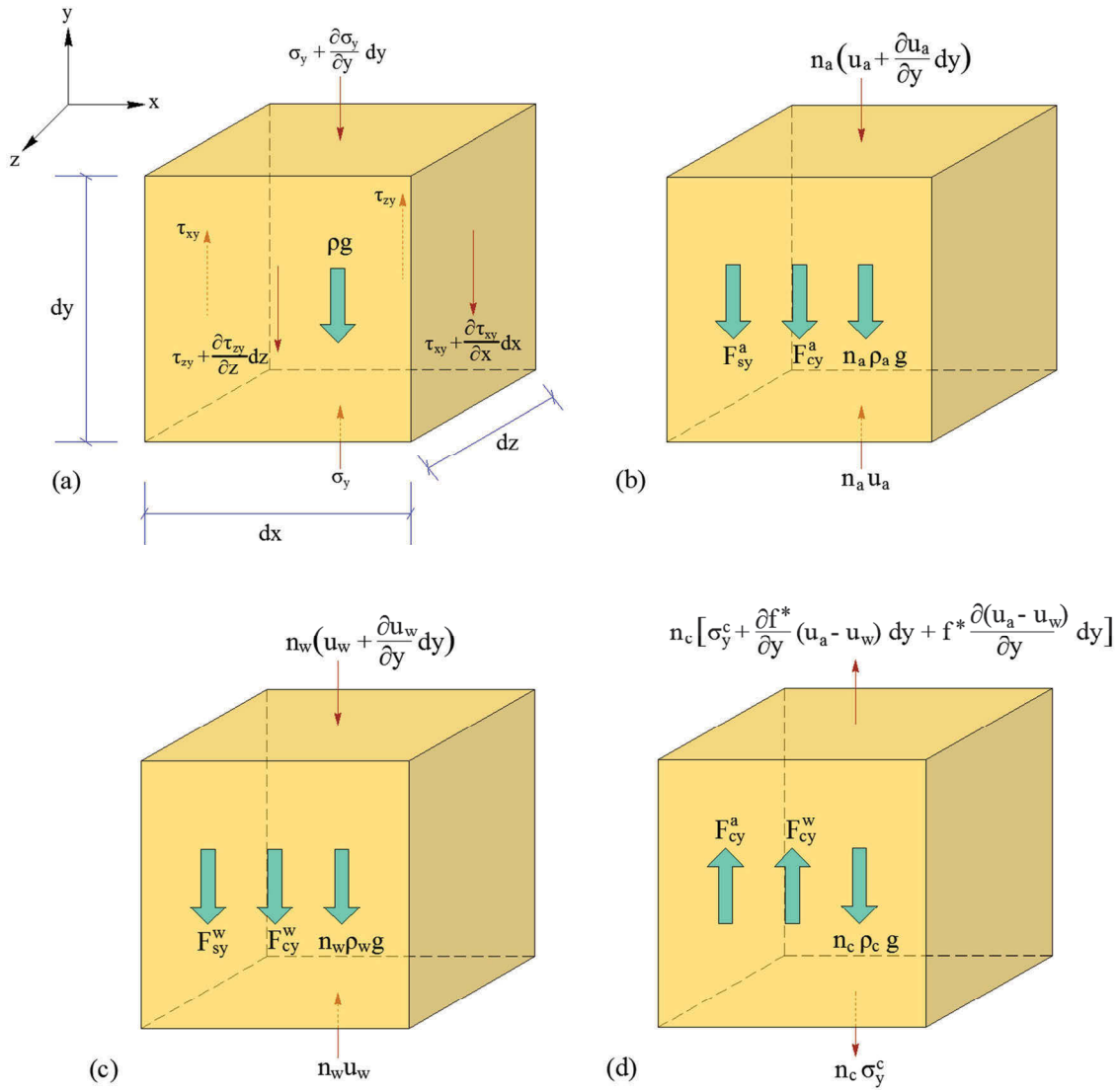

F^a_{sy} = interaction force between air phase and soil particles in the y-direction

F^a_{cy} = interaction force between air phase and contractile skin in the y-direction

F^w_{sy} = interaction force between water phase and soil particles in the y-direction

F^w_{cy} = interaction force between water phase and contractile skin in the y-direction

f^* = interaction between the contractile skin and the soil structure equilibriums

n_a, n_c, n_s, n_w = porosities relative to air, contractile skin, soil particles and water, respectively

ρ_a, ρ_c, ρ_s, ρ_w = densities relative to air, contractile skin, soil particles and water, respectively

σ_y = total normal stress in the y-direction

σ^c_y = normal component of stress in the contractile skin on the y-direction

Figure 2.11. Components for force equilibrium of (a) soil element, (b) air phase, (c) water phase and (d) contractile skin in the y-direction (modified after Fredlund & Rahardjo 1993)

Then, equilibrium equations of soil structure in the y-direction can be rewritten by incorporating Equation [2-12] and subsequently obtaining the resultant forces of independent phases, yielding in:

$$\frac{\partial \tau_{xy}}{\partial x} + \frac{\partial (\sigma_y - u_w)}{\partial y} + (n_a + n_c f^*) \frac{\partial (u_a - u_w)}{\partial y} + \frac{\partial \tau_{zy}}{\partial z} + (n_c + n_s) \frac{\partial u_w}{\partial y} + n_s \rho_s g - F_{sy}^a - F_{sy}^w + n_c (u_a - u_w) \frac{\partial f^*}{\partial y} = 0 \quad [2\text{-}13]$$

Three stress variables, including $(\sigma_y - u_w)$, $(u_a - u_w)$ and (u_w), are extracted from Equation [2-13] and can be used to describe the stress state of unsaturated soils. However, the stress variable (u_w) is disregarded when incompressible soil particles are considered in the analysis (Fredlund & Rahardjo 1993). Therefore, only two possible stress state variables $(\sigma_y - u_w)$ and $(u_a - u_w)$ can be selected for further constitutive formulation.

On the other hand, if the total normal stress in the y-direction (σ_y) is used as a reference, Equation [2-10] can be rearranged as follows:

$$\frac{\partial \tau_{xy}}{\partial x} + (n_a - n_c f^*) \frac{\partial (\sigma_y - u_a)}{\partial y} + (n_w + n_c f^*) \frac{\partial (\sigma_y - u_w)}{\partial y} + (n_c + n_s) \frac{\partial \sigma_y}{\partial y} + n_s \rho_s g - F_{sy}^a - F_{sy}^w + n_c (u_a - u_w) \frac{\partial f^*}{\partial y} = 0 \quad [2\text{-}14]$$

The stress variables $(\sigma_y - u_a)$, $(\sigma_y - u_w)$ and (σ_y) are obtained from Equation [2-14] and can be referred as stress state variables of unsaturated soils. However, the stress variable (σ_y) can be neglected when considering the incompressible soils (Fredlund & Rahardjo 1993). Thus, the available stress state variables for constitutive models are $(\sigma - u_a)$ and $(\sigma - u_w)$.

In a limit of incompressible soil particles, the total equilibrium associated with the soil structure presented in Equations [2-10], [2-13] and [2-14] introduce three combinations of stress variables that principally control the volumetric and shear deformations of unsaturated soils. Specific combinations of stress variables are adopted depending upon the selected referential stress such as u_a, u_w and σ. Table 2.7 summarises different sets of independent stress state variables with corresponding reference pressures.

Table 2.7. Stress state variables depending on each referential pressure (Fredlund et al. 2012)

Reference pressures	**Stress state variables**
Pore-air pressure, u_a	$(\sigma - u_a)$ and $(u_a - u_w)$
Pore-water pressure, u_w	$(\sigma - u_w)$ and $(u_a - u_w)$
Total normal stress, σ	$(\sigma - u_a)$ and $(\sigma - u_w)$

It is worth noting that, if both compressible soil grains and pore fluid are considered in the equilibrium equations, more than two stress state variables are needed to describe the behaviour of unsaturated soils (Ng & Menzies 2007). From Table 2.7, the pair of net stress $(\sigma - u_a)$ and matric suction $(u_a - u_w)$ has been commonly adopted for recent consolidation studies (Fredlund & Morgenstern 1977; Fredlund & Hasan 1979; Fredlund et al. 2012). Some advantages for selecting these stress variables are presented as follows:

- Effects due to changes in the total normal stress (σ) and pore-water pressure (u_w) are independent (Fredlund et al. 2012);
- In most practical problems, the pore-air pressure (u_a) is zero (Ng & Menzies 2007; Fredlund et al. 2012) and as the result, the net stress and suction can be further simplified to the total normal stress and negative pore-water pressure, respectively; and
- The negative pore-water pressure may not be easily measured, therefore selecting the stress variables $(\sigma - u_a)$ and $(u_a - u_w)$ would reduce an uncertainty in the value of stress state variables (Ng & Menzies 2007).

The alternative combination of stress variables $(\sigma - u_w)$ and $(u_a - u_w)$ can also be adopted for some research as it allows an easier transition from unsaturated soil state to fully saturated state. However, this transition has a very minor contribution to the problem solving (Wheeler & Karube 1996). Furthermore, Ng & Menzies (2007) also

added that adopting the two alternative stress variables may lead to practical difficulties since the negative pore-water pressure is not easily determined. Thus, the pair of net stress $(\sigma - u_a)$ and matric suction $(u_a - u_w)$ still has been the most satisfactory combination for practical analyses (Fredlund 1987). For the sake of generality, this thesis will adopt the stress state variables $(\sigma - u_a)$ and $(u_a - u_w)$ for the analytical development in subsequent chapters.

2.4. Volume-Mass Constitutive Relation

2.4.1. Continuity requirement

When a soil is subjected to an external loading, the volume change of soil element is considered to be equal to the sum of volume changes related to each independent phase (Fredlund et al. 2012). If the soil particles are assumed to be incompressible and the contractile skin is considered as part of water phase, the continuity condition for unsaturated soil is presented as follows:

$$\frac{\Delta V_v}{V_0} = \frac{\Delta V_a}{V_0} + \frac{\Delta V_w}{V_0} \qquad [2\text{-}15]$$

where V_0 is the total volume of unsaturated soil element before loading; ΔV_v is the volume change relative to voids of soil element due to loading; ΔV_a is the volume change relative to the air phase due to loading; and ΔV_w is the volume change relative to the water phase due to loading. The continuity requirement, presented in Equation [2-15], is proposed by Fredlund & Hasan (1979). It should be noted that the continuity condition presented in Equation [2-15] is only valid under the assumption of incompressible soil particles (Fredlund & Hasan 1979). The total volume change and water volume change can be practically measured in the laboratory while the air volume change is computed by taking the difference of measured values (Fredlund et al. 2012). The volumetric strain, denoted as ε_v, is defined as a ratio of volume change of voids (ΔV_v) and the initial volume of the element (V_0) is presented below:

$$\varepsilon_v = \frac{\Delta V_v}{V_0} \qquad [2\text{-}16]$$

Alternatively, by considering the 3D Cartesian coordinates (x, y, z), the volumetric strain can also be expressed by adding the normal strain components or adding all partial derivatives of displacement, resulting in:

$$\varepsilon_v = \varepsilon_x + \varepsilon_y + \varepsilon_z = \frac{\partial u}{\partial x} + \frac{\partial v}{\partial y} + \frac{\partial w}{\partial z} \quad [2\text{-}17]$$

where ε_x is the normal strain in the x-direction; ε_y is the normal strain in the y-direction; ε_z is the normal strain in the z-direction; u is the displacement in x-domain; v is the displacement in y-domain; and w is the displacement in z-domain.

2.4.2. Volume-mass constitutive models for unsaturated soils

Considering an isotropic and linearly elastic soil structure, the stress-strain constitutive relations for unsaturated soils can be expressed in terms of stress state variables, as presented in Section 2.3.2, while incorporating a generalised Hooke's law (Biot 1941). Fredlund & Morgenstern (1977) suggested that the net stress $(\sigma - u_a)$ and suction $(u_a - u_w)$ are the most appropriate stress variables for the constitutive formulation. The stress-strain constitutive equations associated with the strains in the x-, y- and z-directions are presented as shown below:

$$\varepsilon_x = \frac{\sigma_x - u_a}{E} - \frac{\mu}{E}(\sigma_y + \sigma_z - 2u_a) + \frac{u_a - u_w}{H} \quad [2\text{-}18a]$$

$$\varepsilon_y = \frac{\sigma_y - u_a}{E} - \frac{\mu}{E}(\sigma_x + \sigma_z - 2u_a) + \frac{u_a - u_w}{H} \quad [2\text{-}18b]$$

$$\varepsilon_z = \frac{\sigma_z - u_a}{E} - \frac{\mu}{E}(\sigma_x + \sigma_y - 2u_a) + \frac{u_a - u_w}{H} \quad [2\text{-}18c]$$

where E is the modulus of elasticity for the soil structure with respect to a change in the net stress; H is the modulus of elasticity for the soil structure with respect to a change in the matric suction; and μ is the Poisson's ratio.

Theoretically, the elastic modulus of the soil structure is described as a ratio between changes in the normal stress ($d\sigma$) and strain ($d\varepsilon$). Figure 2.12 illustrates the nonlinear stress-strain relationship of a soil on both stress-strain planes $[(\sigma - u_a), \varepsilon_v]$ and $[(u_a - u_w), \varepsilon_v]$. For the sign convention, both moduli of elasticity E and H are considered to be negative, as clearly shown in Figure 2.12. Since the stress-strain curve is nonlinear, an incremental analysis should be applied to the constitutive study. The

nonlinear curve can be treated as a linear curve when considering small stress and strain increments. It is worth noting that the incremental process adopting small increments of stress and strain can be practically used to evaluate the linearly elastic behaviour of a soil. The incremental form is applied to the stress-strain constitutive relations presented in Equations [2-18] as follows:

$$d\varepsilon_x = \frac{d(\sigma_x - u_a)}{E} - \frac{\mu}{E} d(\sigma_y + \sigma_z - 2u_a) + \frac{d(u_a - u_w)}{H} \quad [2\text{-}19a]$$

$$d\varepsilon_y = \frac{d(\sigma_y - u_a)}{E} - \frac{\mu}{E} d(\sigma_x + \sigma_z - 2u_a) + \frac{d(u_a - u_w)}{H} \quad [2\text{-}19b]$$

$$d\varepsilon_z = \frac{d(\sigma_z - u_a)}{E} - \frac{\mu}{E} d(\sigma_x + \sigma_y - 2u_a) + \frac{d(u_a - u_w)}{H} \quad [2\text{-}19c]$$

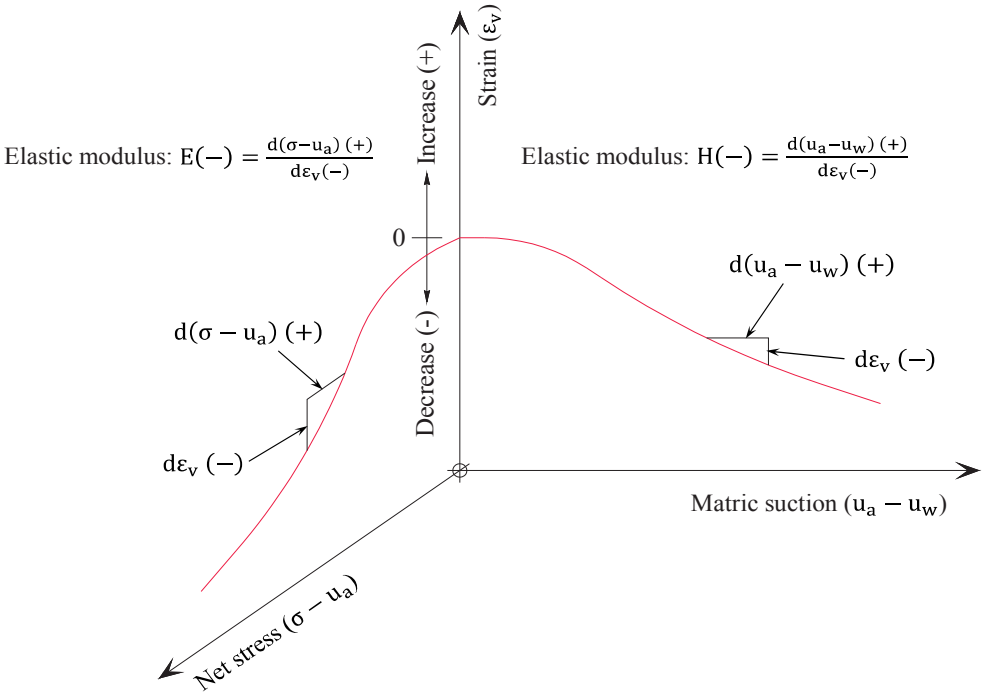

Figure 2.12. A nonlinear stress-strain relationships and sign convention for volumetric deformation properties

The volumetric strain increment of the soil is constituted by the sum of normal strain increments in the x-, y- and z-directions, presented in Equations [2-19a] – [2-19c], resulting in the constitutive equation that links the stress and deformation state variables:

$$d\varepsilon_v = \frac{dV_v}{V_0} = m_1^s d\left(\frac{\sigma_x+\sigma_y+\sigma_z}{3} - u_a\right) + m_2^s d(u_a - u_w) \quad [2\text{-}20]$$

The terms m_1^s and m_2^s presented in Equation [2-20] are defined as *volume change coefficients of soil structure* with respect to the net stress $(\sigma - u_a)$ and matric suction $(u_a - u_w)$, respectively. It should be noted that a pair of volume change coefficients m_1^s and m_2^s are considered as slopes of the constitutive surfaces at a particular stress point (Figure 2.13(a)), and may vary within different stress increments (Fredlund et al. 2012). When considering the general 3D loading condition, these coefficients can be expressed in terms of elastic moduli (E and H) and Poisson's ratio (μ) as follows:

$$m_1^s = \frac{\partial(\Delta V_v/V_0)}{\partial(\sigma_{mean}-u_a)} = 3\left(\frac{1-2\mu}{E}\right) \quad [2\text{-}21a]$$

$$m_2^s = \frac{\partial(\Delta V_v/V_0)}{\partial(u_a-u_w)} = \frac{3}{H} \quad [2\text{-}21b]$$

where $\sigma_{mean} = (\sigma_x + \sigma_y + \sigma_z)/3$. Assuming an incompressible water phase, Fredlund et al. (2012) developed the water phase constitutive equation based on a linear combination of the stress state variables:

$$\frac{dV_w}{V_0} = m_1^w d\left(\frac{\sigma_x+\sigma_y+\sigma_z}{3} - u_a\right) + m_2^w d(u_a - u_w) \quad [2\text{-}22]$$

The terms m_1^w and m_2^w presented in Equation [2-22] are called *volume change coefficients of water* with respect to the net stress $(\sigma - u_a)$ and matric suction $(u_a - u_w)$, respectively. These coefficients are graphically presented as slopes of the constitutive surface for the water phase at a stress point (Figure 2.13(b)), whose equations are expressed as below:

$$m_1^w = \frac{\partial(\Delta V_w/V_0)}{\partial(\sigma_{mean}-u_a)} = \frac{3}{E_w} \quad [2\text{-}23a]$$

$$m_2^w = \frac{\partial(\Delta V_w/V_0)}{\partial(u_a-u_w)} = \frac{1}{H_w} \quad [2\text{-}23b]$$

where E_w is the modulus of elasticity for water phase with respect to a change in the net stress; and H_w is the modulus of elasticity for water phase with respect to a change in the matric suction. As suggested by Fredlund & Hasan (1979), the volume change of air can only be determined on a basis of continuity requirement, as shown in Equation [2-

15]. Thus, the constitutive equation for the air phase is obtained by taking the difference between the volume changes of soil structure and water, giving:

$$\frac{dV_a}{V_0} = m_1^a d\left(\frac{\sigma_x+\sigma_y+\sigma_z}{3} - u_a\right) + m_2^a d(u_a - u_w) \quad [2\text{-}24]$$

Based on the continuity requirement at a particular stress point, the volume change coefficients must satisfy following conditions:

$$m_1^s = m_1^a + m_1^w \quad [2\text{-}25a]$$

$$m_2^s = m_2^a + m_2^w \quad [2\text{-}25b]$$

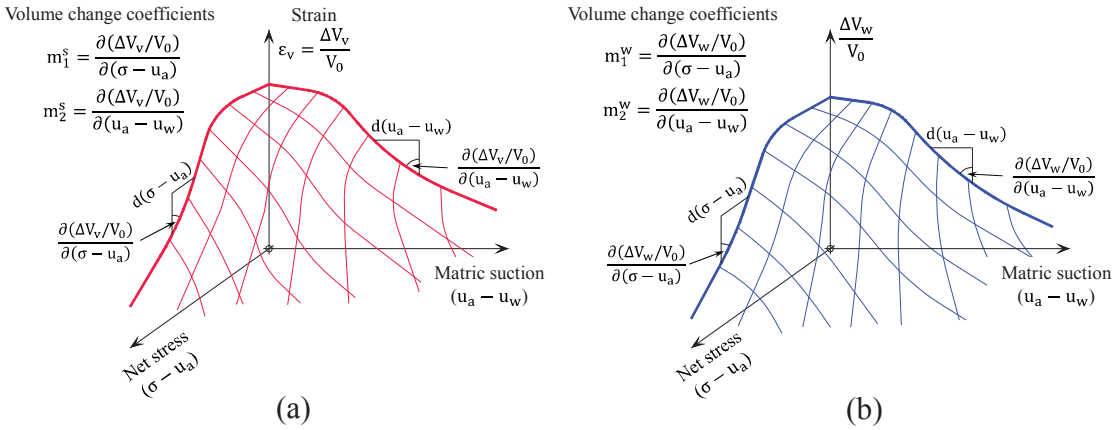

Figure 2.13. Constitutive surfaces for: (a) soil structure and (b) water phase (modified after Fredlund et al. 2012)

The constitutive relations of soil structure, water and air phases under the general 3D loading condition ($d\sigma_x \neq d\sigma_y \neq d\sigma_z$) are formulated in Equations [2-20], [2-22] and [2-24]. This stress-strain formulation can be practically applied to a several other loading conditions such as isotropic loading ($d\sigma_x = d\sigma_y = d\sigma_z = d\sigma_3$), uniaxial loading ($d\sigma_x = d\sigma_y = 0$), triaxial loading ($d\sigma_x = d\sigma_y = d\sigma_3$), K_0 loading (1D loading) ($d\varepsilon_x = d\varepsilon_y = 0$), two-dimensional (2D) plane strain loading ($d\varepsilon_y = 0$), and 2D plane stress loading ($d\sigma_y = 0$). Table 2.8 summarises constitutive equations along with volume change coefficients with respect to the soil structure and water phase for various loading conditions.

Table 2.8. Summary of constitutive equations for different loading conditions (modified after Fredlund et al. 2012)

Loading Conditions	**Constitutive Equations and Volume Change Coefficients for Soil Structure**	**Constitutive Equations and Volume Change Coefficients for Water Phase**
General 3D loading $(d\sigma_x \neq d\sigma_y \neq d\sigma_z)$	$\frac{dV_v}{V_0} = m_1^s d\left(\frac{\sigma_x+\sigma_y+\sigma_z}{3} - u_a\right) + m_2^s d(u_a - u_w)$ $m_1^s = 3\left(\frac{1-2\mu}{E}\right)$ and $m_2^s = \frac{3}{H}$	$\frac{dV_w}{V_0} = m_1^w d\left(\frac{\sigma_x+\sigma_y+\sigma_z}{3} - u_a\right) + m_2^w d(u_a - u_w)$ $m_1^w = \frac{3}{E_w}$ and $m_2^w = \frac{1}{H_w}$
Isotropic 3D loading $(d\sigma_x = d\sigma_y = d\sigma_z = d\sigma_3)$	$\frac{dV_v}{V_0} = m_1^s d(\sigma_3 - u_a) + m_2^s d(u_a - u_w)$ $m_1^s = 3\left(\frac{1-2\mu}{E}\right)$ and $m_2^s = \frac{3}{H}$	$\frac{dV_w}{V_0} = m_1^w d(\sigma_3 - u_a) + m_2^w d(u_a - u_w)$ $m_1^w = \frac{3}{E_w}$ and $m_2^w = \frac{1}{H_w}$
Uniaxial 3D loading $(d\sigma_x = d\sigma_y = 0)$	$\frac{dV_v}{V_0} = m_1^s d\left(\frac{\sigma_z}{3} - u_a\right) + m_2^s d(u_a - u_w)$ $m_1^s = 3\left(\frac{1-2\mu}{E}\right)$ and $m_2^s = \frac{3}{H}$	$\frac{dV_w}{V_0} = m_1^w d\left(\frac{\sigma_z}{3} - u_a\right) + m_2^w d(u_a - u_w)$ $m_1^w = \frac{3}{E_w}$ and $m_2^w = \frac{1}{H_w}$
Triaxial 3D loading $(d\sigma_x = d\sigma_y = d\sigma_3)$	$\frac{dV_v}{V_0} = m_1^s \left[d(\sigma_3 - u_a) + d\left(\frac{\sigma_1-\sigma_3}{3}\right)\right] + m_2^s d(u_a - u_w)$ $m_1^s = 3\left(\frac{1-2\mu}{E}\right)$ and $m_2^s = \frac{3}{H}$	$\frac{dV_w}{V_0} = m_1^w \left[d(\sigma_3 - u_a) + d\left(\frac{\sigma_1-\sigma_3}{3}\right)\right] + m_2^w d(u_a - u_w)$ $m_1^w = \frac{3}{E_w}$ and $m_2^w = \frac{1}{H_w}$

Table 2.8. Summary of constitutive equations for different loading conditions (continued)

Loading Conditions	**Constitutive Equations and Volume Change Coefficients for Soil Structure**	**Constitutive Equations and Volume Change Coefficients for Water Phase**
K_0 loading (1D loading)	$\frac{dV_v}{V_0} = m_1^s d(\sigma_z - u_a) + m_2^s d(u_a - u_w)$	$\frac{dV_w}{V_0} = m_1^w d(\sigma_z - u_a) + m_2^w d(u_a - u_w)$
$(d\varepsilon_x = d\varepsilon_y = 0)$	$m_1^s = \frac{(1+\mu)(1-2\mu)}{E(1-\mu)}$ and $m_2^s = \frac{1+\mu}{H(1-\mu)}$	$m_1^w = \frac{1+\mu}{E_w(1-\mu)}$ and $m_2^w = \frac{1}{H_w} - \frac{2(E/H)}{E_w(1-\mu)}$
2D plane strain loading	$\frac{dV_v}{V_0} = m_1^s d\left(\frac{\sigma_x+\sigma_z}{2} - u_a\right) + m_2^s d(u_a - u_w)$	$\frac{dV_w}{V_0} = m_1^w d\left(\frac{\sigma_x+\sigma_z}{2} - u_a\right) + m_2^w d(u_a - u_w)$
$(d\varepsilon_y = 0)$	$m_1^s = \frac{2(1+\mu)(1-2\mu)}{E}$ and $m_2^s = 2\left(\frac{1+\mu}{H}\right)$	$m_1^w = 2\left(\frac{1+\mu}{E_w}\right)$ and $m_2^w = \frac{1}{H_w} - \frac{(E/H)}{E_w}$
2D plane stress loading	$\frac{dV_v}{V_0} = m_1^s d\left(\frac{\sigma_x+\sigma_z}{2} - \frac{3}{2}u_a\right) + m_2^s d(u_a - u_w)$	$\frac{dV_w}{V_0} = m_1^w d\left(\frac{\sigma_x+\sigma_z}{2} - \frac{3}{2}u_a\right) + m_2^w d(u_a - u_w)$
$(d\sigma_y = 0)$	$m_1^s = 2\left(\frac{1-2\mu}{E}\right)$ and $m_2^s = \frac{3}{H}$	$m_1^w = \frac{2}{E_w}$ and $m_2^w = \frac{1}{H_w}$

2.4.3. Uniqueness of constitutive surfaces

Series of experiments were rigorously conducted to examine the uniqueness of constitutive surfaces associated with the soil structure and water phase. The term "*uniqueness*" indicates that the stress state variables and volume change properties can be used to form only one predictive framework such that values of which are reasonably equal to measured values (Fredlund & Morgenstern 1977). In other words, the constitutive relationships presented in Equations [2-20] and [2-22] should be proven valid by comparing the predicted results with experimental results. According to Fredlund et al. (2012), the constitutive surfaces can be concluded unique if identical samples (with similar soil properties) which approach the same final stress point would experience relatively similar volume changes irrespective of history of stress paths.

The uniqueness of constitutive surfaces, however, could not be easily inspected due to the hysteresis associated with the soil structure (i.e., loading and unloading curves) and contractile skin (i.e., drying and wetting curves). It has been found that increases and decreases in loading or water content would lead to different constitutive surfaces (Fredlund et al. 2012), as shown in Figure 2.14. Thus, volume change coefficients with respect to the soil structure (i.e., m_1^s and m_2^s) and water (i.e., m_1^w and m_2^w) would also change corresponding to those constitutive slopes. As suggested by Fredlund et al.

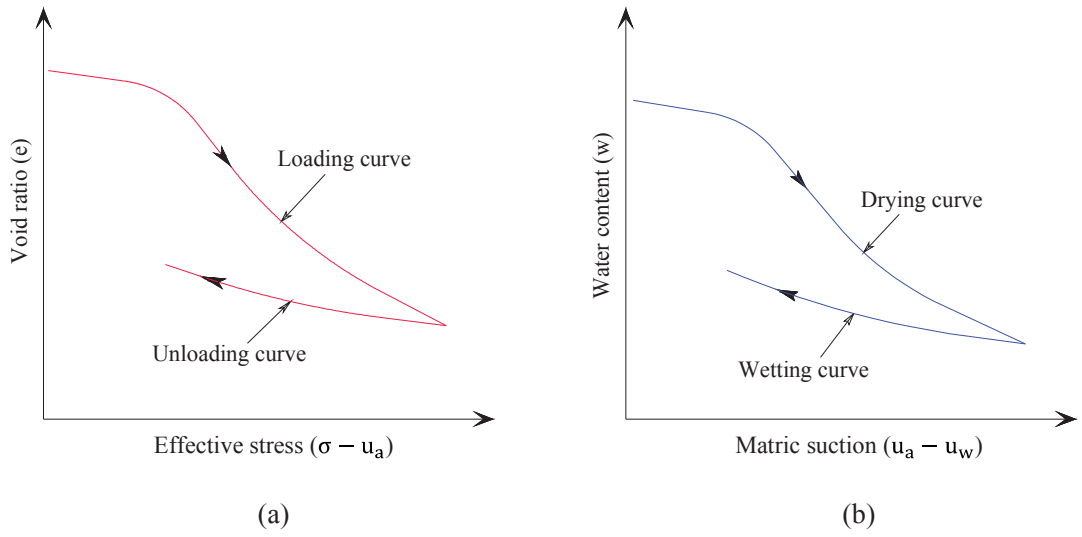

Figure 2.14. Hysteresis associated with (a) soil structure and (b) contractile skin (after Fredlund et al. 2012)

(2012), the uniqueness of loading and unloading constitutive surfaces or wetting and drying constitutive surfaces can be verified separately.

A number of triaxial (isotropic loading) and oedometer (K_0 loading) experiments were conducted by Fredlund & Morgenstern (1977) to verify the uniqueness of the constitutive surfaces. Three undisturbed Regina clay and a compacted kaolin with the same initial volume-mass properties were adopted for verification purposes. These soil samples were subjected to very small stress increments (i.e., $d(\sigma - u_a)$ and $d(u_a - u_w)$) in order to determine volume change coefficients and vertical strain of soils, and the predicted deformation was then compared with the measured deformation. Figure 2.15 illustrates various stress paths to predict the coefficients of volume change and vertical deformation. It should be noted that these soil samples were first loaded to the same initial stress point located at O, as presented in Figure 2.15. The sample was then subjected to a very small increase in net stress $d(\sigma - u_a)$ and constant matric suction (i.e, $d(u_a - u_w) = 0$), as clearly shown from the stress path OA. Note that this experimental procedure was regulated by increasing the total normal stress (σ) while maintaining the same pore-water pressure (u_w). Once the stress path was achieved, a vertical strain (i.e., $d\varepsilon_v$) of the deformed sample was measured. Consequently, the volume change coefficient with respect to the net stress increment (m_1^s) could be evaluated as:

$$m_1^s = \frac{d\varepsilon_v}{d(\sigma - u_a)} \qquad [2\text{-}26]$$

Conversely, another clayey sample was subjected to a very small increase in matric suction $d(u_a - u_w)$ and constant net stress (i.e, $d(\sigma - u_a) = 0$), as indicated by the stress path OB. This procedure could be achieved by decreasing the pore-water pressure (u_w) while keeping the total normal stress (σ) unchanged. A vertical strain ($d\varepsilon_v$) was measured from the experiment and then the volume change coefficient with respect to a change in matric suction (m_2^s) could be determined as follows:

$$m_2^s = \frac{d\varepsilon_v}{d(u_a - u_w)} \qquad [2\text{-}27]$$

It is worth noting that the coefficients m_1^s and m_2^s have negative signs referring to the sign convention presented in Figure 2.12. Unlike previous experiments, a third sample

was subjected to small increases in both net stress $d(\sigma - u_a)$ and matric suction $d(u_a - u_w)$, as demonstrated by stress path OC. The experimental procedure were conducted by simultaneously increasing the total stress (σ) and decreasing the pore-water pressure (u_w). By adopting the values of volume change coefficients m_1^s and m_2^s presented in Equations [2-26] and [2-27], respectively, the vertical deformation of clayey soil (dV_w/V_0) in a particular stress increment could be predicted by:

$$d\varepsilon_v = m_1^s d(\sigma - u_a) + m_2^s d(u_a - u_w) \qquad [2\text{-}28]$$

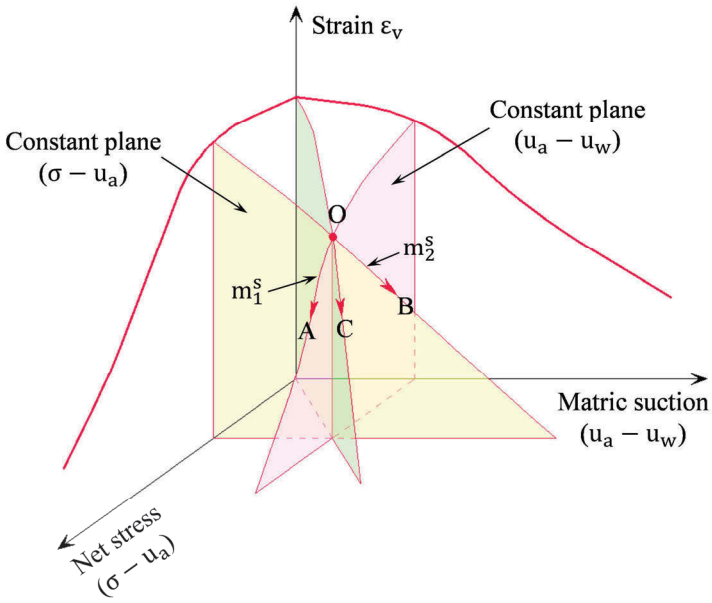

Figure 2.15. Stress paths for determining volume change coefficients and vertical deformation (modified after Fredlund et al. 2012)

Similarly, measurements of volume change of water could be obtained to determine m_1^w and m_2^w, and deformation state variable associated with water (dV_w/V_0). Note that the coefficients m_1^w and m_2^w are also negative due to the sign convention. The predicted volume changes related to the soil structure and water phase were subsequently compared with the measured values using the best-fit straight line technique (Neville & Kennedy 1964). As reported by Fredlund & Morgenstern (1977), predictions for the volume change with respect to the soil structure and water phase are in a relatively good agreement with volume change measurements, indicating that the constitutive surfaces are unique. The constitutive models introduced by Fredlund & Morgenstern (1977) will be adopted for analytical derivations in subsequent chapters of this thesis.

2.5. Elastoplastic (EP) constitutive models for unsaturated soils

2.5.1. Introduction

While the main contribution in this thesis is to estimate the time-dependent settlement of an unsaturated soil stratum due to the pore fluid flows, it is essential to introduce alternative frameworks to evaluate the volume change of unsaturated soils. Particularly, these frameworks have been constituted to describe the EP deformation of soils under isotropic loading conditions. The constitutive EP models have progressed vigorously since the inception of Barcelona Basic Model (BBM) proposed by Alonso et al. (1990). Some features associated with wetting-induced volume change issues (e.g. collapsible and expansive soils) can also be captured in EP models. As discussed in Section 2.2, significant volume change upon saturation may lead to critical failures to structures and foundations and possibly cause fatalities (Ng & Menzies 2007; Sheng 2011; Fredlund et al. 2012).

According to Sheng (2011), a satisfactory EP equation should not only provide a smooth transition between different soil states but also is applicable for a whole range of suction values. In unsaturated soil mechanics, the EP constitutive models can be developed based on three typical categories: (1) independent net stress and matric suction approach (Approach 1), (2) combined net stress and matric suction approach (effective stress approach or Approach 2), and (3) SFG (i.e. Sheng-Fredlund-Gens) approach (Approach 3). Nevertheless, there have been controversies on the selection of these approaches for the formulation of EP model since each approach has some certain advantages and disadvantages. Details of these approaches are presented in subsequent sections.

2.5.2. Independent net stress and matric suction approach (Approach 1)

It is noted that the BBM was developed based on Approach 1, in which the changes in net stress and matric suction are considered to be independent. Thus, the compressibility due to net stress change ($\lambda_{v\sigma}$) and the shrinkability due to suction change (λ_{vs}) can be dealt separately as follows:

$$v = N - \lambda_{v\sigma}\ln(\overline{\sigma}_m) - \lambda_{vs}\ln\left(\frac{s+u_{atm}}{u_{atm}}\right) \quad [2\text{-}29]$$

where v is the specific volume; N is the initial specific volume; $\overline{\sigma}_m$ or $(\sigma_m - u_a)$ is the net mean stress under isotropic conditions; and u_{atm} is the atmospheric pressure. Note that the additional term u_{atm} presented in Equation [2-29] helps to avoid the mathematical error when the suction approaches zero (Alonso et al. 1990). Based on experimental results, Toll & Ong (2003) and Gallipoli et al. (2003) reported that an increase in degree of saturation would lead to a decrease in compressibility $\lambda_{v\sigma}$ and an increase in shrinkability λ_{vs}. As the stress variables are presented in a separate manner, the model allows flexibilities in regulating stress paths when conducting laboratory experiments. Besides the BBM proposed by Alonso et al. (1990), some well-known models adopting the similar approach have been studied by Cui & Delage (1996), Chiu & Ng (2003), Georgiadis et al. (2005) and Thu et al. (2007) to name a few.

Despite the above mentioned advantages, a few shortcomings associated to the EP models adopting Approach 1 can also be found. In particular, Approach 1 does not allow smooth transition between unsaturated and saturated states. Obviously, Equation [2-29] cannot recover back to the EP equation for saturated soils which follows the effective stress principle. Furthermore, the inclusion of atmospheric pressure u_{atm} requires large suction values to be investigated. In other words, the atmospheric pressure may make the suction change inconsiderable if the suction value is smaller than the atmospheric pressure (i.e. $s < u_{atm}$). On the other hand, Approach 1 shows that the volume change induced by suction changes can be independent of stress. This point is not supported by Delage & Graham (1995).

2.5.3. Effective stress approach (Approach 2)

The lack of continuity of transition between unsaturated and fully saturated states has made Approach 1 unfavourable for some researchers when they decided to formulate an explanatory EP model. Instead, most constitutive EP models were developed on the basis of effective stress principle (Approach 2). Current EP studies using Approach 2 have been conducted by Kohgo et al. (1993), Bolzon et al. (1996), Loret & Khalili (2000, 2002), Sheng et al. (2004), Pereira et al. (2005), Santagiuliana & Schrefler (2006), Sun et al. (2007), Nuth & Laloui (2008), and Buscarnera & Nova (2009). In this approach, the net mean stress (i.e. $\overline{\sigma}_m$) and a function of matric suction (i.e. $f(s)$) can be

combined as a single effective stress variable (i.e. $\sigma'_m = \overline{\sigma}_m + f(s)$). Thus, a general EP model can be expressed as follows:

$$v = N - \lambda \ln(\sigma'_m) = N - \lambda \ln[\overline{\sigma}_m + f(s)] \quad [2\text{-}30]$$

where λ is the compressibility due to changes in effective stress; and $f(s)$ is the function of suction or the function of both suction and degree of saturation. According to Alonso et al. (1990), the compressibility λ is considered to be a function of the matric suction whereas the initial specific volume N can be treated as either a constant or variable. On the other hand, Wheeler & Sivakumar (1995) and Loret & Khalili (2002) reported that both parameters N and λ can be expressed in terms of suction. Based on experimental results obtained by Wheeler & Sivakumar (1995), the compressibility λ would increase with increasing suction, especially for high plasticity clays (e.g. speswhite kaolin).

One of the important advantages of selecting Approach 2 for the EP formulation is that it provides smooth transition between soil states. In particular, Equation [2-30] can convert back to the EP equation for the case of saturated soils. However, the combination of stress variables in the model may lead to difficulty in defining the compressibility λ due to net stress change and matric suction change. Another argument related to Equation [2-30] shows that a value of compressibility for an arbitrary suction (i.e. $\lambda(s)$) is smaller than that for zero suction (i.e. $\lambda(0)$), indicating that λ increases with decreasing suction. This prediction, however, contradicts with the experimental study conducted by Wheeler & Sivakumar (1995). As suggested by Sheng (2011), the compressibility λ should be simulated in terms of degree of saturation (i.e. $\lambda(S_r)$) to avoid such constraint.

2.5.4. SFG approach (Approach 3)

Sheng et al. (2008) proposed SFG model using Approach 3, which embraces the concepts of Approaches 1 and 2. This special combination would allow the constitutive EP model to be presented in a way that separates two distinctive compressibilities $\lambda_{v\sigma}$ and λ_{vs}, similar to Approach 1, while still accommodating the combined net mean stress and matric suction in the denominator, comparable to Approach 2. This proposed model is expressed in an incremental form as follows:

$$dv = -\lambda_{v\sigma}\frac{d\bar{\sigma}_m}{\bar{\sigma}_m + f(s)} - \lambda_{vs}\frac{ds}{\bar{\sigma}_m + f(s)} \quad [2\text{-}31]$$

The function f(s) in Equation [2-31] can be replaced by the matric suction (i.e. $f(s) = s$). Equation [2-31] covers some shortcomings found in Equations [2-29] and [2-30]. More importantly, Equation [2-31] can also recover to the incremental form of EP model for saturated soils. The SFG model also shows some good agreements with experimental results obtained from Pham et al. (2005). On the other hand, Sheng et al. (2008) defines a simple relationship between compressibilities $\lambda_{v\sigma}$ and λ_{vs} as:

$$\lambda_{vs} = \begin{cases} \lambda_{v\sigma}, & s < s_{sa} \\ \lambda_{v\sigma}\left(\frac{s_{sa}+1}{s+1}\right), & s \geq s_{sa} \end{cases} \quad [2\text{-}32]$$

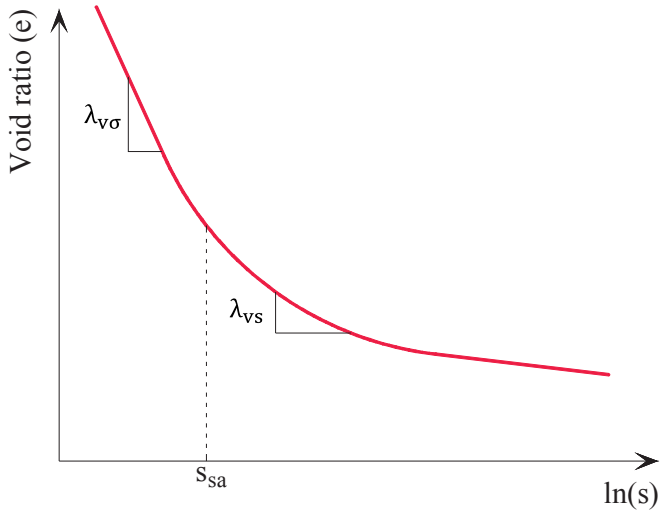

Figure 2.16. Slopes of compressibilities $\lambda_{v\sigma}$ and λ_{vs} in the (e – lns) space (after Sheng et al. 2008)

where s_{sa} is the saturation suction. Note that number "1" is added to the suction in the denominator in Equation [2-32] to avoid the singularity when the suction approaches zero. According to Sheng et al. (2008), Equation [2-32] introduces a continuous function of suction and can be incorporated in Equation [2-31] to determine the volume change of unsaturated soils. However, Sheng et al. (2008) also emphasise that the relationship between compressibilities $\lambda_{v\sigma}$ and λ_{vs} presented in Equation [2-32] may not be a unique approximation that can be applicable to all cases of unsaturated soils. Thus, alternative forms can be used in place of Equation [2-32] to describe such relationship.

Figure 2.16 illustrates compression slopes of $\lambda_{v\sigma}$ and λ_{vs} in the $(e - \ln s)$ space under a constant net stress.

In terms of significance, the SFG model presented in Equation [2-31] has so far been the most complete model describing the volume change of unsaturated soils. The SFG approach, likewise, overcomes some model constraints found in Approaches 1 and 2. One of the most important advantages is that this approach allows the continuous transition between unsaturated state and fully saturated state even when $f(s) = s$. It is however suggested that the term $f(s)$ in the denominator of Equation [2-31] may be expressed as a function of both matric suction and degree of saturation (i.e., $f(s) = S_r s$) to ensure the smooth transition from the unsaturated state to the completely dry state (Sheng 2011). Another main disadvantage shows that the SFG model requires complex integration depending on stress paths. This may limit the range of applications of the SFG model to wider aspects. While previous EP models are presented in much more succinct forms and provide convenient evaluations, the SFG equation may further require rigorous integrations due to different stress paths (Zhang & Lytton 2008), producing a lengthy integral form as shown below:

$$\ln v = \begin{cases} \ln N - \lambda_{v\sigma} \ln\left(\frac{\bar{\sigma}_m + s_0}{\bar{\sigma}_{m_0} + s_0}\right); & ds = 0 \\ \ln N - \lambda_{v\sigma} \ln\left(\frac{\bar{\sigma}_{m_0} + s}{\bar{\sigma}_{m_0} + s_0}\right); & d\bar{\sigma}_m = 0 \;\&\; s < s_{sa} \\ \ln N - \lambda_{v\sigma} \ln\left(\frac{\bar{\sigma}_{m_0} + s_{sa}}{\bar{\sigma}_{m_0} + s_0}\right) - \lambda_{v\sigma}\left(\frac{s_{sa}+1}{\bar{\sigma}_{m_0}-1}\right) \ln\left(\frac{s+1}{\bar{\sigma}_{m_0}+s} \frac{\bar{\sigma}_{m_0}+s_{sa}}{s_{sa}+1}\right); & d\bar{\sigma}_m = 0, \bar{\sigma}_{m_0} \neq 1 \;\&\; s \geq s_{sa} \\ \ln N - \lambda_{v\sigma} \ln\left(\frac{\bar{\sigma}_m + s_{sa}}{\bar{\sigma}_{m_0} + s_0}\right) - \lambda_{v\sigma}\left(1 - \frac{s_{sa}+1}{s+1}\right); & d\bar{\sigma}_m = 0, \bar{\sigma}_{m_0} = 1 \;\&\; s \geq s_{sa} \end{cases} \quad [2\text{-}33]$$

2.6. Consolidation analyses for saturated soils

2.6.1. Classical consolidation theory and its governing equation

Terzaghi (1925) successfully developed the principle of effective stress to describe the 1D consolidation process in fully saturated soils. This classical study has formed a solid foundation for numerous state-of-the-art research and geotechnical designs. In 1D consolidation analyses, the effective stress theory fundamentally involves changes of two local stresses, known as effective normal stress and excess pore-water pressure, induced by external loading.

The concept of effective stress, however, is only applicable to saturated soil mechanics (Craig 2004). Sudden application of external surcharge (q) (e.g., fills, structures, embankments etc.) to a saturated soil stratum generates a notable increase in pore-water pressure, which is defined as *excess pore-water pressure* (Δu_w). This is due to the fact that incompressible pore-water entirely supports the surcharge at the beginning of compression (i.e., $\Delta u_w = q$). Meanwhile, the effective vertical stress (σ'_v) during the early stages remain almost unchanged and equals to an effective stress prior to loading (σ'_{vi}). Development of excess pore-water pressure in the soil stratum would further induce the hydraulic gradient, resulting in flow of water after a certain period of time. Once water begins to dissipate gradually from voids, the effective stress increases to support the surcharge. It should be noted that the excess pore-water pressure dissipation is a time-dependent process which causes the time-dependent settlement of the soil. Very long time after loading, the excess pore-water pressure almost diminishes (i.e., $u_w \approx 0$) while the effective vertical stress approaches the final effective stress that entirely supports the surcharge (i.e., $\sigma'_v = \sigma'_{vf} = q$). The soil stratum would subsequently experience the ultimate consolidation settlement (S_{ult}) and no further deformation of soil can be observed (Coduto et al. 2011). The above mentioned process is regarded as a traditional consolidation theory proposed by Terzaghi (1925, 1943).

Means & Parcher (1963) further suggested that the rate of settlement is significantly affected by soil textures and hydraulic conductivity. For coarse-grained soils (e.g., gravels, cobbles and coarse sands), the consolidation settlement occurs almost immediately due to their high permeability coefficients. In contrary, it takes considerable amount of time for fine-grained geomaterials (e.g., clays, silts and fine sands) to settle as the result of extremely small permeability coefficients. In the 1D consolidation, water is assumed to flow in one direction (e.g. usually vertical direction) only. Additionally, the width of soil stratum is assumed to be indefinite and therefore the soil deformation occurs only vertically (Coduto et al. 2011). The consolidation rate also depends on the drainage distances of water flow. If the consolidating soil consists of a permeable top and an impermeable base, under an external applied load, water will travel upward and the drainage path (H_{dr}) is equivalent to the thickness of the soil (i.e., $H_{dr} = H$). This case is termed the *one-way drainage boundary condition*. When the consolidating soil is sandwiched by much more permeable strata, water is able to drain

both directions, either upward or downward. The drainage path is therefore considered to be only a half of the soil thickness (i.e., $H_{dr} = H/2$). This case is known as the *two-way drainage boundary condition*. Figure 2.17 illustrates typical one-way and two-way drainage boundary conditions. Note that, due to the shorter drainage path, settlement in the two-way drainage system may proceed approximately four times faster than that in the corresponding one-way drainage system (Terzaghi 1943; Venkatramaiah 2006; Coduto et al. 2011).

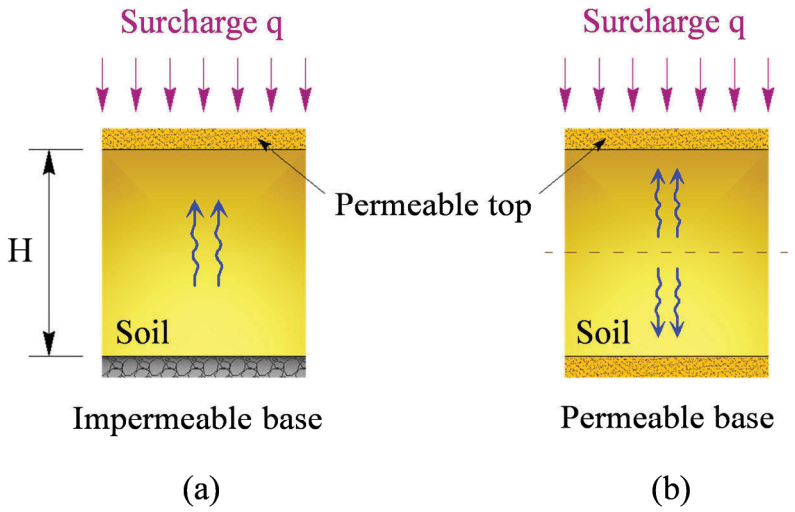

Figure 2.17. Soil stratum under (a) the one-way drainage boundary condition and (b) the two-way drainage boundary condition

The complex nature of soil may lead to computational difficulties. To ensure a predictive equation for the 1D consolidation of fully saturated soil is achievable, additional assumptions made by Terzaghi (1925, 1943) are as follows:

- The soil is homogenous;
- The soil is fully saturated ($S_r = 1$);
- Pore-water and solid particles are incompressible;
- Darcy's law is adopted to describe the water flow;
- No creep occurs simultaneously with the consolidation process;
- Soil deformation happens in the vertical direction only (z-direction);
- Relationship between void ratio and effective stress ($e - \sigma'_v$) is independent of time;
- Soil properties such as coefficients of volume change (m_v) and permeability (k) are treated constant throughout the consolidation.

Terzaghi (1925) mathematically developed a governing equation that describes the dissipation of excess pore-water pressure in response to consolidation. Assuming that water flows upward through a soil element (Figure 2.18), hydraulic gradients at the top and bottom of the element can be expressed in terms of excess pore pressure as shown below:

$$i_z = \frac{1}{\gamma_w}\frac{du_w}{dz} \qquad \text{(at the top)} \qquad [2\text{-}34a]$$

$$i_{z+dz} = \frac{1}{\gamma_w}\left(\frac{du_w}{dz} + \frac{d^2u_w}{dz^2}dz\right) \qquad \text{(at the bottom)} \qquad [2\text{-}34b]$$

where γ_w is the water unit weight; i_z and i_{z+dz} are the hydraulic gradients at the top and bottom of the soil element, respectively. By adopting Darcy's law, volumes of water entering and water leaving the element are derived while incorporating Equation [2-34], resulting in:

$$dV_{we} = \frac{k}{\gamma_w}\left(\frac{du_w}{dz} + \frac{d^2u_w}{dz^2}dz\right)dA\,dt \qquad [2\text{-}35a]$$

$$dV_{wl} = \frac{k}{\gamma_w}\frac{du_w}{dz}\,dA\,dt \qquad [2\text{-}35b]$$

where V_{we} and V_{wl} are the volumes of water entering and water leaving the soil element, respectively; and $dA = dx\,dy$, is the change in cross-sectional area. The net

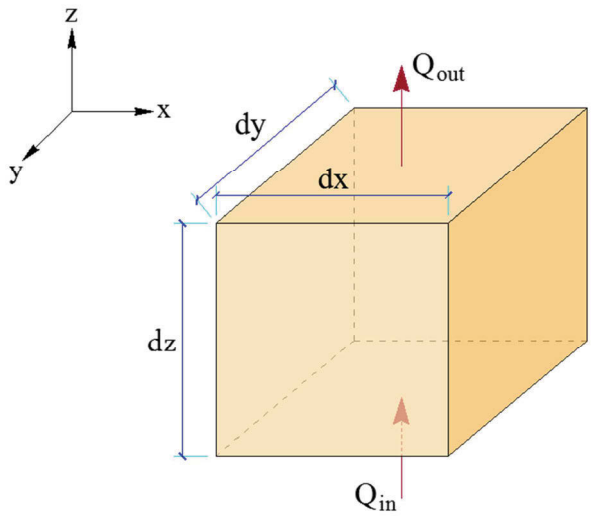

Figure 2.18. One-dimensional flow through the soil element (after Budhu 2008)

flux of water is determined by taking the difference between volumes of water entering (i.e., Equation [2-35a]) and water leaving (i.e., Equation [2-35b]) the element, giving:

$$dV = \frac{k}{\gamma_w}\frac{d^2u_w}{dz^2}\,dz\,dA\,dt \qquad [2\text{-}36]$$

According to Budhu (2008), the change in effective normal stress in a particular depth would be equal to the change in excess pore-water pressure at that depth (i.e., $d\sigma'_z = du_w$). As the result, the net flux of water can be alternatively expressed in terms of volume change coefficients (m_v) as follows:

$$dV = m_v\,du\,dz\,dA \qquad [2\text{-}37]$$

Combining Equations [2-36] and [2-37] results in the governing equation capturing the flow of pore-water in the soil element, as shown below:

$$\frac{\partial u_w}{\partial t} = c_v\frac{\partial^2 u_w}{\partial z^2} \qquad [2\text{-}38]$$

where $c_v = k/(\gamma_w\,m_v)$, is the coefficient of consolidation. Equation [2-38] is written under the partial differential equation (PDE) which relates to three quantities: (1) excess pore-water pressure induced by surcharge (Δu_w), (2) investigated depth (z) that is measured from the top of consolidating soil to the point of interest, and (3) time of consolidation (t) starting from the immediate application of load. The governing equation of flow proposed by Terzaghi (1925) is very similar to the heat diffusion equation in mechanical engineering, except that pore pressure parameter (u_w) replaces temperature (T) and the consolidation coefficient (c_v) replaces the heat factor (K). Besides, volume change (m_v) and permeability (k) coefficients presented in Equation [2-38] are assumed to be constant throughout the consolidation for the sake of simple computation. However, this assumption may not be strictly accurate for some practical cases. Note that both m_v and k are nonlinear properties that change in response to consolidation, resulting in variations in c_v. The assumption may be acceptable for the small stress increment or transient loading process, in which m_v and k do not significantly change (Budhu 2008).

2.6.2. Solution to consolidation of saturated soils

Solving for the PDE presented in Equation [2-38] requires a homogeneous boundary condition, either one-way or two-way drainage condition, and an initial condition. Many clay strata in nature usually consist of pervious top surface that facilitates water drainage and impervious bedrock (Venkatramaiah 2006). With such occurrences, the boundary condition for the one-way drainage system is often considered in the formulation. It should be also noted that the initial condition is highly dependent of loaded area, external loading condition and layer thickness (Jumikis 1969). If the external loading is considered to be indefinite and uniform or the soil stratum is relatively thin, the initial excess pore pressure may be distributed uniformly with depth. However, if the loaded area is small or the soil stratum is too thick, the initial excess pore pressure may decrease with depth. In this case, a simple simulation for the initial condition is a triangular distribution of initial excess pore pressure. Irregular loading applied to the ground surface also results in variations of initial condition. For simplification, the classical solution derived by Terzaghi (1925) captured the uniform initial condition. Based on existing literature (Terzaghi 1943; Venkatramaiah 2006; Verruijt & Van Baars 2007; Budhu 2008; Coduto et al. 2011), the boundary condition related to one-way drainage system and the uniform initial condition are:

- Boundary condition: $u_w(0,t) = \left[\frac{du_w(z,t)}{dz}\right]_{z=H} = 0, \qquad t \in [0,\infty)$ [2-39]
- Initial condition: $u_w(z,0) = \Delta u_w^0, \qquad z \in (0,H]$ [2-40]

Similar to solving the heat transfer equation, Terzaghi (1925) adopted the separation of variables and Fourier sine series to solve the governing flow equation (i.e., Equation [2-38]) while incorporating the boundary and initial conditions (i.e., Equations [2-39] and [2-40], respectively). Thus, the solution predicting excess pore pressure dissipation is obtained as follows:

$$\Delta u_w(z,t) = \sum_{m=0}^{\infty} \frac{2\Delta u_w^0}{M} \sin\left(\frac{M\,z}{H_{dr}}\right) e^{(-M^2 T_v)} \qquad [2\text{-}41]$$

where $M = (2m + 1)\pi/2$, $(m = 0, 1, 2, ...)$; and $T_v = c_v t/(H_{dr})^2$, is the time factor. To illustrate the 1D consolidation in an instructive manner, a series of excess pore-water pressure curves for different time factor T_v at a particular depth z is graphically presented in Figure 2.19. These curves are called *pore pressure isochrones* whose patterns are practically governed by both boundary and initial conditions. As observed in Figure 2.19, excess pore-water pressure isochrones are perpendicular at the base of the soil stratum satisfying the one-way drainage boundary condition presented in Equation [2-39]. Additionally, the pore pressure isochrones also follow the initial condition in Equation [2-40]. In particular, when T_v approaches zero, excess pore-water pressures are equal to initial values and are uniformly distributed along the soil depth, except for the top surface.

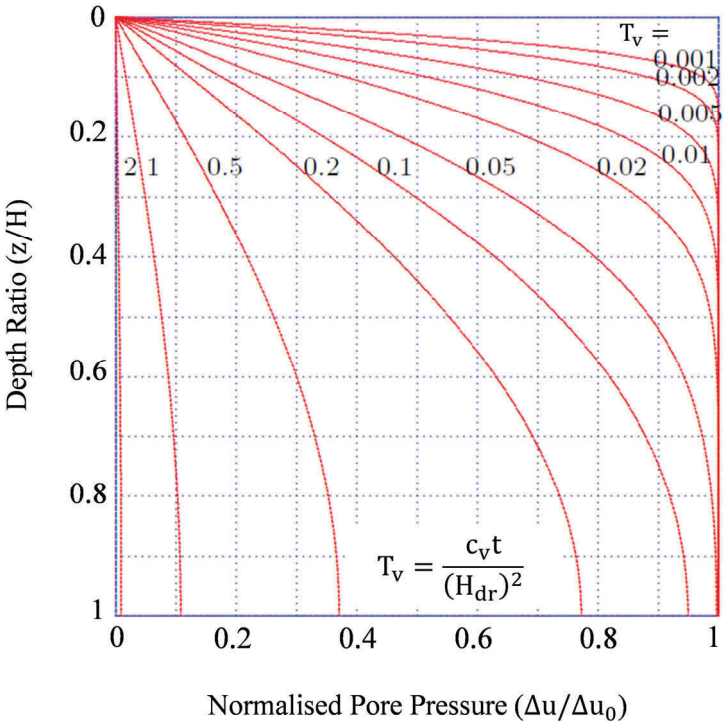

Figure 2.19. Typical excess pore pressure isochrones under one-way drainage system (after Verruijt & Van Baars 2007)

In many geotechnical investigations, it is also useful to analyse the 1D consolidation problems in terms of the average degree of consolidation, denoted as U (Budhu 2008). The average degree of consolidation can be referred as the average settlement over the

entire soil stratum at a particular time (Venkatramaiah 2006). The formulation of the degree of consolidation involves integrating Equation [2-41] against the depth z, giving:

$$U = 1 - \sum_{m=0}^{\infty} \frac{2}{M^2} e^{(-M^2 T_v)} \qquad [2\text{-}42]$$

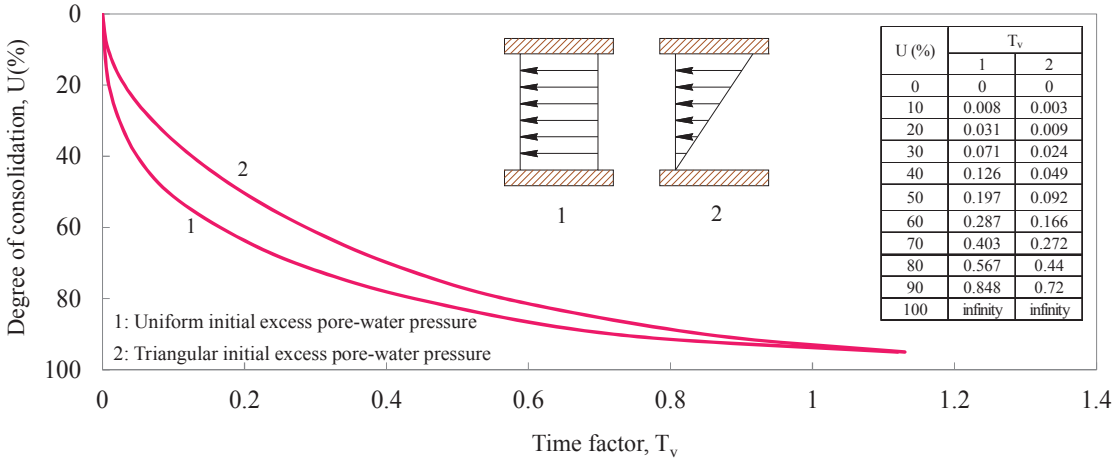

U (%)	T_v	
	1	2
0	0	0
10	0.008	0.003
20	0.031	0.009
30	0.071	0.024
40	0.126	0.049
50	0.197	0.092
60	0.287	0.166
70	0.403	0.272
80	0.567	0.44
90	0.848	0.72
100	infinity	infinity

Figure 2.20. Average degree of consolidation (U) versus time factor (T_v) for uniform and triangular initial conditions (modified after Taylor 1948, Venkatramaiah 2006, and Budhu 2008)

Equation [2-42] presents the settlement response of the entire soil stratum and is a function of time only. Note that consolidation in the two-way drainage system proceeds much faster than that in the corresponding one-way drainage system. For uniform initial conditions, settlement curves, U, are all the same irrespective of different drainage systems (Venkatramaiah 2006). However, values of degree of consolidation would vary due to different initial conditions. Figure 2.20 presents settlement patterns for uniform and triangular distributions of initial excess pore pressures based on available literature (Taylor 1948; Venkatramaiah 2006; Budhu 2008).

The 1D consolidation theory for fully saturated soils proposed by Terzaghi (1925) has motivated numerous well-recognised studies in geotechnical field. Olson (1977) extended the traditional consolidation model by including a simple ramp loading. Zhu & Yin (1998) later conducted similar study to obtain excess pore pressures and degree of consolidation induced by the depth-dependent ramped loading. Morris (2002, 2005) presented both numerical and analytical methods to derive solutions predicting the

average degree of consolidation for linear finite-strain 1D consolidation of initially unconsolidated soils. Xie & Leo (2004) introduced explicit analytical solutions for the large-strain consolidation in thick and thin strata. In this study, Xie & Leo (2004) found that the large-strain consolidation proceed more quickly than the small-strain consolidation. Xie et al. (2002), on the other hand, expanded the consolidation study from a single-layered soil to double-layered soil and estimated the excess pore pressures and average degree of consolidation. All these and many more studies have been recently conducted to improve the reliability of consolidation models. The study of interest has also been rigorously updated to capture mechanical behaviours of problematic soils located in unsaturated regions.

2.6.3. Axisymmetric consolidation and its polar governing equation

In major ground improvement projects, vertical drain assisted preloading has been considered to be a cost-effective method to accelerate drainage in soil deposits and shorten the consolidation process. Vertical drain consolidation can be modelled assuming axisymmetry around the drain. The basic theory of the axisymmetric consolidation was developed based on the traditional consolidation theory proposed by Terzaghi (1925). Figure 2.21 depicts two idealistic cases of drain well system, namely vertical sand drains (Figure 2. 21(a)) and prefabricated vertical drains (PVDs) with smear effects (Figure 2. 21(b)), in a saturated soil stratum.

Dimensions of the typical sand drain primarily include a depth (H), a radius of the influence zone (r_e), and a drain well radius (r_w) located at the centre of the influence zone, as shown in Figure 2. 21(a). Axisymmetric consolidation induced by sand drain follows a simple principle such that, when a constant loading is applied to the soil, the pore-water will dissipate through the radial boundary of drain well and through the permeable boundaries of soil stratum. However, installation of PVDs using close-ended mandrels has reportedly disturbed the surrounding soil and generated some operational issues (Holtz 1987). The remolded soil caused by mandrels may possess the reduced hydraulic conductivity and moisture content, thus impeding the flow of pore-water into the drain system and the consolidation would be eventually delayed (Holtz & Holm 1973; Basu & Prezzi 2007). The disturbed zone is usually referred to as *smear zone* that is located immediately adjacent to the drain, as depicted in Figure 2.21(b). Several

studies conducted by Holtz & Holm (1973), Jamiolkowski et al. (1983), Hansbo (1986, 1987), Mesri et al. (1994), Chai & Miura (1999), Perera et al. (2014), and Indraratna et al. (2014) report that radius of smear zone, measured from the centre of drain well to the smear boundary (r_s), may be equal to or increase up to four times the equivalent radius of mandrel ($r_{m,eq}$). However, the smear radius can also be determined through other factors such as in situ conditions, field explorations and data obtained from case histories (Hird & Moseley 2000).

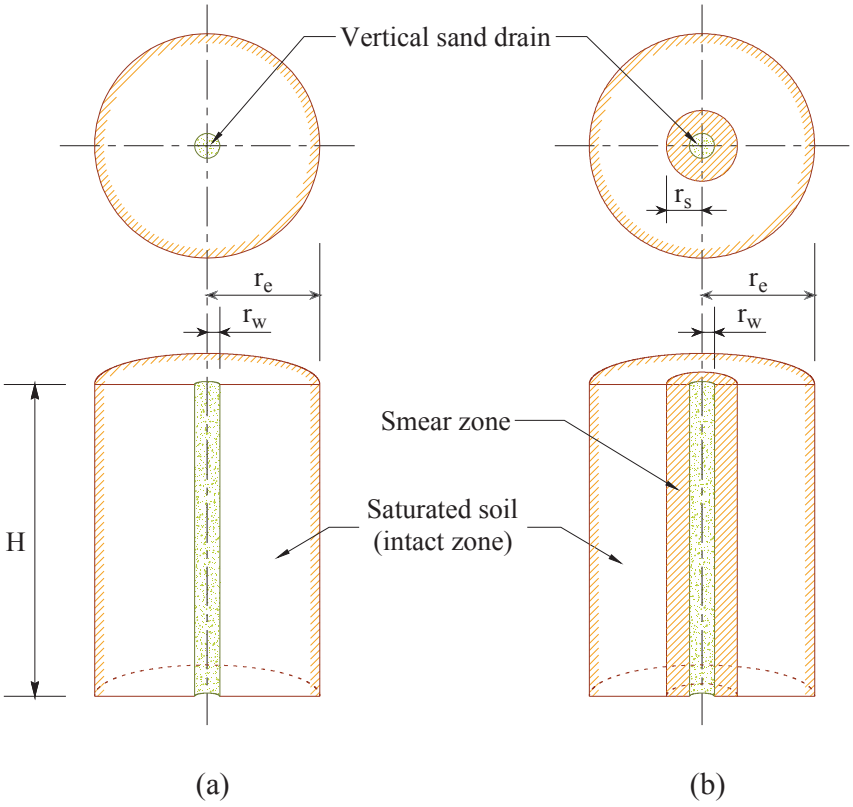

Figure 2.21. Typical drain well installed in saturated soil stratum: (a) vertical sand drains and (b) PVDs with smear effects

Vertical drain wells can be installed in square or triangular patterns depending on different design purposes. According to Indraratna & Bamunawita (2002), the square pattern allows simple and easy installation of vertical drain. However, Barron (1948) suggested that it is more economical to install drain wells in the triangular pattern. Furthermore, the triangular pattern also provides uniform consolidation between drain wells (Indraratna & Bamunawita 2002). Figure 2.22 illustrates the layout of typical

drain well patterns. A centre to centre distance between adjacent drains is called *drain spacing* (S) determining the influence zone radius (r_e) as follows:

- Square pattern: $r_e = 0.546S$ [2-43a]
- Triangular pattern: $r_e = 0.525S$ [2-43b]

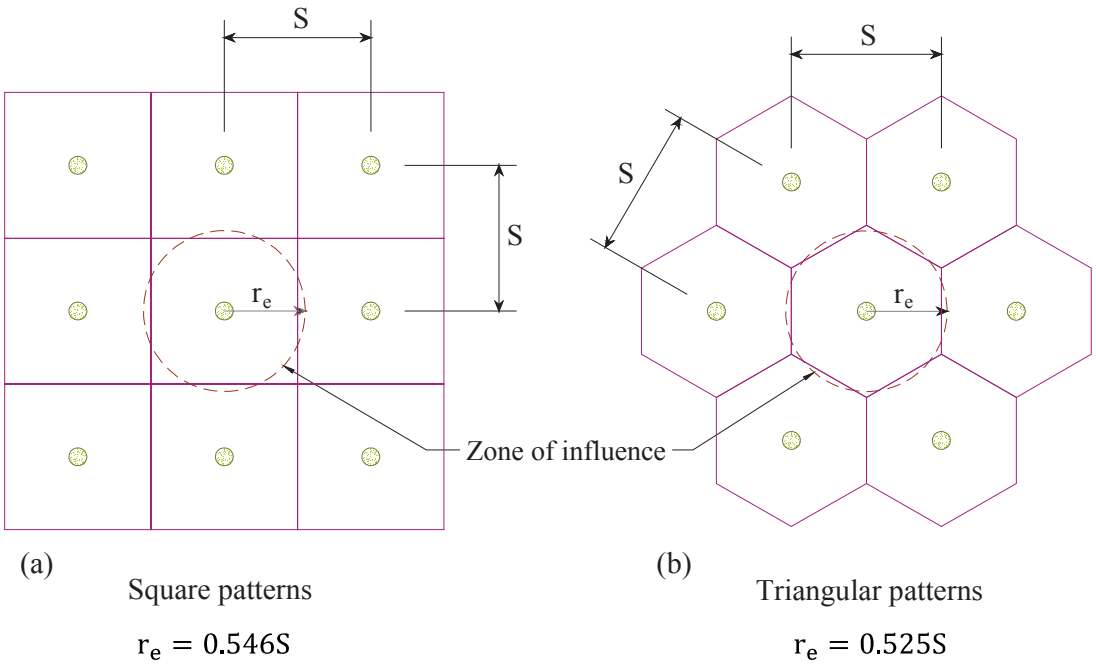

Figure 2.22. Plan of drain well systems: (a) square patterns and (b) triangular patterns

According to Holtz (1987), the desirable range of drain spacing (S) ranges from 1.2m to 3.6m. In other words, the radius of the influence zone (r_e) should be within approximately 0.65 – 2.0m for the square patterns or 0.6 – 1.9m for the triangular patterns. Additionally, design dimensions of drain well radius r_w are presented in Table 2.9 (Holtz et al. 1991; Smoltczyk 2003).

Theoretical complexities of axisymmetric consolidation problems can account for *free strain* and *equal strain* hypotheses. As assumed by Barron (1948), the free strain consolidation due to uniform loading does not consider the stress redistribution by arching of the fill. This assumption indicates that the consolidation process induced by vertical drains is independent of shear strains. Contrariwise, the equal strain consolidation allows the soil adjacent to the drain to consolidate more quickly compared

to the soil further away from the drain (Barron 1948). Thus, differential settlement is developed over the circular zone, influencing the stress redistribution and consolidation rate. Furthermore, shear strains also affects the consolidation process if the equal strain condition is considered. Of these hypotheses, the equal strain case is favoured over the free strain case because of its decent accuracy and practical applications (Barron 1948). On the other hand, problems associated with smear zone and well resistance may also contribute to a wide range of research possibilities.

Table 2.9. Dimensions of various types of vertical drain (modified after Holtz et al. 1991, and Smoltczyk 2003)

Types of Vertical Drain	**Radius (r_w)**
Sand drain (in situ)	0.1 – 0.3m
Sand drain (prefabricated)	0.03 – 0.075m
Prefabricated drains (plastics, cardboard etc.)	0.025 – 0.05m

A governing equation for the flow of pore-water under axisymmetric conditions is obtained from the polar transformation of Terzaghi's classical consolidation equation (Punmia & Jain 2005). Likewise, for the case of axial symmetry on a horizontal 2D plane, Cartesian coordinates (x, y) must be transformed into polar coordinates (r, θ) as follows:

$$r = \sqrt{x^2 + y^2} \qquad [2\text{-}44a]$$

$$\theta = \tan^{-1}\left(\frac{y}{x}\right) \qquad [2\text{-}44b]$$

The net flux of pore-water in the horizontal 2D plane is determined using Darcy's law, leading to:

$$\frac{\partial\left(\frac{\Delta V}{V_0}\right)}{\partial t} = \frac{k_r}{\gamma_w}\left(\frac{d^2u_w}{dx^2} + \frac{d^2u_w}{dy^2}\right) \qquad [2\text{-}45]$$

owing to the following assumption:

$$k_x = k_y = k_r \qquad [2\text{-}46]$$

where k_x and k_y are the coefficients of permeability in the x- and y-directions; and k_r is the coefficient of permeability in the radial direction. Rigorous procedure is conducted combining Equations [2-44] – [2-46], the polar governing equation describing the flow of pore-water in the domain $r \in [r_w, r_e]$ is:

$$\frac{\partial u_w}{\partial t} = c_{v_r}\left(\frac{\partial^2 u_w}{\partial r^2} + \frac{1}{r}\frac{\partial u_w}{\partial r}\right) \qquad [2\text{-}47]$$

where $c_{v_r} = k_r/(\gamma_w m_v)$ is the coefficient of consolidation under axisymmetric conditions. The coefficient c_{v_r} is equivalent to c_v as presented in Equation [2-38]. Equation [2-47] describes the flow of pore-water in the radial direction only without considering the effects of smear zone. For the sake of simplicity, soil properties such as coefficient of volume change (m_v) and permeability (k_r) are assumed to be constant during the radial consolidation, leading to constant c_{v_r}. This assumption may be only valid in a transient process of radial consolidation.

2.6.4. Solution to radial consolidation of saturated soils

Several analytical and numerical approaches were proposed to solve PDE presented in Equation [2-47]. By discarding the smear effects, radial boundary condition generally assumes that the outer boundary of influence zone of the soil (r_e) is impermeable whereas the boundary of the drain cylinder (r_w) is permeable to water. In addition, the uniform initial condition for the radial consolidation is adopted similar to Equation [2-40], except that the depth z is replaced by the radius r. Thus, both boundary and initial conditions are presented as follows:

- Boundary condition: $u_w(r_w, t) = \left[\frac{du_w(r,t)}{dz}\right]_{r=r_e} = 0, \qquad t \in [0, \infty)$ [2-48]
- Initial condition: $u_w(r, 0) = \Delta u_w^0, \qquad r \in (r_w, r_e]$ [2-49]

Barron (1948) first introduced solutions based on both free strain and equal strain conditions to estimate the radial consolidation in saturated soils. Yoshikuni & Nakanodo (1974) later developed an analytical solution for free strain consolidation adopting radial and vertical flows of water, while considering the well resistance. This work was followed by Onoue (1988), whose study expanded the field of interest from single layer soils to multi-layered soils. Among significant research studies, the semi-analytical solution presented by Onoue (1988) has been one of the most rigorous solutions under the free strain condition. However, many recent methods for analysing consolidation assisted by vertical drain wells have adapted the simplified theory given by Hansbo (1981) under the case of equal strain. Table 2.10 summarises the proposed equations for the degree of consolidation (U_r) given by the aforementioned authors. Figure 2.23 also demonstrates the U_r patterns for different N values (i.e., $N = r_e/r_w$) varying with time factor T_r (i.e., $T_r = c_{v_r}t/(2r_e)^2$) based on Barron (1948) solution.

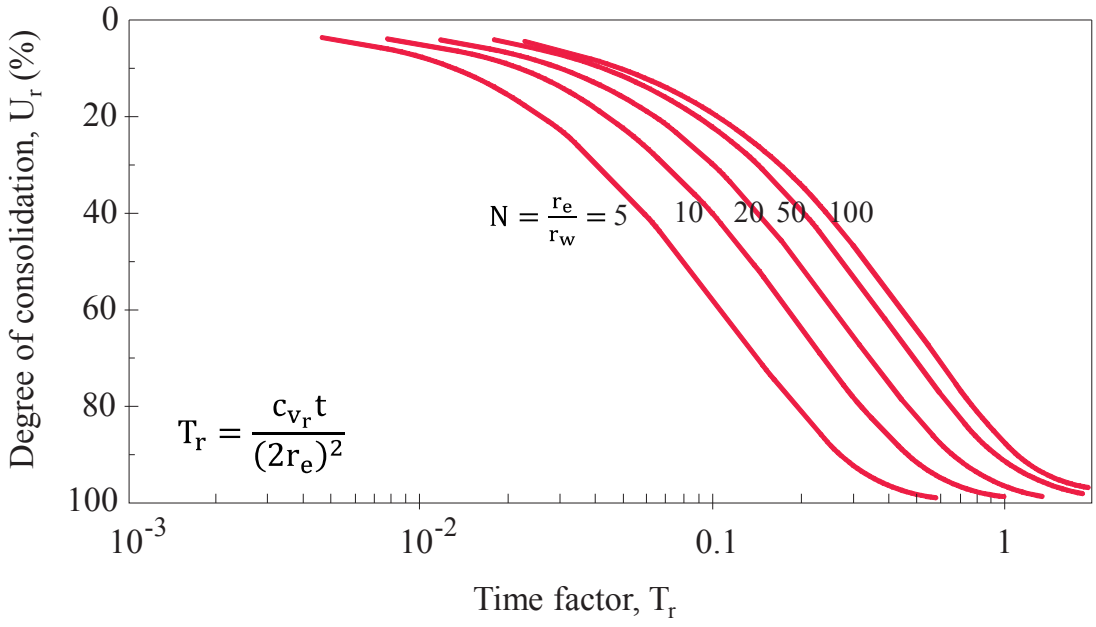

Figure 2.23. Relationship between average degree of consolidation (U_r) and time factor (T_r) obtained from Barron (1948) solution (modified after Barron 1948, after Craig 2004)

Table 2.10. Summary of theoretical solutions for determining the degree of consolidation U_r

Theoretical Solutions for Axisymmetric Consolidation (Average Degree of Consolidation)	**Authors**
$U_r = 1 - e^{-\frac{8T_r}{F(N)}}$ (Equal strain case) where $F(N) = \left(\frac{N^2}{N^2-1}\right)\ln(N) - \left(\frac{3}{4} - \frac{1}{4N^2}\right)$	Barron (1948)
$U_r = 1 - \frac{\Delta\bar{u}_w(T_r)}{\Delta u_w^0}$ (Free strain case) where $\Delta\bar{u}_w(T_r) = \frac{8}{\pi}\left(\frac{N^2}{N^2-1}\right)\left(\frac{1}{L}\right)\sum_{m=0}^{\infty}\sum_{n=0}^{\infty} C_{mn}\left[\frac{m}{(\alpha_{mn}\, r_e)^2}\right] D_0(\alpha_{mn}\, r_e{}^2)\, e^{-\left[4(\alpha_{mn}\, r_e)^2 + \left(\frac{m\pi r_e{}^2}{H}\right)^2\right]T_r}$; $L = \frac{32}{\pi^2}\frac{k_r}{k_w}\left(\frac{H}{2r_w}\right)^2$; $C_{mn} = \frac{8\,\Delta u_0}{\pi}\left(\frac{1}{L}\right)\left[\frac{m}{(\alpha_{mn}\, r_e)^2}\right]\left\{\frac{D_0(\alpha_{mn}\, r_w)}{[D_0(\alpha_{mn}\, r_e)]^2 - \frac{1}{N^2}\left[1+\left(\frac{m^2}{L\,\alpha_{mn}\, r_w}\right)^2\right][D_0(\alpha_{mn}\, r_w)]^2}\right\}$; α_{mn} is the roots of equation: $\frac{D_0(\alpha_{mn}\, r_w)}{\alpha_{mn}\, r_w\, D_1(\alpha_{mn}\, r_w)} = -\frac{L}{m^2}$; and $D_0(\alpha_{mn}\, r) = J_0(\alpha_{mn}\, r) - \left[\frac{J_1(\alpha_{mn}\, r_e)}{Y_1(\alpha_{mn}\, r_e)}\right] J_0(\alpha_{mn}\, r)$	Yoshikuni & Nakanodo (1974)

Table 2.10. Summary of theoretical solutions for determining the degree of consolidation U_r (continued)

Theoretical Solutions for Axisymmetric Consolidation (Average Degree of Consolidation)	**Authors**
$U_r = 1 - e^{-\frac{8T_r}{\mu_s}}$ (Equal strain case) where r_s is the radius measured from the centre of drain well to the smear boundary; $\mu_s = \ln\left(\frac{N}{S}\right) + \left(\frac{k_r}{k_s}\right)\ln(S) - \frac{3}{4} + \pi z(H-z)\left(\frac{k_r}{q_w}\right)$; and $S = \frac{r_s}{r_w}$	Hansbo (1981)
$U_r = \frac{\int_0^1 \int_{1/N}^1 [1-\Delta\bar{u}_w(\eta,\zeta,T_r)]\eta d\eta d\zeta}{\int_0^1 \int_{1/N}^1 \eta d\eta d\zeta}$ (Free strain case) (can be determined using trapezoidal rule) where $\eta = \frac{r}{r_e}$; and $\zeta = \frac{z}{H}$	Onoue (1988)

In an attempt to constitute more realistic models, further studies have included the effects of the smear zone and time-dependent loading (Tang & Onitsuka 2000; Leo 2004; Zhu & Yin 2004; Conte & Troncone 2009; Geng et al. 2010; Lei et al. 2015; Lu et al. 2015), varying radial permeability coefficients (Indraratna et al. 2005a; Walker & Indraratna 2006, 2007), new analysis for soil-drain system conceptually based on the double porosity model (DPM) (Wang & Jiao 2004), vertical drain consolidation with discharge capacity varying linearly with depth and decreasing exponentially with time (Deng et al. 2013), or axisymmetric model including both radial and vertical flows for electro-osmotic consolidation (Wu & Hu 2013). Practical factors which have been observed from installations and operations of drain well system would lead to theoretical variations in developing frameworks for the axisymmetric consolidation. In concerning more thorough models applicable to different soil states, the study of interest has been extensively expanded from saturated soil mechanics to unsaturated soil field (Conte 2006; Qin et al. 2010c; Zhou 2013).

It is also worth mentioning some 2D plane strain consolidation studies associated with vertical drains. Horne (1964) provided analytical solutions to predict the consolidation of a stratified soil under the plane strain and radially symmetrical conditions. In this study, considering the 2D plane strain case, the coefficients of consolidation with respect to the horizontal and vertical flows (i.e., c_x and c_z) were assumed to be functions of the vertical coordinate z only (Horne 1964). On the other hand, Indraratna & Redana (1997) obtained analytical model to quantify the smear effects using the finite element method. The conventional axisymmetric condition was first transformed into an equivalent plane strain system by expressing the equivalent widths (i.e., b_w and b_s) as functions of drain spacing (S). Soil property such as permeability coefficient (k) was likewise adjusted to fit in the plane strain system. Based on the consolidation theory given by Indraratna & Redana (1997), extensive studies conducted by Indraratna and his co-workers (Indraratna et al. 2005b; Indraratna et al. 2005c) derived both analytical and numerical solutions for the plane strain consolidation induced by vertical sand drains and PVDs incorporating the vacuum preloading. In the case of PVDs, the effects of smear zone were also captured in the analytical and numerical modelling.

2.7. Consolidation analyses for unsaturated soils

2.7.1. Consolidation theory and governing equation of flow

An unsaturated soil is the three-phase geomaterial primarily comprised of soil solids, water and air phases. In many theoretical formulations, the contractile skin, which is believed to be the fourth phase in the unsaturated soil, is assumed as part of the water phase (Fredlund et al. 2012). There have been theoretical difficulties in deriving the constitutive frameworks for unsaturated consolidation due to the inclusion of pore-air pressure. Single-valued effective stress variables have been reported to be impractical when predicting mechanical behaviours of problematic soils (Morgenstern 1979; Wheeler & Karube 1996), as discussed in Section 2.3.1. In the late 1970s, Fredlund & Morgenstern (1977) introduced a new set of stress state variables, including $(\sigma - u_a)$, $(\sigma - u_w)$ and $(u_a - u_w)$, through analyses of equilibrium equations for soil structure and independent phases (i.e., air, water and contractile skin). Of these stress variables, net stress $(\sigma - u_a)$ and matric suction $(u_a - u_w)$ are selected to develop the constitutive equations for the air and water phases in the K_0 loading (axial load applied along vertical direction or z-direction) (Fredlund & Hasan 1979) as follows:

$$\frac{\partial\left(\frac{\Delta V_a}{V_0}\right)}{\partial t} = m_1^a \frac{\partial(\sigma_z - u_a)}{\partial t} + m_2^a \frac{\partial(u_a - u_w)}{\partial t} \quad [2\text{-}50a]$$

$$\frac{\partial\left(\frac{\Delta V_w}{V_0}\right)}{\partial t} = m_1^w \frac{\partial(\sigma_z - u_a)}{\partial t} + m_2^w \frac{\partial(u_a - u_w)}{\partial t} \quad [2\text{-}50b]$$

As mentioned in Section 2.4.3, the constitutive relations presented in Equation [2-50] were proven valid for practical applications. In addition, Fredlund & Morgenstern (1977) confirmed that constitutive surfaces associated with the soil structure and water phase are unique due to the good agreement between predicted and measured volume changes. On the other hand, Barden (1965) suggested that the air and water in a soil element flow on the basis of the continuity of fluid phases. In many existing literature, these flows are assumed to be continuous and independent (Qin et al. 2008; Shan et al. 2012; Zhou et al. 2014). Figure 2.24 illustrates upward flows of pore-air and pore-water through an unsaturated soil element. Childs & Collis-George (1950) recommended that the flow of water should follow Darcy's law. Assuming that water is incompressible (i.e., ρ_w is

constant throughout the soil element), the volumes of water entering (V_{we}) and water leaving (V_{wl}) the soil element can be mathematically derived as follows:

$$\frac{\partial V_{we}}{\partial t} = v_w \, dA \qquad [2\text{-}51a]$$

$$\frac{\partial V_{wl}}{\partial t} = \left(v_w + \frac{\partial v_w}{\partial z} dz\right) dA \qquad [2\text{-}51b]$$

where $dA = dx\, dy$, is the unit area of the unsaturated soil element; and v_w is the flow rate of water across the unit area in the z-direction. Besides, Blight (1971) suggested that the air flows in accordance with Fick's law. Note that the air phase is assumed to be continuous and compressible (i.e., ρ_a is not constant throughout the soil element). Thus, the masses of air entering (M_{ae}) and air leaving (M_{al}) the unsaturated soil element are:

$$\frac{\partial M_{ae}}{\partial t} = J_a \, dA \qquad [2\text{-}52a]$$

$$\frac{\partial M_{al}}{\partial t} = \left(J_a + \frac{\partial J_a}{\partial z} dz\right) dA \qquad [2\text{-}52b]$$

where J_a is the mass rate of air across the unit area in the z-direction. The net flux of water in the soil element can be determined by taking the difference between the

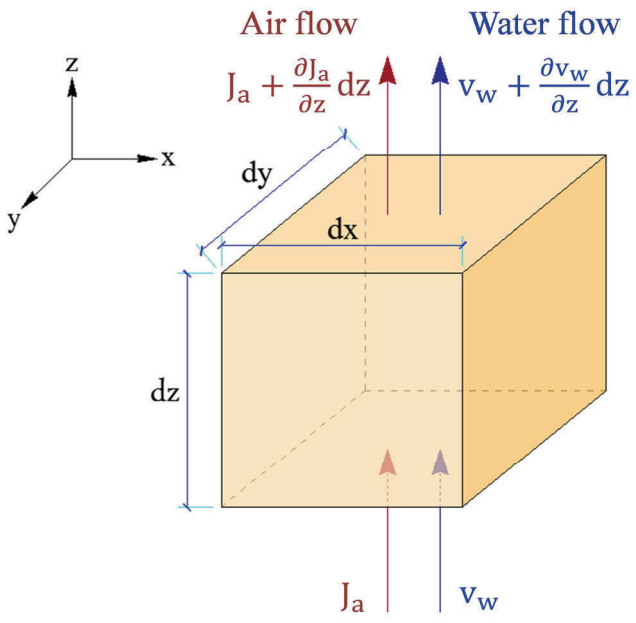

Figure 2.24. Flows of pore-air and pore-water through the unsaturated soil element (modified after Fredlund & Hasan 1979)

volumes of water entering and leaving the soil element. Likewise, under the isothermal condition, the net flux of air is estimated by subtracting the mass of air leaving from the mass of air entering (Fredlund & Hasan 1979). Thus,

$$\frac{\partial\left(\frac{\rho_a V_a}{V_0}\right)}{\partial t} = \frac{\partial J_a}{\partial z} = \frac{k_a}{g}\left[\frac{\partial\left(\frac{\partial u_a}{\partial z}\right)}{\partial z}\right] \quad [2\text{-}53a]$$

$$\frac{\partial\left(\frac{V_w}{V_0}\right)}{\partial t} = \frac{\partial v_w}{\partial z} = \frac{k_w}{\rho_w g}\left[\frac{\partial\left(\frac{\partial u_w}{\partial z}\right)}{\partial z}\right] \quad [2\text{-}53b]$$

where k_a and k_w are the coefficients of permeability with respect to the air and water phases, respectively; ρ_a and ρ_w are the density of air and water, respectively; and g is the gravitational constant. Combining Equations [2-50] and [2-53] while considering the constant loading condition (i.e., $\partial\sigma_z/\partial t = 0$) would lead to the governing equations describing coupled pore-air and pore-water dissipation as follows:

$$\frac{\partial u_a}{\partial t} + C_a\left(\frac{\partial u_w}{\partial t}\right) + c_v^a\left(\frac{\partial^2 u_a}{\partial z^2}\right) = 0 \quad [2\text{-}54a]$$

$$\frac{\partial u_w}{\partial t} + C_w\left(\frac{\partial u_a}{\partial t}\right) + c_v^w\left(\frac{\partial^2 u_w}{\partial z^2}\right) = 0 \quad [2\text{-}54b]$$

in which $C_a = \frac{1}{\left[\left(\frac{m_1^a}{m_2^a}-1\right)-\frac{n(1-S_r)}{m_2^a(u_a+u_{atm})}\right]}$; $c_v^a = \frac{k_a R\Theta}{gM}\frac{1}{\left[m_2^a(u_a+u_{atm})\left(\frac{m_1^a}{m_2^a}-1\right)-n(1-S_r)\right]}$;

$C_w = \left(\frac{m_1^w}{m_2^w}-1\right)$; and $c_v^w = \frac{1}{m_2^w}\left(\frac{k_w}{\gamma_w}\right)$. [2-55]

where C_a and C_w are the interactive constants associated with the air and water phases, respectively; c_v^a and c_v^w are the coefficients of consolidation with respect to the air and water phases, respectively; S_r is the degree of saturation; n is the porosity; u_{atm} is the atmospheric pressure; R is the universal gas constant ($8.31 J.mol^{-1}K^{-1}$); M is the molecular mass of air phase ($0.029 kg.mol^{-1}$); Θ is the absolute temperature; γ_w is the unit weight of water.

According to Fredlund & Hasan (1979), the only drawback in these governing equations (i.e., Equation [2-54]) is that the air phase is assumed continuous throughout the compression even when the degree of saturation (S_r) is high. Nevertheless, this set of governing equations can smoothly convert to the governing equation for saturated soils provided by Terzaghi (1925) or to the equation for dry soils proposed by Blight

(1971). In most models introduced by Fredlund and his co-workers (Fredlund & Hasan 1979; Dakshanamurthy & Fredlund 1980, 1981; Darkshanamurthy et al. 1984; Fredlund et al. 2012), the interactive constants (i.e., C_a and C_w) and coefficients of consolidation (i.e., c_v^a and c_v^w) are assumed to remain unchanged during the consolidation process for the sake of simple evaluation. This assumption may be acceptable for a small stress increment in a transient process, at which all involved properties, such as degree of saturation (S_r), hydraulic conductivity (k_a and k_w), volume change coefficients (m_1^a, m_2^a, m_1^w and m_2^w) and porosity (n) to name a few, do not change considerably. It should be noted that Dakshanamurthy & Fredlund (1980), and Dakshanamurthy et al. (1984) further expanded the 1D equations to the 2D and 3D models, respectively.

2.7.2. Existing models for consolidation in unsaturated soils

The past two decades have witnessed a significant progression in consolidation studies for unsaturated soils. Both analytical and numerical methods have been adopted to derive the consolidation models. Qin et al. (2008) developed an analytical solution to predict the 1D consolidation using Cayley-Hamilton theorem and Laplace transformation technique. The water velocity (v_w) and mass rate of air (J_a) were introduced to the mathematical development, forming fundamental relationships between these terms and pore-air and pore-water pressures. However, the inclusion of v_w and J_a also causes cumbersome computations associated with complex arguments. Although analytical results gave a good agreement with the numerical predictions, the solution may be impractical for use due to the complexity of the obtained equations. Qin et al. (2010a) alternatively presented a semi-analytical solution for the 1D consolidation using Fourier series approximation for Laplace inversion (Crump 1976). Besides, Qin et al. (2010b) further estimated the dissipation rates of excess pore pressures and settlement of unsaturated soil deposits subjected to an exponentially time-dependent loading. In this study, the exponential loading function (with respect to time) generates new consolidation parameters, D_a and D_w, leading to difficulty in deriving the settlement equation. Later, Qin et al. (2014) developed a semi-analytical solution for the consolidation of viscoelastic unsaturated soils. It is reported that the viscosity coefficient (η) has minor impacts on both the excess pore-air and pore-water pressure dissipation rates (Qin et al. 2014).

Shan et al. (2012) provided exact solutions for the unsaturated consolidation using homogeneous and nonhomogeneous boundary conditions. In homogeneous conditions, analytical solutions were obtained by converting the nonhomogeneous governing flow equations into the homogeneous forms. The altered homogeneous equation is presented by:

$$s_i \frac{\partial \psi_i}{\partial t} = \frac{\partial^2 \psi_i}{\partial z^2}, \qquad i = 1,2 \qquad [2\text{-}56]$$

in which s_1 and s_2 can be obtained from the following equation:

$$c_v^a c_v^w s^2 + (c_v^a + c_v^w)s - C_a C_w + 1 = 0 \qquad [2\text{-}57]$$

Similar to the derivation provided by Terzaghi (1925), Equation [2-56] can be solved using the separation of variables method to produce two roots, namely ψ_1 and ψ_2. These alternative solutions constitute excess pore pressures based on relationships presented as follows:

$$\mathbf{u} = \mathbf{A}\boldsymbol{\psi}, \qquad \text{for } s_1 \neq s_2 \qquad [2\text{-}58a]$$

$$\mathbf{u} = \mathbf{B}\boldsymbol{\psi}, \qquad \text{for } s_1 = s_2 \qquad [2\text{-}58b]$$

where $\mathbf{u} = \{u_w, u_a\}^T$; $\boldsymbol{\psi} = \{\psi_1, \psi_2\}^T$;

$$\mathbf{A} = \begin{bmatrix} -1 & -1 \\ a_1 & a_2 \end{bmatrix}; \qquad \mathbf{B} = \begin{bmatrix} 1 & t\frac{\partial}{\partial t} \\ -a_1 & a_3 - a_1 t\frac{\partial}{\partial t} \end{bmatrix};$$

$$a_1 = \frac{c_v^w s_1 + 1}{C_w}; \qquad a_2 = \frac{c_v^w s_2 + 1}{C_w}; \text{ and} \qquad a_3 = \frac{c_v^w s_1}{C_w}. \qquad [2\text{-}59]$$

To obtain Equation [2-58], Shan et al. (2012) used the indirect method which acquires intermediate steps of transforming the nonhomogeneous PDEs to the homogeneous PDEs. In this solution, the authors also captured the effects of exponential and sine wave loading on the consolidation process. Although the analytical method is presented in a constructive manner, the lack of presentation of final equations may lead to the ambiguity in justification, particularly the transition exercise between saturated and unsaturated states. Shan et al. (2014) extensively improved the analytical solutions to predict the consolidation for unsaturated multi-layered soils using the method of undetermined coefficients and orthogonal relation of the eigenfunction. Their

study found that the constant loading exerted to the ground surface of multi-layered soil would generate different excess pore pressures in different layers (Shan et al. 2014).

Zhou et al. (2014), on the other hand, proposed a simple analytical solution for the consolidation of unsaturated soils. The mathematical procedure adopted two alternative variables, namely ϕ_1 and ϕ_2, to transform the nonhomogeneous governing equations to a new set of homogeneous equations. This procedure is comparable to the one proposed by Shan et al. (2012). The alternative set of homogeneous PDEs includes:

$$\frac{\partial \phi_i}{\partial T} = Q_i \frac{\partial^2 \phi_i}{\partial Z^2}, \qquad i = 1,2 \qquad [2\text{-}60]$$

where $Q_1 = \frac{1}{2}\left[A_a + W_w + \sqrt{(A_a - W_w)^2 + 4A_w W_a}\right]$;

$Q_2 = \frac{1}{2}\left[A_a + W_w - \sqrt{(A_a - W_w)^2 + 4A_w W_a}\right]$;

$W_a = \frac{C_w c_v^a \gamma_w m_1^s}{(1 - C_w C_a) k_w}$; $\quad W_w = -\frac{c_v^w \gamma_w m_1^s}{(1 - C_w C_a) k_w}$;

$A_a = -\frac{c_v^a \gamma_w m_1^s}{(1 - C_w C_a) k_w}$; $\quad A_w = \frac{C_a c_v^w \gamma_w m_1^s}{(1 - C_w C_a) k_w}$;

$T = \frac{k_w t}{\gamma_w m_1^s H^2}$; and $\quad Z = \frac{z}{H}$. [2-61]

Zhou et al. (2014) solved the PDEs in Equation [2-60] using the separation of variables method and obtained the roots ϕ_1 and ϕ_2. These solutions can be expressed as functions of excess pore-air and pore-water pressures as follows:

$$\begin{cases} \phi_1 = u_a + c_{21} u_w \\ \phi_2 = c_{12} u_a + u_w \end{cases} \qquad [2\text{-}62]$$

where $c_{12} = (Q_2 - W_w)/A_w$ and $c_{21} = (Q_1 - A_a)/W_a$. Changes in excess pore-air and pore-water pressures can be computed by simultaneously solving Equation [2-62]. For the sake of realistic predictions, the study also incorporated effects of ramped and exponential loadings in the proposed equations. Despite the proposed simple method, analytical procedure given by Zhou et al. (2014) cannot obtain final solutions directly. Moreover, the transition from the obtained solutions to the traditional equation for saturated soils (Terzaghi 1925) may encounter the singularity issues. This indicates that the method is only applicable to the case of unsaturated soils. When the soil becomes saturated, the final solutions may be undefined. Besides the analytical study, Zhou &

Zhao (2014) also provided a numerical approach such as differential quadrature method (DQM) to estimate some complex consolidation problems considering different initial and boundary conditions.

It is also worth mentioning other well-recognised studies associated with the 2D plane strain and axisymmetric consolidation fields. Conte (2004) used the finite element approximation to analyse the plane strain consolidation of a single-layer unsaturated soil. One of the most important findings in this study is that the Mandel-Cryer effect has little impacts on the unsaturated consolidation regardless of values of Poisson's ratio and soil thickness (Conte 2004). This point has been supported by Wong et al. (1998), Vu & Fredlund (2003), and Fredlund et al. (2012).

Previous decades have seen a modest number of studies in relation to the axisymmetric consolidation of unsaturated soils, most of which preferred numerical approaches to deal with the complexity of mathematical equations. Besides the plane strain consolidation study, Conte (2006) also introduced the standard finite element technique to obtain a solution for the coupled consolidation under axisymmetric conditions. Qin et al. (2010c) dealt with the drain well consolidation problem in unsaturated soils using the modified Bessel functions and the Laplace transformation. Zhou & Tu (2012), and Zhou (2013) presented the numerical approach such as DQM to estimate the axisymmetric consolidation behaviour in the unsaturated soil stratum. However, the aforementioned approaches (Conte 2006; Qin et al. 2010c; Zhou & Tu 2012; Zhou 2013) are generally confined to complex numerical procedures. In addition, some prediction methods may be impractical due to the lack of consideration of the vertical flow of air and water phases which occur in the field. Moreover, predictions generated by these methods only cover a simple case when soil is subjected to an external constant loading. In more realistic circumstances, applied loads are rather dynamic and usually vary with time.

2.8. Summary

An unsaturated soil is a three-phase composition generally composed of solid particles, air and water phases. Existing studies (e.g. Fredlund & Morgenstern 1977; Ng & Menzies 2007) have shown that the contractile skin (air-water interface) could be considered as the fourth phase in the soil element. However, contractile skin is

composed of a few thin molecular layers and therefore can be considered as a part of water phase when establishing the volume-mass constitutive models. On the other hand, the contractile skin induces surface traction, which in turn causes a concave curvature on the air-water interface. The radius of curvature, known as meniscus, forms a reverse relationship with matric suction, as demonstrated in Section 2.1.

Soil suction, ψ, is defined as the free energy of soil water and is one of the most important soil properties. The soil suction consists of matric suction component $(u_a - u_w)$ and osmotic suction component (π). Many unsaturated soil problems observed in arid and semi-arid climatic areas are found to significantly affect the matric suction but have minor influence on the osmotic suction (Fredlund et al. 2012). Additionally, experimental studies elucidate that changes in matric suction are very much congruent to changes in the total suction (Krahn & Fredlund 1972). Thus, it can essentially replace the total suction for analysing unsaturated soil mechanics. It is also found that the matric suction change significantly induces the microstructural behaviour of a soil. In particular, the matric suction increase would lead to a bimodal pore-size distribution (PSD) curve, which is ascribed by an increase in the microporosity and a decrease in the macroporosity (Cuisinier & Laloui 2004; Koliji et al. 2006). Effects of matric suction on different pore classes are clearly discussed in Section 2.1. On the other hand, the matric suction has substantial impacts on properties of problematic soil deposits (i.e. collapsible and expansive soils), such as the void ratio (e). It is reported that the decreasing matric suction would lead to a decrease in void ratio for metastable-structured soils and to an increase in void ratio for stable-structured soils (Fredlund 2014). Detailed discussions about problematic soils are presented in Section 2.2.

Terzaghi (1925) proposed a single-valued effective stress variable $(\sigma - u_w)$ based on the effective stress principle, which was used to develop the 1D consolidation theory. However, the single stress variable is only valid for the case of saturated soils but is rather fictive for the case of unsaturated soils. Morgenstern (1979) revealed that single-valued effective equations cannot control both volumetric and shear behaviours of unsaturated soil. Furthermore, Wheeler & Karube (1996) also reported that these proposed equations cannot capture the effects of problematic soils. Therefore, independent stress state variables for constitutive models were recommended by several researchers (Matyas & Radhakrishna 1968; Barden et al. 1969; Fredlund &

Morgenstern 1977). Combination of stress variables, namely $(\sigma - u_a)$, $(\sigma - u_w)$ and $(u_a - u_w)$, were obtained on the basis of equilibrium analyses for a multiphase structure (Fredlund & Morgenstern 1977). The adoption of new stress state variables for unsaturated soils is clearly discussed in Section 2.3.

Fredlund & Morgenstern (1977) proposed a volume-mass constitutive framework based on assumptions of isotropic and linearly elastic soil structure. A set of net stress $(\sigma - u_a)$ and matric suction $(u_a - u_w)$ is usually selected to formulate the constitutive equations for various loading conditions, as presented in Section 2.4. Volume change coefficients for the soil structure (m_1^s and m_2^s) and water phase (m_1^w and m_2^w) associated with changes in stress variables were introduced to the constitutive relations. Verifications for the proposed models were conducted through rigorous laboratory experiments (i.e., oedometer, triaxial tests). In addition, constitutive surfaces for the soil structure and water phase were successfully proven unique as experimental results provided a good agreement with the predictive models (Fredlund & Morgenstern 1977).

Meanwhile, alternative frameworks associated with elastoplastic (EP) behaviour of soils have been developed to predict the total final settlement. The constitutive EP frameworks also capture some features related to wetting-induced volume change issues (e.g. collapsible and expansive soils). These models can be divided in three categories: (1) independent net stress ($\overline{\sigma}$) and matric suction (s) (Approach 1), (2) effective stress approach (Approach 2), and (3) SFG approach (Approach 3). Advantages and disadvantages of each approach were clearly discussed in Section 2.5.

Terzaghi (1925, 1943) introduced a remarkable consolidation theory for fully saturated soils based on the concept of heat diffusion. A derived equation predicting an excess pore-water pressure at particular time and depth was obtained adopting homogeneous drainage boundaries and uniform initial conditions, as shown in Section 2.6. This study provides a solid framework for further formulations of more rigorous settlement models. On the other hand, Barron (1948) transformed the traditional consolidation equation into a polar form to predict the settlement of saturated soils induced by vertical drains. This vertical drain consolidation was analysed assuming axisymmetry around a drain, thus it is also termed axisymmetric consolidation. Predictions of the axisymmetric consolidation are obtained based on free strain and

equal strain hypothesis. According to Barron (1948), equal strain consolidation models are more reliable because of its decent accuracy and simplicity.

Governing equations describing coupled flows of pore-air and pore-water in an unsaturated soil element were originally proposed by Fredlund & Hasan (1979). It is suggested that the flow of air follows Fick's law whereas the water flows in accordance with Darcy's law. Referring to the continuity requirement, the derivation of equation requires assumptions of incompressible soil grains and pore-water, and continuous air phase. The net flux of air and water obtained from changes in mass rate of air (J_a) and water velocity (v_w), respectively, are combined with the constitutive models proposed by Fredlund & Morgenstern (1977), resulting in the governing equations for unsaturated soil consolidation.

Several attempts have been made to solve the governing flow equation provided by Fredlund & Hasan (1979). Among initial studies, Qin et al. (2008) present analytical solution for the 1D consolidation of unsaturated soils using Cayley-Hamilton theorem and Laplace transformation technique. This study reports a good agreement between the analytical predictions and numerical results, indicating that the proposed solution is valid. However, the obtained solution may not be practical for use due to cumbersome equations. On the other hand, Shan et al. (2012) and Zhou et al. (2014) introduced alternative terms, ψ_i and ϕ_i, respectively, to convert the nonlinear nonhomogeneous PDEs into traditional homogeneous PDEs and finally obtain solutions. These indirect methods lead to some uncertainties in mathematical analyses, particularly the transition to the case of saturated soils. Discussions of existing analytical solutions are presented in Section 2.7. The above mentioned analytical methods, however, come across with several constructive ideas, which inspire the ongoing research seeking a precise solution for the consolidation for unsaturated geomaterials. Subsequent chapters will present novel analytical approaches to overcome the shortcomings discussed in the existing solutions.

CHAPTER 3

ANALYTICAL SOLUTION FOR ONE-DIMENSIONAL CONSOLIDATION OF UNSATURATED SOILS USING EIGENFUNCTION EXPANSION METHOD

3.1. Introduction

This chapter proposes a simple but novel analytical solution to predict the dissipations of excess pore-air and pore-water pressures, and the settlement of unsaturated soils during the compression process. The entire procedure refers to 1D consolidation under homogeneous boundary conditions along with the application of uniform and linear distributions of initial excess pore pressures. This study is based on the governing equations originally proposed by Fredlund & Hasan (1979). The method of eigenfunction expansion and the Laplace transform technique are directly applied to solve nonhomogeneous partial differential equations (PDEs), and consequently, the obtained solutions will be presented in two worked examples and verified against other available analytical solutions.

3.2. Governing equations of flow for unsaturated soils

The consolidation theory of unsaturated soils indicates that air and water phases can flow independently. Thus, the flow of air and water should comply with the continuity conditions satisfying Fick's and Darcy's laws, respectively. Considering a referential elevation of a single soil layer in Figure 3.1, for 1D consolidation, the horizontal width is assumed to be infinity and the thickness is denoted as H. A representative soil element has a length:width:depth ratio (x: y: z) of 1: 1: dz, meaning that the depth of the soil element can change. The one-way drainage system demonstrates an upward migration of pore-air and pore-water once an external load is applied to the system. A permeable surface facilitates the dissipation process while the impermeable bedrock

prevents both pore pressures from penetrating through (Figure 3.1(a)). In addition, the two-way drainage boundary condition considers free dissipation of pore-air and pore-water pressures through both permeable surfaces on the top and the base (Figure 3.1(b)).

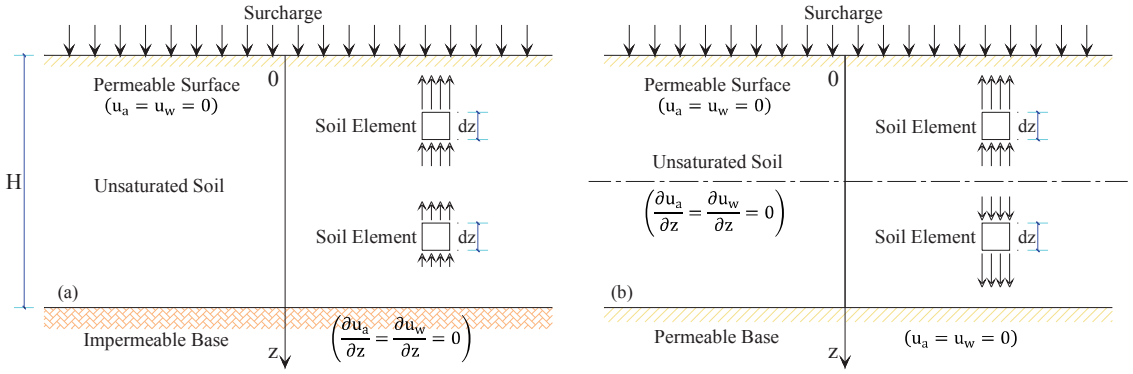

Figure 3.1. A simplified model for one-dimensional elevation of unsaturated soils: (a) one-way drainage system and (b) two-way drainage system

According to Fredlund & Hasan (1979), the constitutive equations illustrating the changes of volume of air (V_a) and water (V_w) with respect to the initial volume of the soil element (V_0) can be expressed as:

$$\frac{\partial\left(\frac{\Delta V_a}{V_0}\right)}{\partial t} = m_1^a \frac{\partial(\sigma - u_a)}{\partial t} + m_2^a \frac{\partial(u_a - u_w)}{\partial t} \quad [3\text{-}1a]$$

$$\frac{\partial\left(\frac{\Delta V_w}{V_0}\right)}{\partial t} = m_1^w \frac{\partial(\sigma - u_a)}{\partial t} + m_2^w \frac{\partial(u_a - u_w)}{\partial t} \quad [3\text{-}1b]$$

where σ is the total pressure; u_a and u_w are excess pore-air and pore-water pressures, respectively; m_1^a and m_1^w are coefficients of air and water volume change with respect to the change of net stress $(\sigma - u_a)$, respectively; and m_2^a and m_2^w are coefficients of air and water volume change with respect to the change of suction $(u_a - u_w)$, respectively.

In addition, the change in air and water volumes can be described by Fick's and Darcy's laws, respectively.

$$\frac{\partial\left(\frac{\Delta V_a}{V_0}\right)}{\partial t} = \frac{k_a R\Theta}{gM(u_a^0 + u_{atm})}\left(\frac{\partial^2 u_a}{\partial z^2}\right) - \frac{n(1 - S_r)}{(u_a^0 + u_{atm})}\left(\frac{\partial u_a}{\partial t}\right) \quad [3\text{-}2a]$$

$$\frac{\partial\left(\frac{\Delta V_w}{V_0}\right)}{\partial t} = \frac{k_w}{\gamma_w}\left(\frac{\partial^2 u_w}{\partial z^2}\right) \quad [3\text{-}2b]$$

where k_a and k_w are air and water permeability coefficients ($m.s^{-1}$), respectively; g is the gravitational acceleration ($\sim 9.8 m.s^{-2}$); u_a^0 and u_w^0 are maximum initial pore-air and pore-water pressures (kPa), respectively; u_{atm} is the atmospheric pressure (kPa); R is the universal air constant ($\sim 8.3 J.mol^{-1}K^{-1}$); $\Theta = (\theta^\circ + 273)$, is the absolute temperature (K); M is the molecular mass of air phase ($\sim 0.029 kg.mol^{-1}$); n is the porosity during consolidation process; S_r is the degree of saturation during consolidation process; and γ_w is water unit weight ($\sim 9.8 kN.m^{-3}$).

The change in total pressure with respect to time in Equations [3-1a] and [3-1b] is set to zero ($\partial\sigma/\partial t = 0$) as a result of constant loading. By combining two pairs of Equations [3-1a] and [3-2a] and Equations [3-1b] and [3-2b], the result demonstrates two nonhomogeneous PDEs of air and water phases dependent on variables z and t, as follows:

$$\frac{\partial u_a}{\partial t} + C_a\left(\frac{\partial u_w}{\partial t}\right) + c_v^a\left(\frac{\partial^2 u_a}{\partial z^2}\right) = 0 \qquad [3\text{-}3a]$$

$$\frac{\partial u_w}{\partial t} + C_w\left(\frac{\partial u_a}{\partial t}\right) + c_v^w\left(\frac{\partial^2 u_w}{\partial z^2}\right) = 0 \qquad [3\text{-}3b]$$

where $C_a = \frac{1}{\left[\left(\frac{m_1^a}{m_2^a}-1\right)-\frac{n(1-S_r)}{m_2^a(u_a^0+u_{atm})}\right]}$, is the interactive constant associated with the air phase;

$c_v^a = \frac{k_a R\Theta}{gM}\frac{1}{\left[m_2^a(u_a^0+u_{atm})\left(\frac{m_1^a}{m_2^a}-1\right)-n(1-S_r)\right]}$, is the coefficient of consolidation with respect to the air phase;

$C_w = \left(\frac{m_1^w}{m_2^w}-1\right)$, is the interactive constant associated with the water phase; and

$c_v^w = \frac{1}{m_2^w}\left(\frac{k_w}{\gamma_w}\right)$, is the coefficient of consolidation with respect to the water phase.

Equations [3-3a] and [3-3b] can be simplified as follows:

$$u_{a,t} + C_a u_{w,t} + c_v^a u_{a,zz} = 0 \qquad [3\text{-}4a]$$

$$u_{w,t} + C_w u_{a,t} + c_v^w u_{w,zz} = 0 \qquad [3\text{-}4b]$$

where $u_{a,t}$ and $u_{w,t}$ are the first order of PDEs of pore-air and pore-water pressures with respect to time, respectively; and $u_{a,zz}$ and $u_{w,zz}$ are the second order of PDEs of pore-air and pore-water pressures with respect to depth, respectively.

3.3. Analytical solution for 1D consolidation

The nature of soils, in general, is some of ambiguity due to the complicated texture assemblage and the lack of homogeneity in particle sizes, making it more difficult in predicting the consolidation characteristics. Before analysing further, some essential assumptions need to be made to allow an ease of handling analytical development, which are listed below:

(1) The entire soil strata are assumed to be homogeneous;
(2) Solid solids and pore-water are incompressible;
(3) Air and water phases are assumed to be continuous;
(4) Environmental influences such as air diffusion through water and temperature change can be neglected;
(5) The loading and deformation happen along vertical direction only (1D consolidation);
(6) Interactive constants and consolidation coefficients with respect to air phase (C_a and c_v^a, respectively) and water phase (C_w and c_v^w, respectively) are assumed to be constant.

Due to variations of permeability, volume change coefficients, degree of saturation (S_r), and porosity (n), the interactive and consolidation coefficients may change during the consolidation process. However, for the sake of simplification, assumption (6) is made to alleviate the complication in obtaining the solutions for the governing equations (i.e. Equation [3-3]). It should be noted that this assumption was also adopted by Shan et al. (2012). Additionally, in the analytical solution provided by Terzaghi (1943), the consolidation coefficient (c_v) was considered to be constant.

In this chapter, the homogeneous boundary conditions, namely one-way and two-way drainage systems, can be mathematically described as follows:

(a) One-way drainage condition:

- $u_a(0,t) = u_w(0,t) = 0;$ $t \geq 0$ [3-5a]
- $\left[\frac{\partial u_a(z,t)}{\partial z}\right]_{z=H} = \left[\frac{\partial u_w(z,t)}{\partial z}\right]_{z=H} = 0;$ $t \geq 0$ [3-5b]

(b) Two-way drainage condition:

- $u_a(0,t) = u_w(0,t) = 0;$ $t \geq 0$ [3-6a]
- $u_a(H,t) = u_w(H,t) = 0;$ $t \geq 0$ [3-6b]

where H is the soil layer thickness.

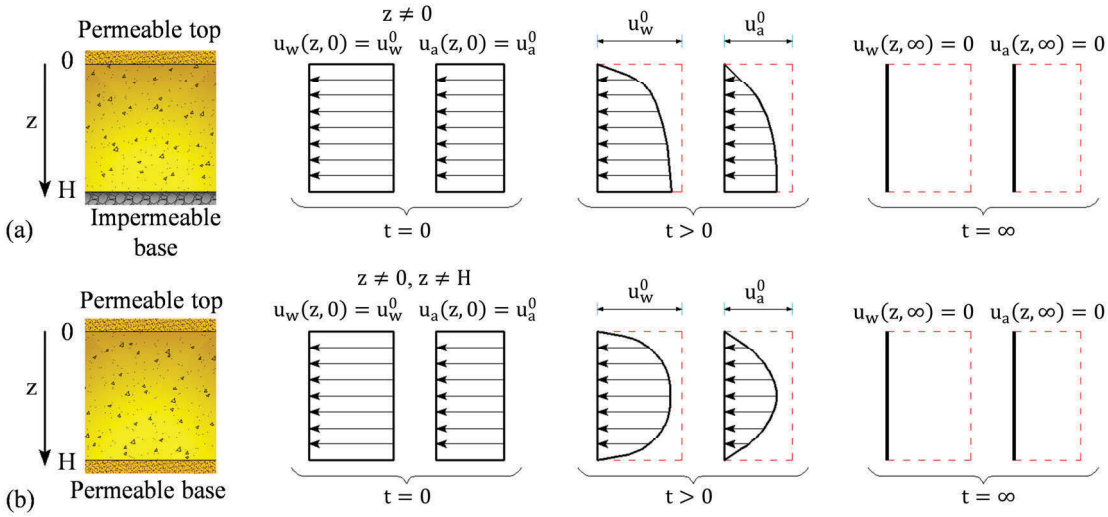

Figure 3.2. Dissipation of excess pore-water and pore-air pressures for (a) one-way drainage system and (b) two-way drainage system

Constant initial excess pore pressures have been assumed in most literature and in the laboratory consolidation tests (Venkatramaiah 2006). Figure 3.2 depicts typical patterns of water and air dissipation under one-way (Figure 3.2(a)) and two-way (Figure 3.2(b)) drainage systems when the constant initial condition is considered. However, this condition is not strictly applicable in the cases of consolidation under small footings or deep soil layers (Venkatramaiah 2006). In this chapter, the initial condition of the soil layer will be presented in mathematical forms which capture the cases of the initial excess pore pressures being uniformly distributed (constant with depth) and linearly

distributed (linearly decreasing with depth). Thus, at $t = 0$, the initial pore-air and pore-water pressures are respectively described in the domain $z \in (0, H)$ as follows:

$$u_a(z, 0) = f_a(z) = u_a^0 \left(1 - \lambda_a \frac{z}{H}\right); \quad [3\text{-}7a]$$

$$u_w(z, 0) = f_w(z) = u_w^0 \left(1 - \lambda_w \frac{z}{H}\right); \quad [3\text{-}7b]$$

where λ_a and λ_w are dimensionless parameters controlling the gradient of distributions of initial excess pore-air and pore-water pressures with depth, respectively.

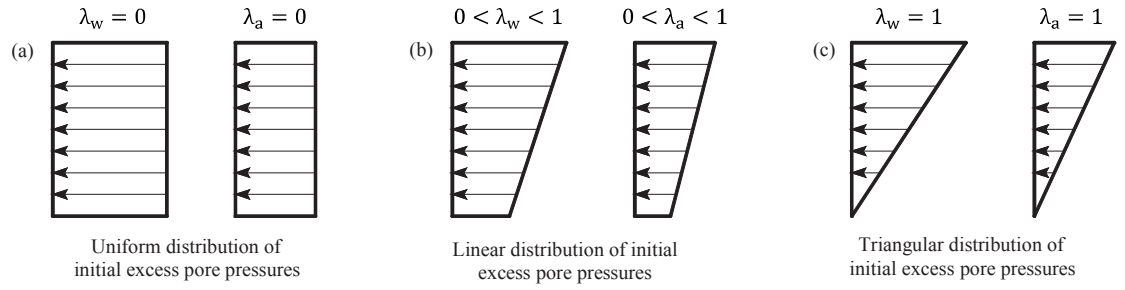

Figure 3.3. Different initial conditions due to the changes of λ_w and λ_a

The parameters λ_a and λ_w act as weighting factors, ranging from 0 to 1. When $\lambda_a = \lambda_w = 0$, $u_a(z, 0)$ and $u_w(z, 0)$ will become u_a^0 and u_w^0, respectively. This means that the distribution of initial pore pressures is uniform throughout the depth. In the case where $0 < \lambda_a < 1$ or $0 < \lambda_w < 1$, the initial excess pore pressures decrease linearly with depth. The triangular distributions of initial pore pressures will be formed when $\lambda_a = \lambda_w = 1$. Figure 3.3 demonstrates the gradient change of distributions of initial pore pressures with variations of λ_a and λ_w.

According to Haberman (2012), to deal with nonhomogeneous problems, the eigenfunction expansion method with homogeneous boundary conditions (Equations [3-5] and [3-6]) employs homogeneous forms for general solutions of $u_a(z, t)$ and $u_w(z, t)$.

$$u_a(z, t) = \sum_{k=0}^{\infty} Z_a(z).T_a(t) \quad [3\text{-}8a]$$

$$u_w(z, t) = \sum_{k=0}^{\infty} Z_w(z).T_w(t) \quad [3\text{-}8b]$$

where $Z_a(z)$ and $Z_w(z)$ are eigenfunctions with respect to the depth z; and $T_a(t)$ and $T_w(t)$ are generalised Fourier coefficients varying with time t.

These general solutions can be written as products of functions of z and functions of t. The functions $Z_a(z)$ and $Z_w(z)$ are subjected to homogeneous boundary conditions and are termed as eigenfunctions. In this study, the eigenfunctions describe natural vibrations and can be presented in trigonometric series, namely ordinary Fourier sine series (Haberman 2012). Additionally, eigenvalues, known as natural frequencies of vibration (λ_k) (with $k = 0, 1, 2, ...$), are determined by the material constants of the system, geometrical factors and boundary conditions. Two pairs of eigenfunctions and eigenvalues can be adopted as follows:

(a) One-way drainage condition:

$$\begin{cases} Z_a^k(z) = Z_w^k(z) = \sin\left[(2k+1)\frac{\pi}{2}\frac{z}{H}\right] \\ \lambda_k = \frac{(2k+1)^2}{H^2}\frac{\pi^2}{4} \end{cases} \quad [3\text{-}9]$$

(b) Two-way drainage condition:

$$\begin{cases} Z_a^k(z) = Z_w^k(z) = \sin\left[k\pi\frac{z}{H}\right] \\ \lambda_k = \frac{k^2\pi^2}{H^2} \end{cases} \quad [3\text{-}10]$$

For the ease of handling the mathematical development in both drainage conditions, term K can be introduced in Equation [3-11], as follows:

$$K = \sqrt{\lambda_k} = \begin{cases} \frac{(2k+1)}{H}\frac{\pi}{2}, & \text{for one} - \text{way drainage} \\ \frac{k\pi}{H}, & \text{for two} - \text{way drainage} \end{cases} \quad [3\text{-}11]$$

Hence, Equations [3-8a] and [3-8b] can be rewritten as follows:

$$u_a(z,t) = \sum_{k=0}^{\infty} T_a^k(t)\sin(Kz) \quad [3\text{-}12a]$$

$$u_w(z,t) = \sum_{k=0}^{\infty} T_w^k(t)\sin(Kz) \quad [3\text{-}12b]$$

Substituting Equations [3-12a] and [3-12b] into the corresponding Equations [3-4a] and [3-4b] gives:

$$\sum_{k=0}^{\infty}\left\{(-C_a)T_{w,t}^k(t)\sin(Kz)\right\} = \sum_{k=0}^{\infty}\left\{\left[T_{a,t}^k(t) - c_v^a(K^2)T_a^k(t)\right]\sin(Kz)\right\} \quad [3\text{-}13a]$$

$$\sum_{k=0}^{\infty}\left\{(-C_w)T_{a,t}^k(t)\sin(Kz)\right\} = \sum_{k=0}^{\infty}\left\{\left[T_{w,t}^k(t) - c_v^w(K^2)T_w^k(t)\right]\sin(Kz)\right\} \quad [3\text{-}13b]$$

Equations [3-13a] and [3-13b] can be truncated to the family of ordinary differential equations (ODEs):

$$(-C_a)T_{w,t}^k(t) = T_{a,t}^k(t) - c_v^a(K^2)T_a^k(t) \quad [3\text{-}14a]$$

$$(-C_w)T_{a,t}^k(t) = T_{w,t}^k(t) - c_v^w(K^2)T_w^k(t) \quad [3\text{-}14b]$$

with $k = 0, 1, 2, ...$

Applying Laplace transform to Equations [3-14a] and [3-14b] yields in:

$$(-C_a)\left[s\overline{T}_w^k(s) - T_w^k(0)\right] = \left[s\overline{T}_a^k(s) - T_a^k(0)\right] - c_v^a(K^2)\overline{T}_a^k(s) \quad [3\text{-}15a]$$

$$(-C_w)\left[s\overline{T}_a^k(s) - T_a^k(0)\right] = \left[s\overline{T}_w^k(s) - T_w^k(0)\right] - c_v^w(K^2)\overline{T}_w^k(s) \quad [3\text{-}15b]$$

with $k = 0, 1, 2, ...$

Rearranging and then simultaneously solving for $\overline{T}_a^k(s)$ and $\overline{T}_w^k(s)$ ($k = 0, 1, 2, ...$) in Equation [3-15] results in:

$$\overline{T}_a^k(s) = \frac{T_a^k(0)(C_wC_a-1)s+c_v^w[C_aT_w^k(0)+T_a^k(0)]K^2}{(C_wC_a-1)s^2+(c_v^w+c_v^a)K^2s-c_v^wc_v^aK^4} \quad [3\text{-}16a]$$

$$\overline{T}_w^k(s) = \frac{T_w^k(0)(C_wC_a-1)s+c_v^a[C_wT_a^k(0)+T_w^k(0)]K^2}{(C_wC_a-1)s^2+(c_v^w+c_v^a)K^2s-c_v^wc_v^aK^4} \quad [3\text{-}16b]$$

It is known that the parameters $T_a^k(0)$ and $T_w^k(0)$ ($k = 0, 1, 2, ...$) are independent of the complex argument s. Thus, taking the inverse Laplace in Equations [3-16a] and [3-16b] leads to:

$$T_a^k(t) = \frac{\Omega\left(e^{\alpha_1K^2t}-e^{\alpha_2K^2t}\right)+\Psi\left(e^{\alpha_1K^2t}+e^{\alpha_2K^2t}\right)}{2\eta} \quad [3\text{-}17a]$$

$$T_w^k(t) = \frac{\Omega'\left(e^{\alpha_1K^2t}-e^{\alpha_2K^2t}\right)+\Psi'\left(e^{\alpha_1K^2t}+e^{\alpha_2K^2t}\right)}{2\eta} \quad [3\text{-}17b]$$

where $\eta = [(c_v^w - c_v^a)^2 + 4c_v^wc_v^aC_wC_a]^{\frac{1}{2}}$;

$\Omega = (c_v^a - c_v^w)T_a^k(0) - 2c_v^wC_aT_w^k(0)$; $\quad \Psi = \eta T_a^k(0)$;

$\Omega' = (c_v^w - c_v^a)T_w^k(0) - 2c_v^aC_wT_a^k(0)$; $\quad \Psi' = \eta T_w^k(0)$;

$T_a^k(0) = \frac{\int_0^H[u_a(z,0)\sin(Kz)]dz}{\int_0^H[\sin^2(Kz)]dz}$; $\quad T_w^k(0) = \frac{\int_0^H[u_w(z,0)\sin(Kz)]dz}{\int_0^H[\sin^2(Kz)]dz}$;

$\alpha_1 = \frac{1}{2}\left(\frac{c_v^w + c_v^a + \eta}{1 - C_w C_a}\right)$; and $\alpha_2 = \frac{1}{2}\left(\frac{c_v^w + c_v^a - \eta}{1 - C_w C_a}\right)$.

Substituting a pair of Equations [3-17a] and [3-17b] into Equations [3-12a] and [3-12b], respectively, results in:

$$u_a(z,t) = \sum_{k=0}^{\infty} \frac{\sin(Kz)}{2\eta}\left[\Omega\left(e^{\alpha_1 K^2 t} - e^{\alpha_2 K^2 t}\right) + \Psi\left(e^{\alpha_1 K^2 t} + e^{\alpha_2 K^2 t}\right)\right] \quad [3\text{-}18a]$$

$$u_w(z,t) = \sum_{k=0}^{\infty} \frac{\sin(Kz)}{2\eta}\left[\Omega'\left(e^{\alpha_1 K^2 t} - e^{\alpha_2 K^2 t}\right) + \Psi'\left(e^{\alpha_1 K^2 t} + e^{\alpha_2 K^2 t}\right)\right] \quad [3\text{-}18b]$$

Equation [3-18] indicates the dissipation of excess pore pressures applicable to both drainage systems. These equations present closed-form solutions and can smoothly convert back to the solution for 1D consolidation in saturated soils (Terzaghi 1943) if properties associated with the air phase are discarded. Moreover, the application of eigenfunction expansion method allows the general solution to be expressed in a series of the eigenfunction of the related homogeneous problem. This means that Equation [3-4] can be solved directly without an intermediate step of converting the nonhomogeneous PDEs to the homogeneous PDEs as performed by Shan et al. (2012) and Zhou et al. (2014).

3.4. Settlement of unsaturated soils

The prediction of the time-dependent soil settlement is a key objective in this study. Settlement rate mainly corresponds to the dissipation rate of pore-air and pore-water pressures with respect to time. Therefore, it is crucial to express the settlement equation under the time domain only. It is also worth noting that when the time approaches infinity, excess pore pressures completely dissipate, and the soil layer will achieve its final settlement.

To obtain the settlement of unsaturated soils, coefficients of volume change with respect to air and water phases are assumed to remain constant during the consolidation process. Fredlund & Hasan (1979) proposed a constitutive equation for the soil structure to link the stress and deformation state variables, as below:

$$\frac{\partial\left(\frac{\Delta V}{V_0}\right)}{\partial t} = \frac{\partial(\varepsilon_v)}{\partial t} = m_1^s \frac{\partial(\sigma - u_a)}{\partial t} + m_2^s \frac{\partial(u_a - u_w)}{\partial t} \quad [3\text{-}19]$$

where ε_v is the volumetric strain; $m_1^s = m_1^w + m_1^a$, is the coefficient of volume change of the soil element with respect to the change in the net stress; and $m_2^s = m_2^w + m_2^a$, is the coefficient of volume change of the soil element with respect to the change in suction.

Considering a static loading, the change in the total stress with respect to time is set at zero ($\partial\sigma/\partial t = 0$), thus:

$$\frac{\partial(\varepsilon_v)}{\partial t} = (m_2^s - m_1^s)\frac{\partial u_a}{\partial t} - m_2^s\frac{\partial u_w}{\partial t} \quad [3\text{-}20]$$

Integrating Equation [3-20] with respect to time t at which $t \in [0, \infty)$, the volumetric strain will be given by:

$$\varepsilon_v(z,t) = (m_2^s - m_1^s)[u_a(z,t) - u_a(z,0)] - m_2^s[u_w(z,t) - u_w(z,0)] \quad [3\text{-}21]$$

The compression of the soil layer can be expressed by integrating Equation [3-21] with respect to depth z at which $z \in [0, H]$.

$$S(t) = \left|\int_0^H \varepsilon_v(z,t)dz\right| = \left|(m_2^s - m_1^s)\left[\int_0^H u_a(z,t)dz - Hu_a^0\left(1 - \frac{\lambda_a}{2}\right)\right] - m_2^s\left[\int_0^H u_w(z,t)dz - Hu_w^0\left(1 - \frac{\lambda_w}{2}\right)\right]\right| \quad [3\text{-}22]$$

Equation [3-22] is a function of time t and can be utilised to predict the settlement of the unsaturated soil deposits.

3.5. Worked examples

This section consists of two worked examples predicting the dissipation rates of excess pore-air and pore-water pressures, and more importantly, the ground surface settlement against elapsed time. Example 1 considers the case of uniformly distributed initial pore pressures, where the parameters λ_a and λ_w are equal to zero. In this worked example, the predictions are presented incorporating various permeability ratios (k_a/k_w). Verification is conducted by comparing the predictions with analytical solutions introduced by Shan et al. (2012). Furthermore, Example 2 adopts linear distributions of initial pore-air and pore-water pressures, where λ_a and λ_w are greater than zero. This

example primarily investigates the variation of dissipation rates of pore pressures and settlement due to the changes in the newly proposed parameters λ_a and λ_w. Both examples include one-way and two-way drainage boundary conditions and will adopt similar properties (Qin et al. 2008; Shan et al. 2012) as follows:

- Material properties: $n = 0.50$; $S_r = 80\%$; $k_w = 10^{-10}ms^{-1}$;
  $H = 10m$; $u_{atm} = 100kPa$;
  $m_1^s = -2.5 \times 10^{-4}kPa^{-1}$; $m_2^s = 0.4m_1^s$;
  $m_1^w = 0.2m_1^s$; $m_2^w = 4m_1^w$.
- Physical properties: $R = 8.314J.mol^{-1}K^{-1}$; $M = 0.029kg.mol^{-1}$;
  $\Theta = (\theta° + 273.16)K$; $\theta° = 20℃$.

In Example 1, the air permeability coefficient (k_a) varies from 10^{-12} to $10^{-7}m/s$ while the water permeability coefficient (k_w) remains constant with the value of $10^{-10}m/s$. The properties, as provided above, can be employed to work out the values of the consolidation coefficients (c_v^a and c_v^w) and the interactive constants (C_a and C_w) presented in Equations (3a) and (3b). In Example 2, the effects of λ_a and λ_w on consolidation of unsaturated soils can be investigated by increasing λ_a from 0 to 1 while maintaining λ_w of 0.25, and vice versa. The investigated subject is an unsaturated soil layer with an infinite width, and depth of $10m$. A static surcharge of $100kPa$ is instantaneously applied on the ground surface and is denoted as q. According to Fredlund & Hasan (1979), the application of surcharge will generate an initial excess pore-air pressure of $20kPa$ and an initial excess pore-water pressure $40kPa$. After a certain time of loading, the air and water tend to flow out of the soil, resulting in the reduction of the soil volume. Therefore, the vertical effective stress begins to increase gradually in order to compensate the pore pressure losses and the ground surface settlement can be observed.

3.5.1. Worked example 1

In this example, uniformly distributed initial excess pore pressures are assumed throughout the soil layer, meaning λ_a and λ_w are equal to zero. Thus, Equations [3-7a] and [3-7b] can be rewritten in a domain $z \in (0, H)$ as follows:

$$u_a(z,0) = u_a^0 = 20\text{kPa} \quad [3\text{-}23a]$$

$$u_w(z,0) = u_w^0 = 40\text{kPa} \quad [3\text{-}23b]$$

Then, Equation [3-18] can be rearranged under one-way and two-way drainage conditions, respectively, as follows:

(a) One-way drainage condition:

$$u_a(z,t) = \sum_{k=0}^{\infty} \frac{\sin(Kz)}{\eta HK}\left[\Omega_1\left(e^{\alpha_1 K^2 t} - e^{\alpha_2 K^2 t}\right) + \Psi_1\left(e^{\alpha_1 K^2 t} + e^{\alpha_2 K^2 t}\right)\right] \quad [3\text{-}24a]$$

$$u_w(z,t) = \sum_{k=0}^{\infty} \frac{\sin(Kz)}{\eta HK}\left[\Omega_1'\left(e^{\alpha_1 K^2 t} - e^{\alpha_2 K^2 t}\right) + \Psi_1'\left(e^{\alpha_1 K^2 t} + e^{\alpha_2 K^2 t}\right)\right] \quad [3\text{-}24b]$$

(b) Two-way drainage condition:

$$u_a(z,t) = \sum_{k=0}^{\infty} \frac{[1-(-1)^k]\sin(Kz)}{\eta HK}\left[\Omega_1\left(e^{\alpha_1 K^2 t} - e^{\alpha_2 K^2 t}\right) + \Psi_1\left(e^{\alpha_1 K^2 t} + e^{\alpha_2 K^2 t}\right)\right] \quad [3\text{-}25a]$$

$$u_w(z,t) = \sum_{k=0}^{\infty} \frac{[1-(-1)^k]\sin(Kz)}{\eta HK}\left[\Omega_1'\left(e^{\alpha_1 K^2 t} - e^{\alpha_2 K^2 t}\right) + \Psi_1'\left(e^{\alpha_1 K^2 t} + e^{\alpha_2 K^2 t}\right)\right] \quad [3\text{-}25b]$$

where $\eta = [(c_v^w - c_v^a)^2 + 4c_v^w c_v^a C_w C_a]^{\frac{1}{2}}$;

$\Omega_1 = (c_v^a - c_v^w)u_a^0 - 2c_v^w C_a u_w^0$; $\Psi_1 = \eta u_a^0$;

$\Omega_1' = (c_v^w - c_v^a)u_w^0 - 2c_v^a C_w u_a^0$; $\Psi_1' = \eta u_w^0$;

$K = \frac{(2k+1)}{H}\frac{\pi}{2}$ for one-way drainage system; or

$= \frac{k\pi}{H}$ for two-way drainage system;

$\alpha_1 = \frac{1}{2}\left(\frac{c_v^w + c_v^a + \eta}{1 - C_w C_a}\right)$; and $\alpha_2 = \frac{1}{2}\left(\frac{c_v^w + c_v^a - \eta}{1 - C_w C_a}\right)$.

In this example, the dissipation process is investigated at $H/2$ (middle of the layer). Figures 3.4(a) and 3.4(b) are correspondingly obtained from Equations [3-24a] and [3-24b], presenting the dissipation rates of the excess pore pressures with respect to time for the one-way drainage system. Figures 3.5(a) and 3.5(b) also describe the change in excess pore pressures generated by Equations [3-25a] and [3-25b] for the two-way drainage system, respectively. The dissipation rates of normalised air (u_a/u_a^0) and normalised water (u_w/u_w^0) pressures are examined with varying permeability ratios (k_a/k_w), ranging from 0.01 to 1000. As observed in Figures 3.4 and 3.5, the pore-water pressure dissipation illustrates a double S-shaped pattern when k_a is greater than $0.1k_w$,

while the pore-air pressure dissipation only forms a single curve throughout the entire dissipation process.

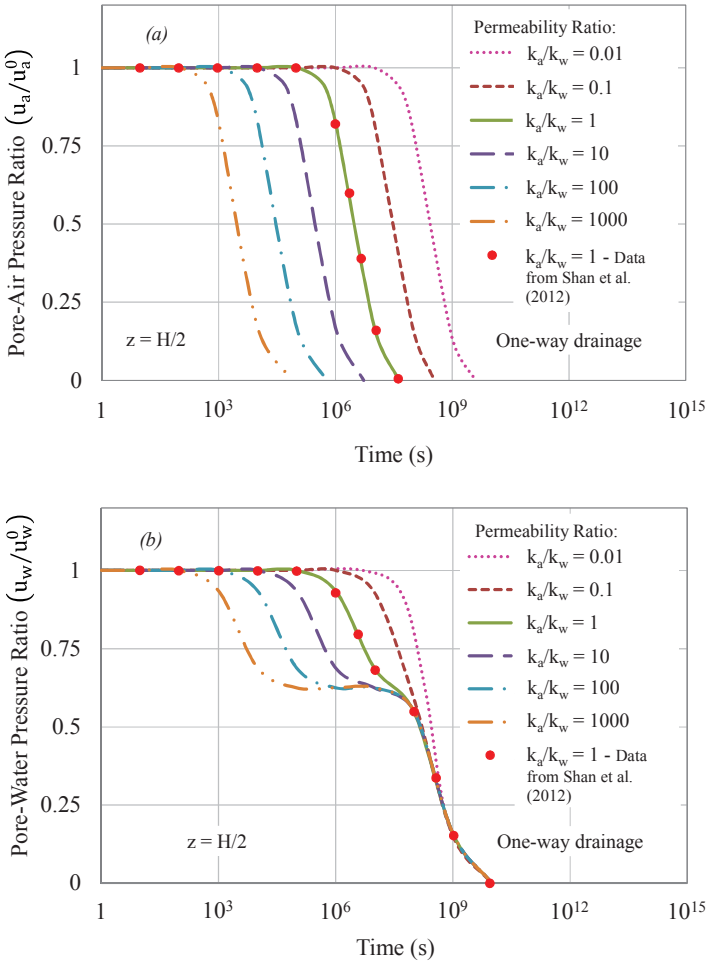

Figure 3.4. Dissipation of pore pressures varying with permeability ratios in one-way drainage system: (a) dissipation of pore-air pressure and (b) dissipation of pore-water pressure

In Figures 3.4(a) and 3.5(a), parallel curves are formed when pore-air pressures with varying k_a/k_w start decreasing. It can be clearly seen that higher k_a/k_w delivers faster dissipation of pore-air pressures. Considering the highest value of k_a/k_w, the pore-air pressure patterns indicate an instantaneous dissipation and require very short time to complete this process. Besides, the dissipation rate of pore-water pressures can be divided into two stages due to its complex curve. By closely examining k_a/k_w of 10 in the one-way drainage system, Figure 3.4(a) shows that the pore-air pressure completely dissipates after 5×10^6s and during this time the water dissipation rate with the similar

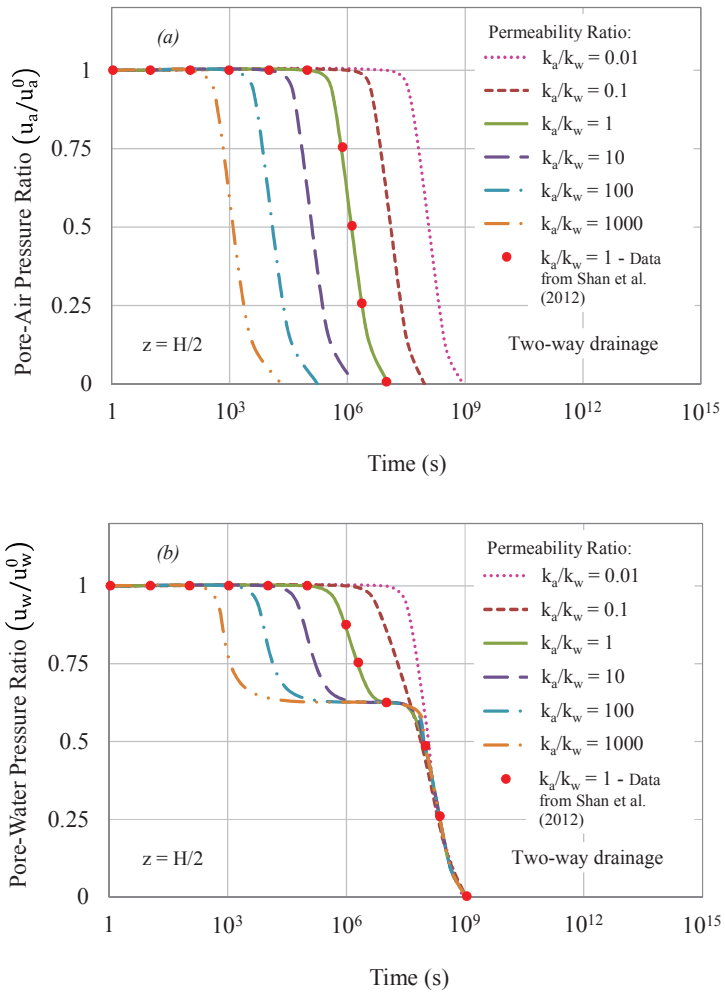

Figure 3.5. Dissipation of pore pressures varying with permeability ratios in two-way drainage system: (a) dissipation of pore-air pressure and (b) dissipation of pore-water pressure

k_a/k_w forms an upper S curve (Figure 3.4(b)). This process is considered as the first stage of dissipation, where significant variation of pore-water pressure patterns can be clearly observed. Figures 3.4(b) and 3.5(b) depict that the rate of water flowing out of the soil at the first stage is more rapid as a result of higher k_a/k_w. The second stage begins after the pore-air pressure completely diminishes. During this stage, the pore-water pressure patterns with different values of k_a/k_w converge into a single curve and fully dissipate at the same time (i.e., 10^{10}s for one-way drainage condition and 10^9s for two-way drainage condition). The dissipation at the second stage is a slow process similar to the consolidation of saturated soils. In comparison to the one-way drainage

condition, the results obtained in the two-way drainage system also share similar patterns for pore-air and pore-water pressures. The only difference is that the two-way drainage system accelerates the dissipation process; therefore the soil layer consolidates more quickly than it does in the one-way drainage system.

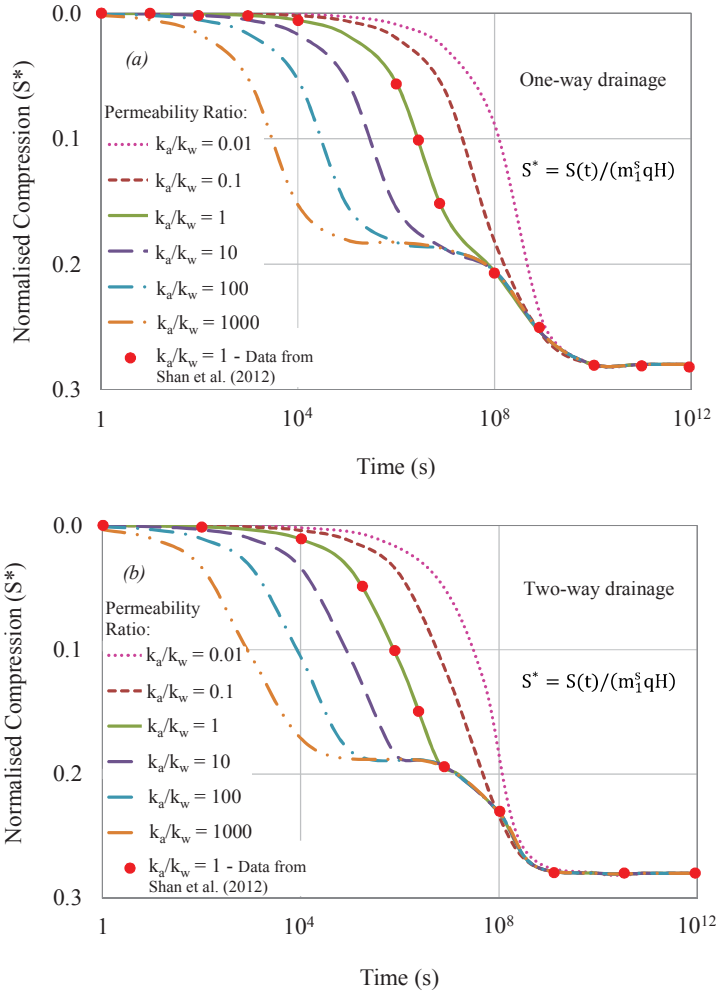

Figure 3.6. Settlement of unsaturated soils varying with permeability ratios: (a) for one-way drainage and (b) for two-way drainage systems

On the other hand, the settlement of the soil layer considering uniformly distributed initial pore pressures can be computed as follows:

$$S(t) = \left|\int_0^H \varepsilon_v(z,t)dz\right| = \left|(m_2^s - m_1^s)\left[\int_0^H u_a(z,t)dz - Hu_a^0\right] - m_2^s\left[\int_0^H u_w(z,t)dz - Hu_w^0\right]\right| \quad [3\text{-}26]$$

where

(a) One-way drainage condition:

$$\int_0^H u_a(z,t)dz = \sum_{k=0}^{\infty}\left(\frac{1}{\eta HK^2}\right)\left[\Omega_1\left(e^{\alpha_1 K^2 t} - e^{\alpha_2 K^2 t}\right) + \Psi_1\left(e^{\alpha_1 K^2 t} + e^{\alpha_2 K^2 t}\right)\right] \quad [3\text{-}27a]$$

$$\int_0^H u_w(z,t)dz = \sum_{k=0}^{\infty}\left(\frac{1}{\eta HK^2}\right)\left[\Omega_1'\left(e^{\alpha_1 K^2 t} - e^{\alpha_2 K^2 t}\right) + \Psi_1'\left(e^{\alpha_1 K^2 t} + e^{\alpha_2 K^2 t}\right)\right] \quad [3\text{-}27b]$$

(b) Two-way drainage condition:

$$\int_0^H u_a(z,t)dz = \sum_{k=0}^{\infty}\left\{\frac{\left[1-(-1)^k\right]^2}{\eta HK^2}\right\}\left[\Omega_1\left(e^{\alpha_1 K^2 t} - e^{\alpha_2 K^2 t}\right) + \Psi_1\left(e^{\alpha_1 K^2 t} + e^{\alpha_2 K^2 t}\right)\right] \quad [3\text{-}28a]$$

$$\int_0^H u_w(z,t)dz = \sum_{k=0}^{\infty}\left\{\frac{\left[1-(-1)^k\right]^2}{\eta HK^2}\right\}\left[\Omega_1'\left(e^{\alpha_1 K^2 t} - e^{\alpha_2 K^2 t}\right) + \Psi_1'\left(e^{\alpha_1 K^2 t} + e^{\alpha_2 K^2 t}\right)\right] \quad [3\text{-}28b]$$

Figure 3.6 represents variations of the normalised settlement (S^*) with time in both one-way drainage (obtained from Equations [3-26] and [3-27]) and two-way drainage (obtained from Equations [3-26] and [3-28]) conditions. The general patterns adequately resemble to the double S curves of the water dissipation rates shown in Figures 3.4(b) and 3.5(b). These double S curves can be easily seen when k_a is higher than $0.1k_w$. This is due to the fact that the settlement in the earlier stage is mainly governed by the dissipation of excess pore pressures, in which air dissipates more quickly than water, whereas the settlement in the later stage is air-free and presents the gradual dissipation of excess pore-water pressure only. It is suggested that considerably higher values of k_a/k_w, let say 10^3 or more, cause a rapid dissipation of air pressure. As a result, the instantaneous settlement occurs and the upper S curve tends to be shifted away to far left. In Figure 3.6, the change in the normalised settlement of the soil layer S^* ($S^* = S(t)/(m_1^s qH)$) is plotted against time t. As observed, the two-way drainage system allows faster settlement than the one-way drainage system as air and water can be squeezed out of the soil from both boundaries.

Furthermore, the verification is conducted by graphically comparing the obtained solution in this study against the analytical solution proposed by Shan et al. (2012). The dissipation rate of excess pore pressures and consolidation settlement with k_a/k_w of 1 are considered for this comparison as shown in Figures 3.4-3.6. As observed, the predictions in this study are in a very good agreement with the reported values by Shan

et al. (2012), confirming that the analytical solution developed in this study can deliver reliable predictions.

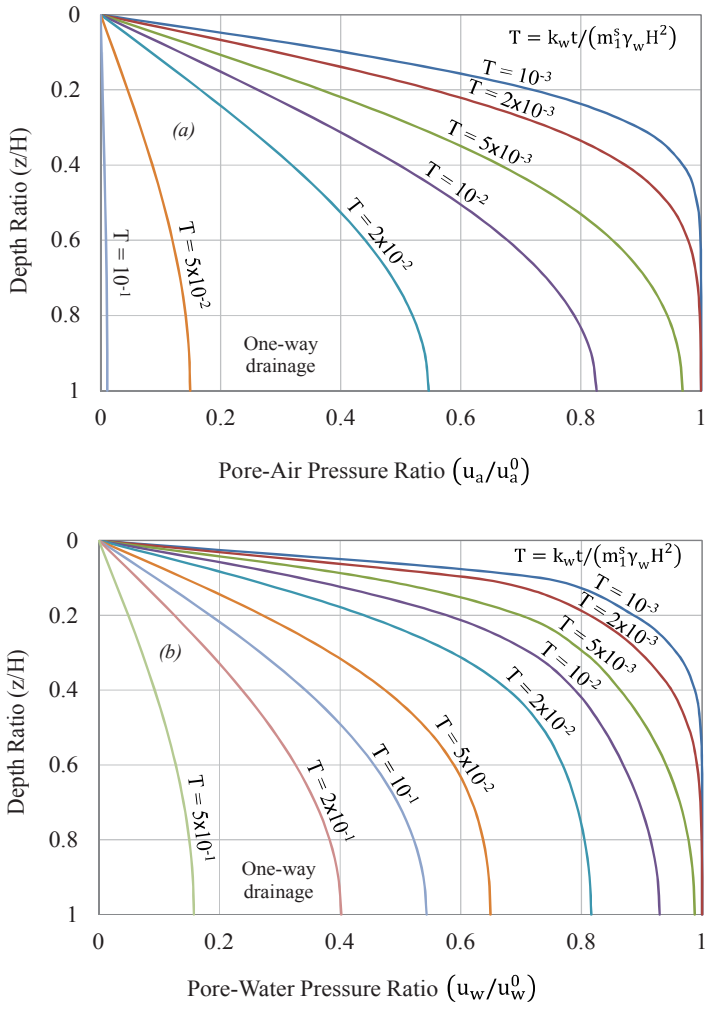

Figure 3.7. Dissipation of pore pressures varying with depth in one-way drainage system: (a) dissipation of pore-air pressure and (b) dissipation of pore-water pressure

Figures 3.7 and 3.8 demonstrate the dissipation of pore pressures with depth at different time factors T ($T = k_w t/(m_1^s \gamma_w H^2)$) for one-way and two-way drainage systems, respectively. The ratio k_a/k_w of 0.1 is taken for the investigation. In general, the results obtained from both drainage systems confirm expected behaviours similar to saturated consolidation. Both graphs provide satisfactory patterns according to the boundary desires and reinforce the principle of consolidation in which pore pressures continuously decrease as time elapses. The dissipation of pore-air pressure appears to be

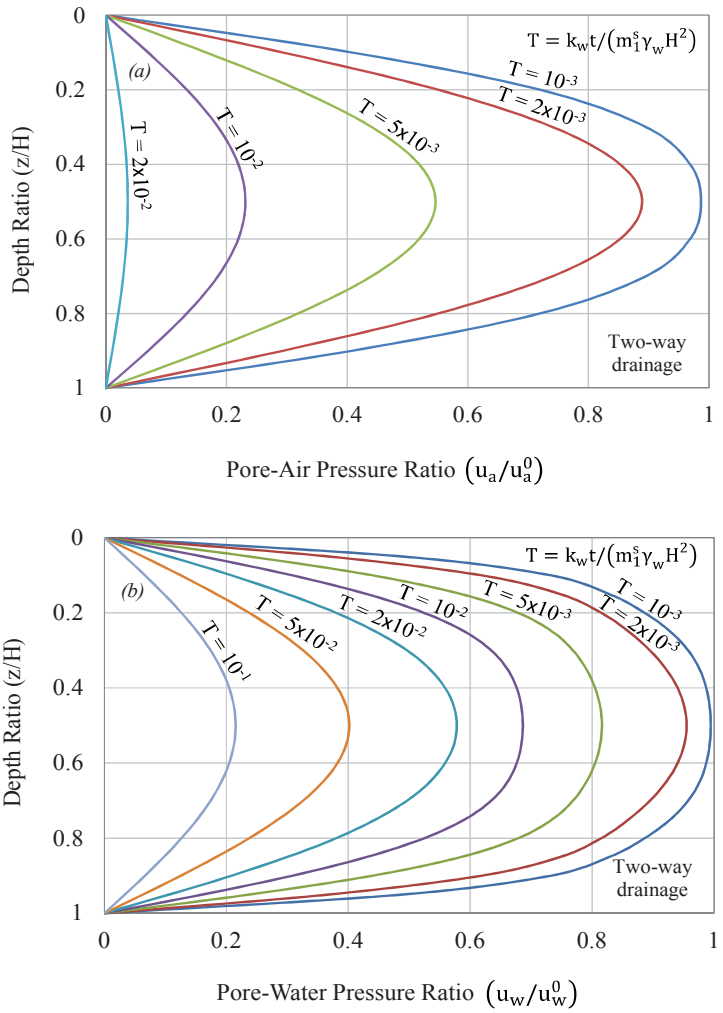

Figure 3.8. Dissipation of pore pressures varying with depth in two-way drainage system: (a) dissipation of pore-air pressure and (b) dissipation of pore-water pressure

faster than that of pore-water pressure. For instance, Figure 3.7 shows that, when $T = 10^{-1}$, the largest u_w/u_w^0 is recorded to be 0.55, whereas largest u_a/u_a^0 is almost zero. This is in a good agreement with the results presented in Figures 3.4 and 3.5.

3.5.2. Worked example 2

Example 2 investigates the dissipation rates of normalised pore-air $(u_a/[u_a^0(1-\lambda_a z/H)])$ and normalised pore-water pressures $(u_w/[u_w^0(1-\lambda_w z/H)])$ as well as the normalised settlement (S^*) considering the linear distribution of initial excess pore

pressures with depth. This condition results in both parameters λ_a and λ_w being greater than zero. In this example, the proposed mathematical forms for initial pore-air and pore-water pressures resemble to Equations [3-7a] and [3-7b]. Hence, the Fourier coefficients $T_w^k(0)$ and $T_a^k(0)$ can be determined using the orthogonality of sine function and Equation [3-18] becomes:

(a) One-way drainage condition:

$$u_a(z,t) = \sum_{k=0}^{\infty} \frac{\sin(Kz)}{\eta(HK)^2}\left[\Omega_2^k\left(e^{\alpha_1 K^2 t} - e^{\alpha_2 K^2 t}\right) + \Psi_2^k\left(e^{\alpha_1 K^2 t} + e^{\alpha_2 K^2 t}\right)\right] \quad [3\text{-}29a]$$

$$u_w(z,t) = \sum_{k=0}^{\infty} \frac{\sin(Kz)}{\eta(HK)^2}\left[\Omega_2'^k\left(e^{\alpha_1 K^2 t} - e^{\alpha_2 K^2 t}\right) + \Psi_2'^k\left(e^{\alpha_1 K^2 t} + e^{\alpha_2 K^2 t}\right)\right] \quad [3\text{-}29b]$$

(b) Two-way drainage condition:

$$u_a(z,t) = \sum_{k=0}^{\infty} \frac{\sin(Kz)}{\eta HK}\left[\Omega_3^k\left(e^{\alpha_1 K^2 t} - e^{\alpha_2 K^2 t}\right) + \Psi_3^k\left(e^{\alpha_1 K^2 t} + e^{\alpha_2 K^2 t}\right)\right] \quad [3\text{-}30a]$$

$$u_w(z,t) = \sum_{k=0}^{\infty} \frac{\sin(Kz)}{\eta HK}\left[\Omega_3'^k\left(e^{\alpha_1 K^2 t} - e^{\alpha_2 K^2 t}\right) + \Psi_3'^k\left(e^{\alpha_1 K^2 t} + e^{\alpha_2 K^2 t}\right)\right] \quad [3\text{-}30b]$$

where $\eta = [(c_v^w - c_v^a)^2 + 4c_v^w c_v^a C_w C_a]^{\frac{1}{2}}$;

$\Omega_2^k = u_a^0(c_v^a - c_v^w)\left[HK - (-1)^k\lambda_a\right] - 2c_v^w C_a u_w^0\left[HK - (-1)^k\lambda_w\right]$;

$\Psi_2^k = \eta u_a^0\left[HK - (-1)^k\lambda_a\right]$;

$\Omega_2'^k = u_w^0(c_v^w - c_v^a)\left[HK - (-1)^k\lambda_w\right] - 2c_v^a C_w u_a^0\left[HK - (-1)^k\lambda_a\right]$;

$\Psi_2'^k = \eta u_w^0\left[HK - (-1)^k\lambda_w\right]$;

$\Omega_3^k = u_a^0(c_v^a - c_v^w)\left[1 + (-1)^k(\lambda_a - 1)\right] - 2c_v^w C_a u_w^0\left[1 + (-1)^k(\lambda_w - 1)\right]$;

$\Psi_3^k = \eta u_a^0\left[1 + (-1)^k(\lambda_a - 1)\right]$;

$\Omega_3'^k = u_w^0(c_v^w - c_v^a)\left[1 + (-1)^k(\lambda_w - 1)\right] - 2c_v^a C_w u_a^0\left[1 + (-1)^k(\lambda_a - 1)\right]$;

$\Psi_3'^k = \eta u_w^0\left[1 + (-1)^k(\lambda_w - 1)\right]$;

$K = \frac{(2k+1)}{H}\frac{\pi}{2}$ for one-way drainage system; or

$= \frac{k\pi}{H}$ for two-way drainage system;

$\alpha_1 = \frac{1}{2}\left(\frac{c_v^w + c_v^a + \eta}{1 - C_w C_a}\right)$; and $\alpha_2 = \frac{1}{2}\left(\frac{c_v^w + c_v^a - \eta}{1 - C_w C_a}\right)$.

This worked example primarily predicts the changes of excess pore-air and pore-water pressures due to variations in λ_a and λ_w. The consolidation process is investigated

at H/2 and the permeability ratio (k_a/k_w) of 1 is adopted throughout the dissipation and settlement analyses (Figures 3.9-3.14). It should be noted that effects of permeability ratio variations have already been discussed in Section 5.1. Figures 3.9(a) and 3.9(b) are used to respectively describe Equations [3-29a] and [3-29b], which demonstrate the dissipation rates of excess pore pressures with increasing λ_a (from 0 to 1) and constant λ_w (0.25) in the one-way drainage system. In contrast, Figures 3.10(a) and 3.10(b) correspond to the similar equations with increasing λ_w (from 0 to 1) and constant λ_a (0.25).

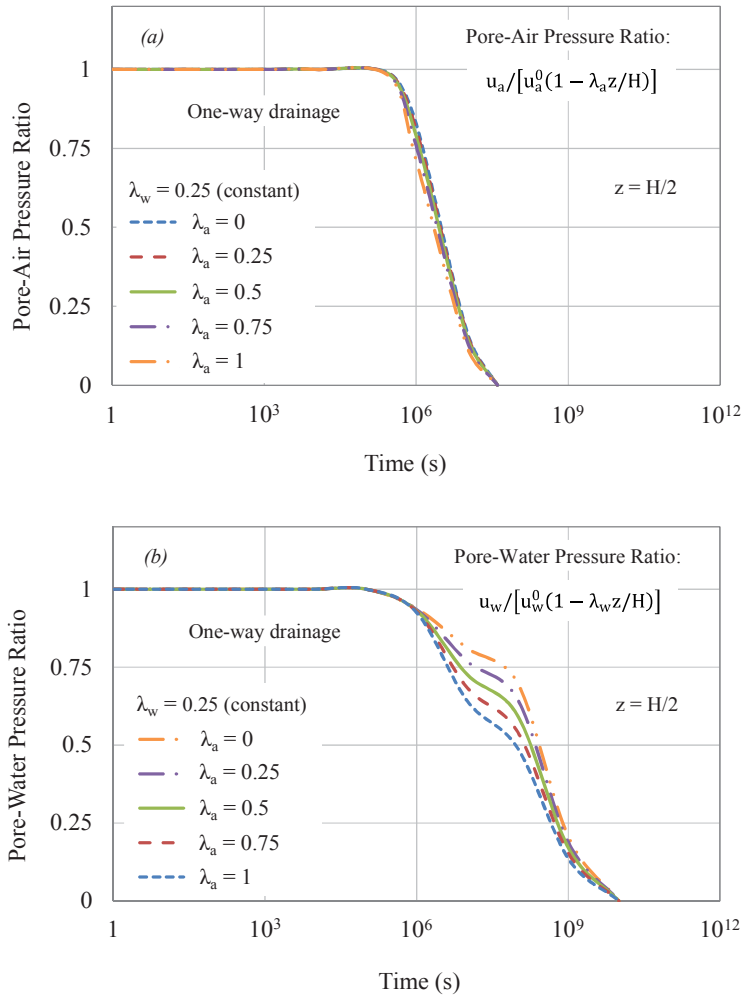

Figure 3.9. Dissipation of pore pressures varying with λ_a in one-way drainage system: (a) dissipation of pore-air pressure and (b) dissipation of pore-water pressure

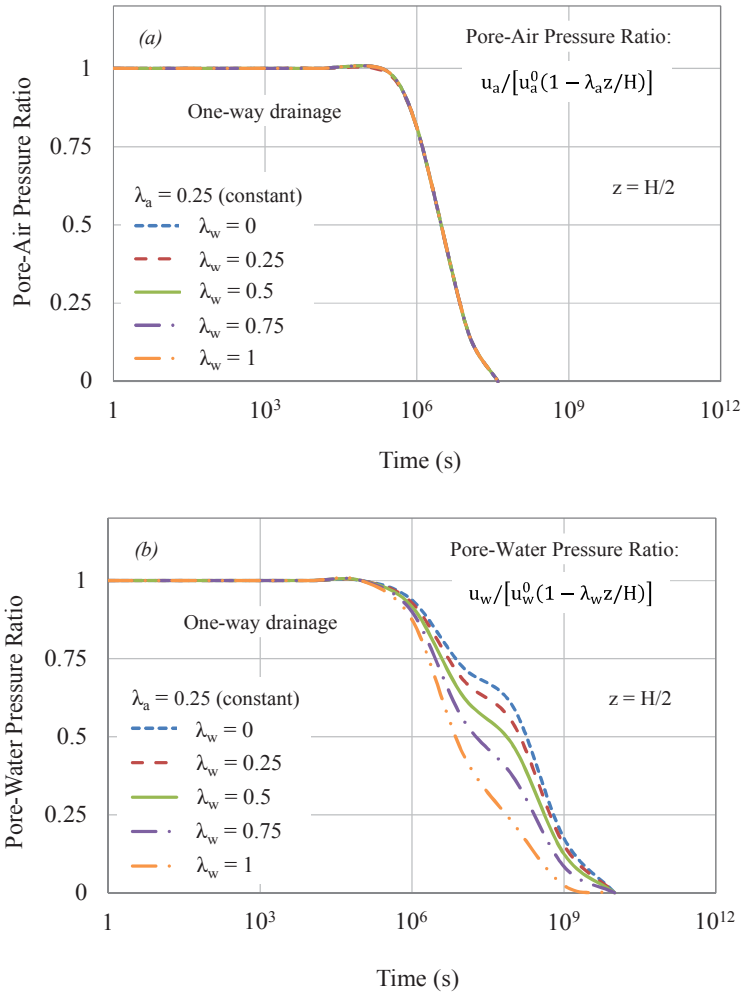

Figure 3.10. Dissipation of pore pressures varying with λ_w in one-way drainage system: (a) dissipation of pore-air pressure and (b) dissipation of pore-water pressure

Figure 3.9(a) demonstrates that the variation in λ_a (while keeping λ_w constant) has minor effects on the pore-air pressure dissipation rate. By a closer examination, all pore-air pressures diminish after 5×10^7s, regardless of values of λ_a. Therefore, it can be concluded that the change in the pore-air pressure is mainly influenced by the change in k_a/k_w (see Figures 3.4(a) and 3.5(a)). Figure 3.9(b) shows slower changes in the pore-water pressure during the first stage of dissipation while considering higher values of λ_a. It is noted that the increasing λ_a causes the decrease in the average pore-air pressure. Thus, when this insignificant pore-air pressure completely dissipates, there is still considerable pore-water pressure remaining in the soil after the first stage. It can be

noted that pore-water pressures with varying λ_a continue dissipating until 10^{10}s (end of the second stage).

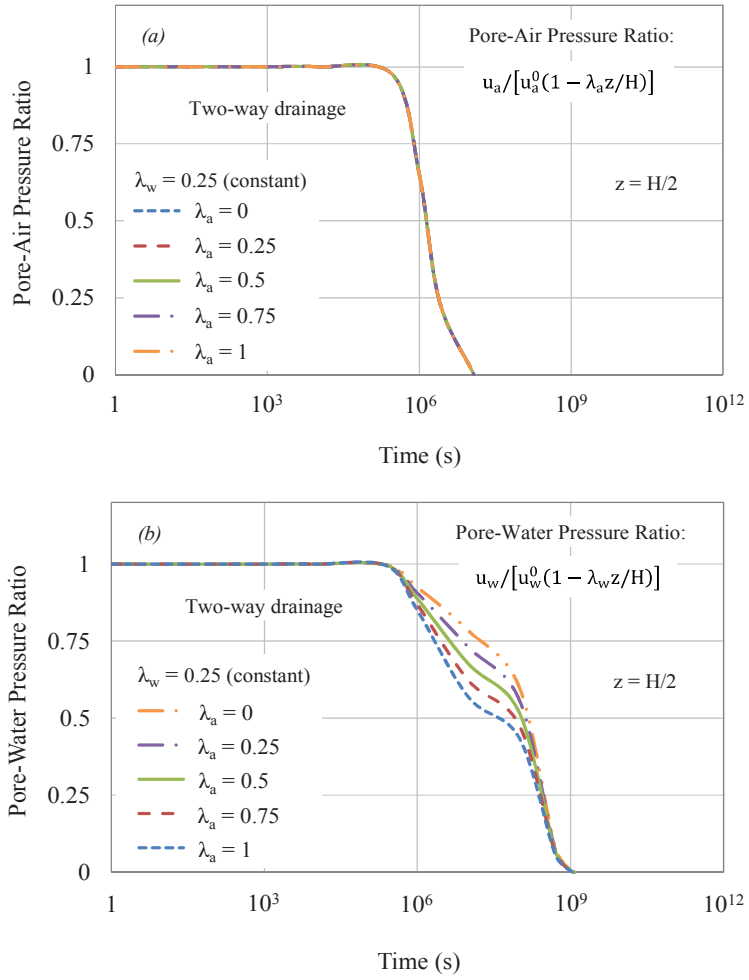

Figure 3.11. Dissipation of pore pressures varying with λ_a in two-way drainage system: (a) dissipation of pore-air pressure and (b) dissipation of pore-water pressure

Effects of increasing λ_w (with constant λ_a) are also investigated on the dissipation rates in the one-way drainage system. Figure 3.10(a) shows that the change in λ_w has no influence on the pore-air pressure ratio. On the other hand, a noticeable decrease in the pore-water pressure ratio due to increasing λ_w can be observed during the first stage of dissipation, as shown in Figure 3.10(b). This can be explained that the insignificant pore-water pressure caused by the higher values of λ_w dissipates along with relatively high pore-air pressure and as a result, when the pore-air pressure has been diminished

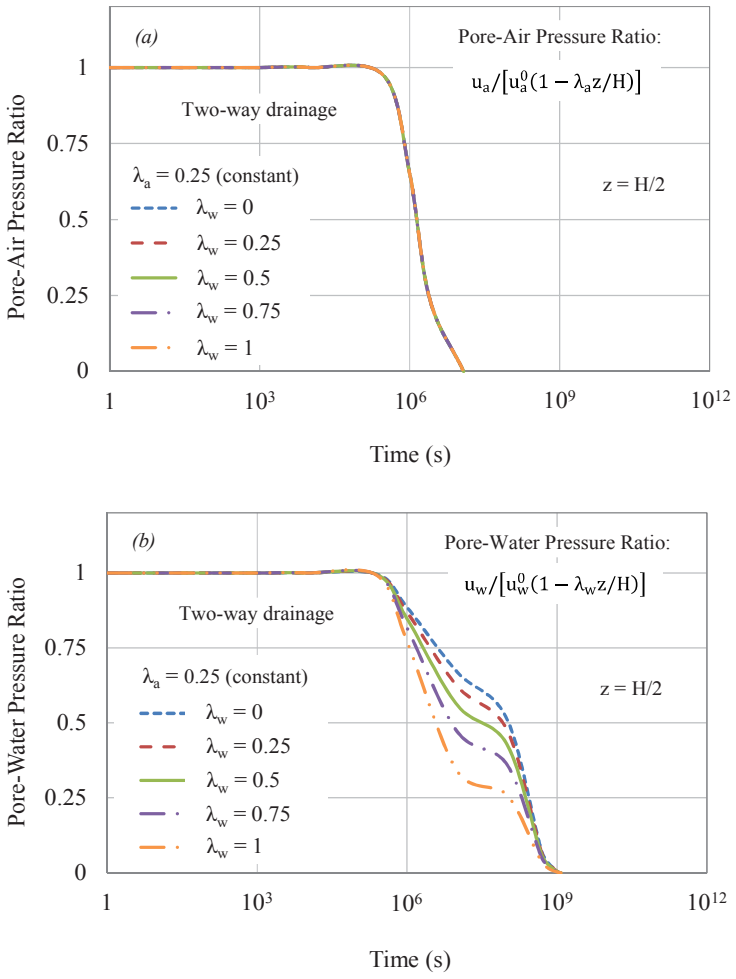

Figure 3.12. Dissipation of pore pressures varying with λ_w in two-way drainage system: (a) dissipation of pore-air pressure and (b) dissipation of pore-water pressure

(after the first stage), the remaining pore-water pressures are reported to be lower with increasing λ_w. For the two-way drainage system, Figures 3.11 and 3.12 present the dissipation rates of pore pressures with varying λ_a (from 0 to 1) and varying λ_w (from 0 to 1), respectively. The results show similar patterns for pore-air and pore-water pressures comparable with the one-way drainage condition. However, the two-way drainage condition allows the consolidation to proceed more rapidly as a result of two permeable boundaries.

When the initial excess pore pressures are distributed linearly with depth, settlement of the unsaturated soil layer can be presented as:

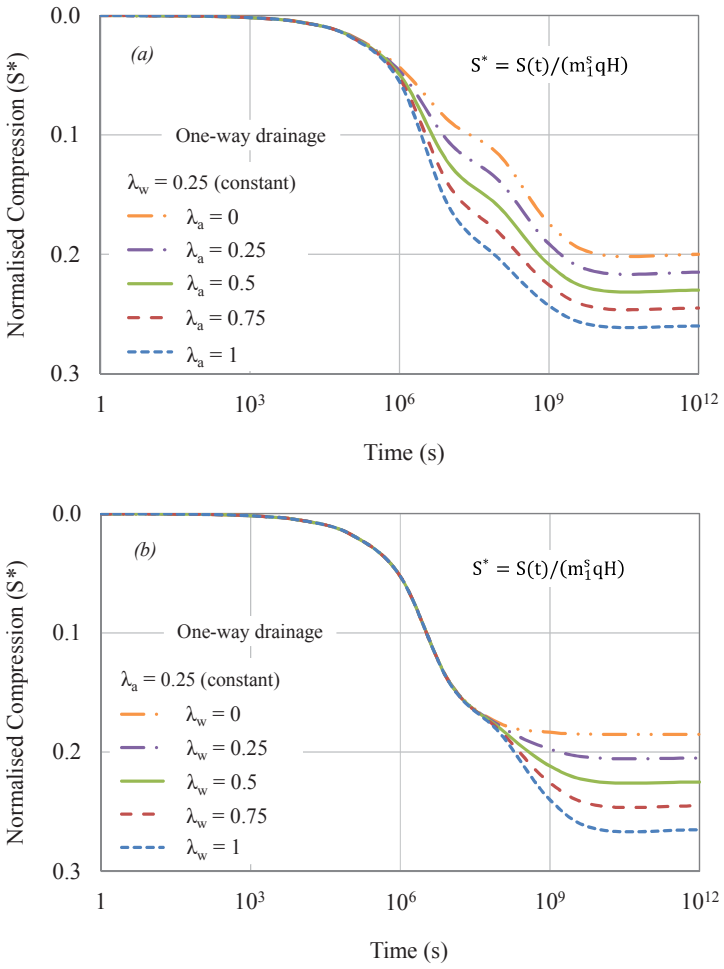

Figure 3.13. Settlement of unsaturated soils due to (a) the variation of λ_a and (b) the variation of λ_w in one-way drainage system

$$S(t) = \left|\int_0^H \varepsilon_v(z,t)dz\right| = \left|(m_2^s - m_1^s)\left[\int_0^H u_a(z,t)dz - Hu_a^0\left(1-\frac{\lambda_a}{2}\right)\right] - m_2^s\left[\int_0^H u_w(z,t)dz - Hu_w^0\left(1-\frac{\lambda_w}{2}\right)\right]\right| \quad [3\text{-}31]$$

where

(a) One-way drainage condition:

$$\int_0^H u_a(z,t)dz = \sum_{k=0}^{\infty}\frac{1}{K}\left[\frac{1}{\eta(HK)^2}\right]\left[\Omega_2^k\left(e^{\alpha_1 K^2 t} - e^{\alpha_2 K^2 t}\right) + \Psi_2^k\left(e^{\alpha_1 K^2 t} + e^{\alpha_2 K^2 t}\right)\right] \quad [3\text{-}32a]$$

$$\int_0^H u_w(z,t)dz = \sum_{k=0}^{\infty}\frac{1}{K}\left[\frac{1}{\eta(HK)^2}\right]\left[\Omega_2'^k\left(e^{\alpha_1 K^2 t} - e^{\alpha_2 K^2 t}\right) + \Psi_2'^k\left(e^{\alpha_1 K^2 t} + e^{\alpha_2 K^2 t}\right)\right] \quad [3\text{-}32b]$$

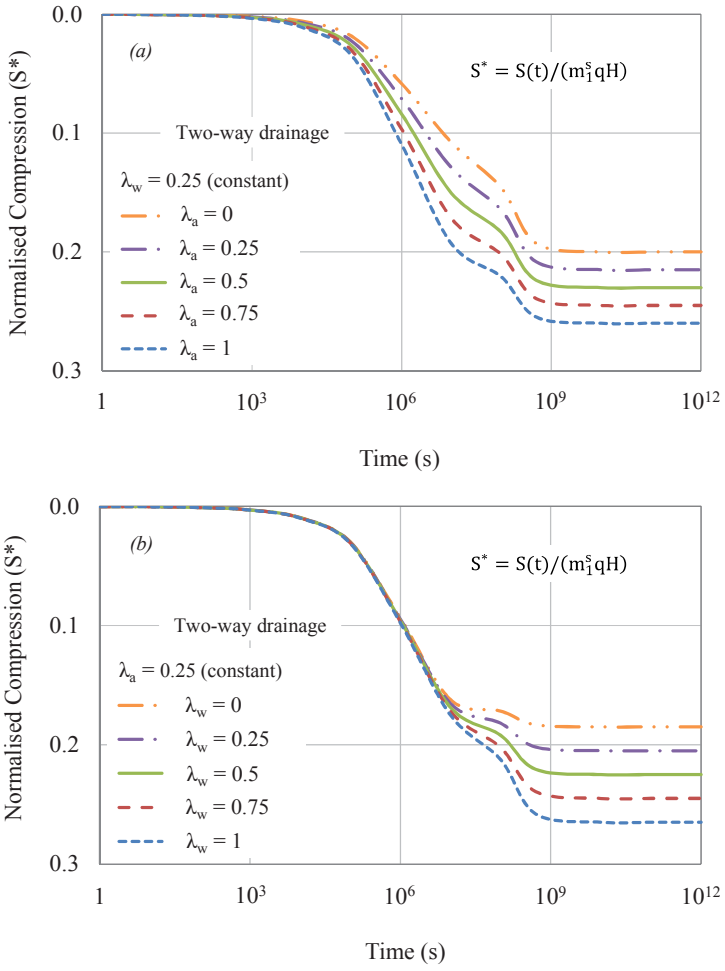

Figure 3.14. Settlement of unsaturated soils due to (a) the variation of λ_a and (b) the variation of λ_w in two-way drainage system

(b) Two-way drainage condition:

$$\int_0^H u_a(z,t)dz = \sum_{k=0}^{\infty}\left[\frac{1-(-1)^k}{\eta HK^2}\right]\left[\Omega_3^k\left(e^{\alpha_1 K^2 t} - e^{\alpha_2 K^2 t}\right) + \Psi_3^k\left(e^{\alpha_1 K^2 t} + e^{\alpha_2 K^2 t}\right)\right] \quad [3\text{-}33a]$$

$$\int_0^H u_w(z,t)dz = \sum_{k=0}^{\infty}\left[\frac{1-(-1)^k}{\eta HK^2}\right]\left[\Omega_3'^k\left(e^{\alpha_1 K^2 t} - e^{\alpha_2 K^2 t}\right) + \Psi_3'^k\left(e^{\alpha_1 K^2 t} + e^{\alpha_2 K^2 t}\right)\right] \quad [3\text{-}33b]$$

Figure 3.13 predicts the settlement of the soil deposit due to varying parameters λ_a and λ_w for the one-way drainage condition. By comparing Figures 3.13(a) and 3.13(b), it becomes apparent that the settlement rate in the early stage is influenced by the λ_a value. In Figure 3.13(a), the normalised compression (S^*) decreases when λ_a increases. It can be noticed that the increasing λ_a reduces the average initial pore-air pressure in

the soil and consequently, less air pressure dissipates resulting in reduced settlement. Figure 3.13(b) demonstrates that the constant λ_a leads to similar normalised compressions at the beginning. Once pore-air pressures completely dissipate, the later stage of consolidation is air-free and the increasing λ_w contributes to reduction of the final settlement. Figure 3.14 predicts the settlement of the soil for the two-way drainage condition. As expected, in this condition, the normalised compressions for both cases (variations in λ_a or λ_w) are predicted to be faster than those for the one-way drainage system.

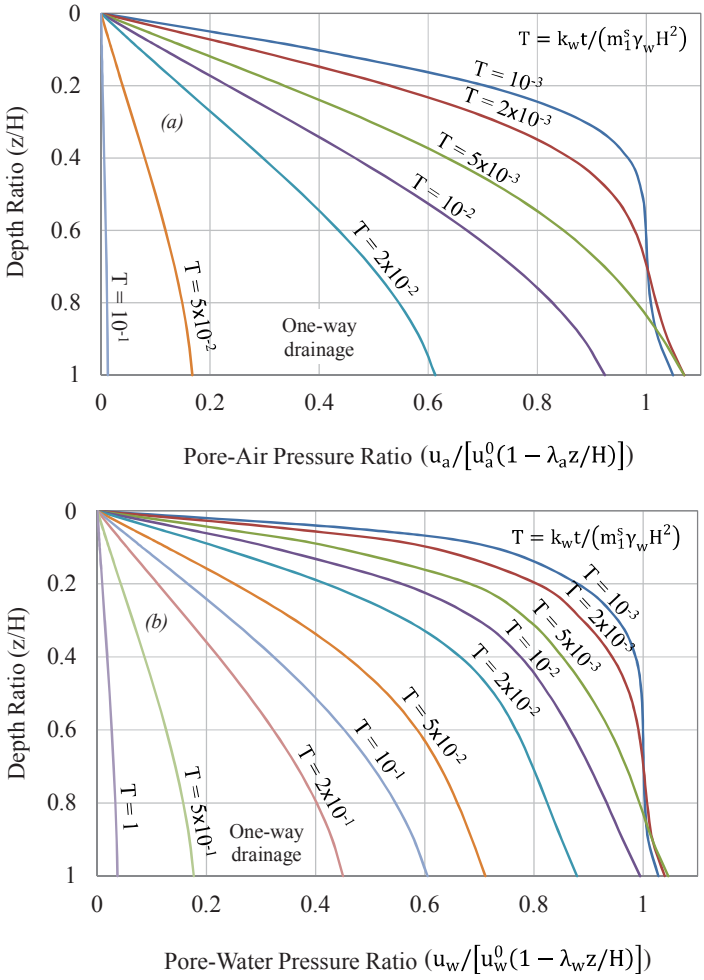

Figure 3.15. Dissipation of pore pressures varying with depth in one-way drainage system: (a) dissipation of pore-air pressure and (b) dissipation of pore-water pressure

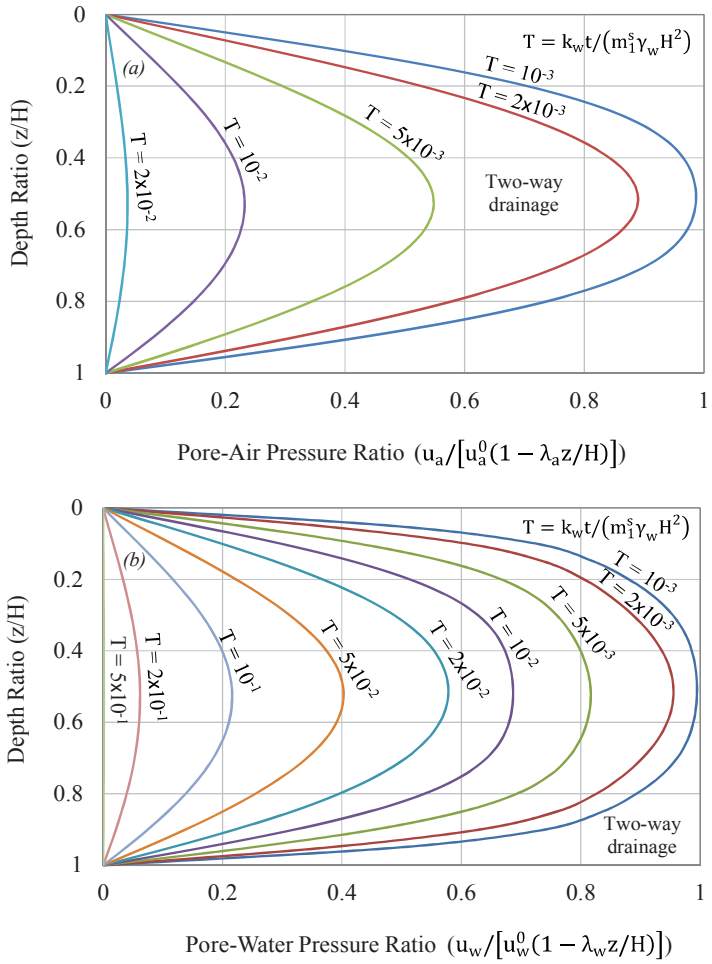

Figure 3.16. Dissipation of pore pressures varying with depth in two-way drainage system: (a) dissipation of pore-air pressure and (b) dissipation of pore-water pressure

Figure 3.15 illustrates the distribution of excess pore pressures with depth for the one-way drainage condition. The adopted value of 0.25 for both λ_a and λ_w indicates that the maximum pore pressures at the near permeable surface are 20kPa (for air) and 40kPa (for water), and pressures at the impervious bedrock boundary are recorded to be 15kPa (for air) and 30kPa (for water). Similar to Example 1, the k_a/k_w value of 0.1 is adopted to obtain the dimensionless solutions. As observed in Figures 3.15(a) and 3.15(b), there are minor increases in pressures at the impervious bedrock boundary in the early stage of consolidation. One of the possible reasons for this is that, under an external surcharge, existing initial pressures may be redistributed throughout the soil stratum so that the pressure equilibrium can be ubiquitously achieved. Such

phenomenon involves dissipation of significant amount of pore pressures through permeable surface, while pushing considerable amount of pressures down to the impermeable base. Thus, it is understandable that the pore-air and pore-water pressure ratios at the bedrock can be more than 1 during the early stage of consolidation. Figure 3.16 depicts the dissipation of pore pressures with depth for the two-way drainage system. The obtained patterns are generally similar to Figure 3.8, in which the pore-air pressure dissipates more quickly than the pore-water pressure.

3.6. Summary

An analytical solution to predict pore-air and pore-water pressures and consolidation settlement of the unsaturated soil layer has been presented in this chapter. The applied procedure is based on homogenous boundary conditions, namely one-way and two-way drainage systems, and two typical cases of initial conditions, including uniform and linear distributions of the initial excess pore pressures. For the analytical development, the eigenfunction expansion and Laplace transform methods are used to obtain an exact solution. The proposed equations allow a great convenience for practical use due to its simplicity. Moreover, the satisfactory verification also adds more creditability to the proposed solution and therefore it can be readily used by practicing geotechnical engineers.

Two worked examples have been introduced in this chapter to predict the 1D consolidation behaviours. In Example 1, majority of graphs mainly illustrate significant effects of the permeability ratio (k_a/k_w) on the dissipation rates of excess pore pressures and final compression with time. As expected, the obtained results show that a higher value of k_a/k_w leads to faster air dissipation and induces double S-shaped patterns for water dissipation and settlement prediction. Moreover, Example 2 also presents the effects of the newly proposed parameters λ_a and λ_w on the dissipation rates of pore pressures and the final settlement with time. In general, varying λ_a or λ_w has insignificant influences on the change of pore-air pressures but cause notable changes in pore-water pressures and settlement. Furthermore, findings of this study show that, for the one-way drainage system, there are minor increases in pore pressures at the impervious bedrock boundary during the early stage of consolidation. This is due to the redistribution of pore pressures in the soil layer under the external surcharge.

CHAPTER 4

ONE-DIMENSIONAL CONSOLIDATION ANALYSIS OF UNSATURATED SOILS SUBJECTED TO TIME-DEPENDENT LOADING

4.1. Introduction

Based on the governing equations originally proposed by Fredlund & Hasan (1979), this paper adopts the eigenfunction expansion and Laplace transform techniques to determine the changes in excess pore pressures and settlement of unsaturated soils due to four external loadings, namely ramping, asymptotic, sinusoid and damped sine wave. Each load is simulated and described using a mathematical equation with respect to time. The analytical procedure refers to homogeneous boundary conditions (i.e. one-way and two-way drainage systems) and constant initial conditions (i.e. uniform distribution of initial excess pore pressures). The proposed solutions will be graphically demonstrated in worked examples hereafter.

4.2. Governing equations for unsaturated soils

Typical unsaturated soils primarily consist of three fundamental phases including solid skeleton (soil), liquid (water) and gas (air). According to Barden (1965), the three different elements of such soils can be distinguished on the basis of continuity of the fluid phases. For instance, in a case of high degree of saturation (S_r), the water phase is continuous and the air phase is discontinuous. For reduced values of S_r, both phases may be continuous, whilst much smaller S_r indicates that water phase is discontinuous and the air phase is continuous. The analysis of consolidation should be carried out using a specific approach for each of these cases.

Considering traditional assumptions in Terzaghi (1943) consolidation theory, Fredlund & Hasan (1979) governing equations indicate that air and water phases are

continuous and flow independently along the vertical direction (z-direction). Fredlund & Hasan (1979) described the flows of air and water using the continuity conditions satisfying Fick's and Darcy's laws, respectively, as summarised in Equations [4-1a] and [4-1b].

$$\frac{\partial\left(\frac{\Delta V_a}{V_0}\right)}{\partial t} = \frac{k_a R\Theta}{gM\left(u_a^0+u_{atm}\right)}\left(\frac{\partial^2 u_a}{\partial z^2}\right) - \frac{n(1-S_r)}{\left(u_a^0+u_{atm}\right)}\left(\frac{\partial u_a}{\partial t}\right) \quad [4\text{-}1a]$$

$$\frac{\partial\left(\frac{\Delta V_w}{V_0}\right)}{\partial t} = \frac{k_w}{\gamma_w}\left(\frac{\partial^2 u_w}{\partial z^2}\right) \quad [4\text{-}1b]$$

where k_a and k_w are air and water permeability coefficients ($m.s^{-1}$), respectively; g is the gravitational acceleration ($\sim 9.8 m.s^{-2}$); u_a^0 and u_w^0 are initial pore-air and pore-water pressures (kPa), respectively; u_{atm} is the atmospheric pressure (kPa); R is the universal air constant ($\sim 8.3 J.mol^{-1}K^{-1}$); $\Theta = (\theta^\circ + 273)$, is the absolute temperature (K); M is the molecular mass of air phase ($\sim 0.029 kg.mol^{-1}$); n is the porosity during consolidation process; S_r is the degree of saturation during consolidation process; and γ_w is the unit weight of water ($\sim 9.8 kN.m^{-3}$).

According to Fredlund & Morgenstern (1977), the constitutive relationship presenting changes in the volumes of air (V_a) and water (V_w) with respect to the initial volume of the soil element (V_0) can be expressed as:

$$\frac{\partial\left(\frac{\Delta V_a}{V_0}\right)}{\partial t} = m_1^a \frac{\partial(\sigma-u_a)}{\partial t} + m_2^a \frac{\partial(u_a-u_w)}{\partial t} \quad [4\text{-}2a]$$

$$\frac{\partial\left(\frac{\Delta V_w}{V_0}\right)}{\partial t} = m_1^w \frac{\partial(\sigma-u_a)}{\partial t} + m_2^w \frac{\partial(u_a-u_w)}{\partial t} \quad [4\text{-}2b]$$

where σ is the total stress; u_a and u_w are excess pore-air and pore-water pressures, respectively; m_1^a and m_1^w are coefficients of air and water volume change with respect to the change of net stress $(\sigma - u_a)$, respectively; and m_2^a and m_2^w are coefficients of air and water volume change with respect to the change of suction $(u_a - u_w)$, respectively.

Combining two pairs of Equations [4-1a] and [4-2a], and Equations [4-1b] and [4-2b] results in inhomogeneous PDEs of air and water phases, dependent on variables z and t. The simplified equations of flow are presented as follows:

$$u_{a,t} + c_v^a u_{a,zz} + C_a u_{w,t} - c_\sigma^a \sigma_{,t} = 0 \quad [4\text{-}3a]$$

$$u_{w,t} + c_v^w u_{w,zz} + C_w u_{a,t} - c_\sigma^w \sigma_{,t} = 0 \quad [4\text{-}3b]$$

where $u_{a,t}$ and $u_{w,t}$ are the first order PDEs of pore-air and pore-water pressures with respect to time, respectively; $u_{a,zz}$ and $u_{w,zz}$ are the second order PDEs of pore-air and pore-water pressures with respect to depth, respectively; and $\sigma_{,t}$ are the first order PDE of the total stress with respect to time. Additionally,

$$C_a = \frac{1}{\left[\left(\frac{m_1^a}{m_2^a} - 1\right) - \frac{n(1-S_r)}{m_2^a(u_a^0 + u_{atm})}\right]}; \quad [4\text{-}4a]$$

$$c_v^a = \frac{k_a R\Theta}{gM} \frac{1}{\left[m_2^a(u_a^0 + u_{atm})\left(\frac{m_1^a}{m_2^a} - 1\right) - n(1-S_r)\right]}; \quad [4\text{-}4b]$$

$$c_\sigma^a = \frac{1}{\left[\left(1 - \frac{m_2^a}{m_1^a}\right) - \frac{n(1-S_r)}{m_1^a(u_a^0 + u_{atm})}\right]}; \quad [4\text{-}4c]$$

$$C_w = \left(\frac{m_1^w}{m_2^w} - 1\right); \quad [4\text{-}4d]$$

$$c_v^w = \frac{1}{m_2^w}\left(\frac{k_w}{\gamma_w}\right); \text{ and} \quad [4\text{-}4e]$$

$$c_\sigma^w = \frac{m_1^w}{m_2^w}. \quad [4\text{-}4f]$$

Equation [4-3] is employed to investigate the deformation of an unsaturated soil deposit due to the dissipation of excess pore-air and pore-water pressures. Since the total pressure is varying with time, the term $\partial\sigma/\partial t \neq 0$ and two consolidation parameters, c_σ^a and c_σ^w, have been introduced to Equation [4-3], influencing the patterns of normalised excess pore pressures and the normalised settlement.

4.3. Analytical formulations for 1D consolidation

The actual soil properties influencing deformation of the ground are relatively ambiguous due to the complicated texture assemblage and the lack of homogeneity of the soil. These may result in a difficulty in predicting the consolidation characteristics. Therefore, some additional assumptions helping to obtain solutions must be made for simplicity as follows:

(1) The entire soil strata are assumed to be homogeneous;
(2) The flows of air and water phases are assumed to be continuous and independent;

(3) Solid skeleton and water phase are incompressible;
(4) Effects of environmental factors such as air diffusion and temperature change are ignored;
(5) The vertical loading and deformations are only along z-direction; and
(6) Consolidation parameters with respect to air phase (C_a, c_v^a and c_σ^a) and water phase (C_w, c_v^w and c_σ^w) are assumed to be constant during the loading process.

It should be noted that, during the loading process, consolidation parameters may change due to the variation of permeability, degree of saturation (S_r), porosity (n) and volume change coefficients. In particular, the permeability coefficients are considered as nonlinear functions of degree of saturation and water content (Fredlund et al. 2012). Consideration of highly nonlinear behaviours in the mathematical procedure, however, may be subjected to the numerical analysis, as a closed-form analytical solution may not be achievable. To obtain the exact analytical solution, for simplicity, Assumption (6) is justified to alleviate the complication in obtaining the exact solutions for the governing equations (i.e. Equation [4-3]). Furthermore, constant soil properties have been adopted in several studies in literature, some of which are conducted by Qin et al. (2010b), Shan et al. (2012), and Zhou et al. (2014).

4.3.1. Boundary and initial conditions

Figure 4.1 illustrates a referential profile of a homogeneous soil with an infinite width and a thickness H. A representative soil element in 1-D consolidation located at (x: y: z) has dimensions of $1: 1: dz$, indicating that the depth of the soil element can change. In Figure 4.1(a), the one-way drainage boundary system can be described as a soil profile with a permeable top surface and an impervious base. Soon after the application of external loads, excess pore-air and pore-water pressures move towards the permeable top surface but cannot dissipate through the impermeable base of the soil layer. In addition, the two-way drainage system consists of two permeable boundary surfaces as shown in Figure 4.1(b). This system allows free dissipation of pore pressures through permeable surfaces on the top and the base. Both boundary conditions can be mathematically presented as follows:

(a) One-way drainage condition:
$$\begin{cases} u_a(0,t) = u_w(0,t) = 0 \\ (u_{a,z})_{z=H} = (u_{w,z})_{z=H} = 0 \end{cases}; \quad t \geq 0 \qquad [4\text{-}5a]$$

(b) Two-way drainage condition:
$$\begin{cases} u_a(0,t) = u_w(0,t) = 0 \\ u_a(H,t) = u_w(H,t) = 0 \end{cases}; \quad t \geq 0 \qquad [4\text{-}5b]$$

where H is the soil layer thickness.

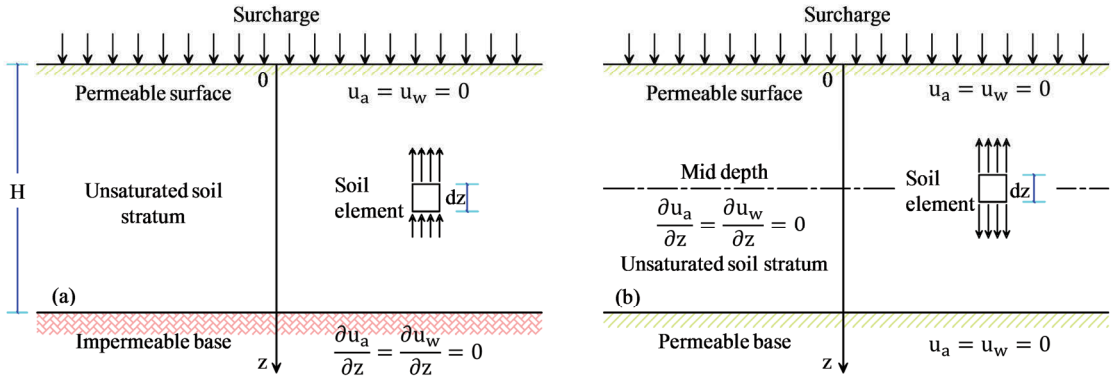

Figure 4.1. Simplified unsaturated soil profiles for (a) one-way drainage system; and (b) two-way drainage system

In this study, a uniform distribution of initial excess pore pressures generated by the external loading applied on the ground surface is adopted. For both drainage systems, the initial pore pressures in the domain $z \in (0, H)$ can be presented as below:

$$\begin{cases} u_a(z,0) = u_a^0 \\ u_w(z,0) = u_w^0 \end{cases} \qquad [4\text{-}6]$$

where u_a^0 and u_w^0 are values of the excess pore-air and pore-water pressures when $t = 0$, respectively.

4.3.2. Analytical procedure

The eigenfunction expansion method can be applied to inhomogeneous differential problems involved with piecewise smooth functions (Haberman 2012). This method uses homogeneous forms for general solutions of $u_a(z,t)$ and $u_w(z,t)$, as follows:

$$u_a(z,t) = \sum_{k=0}^{\infty} Z_a(z).T_a(t) \quad [4\text{-}7a]$$

$$u_w(z,t) = \sum_{k=0}^{\infty} Z_w(z).T_w(t) \quad [4\text{-}7b]$$

where $Z_a(z)$ and $Z_w(z)$ are eigenfunctions with respect to the depth z; and $T_a(t)$ and $T_w(t)$ are generalised Fourier coefficients varying with time t.

Considering the homogeneous boundary conditions, the eigenfunction expansion method is employed to solve the inhomogeneous PDEs (i.e. Equations [4-3a] and [4-3b]) by expanding the general solutions in a series of the eigenfunctions of the related homogeneous problem. In most cases, the eigenfunctions will be expressed in an ordinary Fourier sine or cosine series depending on different drainage boundary conditions. According to Haberman (2012) for general homogeneous problems, the eigenvalue, denoted by λ, is found to be $\lambda_k = [(2k+1)\pi/(2H)]^2$ $(k = 0, 1, 2 ...)$ for the one-way drainage condition and $\lambda_k = (k\pi/H)^2$ for the two-way drainage condition. Considering the above mentioned eigenvalues, the corresponding eigenfunctions for one-way and two-way drainage conditions are $Z(z) = \sin[(2k+1)\pi z/(2H)]$ and $Z(z) = \sin(k\pi z/H)$, respectively. Assuming $K = \sqrt{\lambda_k}$ $(k = 0, 1, 2, ...)$, Equations [4-7a] and [4-7b] can be rewritten as follows:

$$u_a(z,t) = \sum_{k=0}^{\infty} T_a(t) \sin(K z) \quad [4\text{-}8a]$$

$$u_w(z,t) = \sum_{k=0}^{\infty} T_w(t) \sin(K z) \quad [4\text{-}8b]$$

where $K = \frac{(2k+1)}{H}\frac{\pi}{2}$, for the one-way drainage boundary condition; and

$= \frac{k\pi}{H}$, for the two-way drainage boundary condition. [4-9]

The analytical development may encounter a difficulty in determining the generalised Fourier coefficients, $T_a(t)$ and $T_w(t)$, by substituting Equation [4-8] into Equation [4-3]. Additionally, an idea of taking second order derivatives of Equation [4-8] with respect to depth z is irrational as $u(z,t)$ and $Z(z)$ do not satisfy the same homogeneous boundary conditions (i.e. $u_{,zz}(z,t) \neq \sum_{k=0}^{\infty} Z_{,zz}(z)T(t)$). However, the term-by-term differentiations with respect to time t in Equation [4-8] are valid and will result in:

$$u_{a,t}(z,t) = \sum_{k=0}^{\infty} T_{a,t}(t)\sin(K\,z) \quad [4\text{-}10a]$$

$$u_{w,t}(z,t) = \sum_{k=0}^{\infty} T_{w,t}(t)\sin(K\,z) \quad [4\text{-}10b]$$

Combining two pairs of Equations [4-3a] and [4-10a] and Equations [4-3b] and [4-10b] gives:

$$\sum_{k=0}^{\infty} T_{a,t}(t)\sin(K\,z) = -c_v^a u_{a,zz}(z,t) - C_a u_{w,t}(z,t) + c_\sigma^a \sigma_{,t}(t) \quad [4\text{-}11a]$$

$$\sum_{k=0}^{\infty} T_{w,t}(t)\sin(K\,z) = -c_v^w u_{w,zz}(z,t) - C_w u_{a,t}(z,t) + c_\sigma^w \sigma_{,t}(t) \quad [4\text{-}11b]$$

By computing orthogonalities of sine functions, the Equation [4-11] becomes:

$$T_{a,t}^k(t) = c_v^a(K)^2\, T_a(t) - C_a\, T_{w,t}(t) + D_k c_\sigma^a \sigma_{,t}(t) \quad [4\text{-}12a]$$

$$T_{w,t}^k(t) = c_v^w(K)^2\, T_w(t) - C_w\, T_{a,t}(t) + D_k c_\sigma^w \sigma_{,t}(t) \quad [4\text{-}12b]$$

where $D_k = \int_0^H \sin(K\,z)dz \,/\, \int_0^H \sin^2(K\,z)dz$ $(k = 0, 1, 2, ...)$. The term D_k becomes $D_k = 2/(H\,K)$ for the one-way drainage condition; or $D_k = 2\left[1-(-1)^k\right]/(H\,K)$ for the two-way drainage condition. As a reminder, the term K was defined in Equation [4-9].

To solve the first order derivatives, Equations [4-12a] and [4-12b] are converted into Laplace transformed equations with a complex variable s.

$$\left[s\overline{T}_a^k(s) - T_a^k(0)\right] = c_v^a(K)^2\, \overline{T}_a^k(s) - C_a\left[s\overline{T}_w^k(s) - T_w^k(0)\right] + D_k c_\sigma^a[s\overline{\sigma}(s) - \sigma(0)] \quad [4\text{-}13a]$$

$$\left[s\overline{T}_w^k(s) - T_w^k(0)\right] = c_v^w(K)^2\, \overline{T}_w^k(s) - C_w\left[s\overline{T}_a^k(s) - T_a^k(0)\right] + D_k c_\sigma^w[s\overline{\sigma}(s) - \sigma(0)] \quad [4\text{-}13b]$$

where $\overline{T}_a^k(s)$, $\overline{T}_w^k(s)$ $(k = 0, 1, 2, ...)$ and $\overline{\sigma}(s)$ are Laplace transformed functions with complex argument s.

On the other hand, the initial generalised Fourier coefficients $T_a^k(0)$ and $T_w^k(0)$ can be computed based on the mentioned initial conditions (Equation [4-6]) as follows:

$$T_a^k(0) = \frac{\int_0^H [u_a(z,0)\sin(K\,z)]dz}{\int_0^H [\sin^2(K\,z)]dz} = D_k u_a^0 \qquad [4\text{-}14a]$$

$$T_w^k(0) = \frac{\int_0^H [u_w(z,0)\sin(K\,z)]dz}{\int_0^H [\sin^2(K\,z)]dz} = D_k u_w^0 \qquad [4\text{-}14b]$$

The obtained $T_a^k(0)$ and $T_w^k(0)$ ($k = 0, 1, 2, ...$) are then substituted into Equation [4-13]. For the ease of calculations, these Laplace transformed equations can be rearranged and written in a matrix form as follows:

$$\boldsymbol{\mathcal{A}}\boldsymbol{\mathcal{T}} = D_k(\boldsymbol{\mathcal{B}} + \boldsymbol{\mathcal{C}}) \qquad [4\text{-}15]$$

where $\boldsymbol{\mathcal{A}} = \begin{bmatrix} s - c_v^a(K)^2 & sC_a \\ sC_w & s - c_v^w(K)^2 \end{bmatrix}$; $\boldsymbol{\mathcal{B}} = \begin{Bmatrix} u_a^0 + C_a u_w^0 \\ C_w u_a^0 + u_w^0 \end{Bmatrix}$;

$$\boldsymbol{\mathcal{C}} = \begin{Bmatrix} c_\sigma^a \\ c_\sigma^w \end{Bmatrix}[s\bar{\sigma}(s) - \sigma(0)]; \quad \text{and} \quad \boldsymbol{\mathcal{T}} = \begin{Bmatrix} \bar{T}_a^k(s) \\ \bar{T}_w^k(s) \end{Bmatrix}. \qquad [4\text{-}16]$$

Solving for $\bar{T}_a^k(s)$ and $\bar{T}_w^k(s)$ ($k = 0, 1, 2, ...$) yields in:

$$\boldsymbol{\mathcal{T}} = D_k(\boldsymbol{\mathcal{A}}^{-1}\boldsymbol{\mathcal{B}} + \boldsymbol{\mathcal{A}}^{-1}\boldsymbol{\mathcal{C}}) \qquad [4\text{-}17]$$

where $\boldsymbol{\mathcal{A}}^{-1}\boldsymbol{\mathcal{B}} = \begin{Bmatrix} \frac{u_a^0\,(C_wC_a-1)s + c_v^w(C_a u_w^0 + u_a^0)\,(K)^2}{(C_wC_a-1)s^2 + (c_v^w + c_v^a)\,(K)^2 s - c_v^w c_v^a\,(K)^4} \\ \frac{u_w^0\,(C_wC_a-1)s + c_v^a(C_w u_a^0 + u_w^0)\,(K)^2}{(C_wC_a-1)s^2 + (c_v^w + c_v^a)\,(K)^2 s - c_v^w c_v^a\,(K)^4} \end{Bmatrix}$; and

$$\boldsymbol{\mathcal{A}}^{-1}\boldsymbol{\mathcal{C}} = \begin{Bmatrix} \frac{(C_a c_\sigma^w - c_\sigma^a)s + c_v^w c_\sigma^a\,(K)^2}{(C_wC_a-1)s^2 + (c_v^w + c_v^a)\,(K)^2 s - c_v^w c_v^a\,(K)^4} \\ \frac{(C_w c_\sigma^a - c_\sigma^w)s + c_v^a c_\sigma^w\,(K)^2}{(C_wC_a-1)s^2 + (c_v^w + c_v^a)\,(K)^2 s - c_v^w c_v^a\,(K)^4} \end{Bmatrix}[s\bar{\sigma}(s) - \sigma(0)]. \qquad [4\text{-}18]$$

Then, taking the Laplace inverse of Equation [4-17] results in:

$$\mathcal{L}^{-1}\{\boldsymbol{\mathcal{T}}\} = D_k\left\{\mathcal{L}^{-1}\{\boldsymbol{\mathcal{A}}^{-1}\boldsymbol{\mathcal{B}}\} + \mathcal{L}^{-1}\{\boldsymbol{\mathcal{A}}^{-1}\boldsymbol{\mathcal{C}}\}\right\} \qquad [4\text{-}19]$$

where $\mathcal{L}^{-1}\{\boldsymbol{\mathcal{T}}\} = \begin{Bmatrix} T_a^k(t) \\ T_w^k(t) \end{Bmatrix}$;

$$\mathcal{L}^{-1}\{\boldsymbol{\mathcal{A}}^{-1}\boldsymbol{\mathcal{B}}\} = \begin{Bmatrix} \frac{\omega\left[e^{\alpha_1(K)^2 t} - e^{\alpha_2(K)^2 t}\right] + \psi\left[e^{\alpha_1(K)^2 t} + e^{\alpha_2(K)^2 t}\right]}{2\eta} \\ \frac{\omega'\left[e^{\alpha_1(K)^2 t} - e^{\alpha_2(K)^2 t}\right] + \psi'\left[e^{\alpha_1(K)^2 t} + e^{\alpha_2(K)^2 t}\right]}{2\eta} \end{Bmatrix};$$

$$\eta = [(c_v^w - c_v^a)^2 + 4c_v^w c_v^a C_w C_a]^{\frac{1}{2}};$$

$$\omega = (c_v^a - c_v^w)\, u_a^0 - 2c_v^w C_a\, u_w^0; \qquad \omega' = (c_v^w - c_v^a)\, u_w^0 - 2c_v^a C_w\, u_a^0;$$

$$\psi = \eta\, u_a^0; \qquad \psi' = \eta\, u_w^0;$$

$$\alpha_1 = \frac{1}{2}\left(\frac{c_v^w + c_v^a + \eta}{1 - C_w C_a}\right); \quad \text{and} \quad \alpha_2 = \frac{1}{2}\left(\frac{c_v^w + c_v^a - \eta}{1 - C_w C_a}\right). \qquad [4\text{-}20]$$

In Equation [4-19], the term $\mathcal{L}^{-1}\{\boldsymbol{\mathcal{A}}^{-1}\boldsymbol{\mathcal{C}}\}$ follows different time-dependent loading functions and will be discussed further in subsequent sections. The final generalised solution describing the dissipation of excess pore pressures can be deducted as follows:

$$\boldsymbol{\mathcal{U}} = \sum_{k=0}^{\infty} \sin(K\,z)\left\{\mathcal{L}^{-1}\{\boldsymbol{\mathcal{T}}\}\right\} = \sum_{k=0}^{\infty} D_k \sin(K\,z)\left\{\mathcal{L}^{-1}\{\boldsymbol{\mathcal{A}}^{-1}\boldsymbol{\mathcal{B}}\} + \mathcal{L}^{-1}\{\boldsymbol{\mathcal{A}}^{-1}\boldsymbol{\mathcal{C}}\}\right\} \quad [4\text{-}21]$$

where $\boldsymbol{\mathcal{U}} = \begin{Bmatrix} u_a(z,t) \\ u_w(z,t) \end{Bmatrix}$;

One-way drainage condition: $\begin{cases} K = \frac{(2k+1)}{H}\frac{\pi}{2} \\ D_k = \frac{2}{H\,K} \end{cases}$ $(k = 0, 1, 2, \ldots)$; and

Two-way drainage condition: $\begin{cases} K = \frac{k\pi}{H} \\ D_k = \frac{2[1-(-1)^k]}{H\,K} \end{cases}$ $(k = 0, 1, 2, \ldots)$. [4-22]

For fully saturated soils ($S_r = 1$), under constant uniform loading (i.e. $\mathcal{L}^{-1}\{\boldsymbol{\mathcal{A}}^{-1}\boldsymbol{\mathcal{C}}\} = 0$), the coefficient of permeability and the initial pressure with respect to air phase (k_a and u_a^0, respectively) become zero, resulting in the consolidation parameters C_a and c_v^a equal to zero. In addition, the coefficients of volume change of water m_1^w and m_2^w are equal to the conventional volume change m_v. Thus, Equation [4-21] will transform into Equation [4-23]:

$$u_w(z,t) = \sum_{k=0}^{\infty} D_k\, u_w^0 \sin(K\,z) e^{c_v^w (K)^2 t} \qquad [4\text{-}23]$$

The coefficient of consolidation with respect to water phase (c_v^w) in Equation [4-23] is negative due to the negative coefficient of volume change. It is noticed that Equation [4-23] is similar to the consolidation equation originally proposed by Terzaghi (1943) for saturated soils.

4.3.3. Settlement of the unsaturated soil layer

Fredlund & Hasan (1979) proposed a constitutive equation for the soil structure to link the stress and deformation state variables, as below:

$$\frac{\partial(\varepsilon_v)}{\partial t} = m_1^s \frac{\partial \sigma}{\partial t} + (m_2^s - m_1^s)\frac{\partial u_a}{\partial t} - m_2^s \frac{\partial u_w}{\partial t} \quad [4\text{-}24]$$

where ε_v is the volumetric strain; $m_1^s = m_1^w + m_1^a$, is the coefficient of volume change of the soil element with respect to the change in the net stress $(\sigma - u_a)$; and $m_2^s = m_2^w + m_2^a$, is the coefficient of volume change of the soil element with respect to the change in the matric suction $(u_a - u_w)$.

It is assumed that the volume change coefficients of the soil are constant during the consolidation process. The volumetric strain is determined by integrating Equation [4-24] with respect to time, thus:

$$\varepsilon_v(z,t) = m_1^s[\sigma(t) - \sigma(0)] + (m_2^s - m_1^s)[u_a(z,t) - u_a(z,0)] - m_2^s[u_w(z,t) - u_w(z,0)] \quad [4\text{-}25]$$

Then, the settlement of the soil layer can be obtained by:

$$S(t) = \left|\int_0^H \varepsilon_v(z,t)dz\right| = \left|m_1^s H\,[\sigma(t) - \sigma_0] + (m_2^s - m_1^s)\left[\int_0^H u_a(z,t)dz - H\,u_a^0\right] - m_2^s\left[\int_0^H u_w(z,t)dz - H\,u_w^0\right]\right| \quad [4\text{-}26]$$

Equation [4-26] presents the time-dependent settlement (vertical deformation) of the unsaturated soil deposit due to an applied time-dependent load. Functions $u_a(z,t)$ and $u_w(z,t)$ required to estimate the time-dependent settlement can be obtained from Equation [4-21]. It is worth mentioning that the influences of soil cementation and visco-plastic behaviour on the time-dependent deformation of soil may be major interests in geotechnical engineering (Nguyen et al. 2014; Le et al. 2015). This study, however, has not included these mentioned studies.

4.4. Worked examples

This study presents four time-dependent loadings adapting from ramped (linear), asymptotic, sinusoidal and damped sine wave functions (see Figure 4.2). Such loadings

applied on the unsaturated soil deposit surface contribute to the changes in the interparticle stresses due to the dissipation of excess pore pressures and eventually the soil settlement. In this section, the analytical development incorporating the mentioned loading functions are presented to derive exact solutions predicting 1-D consolidation behaviour of unsaturated soils. The effects of air to water permeability ratio k_a/k_w are investigated through analysing the patterns of the normalised pore pressures u_a/u_{atm} and u_w/u_{atm} as well as the normalised settlement (S^*). Furthermore, this study also examines the effects of loading parameter of each loading function on the change in normalised pore pressures and the settlement. The following material properties are adopted in this study and it is assumed that these properties remain constant during the loading process:

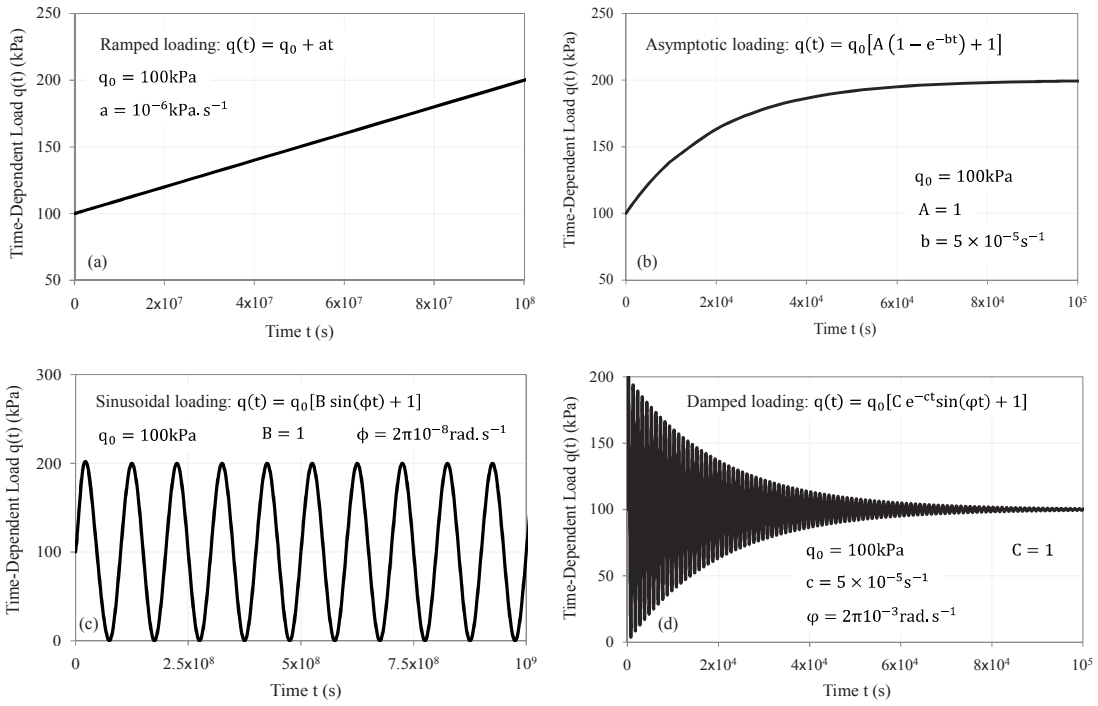

Figure 4.2. Time-dependent loadings: (a) ramping, (b) asymptotic, (c) sinusoid, and (d) damped sine wave

- Material properties: $n = 0.50$; $S_r = 80\%$; $k_w = 10^{-10}ms^{-1}$;
  $H = 10m$; $u_{atm} = 100kPa$; $q_0 = 100kPa$;
  $u_a^0 = 20kPa$; $u_w^0 = 40kPa$;
  $m_1^s = -2.5 \times 10^{-4}kPa^{-1}$; $m_2^s = 0.4m_1^s$;
  $m_1^w = 0.2m_1^s$; $m_2^w = 4m_1^w$. [4-27]

- Physical properties: $R = 8.314 J.mol^{-1}K^{-1}$;
  $M = 0.029 kg.mol^{-1}$;
  $\Theta = (\theta° + 273.16)K$; $\theta° = 20℃$. [4-28]

The application of an external load on the ground surface leads to an instantaneous undrained compression and induces excess pore pressures. Such induced pressures form the initial conditions for the compression process. According to Fredlund & Hasan (1979) and Fredlund et al. (2012), under isotropic conditions, an initial loading $q_0 = 100kPa$ will generate an initial excess pore-air pressure $u_a^0 = 20kPa$ and an initial excess pore-water pressure $u_w^0 = 40kPa$. In this study, the unsaturated homogeneous soil stratum consists of an infinite width and depth $H = 10m$. For the permeability ratio, the air permeability (k_a) is varying from 10^{-12} to $10^{-7} m/s$ whereas the water permeability (k_w) is assumed to be constant and equal to $10^{-10} m/s$. The properties provided in Equations [4-27] and [4-28] are employed to determine the values of the consolidation parameters with respect to the air phase (C_a, c_v^a and c_σ^a) and the water phase (C_w, c_v^w and c_σ^w).

4.4.1. Ramped Loading

The ground surface of the unsaturated soil deposits is sometimes subjected to an external ramped loading (loading varying linearly with time). This loading may be used to simulate the influence of construction time to the consolidation process. The general loading function is given by:

$$q(t) = q_0 + at \quad [4-29]$$

where $q_0 = 100kPa$, is the initial surcharge; 'a' is the load function parameter acting as the linear load rate ($kPa.s^{-1}$). Along with the initial surcharge q_0, the additional load rate $a = 10^{-6}\ kPa.s^{-1}$ is continuously applied on the unsaturated ground as time elapses (Figure 4.2(a)). Equation [4-29] can be substituted to the Laplace transformed $\boldsymbol{\mathcal{A}^{-1}\mathcal{C}}$ presented in Equation [4-18]. The term $\mathcal{L}^{-1}\{\boldsymbol{\mathcal{A}^{-1}\mathcal{C}}\}$ incorporating the ramped loading function is then obtained as follows:

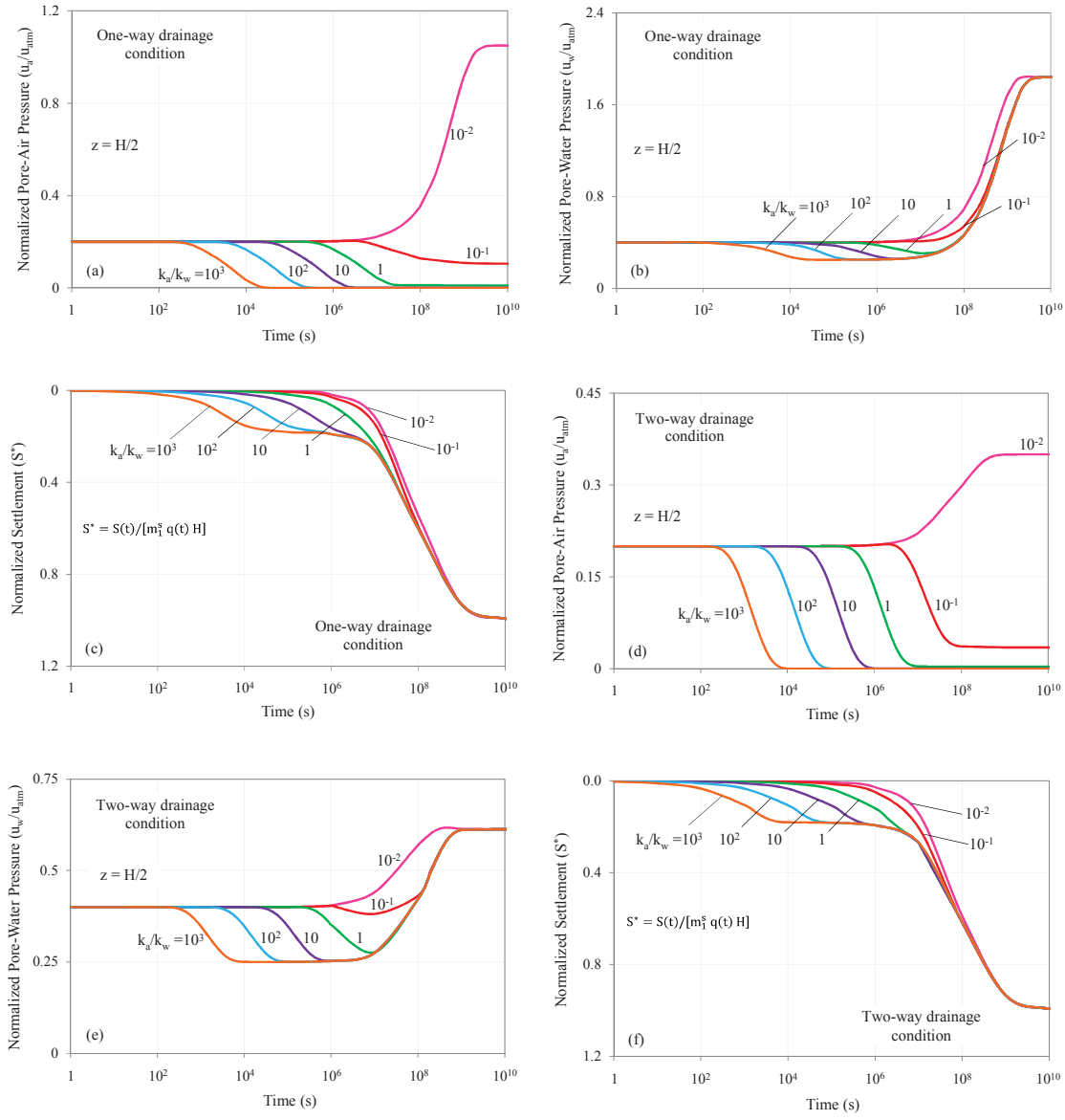

Figure 4.3. Variations in excess pore pressures and settlement with different k_a/k_w due to the ramped loading for (a–c) one-way and (d–f) two-way drainage conditions

$$\mathcal{L}^{-1}\{\boldsymbol{\mathcal{A}}^{-1}\boldsymbol{\mathcal{C}}\} = \begin{Bmatrix} \frac{X_1}{(K)^2}\left[\frac{e^{\alpha_1(K)^2 t}(\alpha_1+\beta)}{\alpha_1(\alpha_1-\alpha_2)} + \frac{e^{\alpha_2(K)^2 t}(\alpha_2+\beta)}{\alpha_2(\alpha_2-\alpha_1)} + \frac{\beta}{\alpha_1\alpha_2}\right] \\ \frac{X_1'}{(K)^2}\left[\frac{e^{\alpha_1(K)^2 t}(\alpha_1+\beta')}{\alpha_1(\alpha_1-\alpha_2)} + \frac{e^{\alpha_2(K)^2 t}(\alpha_2+\beta')}{\alpha_2(\alpha_2-\alpha_1)} + \frac{\beta'}{\alpha_1\alpha_2}\right] \end{Bmatrix} \quad [4\text{-}30]$$

where $\eta = [(c_v^w - c_v^a)^2 + 4c_v^w c_v^a C_w C_a]^{\frac{1}{2}}$;

$$X_1 = \frac{a(C_a c_\sigma^w - c_\sigma^a)}{C_a C_w - 1}; \qquad X_1' = \frac{a(C_w c_\sigma^a - c_\sigma^w)}{C_a C_w - 1};$$

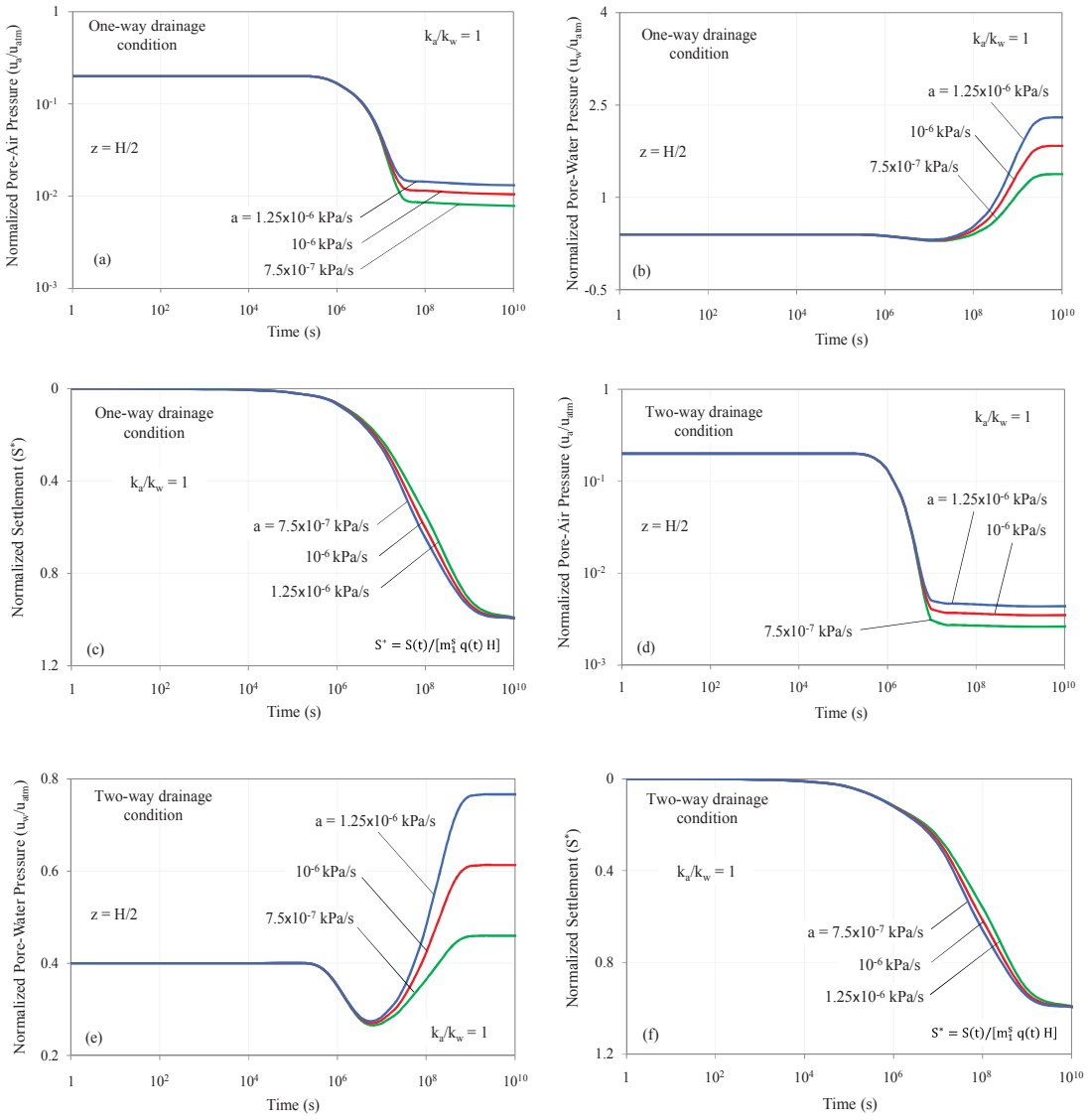

Figure 4.4. Excess pore pressures and settlement ($k_a/k_w = 1$) with different values of the loading rate a due to the ramped loading for (a–c) one-way and (d–f) two-way drainage conditions

$$\alpha_1 = \frac{1}{2}\left(\frac{c_v^w + c_v^a + \eta}{1 - C_w C_a}\right); \qquad \alpha_2 = \frac{1}{2}\left(\frac{c_v^w + c_v^a - \eta}{1 - C_w C_a}\right);$$

$$\beta = \frac{c_\sigma^a c_v^w}{C_a c_\sigma^w - c_\sigma^a}; \text{ and} \qquad \beta' = \frac{c_\sigma^w c_v^a}{C_w c_\sigma^a - c_\sigma^w}. \qquad [4\text{-}31]$$

Then, Equation [4-30] can be substituted back to Equation [4-21] to estimate the change in excess pore pressures under the ramped loading. The complete equations $u_a(z,t)$ and $u_w(z,t)$ are shown in Equations [A-1a] and [A-1b] in Appendix A.

In this example, the effects of permeability ratio k_a/k_w on the excess pore pressure dissipation and consolidation settlement are investigated at the depth $H/2 = 5m$ for the one-way (Figures 4.3(a – c)) and for the two-way (Figures 4.3(d – f)) drainage conditions. It is observed that the application of ramped loading on the ground surface contributes to the significant increase in the excess pore-water pressure after $10^6 s$. This increase is a result of the slow dissipation of excess pore-water pressure. Likewise, when $k_a/k_w > 1$, the excess pore-air pressure dissipation is also considerably increasing due to its slow dissipation rate. When k_a/k_w exceeds 1, the excess pore-air pressure is fully dissipated before $10^6 s$, as a result, the external ramping load will have little effect on the change of excess pore-air pressure.

On the other hand, Figures 4.3(c) and 4.3(f) present the normalised settlement (i.e., $S^* = S(t)/[m_1^s\, q(t)\, H]$) of the unsaturated soil deposit subjected to the ramped loading. In the early stages of compression, different values of k_a/k_w result in variations in settlement patterns. During this stage, it can be seen that the settlement patterns form inverse S curves when $k_a/k_w > 1$. This is due to the fact that the compression of the soil deposit in the early stages is governed by the dissipation of both excess pore-air and pore-water pressures, in which air dissipates faster than water, whilst the compression in the later stage is only controlled by excess pore-water pressure as a result of the quick dissipation of the pore-air pressure. Before $10^6 s$, the settlement patterns resemble to those induced by a constant loading. However, after $10^6 s$, the unsaturated soil layer suffers from a dramatic reduction in the volume due to the linearly increasing load. These settlement patterns then converge into a single curve and continue to increase until they remain unchanged after a long time. In comparison to the one-way drainage condition (Figures 4.3(a – c)), the results obtained in the two-way drainage system (Figures 4.3(d – f)) also share similar dissipation and settlement patterns. The major difference is that the dissipation process and the consolidation settlement in the two-way drainage system proceed more quickly than the one-way drainage system.

Variations in the loading rate 'a', ranging from 7.5×10^{-7} to 1.25×10^{-6} kPa. s^{-1}, also significantly influences the 1-D consolidation behaviour. The normalised pressures and settlement of the unsaturated soil subjected to the ramped loading with various load rates are presented in Figures 4.4(a – c) for the one-way drainage condition and in

Figures 4.4(d – f) for the two-way drainage condition. The permeability ratio k_a/k_w of 1 is adopted in this analysis. It is noticed that a higher loading rate 'a' leads to higher external load at a particular time, generating larger excess pore pressures during the compression process. Such increase in pressure is clearly observed in both excess pore-air and pore-water pressure dissipation. Furthermore, faster settlement rate can be observed at the later stages of consolidation due to higher external loads. However, the settlement patterns approach a similar value after a very long time, regardless of values of 'a'.

4.4.2. Asymptotic Loading

During construction, it is often observed that an external loading continuously increases before approaching an asymptote. The general asymptotic function can be mathematically simulated as follows:

$$q(t) = q_0\left[A\left(1 - e^{-bt}\right) + 1\right] \qquad [4\text{-}32]$$

where 'A' is the dimensionless parameter influencing the load magnitude; and 'b' is the loading parameter controlling the rate of asymptotic loading (s^{-1}). Figure 4.2(b) depicts the loading varying exponentially with time when $b = 5 \times 10^{-5} s^{-1}$ and $A = 1$. The asymptotic function presented in Equation [4-32] can be now substituted to the Laplace transformed $\boldsymbol{\mathcal{A}^{-1}\mathcal{C}}$ as shown in Equation [4-18]. The term $\mathcal{L}^{-1}\{\boldsymbol{\mathcal{A}^{-1}\mathcal{C}}\}$ incorporating the asymptotic loading is now presented below:

$$\mathcal{L}^{-1}\{\boldsymbol{\mathcal{A}^{-1}\mathcal{C}}\} = \begin{Bmatrix} X_2\left\{\frac{e^{-bt}[\beta(K)^2 - b]}{[b+\alpha_1(K)^2]\,[b+\alpha_2(K)^2]} + \frac{e^{\alpha_1(K)^2 t}(\alpha_1+\beta)}{[b+\alpha_1(K)^2]\,(\alpha_1-\alpha_2)} + \frac{e^{\alpha_2(K)^2 t}(\alpha_2+\beta)}{[b+\alpha_2(K)^2]\,(\alpha_2-\alpha_1)}\right\} \\ X_2'\left\{\frac{e^{-bt}[\beta'(K)^2 - b]}{[b+\alpha_1(K)^2]\,[b+\alpha_2(K)^2]} + \frac{e^{\alpha_1(K)^2 t}(\alpha_1+\beta')}{[b+\alpha_1(K)^2]\,(\alpha_1-\alpha_2)} + \frac{e^{\alpha_2(K)^2 t}(\alpha_2+\beta')}{[b+\alpha_2(K)^2]\,(\alpha_2-\alpha_1)}\right\} \end{Bmatrix} \qquad [4\text{-}33]$$

where $X_2 = \frac{bq_0A(C_a c_\sigma^w - c_\sigma^a)}{C_a C_w - 1}$; and $\quad X_2' = \frac{bq_0A(C_w c_\sigma^a - c_\sigma^w)}{C_a C_w - 1}$. $\qquad [4\text{-}34]$

Equation [4-33] can be substituted back in Equation [4-21] to estimate the change in excess pore pressures due to the defined asymptotic loading. The detailed equations $u_a(z,t)$ and $u_w(z,t)$ for asymptotic loading are given in Equations [A-2a] and [A-2b] in Appendix A.

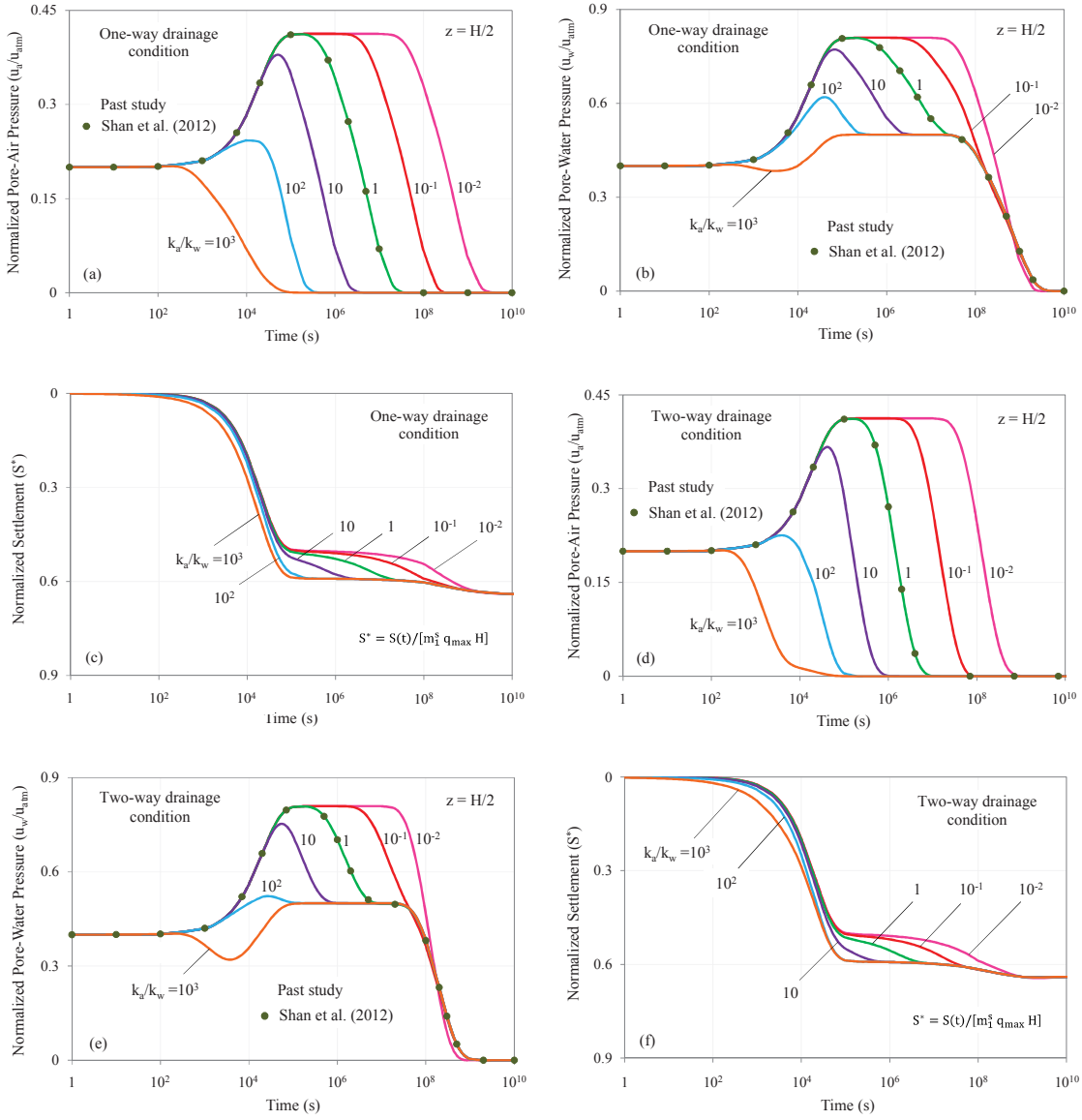

Figure 4.5. Variations in excess pore pressures and settlement with different k_a/k_w due to the asymptotic loading for (a–c) one-way and (d–f) two-way drainage conditions

The changes in excess pore pressures and consolidation settlement are investigated at the depth $H/2$ for one-way (Figures 4.5(a – c)) and two-way (Figures 4.5(d – f)) drainage conditions. As observed in Figure 4.2(b), the external loading gradually increases until approaching the constant $q_{max} = 200\text{kPa}$, doubling the value of the initial surcharge q_0. Likewise, excess pore pressures with $k_a/k_w < 10$ exponentially increase due to the slow dissipation process. Once the loading approaches the asymptote

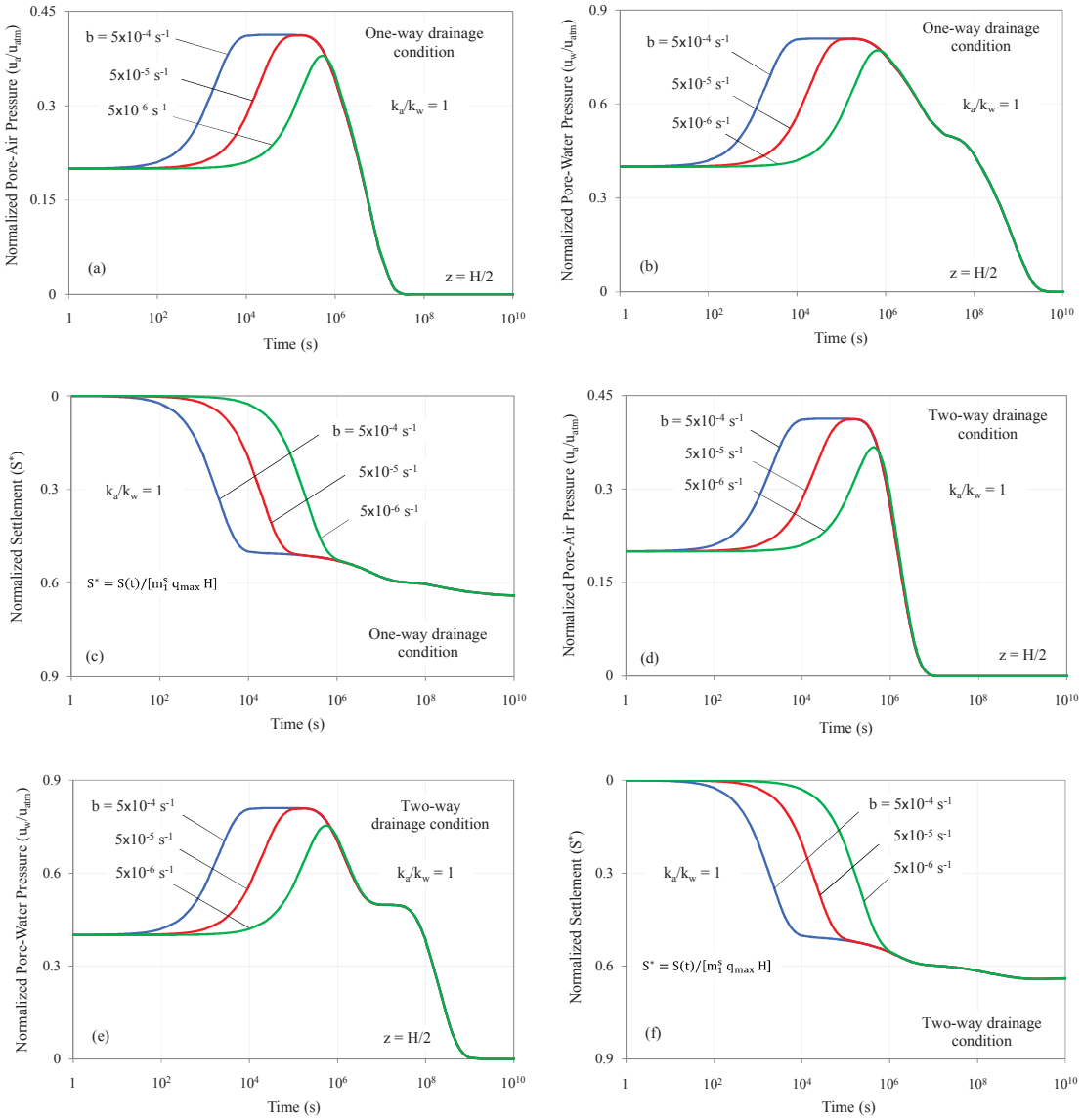

Figure 4.6. Excess pore pressures and settlement ($k_a/k_w = 1$) with different values of the parameter b due to the asymptotic loading for (a–c) one-way and (d–f) two-way drainage conditions

(i.e. $q_{max} = 200$kPa), these pressures begin to decrease. It can be noticed that higher values of k_a/k_w (greater than 10) lead to faster dissipation of excess pore-air pressure and as a consequence, the pressure tends to dissipate before 10^5s. The validation exercise between the dissipation predictions presented in Equation [4-42] and the existing solution proposed by Shan et al. (2012) has been conducted in Figures 4.5(a – b) and 4.5(d – e). By examining $k_a/k_w = 1$, the analytical solution in this study has a

similar result compared to that of the solution in literature (Shan et al. 2012), confirming that the proposed solution is valid.

Figures 4.5(c) and 4.5(f) present the normalised settlement (i.e. $S^* = S(t)/(m_1^s\, q_{max}\, H)$) of the unsaturated soil deposit due to the asymptotic loading. As observed, the normalised settlement abruptly increases due to the rapidly increasing external load in the early stages. When the loading approaches the asymptote, the settlement gradually increases whilst forming inverse S-shaped curves, as expected for the constant loading. It can be noticed that the two-way drainage system delivers faster settlement rate than the one-way drainage system due to the free dissipation of air and water in both drainage boundaries. For instance, the soil deposit consisting of double drainage boundaries approaches the final settlement at 10^9s whilst the corresponding time in one-way drainage system is 10^{10}s.

The investigation also accentuates on the effects of parameter 'b' on the 1-D consolidation behaviour. Various values of 'b', ranging from 5×10^{-4} to $5 \times 10^{-6}s^{-1}$ are adopted for this investigation. Considering the permeability ratio $k_a/k_w = 1$, normalised pore pressures take shorter time to achieve its highest value as 'b' increases (Figures 4.6(a – b) and 4.6(d – e)). When the parameter 'b' is small, the maximum value of the excess pore pressure tends to decrease due to the slower loading rate. This behaviour can be seen in both excess pore-air and pore-water pressures. In the early stages of consolidation, the compression of the soil subjected to the asymptotic loading having higher 'b' values also tend to proceed more quickly than those having smaller 'b' values (Figures 4.6(c) and 4.6(f)).

4.4.3. Sinusoidal Loading

Sinusoidal (sine wave) function describes a smooth repetitive oscillation and can be taken as a possible repetitive external loading applied on the unsaturated soil deposit. The general function is mathematically presented as follows:

$$q(t) = q_0[B\ \sin(\phi t) + 1] \qquad [4\text{-}35]$$

where 'B' is the dimensionless parameter influencing the loading amplitude; and 'ϕ' is the angular frequency ($rad.s^{-1}$). The sinusoidal function depicted in Figure 4.2(c)

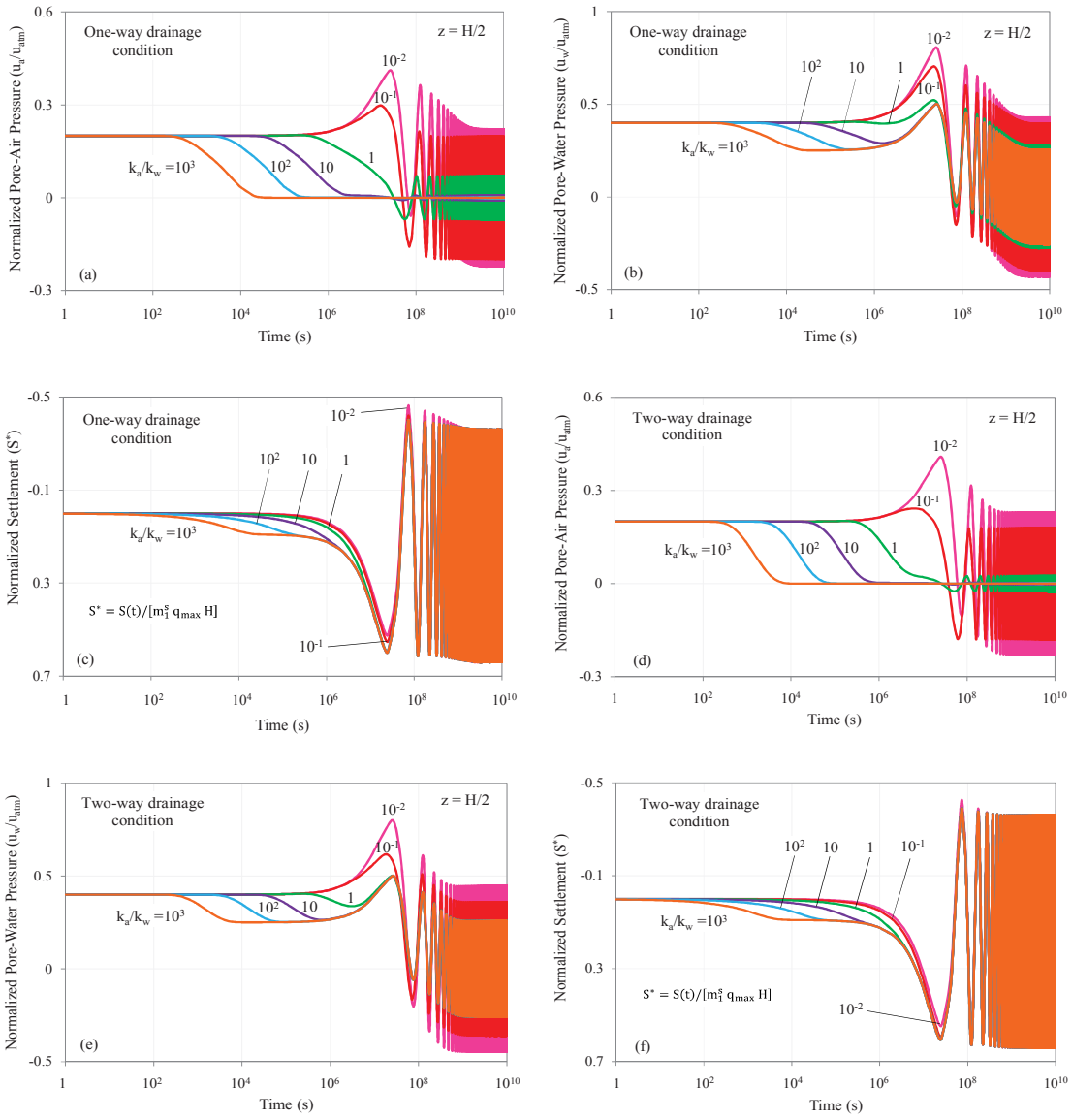

Figure 4.7. Variations in excess pore pressures and settlement with different k_a/k_w due to the sinusoidal loading for (a–c) one-way and (d–f) two-way drainage conditions

consists of a peak to peak amplitude of $2q_0$ (i.e. 200kPa) with an angular frequency $\phi = 2\pi 10^{-8}$ rad.s^{-1} and $B = 1$. A possible application for the case study with small ϕ can be regarded as the compression induced by the storage tanks and silos. For instance, in a water storage tank, the liquid weight may gradually reduce to zero when the tank is emptied as the result of domestic uses and then approach the maximum value (i.e. 200kPa) when the tank is gradually filled with water to replenish its supply. It is worth

mentioning that filling and emptying large tanks and silos usually occur with a very slow rate. The change in the liquid weight may be assumed to be periodic and therefore can be simulated as the sinusoidal loading function. Obviously, by increasing the value of ϕ in Equation [4-35], it is possible to generate results with a shorter period. For example, the cyclic loads generated by heavy trains or road traffic can be simulated with higher ϕ values.

The sinusoidal function in Equation [4-35] can be substituted to the Laplace transformed $\boldsymbol{\mathcal{A}^{-1}\mathcal{C}}$ as shown in Equation [4-18]. The term $\mathcal{L}^{-1}\{\boldsymbol{\mathcal{A}^{-1}\mathcal{C}}\}$ incorporating the sinusoidal loading is now obtained as below:

$$\mathcal{L}^{-1}\{\boldsymbol{\mathcal{A}^{-1}\mathcal{C}}\} = \begin{Bmatrix} X_3\left\{\frac{e^{\alpha_1(K)^2 t}\alpha_1(K)^2(\alpha_1+\beta)}{\{[\alpha_1(K)^2]^2+\phi^2\}(\alpha_1-\alpha_2)}+\frac{e^{\alpha_2(K)^2 t}\alpha_2(K)^2(\alpha_2+\beta)}{\{[\alpha_2(K)^2]^2+\phi^2\}(\alpha_2-\alpha_1)}+\frac{\zeta_1^k\cos(\phi t)+\zeta_2^k\sin(\phi t)}{\{[\alpha_1(K)^2]^2+\phi^2\}\{[\alpha_2(K)^2]^2+\phi^2\}}\right\} \\ X_3'\left\{\frac{e^{\alpha_1(K)^2 t}\alpha_1(K)^2(\alpha_1+\beta')}{\{[\alpha_1(K)^2]^2+\phi^2\}(\alpha_1-\alpha_2)}+\frac{e^{\alpha_2(K)^2 t}\alpha_2(K)^2(\alpha_2+\beta')}{\{[\alpha_2(K)^2]^2+\phi^2\}(\alpha_2-\alpha_1)}+\frac{\zeta_1'^k\cos(\phi t)+\zeta_2'^k\sin(\phi t)}{\{[\alpha_1(K)^2]^2+\phi^2\}\{[\alpha_2(K)^2]^2+\phi^2\}}\right\} \end{Bmatrix} \quad [4\text{-}36]$$

where $X_3 = \frac{q_0 B\phi(C_a c_\sigma^w - c_\sigma^a)}{C_a C_w - 1}$; $\quad X_3' = \frac{q_0 B\phi(C_w c_\sigma^a - c_\sigma^w)}{C_a C_w - 1}$;

$$\zeta_1^k = (K)^2\,[\alpha_1\alpha_2\beta\,(K)^4 - (\alpha_1+\alpha_2+\beta)\phi^2];$$
$$\zeta_1'^k = (K)^2\,[\alpha_1\alpha_2\beta'\,(K)^4 - (\alpha_1+\alpha_2+\beta')\phi^2];$$
$$\zeta_2^k = \phi\,\{\phi^2 - [\beta(\alpha_1+\alpha_2)+\alpha_1\alpha_2]\,(K)^4\};\text{ and}$$
$$\zeta_2'^k = \phi\,\{\phi^2 - [\beta'(\alpha_1+\alpha_2)+\alpha_1\alpha_2]\,(K)^4\}. \quad [4\text{-}37]$$

The term $\mathcal{L}^{-1}\{\boldsymbol{\mathcal{A}^{-1}\mathcal{C}}\}$ obtained from Equation [4-36] can be then substituted back to Equation [4-21] to estimate the change in excess pore pressures under the sinusoidal loading. The detailed equations $u_a(z,t)$ and $u_w(z,t)$ for sinusoidal loading are presented in Equations [A-3a] and [A-3b] in Appendix A.

The excess pore pressure dissipation and consolidation settlement are investigated at the depth $H/2$ for one-way (Figures 4.7(a – c)) and two-way (Figures 4.7(d – f)) drainage conditions. The typical sinusoidal loading function includes loading-unloading curves, generating similar impacts on the dissipation patterns. In specific, the excess pore pressures increase during the loading process (i.e. stress path from 0 to 200kPa) and decrease during the unloading process (i.e. stress path from 200kPa to 0) whilst still dissipate due to the average loading (i.e. $q_0 = 100$kPa) at a very slow rate. As

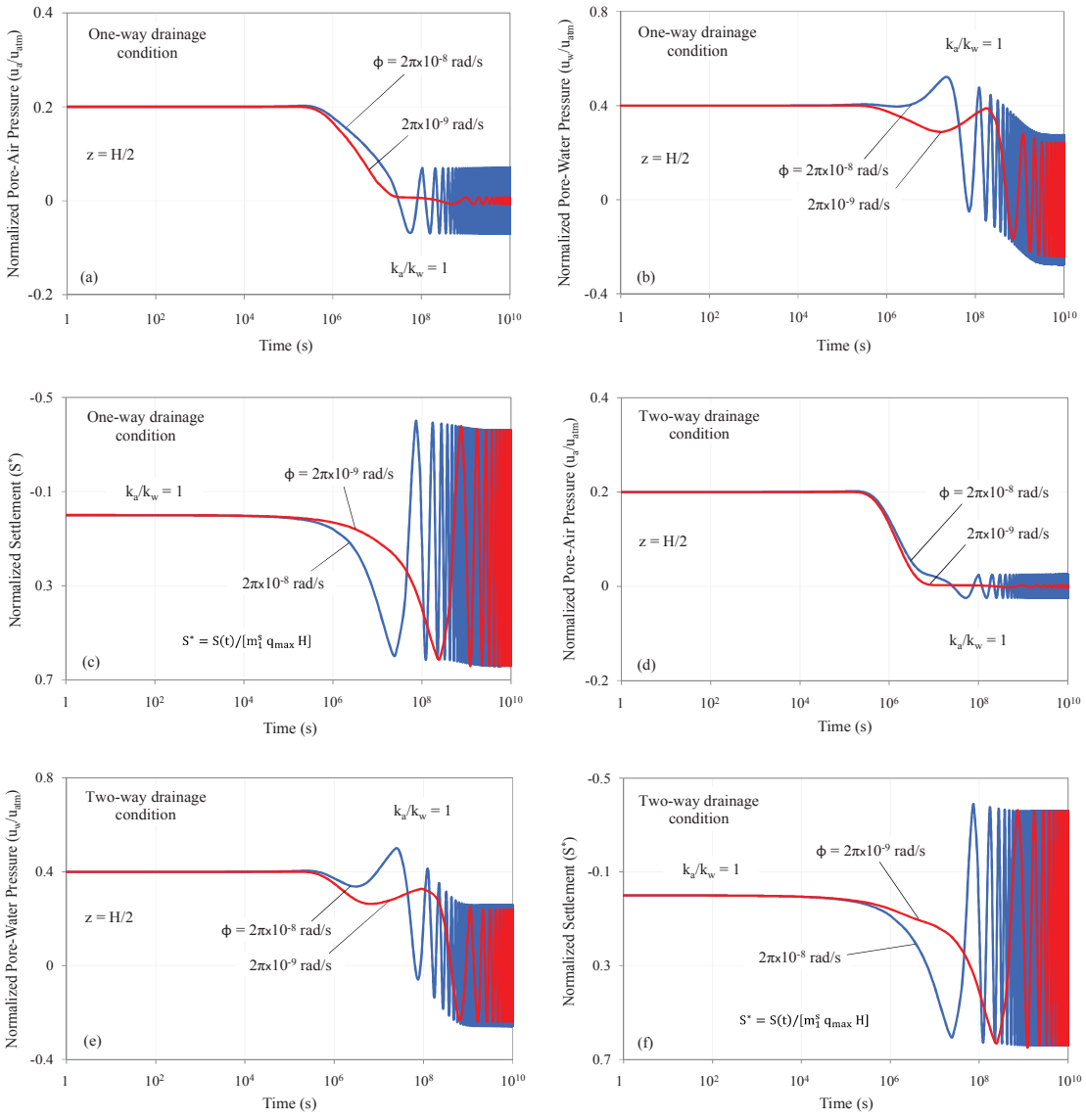

Figure 4.8. Excess pore pressures and settlement ($k_a/k_w = 1$) with different values of the angular frequency ϕ due to the sinusoidal loading for (a–c) one-way and (d–f) two-way drainage conditions

observed in Figures 4.7(a – b) and 4.7(d – e), when the consolidation duration is significant (e.g. $t > 10^7$s), the excess pore pressures become negative due to the unloading process, as a result of the decreasing total stress. On the other hand, the loading-unloading process presents repetitive oscillations with amplitudes dependent on the dissipation rate of excess pore pressures. It can be noticed that the higher values of k_a/k_w (greater than 1) lead to insignificant excess pore-air pressure remaining in the soil after 10^6s due to the high excess pore pressure dissipation rate. This results in a

smaller amplitude in the excess pore-air pressure pattern, indicating that the external sinusoidal loading has little effects on the excess pore-air pressure dissipation process when $k_a/k_w > 1$. Considering the higher value of k_a/k_w (e.g. 10^3) the excess pore-air pressure diminishes before 10^6s whereas the excess pore-water pressure still continues oscillating due to the slow pore-water pressure dissipation process.

Figures 4.7(c) and 4.7(f) illustrate the normalised settlement (i.e. $S^* = S(t)/(m_1^s q_{max} H)$) of the unsaturated soil layer subjected to the sinusoidal loading. The compression patterns form inverse S curves in the early stages of consolidation and then oscillate indefinitely after 10^6s. The unsaturated soil deposit settles and expands in response to the loading and unloading processes, respectively. This phenomenon indicates that air and water are squeezed out during loading process and then absorbed in during unloading process; hence, the soil volume continuously changes with time.

The effects of angular frequency 'ϕ' on the consolidation pattern can be clearly demonstrated for one-way (Figures 4.8(a – c)) and two-way (Figures 4.8(d – f)) drainage systems, when particular frequencies of $2\pi 10^{-8}$ and $2\pi 10^{-9}\,\mathrm{rad.\,s^{-1}}$ are investigated. For $k_a/k_w = 1$, the smaller 'ϕ' ($2\pi 10^{-9}\,\mathrm{rad.\,s^{-1}}$) delivers slower loading-unloading rate, allowing more time for the excess pore-air pressure to dissipate. The inconsiderable excess pore-air pressure remaining in the soil after a long period of time (e.g. 10^8s), may result in a smaller peak to peak amplitude in the pressure pattern. In contrary, the increasing 'ϕ' does not only induce a significant amplitude but also contributes to more loading-unloading cycles for excess pore pressures. On the other hand, at the early stages of consolidation, it is noticed that the unsaturated soil deposit settles more quickly when 'ϕ' increases.

4.4.4. Damped Sine Wave Loading

The damped sine wave loading is described as a sinusoidal function with its amplitude approaching zero when time increases. In engineering practice, soil deposits beneath the ground may be subjected to damped and cyclic loadings as the result of traffic loads. A damped wave function can be a good representative to describe such external loadings. The general damped sine wave loading can be simulated as below:

$$q(t) = q_0[C\, e^{-ct} \sin(\varphi t) + 1] \qquad [4\text{-}38]$$

where 'C' is the dimensionless parameter influencing the loading amplitude; 'c' is the loading parameter controlling damping rate (s^{-1}); and 'φ' is the angular frequency ($rad.s^{-1}$). The damped sine wave loading depicted in Figure 4.2(d) consists of an angular frequency $\varphi = 2\pi 10^{-3}\,rad.s^{-1}$ whilst adopting the damping parameter $c = 5 \times 10^{-5} s^{-1}$ and $C = 1$. The damped function presented in Equation [4-38] can be substituted to the Laplace transformed $\boldsymbol{\mathcal{A}^{-1}\mathcal{C}}$ as shown in Equation [4-18]. The term $\mathcal{L}^{-1}\{\boldsymbol{\mathcal{A}^{-1}\mathcal{C}}\}$ incorporating the damped loading can be presented as follows:

$$\mathcal{L}^{-1}\{\boldsymbol{\mathcal{A}^{-1}\mathcal{C}}\} = \begin{Bmatrix} X_4 \left\{ \frac{e^{\alpha_1 (K)^2 t}\alpha_1 (K)^2(\alpha_1+\beta)}{\{[\alpha_1 (K)^2+c]^2+\varphi^2\}(\alpha_1-\alpha_2)} + \frac{e^{\alpha_2 (K)^2 t}\alpha_2 (K)^2(\alpha_2+\beta)}{\{[\alpha_2 (K)^2+c]^2+\varphi^2\}(\alpha_2-\alpha_1)} + \frac{e^{-ct}[\xi_1^k \cos(\varphi t)+\xi_2^k \sin(\varphi t)]}{\varphi\{[\alpha_1 (K)^2+c]^2+\varphi^2\}\{[\alpha_2 (K)^2+c]^2+\varphi^2\}} \right\} \\ X_4' \left\{ \frac{e^{\alpha_1 (K)^2 t}\alpha_1 (K)^2(\alpha_1+\beta')}{\{[\alpha_1 (K)^2+c]^2+\varphi^2\}(\alpha_1-\alpha_2)} + \frac{e^{\alpha_2 (K)^2 t}\alpha_2 (K)^2(\alpha_2+\beta')}{\{[\alpha_2 (K)^2+c]^2+\varphi^2\}(\alpha_2-\alpha_1)} + \frac{e^{-ct}[\xi_1'^k \cos(\varphi t)+\xi_2'^k \sin(\varphi t)]}{\varphi\{[\alpha_1 (K)^2+c]^2+\varphi^2\}\{[\alpha_2 (K)^2+c]^2+\varphi^2\}} \right\} \end{Bmatrix} \quad [4\text{-}39]$$

where $X_4 = \frac{q_0 C\varphi(C_a c_\sigma^w - c_\sigma^a)}{C_a C_w - 1}$; $\quad X_4' = \frac{q_0 C\varphi(C_w c_\sigma^a - c_\sigma^w)}{C_a C_w - 1}$;

$$\xi_1^k = -\varphi\,(K)^2[(c^2+\varphi^2)(\alpha_1+\alpha_2+\beta) + 2c\alpha_1\alpha_2\,(K)^2 - \alpha_1\alpha_2\beta\,(K)^4];$$

$$\xi_1'^k = -\varphi\,(K)^2[(c^2+\varphi^2)(\alpha_1+\alpha_2+\beta') + 2c\alpha_1\alpha_2\,(K)^2 - \alpha_1\alpha_2\beta'\,(K)^4];$$

$$\xi_2^k = (c^2+\varphi^2)^2 + c(\alpha_1+\alpha_2-\beta)(c^2+\varphi^2)\,(K)^2 + [(c^2-\varphi^2)\alpha_1\alpha_2 - \beta(\alpha_1+\alpha_2)(c^2+\varphi^2)]\,(K)^4 - c\alpha_1\alpha_2\beta\,(K)^6; \text{ and}$$

$$\xi_2'^k = (c^2+\varphi^2)^2 + c(\alpha_1+\alpha_2-\beta')(c^2+\varphi^2)\,(K)^2 + [(c^2-\varphi^2)\alpha_1\alpha_2 - \beta'(\alpha_1+\alpha_2)(c^2+\varphi^2)]\,(K)^4 - c\alpha_1\alpha_2\beta'\,(K)^6. \quad [4\text{-}40]$$

The term $\mathcal{L}^{-1}\{\boldsymbol{\mathcal{A}^{-1}\mathcal{C}}\}$ obtained from Equation [4-39] will be substituted to Equation [4-21] to determine the dissipation of excess pore pressures due to the damped sine wave loading. The complete equations $u_a(z,t)$ and $u_w(z,t)$ for damped loading are presented in Equations [A-4a] and [A-4b] in Appendix A.

The excess pore pressure dissipation and settlement induced by damped sine wave loading are investigated at the depth $H/2$ for one-way (Figures 4.9(a – c)) and two-way (Figures 4.9(d – f)) drainage systems. Similar to the sinusoidal loading, the damped sine wave function consists of oscillations with peak to peak amplitude of about $2q_0$ at the very beginning; then, the amplitude exponentially decreases and approaches zero and the external loading becomes constant ($q_0 = 100kPa$). Correspondingly, excess pore pressure dissipation patterns appear to oscillate due to the loading-unloading process at

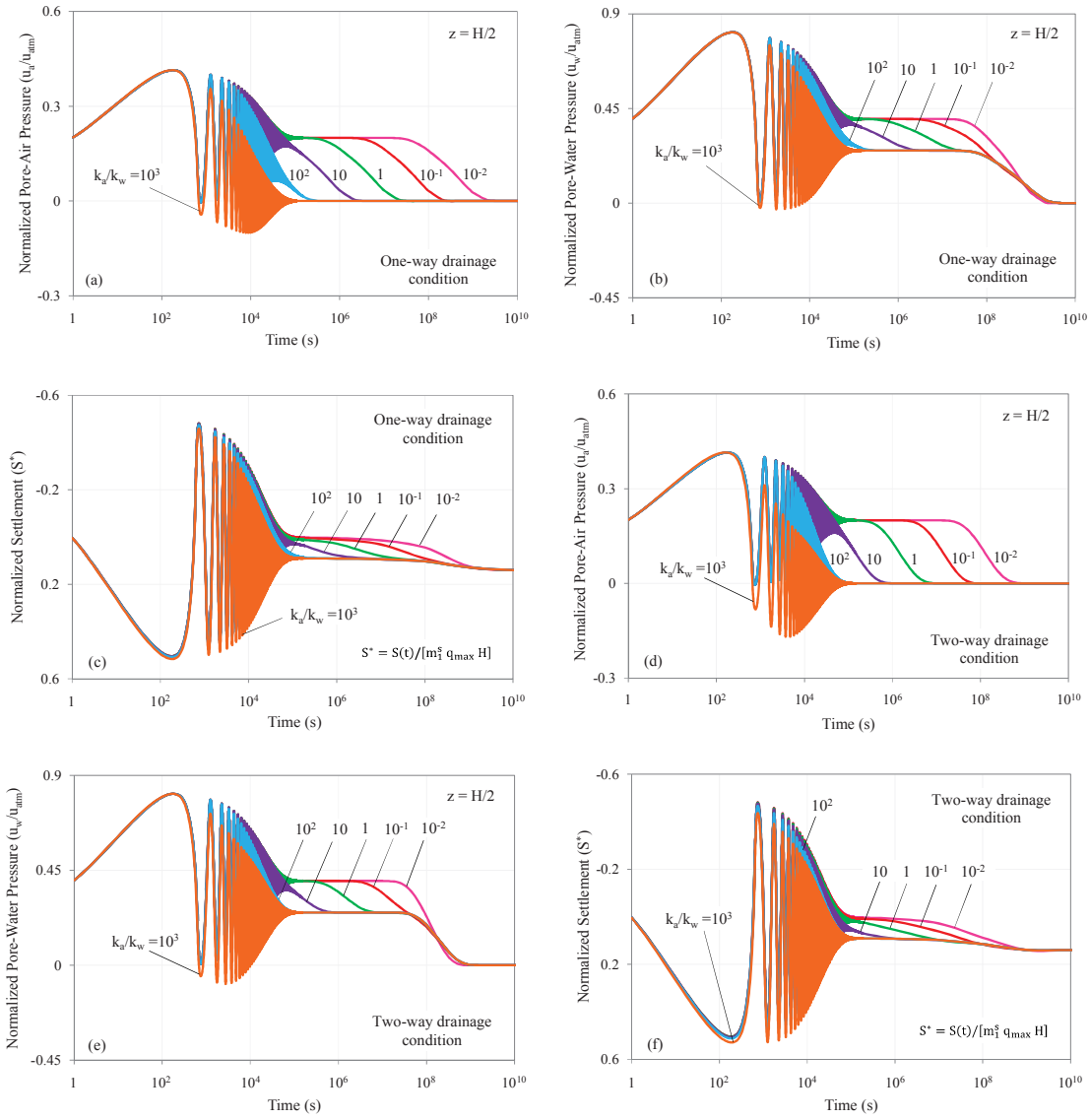

Figure 4.9. Variations in excess pore pressures and settlement with different k_a/k_w due to the damped sine wave loading for (a–c) one-way and (d–f) two-way drainage conditions

the early stages and then gradually dissipate after 10^5s. The change in pressure at later stages resembles to that previously proposed in literature (Qin et al. 2008; Shan et al. 2012; Zhou et al. 2014), in which the dissipation of the excess pore-air pressure presents a typical single inverse S curve whilst the excess pore-water pressure forms double inverse S curves when $k_a/k_w > 1$.

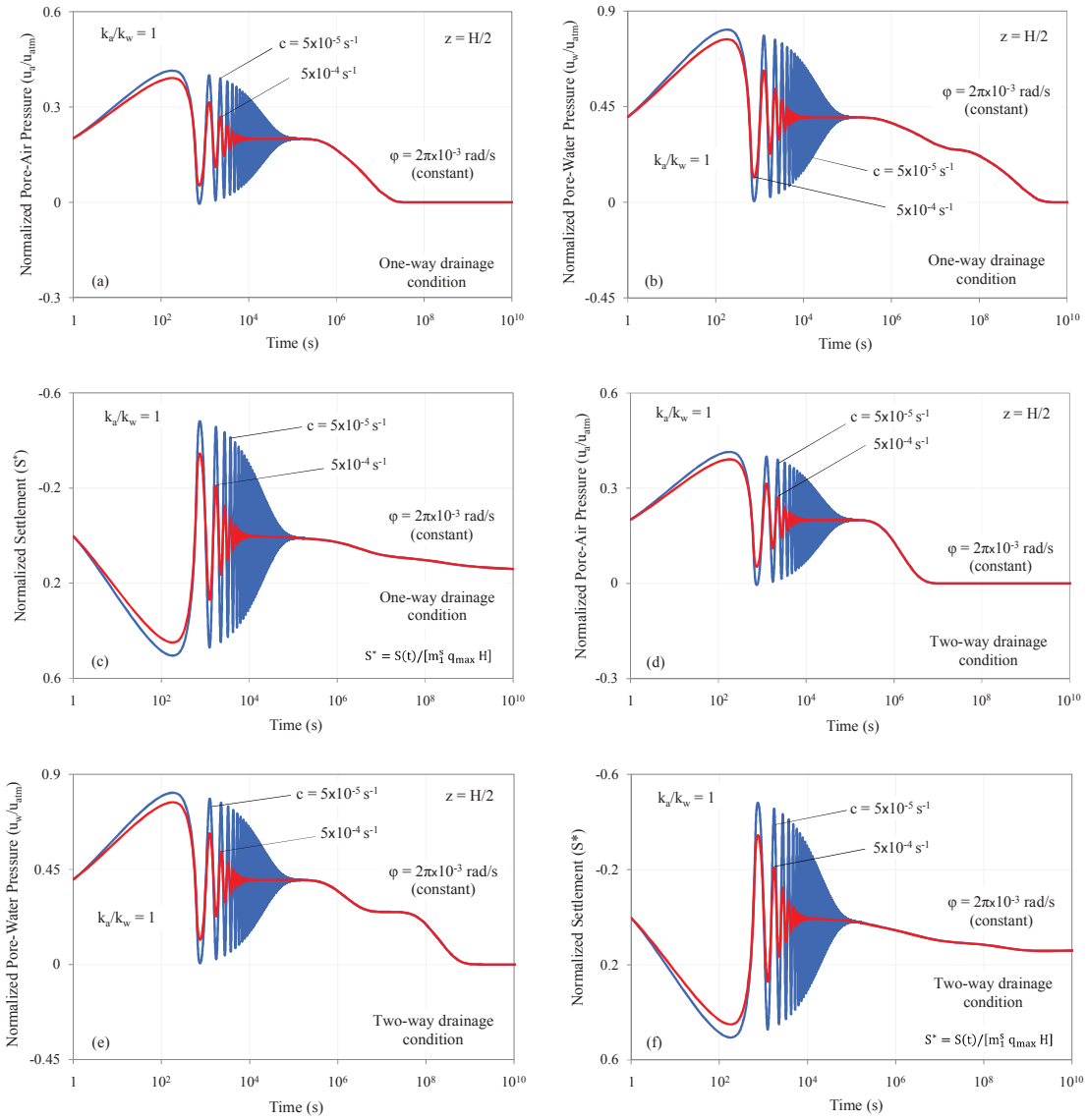

Figure 4.10. Excess pore pressures and settlement ($k_a/k_w = 1$) with different values of the parameter c due to the damped sine wave loading for (a–c) one-way and (d–f) two-way drainage conditions

Figures 4.9(c) and 4.9(f) depict the normalised settlement (i.e. $S^* = S(t)/(m_1^s q_{max} H)$) of the unsaturated soil layer due to the damped sine wave loading. The compression patterns initially show oscillations with decreasing amplitude. As the damped sine wave loading stabilises (the amplitude approaches zero), the compression patterns resemble to the patterns proposed for the constant loading. It is also noticed that the two-way drainage condition results in higher settlement rate in comparison to the one-way drainage condition.

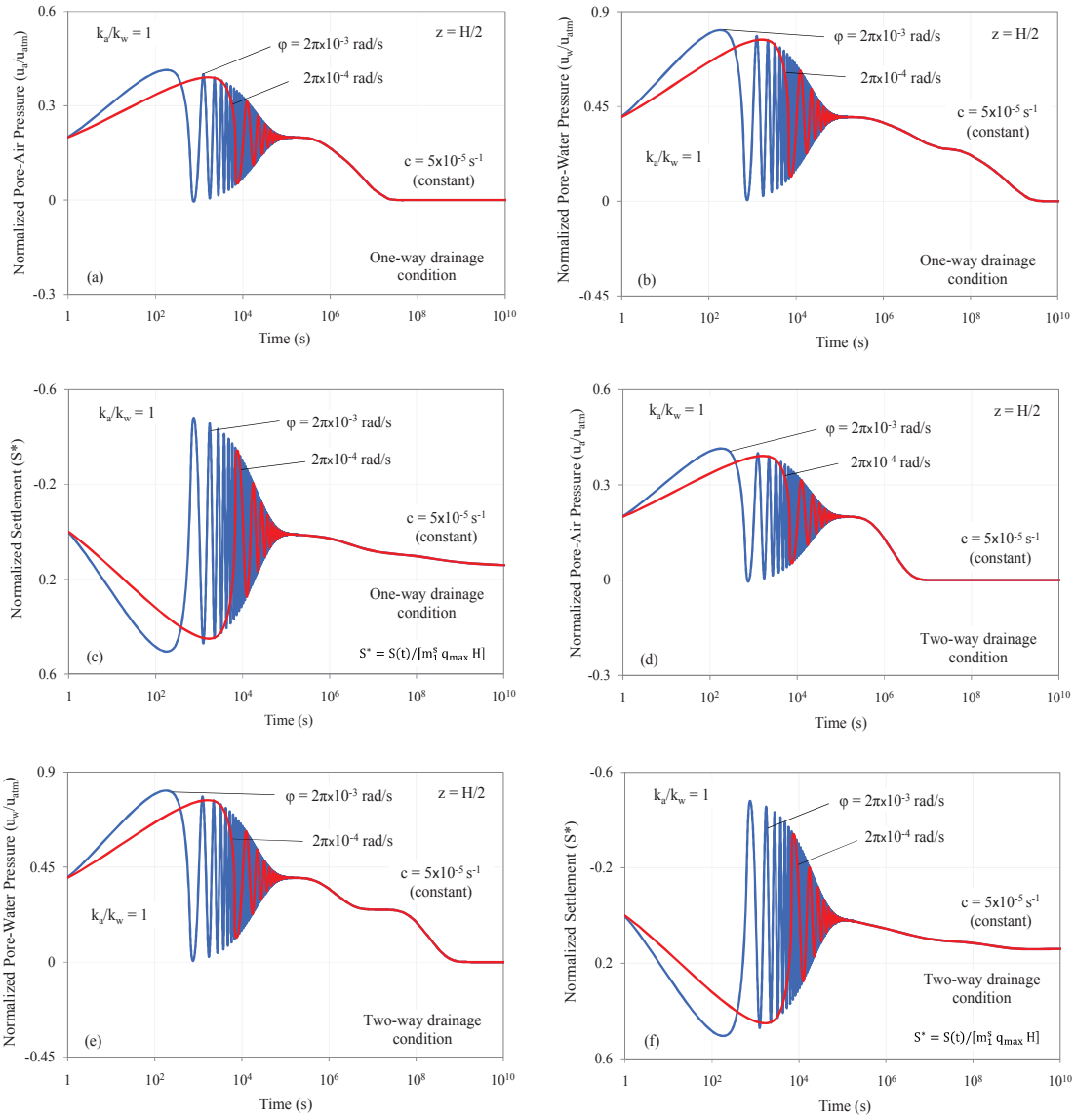

Figure 4.11. Excess pore pressures and settlement ($k_a/k_w = 1$) with different values of the angular frequency φ due to the damped sine wave loading for (a–c) one-way and (d–f) two-way drainage conditions

The significant effects of the damping parameter 'c' (5×10^{-4} and $5 \times 10^{-5}s^{-1}$) and the angular frequency 'φ' ($2\pi10^{-2}$ and $2\pi10^{-3}$ rad. s^{-1}) on 1-D consolidation can be demonstrated in Figures 4.10(a – f) and Figures 4.11(a – f), respectively. Considering $k_a/k_w = 1$, when 'c' is varying whilst 'φ' is constant, the higher value of 'c' (i.e. $5 \times 10^{-4}s^{-1}$) accelerates the damping process, in which the load amplitude approaches zero much faster than that with smaller 'c' (i.e. $5 \times 10^{-5}s^{-1}$). Likewise, excess pore

pressures with the higher ‘c’ tend to stabilise more quickly before being dissipated. On the other hand, during the early stages of consolidation, more loading-unloading cycles in the excess pore pressure and compression patterns are observed as ‘φ’ increases whilst c remains unchanged. The effects of ‘φ’ is similar to those of ‘ϕ’ in the sinusoidal loading function. Once the load amplitude approaches zero, the consolidation behaviour is no longer influenced by parameters ‘c’ and ‘φ’.

4.5. Summary

This paper introduces the application of eigenfunction expansion and Laplace transform techniques to determine excess pore pressures and 1-D settlement of the unsaturated soil layer subjected to various time-dependent loadings. In this study, the homogeneous boundary conditions (one-way and two-way drainage systems) and the uniformly distributed initial pore pressures are adopted for the analytical development. The general solution consisting of the eigenfunctions is employed. Once the first order derivatives with respect to time are obtained, exact solutions can be computed using Laplace transform and Laplace inverse methods. When the soil is in saturated state, the proposed final solution can be simplified and transformed into the classical Terzaghi’s consolidation equation. This shows that the proposed solution is applicable for different soil states. Moreover, the validation has been conducted in the worked examples suggesting the proposed solution is valid for use.

Loading functions (i.e. ramped, asymptotic, sinusoidal, and damped sine wave loadings) varying with time are mathematically simulated in different worked examples. Closed-form analytical solutions to predict variations of the excess pore-air and pore-water pressures as well as the ground surface settlement with time have been developed. Through the analytical solutions, the 1-D consolidation behaviour reveals that the application of time-dependent loads has less significant impacts on the excess pore-air pressure as k_a/k_w increases. In contrary, the excess pore-water pressure patterns varying with k_a/k_w are significantly influenced by particular loading functions. It is also concluded that the dissipation process of excess pore pressures and settlement in the two-way drainage system proceed faster than those in the one-way drainage system. Besides, the effects of loading parameters (‘a’, ‘b’, ‘c’, ‘ϕ’ and ‘φ’) presented in the mentioned loading functions were also investigated. In most cases, particularly in the

early stages of loading or consolidation process, changes in the loading function parameters lead to significant changes in excess pore pressures and the predicted settlement. More specifically, for ramped and asymptotic loadings, excess pore pressure dissipation rates generally increase with increasing loading rates a and b; whilst higher angular frequencies 'ϕ' or 'φ', presented in sinusoidal and damped sine wave loadings, contribute to more loading-unloading cycles for excess pore pressures and the ground surface settlement. Additionally, higher damping rate 'c', shown in the damped sine wave loading, accelerates the damping process for the excess pore pressures and the settlement.

CHAPTER 5

ANALYTICAL SOLUTION TO ONE-DIMENSIONAL CONSOLIDATION IN UNSATURATED SOIL DEPOSIT INCORPORATING TIME-DEPENDENT TEMPERATURE VARIATIONS

5.1. Introduction

Referring to the experiment-based research conducted by Alsherif & McCartney (2015), there is realisation that changes in temperature induce pronounced impacts on the deformation behaviour of compacted and unsaturated soils. This paper presents an analytical solution to the 1D consolidation of unsaturated soil deposit induced by the temperature varying with time and depth. The governing flow equations that capture the temperature change are adopted from Dakshanamurthy & Fredlund (1981). Fourier sine series and Laplace transformation techniques are employed to obtain final solutions. Effects of temperature varying linearly, exponentially and diurnally on changes in pore pressures and soil deformation are highlighted. This paper also investigates combined effects of temperature change and constant loading on the consolidation behaviour. Furthermore, effects of thermal parameters influencing the consolidation process are investigated and discussed. This proposed analytical solution can be used to validate the future numerical and experimental results for the 1D consolidation of unsaturated soils induced by temperature variations.

5.2. Governing flow equations in unsaturated soils

As suggested by Barden (1965), the flows of air and water can be described in accordance with the continuity of fluid phases. When the degree of saturation (S_r) is high, the water phase is considered to be continuous whereas the air phase is not; when S_r reduces, both air and water media may be continuous; and for lower S_r, the air phase

is considered to be continuous while the water phase is not. In existing literature (Qin et al. 2008; Shan et al. 2012; Zhou et al. 2014), flows of air and water can be assumed continuous and independent. It should be also noted that Fick's law can be used to present the air flow (Blight 1971) while Darcy's law describes the water flow (Childs & Collis-George 1950).

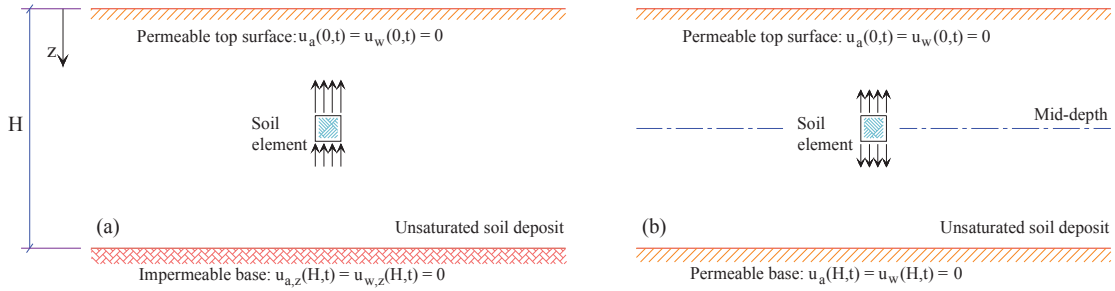

Figure 5.1. Single layer soil profile under: (a) the one-way drainage system and (b) the two-way drainage system

A single layer soil consisting of an infinite width and a definable thickness H is depicted in Figure 5.1. Considering the 1D consolidation theory, it is assumed that air and water only flow in the vertical direction only (i.e. z-direction). Figure 5.1(a) illustrates a typical one-way drainage system, in which the ground surface is pervious whereas the base is impervious to air and water. Figure 5.1(b), on the other hand, presents a two-way drainage system where the surface and base of the soil are pervious to both phases. Following Fredlund & Hasan (1979), the constitutive equations with respect to the air and water phases can be presented as shown below:

$$\frac{\partial\left(\frac{\Delta V_a}{V_0}\right)}{\partial t} = m_1^a \frac{\partial(\sigma_z - u_a)}{\partial t} + m_2^a \frac{\partial(u_a - u_w)}{\partial t} \quad [5\text{-}1a]$$

$$\frac{\partial\left(\frac{\Delta V_w}{V_0}\right)}{\partial t} = m_1^w \frac{\partial(\sigma_z - u_a)}{\partial t} + m_2^w \frac{\partial(u_a - u_w)}{\partial t} \quad [5\text{-}1b]$$

where σ_z is the total pressure (kPa); u_a and u_w are the excess pore-air and pore-water pressures (kPa), respectively; m_1^a and m_1^w are the coefficients of air and water volume change with respect to the change of net stress (kPa^{-1}), respectively; and m_2^a and m_2^w are the coefficients of air and water volume change with respect to the change of suction (kPa^{-1}), respectively. The change in air and water volumes can be described in

accordance with Fick's and Darcy's laws, respectively, while capturing the non-isothermal condition (Dakshanamurthy & Fredlund 1981), as follows:

$$\frac{\partial\left(\frac{\Delta V_a}{V_0}\right)}{\partial t} = \frac{k_a R\Theta}{gM\left(u_a^0+u_{atm}\right)}\left(\frac{\partial^2 u_a}{\partial z^2}\right) - \frac{n(1-S_r)}{\left(u_a^0+u_{atm}\right)}\left(\frac{\partial u_a}{\partial t}\right) + \frac{n(1-S_r)}{\Theta}\left(\frac{\partial \Theta}{\partial t}\right) \quad [5\text{-}2a]$$

$$\frac{\partial\left(\frac{\Delta V_w}{V_0}\right)}{\partial t} = \frac{k_w}{\gamma_w}\left(\frac{\partial^2 u_w}{\partial z^2}\right) \quad [5\text{-}2b]$$

where k_a and k_w are the air and water permeability coefficients (m/s), respectively; g is the gravitational acceleration (i.e. $9.81\ m/s^2$); u_a^0 is the initial pore-air and pore-water pressures (kPa); u_{atm} is the atmospheric pressure (kPa); R is the universal air constant (i.e. $8.3\ J/(mol.\ K)$); $\Theta = \theta^\circ + 273.16$, is the absolute temperature (K); θ° is the average temperature of the soil profile (i.e. $25^\circ C$); M is the molecular mass of air (i.e. $0.03\ kg/mol$); n is the porosity; S_r is the degree of saturation; and γ_w is the water unit weight (i.e. $9.81\ kN/m^3$).

Due to a constant applied load, the change in total stress with respect to time, as presented in Equations [5-1a] and [5-1b], is set as zero (i.e. $\partial\sigma_z/\partial t = 0$). Combining two pairs of Equations [5-1a] and [5-2a] as well as [5-1b] and [5-2b] results in PDEs for air and water flows, as presented by Dakshanamurthy & Fredlund (1981):

$$\frac{\partial u_a}{\partial t} + C_a\left(\frac{\partial u_w}{\partial t}\right) + C_\Theta\left(\frac{\partial \Theta}{\partial t}\right) + c_v^a\left(\frac{\partial^2 u_a}{\partial z^2}\right) = 0 \quad [5\text{-}3a]$$

$$\frac{\partial u_w}{\partial t} + C_w\left(\frac{\partial u_a}{\partial t}\right) + c_v^w\left(\frac{\partial^2 u_w}{\partial z^2}\right) = 0 \quad [5\text{-}3b]$$

where $C_a = \frac{1}{\left[\left(\frac{m_1^a}{m_2^a}-1\right)-\frac{n(1-S_r)}{m_2^a\left(u_a^0+u_{atm}\right)}\right]}$;

$c_v^a = \frac{k_a R\Theta}{gM}\frac{1}{\left[m_2^a\left(u_a^0+u_{atm}\right)\left(\frac{m_1^a}{m_2^a}-1\right)-n(1-S_r)\right]}$;

$C_\Theta = \frac{1}{\Theta\left[\frac{m_2^a\left(\frac{m_1^a}{m_2^a}-1\right)}{n(1-S_r)}-\frac{1}{u_a^0+u_{atm}}\right]}$;

$C_w = \left(\frac{m_1^w}{m_2^w}-1\right)$; and

$c_v^w = \frac{1}{m_2^w}\left(\frac{k_w}{\gamma_w}\right)$. [5-4]

Equations [5-3a] and [5-3b] can be further simplified as follows:

$$u_{a,t} + C_a u_{w,t} + C_\Theta \Theta_{,t} + c_v^a u_{a,zz} = 0 \quad [5\text{-}5a]$$

$$u_{w,t} + C_w u_{a,t} + c_v^w u_{w,zz} = 0 \quad [5\text{-}5b]$$

where $u_{a,t}$ and $u_{w,t}$ are the first order of PDEs of pore-air and pore-water pressures with respect to time, respectively; and $u_{a,zz}$ and $u_{w,zz}$ are the second order of PDEs of pore-air and pore-water pressures with respect to depth, respectively.

Equations [5-5a] and [5-5b] describe the continuous and independent dissipation of excess pore-air (u_a) and pore-water (u_w) pressures due to changes in temperature and constant loading. Solutions for Equations [5-5a] and [5-5b] would present functions of depth z and time t.

5.3. Analytical solution

A typical unsaturated soil is usually sophisticated in nature due to its nonlinear properties and intricate phase relationships within a soil element. Consideration of complex properties in the mathematical procedure may result in arduous numerical analyses, and analytical approaches may not be achievable. In order to alleviate difficulties in obtaining the analytical solution, following assumptions should be made:

(1) The soil stratum is homogeneous;
(2) The soil grains and water are incompressible;
(3) Flows of air and water phases are continuous and independent;
(4) Air diffusion through water is neglected;
(5) Soil deformation only occurs in the vertical direction (z-direction);
(6) Consolidation coefficients with respect to the air phase (C_a, C_Θ and c_v^a, respectively) and the water phase (C_w and c_v^w, respectively) are assumed to be constant.

Note that Assumption (6) may not be applicable to some cases. In engineering practice, an application of external load may result in changes in soil properties such as permeability coefficients (k_a and k_w), porosity (n) and degree of saturation (S_r) to name a few. This means the consolidation coefficients may eventually change, but it may be

acceptable to consider the consolidation coefficients to be constant during a transient process at a particular loading increment.

5.3.1. Boundary and initial conditions

The homogeneous boundary conditions, namely one-way and two-way drainage systems, are presented as follows:

(c) One-way drainage condition:

$$u_a(0,t) = u_w(0,t) = u_{a,z}(H,t) = u_{w,z}(H,t) = 0, \qquad t \geq 0 \qquad [5\text{-}6]$$

(d) Two-way drainage condition:

$$u_a(0,t) = u_w(0,t) = u_a(H,t) = u_w(H,t) = 0, \qquad t \geq 0 \qquad [5\text{-}7]$$

where H is the thickness of the soil. Referring to existing literature (Craig 2004; Venkatramaiah 2006; Coduto et al. 2011), the initial conditions for both one-way and two-way drainage systems are:

$$\begin{cases} u_a(z,0) = u_a^0 \\ u_w(z,0) = u_w^0 \end{cases}, \qquad z \in (0,H) \qquad [5\text{-}8]$$

where u_a^0 and u_w^0 are the initial excess pore-air and pore-water pressures (kPa). Note that the initial excess pore pressures are distributed uniformly along the soil depth, except for the permeable boundaries.

5.3.2. Excess pore pressure dissipation and settlement

First, the Fourier sine series can be introduced as general solutions for Equations [5-5a] and [5-5b]:

$$u_a(z,t) = \sum_{k=0}^{\infty} T_a^k(t) \sin(K\,z) \qquad [5\text{-}9a]$$

$$u_w(z,t) = \sum_{k=0}^{\infty} T_w^k(t) \sin(K\,z) \qquad [5\text{-}9b]$$

where $K = \frac{(2k+1)}{H}\frac{\pi}{2}$ for the one-way drainage condition ($k = 0, 1, 2, ...$); or

$= \frac{k\pi}{H}$ for the two-way drainage condition ($k = 0, 1, 2, ...$). [5-10]

In addition, the general thermal equation is proposed as functions of depth z and time t, as follows:

$$\Theta(z,t) = \sum_{k=0}^{\infty} \vartheta^k(t)\sin(K\,z) \qquad [5\text{-}11]$$

$$\text{where } \vartheta^k(t) = \frac{\int_0^H \Theta(z,t)\sin(K\,z)\,dz}{\int_0^H \sin^2(K\,z)\,dz}. \qquad [5\text{-}12]$$

Substituting Equations [5-9] – [5-12] into Equation [5-5] gives:

$$\left[T_{a,t}^k(t) + C_a T_{w,t}^k(t) + C_\Theta \vartheta_{,t}^k - c_v^a (K)^2 T_a^k(t)\right]\sum_{k=0}^{\infty}\sin(K\,z) = 0 \qquad [5\text{-}13a]$$

$$\left[T_{w,t}^k(t) + C_w T_{a,t}^k(t) - c_v^w (K)^2 T_w^k(t)\right]\sum_{k=0}^{\infty}\sin(K\,z) = 0 \qquad [5\text{-}13b]$$

Truncating Equation [5-13] results in:

$$T_{a,t}^k(t) + C_a T_{w,t}^k(t) + C_\Theta \vartheta_{,t}^k - c_v^a (K)^2 T_a^k(t) = 0 \qquad [5\text{-}14a]$$

$$T_{w,t}^k(t) + C_w T_{a,t}^k(t) - c_v^w (K)^2 T_w^k(t) = 0 \qquad [5\text{-}14b]$$

Applying the Laplace transformation to Equations [5-14a] and [5-14b] yields:

$$\left[s\overline{T}_a^k(s) - T_a^k(0)\right] + C_a\left[s\overline{T}_w^k(s) - T_w^k(0)\right] + C_\Theta\left[s\bar{\vartheta}^k(s) - \vartheta^k(0)\right] - c_v^a (K)^2\overline{T}_a^k(s) = 0 \qquad [5\text{-}15a]$$

$$\left[s\overline{T}_w^k(s) - T_w^k(0)\right] + C_w\left[s\overline{T}_a^k(s) - T_a^k(0)\right] - c_v^w (K)^2\overline{T}_w^k(s) = 0 \qquad [5\text{-}15b]$$

where $\overline{T}_a^k(s)$, $\overline{T}_w^k(s)$ and $\bar{\vartheta}^k(s)$ $(k = 1, 2, 3, ...)$ are Laplace transformed terms with the subjugate variable s. Solving for $\overline{T}_a^k(s)$ and $\overline{T}_w^k(s)$ and then presenting the results in a simplified matrix form as shown below:

$$\mathbf{T} = \mathbf{A} + \mathbf{B} \qquad [5\text{-}16]$$

$$\text{where } \mathbf{T} = \begin{Bmatrix} \overline{T}_a^k(s) \\ \overline{T}_w^k(s) \end{Bmatrix};$$

$$\mathbf{A} = \begin{Bmatrix} \dfrac{T_a^k(0)(C_w C_a - 1)s + c_v^w\left[C_a T_w^k(0) + T_a^k(0)\right](K)^2}{(C_w C_a - 1)s^2 + (c_v^w + c_v^a)(K)^2 s - c_v^w c_v^a (K)^4} \\ \dfrac{T_w^k(0)(C_w C_a - 1)s + c_v^a\left[C_w T_a^k(0) + T_w^k(0)\right](K)^2}{(C_w C_a - 1)s^2 + (c_v^w + c_v^a)(K)^2 s - c_v^w c_v^a (K)^4} \end{Bmatrix}; \text{ and}$$

$$\mathbf{B} = \begin{Bmatrix} \frac{C_\Theta[s - c_v^w(K)^2][s\bar{\vartheta}^k(s) - \vartheta^k(0)]}{(C_w C_a - 1)s^2 + (c_v^w + c_v^a)(K)^2 s - c_v^w c_v^a (K)^4} \\ -\frac{C_w C_\Theta[s\bar{\vartheta}^k(s) - \vartheta^k(0)]s}{(C_w C_a - 1)s^2 + (c_v^w + c_v^a)(K)^2 s - c_v^w c_v^a (K)^4} \end{Bmatrix}. \quad [5\text{-}17]$$

Besides, the terms $T_a^k(0)$ and $T_w^k(0)$ can be obtained using the orthogonality of sine functions as follows:

$$T_a^k(0) = \frac{\int_0^H [u_a(z,0)\sin(K z)]dz}{\int_0^H [\sin^2(K z)]dz} = \varpi^k u_a^0 \quad [5\text{-}18a]$$

$$T_w^k(0) = \frac{\int_0^H [u_w(z,0)\sin(K z)]dz}{\int_0^H [\sin^2(K z)]dz} = \varpi^k u_w^0 \quad [5\text{-}18b]$$

where $\varpi^k = \frac{2}{HK}$ for the one-way drainage condition ($k = 0, 1, 2, ...$); or

$= \frac{2[1-(-1)^k]}{HK}$ for the two-way drainage condition ($k = 0, 1, 2, ...$). [5-19]

Combining Equations [5-16] – [5-19] and then taking the Laplace inverse gives:

$$\mathcal{L}^{-1}\{\mathbf{T}\} = \mathcal{L}^{-1}\{\mathbf{A}\} + \mathcal{L}^{-1}\{\mathbf{B}\} \quad [5\text{-}20]$$

where $\mathcal{L}^{-1}\{\mathbf{T}\} = \begin{Bmatrix} T_a^k(t) \\ T_w^k(t) \end{Bmatrix}$;

$$\mathcal{L}^{-1}\{\mathbf{A}\} = \begin{Bmatrix} \frac{\varpi^k\left[\Omega\left(e^{\alpha_1^k t} - e^{\alpha_2^k t}\right) + \Psi\left(e^{\alpha_1^k t} + e^{\alpha_2^k t}\right)\right]}{2\eta} \\ \frac{\varpi^k\left[\Omega'\left(e^{\alpha_1^k t} - e^{\alpha_2^k t}\right) + \Psi'\left(e^{\alpha_1^k t} + e^{\alpha_2^k t}\right)\right]}{2\eta} \end{Bmatrix};$$

$\eta = [(c_v^w - c_v^a)^2 + 4c_v^w c_v^a C_w C_a]^{\frac{1}{2}}$;

$\Omega = (c_v^a - c_v^w)u_a^0 - 2c_v^w C_a u_w^0$; $\Omega' = (c_v^w - c_v^a)u_w^0 - 2c_v^a C_w u_a^0$;

$\Psi = \eta u_a^0$; $\Psi' = \eta u_w^0$;

$\alpha_1^k = \frac{1}{2}\left(\frac{c_v^w + c_v^a + \eta}{1 - C_w C_a}\right)(K)^2$; and $\alpha_2^k = \frac{1}{2}\left(\frac{c_v^w + c_v^a - \eta}{1 - C_w C_a}\right)(K)^2$. [5-21]

It should be noted that the term $\mathcal{L}^{-1}\{\mathbf{B}\}$ follows different thermal equations, which will be discussed in a subsequent section. Substituting Equation [5-20] back into Equation [5-9] would provide solutions for excess pore pressure dissipation:

$$u_a(z,t) = \sum_{k=0}^{\infty} \left\{ \frac{\varpi^k \left[\Omega \left(e^{\alpha_1^k t} - e^{\alpha_2^k t} \right) + \Psi \left(e^{\alpha_1^k t} + e^{\alpha_2^k t} \right) \right]}{2\eta} + \mathcal{L}^{-1}\{\mathbf{B}\} \right\} \sin(K z) \quad [5\text{-}22a]$$

$$u_w(z,t) = \sum_{k=0}^{\infty} \left\{ \frac{\varpi^k \left[\Omega' \left(e^{\alpha_1^k t} - e^{\alpha_2^k t} \right) + \Psi' \left(e^{\alpha_1^k t} + e^{\alpha_2^k t} \right) \right]}{2\eta} + \mathcal{L}^{-1}\{\mathbf{B}\} \right\} \sin(K z) \quad [5\text{-}22b]$$

Note that the term $\mathcal{L}^{-1}\{\mathbf{B}\}$ equals zero when the temperature becomes constant. Thus, Equation [5-22], as presented under the non-isothermal condition, can convert to excess pore pressure equations under the isothermal condition, as shown below:

$$u_a(z,t) = \sum_{k=0}^{\infty} \left\{ \frac{\varpi^k \left[\Omega \left(e^{\alpha_1^k t} - e^{\alpha_2^k t} \right) + \Psi \left(e^{\alpha_1^k t} + e^{\alpha_2^k t} \right) \right]}{2\eta} \right\} \sin(K z) \quad [5\text{-}23a]$$

$$u_w(z,t) = \sum_{k=0}^{\infty} \left\{ \frac{\varpi^k \left[\Omega' \left(e^{\alpha_1^k t} - e^{\alpha_2^k t} \right) + \Psi' \left(e^{\alpha_1^k t} + e^{\alpha_2^k t} \right) \right]}{2\eta} \right\} \sin(K z) \quad [5\text{-}23b]$$

On the other hand, Fredlund et al. (2012), and Fredlund & Hasan (1979) introduced the constitutive model for the soil structure linking stress and deformation state variables as follows:

$$\frac{\partial \varepsilon_v}{\partial t} = m_1^s \frac{\partial (\sigma - u_a)}{\partial t} + m_2^s \frac{\partial (u_a - u_w)}{\partial t} \quad [5\text{-}24]$$

where ε_v is the volumetric strain; m_1^s is the coefficient of volume change of soil particle with respect to the change in the net stress (kPa^{-1}); and m_2^s is the coefficient of volume change of soil particle with respect to the change in suction (kPa^{-1}). The volumetric strain can be determined by integrating Equation [5-24] against time t while considering the constant loading condition (i.e. $\partial\sigma/\partial t = 0$), resulting in:

$$\varepsilon_v(z,t) = (m_2^s - m_1^s)[u_a(z,t) - u_a^0] - m_2^s[u_w(z,t) - u_w^0] \quad [5\text{-}25]$$

Then, the settlement of unsaturated soil layer can be obtained by:

$$S(t) = \int_0^H \varepsilon_v(z,t)dz = (m_2^s - m_1^s)\left[\int_0^H u_a(z,t)dz - Hu_a^0\right] - m_2^s\left[\int_0^H u_w(z,t)dz - Hu_w^0\right] \quad [5\text{-}26]$$

Equation [5-26] predicts the time-dependent settlement of unsaturated soil deposit. According to Fredlund et al. (Fredlund et al. 2012), it should be noted that the volume change of soil particles should satisfy $m_1^s = m_1^w + m_1^a$ and $m_2^s = m_2^w + m_2^a$.

5.3.3. Thermal equations

Temperature variations can be simulated as functions of depth z and time t. In this study, it is assumed that the temperature decreases with depth while varying linearly, exponentially or diurnally with time. Three adopted thermal equations are presented as follows:

Linear: $$\Theta(z,t) = 273.16 + (\theta^\circ + a\,t)\left(1 - \xi\,\frac{z}{H}\right) \quad [5\text{-}27a]$$

Exponential: $$\Theta(z,t) = 273.16 + [\theta^\circ + A\,(1 - e^{-b\,t})]\left(1 - \xi\,\frac{z}{H}\right) \quad [5\text{-}27b]$$

Diurnal sine wave: $$\Theta(z,t) = 273.16 + \left\{\theta^\circ + A_d \sin\left[\omega_d(t - t_0) - \frac{z}{d_d} - \frac{\pi}{2}\right] e^{-\frac{z}{d_d}}\right\} \quad [5\text{-}27c]$$

where 'a' is the thermal parameter presented in the linear thermal equation (°C/s); 'b' is the thermal parameter presented in the exponential thermal equation (s^{-1}); A is the dimensionless parameter presented in the exponential thermal equation; ξ is the gradient that controls the linear distribution of temperature throughout the soil profile; A_d is the amplitude of the surface temperature fluctuation (°C); $d_d = (2D_h/\omega_d)^{1/2}$, is the characteristic depth (m); ω_d is the angular frequency for the diurnal sine wave (s^{-1}); D_h is the heat diffusivity (m^2/s); t_0 is the time lag from an arbitrary starting time (s).

Variations in soil temperature are primarily induced by the air temperature and heat from solar radiation. Referring to Hillel (2003), in frost-free areas the soil temperature profile may vary from season to season, particularly the temperature increases with depth during winter and generally decreases with depth during summer. Temperature distributions throughout the soil profile in typical seasons are presented in Figure 5.2. For the sake of simplicity, this study only examines the temperature decreasing with depth. In relation, the parameter ξ, as adopted in Equations [5-27a] and [5-27b], would range from 0 to 1, simulating a linear reduction of temperature along the soil depth. It

should be noted that the soil temperature profile is uniform with depth when $\xi = 0$, or no thermal impact on the base of soil is reported when $\xi = 1$.

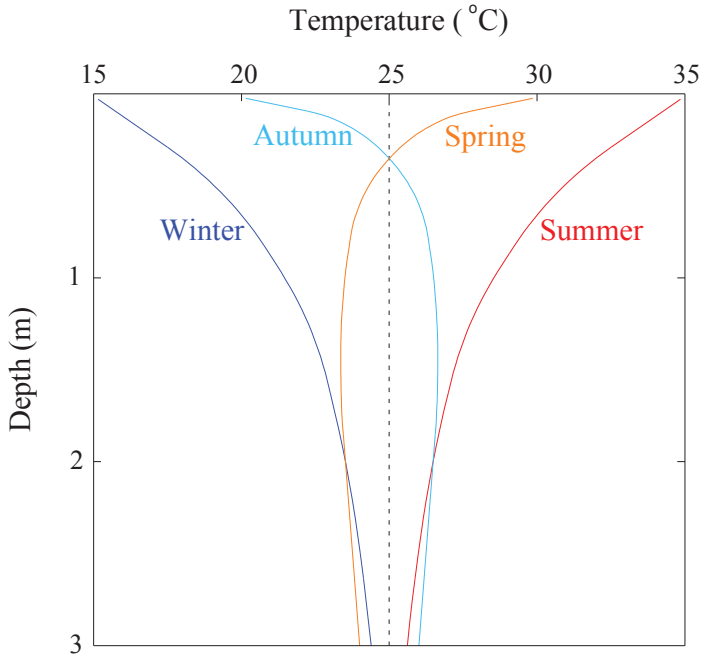

Figure 5.2. Temperature distributions along depth (modified after Hillel 2003)

On the other hand, in real practice, the soil temperature is prone to fluctuate diurnally due to a regular periodic succession of days and nights (Marshall et al. 1996; Wu & Nofziger 1999; Hillel 2003). In this study, assuming that climatic irregularities (e.g. rainstorms, drought, cloudiness etc.) are neglected, Equation [5-27c] adopts the sinusoidal function recommended by Hillel (2003) to present the periodic temperature wave. Since heat is conducted throughout the soil profile at a very slow rate, the soil temperature would experience the damping and retarding phenomena at each succeeding depth (Hillel 2003). By examining Equation [5-27c], at a particular depth z, the soil temperature reduces by a factor e^{z/d_d} (damping) and the peak temperature is delayed by z/d_d (retarding) compared to that at the ground surface. Time-dependent linear, exponential and diurnal temperature variations at various depths are depicted in Figure 5.3.

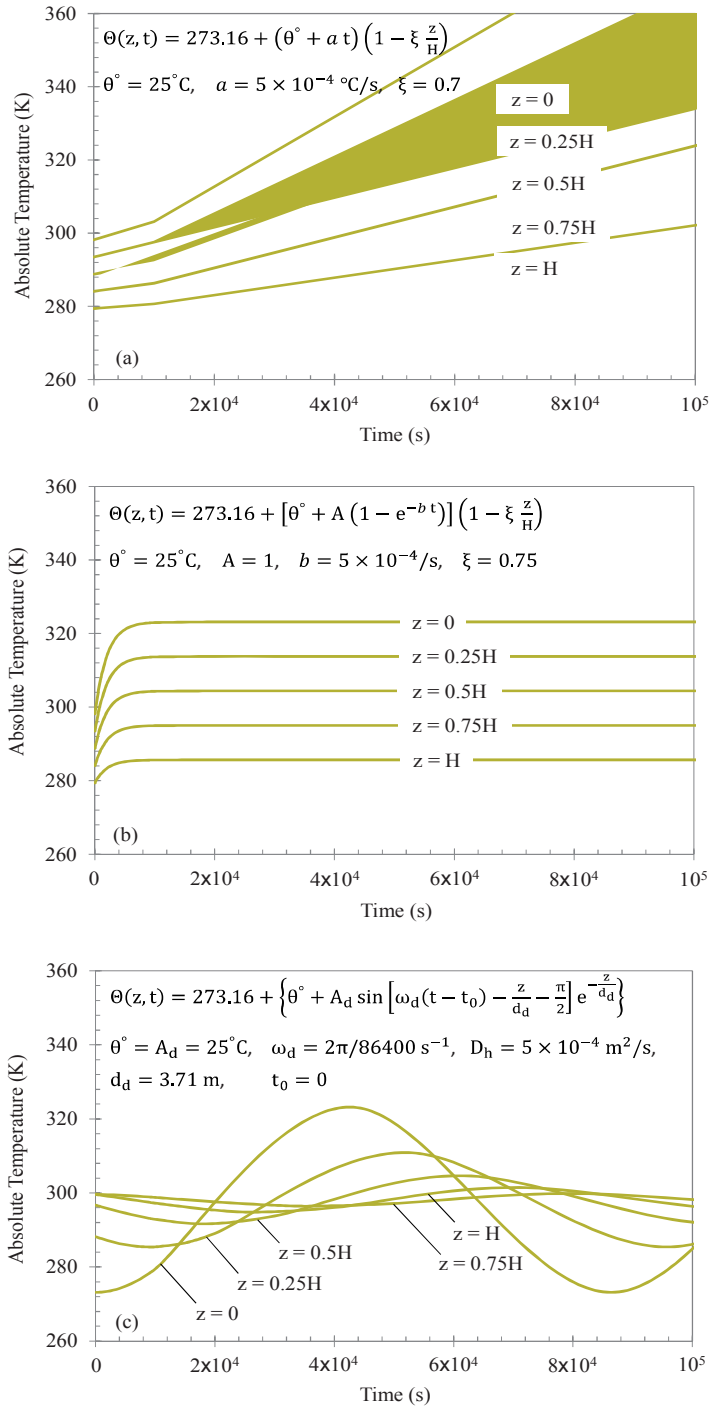

Figure 5.3. Simulated temperature changes with depth while considering (a) linear, (b) exponential and (c) diurnal variations with time

By alternatively substituting Equations [5-27a] – [5-27c] into Equation [5-11], the term $\mathcal{L}^{-1}\{\mathbf{B}\}$ then can be determined through the analytical procedure presented in

Equations [5-11] – [5-22]. Full solutions for predicting excess pore pressure dissipation rates under non-isothermal conditions are presented in Appendix B.

5.4. Examples

Two main examples are presented in this study, both of which investigate the effect of temperature variation only and combined effects of temperature and constant loading on 1D consolidation of unsaturated soil deposit. Example 1 mainly studies excess pore-air and pore-water dissipation and consolidation settlement due to the time-dependent linear, exponential and diurnal temperature simulations. Example 2, on the other hand, highlights the influence of thermal parameters, presented in Equations [27a] – [27c], on the dissipation rates and settlement. Based on the existing literature (Qin et al. 2008; Shan et al. 2012; Zhou et al. 2014), the properties of unsaturated soil are as follows:

- Material properties: $m_1^s = -2.5 \times 10^{-4}\ \text{kPa}^{-1}$, $m_2^s = 0.4m_1^s$, $m_1^w = 0.2m_1^s$, $m_2^w = 4m_1^w$, $n = 0.50$, $S_r = 80\%$, $k_w = 10^{-10}\ \text{m/s}$, $k_a/k_w = 10$, $H = 10\text{m}$; [5-28]

- Physical properties: $R = 8.314\ \text{J/(mol. K)}$, $M = 0.029\ \text{kg/mol}$, $\Theta = (\theta^\circ + 273.16)\ \text{K}$, $\theta^\circ = 25℃$, $u_{atm} = 100\ \text{kPa}$; [5-29]

- Initial stresses: $u_a^0 = 20\ \text{kPa}$, $u_w^0 = 40\ \text{kPa}$, $q_0 = 100\ \text{kPa}$. [5-30]

Soil properties provided in Equations [5-28] – [5-30] are used to obtain consolidation coefficients for the air phase (C_a, C_Θ and c_v^a) and for the water phase (C_w and c_v^w). Note that Equation [5-30] is only applicable to the consolidation process, in which combined effects of temperature and constant loading are considered. A sudden application of load results in an instantaneous compression, which in turn induces excess pore pressures within a soil. According to Fredlund et al. (2012), the constant load q_0 (i.e. 100kPa) applied to the ground surface generates an initial excess pore-air pressure (u_a^0) of 20kPa and an initial excess pore-water pressure (u_w^0) of 40kPa. When only the temperature

variation is considered and no load is applied to the soil, both initial excess pore pressures would be equal to zero and time-dependent changes in excess pore pressures only correspond to changes in temperature.

For the sake of generality, when investigating the effect of temperature variation only, the normalised pore pressures, u_a/u_{atm} and u_w/u_{atm}, and normalised soil deformation S^* (i.e. $S^* = S(t)/(m_1^s u_{atm} H)$) are adopted. On the other hand, when combined effects of temperature and constant loading are considered, normalised excess pore pressures, u_a/u_a^0 and u_w/u_w^0, and normalised settlement S^* (i.e. $S^* = S(t)/(m_1^s q_0 H)$) are obtained. Moreover, results and discussions in each example are only based on the one-way drainage boundary system.

5.4.1. Example 1

5.4.1.1. Linear temperature variation

In this section the linear thermal parameter $a = 5 \times 10^{-4}\ ℃/s$ and the gradient $\xi = 0.75$ are used for evaluation and further analyses. Thus, Equation [5-27a] with adopted parameters can be incorporated in the analytical procedure to obtain Equation [B-1] in Appendix B.

Based on Equation [B-1], Figures 5.4(a) and 5.4(b) illustrate changes in pore-air (u_a/u_{atm}) and pore-water (u_w/u_{atm}) pressures at various depths, respectively, influenced by the time-dependent linear temperature while excluding the external applied load. By adopting a logarithmic time-scale, it can be observed that the pore-air pressures begin to increase rapidly at about 10^4s due to a significant increase in temperature, as shown in Figure 5.4(a). Referring to the ideal gas law, the increasing heat would lead to a notable reduction in the density of air (ρ_a), which in turn causes the air to expand within the soil. Under an undrained condition, the pore-air pressure increases considerably as a result of expansion of air in the soil. Initially, the pore-air pressures near the ground surface (i.e. $z \leq 0.5H$) tend to increase more quickly compared to those at lower depths. Since the permeable surface facilitates the dissipation process, the dissipation of excess pore-air pressure occurring near the surface would subsequently decelerate the increase in the pore pressure. After 10^6s, at any depth, the excess pore-air pressure curves remain unchanged while the temperature

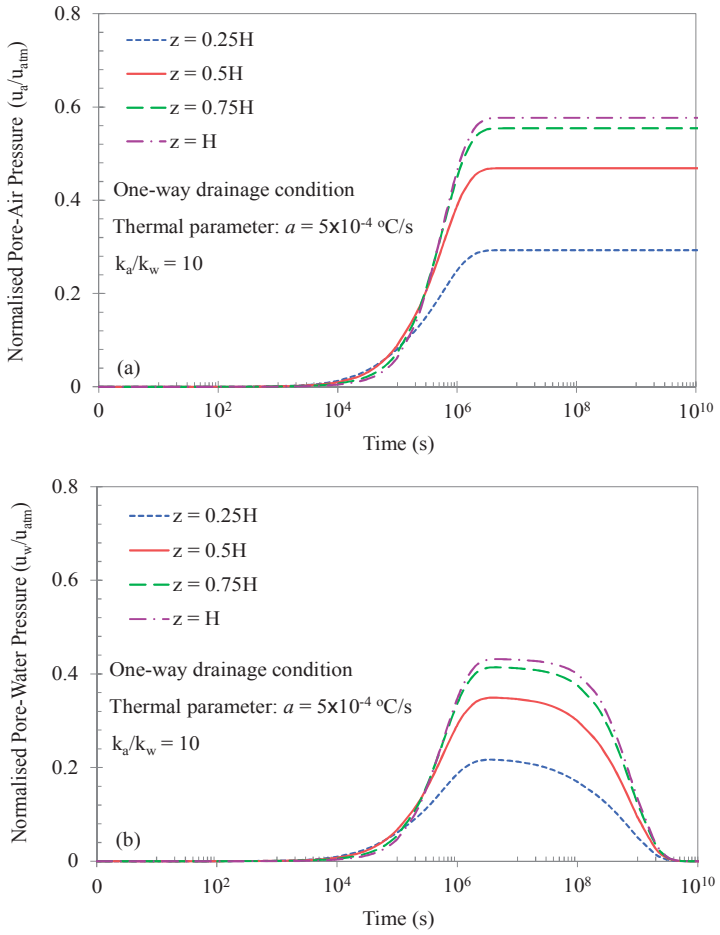

Figure 5.4. Changes in (a) pore-air and (b) pore-water pressures induced by the effect of time-dependent linear temperature

continues to increase, indicating that the dissipation rate and increase rate due to heat are counterbalanced. As shown in Figure 5.4(b), the pore-water pressures also start to increase rapidly at about 10^4s. Similar to Figure 5.4(a), the pore-water pressure near the ground surface initially increases at a quicker rate and then decelerates due to the significant dissipation. The excess pore-water pressure curves at various depths eventually dissipate at almost the same time (i.e. after 10^9s). It should be noted that the non-isothermal effect on pore-air and pore-water pressures is less evident with depth.

Figures 5.5(a) and 5.5(b) demonstrate changes in excess pore-air (u_a/u_a^0) and pore-water (u_w/u_w^0) pressures at various depths, respectively, induced by combined effects of time-dependent linear temperature and applied external load (q_0). In general, it can be observed that excess pore-air and pore-water pressures increase noticeably after

about 10^4s. At the later stages of consolidation, the excess pore-air pressures remain constant since the dissipation rate and increase rate due to the increasing temperature are counterbalanced (Figure 5.5(a)). In contrary, the excess pore-water pressures at various depths are fully dissipated at almost the same time (i.e. after 10^9s) (Figure 5.5(b)).

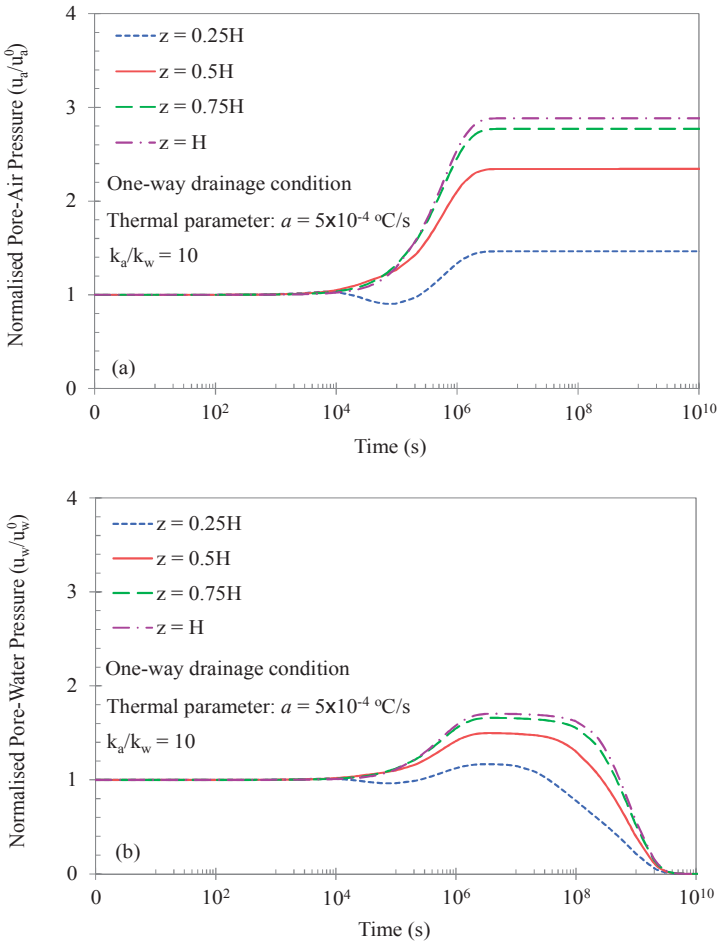

Figure 5.5. Changes in (a) excess pore-air and (b) excess pore-water pressures induced by combined effects of time-dependent linear temperature and constant loading

Figures 5.6(a) and 5.6(b) present the deformation of unsaturated soil stratum induced by the effect of time-dependent linear temperature variation (i.e. $S^* = S(t)/(m_1^s u_{atm} H)$) and by combined effects of temperature change and external applied load (q_0) (i.e. $S^* = S(t)/(m_1^s q_0 H)$), respectively. As shown in Figure 5.6(a), the soil begins to expand after 10^4s due to the significantly increasing temperature. The expansion of soil is

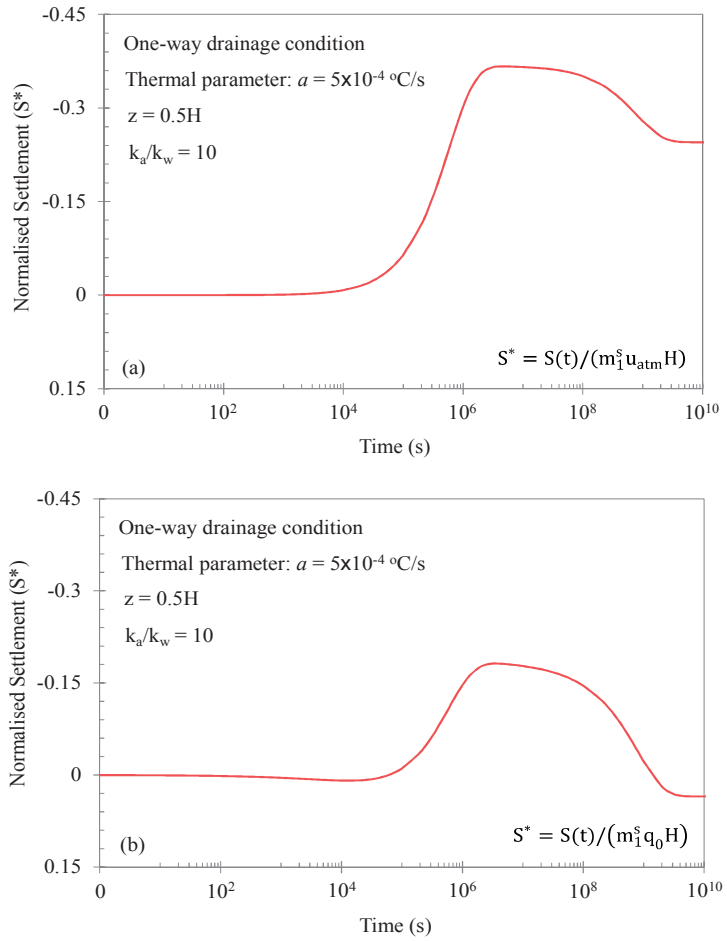

Figure 5.6. Deformation of soil due to (a) the time-dependent linear temperature only and (b) the time-dependent linear temperature and constant loading

governed by increases in pore-air and pore-water pressures. After about 10^6s, the soil gradually retracts as the excess pore-water pressure dissipates and only excess pore-air pressure governs the soil deformation during this stage. No further change in the soil stratum can be observed after approximately 10^9s. Similarly, Figure 5.6(b) first illustrates a notable expansion of soil due to increases in excess pore pressures. The soil later settles as the excess pore-water pressure diminishes whereas the excess pore-air pressure remains constant at the later stages of consolidation. It is noted that the soil expansion due to heat would be much attenuated by the applied constant load (q_0), which eventually results in soil settlement. In the adopted case, the consolidation settlement completes after about 10^9s.

5.4.1.2. Exponential temperature variation

In this study, thermal parameters $A = 1$, $b = 5 \times 10^{-4}/s$ and $\xi = 0.75$ are adopted for further investigation. Equation [5-27b] with the adopted parameters can be incorporated in the analytical procedure to obtain Equation [B-3], as presented in Appendix B.

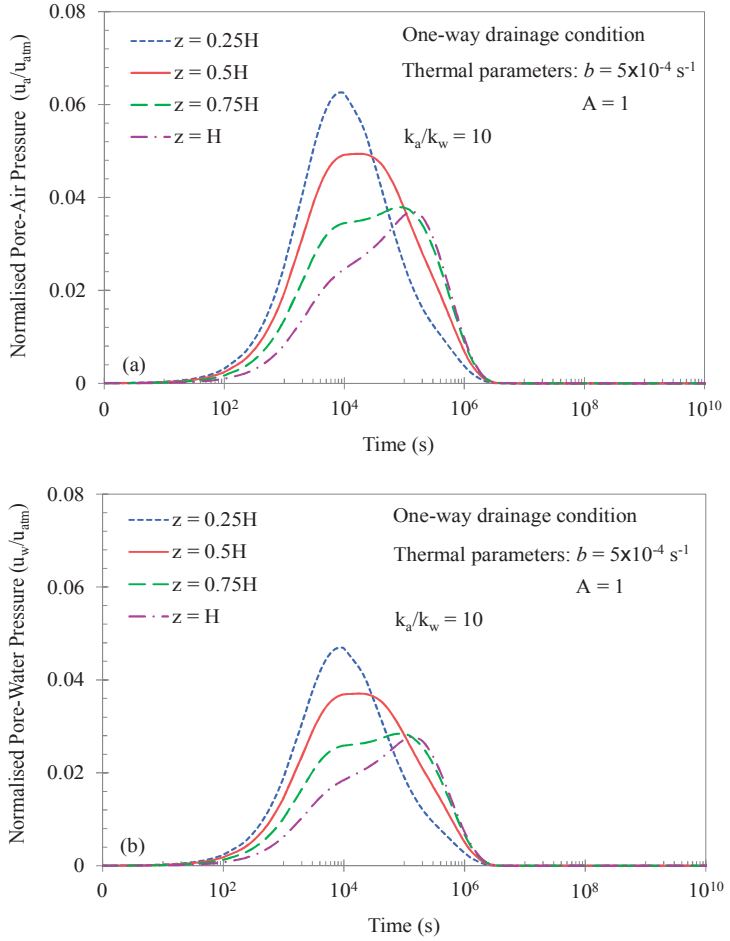

Figure 5.7. Changes in (a) pore-air and (b) pore-water pressures induced by the effect of time-dependent exponential temperature

As estimated from Equation [B-3], Figures 5.7(a) and 5.7(b) depict changes in pore-air (u_a/u_{atm}) and pore-water (u_w/u_{atm}) pressures at various depths, respectively, caused by the time-dependent exponential temperature variation while excluding the external applied load. As observed, the increasing temperature results in notable increases in pore-air and pore-water pressures, in particular pore pressures near the ground surface (i.e. $z \leq 0.5H$) tend to increase faster than those at lower depths. When

the temperature approaches the asymptote (i.e. $\theta^{\circ}_{max} = 50°C$), pore pressures near the surface would attain the peak values at about 10^4s and then dissipate a short time afterwards. In contrast, it takes longer time for the pore-air and pore-water pressures at lower depths to achieve the peak values prior to the dissipation. It should be noted that the permeable surface of unsaturated soil facilitates the drainage of air and water, resulting in significant dissipation at the top soil deposit. Thus, excess pore pressures near the ground surface are prone to dissipate more quickly. However, the dissipation completes at almost the same time (i.e. after 10^6s) regardless of different depths.

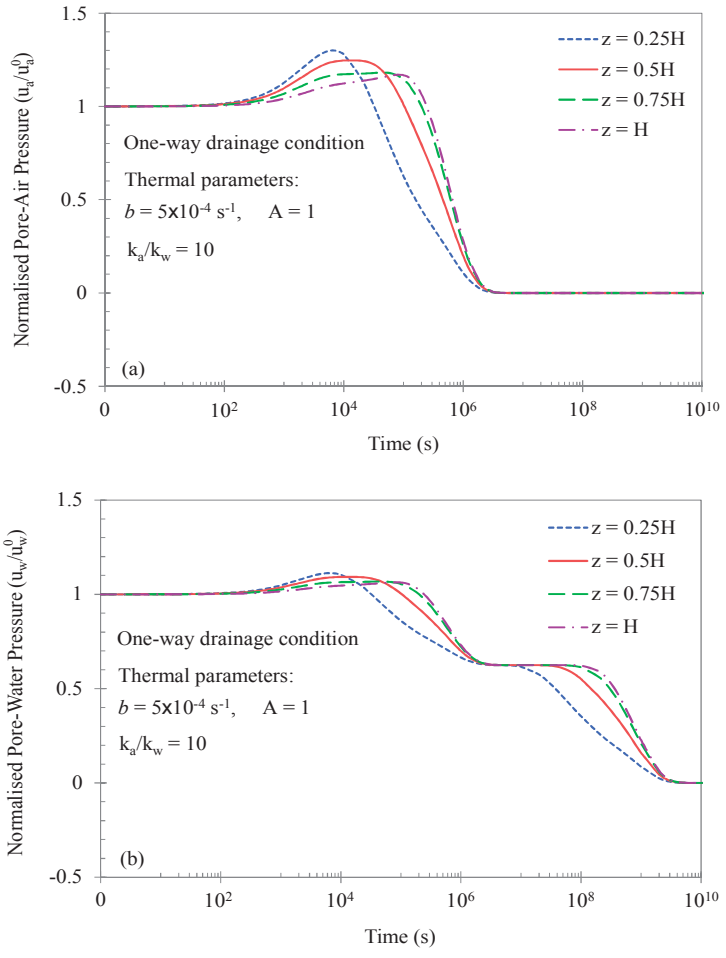

Figure 5.8. Changes in (a) excess pore-air and (b) excess pore-water pressures induced by combined effects of time-dependent exponential temperature and constant loading

On the other hand, Figures 5.8(a) and 5.8(b) present changes in excess pore-air (u_a/u_a^0) and pore-water (u_w/u_w^0) pressures at various depths, respectively, induced by

combined effects of time-dependent exponential temperature variation and external applied load (q_0). It is observed that the exponentially increasing temperature induces moderate increases in excess pore-air and pore-water pressures at the early stages of consolidation. During these stages, it takes shorter time for excess pore pressures near the ground surface to attain the peak values as the temperature approaches the asymptote. It is also worth mentioning that the peak values may reduce with depth. Since there are no temperature changes after 10^4s, excess pore pressures would eventually dissipate resembling to those under the isothermal condition.

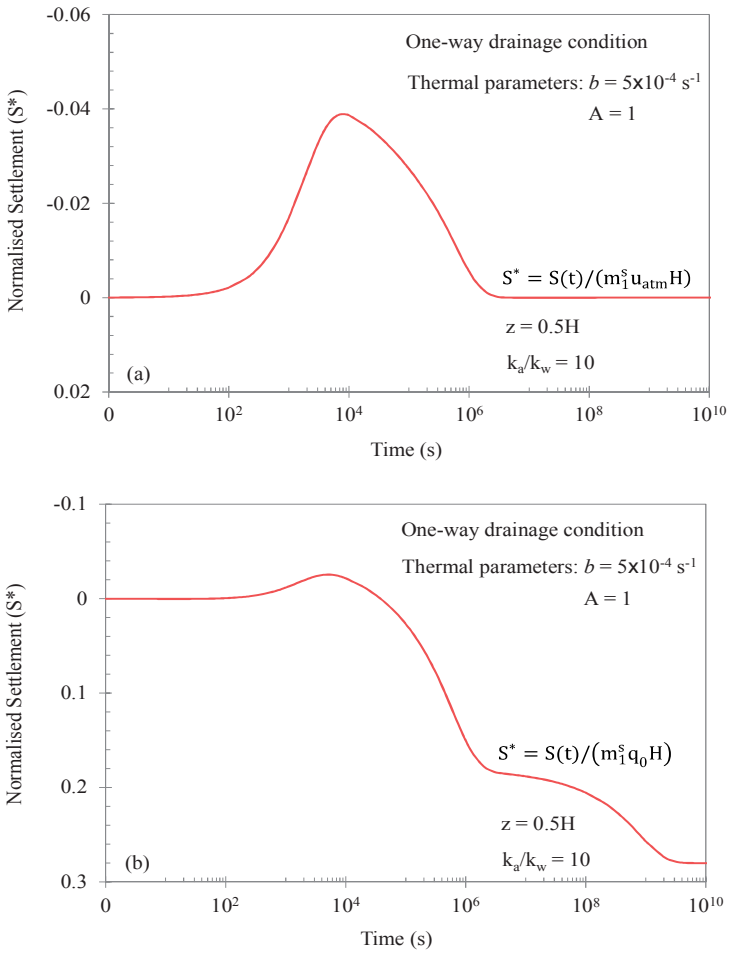

Figure 5.9. Deformation of soil due to (a) the time-dependent exponential temperature only and (b) the time-dependent exponential temperature and constant loading

Figures 5.9(a) and 5.9(b) show the deformation of unsaturated soil stratum induced by the effect of time-dependent exponential temperature variation (i.e. $S^* =$

$S(t)/(m_1^s u_{atm} H)$) and by combined effects of temperature change and external applied load (q_0) (i.e. $S^* = S(t)/(m_1^s q_0 H)$), respectively. As observed in Figure 5.9(a), the soil initially expands as the temperature increases, and then retracts to its original thickness once the temperature becomes constant. This is due to the fact that the soil deformation is ascribed initially to increases in pore pressures and subsequently to the dissipation of excess pore pressures. When the constant loading is considered in the analysis, a slight expansion of soil can be observed during the early stages of consolidation, as shown in Figure 5.9(b). It can be noted that the settlement pattern resembles to that under the isothermal condition when the temperature remains unchanged.

5.4.1.3. Diurnal temperature variation

This example adopts parameters $A_d = 25℃$, $\omega_d = 2\pi/86400\ s^{-1}$, $D_h = 5 \times 10^{-4}\ m^2/s$, and $t_0 = 0$ for the investigation. Based on the adopted values of angular frequency ω_d and heat diffusivity D_h, the characteristic depth d_d is estimated to be $3.71m$. Thus, Equation [5-27c] with the above mentioned parameters can be incorporated in the analytical procedure to obtain Equation [B-5], as presented in Appendix B.

Referring to Equation [B-5], Figures 5.10(a) and 5.10(b) demonstrate changes in pore-air (u_a/u_{atm}) and pore-water (u_w/u_{atm}) pressures at various depths, respectively, induced by the time-dependent diurnal temperature variation while excluding the external loading. It can be observed that both excess pore-air and pore-water pressure patterns consist of harmonic oscillations, corresponding to a regular succession of days and nights. These oscillations are characterised by the periodic absorption and release of heat throughout the soil profile. As the heat transmission through the soil is a relatively slow process, the soil temperature wave would experience the damping and retarding phenomena (Hillel 2003), which are also clearly captured in pore-air and pore-water pressure curves. As observed, the peak pore pressures at lower depths are damped and shifted progressively in time. Both pore pressure patterns exhibit indefinite oscillations due to the diurnal temperature wave.

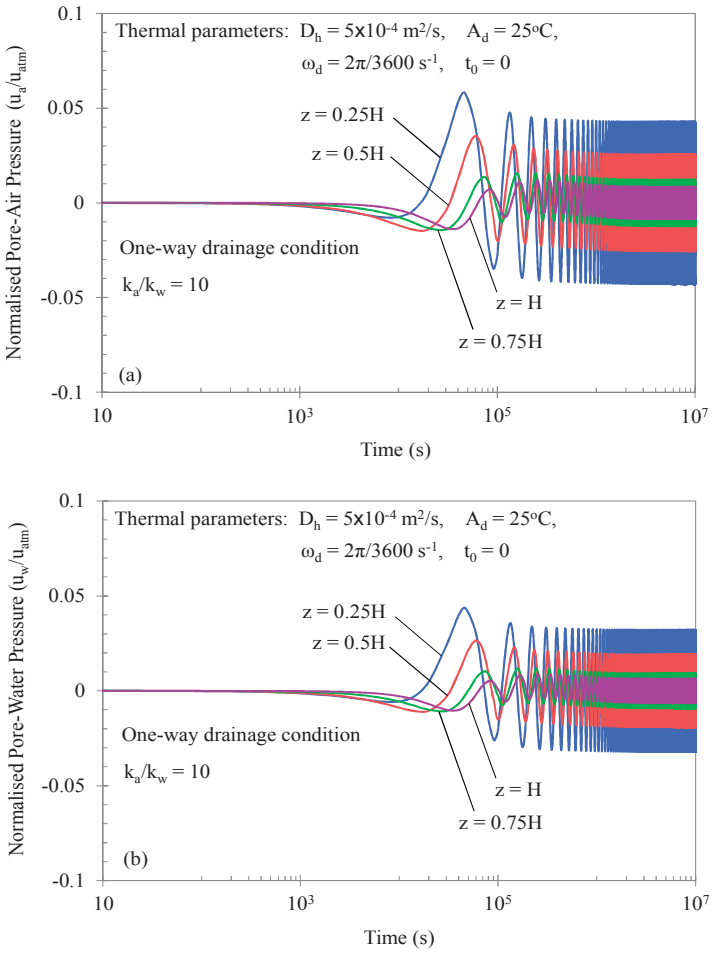

Figure 5.10. Changes in (a) pore-air and (b) pore-water pressures induced by the effect of time-dependent diurnal temperature variation

Figures 5.11(a) and 5.11(b) illustrate changes in excess pore-air (u_a/u_a^0) and pore-water (u_w/u_w^0) pressures at various depths, respectively, caused by combined effects of time-dependent diurnal temperature variation and external loading (q_0). It can be observed that both excess pore-air and pore-water pressure curves oscillate indefinitely while dissipating gradually with time. Similar to Figure 5.10, the amplitude of excess pore pressure oscillation decreases (damping) whereas the phase lag of peak pore pressure increases (retarding) at each succeeding depth.

Figures 5.12(a) and 5.12(b) depict the deformation of unsaturated soil stratum induced by the effect of time-dependent diurnal temperature variation (i.e. $S^* = S(t)/(m_1^s u_{atm} H)$) and by combined effects of temperature variation and external loading (q_0) (i.e. $S^* = S(t)/(m_1^s q_0 H)$), respectively. It is predicted that the deformation

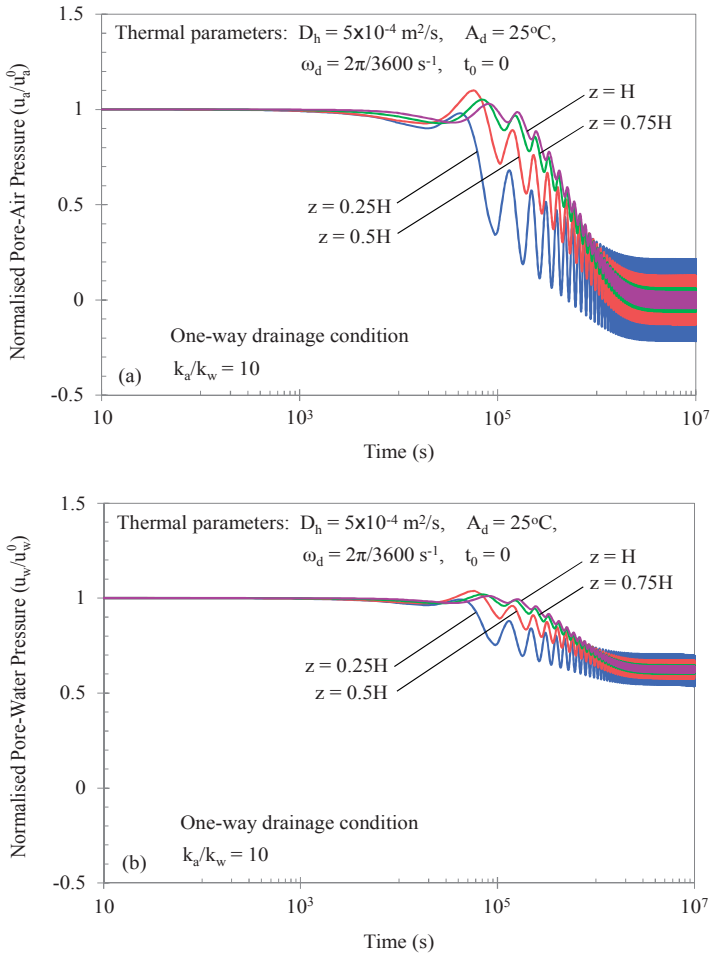

Figure 5.11. Changes in (a) excess pore-air and (b) excess pore-water pressures induced by combined effects of time-dependent diurnal temperature variation and constant loading

of soil is mainly governed by indefinite changes in pore-air and pore-water pressures (Figure 5.12(a)). In particular, the soil continuously expands and retracts corresponding to the periodic temperature waves. On the other hand, when the temperature wave and constant loading are considered in the analysis, the settlement curve would increase and fluctuate simultaneously (Figure 5.12(b)).

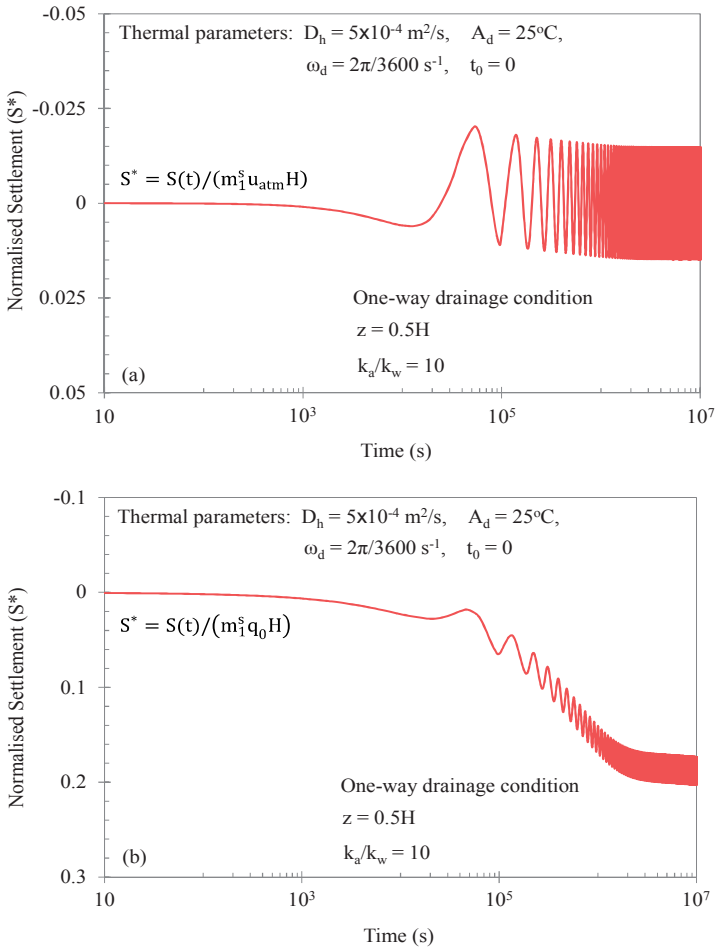

Figure 5.12. Deformation of soil due to (a) the time-dependent diurnal temperature variation only and (b) the time-dependent diurnal temperature variation and constant loading

5.4.2. Example 2

5.4.2.1. Effects of linear thermal parameter 'a'

In this parametric study, different values for the linear thermal parameter 'a', ranging from 2.5×10^{-4} to 7.5×10^{-4} ℃/s, are adopted for the analysis. Moreover, the 1D consolidation behaviours of unsaturated soil deposit, in terms of excess pore pressures and consolidation settlement, are investigated at $z = 0.5H$.

The significant effect of thermal parameter 'a' on changes in pore-air (u_a/u_{atm}) and pore-water (u_w/u_{atm}) pressures are presented in Figures 5.13(a) and 5.13(b), respectively, while excluding the external loading in the analysis. As observed, higher

values of 'a' would accelerate the linear increase in temperature, which in turn leads to more pronounced increases in pore-air and pore-water pressures. It is also predicted that pore pressures tend to increase more quickly with increasing 'a'. After about 10^6s, the excess pore-air pressures attain the maximum values and then remain constant. Obviously, the maximum values become larger as 'a' increases. Excess pore-water pressures, on the other hand, initially increase due to the increasing temperature but later fully dissipate at almost the same time (i.e. after 10^9s) regardless of values of 'a'.

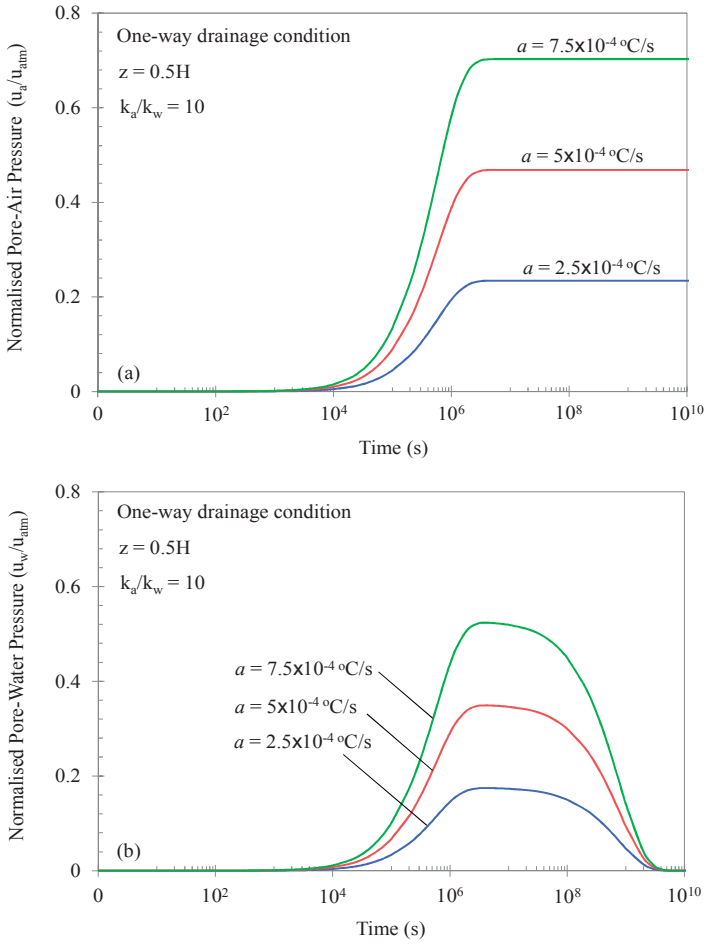

Figure 5.13. Effect of linear thermal parameter 'a' on changes in (a) pore-air and (b) pore-water pressures

Figures 5.14(a) and 5.14(b), on the other hand, illustrate the influence of thermal parameter 'a' on changes in excess pore-air (u_a/u_a^0) and pore-water (u_w/u_w^0) pressures, respectively, while considering the external applied load (q_0) in the analysis. It is obvious that higher values of 'a' would lead to more pronounced increases in excess

pore-air and pore-water pressures after 10^4s. Similar to Figure 5.13, at the later stages of consolidation, the excess pore-air pressures remain unchanged whereas excess pore-water pressures gradually dissipate and are fully dissipated after about 10^9s irrespective of adopted values of 'a'.

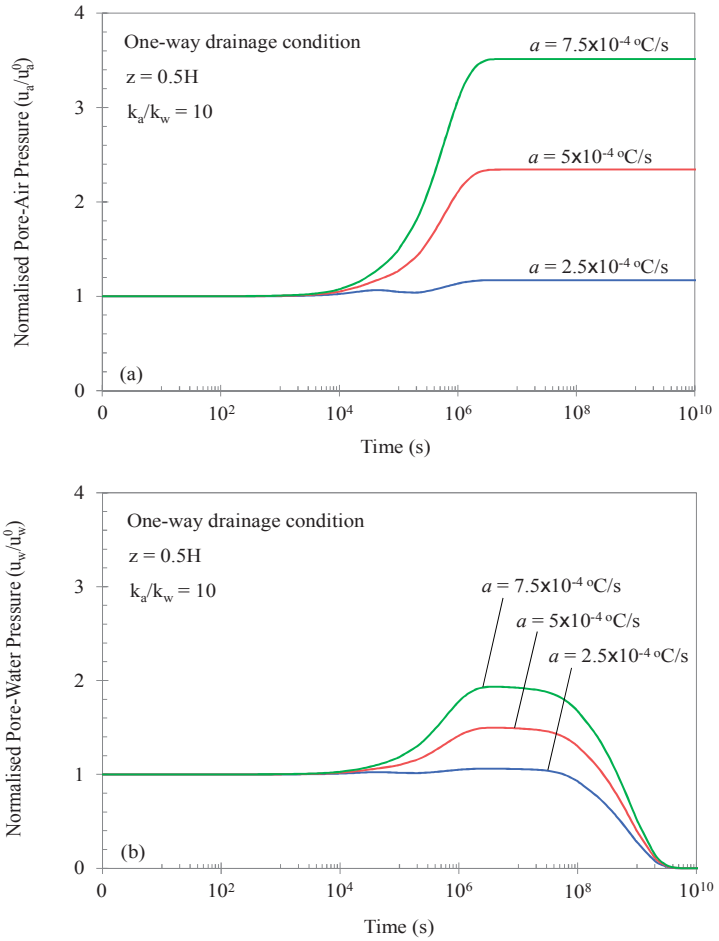

Figure 5.14. Combined effects of linear thermal parameter 'a' and constant loading on changes in (a) excess pore-air and (b) excess pore-water pressures

The effect of thermal parameter 'a' on the deformation of unsaturated soil deposit, including or excluding the external applied load (q_0) is investigated in Figure 5.15. When the applied load is discarded in the analysis, the soil expands more significantly since 'a' increases, as presented in Figure 5.15(a). After 10^6s, the soil begins to retract due to the dissipation of excess pore-water pressure. It can be noted that the retraction in the soil is less considerable when 'a' decreases. No further deformation of unsaturated soil occurs after about 10^9s. When the constant loading is considered, similar soil

deformation is predicted in Figure 5.15(b), in which the soil first expands and then retracts more considerably with increasing 'a'.

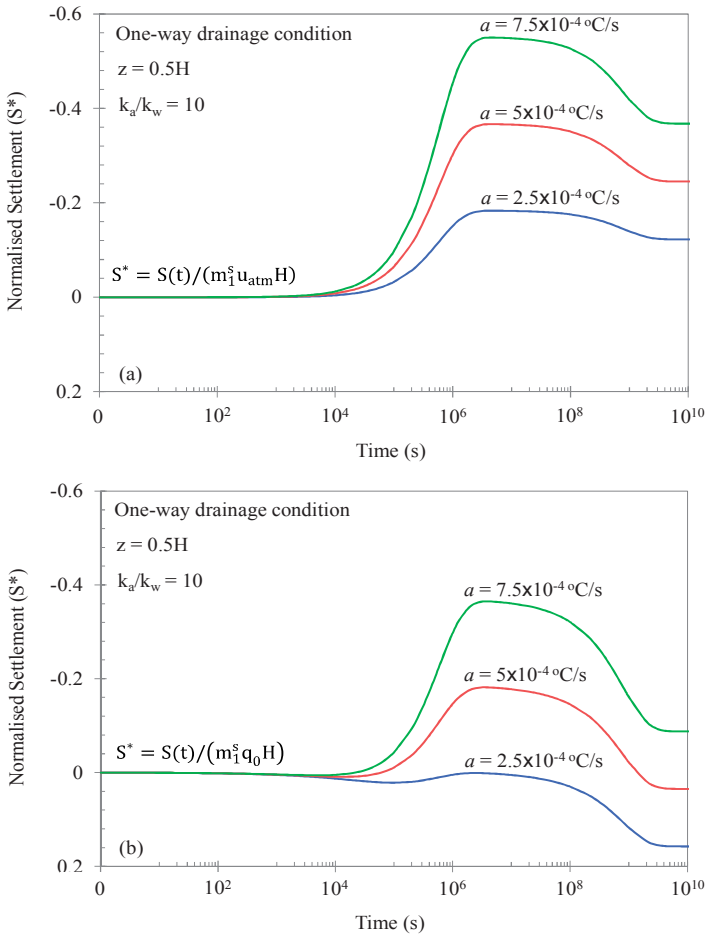

Figure 5.15. Deformation of soil due to (a) the linear thermal parameter 'a' without considering constant loading and (b) the linear thermal parameter 'a' while considering constant loading

5.4.2.2. Effects of exponential thermal parameter 'b'

In this section, different values for the exponential thermal parameter 'b', ranging from 5×10^{-3} to 5×10^{-5}/s, are adopted for further analysis. It should be noted that excess pore-air and pore-water pressures and consolidation settlement are investigated at $z = 0.5H$.

Figures 5.16(a) and 5.16(b) illustrate the effects of thermal parameter 'b' on changes in pore-air (u_a/u_{atm}) and pore-water (u_w/u_{atm}) pressures, respectively, while

excluding the external applied load (q_0) in the analysis. As observed, it takes shorter time for the pore-air and pore-water pressures to attain the maximum values as 'b' increases. In contrast, smaller 'b' values decelerate the increases in pore pressures, which noticeably dissipate before approaching the maximum value. After the temperature approaches the asymptote (i.e. $\theta^{\circ}_{max} = 50°C$), both excess pore pressures are prone to dissipate at the same rate regardless of 'b' values.

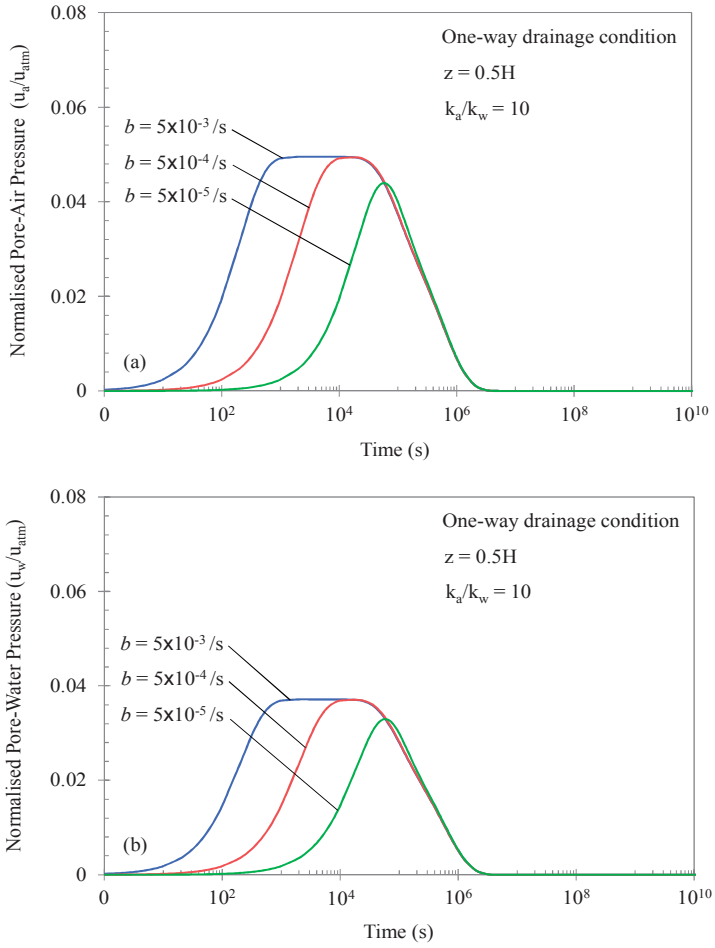

Figure 5.16. Effect of exponential thermal parameter 'b' on changes in (a) pore-air and (b) pore-water pressures

Figures 5.17(a) and 5.17(b) demonstrate the effect of thermal parameter 'b' on changes in excess pore-air (u_a/u_a^0) and pore-water (u_w/u_w^0) pressures, respectively, while including the external applied load (q_0) in the analysis. During the early stages of consolidation, it is predicted that excess pore-air and pore-water pressures increase and attain the maximum values with a quicker rate as 'b' increases. When parameter 'b'

becomes very small (i.e. $b < 5 \times 10^{-5}/\mathrm{s}$), the additional increases in excess pore pressures at the early stages would be very much attenuated. During the later stages of consolidation, at which the temperature approaches the asymptote and stays constant afterwards, dissipation of excess pore pressures is almost independent of 'b' values and is mainly controlled by the applied load.

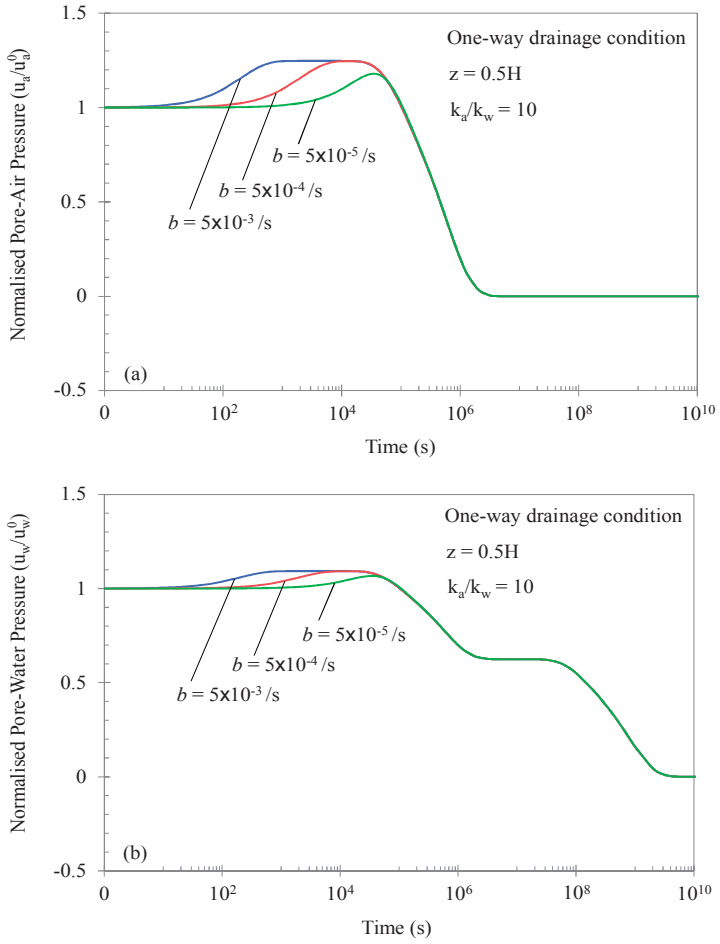

Figure 5.17. Combined effects of exponential thermal parameter 'b' and constant loading on changes in (a) excess pore-air and (b) excess pore-water pressures

Besides, the effect of thermal parameter 'b' on the deformation of unsaturated soil including or excluding the external applied load (q_0) is investigated in Figure 5.18. When the applied load is excluded from the analysis, increasing 'b' value induces further soil expansion, as presented in Figure 5.18(a). It should be noted that the predicted peak settlement reduces as 'b' decreases. Once the temperature approaches the asymptote, the soil begins to retract at similar rate regardless of 'b' values. In the

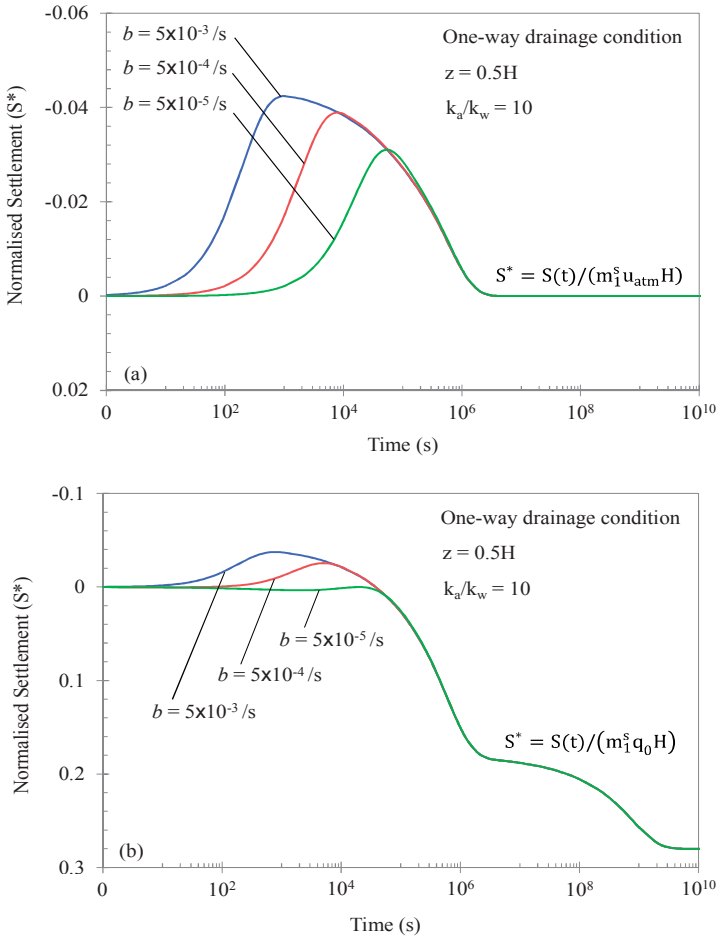

Figure 5.18. Deformation of soil due to (a) the exponential thermal parameter 'b' without considering constant loading and (b) the exponential thermal parameter 'b' while considering constant loading

case when the external loading is considered, higher values of 'b' result in more considerable expansion of soil at the early stages, as shown in Figure 5.18(b). However, the influence of parameter 'b' on the settlement rate is insignificant during the later stages of consolidation.

5.4.2.3. Effects of heat diffusivity D_h

This section adopts different values for the heat diffusivity D_h, including 5×10^{-4} and 5×10^{-5} m^2/s, for further analysis. It is noted that excess pore-air and pore-water pressures and consolidation settlement are investigated at $z = 0.5H$.

Figures 5.19(a) and 5.19(b) present the effect of heat diffusivity D_h on changes in pore-air (u_a/u_{atm}) and pore-water (u_w/u_{atm}) pressures, respectively, while excluding the external loading (q_0) in the analysis. The smaller D_h value implies that the heat transmission would proceed more slowly throughout the soil profile, exhibiting clear damping and retarding effects on pore pressures. Evidently, by considering the smaller

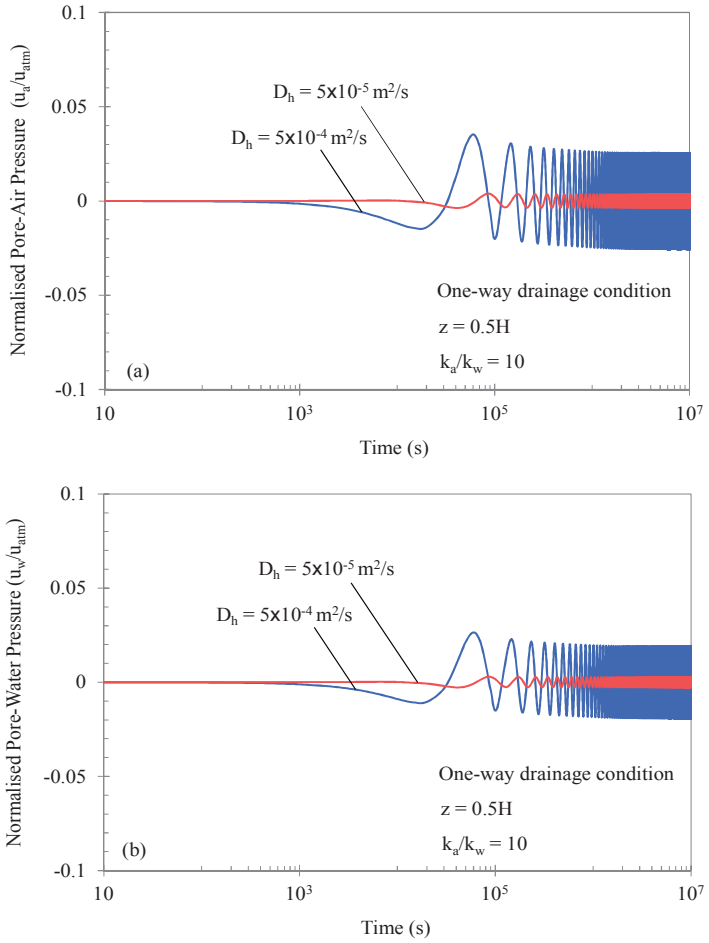

Figure 5.19. Effect of heat diffusivity D_h on changes in (a) pore-air and (b) pore-water pressures

D_h value, amplitudes of excess pore-air and pore-water pressure oscillations significantly reduce (damping) while the peak excess pore pressures are shifted in time (retarding). It is worth mentioning that, when D_h value becomes very small (i.e. $D_h < 5 \times 10^{-5}$ m^2/s), the effect of diurnal temperature wave is less evident and can be practically ignored.

Figures 5.20(a) and 5.20(b) show the effect of heat diffusivity D_h on changes in excess pore-air (u_a/u_a^0) and pore-water (u_w/u_w^0) pressures, respectively, while considering the external loading (q_0) in the analysis. As observed, by adopting the smaller D_h value, excess pore pressures would undergo the damping and retarding phenomena, similar to observations made in Figure 5.19. In addition, when the external load is applied on the surface of unsaturated soil deposit, these excess pore pressures oscillate and dissipate simultaneously.

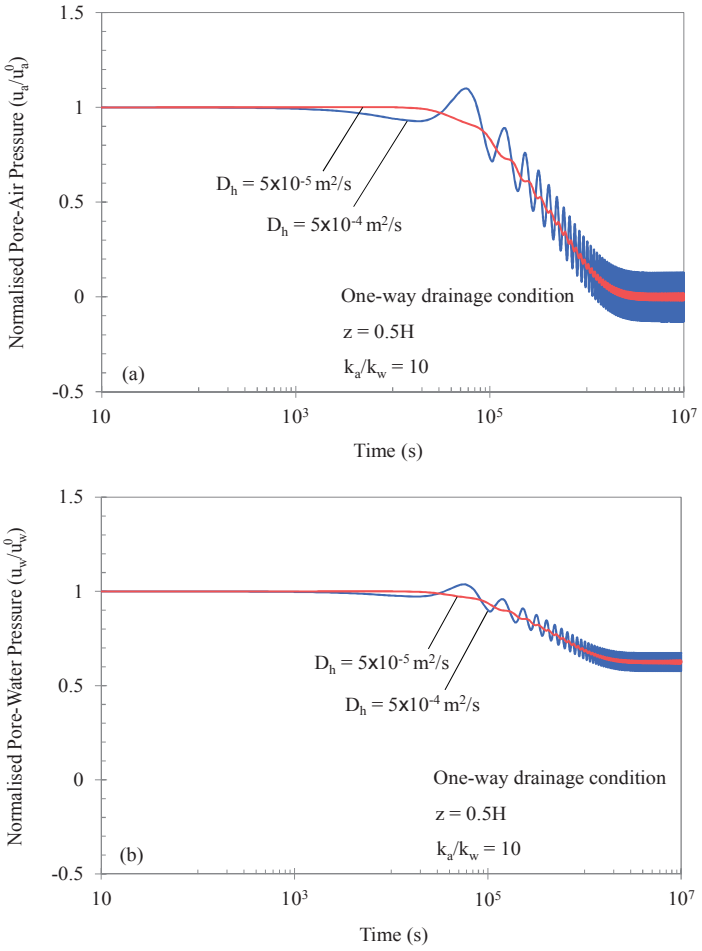

Figure 5.20. Combined effects of heat diffusivity D_h and constant loading on changes in (a) excess pore-air and (b) excess pore-water pressures

The significant effect of heat diffusivity D_h on the deformation of unsaturated soil is investigated in Figure 5.21. When there is no external loading, the smaller D_h value results in insignificant oscillations in the settlement, indicating that a very small amount of heat may be absorbed and released at the mid-depth (Figure 5.21(a)). Similarly, when

the external loading is considered, the amplitude of settlement is significantly attenuated as a result of adopting the smaller D_h value (Figure 5.21(b)).

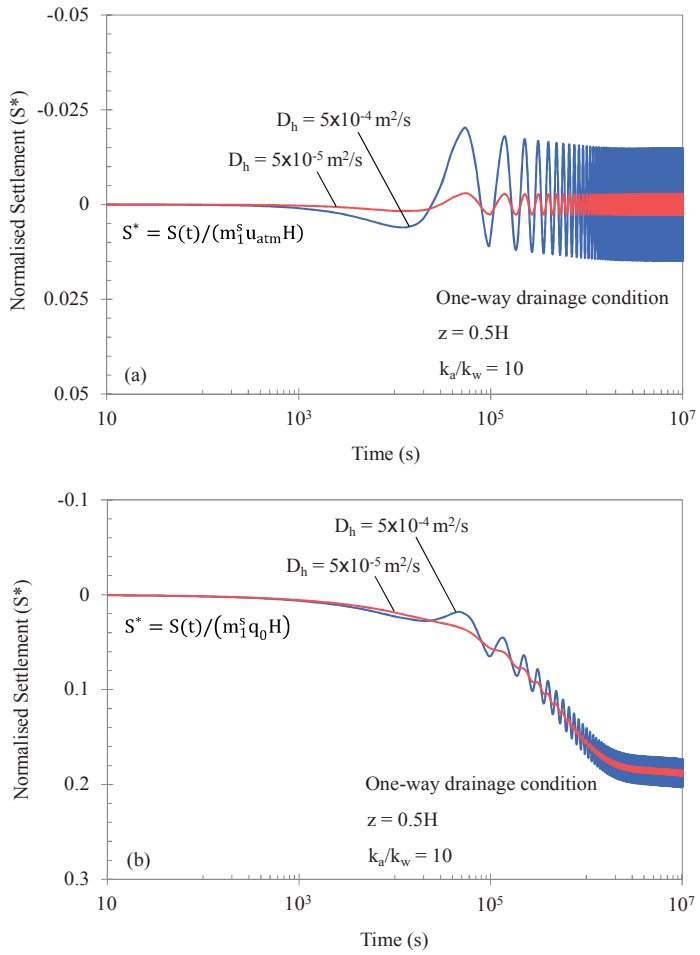

Figure 5.21. Deformation of soil due to (a) the heat diffusivity D_h without considering constant loading and (b) the heat diffusivity D_h while considering constant loading

5.5. Summary

Experimental studies demonstrate that changes in temperature influence the deformation of unsaturated soils significantly, resulting in an essential need to develop a predictive model for unsaturated consolidation capturing the non-isothermal effects. This paper presents an analytical solution to predict the 1D consolidation of unsaturated soil deposit induced by temperature varying with depth and time. The governing equations of flow, incorporating the temperature variation effects, were first adopted. The

mathematical procedure adopted homogeneous drainage boundary conditions such as one-way and two-way drainage systems, while considering uniform initial condition. Fourier sine series and Laplace transformation technique were employed to obtain the closed-form analytical solutions.

Time-dependent thermal functions, namely linear, exponential and diurnal sine wave, were mathematically simulated and then incorporated in the proposed solutions. Changes in excess pore pressures and settlement induced by the effect of temperature variation only and by combined effects of temperature variation and constant loading were investigated. Considering the time-dependent linear temperature, excess pore-air pressure attains a constant value while the excess pore-water pressure fully dissipates during the later stages. It was also predicted that excess pore-air and pore-water pressures near the ground surface tend to increase more quickly due to the exponentially increasing temperature and then fully dissipate as the temperature approaches a constant value. The diurnal temperature wave, on the other hand, highlights the damping and retarding phenomena that can be observed from excess pore pressure oscillations. Parametric studies were also conducted by investigating effects of thermal parameters 'a' and 'b', and heat diffusivity D_h on the 1D consolidation of unsaturated soil deposit. It was observed that increases in 'a' and 'b' accelerate the increases in excess pore pressures, whereas the smaller D_h value leads to notable damping and retarding of predicted excess pore pressures.

CHAPTER 6

A CLOSED FORM ANALYTICAL SOLUTION FOR TWO-DIMENSIONAL PLANE STRAIN CONSOLIDATION OF UNSATURATED SOIL STRATUM

6.1. Introduction

In an attempt to constitute a more reliable prediction model, this study develops a solution for the two-dimensional (2D) plane strain consolidation theory given by Dakshanamurthy & Fredlund (1980). Eigenfunction expansion and Laplace transformation methods are adopted in the analytical procedure along with the homogeneous drainage boundary conditions. This study proposes final solutions capturing uniform and linear distributions of the initial excess pore pressures under a constant surcharge. Following the proposed analytical solutions, two worked examples are introduced and predictions in terms of time-dependent excess pore pressures and degree of consolidation for 2D consolidation are graphically presented in this chapter.

6.2. Transient flow equations for 2D consolidation theory

The flows of air and water can be presented on the basis of continuity of the fluid phases. The air and water phases may be assumed to flow independently and continuously for simple evaluations. Childs & Collis-George (1950) suggested the water flux in unsaturated soil would satisfy Darcy's law, similar to the saturated soil practice. The air flux, on the other hand, should comply with Fick's law, as suggested by Blight (1971). Considering the flux in y-axis is discarded, the net flux of air and water per unit volume of the soil element can be summarised in the 2D coordinates (x, z) as follows:

$$\frac{\partial\left(\frac{\Delta V_a}{V_0}\right)}{\partial t} = \frac{R\Theta}{gM\left(u_a^0+u_{atm}\right)}\left[k_{a_x}\left(\frac{\partial^2 u_a}{\partial x^2}\right)+k_{a_z}\left(\frac{\partial^2 u_a}{\partial z^2}\right)\right]-\frac{n(1-S_r)}{\left(u_a^0+u_{atm}\right)}\left(\frac{\partial u_a}{\partial t}\right) \qquad [6\text{-}1a]$$

$$\frac{\partial\left(\frac{\Delta V_w}{V_0}\right)}{\partial t} = \frac{1}{\gamma_w}\left[k_{w_x}\left(\frac{\partial^2 u_w}{\partial x^2}\right) + k_{w_z}\left(\frac{\partial^2 u_w}{\partial z^2}\right)\right] \quad [6\text{-}1b]$$

where k_{a_x} and k_{w_x} are coefficients of air and water permeability in x-direction ($m.s^{-1}$), respectively; k_{a_z} and k_{w_z} are coefficients of air and water permeability in z-direction ($m.s^{-1}$), respectively; g is the gravitational acceleration ($\sim 9.8 m.s^{-2}$); u_a^0 is the initial pore-air pressure (kPa), respectively; u_{atm} is the atmospheric pressure (kPa); R is the universal air constant ($\sim 8.3 J.mol^{-1}K^{-1}$); $\Theta = (\theta^{\circ} + 273)$, is the absolute temperature (K); M is the molecular mass of air phase ($\sim 0.029 kg.mol^{-1}$); n is the porosity during consolidation process; S_r is the degree of saturation during consolidation process; and γ_w is the unit weight of water ($\sim 9.8 kN.m^{-3}$).

According to Dakshanamurthy & Fredlund (1980), the constitutive equations illustrating the volume changes of air (V_a) and water (V_w) with respect to the initial volume of the soil element (V_0) can be expressed as:

$$\frac{\partial\left(\frac{\Delta V_a}{V_0}\right)}{\partial t} = m_1^a \frac{\partial}{\partial t}\left(\frac{\sigma_x+\sigma_z}{2} - u_a\right) + m_2^a \frac{\partial(u_a - u_w)}{\partial t} \quad [6\text{-}2a]$$

$$\frac{\partial\left(\frac{\Delta V_w}{V_0}\right)}{\partial t} = m_1^w \frac{\partial}{\partial t}\left(\frac{\sigma_x+\sigma_z}{2} - u_a\right) + m_2^w \frac{\partial(u_a - u_w)}{\partial t} \quad [6\text{-}2b]$$

where σ_x and σ_z are the total stresses in x- and z-directions, respectively; u_a and u_w are excess pore-air and pore-water pressures, respectively; m_1^a and m_1^w are coefficients of air and water volume change with respect to the change of net stress $(\sigma - u_a)$, respectively; and m_2^a and m_2^w are coefficients of air and water volume change with respect to the change of suction $(u_a - u_w)$, respectively.

The total stresses provided in Equations [6-2a] and [6-2b] are assumed to be constant (i.e. $\partial\sigma_x/\partial t = \partial\sigma_z/\partial t = 0$) during the transient process (Dakshanamurthy & Fredlund 1980; Fredlund 1984). Equations [6-1a] and [6-1b] can be equated to Equations [6-2a] and [6-2b], respectively, resulting in the continuity equations as shown (Dakshanamurthy & Fredlund 1980):

$$\frac{\partial u_a}{\partial t} + C_a\left(\frac{\partial u_w}{\partial t}\right) + c_{v_x}^a\left(\frac{\partial^2 u_a}{\partial x^2}\right) + c_{v_z}^a\left(\frac{\partial^2 u_a}{\partial z^2}\right) = 0 \quad [6\text{-}3a]$$

$$\frac{\partial u_w}{\partial t} + C_w\left(\frac{\partial u_a}{\partial t}\right) + c_{v_x}^w\left(\frac{\partial^2 u_w}{\partial x^2}\right) + c_{v_z}^w\left(\frac{\partial^2 u_w}{\partial z^2}\right) = 0 \quad [6\text{-}3b]$$

where C_a and C_w are the interactive constants associated with the air and water phases, respectively; $c_{v_x}^a$ and $c_{v_x}^w$ are the coefficients of consolidation with respect to the air and water phases in x-direction; $c_{v_z}^a$ and $c_{v_z}^w$ are the coefficients of consolidation with respect to the air and water phases in z-direction. Additionally, the consolidation parameters are:

$$C_a = \frac{1}{\left[\left(\frac{m_1^a}{m_2^a}-1\right)-\frac{n(1-S_r)}{m_2^a(u_a^0+u_{atm})}\right]}; \quad [6\text{-}4a]$$

$$c_{v_x}^a = \frac{k_{a_x}R\Theta}{gM}\frac{1}{\left[m_2^a(u_a^0+u_{atm})\left(\frac{m_1^a}{m_2^a}-1\right)-n(1-S_r)\right]}; \quad [6\text{-}4b]$$

$$c_{v_z}^a = \frac{k_{a_z}R\Theta}{gM}\frac{1}{\left[m_2^a(u_a^0+u_{atm})\left(\frac{m_1^a}{m_2^a}-1\right)-n(1-S_r)\right]}; \quad [6\text{-}4c]$$

$$C_w = \left(\frac{m_1^w}{m_2^w}-1\right); \quad [6\text{-}4d]$$

$$c_{v_x}^w = \frac{1}{m_2^w}\left(\frac{k_{w_x}}{\gamma_w}\right); \quad [6\text{-}4e]$$

$$c_{v_z}^w = \frac{1}{m_2^w}\left(\frac{k_{w_z}}{\gamma_w}\right). \quad [6\text{-}4f]$$

Equations [6-3a] and [6-3b] can be rewritten in simplified forms as follows:

$$u_{a,t} + C_a u_{w,t} + c_{v_x}^a u_{a,xx} + c_{v_z}^a u_{a,zz} = 0 \quad [6\text{-}5a]$$

$$u_{w,t} + C_w u_{a,t} + c_{v_x}^w u_{w,xx} + c_{v_z}^w u_{w,zz} = 0 \quad [6\text{-}5b]$$

where $u_{a,t}$ and $u_{w,t}$ are the first order of PDEs of excess pore-air and pore-water pressures against time t, respectively; $u_{a,zz}$ and $u_{w,zz}$ are the second order of PDEs of pore-air and pore-water pressures against depth z, respectively; and $u_{a,xx}$ and $u_{w,xx}$ are the second order of PDEs of pore-air and pore-water pressures against length x, respectively.

Equations [6-5a] and [6-5b] are the 2D plane strain governing equations describing dissipation of excess pore-air and pore-water pressures in the soil deposits and are presented under inhomogeneous PDEs. Final solutions u_a and u_w are compound functions of length x, depth z, and time t.

6.3. Analytical solution for 2D unsaturated consolidation equations

Soil properties vary during the consolidation and this may involve the changes of permeability coefficients, degree of saturation (S_r), porosity (n) and numerous other properties. For the ease of mathematical derivations, some additional assumptions should be made along with those of Terzaghi's consolidation theory (1943):

(1) The soil stratum is assumed to be homogeneous;
(2) The flows of air and water are assumed to be continuous and independent;
(3) Solid skeleton and water phase are incompressible;
(4) Effects of environmental factors such as air diffusion and temperature change can be disregarded;
(5) Deformations of a soil stratum happens along x- and z-directions;
(6) Consolidation parameters with respect to air phase (C_a, $c_{v_x}^a$ and $c_{v_z}^a$) and water phase (C_w, $c_{v_x}^w$ and $c_{v_z}^w$) are assumed to be constant during the loading process.

The above mentioned assumptions may not be completely accurate for some cases, especially Assumption (6). The consolidation parameters may change due to the variation of the soil properties such as permeability, degree of saturation (S_r), and porosity (n). However, it may be acceptable to assume that these parameters are constant during the transient process for a particular stress increment. The assumption (6) is adjusted in such way that alleviates the complication in obtaining the solutions for Equation [6-5].

6.3.1. Boundary and initial conditions

Figure 6.1 illustrates a referential profile of a homogeneous soil stratum with a finite depth H (in z-direction). A length L is considered to be the spacing between two installed vertical drains that facilitate horizontal drainage (in x-direction). Representative soil elements have the length:width:depth ratio of dx:1:dz corresponding to coordinates (x, y, z), indicating that the length and depth of the soil are variables. Figure 6.1(a) shows the typical drainage boundary system consisting of a permeable top surface and an impervious bedrock along z-direction. Figure 6.1(b) demonstrates the drainage system with double drainage paths allowing free drainage from both top and

base boundaries of the soil stratum. The horizontal drainage in this study takes place through two side boundaries defined by vertical sand drains. Homogeneous boundary conditions can be summarised in Equations [6-6a] and [6-6b]:

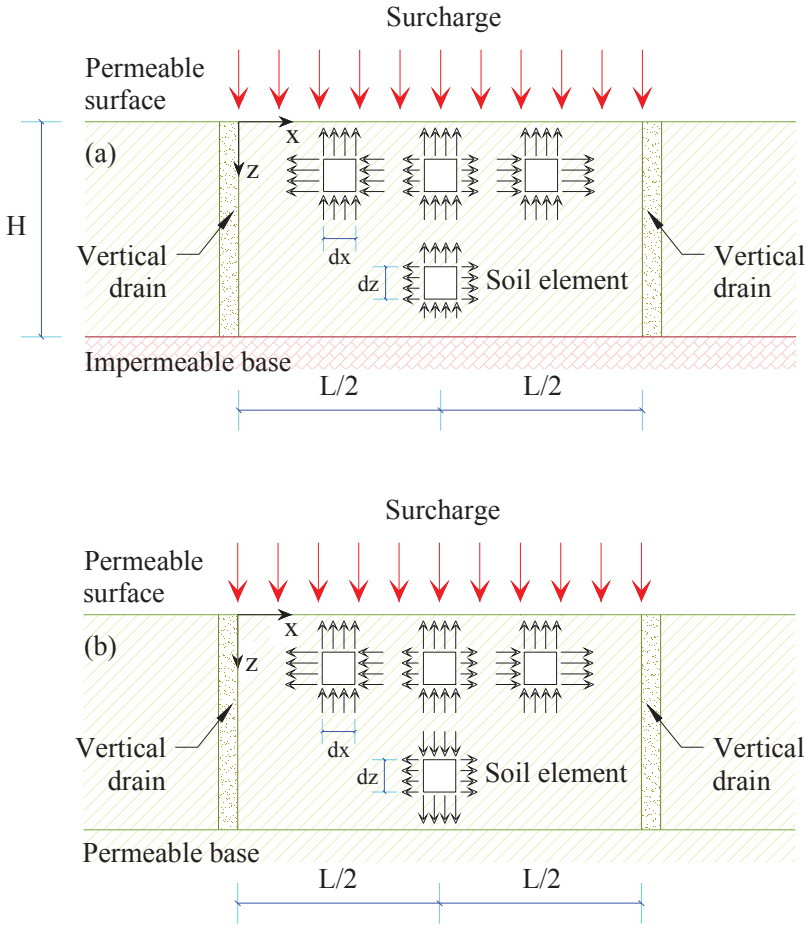

Figure 6.1. The profile of the homogeneous soil stratum representing (a) top drainage boundary system and (b) top-base drainage boundary system

(a) Top drainage (one-way drainage along depth) boundary condition ($t \geq 0$):

- $u_a(0,z,t) = u_w(0,z,t) = u_a(L,z,t) = u_w(L,z,t) = 0$;
- $u_a(x,0,t) = u_w(x,0,t) = u_{a,z}(x,H,t) = u_{w,z}(x,H,t) = 0$. [6-6a]

(b) Top-base drainage (two-way drainage along depth) boundary condition ($t \geq 0$):

- $u_a(0,z,t) = u_w(0,z,t) = u_a(L,z,t) = u_w(L,z,t) = 0$;
- $u_a(x,0,t) = u_w(x,0,t) = u_a(x,H,t) = u_w(x,H,t) = 0$. [6-6b]

The consolidation subjected to the uniform initial condition has been frequently reported in the literature and consolidation experiments (Venkatramaiah 2006; Qin et al. 2008; Zhou et al. 2014). However, this condition may not be strictly accurate in engineering practice, particularly when the size of the loaded area on the ground surface is small, in comparison to the thickness of the soil deposit. To be more realistic, the initial conditions can be mathematically simulated by introducing two dimensionless parameters ζ_a and ζ_w to capture distributions of the initial excess pore pressures with depth. When $t = 0$, the initial excess pore-air and pore-water pressures are respectively presented in the domains $x \in (0, L)$ and $z \in (0, H)$ as follows:

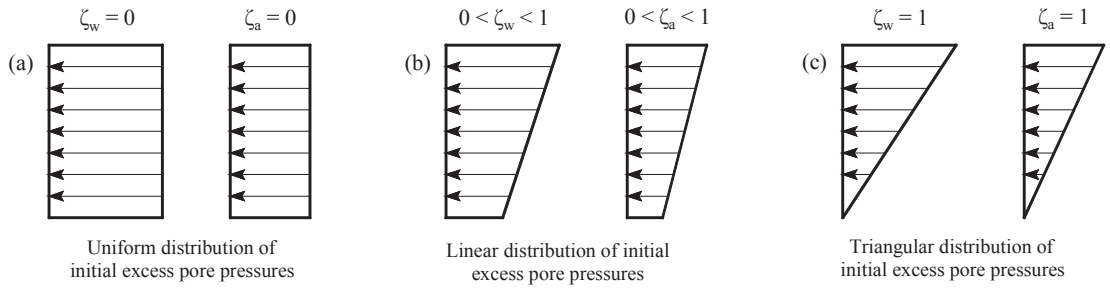

Figure 6.2. Different distributions of initial excess pore pressures along depth: (a) uniform distribution, (b) trapezoidal distribution and (c) triangular distribution

$$u_a(x, z, 0) = u_a^0 \left(1 - \zeta_a \frac{z}{H}\right); \quad [6\text{-}7a]$$

$$u_w(x, z, 0) = u_w^0 \left(1 - \zeta_w \frac{z}{H}\right); \quad [6\text{-}7b]$$

where u_a^0 and u_w^0 are maximum initial pore-air and pore-water pressures (kPa), respectively. The introduction of the newly proposed parameters ζ_a and ζ_w is to control the gradient of variations of excess pore-air and pore-water pressures with depth, respectively. Both parameters range from 0 to 1 and initial pore pressures may vary with depth corresponding to the variations of these parameters. For instance, when $\zeta_a = \zeta_w = 0$, the distribution of initial excess pore pressures is uniform along z-direction; when both ζ_a and ζ_w are in between 0 and 1, the initial excess pore pressures decrease linearly with depth; and when $\zeta_a = \zeta_w = 1$, the triangular distribution will be formed with zero initial pressures at $z = H$. A schematic distribution of initial excess pore pressures due to variations of ζ_a and ζ_w is presented in Figure 6.2.

6.3.2. Eigenfunction expansion and Laplace transformation methods

Based on the eigenfunction expansion method for a higher dimensional PDE, the general solutions for the set of nonlinear inhomogeneous equations (i.e. Equations [6-5a] and [6-5b]) incorporating homogeneous drainage boundary conditions (i.e. Equations [6-6a] and [6-6b]) can be presented in homogeneous forms as below:

$$u_a(x,z,t) = \sum_{i=0}^{\infty}\sum_{j=0}^{\infty} X_a(x)Z_a(z)T_a(t) \quad [6\text{-}8a]$$

$$u_w(x,z,t) = \sum_{i=0}^{\infty}\sum_{j=0}^{\infty} X_w(x)Z_w(z)T_w(t) \quad [6\text{-}8b]$$

where $X_a(x)$ and $X_w(x)$ are eigenfunctions in the domain x with respect to air and water phases, respectively; $Z_a(x)$ and $Z_w(x)$ are eigenfunctions in the domain z with respect to air and water phases, respectively; and $T_a(t)$ and $T_w(t)$ are generalised Fourier coefficients for air and water, respectively, varying against t.

The above solutions are written as products of functions of x, z and t. The functions of x and z, known as eigenfunctions, are derived based on the homogeneous boundary conditions and consist of Fourier sine series (Haberman 2012). The eigenvalues corresponding to particular sine functions are determined by the material constants of the system, geometrical factors and boundary conditions. It can be noted that eigenfunctions describe the natural vibrations and their eigenvalues present the natural frequencies of vibration. In this study, the eigenvalues are categorised into two terms Λ^{ij} and λ^{ij} representing two distinctive permeability conditions. The term Λ^{ij} ($i = 0, 1, 2, ...$; and $j = 0, 1, 2, ...$) introduces an isotropic permeability condition ($k_x = k_z$) to the soil system, whereas λ^{ij} presents an anisotropic permeability condition ($k_x \neq k_z$). Based on the solution of heat diffusion, the sets of eigenfunctions and eigenvalues are shown as below:

(a) Isotropic permeability condition ($k_x = k_z$):

$$\begin{cases} X_a^i(x) = X_w^i(x) = \sin(Ix) \\ Z_a^j(z) = Z_w^j(z) = \sin(Jz) \\ \Lambda^{ij} = (I)^2 + (J)^2 \end{cases} \quad [6\text{-}9a]$$

(b) Anisotropic permeability condition ($k_x \neq k_z$): $\begin{cases} X_a^i(x) = X_w^i(x) = \sin(Ix) \\ Z_a^j(z) = Z_w^j(z) = \sin(Jz) \\ \lambda_a^{ij} = k_{a_x}(I)^2 + k_{a_z}(J)^2 \\ \lambda_w^{ij} = k_{w_x}(I)^2 + k_{w_z}(J)^2 \end{cases}$ [6-9b]

where

$I = \frac{i\pi}{L}$, for double side drainage condition over domain x ($i = 0, 1, 2, ...$);

and

$J = \frac{(2j+1)\pi}{2H}$, for top drainage condition over domain z ($j = 0, 1, 2, ...$); or

$= \frac{j\pi}{H}$, for top-base drainage condition over domain z. [6-10]

Equation [6-8] then can be rewritten whilst incorporating the eigenfunctions given in Equation [6-9]:

$u_a(x, z, t) = \sum_{i=0}^{\infty} \sum_{j=0}^{\infty} \sin(Ix)\sin(Jz)T_a(t)$ [6-11a]

$u_w(x, z, t) = \sum_{i=0}^{\infty} \sum_{j=0}^{\infty} \sin(Ix)\sin(Jz)T_w(t)$ [6-11b]

The above homogeneous solutions can be substituted into Equations [6-5a] and [6-5b], and the expansion of the governing equations yields in:

(a) Isotropic permeability condition ($k_x = k_z$):

$\sum_{i=0}^{\infty} \sum_{j=0}^{\infty} \sin(Ix)\sin(Jz) \left[T_{a,t}^{ij}(t) + C_a T_{w,t}^{ij}(t) - c_{v_1}^a (\Lambda^{ij}) T_a^{ij}(t)\right] = 0$ [6-12a]

$\sum_{i=0}^{\infty} \sum_{j=0}^{\infty} \sin(Ix)\sin(Jz) \left[T_{w,t}^{ij}(t) + C_w T_{a,t}^{ij}(t) - c_{v_1}^w (\Lambda^{ij}) T_w^{ij}(t)\right] = 0$ [6-12b]

(b) Anisotropic permeability condition ($k_x \neq k_z$):

$\sum_{i=0}^{\infty} \sum_{j=0}^{\infty} \sin(Ix)\sin(Jz) \left[T_{a,t}^{ij}(t) + C_a T_{w,t}^{ij}(t) - c_{v_2}^a (\lambda_a^{ij}) T_a^{ij}(t)\right] = 0$ [6-13a]

$\sum_{i=0}^{\infty} \sum_{j=0}^{\infty} \sin(Ix)\sin(Jz) \left[T_{w,t}^{ij}(t) + C_w T_{a,t}^{ij}(t) - c_{v_2}^w (\lambda_w^{ij}) T_w^{ij}(t)\right] = 0$ [6-13b]

where $c_{v_1}^a = \frac{k_a R\Theta}{gM} \frac{1}{\left[m_2^a (u_a^0 + u_{atm})\left(\frac{m_1^a}{m_2^a} - 1\right) - n(1 - S_r)\right]}$; $c_{v_1}^w = \frac{1}{m_2^w}\left(\frac{k_w}{\gamma_w}\right)$;

$c_{v_2}^a = \frac{R\Theta}{gM} \frac{1}{\left[m_2^a (u_a^0 + u_{atm})\left(\frac{m_1^a}{m_2^a} - 1\right) - n(1 - S_r)\right]}$; and $c_{v_2}^w = \frac{1}{m_2^w}\left(\frac{1}{\gamma_w}\right)$. [6-14]

Truncating Equations [6-12] and [6-13] to a set of ordinary differential equations (ODEs) gives:

(a) Isotropic permeability condition ($k_x = k_z$):

$$T_{a,t}^{ij}(t) + C_a T_{w,t}^{ij}(t) - c_{v_1}^{a}\left(\Lambda^{ij}\right)T_a^{ij}(t) = 0 \qquad [6\text{-}15a]$$

$$T_{w,t}^{ij}(t) + C_w T_{a,t}^{ij}(t) - c_{v_1}^{w}\left(\Lambda^{ij}\right)T_w^{ij}(t) = 0 \qquad [6\text{-}15b]$$

with $i = 0, 1, 2, ...$; and $j = 0, 1, 2, ...$

(b) Anisotropic permeability condition ($k_x \neq k_z$):

$$T_{a,t}^{ij}(t) + C_a T_{w,t}^{ij}(t) - c_{v_2}^{a}\left(\lambda_a^{ij}\right)T_a^{ij}(t) = 0 \qquad [6\text{-}16a]$$

$$T_{w,t}^{ij}(t) + C_w T_{a,t}^{ij}(t) - c_{v_2}^{w}\left(\lambda_w^{ij}\right)T_w^{ij}(t) = 0 \qquad [6\text{-}16b]$$

with $i = 0, 1, 2, ...$; and $j = 0, 1, 2, ...$

Then, the Laplace transformation method is applied to Equations [6-15] and [6-16]. The variable t is converted to the complex argument s. For the sake of simplicity, a new set of Laplace transformed equations can be presented under a matrix form as follows:

$$\mathbf{A}.\mathbf{T} = \mathbf{B} \qquad [6\text{-}17]$$

where $\mathbf{A} = \begin{bmatrix} s - c_{v_1}^{a}\Lambda^{ij} & sC_a \\ sC_w & s - c_{v_1}^{w}\Lambda^{ij} \end{bmatrix}$, for $k_x = k_z$; or

$= \begin{bmatrix} s - c_{v_2}^{a}\lambda_a^{ij} & sC_a \\ sC_w & s - c_{v_2}^{w}\lambda_w^{ij} \end{bmatrix}$, for $k_x \neq k_z$;

$\mathbf{B} = \begin{Bmatrix} T_a^{ij}(0) + C_a T_w^{ij}(0) \\ C_w T_a^{ij}(0) + T_w^{ij}(0) \end{Bmatrix}$; and $\mathbf{T} = \begin{Bmatrix} \overline{T}_a^{ij}(s) \\ \overline{T}_w^{ij}(s) \end{Bmatrix}$. [6-18]

Solving for $\overline{T}_a^{ij}(s)$ and $\overline{T}_w^{ij}(s)$ ($i = 0, 1, 2, ...$; and $j = 0, 1, 2, ...$) presented in Equation [6-17] results in:

$$\mathbf{T} = \mathbf{A^{-1}B} \qquad [6\text{-}19]$$

where $\mathbf{A^{-1}B} = \begin{Bmatrix} \frac{T_a^{ij}(0)(C_aC_w-1)s+c_{v_1}^w\left[C_aT_w^{ij}(0)+T_a^{ij}(0)\right]\Lambda^{ij}}{(C_wC_a-1)s^2+\left(c_{v_1}^a+c_{v_1}^w\right)\Lambda^{ij}s-c_{v_1}^ac_{v_1}^w\left(\Lambda^{ij}\right)^2} \\ \frac{T_w^{ij}(0)(C_aC_w-1)s+c_{v_1}^a\left[C_wT_a^{ij}(0)+T_w^{ij}(0)\right]\Lambda^{ij}}{(C_wC_a-1)s^2+\left(c_{v_1}^a+c_{v_1}^w\right)\Lambda^{ij}s-c_{v_1}^ac_{v_1}^w\left(\Lambda^{ij}\right)^2} \end{Bmatrix}$, for $k_x = k_z$; or

$= \begin{Bmatrix} \frac{T_a^{ij}(0)(C_aC_w-1)s+c_{v_2}^w\left[C_aT_w^{ij}(0)+T_a^{ij}(0)\right]\lambda_w^{ij}}{(C_wC_a-1)s^2+\left(c_{v_2}^a\lambda_a^{ij}+c_{v_2}^w\lambda_w^{ij}\right)s-c_{v_2}^ac_{v_2}^w\lambda_a^{ij}\lambda_w^{ij}} \\ \frac{T_w^{ij}(0)(C_aC_w-1)s+c_{v_2}^a\left[C_wT_a^{ij}(0)+T_w^{ij}(0)\right]\lambda_a^{ij}}{(C_wC_a-1)s^2+\left(c_{v_2}^a\lambda_a^{ij}+c_{v_2}^w\lambda_w^{ij}\right)s-c_{v_2}^ac_{v_2}^w\lambda_a^{ij}\lambda_w^{ij}} \end{Bmatrix}$, for $k_x \neq k_z$. [6-20]

It can be noticed that $T_a^{ij}(0)$ and $T_w^{ij}(0)$ $(i = 0, 1, 2, ...;$ and $j = 0, 1, 2, ...)$ are independent of the variable s. They can be obtained using initial conditions provided in Equation [6-7]. The generalised Fourier coefficients for air and water can be obtained by taking Laplace inverse of Equation [6-19], leading to:

$$\mathcal{L}^{-1}\{\mathbf{T}\} = \mathcal{L}^{-1}\{\mathbf{A^{-1}B}\} \quad [6\text{-}21]$$

Where $\mathcal{L}^{-1}\{\mathbf{T}\} = \begin{Bmatrix} T_a^{ij}(t) \\ T_w^{ij}(t) \end{Bmatrix}$ $(i = 0, 1, 2, ...;$ and $j = 0, 1, 2, ...)$; and

$$\mathcal{L}^{-1}\{\mathbf{A^{-1}B}\} = \begin{Bmatrix} \frac{\Omega\left(e^{\alpha_1\Lambda^{ij}t}-e^{\alpha_2\Lambda^{ij}t}\right)+\Psi\left(e^{\alpha_1\Lambda^{ij}t}+e^{\alpha_2\Lambda^{ij}t}\right)}{2\eta} \\ \frac{\Omega'\left(e^{\alpha_1\Lambda^{ij}t}-e^{\alpha_2\Lambda^{ij}t}\right)+\Psi'\left(e^{\alpha_1\Lambda^{ij}t}+e^{\alpha_2\Lambda^{ij}t}\right)}{2\eta} \end{Bmatrix}, \quad \text{for } k_x = k_z; \text{ or}$$

$$= \begin{Bmatrix} \frac{\omega\left(e^{\alpha_1^{ij}t}-e^{\alpha_2^{ij}t}\right)+\psi\left(e^{\alpha_1^{ij}t}+e^{\alpha_2^{ij}t}\right)}{2\eta^{ij}} \\ \frac{\omega'\left(e^{\alpha_1^{ij}t}-e^{\alpha_2^{ij}t}\right)+\psi'\left(e^{\alpha_1^{ij}t}+e^{\alpha_2^{ij}t}\right)}{2\eta^{ij}} \end{Bmatrix}, \quad \text{for } k_x \neq k_z; \quad [6\text{-}22]$$

with $\eta = \left[\left(c_{v_1}^a - c_{v_1}^w\right)^2 + 4c_{v_1}^ac_{v_1}^wC_wC_a\right]^{\frac{1}{2}}$;

$\eta^{ij} = \left[\left(c_{v_2}^a\lambda_a^{ij} - c_{v_2}^w\lambda_w^{ij}\right)^2 + 4c_{v_2}^ac_{v_2}^wC_wC_a\lambda_a^{ij}\lambda_w^{ij}\right]^{\frac{1}{2}}$;

$\alpha_1 = \frac{1}{2}\left(\frac{c_{v_1}^a+c_{v_1}^w+\eta}{1-C_wC_a}\right)$; $\alpha_2 = \frac{1}{2}\left(\frac{c_{v_1}^a+c_{v_1}^w-\eta}{1-C_wC_a}\right)$;

$\alpha_1^{ij} = \frac{1}{2}\left(\frac{c_{v_2}^a\lambda_a^{ij}+c_{v_2}^w\lambda_w^{ij}+\eta^{ij}}{1-C_wC_a}\right)$; $\alpha_2^{ij} = \frac{1}{2}\left(\frac{c_{v_2}^a\lambda_a^{ij}+c_{v_2}^w\lambda_w^{ij}-\eta^{ij}}{1-C_wC_a}\right)$;

$\Omega = \left(c_{v_1}^a - c_{v_1}^w\right)T_a^{ij}(0) - 2c_{v_1}^wC_aT_w^{ij}(0)$; $\Psi = \eta T_a^{ij}(0)$;

$\Omega' = \left(c_{v_1}^w - c_{v_1}^a\right)T_w^{ij}(0) - 2c_{v_1}^aC_wT_a^{ij}(0)$; $\Psi' = \eta T_w^{ij}(0)$;

$$\omega = \left(c_{v_2}^{a}\lambda_{a}^{ij} - c_{v_2}^{w}\lambda_{w}^{ij}\right)T_{a}^{ij}(0) - 2c_{v_2}^{w}C_{a}\lambda_{w}^{ij}T_{w}^{ij}(0); \qquad \psi = \eta^{ij}T_{a}^{ij}(0);$$

$$\omega' = \left(c_{v_2}^{w}\lambda_{w}^{ij} - c_{v_2}^{a}\lambda_{a}^{ij}\right)T_{w}^{ij}(0) - 2c_{v_2}^{a}C_{w}\lambda_{a}^{ij}T_{a}^{ij}(0); \qquad \psi' = \eta^{ij}T_{w}^{ij}(0);$$

$$T_{a}^{ij}(0) = \frac{\int_0^H \int_0^L \left\{\left[u_a^0\left(1-\zeta_a\frac{z}{H}\right)\right]\sin(Ix)\sin(Jz)\right\}dxdz}{\int_0^H \int_0^L [\sin^2(Ix)\sin^2(Jz)]dxdz}; \text{ and}$$

$$T_{w}^{ij}(0) = \frac{\int_0^H \int_0^L \left\{\left[u_w^0\left(1-\zeta_w\frac{z}{H}\right)\right]\sin(Ix)\sin(Jz)\right\}dxdz}{\int_0^H \int_0^L [\sin^2(Ix)\sin^2(Jz)]dxdz}. \qquad [6\text{-}23]$$

By substituting the obtained Fourier coefficients $T_{a}^{ij}(t)$ and $T_{w}^{ij}(t)$ into Equation [6-11], the finalised solutions will be:

(a) Isotropic permeability condition ($k_x = k_z$):

$$u_a(x,z,t) = \sum_{i=0}^{\infty}\sum_{j=0}^{\infty}\sin(Ix)\sin(Jz)\left[\frac{\Omega\left(e^{\alpha_1\Lambda^{ij}t} - e^{\alpha_2\Lambda^{ij}t}\right) + \Psi\left(e^{\alpha_1\Lambda^{ij}t} + e^{\alpha_2\Lambda^{ij}t}\right)}{2\eta}\right] \qquad [6\text{-}24a]$$

$$u_w(x,z,t) = \sum_{i=0}^{\infty}\sum_{j=0}^{\infty}\sin(Ix)\sin(Jz)\left[\frac{\Omega'\left(e^{\alpha_1\Lambda^{ij}t} - e^{\alpha_2\Lambda^{ij}t}\right) + \Psi'\left(e^{\alpha_1\Lambda^{ij}t} + e^{\alpha_2\Lambda^{ij}t}\right)}{2\eta}\right] \qquad [6\text{-}24b]$$

(b) Anisotropic permeability condition ($k_x \neq k_z$):

$$u_a(x,z,t) = \sum_{i=0}^{\infty}\sum_{j=0}^{\infty}\sin(Ix)\sin(Jz)\left[\frac{\omega\left(e^{\alpha_1^{ij}t} - e^{\alpha_2^{ij}t}\right) + \psi\left(e^{\alpha_1^{ij}t} + e^{\alpha_2^{ij}t}\right)}{2\eta^{ij}}\right] \qquad [6\text{-}25a]$$

$$u_w(x,z,t) = \sum_{i=0}^{\infty}\sum_{j=0}^{\infty}\sin(Ix)\sin(Jz)\left[\frac{\omega'\left(e^{\alpha_1^{ij}t} - e^{\alpha_2^{ij}t}\right) + \psi'\left(e^{\alpha_1^{ij}t} + e^{\alpha_2^{ij}t}\right)}{2\eta^{ij}}\right] \qquad [6\text{-}25b]$$

Equations [6-24] and [6-25] present closed-form solutions to simulate the dissipation process of excess pore-air and pore-water pressures under a constant and uniform load. Complete analytical solutions capturing both uniformly and linearly distributed initial excess pore pressures are presented in Appendix C. The application of eigenfunction expansion provides a direct and simple computation to solve inhomogeneous equations given by Dakshanamurthy & Fredlund (1980). This method allows the general solutions to be expressed in a series of the eigenfunctions of the related homogeneous problem and thus providing the convenience in handling the nonlinear problem. For the anisotropic soil, if the horizontal permeability coefficient (k_x) is equal to the vertical permeability coefficient (k_z), Equation [6-25] then becomes similar to Equation [6-24].

Furthermore, when the soil is in a fully saturated state, the coefficient of permeability, the initial excess pore pressure and all consolidation parameters with respect to air phase will be zero. In addition, the coefficients of volume change of water m_1^w and m_2^w are equal to the classical volume change coefficient, m_v. As a result, Equation [6-24] will be converted to the conventional 2D consolidation equation for saturated soils. Considering the uniform distribution of excess pore-water pressure ($\zeta_w = 0$) and the typical top drainage boundary condition, Equation [6-25] predicting the excess pore-water pressure dissipation can be presented as follows:

$$u_w(x,z,t) = \sum_{i=0}^{\infty}\sum_{j=0}^{\infty}\frac{8[1-(-1)^i]u_w^0}{(i\pi)[(2j+1)\pi]}\sin\left(\frac{i\pi x}{L}\right)\sin\left[\frac{(2j+1)\pi z}{2H}\right]e^{c_{v_2}^w\left\{k_{w_x}\left(\frac{i\pi}{L}\right)^2+k_{w_z}\left[\frac{(2j+1)\pi}{2H}\right]^2\right\}t} \quad [6\text{-}26]$$

Assuming the horizontal length is boundless, the coefficient of water permeability in x-direction (k_{w_x}) will be discarded and Equation [6-26] will become Terzaghi's traditional equation for 1D consolidation for fully saturated soils.

6.4. Average degree of consolidation of 2D unsaturated soil system

In this study, the coefficients of volume change with respect to air and water phases are assumed to be constant during the consolidation for a particular stress increment, similar to the traditional assumptions for Terzaghi's consolidation theory (1943). Under the constant loading, the constitutive model for 2D plane strain deformation proposed by Dakshanamurthy & Fredlund (1980) can be rearranged as below:

$$\frac{\partial\left(\frac{\Delta V}{V_0}\right)}{\partial t} = \frac{\partial(\varepsilon_v)}{\partial t} = (m_2^s - m_1^s)\frac{\partial u_a}{\partial t} - m_2^s\frac{\partial u_w}{\partial t} \quad [6\text{-}27]$$

where ε_v is the volumetric strain; $m_1^s = m_1^w + m_1^a$, is the coefficient of volume change of the soil element with respect to the change in the net stress; and $m_2^s = m_2^w + m_2^a$, is the coefficient of volume change of the soil element with respect to the change in suction. The volumetric strain can be obtained by integrating Equation [6-27] against time t at which $t \in [0, \infty)$:

$$\varepsilon_v(x,z,t) = (m_2^s - m_1^s)[u_a(x,z,t) - u_a(x,z,0)] - m_2^s[u_w(x,z,t) - u_w(x,z,0)] \quad [6\text{-}28]$$

The average degree of consolidation, denoted as $\overline{U}$, can be determined based on the volumetric strain ε_v provided in Equation [6-28]:

$$\overline{U} = \frac{S_t}{S_\infty} = \left| \frac{\int_0^H \int_0^L \varepsilon_v(x,z,t)\,dx\,dz}{\int_0^H \int_0^L \varepsilon_v(x,z,\infty)\,dx\,dz} \right| \quad [6\text{-}29]$$

where S_t is the ground surface settlement corresponding to time t; and

S_∞ is the final ground surface settlement when time t approaches infinity.

Equation [6-29] represents a function of time t describing the settlement response of the unsaturated soil deposit subjected to a constant load at a particular time.

6.5. Worked examples

This study provides two worked examples investigating 2D consolidation behaviour against the applications of uniformly and linearly distributed initial excess pore pressures with depth. Each example considers both top and top-base drainage boundary conditions whilst adopting the following soil properties (Qin et al. 2008; Qin et al. 2010c; Shan et al. 2012; Ho et al. 2013; Zhou et al. 2014):

- Material properties:

$$\begin{aligned} &n = 0.50; \quad S_r = 80\%; \quad k_w = 10^{-10}\mathrm{ms}^{-1}; \\ &L = 2\mathrm{m}; \quad H = 5\mathrm{m}; \quad u_{atm} = 100\mathrm{kPa}; \\ &u_a^0 = 20\mathrm{kPa}; \quad u_w^0 = 40\mathrm{kPa}; \quad q_0 = 100\mathrm{kPa}; \\ &m_1^s = -5 \times 10^{-4}\mathrm{kPa}^{-1}; \quad m_2^s = 0.2m_1^s; \\ &m_1^w = 0.1m_1^s; \quad m_2^w = 4m_1^w. \end{aligned} \quad [6\text{-}30]$$

- Physical properties:

$$\begin{aligned} &R = 8.314\mathrm{J.mol}^{-1}\mathrm{K}^{-1}; \quad M = 0.029\mathrm{kg.mol}^{-1}; \\ &\Theta = (\theta^\circ + 273.16)\mathrm{K}; \quad \theta^\circ = 20^\circ\mathrm{C}. \end{aligned} \quad [6\text{-}31]$$

The sudden application of load to an unsaturated soil stratum results in instantaneous undrained compression and consequently, immediate increase in pore pressures, known as initial excess pore pressures. Based on the existing estimations provided by Fredlund & Hasan (1979), and Conte (2004), an external loading $q_0 = 100\mathrm{kPa}$ may immediately generate an initial excess pore-air pressure $u_a^0 = 20\mathrm{kPa}$ and an initial excess pore-water pressure $u_w^0 = 40\mathrm{kPa}$. Detailed explanation regarding the estimation of the initial excess pore pressures is presented in Appendix D. It is assumed that these initial excess

pore pressures are ubiquitous of values u_a^0 and u_w^0 in the soil deposit, except for permeable boundaries. All the given parameters in Equations [6-30] and [6-31] are employed to obtain the consolidation coefficients presented in Equation [6-4].

Example 1 investigates effects of air to the water permeability ratio, k_a/k_w (isotropic permeability ratio), and the horizontal to vertical permeability ratio, k_x/k_z (anisotropic permeability ratio), on the 2D consolidation process. The ratio k_a/k_w varies in the range of 10^{-2} to 10^3, in which k_a is a variable while k_w is kept constant (i.e. $k_{w_x} = k_{w_z} = 10^{-10} ms^{-1}$). Similarly, assuming the diagonal permeability k_{xz} is zero, the ratio k_x/k_z changes from 1 to 10 as k_x increases whilst k_z remains unchanged (i.e. $k_{a_z} = 10^{-9} ms^{-1}$ and $k_{w_z} = 10^{-10} ms^{-1}$). In this investigation, the uniform distribution of initial excess pore pressures is employed for both isotropic and anisotropic permeability conditions ($\zeta_a = \zeta_w = 0$). In contrast, Example 2 adopts linear distribution of initial pore pressures, in which ζ_a and ζ_w are in the range between 0 and 1. Example 2 is to study the variations of the dissipation rates as well as the degree of consolidation due to the changes in ζ_a and ζ_w. It should be noted that, although soil cementation and visco-plastic behaviour can significantly influence the time-dependent deformation of soil (Nguyen et al. 2014; Le et al. 2015), these areas have not been captured in this study.

6.5.1. Worked example 1

In this example, the uniform distribution of initial excess pore pressures is applied throughout the soil depth. This means that the dimensionless parameters ζ_a and ζ_w can be discarded and Equation [6-7] then becomes:

$$u_a(x, z, 0) = u_a^0 \quad [6\text{-}32a]$$

$$u_w(x, z, 0) = u_w^0 \quad [6\text{-}32b]$$

The terms $T_a^{ij}(0)$ and $T_w^{ij}(0)$ can be determined using the orthogonality of sine function based on Equations [6-32a] and [6-32b], respectively. The obtained $T_a^{ij}(0)$ and $T_w^{ij}(0)$ are then substituted into Equations [6-24] and [6-25]. A complete set of equations $u_a(x, z, t)$ and $u_w(x, z, t)$ are presented in Equations [C-1] – [C-3] in Appendix C. Equations [C-1] and [C-2] predict the dissipation process of excess pore pressures adopting isotropic and anisotropic permeability conditions, respectively. For

the graphical presentation, the point of investigation is located at x = 1m (i.e. x/L = 0.5) and z = 4m (i.e. z/H = 0.8). Figures 6.3 and 6.4 obtained from Equation [C-1] depict the changes in normalised excess pore pressures (i.e. u_a/u_a^0 and u_w/u_w^0) against different values of k_a/k_w, whilst Figures 6.5 and 6.6 obtained from Equation [C-2] show the changes in excess pore pressures investigating variations of k_x/k_z.

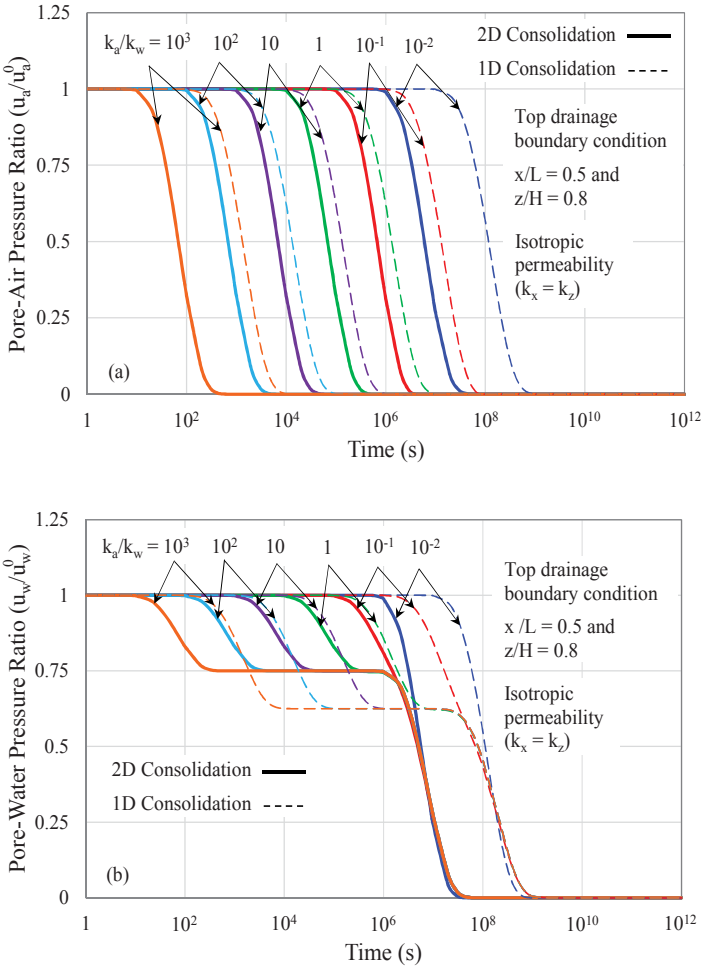

Figure 6.3. Dissipation of (a) excess pore-air and (b) excess pore-water pressures varying with k_a/k_w under top drainage boundary condition

Figures 6.3(a) and 6.4(a) illustrate a group of parallel curves of excess pore-air pressure for different values of k_a/k_w. It can be observed that higher values of k_a/k_w result in a higher dissipation rate of excess pore-air pressure. This graphically indicates that the normalised curves are shifted to the left. Figures 6.3(b) and 6.4(b) show the typical double inverse S curves demonstrating the dissipation pattern for water. The

dissipation process can be separated into two stages due to the distinctive double S-shaped pattern. It is observed that the required time for an upper inverse S curve to be formed, is about the same time that the excess pore-air pressure is fully dissipated. During this time, the process is identified as the first stage of dissipation. The second stage begins when different curves tend to converge into a single curve. Besides, the consideration of the horizontal drainage in 2D consolidation helps to accelerate the changes in excess pore pressures. This indicates that the consolidation with both vertical and horizontal drainage conditions proceeds more quickly than that with vertical drainage condition as expected (see Figures 6.3 and 6.4).

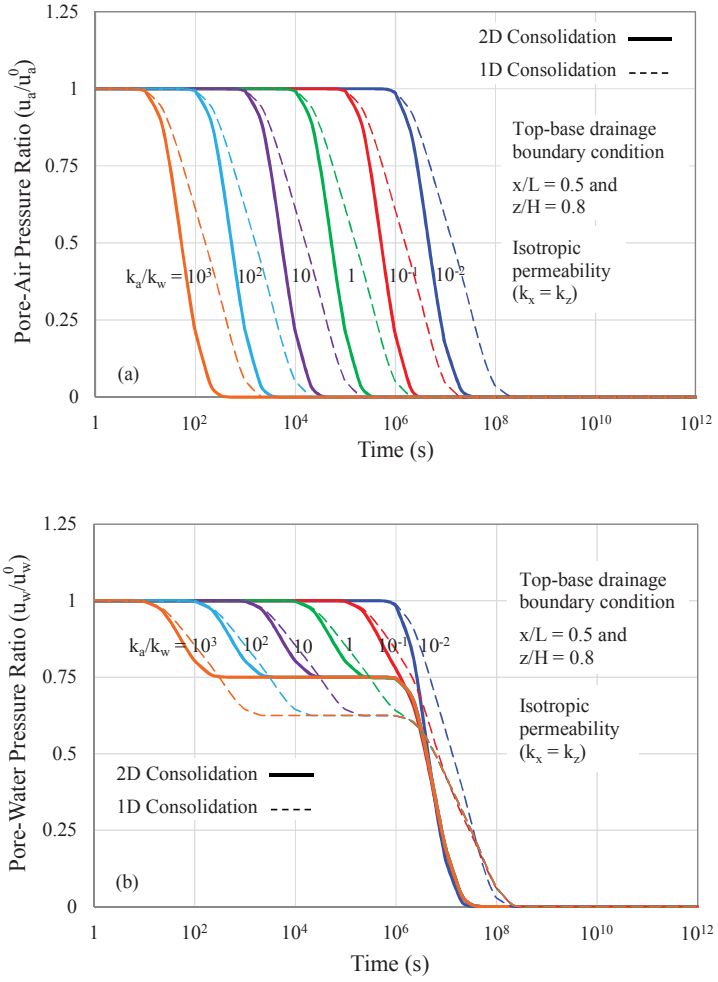

Figure 6.4. Dissipation of (a) excess pore-air and (b) excess pore-water pressures varying with k_a/k_w under top-base drainage boundary condition

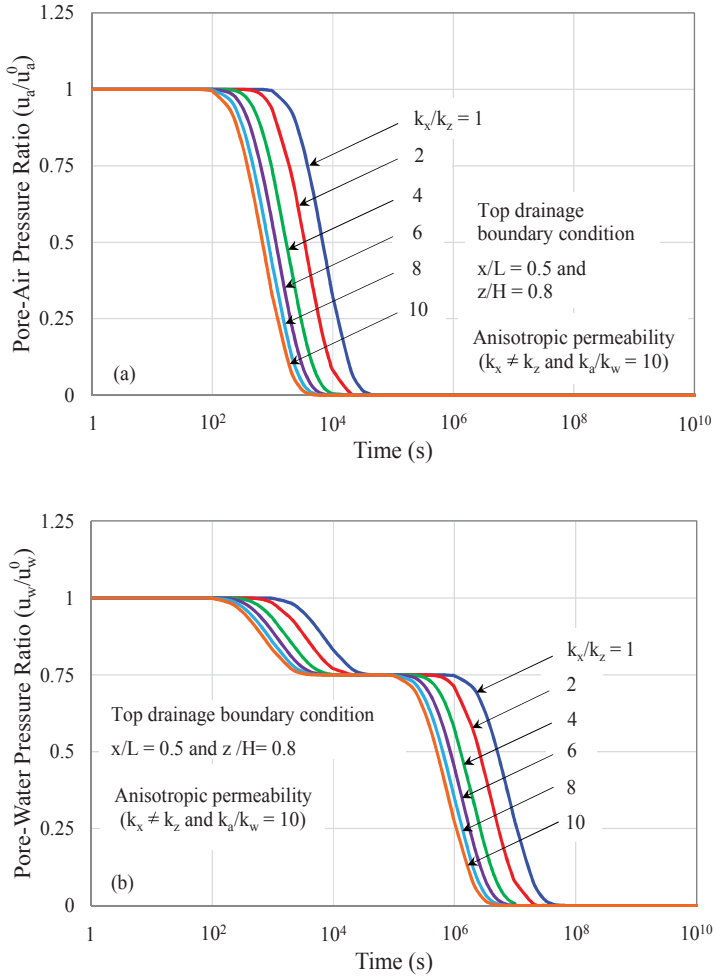

Figure 6.5. Dissipation of (a) excess pore-air and (b) excess pore-water pressures varying with k_x/k_z under top drainage boundary condition

For the analysis of anisotropic permeability condition, when considering $k_x/k_z = k_{a_x}/k_{a_z} = k_{w_x}/k_{w_z}$ whilst k_{a_z} and k_{w_z} are constant, it is obvious that different values of k_x/k_z significantly influence the dissipation rate for both air and water phases. As evidenced in Figures 6.5 and 6.6, the dissipation process with higher k_x/k_z (eg. 8 – 10) tends to progress relatively faster than that of smaller k_x/k_z, but it may also reduce the effects of vertical drainage on the dissipation. This can be explained that the vertical drains installed in the soil stratum provides shorter drainage path in the horizontal dimension and allows appreciably large amount of excess pore-air and pore-water pressures to be horizontally dissipated. As the result, when k_x/k_z increases, the rate of dissipation in the top drainage condition is found to be very similar to that in the top-

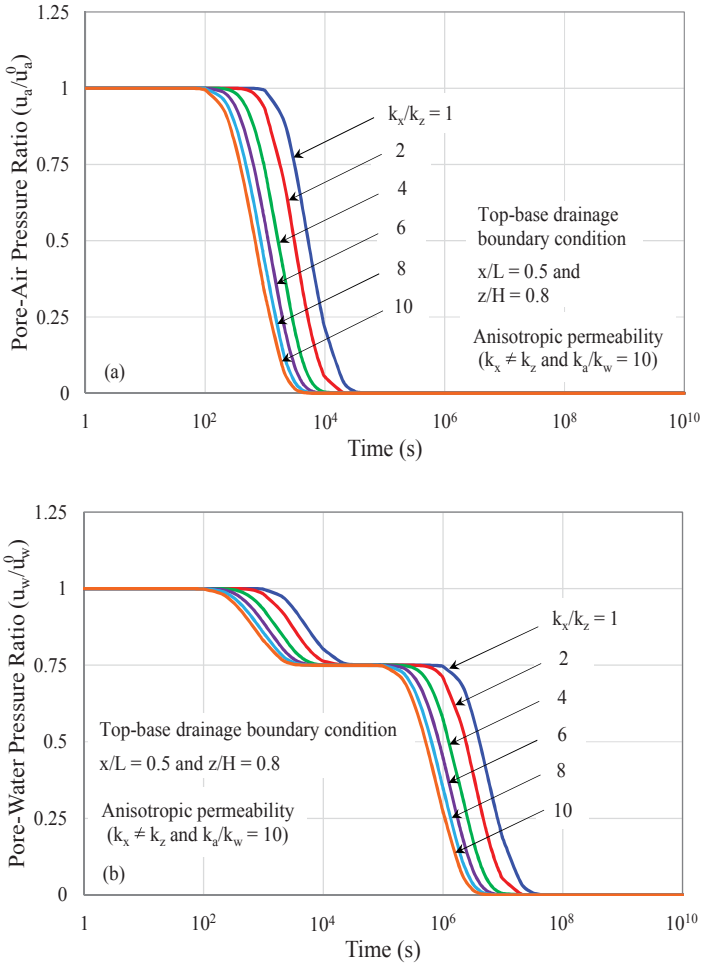

Figure 6.6. Dissipation of (a) excess pore-air and (b) excess pore-water pressures varying with k_x/k_z under top-base drainage boundary condition

base drainage condition. For instance, by examining k_x/k_z of 10 in Figures 6.5 and 6.6, the excess pore pressures under both boundary conditions are reported to diminish at almost the same time (i.e. 5×10^3s for pore-air pressure and 10^7s for pore-water pressure).

The average degree of consolidation ($\bar{U}$) can be determined by combining Equations [6-29] and [6-32]. A complete set of equations to predict $\bar{U}$ is presented in Equations [C-4] – [C-8] in Appendix C. Figures 6.7 and 6.8 illustrate the variation patterns of $\bar{U}$ against time factor T for isotropic and anisotropic permeability conditions, respectively. In this study, the time factor T is defined as $T = k_w t/(m_1^s \gamma_w H^2)$ for the isotropic permeability and $T = k_{w_z} t/(m_1^s \gamma_w H^2)$ for the anisotropic permeability. Similar to the

excess pore-water pressure, the pattern of $\overline{U}$ can be divided into two stages based on the typical double S curve. The first stage includes simultaneous dissipation of both excess pore-air and pore-water pressures, whereas later stages only present an air-free consolidation similar to that of saturated soils. For the case of isotropic permeability ($k_x = k_z$), the double S curve can be easily identified when k_a/k_w is greater than 0.1. The higher k_a/k_w may also result in more rapid dissipation of pore-air pressure and induces an instantaneous rate of consolidation at the beginning of the loading process. With an assistance of vertical drains, the soil stratum is prone to settle more quickly than that in the 1D field (see Figure 6.7). Based on numerical predictions reported in Figures 6.3, 6.4 and 6.7, it can be observed that the consolidation rate in the top-base drainage condition is slightly faster compared to that in the top drainage condition only. However, since the adopted vertical drain spacing ($L = 2m$) is smaller than the soil depth ($H = 5m$), the horizontal consolidation is more significant than the vertical consolidation. Thus, effects of vertical drainage are much attenuated since horizontal drainage is introduced to the soil system. This indicates that larger amount of excess pore pressures preferably dissipate through horizontal boundaries in this case study. An equivalent concept can be seen in Figure 6.8. The increase in k_x/k_z accelerates the consolidation process, but it may as well hinder the dissipation through vertical boundaries, resulting in similar consolidation rate in both top and top-base drainage conditions.

In this study, for the sake of simplicity, the Mandel-Cryer effect has been neglected in the computation process. The Mandel-Cryer effect, which induces an additional increase in excess pore-water pressure prior to dissipation, is often captured in the coupled consolidation theory for fully saturated soils (Mandel 1953; Cryer 1963). This may consequently reduce the consolidation rate as the Poisson's ratio decreases. This aspect was pointed out in the coupled solution provided by Gibson (1970). However, according to Wong et al. (1998), Vu (2008), and Conte (2004), the Mandel-Cryer effect is considered to be minimal in unsaturated soils. Based on the coupled solution proposed by Wong et al. (1998), under a constant loading, the maximum increase in pore-water pressure in a specimen, induced by the mentioned effect, is relatively small. Vu (2008) investigated the volume change problems in expansive soils considering variations of matric suction due to moisture infiltration and confirmed that the Mandel-

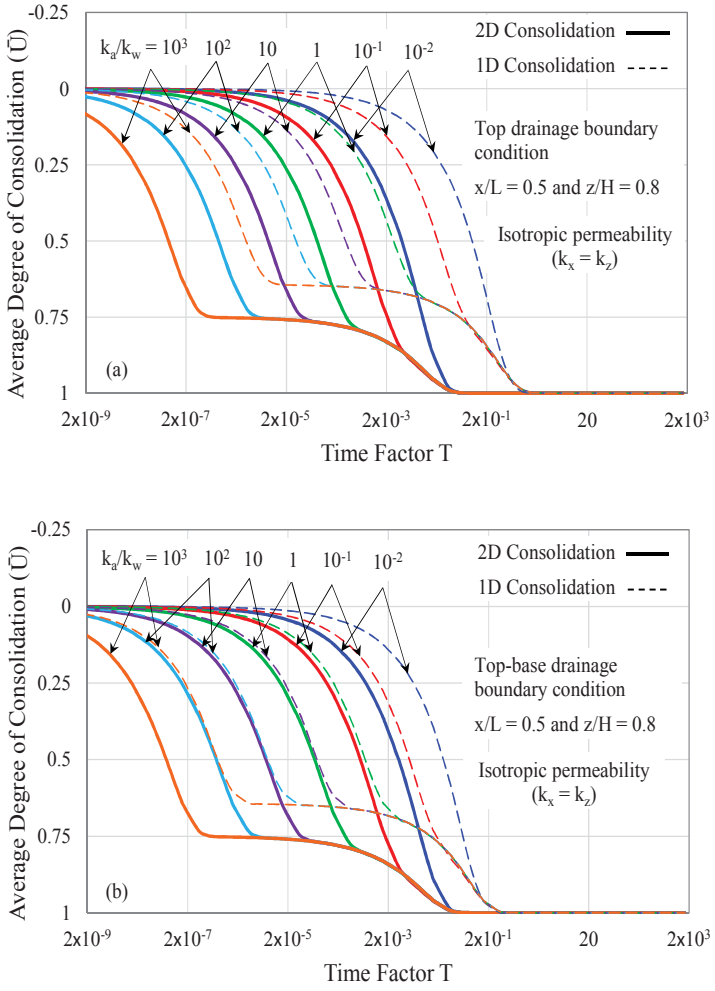

Figure 6.7. Average degree of consolidation varying with k_a/k_w under (a) top drainage and (b) top-base drainage boundary conditions

Cryer effect would play a little role in the study. Through the numerical analysis, Conte (2004) further reported that this effect may be significantly alleviated when the depth of the soil increases or the Poisson's ratio decreases. Moreover, Conte (2004) numerically demonstrated the insignificant difference in the degree of consolidation in both coupled and uncoupled solutions for unsaturated soils, indicating that the simple uncoupled solution may generally provide a valid approximation to the coupled theory.

Examining the isotropic permeability consolidation only ($k_x = k_z$), Figures 6.9 and 6.10 illustrate excess pore pressure isochrones varying with T (in both domains x and z) under the top and top-base drainage boundary systems, respectively. The ratio k_a/k_w of

0.1 is considered for this analysis. The pore-air and pore-water pressure isochrones represent typical patterns induced by the uniform distribution of initial pore pressures along z-direction. These sets of isochrones satisfy both drainage boundary conditions and confirm the traditional consolidation theory in which excess pore pressures gradually dissipate as time increases (Figures 6.9(a) and 6.10(a)). For the x-direction, the pore pressure isochrones are influenced by the double side drainage due to the vertical sand drains, in which pressures at the left (x = 0) and right (x = L) boundaries are zero (Figures 6.9(b) and 6.10(b)).

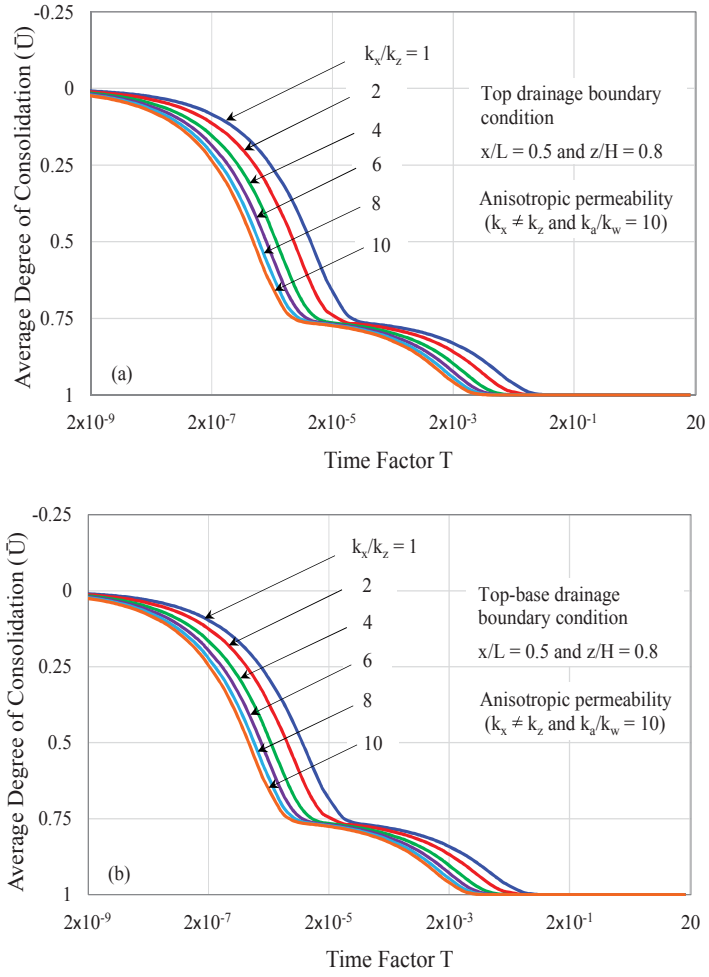

Figure 6.8. Average degree of consolidation varying with k_x/k_z under (a) top drainage and (b) top-base drainage boundary conditions

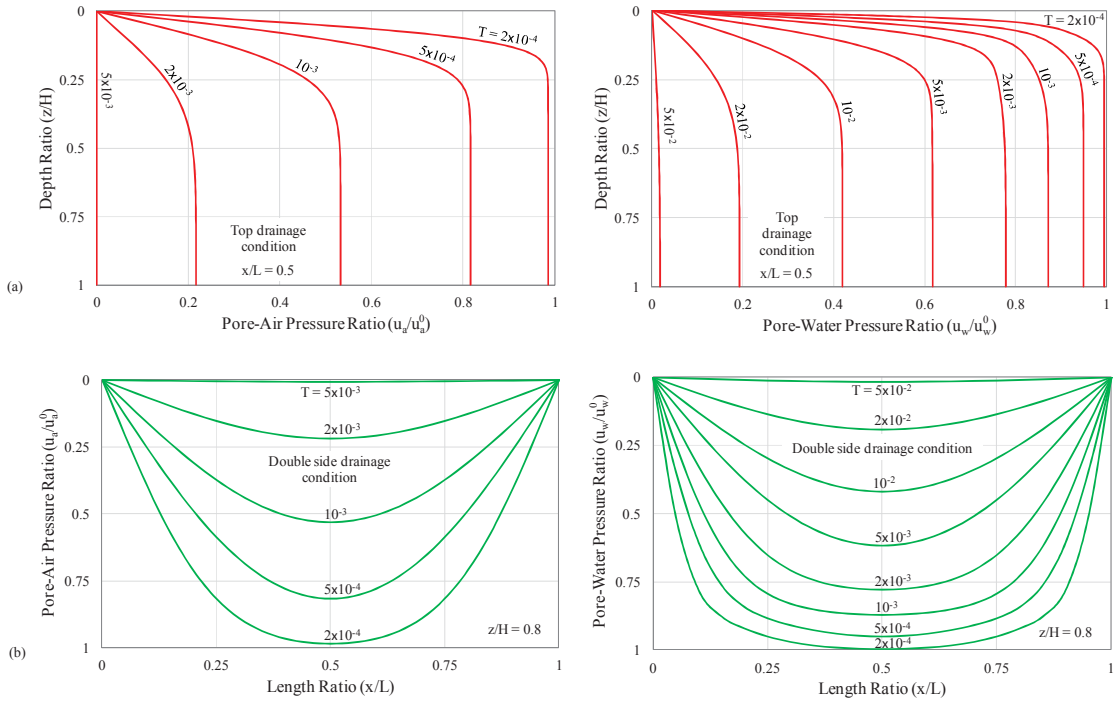

Figure 6.9. Excess pore pressure isochrones against (a) depth ratio and (b) length ratio due to effects of k_a/k_w under top drainage boundary condition

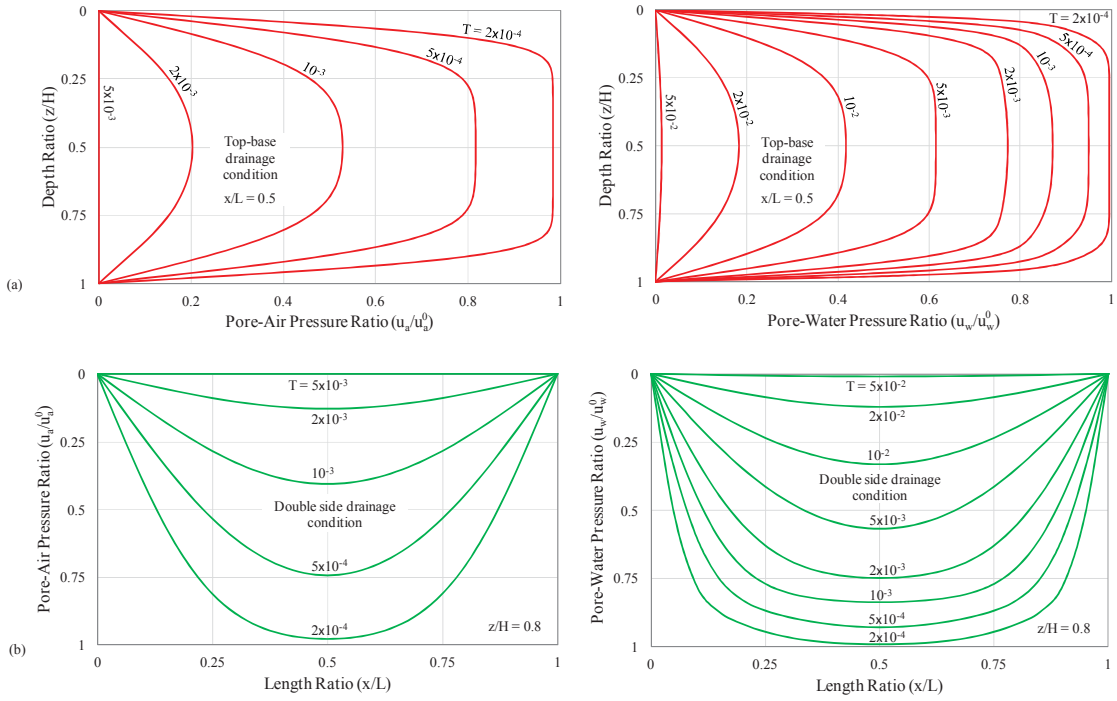

Figure 6.10. Excess pore pressure isochrones against (a) depth ratio and (b) length ratio due to effects of k_a/k_w under top-base drainage boundary condition

6.5.2. Worked example 2

Example 2 generally analyses the effects of the proposed parameters ζ_a and ζ_w, introduced in Equation [6-7], on the 2D consolidation process. The initial excess pore pressures are assumed to be distributed linearly with depth, thus, the simulated initial conditions will have ζ_a and ζ_w greater than 0. The variations of normalised excess pore-air $(u_a/[u_a^0(1-\zeta_a z/H)])$ and pore-water $(u_w/[u_w^0(1-\zeta_w z/H)])$ pressures as well as the average degree of consolidation $(\bar{U})$ will be analysed in this study. The Fourier coefficients $T_a^{ij}(0)$ and $T_w^{ij}(0)$ can be computed using the orthogonality of the sine function based on Equation [6-7]. A complete set of equations for $u_a(x,z,t)$ and

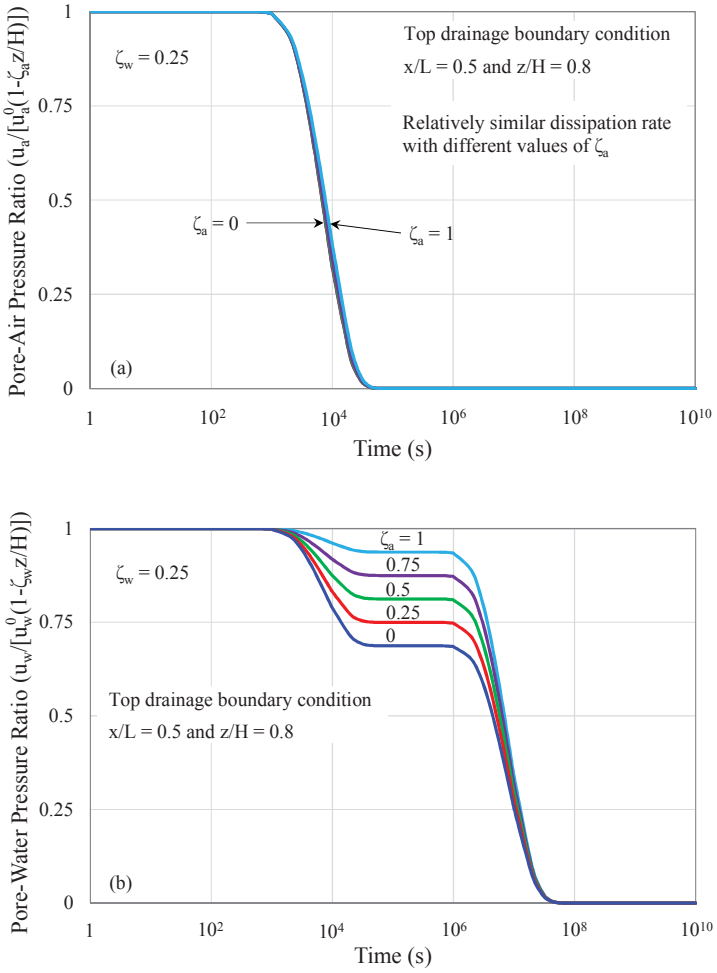

Figure 6.11. Dissipation of (a) excess pore-air and (b) excess pore-water pressures varying with ζ_a under top drainage boundary condition

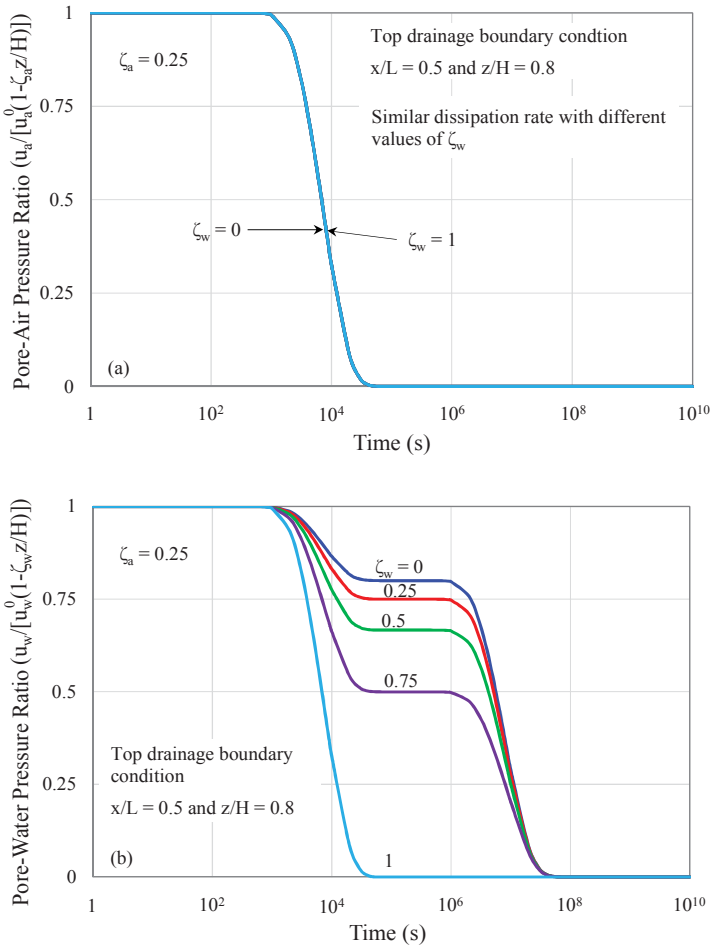

Figure 6.12. Dissipation of (a) excess pore-air and (b) excess pore-water pressures varying with ζ_w under top drainage boundary condition

$u_w(x, z, t)$ are presented in Equations [C-9] – [C-12] in Appendix C. Equations [C-9] and [C-10] estimate the dissipation of excess pore pressures adopting isotropic and anisotropic permeability conditions, respectively. For the sake of the graphical representation, this worked example only highlights the isotropic permeability condition. The location of an investigated point is similar to Section 5.1 and $k_a/k_w = 10$. Under the top drainage boundary condition, Figure 6.11 illustrates the changes in excess pore pressures with increasing ζ_a (from 0 to 1) and constant ζ_w (0.25), whereas Figure 6.12 investigates a reverse effect of ζ_a and ζ_w on the changes in excess pore pressures. Besides, Figures 6.13 and 6.14 are plotted to investigate the same effects for the top-base drainage boundary system.

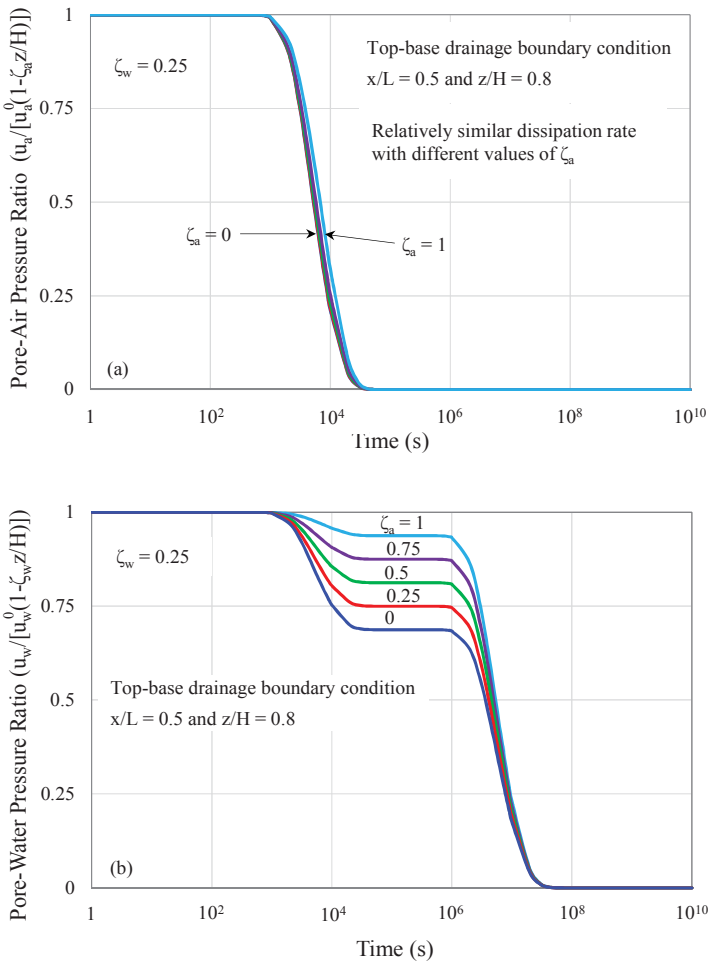

Figure 6.13. Dissipation of (a) excess pore-air and (b) excess pore-water pressures varying with ζ_a under top-base drainage boundary condition

As shown in Figure 6.11(a), variations in ζ_a (whilst ζ_w is constant) have insignificant effects on the dissipation rate of excess pore-air pressure. It can be observed that the excess pore-air pressure curves with different values of ζ_a almost overlap, and the full dissipation is achieved at the same time (i.e. about 5×10^4s). In fact, increasing ζ_a leads to reduction of the average initial pore-air pressure, and the initial pore-water pressure becomes more considerable at the beginning of the dissipation process. Thus, the insignificant excess pore-air pressure may result in a relatively slower change in the pore-water pressure during the first stage (Figure 6.11(b)). At the second stage, pore-water pressures (adopting different values of ζ_a) diminish with almost the same rate.

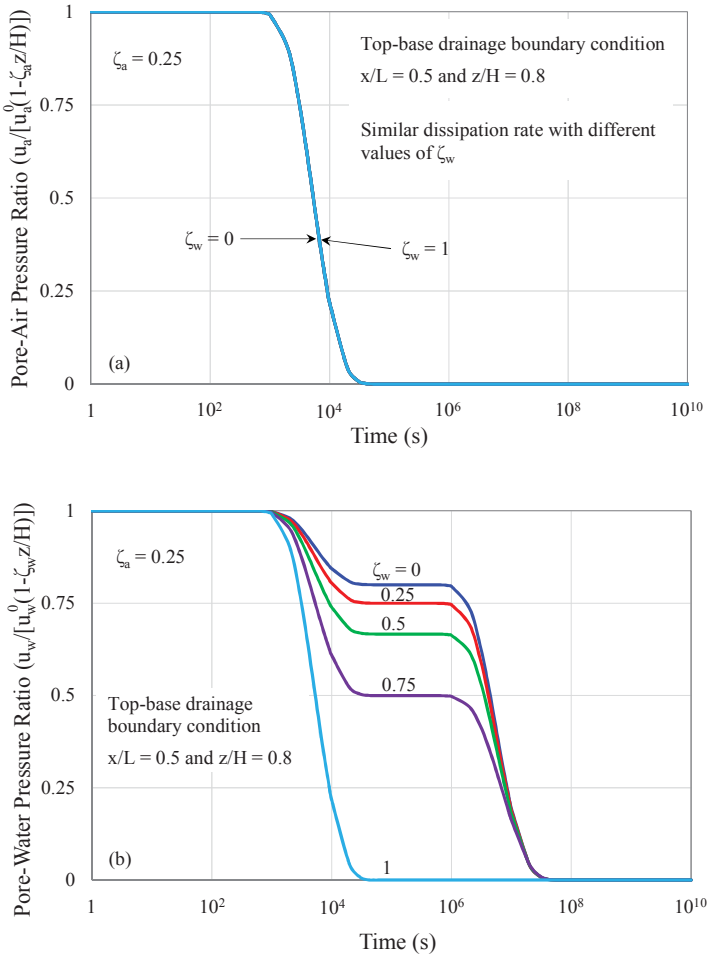

Figure 6.14. Dissipation of (a) excess pore-air and (b) excess pore-water pressures varying with ζ_w under top-base drainage boundary condition

Example 2 investigates the effects of ζ_w on the dissipation of excess pore pressures. As illustrated in Figure 6.12(a), the data obtained from Equation [C-9] indicates that the variations in ζ_w (whilst ζ_a is constant) have insignificant effects on the excess pore-air pressure. However, it is observed that the increase in ζ_w accelerates the excess pore-water pressure dissipation during the first stage. Similar to the effects of ζ_a, the increasing ζ_w reduces the average initial pore-water pressure, and that eventually becomes less significant compared to the initial pore-air pressure, leading to a quicker rate of excess pore-water pressure dissipation at the first stage. When $\zeta_w = 1$, the excess pore-water pressure is fully dissipated before the excess pore-air pressure diminishes (Figure 6.12(b)). Figures 6.13 and 6.14 demonstrate the similar consolidation behaviour in the top-base drainage boundary condition. As expected, the inclusion of both

horizontal and vertical drainage in the soil increases the dissipation rate of excess pore-air and pore-water pressures.

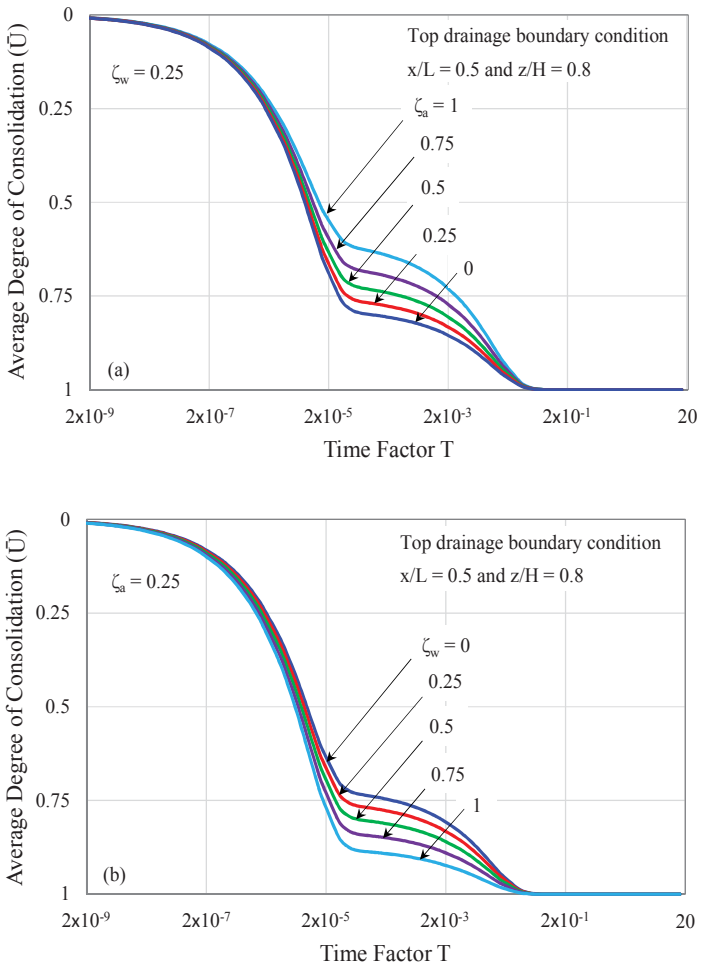

Figure 6.15. Average degree of consolidation varying with (a) ζ_a and (b) ζ_w under top drainage boundary condition

The average degree of consolidation ($\bar{U}$) can be estimated by combining Equations [6-7] and [6-29]. A complete set of equations to predict $\bar{U}$ is presented in Equations [C-13] – [C-17] in Appendix C. Figure 6.15 predicts the variation of $\bar{U}$ against the time factor T incorporating the effects of ζ_a and ζ_w under the top drainage condition whereas Figure 6.16 shows similar study under the top-base drainage condition. It is apparent that noticeable changes in $\bar{U}$ occur in the later stages of consolidation. In particular, the increasing ζ_a decelerates the consolidation whereas the increasing ζ_w accelerates the

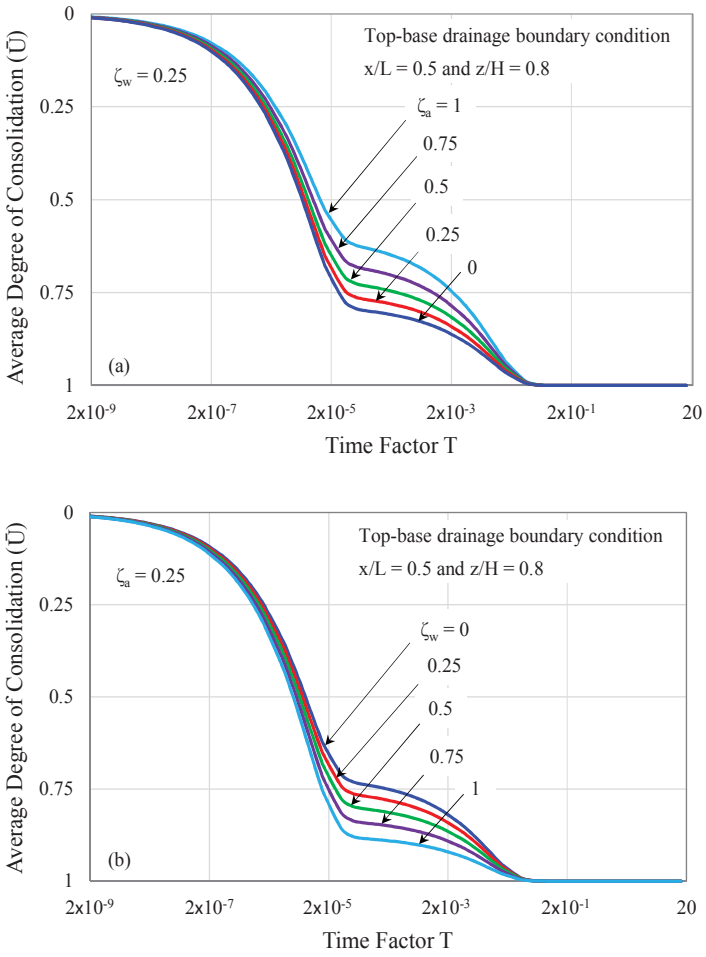

Figure 6.16. Average degree of consolidation varying with (a) ζ_a and (b) ζ_w under top-base drainage boundary condition

consolidation process (Figure 6.15). Such behaviour is mainly due to the impact of ζ_a and ζ_w on the dissipation rate of excess pore pressures, which was explained earlier. Similar time-dependent variations of $\bar{U}$ can be observed in Figure 6.16. The consolidation ends at about the same time regardless of values of ζ_a and ζ_w (i.e. before 10^8s for both top and top-base drainage conditions).

Figures 6.17 and 6.18 introduce the excess pore pressure isochrones (along x- and z-directions) under the top and top-base drainage boundary conditions, respectively, whilst $\zeta_a = \zeta_w = 0.5$ and the ratio $k_a/k_w = 0.1$ are adopted. Figure 6.17(a) shows some minor increases in excess pore-air and pore-water pressures at the impervious boundary ($z = H$). This phenomenon happens as the result of redistribution of the

existing initial excess pore pressures to achieve the pressure equilibrium throughout the soil stratum. Under the instantaneous loading, the soil medium only allows some excess pore pressures to dissipate through the permeable top surface at the very early stages of the consolidation, whilst the remaining excess pore pressures are pushed down towards the impervious base. This explains why the excess pore-air and pore-water pressure ratios are greater than 1 at z = H at the early stages. As time elapses, the pore pressure isochrones are believed to recover to their original pattern as presented in Figure 6.8. Additionally, Figure 6.17(b) presents a set of pore pressure isochrones along the x-axis. It can be observed that pressures are zero at x = 0 and x = L due to two vertical sand drains. Unlike the top drainage condition, the isochrones in top-base drainage condition (over z-direction) do not exceed 1 as the result of shorter drainage path (Figure 6.18).

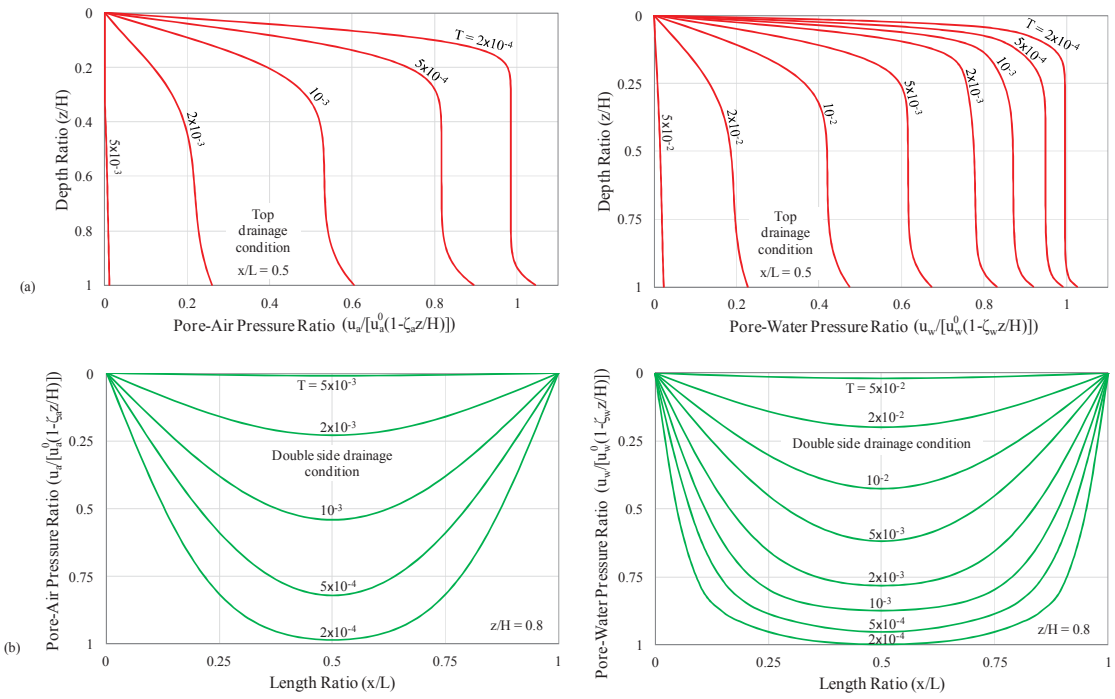

Figure 6.17. Excess pore pressure isochrones against (a) depth ratio and (b) length ratio due to effects of ζ_a and ζ_w under top drainage boundary condition

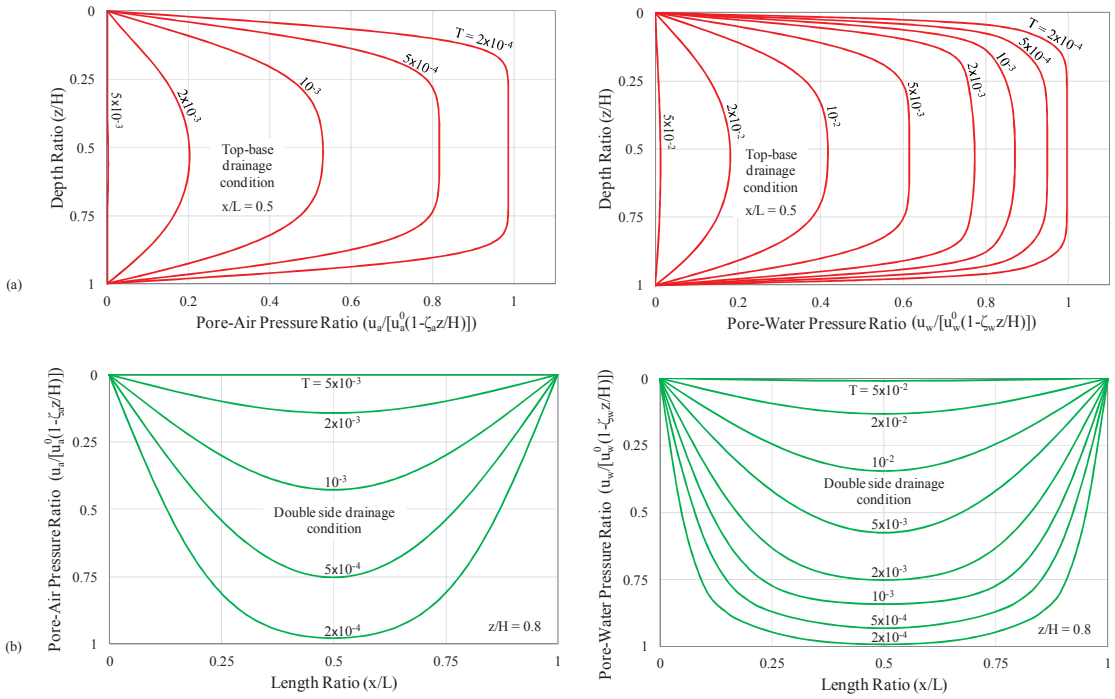

Figure 6.18. Excess pore pressure isochrones against (a) depth ratio and (b) length ratio due to effects of ζ_a and ζ_w under top-base drainage boundary condition

6.6. Summary

This study has provided a closed form analytical solution for the 2D plane strain consolidation of unsaturated soils using the eigenfunction expansion and Laplace transform techniques. The analytical development captures the applications of uniform and linear distributions of initial excess pore pressures. At first, the eigenfunctions and eigenvalues are determined based on the homogeneous boundary conditions. By substituting these eigenfunctions into the given governing equations of flow, the new ordinary differential equations are derived. Then, the Laplace transform method is applied to obtain an exact solution for the newly derived differential equations.

Two worked examples have been introduced in this study. Example 1 has investigated the effects of both isotropic and anisotropic permeability conditions capturing the uniformly distributed initial pore pressures. As expected, for the isotropic permeability, the change in k_a/k_w results in the typical double S-shaped curves for the excess pore-water pressure dissipation and average degree of consolidation, and single curves for the excess pore-air pressure dissipation. For the anisotropic permeability, it

has been observed that the increase in k_x/k_z results in slightly faster 2D consolidation rate. In addition, the consolidation rate of the top drainage boundary system has been found to be similar to that of the top-base drainage system as k_x/k_z increases. Example 2 has presented the consolidation process when considering the linearly distributed initial pore pressures. In this example, the effects of both initial pore-air and pore-water pressure distributions have been investigated. Generally, the distribution of initial excess pore pressures has insignificant effects on the excess pore-air dissipation but significantly influences the excess pore-water pressure dissipation rate. Two sets of isochrones along x- and z-directions have been presented in both examples. For the case of linearly distributed initial pore pressures, several minor increases in excess pore pressures have been observed at the impervious base boundary during the early stages of consolidation. This phenomenon occurs to redistribute the pore pressures in the soil stratum under the external surcharge.

CHAPTER 7

ANALYTICAL SOLUTION FOR THE TWO-DIMENSIONAL PLANE STRAIN CONSOLIDATION OF AN UNSATURATED SOIL STRATUM SUBJECTED TO TIME-DEPENDENT LOADING

7.1. Introduction

Having realised a limited analytical study about 2D plane strain consolidation system, particularly for unsaturated soils subjected to different types of loading, this chapter introduces a closed-form analytical solution predicting the dissipation of excess pore-air and pore-water pressures and settlement using the continuity equations proposed by Dakshanamurthy & Fredlund (1980). The mathematical development adopts eigenfunction expansion and Laplace transformation methods along with homogeneous drainage boundary conditions and uniform initial conditions. Four different time-dependent loadings, namely, ramping, asymptotic, sinusoid and damped sine wave, are simulated and incorporated into the solution. Examples for mentioned loading cases and validation for ramped loading will be provided hereafter.

7.2. Governing equations of 2D plane-strain consolidation

The typical unsaturated soil is a three-phase geomaterial primarily consisting of air, water and soil skeleton. Immediately after the surcharge, the excess pore-air and pore-water pressures can be generated and gradually dissipated with time through permeable boundaries. This phenomenon eventually results in a considerable reduction in the soil volume. The following continuity equations for 2D consolidation of unsaturated soils in the Cartesian coordinate system (x, z) are conceptually based on the model proposed by Dakshanamurthy & Fredlund (1980):

$$\frac{\partial u_a}{\partial t} + C_a\left(\frac{\partial u_w}{\partial t}\right) + c^a_{v_x}\left(\frac{\partial^2 u_a}{\partial x^2}\right) + c^a_{v_z}\left(\frac{\partial^2 u_a}{\partial z^2}\right) - c^a_\sigma\left[\frac{\partial(\sigma_x+\sigma_z)}{\partial t}\right] = 0 \qquad [7\text{-}1a]$$

$$\frac{\partial u_w}{\partial t} + C_w\left(\frac{\partial u_a}{\partial t}\right) + c_{v_x}^w\left(\frac{\partial^2 u_w}{\partial x^2}\right) + c_{v_z}^w\left(\frac{\partial^2 u_w}{\partial z^2}\right) - c_\sigma^w\left[\frac{\partial(\sigma_x+\sigma_z)}{\partial t}\right] = 0 \quad [7\text{-}1b]$$

where σ_x and σ_z is the total stress in x- and z-directions, respectively (kPa); u_a and u_w are excess pore-air and pore-water pressures, respectively (kPa); C_a and C_w are interactive constants with respect to air and water phases, respectively; $c_{v_x}^a$, $c_{v_z}^a$ and c_σ^a are the consolidation coefficients for air phases (m^2/s); and $c_{v_x}^w$, $c_{v_z}^w$ and c_σ^w are the consolidation coefficients for water phases (m^2/s). The consolidation parameters can be expressed as follows:

$$C_a = \frac{1}{\left[\left(\frac{m_1^a}{m_2^a}-1\right)-\frac{n(1-S_r)}{m_2^a(u_a^0+u_{atm})}\right]} \quad [7\text{-}2a]$$

$$c_{v_x}^a = \frac{k_{a_x}R\Theta}{gM}\frac{1}{\left[m_2^a(u_a^0+u_{atm})\left(\frac{m_1^a}{m_2^a}-1\right)-n(1-S_r)\right]} \quad [7\text{-}2b]$$

$$c_{v_z}^a = \frac{k_{a_z}R\Theta}{gM}\frac{1}{\left[m_2^a(u_a^0+u_{atm})\left(\frac{m_1^a}{m_2^a}-1\right)-n(1-S_r)\right]} \quad [7\text{-}2c]$$

$$c_\sigma^a = \frac{1}{2\left[\left(1-\frac{m_2^a}{m_1^a}\right)-\frac{n(1-S_r)}{m_1^a(u_a^0+u_{atm})}\right]} \quad [7\text{-}2d]$$

$$C_w = \left(\frac{m_1^w}{m_2^w}-1\right) \quad [7\text{-}2e]$$

$$c_{v_x}^w = \frac{1}{m_2^w}\left(\frac{k_{w_x}}{\gamma_w}\right) \quad [7\text{-}2f]$$

$$c_{v_z}^w = \frac{1}{m_2^w}\left(\frac{k_{w_z}}{\gamma_w}\right) \quad [7\text{-}2g]$$

$$c_\sigma^w = \frac{m_1^w}{2m_2^w} \quad [7\text{-}2h]$$

where k_{a_x} and k_{w_x} are coefficients of air and water permeability in x-direction (m/s), respectively; k_{a_z} and k_{w_z} are coefficients of air and water permeability in z-direction, respectively; g is the gravitational acceleration ($\sim 9.8 m/s^2$); u_a^0 is the initial pore-air pressure; u_{atm} is the atmospheric pressure; R is the universal air constant ($\sim 8.3 J.mol^{-1}K^{-1}$); $\Theta = (\theta^\circ + 273)$, is the absolute temperature (K); M is the molecular mass of air phase ($\sim 0.029 kg/mol$); n is the soil porosity; S_r is the degree of saturation; γ_w is the unit weight of water ($\sim 9.8 kN/m^3$); m_1^a and m_1^w are coefficients of air and water volume change with respect to the change of net stress (kPa^{-1}), respectively; and m_2^a and m_2^w are coefficients of air and water volume change with respect to the change

of suction, respectively. Equations [7-1a] and [7-1b] can be rewritten in simplified forms as follows:

$$u_{a,t} + C_a u_{w,t} + c_{v_x}^a u_{a,xx} + c_{v_z}^a u_{a,zz} - c_\sigma^a\left(\sigma_{x,t} + \sigma_{z,t}\right) = 0 \qquad [7\text{-}3a]$$

$$u_{w,t} + C_w u_{a,t} + c_{v_x}^w u_{w,xx} + c_{v_z}^w u_{w,zz} - c_\sigma^w\left(\sigma_{x,t} + \sigma_{z,t}\right) = 0 \qquad [7\text{-}3b]$$

Equations [7-3a] and [7-3b] are a set of continuity equations describing flows of air and water phases. It should be noted that when the applied surcharge is time-dependent, $\partial\sigma_x/\partial t \neq 0$ and $\partial\sigma_z/\partial t \neq 0$. The continuity equations consist of three variables, x (horizontal direction), z (vertical direction) and t (time); and can be presented under PDEs.

7.3. Analytical solution for excess pore pressure dissipation

The vertical drain assisted preloading is one of the most commonly used ground improvement methods in geotechnical practice to shorten the duration of soil consolidation by facilitating the drainage characteristics in soils. According to Horne (1964), and Walker & Indraratna (2009), the drainage in horizontal direction, induced by vertical drains, may proceed much faster due to the reduced drainage path and consideration of the horizontal permeability. This study presents a referential profile of an unsaturated soil stratum with a finite thickness H and two vertical drains, whose internal space is denoted as L (see Figure 7.1). Figure 7.1(a) demonstrates a homogeneous soil stratum with a pervious ground surface and impervious bedrock, allowing air and water phases to dissipate through the top (pervious ground surface) and the lateral (vertical drains) boundaries. Figure 7.1(b) shows a soil system consisting of both pervious top and base, indicating free drainage from all boundaries. The two mentioned drainage boundary conditions can be presented as below:

- Vertical boundary:

(a) Top drainage:

$$u_a(x,0,t) = u_w(x,0,t) = 0;$$
$$u_{a,z}(x,H,t) = u_{w,z}(x,H,t) = 0; \qquad [7\text{-}4a]$$

(b) Top and base drainage:

$$u_a(x,0,t) = u_w(x,0,t) = 0;$$
$$u_a(x,H,t) = u_w(x,H,t) = 0; \qquad [7\text{-}4b]$$

- Lateral boundary: $u_a(0,z,t) = u_w(0,z,t) = 0;$

$u_a(L,z,t) = u_w(L,z,t) = 0.$ [7-4c]

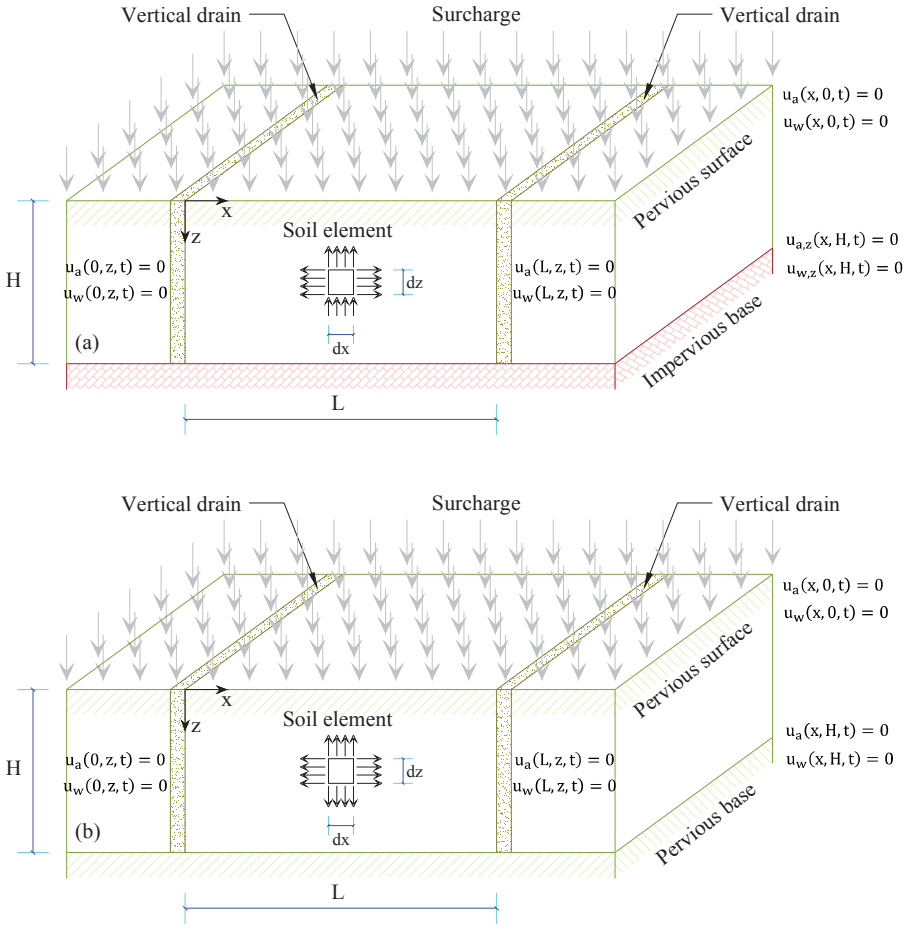

Figure 7.1. The profile of the homogeneous soil stratum representing (a) top drainage boundary system and (b) top-base drainage

It is assumed that, immediately after the loading ($t = 0$), the uniformly distributed initial excess pore-air and pore-water pressures are generated, in the domain $x \in (0, L)$ and $z \in (0, H)$:

$$u_a(x,z,0) = u_a^0 \quad [7\text{-}5a]$$

$$u_w(x,z,0) = u_w^0 \quad [7\text{-}5b]$$

where u_a^0 and u_w^0 are the initial excess pore-air and pore-water pressures ubiquitous along the soil depth, respectively. Unsaturated soils are complex in nature and lack

homogeneity due to their texture assemblage. For simplicity, the following assumptions should be made:

(1) The homogeneous soil is considered throughout the entire stratum;
(2) Solid skeleton and water are incompressible phases;
(3) Environmental factors such as air diffusion and temperature change are neglected;
(4) The air and water flows continuously and independently;
(5) The external loading is boundless and uniformly distributed, thus the settlement induced by the external loading is considered to occur along the vertical direction; and
(6) Consolidation parameters with respect to air phase (C_a, c_v^a and c_σ^a) and water phase (C_w, c_v^w and c_σ^w) are assumed constant during the loading process.

Assumption (5) may be applicable for both flexible and rigid foundations when the loaded area is significantly large (see Figure 7.1). Thus, although the horizontal and vertical drainage conditions are considered in the 2D consolidation, it is acceptable to assume that the settlement occurs along the vertical direction as the external loading is boundless and uniform. Assumption (6), on the other hand, may not be strictly accurate for some cases as the consolidation parameters may vary due to the changes of the soil properties such as permeability coefficients (k_a and k_w), degree of saturation (S_r), and porosity (n). It should be also noted that the permeability coefficients are functions of both water content and degree of saturation (Dakshanamurthy & Fredlund 1980; Fredlund et al. 2012). However, to achieve the closed-form solution in this study, it is necessary to assume these soil properties remain constant during the loading process. Moreover, in consolidation studies for unsaturated soils, constant properties have been already adopted in several existing analytical methods proposed by Qin et al. (2008; 2010b), Shan et al. (2012), and Zhou et al. (2014).

General solutions to Equations [7-3a] and [7-3b] can be expanded using the Fourier sine series of the related homogeneous problems (Haberman 2012), thus,

$$u_a(x,z,t) = \sum_{i=0}^{\infty}\sum_{j=0}^{\infty}\sin(Ix)\sin(Jz)T_a(t) \quad [7\text{-}6a]$$

$$u_w(x,z,t) = \sum_{i=0}^{\infty}\sum_{j=0}^{\infty}\sin(Ix)\sin(Jz)T_w(t) \quad [7\text{-}6b]$$

where $T_a(t)$ and $T_w(t)$ are generalised Fourier coefficients for air and water, respectively, varying against t;

$I = \frac{i\pi}{L}$, for lateral drainage condition over domain x ($i = 0, 1, 2, ...$); and

$J = \frac{(2j+1)\pi}{2H}$, for top drainage condition over domain z ($j = 0, 1, 2, ...$); or

$= \frac{j\pi}{H}$, for top and base drainage condition over domain z. [7-7]

The Fourier sine functions, also known as eigenfunctions, of variables x and z are obtained based on the drainage boundary conditions provided in Equation [7-4]. The term-by-term differentiations with respect to time t in Equation [7-6] yield in:

$$u_{a,t}(x,z,t) = \sum_{i=0}^{\infty}\sum_{j=0}^{\infty}\sin(Ix)\sin(Jz)T_{a,t}(t) \quad [7\text{-}8a]$$

$$u_{w,t}(x,z,t) = \sum_{i=0}^{\infty}\sum_{j=0}^{\infty}\sin(Ix)\sin(Jz)T_{w,t}(t) \quad [7\text{-}8b]$$

Substituting Equations [7-8a] and [7-8b] into Equations [7-3b] and [7-3b], respectively, gives:

$$\sum_{i=0}^{\infty}\sum_{j=0}^{\infty}\sin(Ix)\sin(Jz)T_{a,t}(t) = c_{\sigma}^{a}\left[\sigma_{x,t}(t)+\sigma_{z,t}(t)\right] - \left[C_a u_{w,t} + c_{v_x}^{a}u_{a,xx} + c_{v_z}^{a}u_{a,zz}\right] \quad [7\text{-}9a]$$

$$\sum_{i=0}^{\infty}\sum_{j=0}^{\infty}\sin(Ix)\sin(Jz)T_{w,t}(t) = c_{\sigma}^{w}\left[\sigma_{x,t}(t)+\sigma_{z,t}(t)\right] - \left[C_w u_{a,t} + c_{v_x}^{w}u_{w,xx} + c_{v_z}^{w}u_{w,zz}\right] \quad [7\text{-}9b]$$

By computing orthogonality of sine functions, Equation [7-9] can be presented as follows:

(a) Isotropic permeability condition ($k_x = k_z$):

$$T_{a,t}^{ij}(t) + C_a T_{w,t}^{ij}(t) - c_{v_1}^{a}\left(\Lambda^{ij}\right)T_a^{ij}(t) - \varpi_{ij}c_{\sigma}^{a}\left[\sigma_{x,t}(t)+\sigma_{z,t}(t)\right] = 0 \quad [7\text{-}10a]$$

$$T_{w,t}^{ij}(t) + C_w T_{a,t}^{ij}(t) - c_{v_1}^{w}\left(\Lambda^{ij}\right)T_w^{ij}(t) - \varpi_{ij}c_{\sigma}^{w}\left[\sigma_{x,t}(t)+\sigma_{z,t}(t)\right] = 0 \quad [7\text{-}10b]$$

(b) Anisotropic permeability condition ($k_x \neq k_z$):

$$T_{a,t}^{ij}(t) + C_a T_{w,t}^{ij}(t) - c_{v_2}^{a}\left(\lambda_a^{ij}\right)T_a^{ij}(t) - \varpi_{ij}c_{\sigma}^{a}\left[\sigma_{x,t}(t)+\sigma_{z,t}(t)\right] = 0 \quad [7\text{-}11a]$$

$$T_{w,t}^{ij}(t) + C_w T_{a,t}^{ij}(t) - c_{v_2}^{w}\left(\lambda_w^{ij}\right)T_w^{ij}(t) - \varpi_{ij}c_{\sigma}^{w}\left[\sigma_{x,t}(t)+\sigma_{z,t}(t)\right] = 0 \quad [7\text{-}11b]$$

with $i = 0, 1, 2, ...$; and $j = 0, 1, 2, ...$

where $c_{v_1}^a = \frac{R\Theta}{gM}\frac{k_a}{\left[m_2^a(u_a^0+u_{atm})\left(\frac{2m_1^a}{m_2^a}-1\right)-n(1-S_r)\right]}$; $c_{v_1}^w = \frac{1}{m_2^w}\left(\frac{k_w}{\gamma_w}\right)$;

$c_{v_2}^a = \frac{R\Theta}{gM}\frac{1}{\left[m_2^a(u_a^0+u_{atm})\left(\frac{2m_1^a}{m_2^a}-1\right)-n(1-S_r)\right]}$; $c_{v_2}^w = \frac{1}{m_2^w}\left(\frac{1}{\gamma_w}\right)$;

$\lambda_a^{ij} = k_{a_x}(I)^2 + k_{a_z}(J)^2$; $\lambda_w^{ij} = k_{w_x}(I)^2 + k_{w_z}(J)^2$;

$\Lambda^{ij} = (I)^2 + (J)^2$;

$\varpi^{ij} = \frac{4[1-(-1)^i]}{HLIJ}$, for the top drainage condition; or

$= \frac{4[1-(-1)^i][1-(-1)^j]}{HLIJ}$, for the top and base drainage condition. [7-12]

The terms Λ^{ij} and λ^{ij} ($i = 0, 1, 2, ...$; and $j = 0, 1, 2, ...$), known as separation constants, introduce an isotropic permeability condition ($k_x = k_z$) and an anisotropic permeability condition ($k_x \neq k_z$) to the soil stratum, respectively. Equations [7-10] and [7-11] are now ODEs with a variable t. To solve the first order derivatives, Equations [7-10] and [7-11] are converted into Laplace transformed equations with a complex subjugate s:

(a) Isotropic permeability condition ($k_x = k_z$):

$$\left[s\overline{T}_a^{ij}(s) - T_a^{ij}(0)\right] + C_a\left[s\overline{T}_w^{ij}(s) - T_w^{ij}(0)\right] - c_{v_1}^a\left(\Lambda^{ij}\right)\overline{T}_a^{ij}(s) - \varpi_{ij}c_\sigma^a(1+K)[s\overline{\sigma}_z(s) - \sigma(0)] = 0; \quad [7\text{-}13a]$$

$$\left[s\overline{T}_w^{ij}(s) - T_w^{ij}(0)\right] + C_w\left[s\overline{T}_a^{ij}(s) - T_a^{ij}(0)\right] - c_{v_1}^w\left(\Lambda^{ij}\right)\overline{T}_w^{ij}(s) - \varpi_{ij}c_\sigma^w(1+K)[s\overline{\sigma}_z(s) - \sigma(0)] = 0; \quad [7\text{-}13b]$$

(b) Anisotropic permeability condition ($k_x \neq k_z$):

$$\left[s\overline{T}_a^{ij}(s) - T_a^{ij}(0)\right] + C_a\left[s\overline{T}_w^{ij}(s) - T_w^{ij}(0)\right] - c_{v_2}^a\left(\lambda_a^{ij}\right)\overline{T}_a^{ij}(s) - \varpi_{ij}c_\sigma^a(1+K)[s\overline{\sigma}_z(s) - \sigma(0)] = 0; \quad [7\text{-}14a]$$

$$\left[s\overline{T}_w^{ij}(s) - T_w^{ij}(0)\right] + C_w\left[s\overline{T}_a^{ij}(s) - T_a^{ij}(0)\right] - c_{v_2}^w\left(\lambda_w^{ij}\right)\overline{T}_w^{ij}(s) - \varpi_{ij}c_\sigma^w(1+K)[s\overline{\sigma}_z(s) - \sigma(0)] = 0; \quad [7\text{-}14b]$$

where $\overline{T}_a^{ij}(s)$, $\overline{T}_w^{ij}(s)$ $(i = 0, 1, 2, ...;$ and $j = 0, 1, 2, ...)$ and $\overline{\sigma}_z(s)$ are Laplace transformed functions with complex argument s; and $K = d\sigma_x/d\sigma_z$, describes the ratio of the changes in horizontal and vertical stresses at a point. Based on the elastic theory introduced by Jumikis (1969), these changes depend on the applied loads, point of investigation, and dimensions of the foundation. In the 2D consolidation, when the external loading is considered to be uniform and boundless (Assumption (5)), the K value may be assumed constant throughout the compression process. However, under a non-uniform loading, K value may change during the consolidation due to the lateral deformation of the soil.

The terms $T_a^{ij}(0)$ and $T_w^{ij}(0)$ can be determined using orthogonality of sine functions based on Equation [7-5]:

$$T_a^{ij}(0) = \frac{\int_0^H \int_0^L \{u_a^0 \sin(Ix)\sin(Jz)\}dxdz}{\int_0^H \int_0^L [\sin^2(Ix)\sin^2(Jx)]dxdz} = \varpi_{ij} u_a^0; \qquad [7\text{-}15a]$$

$$T_w^{ij}(0) = \frac{\int_0^H \int_0^L \{u_w^0 \sin(Ix)\sin(Jz)\}dxdz}{\int_0^H \int_0^L [\sin^2(Ix)\sin^2(Jx)]dxdz} = \varpi_{ij} u_w^0. \qquad [7\text{-}15b]$$

The terms $T_a^{ij}(0)$ and $T_w^{ij}(0)$ obtained from Equation [7-15] now can be substituted back into Equations [7-13] and [7-14], which are now rewritten in a matrix form as below:

$$\mathbf{A}.\mathbf{T} = \varpi_{ij}(\mathbf{B} + \mathbf{C}) \qquad [7\text{-}16]$$

where $\mathbf{A} = \begin{bmatrix} s - c_{v_1}^a \Lambda^{ij} & sC_a \\ sC_w & s - c_{v_1}^w \Lambda^{ij} \end{bmatrix}$, for $k_x = k_z$; or

$= \begin{bmatrix} s - c_{v_2}^a \lambda_a^{ij} & sC_a \\ sC_w & s - c_{v_2}^w \lambda_w^{ij} \end{bmatrix}$, for $k_x \neq k_z$;

$\mathbf{B} = \begin{Bmatrix} u_a^0 + C_a u_w^0 \\ C_w u_a^0 + u_w^0 \end{Bmatrix}$; $\mathbf{C} = (1 + K)\begin{Bmatrix} c_\sigma^a \\ c_\sigma^w \end{Bmatrix}[s\overline{\sigma}_z(s) - \sigma(0)]$; and

$\mathbf{T} = \begin{Bmatrix} \overline{T}_a^{ij}(s) \\ \overline{T}_w^{ij}(s) \end{Bmatrix}$. $\qquad [7\text{-}17]$

Solving for $\overline{T}_a^{ij}(s)$ and $\overline{T}_w^{ij}(s)$ ($i = 0, 1, 2, ...; j = 0, 1, 2, ...$) results in:

$$\mathbf{T} = \varpi_{ij}(\mathbf{A}^{-1}.\mathbf{B} + \mathbf{A}^{-1}.\mathbf{C}) \qquad [7\text{-}18]$$

where

(a) Isotropic permeability condition ($k_x = k_z$):

$$\mathbf{A}^{-1}.\mathbf{B} = \begin{Bmatrix} \frac{u_a^0(C_aC_w-1)s+c_{v_1}^w(C_au_w^0+u_a^0)\Lambda^{ij}}{(C_wC_a-1)s^2+(c_{v_1}^a+c_{v_1}^w)\Lambda^{ij}s-c_{v_1}^ac_{v_1}^w(\Lambda^{ij})^2} \\ \frac{u_w^0(C_aC_w-1)s+c_{v_1}^a(C_wu_a^0+u_w^0)\Lambda^{ij}}{(C_wC_a-1)s^2+(c_{v_1}^a+c_{v_1}^w)\Lambda^{ij}s-c_{v_1}^ac_{v_1}^w(\Lambda^{ij})^2} \end{Bmatrix};$$

$$\mathbf{A}^{-1}.\mathbf{C} = \begin{Bmatrix} \frac{(1+K)[(C_ac_\sigma^w-c_\sigma^a)s+c_{v_2}^wc_\sigma^a\Lambda^{ij}]}{(C_wC_a-1)s^2+(c_{v_1}^a+c_{v_1}^w)\Lambda^{ij}s-c_{v_1}^ac_{v_1}^w(\Lambda^{ij})^2} \\ \frac{(1+K)[(C_wc_\sigma^a-c_\sigma^w)s+c_{v_2}^ac_\sigma^w\Lambda^{ij}]}{(C_wC_a-1)s^2+(c_{v_1}^a+c_{v_1}^w)\Lambda^{ij}s-c_{v_1}^ac_{v_1}^w(\Lambda^{ij})^2} \end{Bmatrix}[s\overline{\sigma}_z(s)-\sigma(0)]; \qquad [7\text{-}19]$$

(b) Anisotropic permeability condition ($k_x \neq k_z$):

$$\mathbf{A}^{-1}.\mathbf{B} = \begin{Bmatrix} \frac{u_a^0(C_aC_w-1)s+c_{v_2}^w(C_au_w^0+u_a^0)\lambda_w^{ij}}{(C_wC_a-1)s^2+\left(c_{v_2}^a\lambda_a^{ij}+c_{v_2}^w\lambda_w^{ij}\right)s-c_{v_2}^ac_{v_2}^w\lambda_a^{ij}\lambda_w^{ij}} \\ \frac{u_w^0(C_aC_w-1)s+c_{v_2}^a(C_wu_a^0+u_w^0)\lambda_a^{ij}}{(C_wC_a-1)s^2+\left(c_{v_2}^a\lambda_a^{ij}+c_{v_2}^w\lambda_w^{ij}\right)s-c_{v_2}^ac_{v_2}^w\lambda_a^{ij}\lambda_w^{ij}} \end{Bmatrix};$$

$$\mathbf{A}^{-1}.\mathbf{C} = \begin{Bmatrix} \frac{(1+K)\left[(C_ac_\sigma^w-c_\sigma^a)s+c_{v_2}^wc_\sigma^a\lambda_w^{ij}\right]}{(C_wC_a-1)s^2+\left(c_{v_2}^a\lambda_a^{ij}+c_{v_2}^w\lambda_w^{ij}\right)s-c_{v_2}^ac_{v_2}^w\lambda_a^{ij}\lambda_w^{ij}} \\ \frac{(1+K)\left[(C_wc_\sigma^a-c_\sigma^w)s+c_{v_2}^ac_\sigma^w\lambda_a^{ij}\right]}{(C_wC_a-1)s^2+\left(c_{v_2}^a\lambda_a^{ij}+c_{v_2}^w\lambda_w^{ij}\right)s-c_{v_2}^ac_{v_2}^w\lambda_a^{ij}\lambda_w^{ij}} \end{Bmatrix}[s\overline{\sigma}_z(s)-\sigma(0)]. \qquad [7\text{-}20]$$

Then, taking the Laplace inverse of Equation [7-18] gives:

$$\mathcal{L}^{-1}\{\mathbf{T}\} = \varpi_{ij}\left\{\mathcal{L}^{-1}\{\mathbf{A}^{-1}.\mathbf{B}\} + \mathcal{L}^{-1}\{\mathbf{A}^{-1}.\mathbf{C}\}\right\} \qquad [7\text{-}21]$$

where $\mathcal{L}^{-1}\{\mathbf{T}\} = \begin{Bmatrix} T_a^{ij}(t) \\ T_w^{ij}(t) \end{Bmatrix}$;

(a) Isotropic permeability condition ($k_x = k_z$):

$$\mathcal{L}^{-1}\{\mathbf{A}^{-1}.\mathbf{B}\} = \begin{Bmatrix} \frac{\Omega\left(e^{\alpha_1\Lambda^{ij}t}-e^{\alpha_2\Lambda^{ij}t}\right)+\Psi\left(e^{\alpha_1\Lambda^{ij}t}+e^{\alpha_2\Lambda^{ij}t}\right)}{2\eta} \\ \frac{\Omega'\left(e^{\alpha_1\Lambda^{ij}t}-e^{\alpha_2\Lambda^{ij}t}\right)+\Psi'\left(e^{\alpha_1\Lambda^{ij}t}+e^{\alpha_2\Lambda^{ij}t}\right)}{2\eta} \end{Bmatrix};$$

$$\eta = \left[\left(c_{v_1}^a - c_{v_1}^w\right)^2 + 4c_{v_1}^a c_{v_1}^w C_w C_a\right]^{\frac{1}{2}};$$

$$\alpha_1 = \frac{1}{2}\left(\frac{c_{v_1}^a + c_{v_1}^w + \eta}{1-C_wC_a}\right); \qquad \alpha_2 = \frac{1}{2}\left(\frac{c_{v_1}^a + c_{v_1}^w - \eta}{1-C_wC_a}\right);$$

$$\Omega = \left(c_{v_1}^a - c_{v_1}^w\right)u_a^0 - 2c_{v_1}^w C_a u_w^0; \qquad \Psi = \eta u_a^0;$$

$$\Omega' = \left(c_{v_1}^w - c_{v_1}^a\right)u_w^0 - 2c_{v_1}^a C_w u_a^0; \qquad \Psi' = \eta u_w^0; \qquad [7\text{-}22]$$

(b) Anisotropic permeability condition ($k_x \neq k_z$):

$$\mathcal{L}^{-1}\{\mathbf{A}^{-1}.\mathbf{B}\} = \begin{Bmatrix} \frac{\omega\left(e^{\alpha_1^{ij}t}-e^{\alpha_2^{ij}t}\right)+\psi\left(e^{\alpha_1^{ij}t}+e^{\alpha_2^{ij}t}\right)}{2\eta^{ij}} \\ \frac{\omega'\left(e^{\alpha_1^{ij}t}-e^{\alpha_2^{ij}t}\right)+\psi'\left(e^{\alpha_1^{ij}t}+e^{\alpha_2^{ij}t}\right)}{2\eta^{ij}} \end{Bmatrix};$$

$$\eta^{ij} = \left[\left(c_{v_2}^a\lambda_a^{ij} - c_{v_2}^w\lambda_w^{ij}\right)^2 + 4c_{v_2}^a c_{v_2}^w C_w C_a \lambda_a^{ij}\lambda_w^{ij}\right]^{\frac{1}{2}};$$

$$\alpha_1^{ij} = \frac{1}{2}\left(\frac{c_{v_2}^a\lambda_a^{ij} + c_{v_2}^w\lambda_w^{ij} + \eta^{ij}}{1-C_wC_a}\right); \qquad \alpha_2^{ij} = \frac{1}{2}\left(\frac{c_{v_2}^a\lambda_a^{ij} + c_{v_2}^w\lambda_w^{ij} - \eta^{ij}}{1-C_wC_a}\right);$$

$$\omega = \left(c_{v_2}^a\lambda_a^{ij} - c_{v_2}^w\lambda_w^{ij}\right)u_a^0 - 2c_{v_2}^w C_a\lambda_w^{ij}u_w^0; \quad \psi = \eta^{ij}u_a^0;$$

$$\omega' = \left(c_{v_2}^w\lambda_w^{ij} - c_{v_2}^a\lambda_a^{ij}\right)u_w^0 - 2c_{v_2}^a C_w\lambda_a^{ij}u_a^0; \quad \psi' = \eta^{ij}u_w^0. \qquad [7\text{-}23]$$

In Equation [7-21], the term $\mathcal{L}^{-1}\{\mathbf{A}^{-1}.\mathbf{C}\}$ follows different time-dependent loading functions and will be determined in Section 5. The final solution describing the dissipation of excess pore pressures can be deduced as follows:

$$\mathbf{U} = \sum_{i=0}^{\infty}\sum_{j=0}^{\infty}\varpi_{ij}\sin(Ix)\sin(Jz)\left\{\mathcal{L}^{-1}\{\mathbf{A}^{-1}.\mathbf{B}\} + \mathcal{L}^{-1}\{\mathbf{A}^{-1}.\mathbf{C}\}\right\} \qquad [7\text{-}24]$$

where $\mathbf{U} = \begin{Bmatrix} u_a(x,z,t) \\ u_w(x,z,t) \end{Bmatrix}$. [7-25]

It should be noted that, when the term $\mathcal{L}^{-1}\{\mathbf{A}^{-1}.\mathbf{C}\}$ is equal to zero, Equation [7-24] will predict the change in excess pore pressures only restricted to a special case of constant loading.

7.4. Normalised settlement of 2D unsaturated soil consolidation

Assuming coefficients of volume change for the air and water phases are constant during the consolidation for a particular stress increment, the constitutive model for 2D plane strain condition proposed by Dakshanamurthy & Fredlund (1980) is derived as below:

$$\frac{\partial\left(\frac{\Delta V}{V_0}\right)}{\partial t} = \frac{\partial(\varepsilon_v)}{\partial t} = m_1^s\left(\frac{1+K}{2}\right)\frac{\partial\sigma_z}{\partial t} + (m_2^s - m_1^s)\frac{\partial u_a}{\partial t} - m_2^s\frac{\partial u_w}{\partial t} \qquad [7\text{-}26]$$

where ε_v is the volumetric strain; m_1^s, is the coefficient of volume change of the soil element with respect to the change in the net stress (kPa^{-1}); and m_2^s, is the coefficient of volume change of the soil element with respect to the change in suction.

Integrating Equation [7-26] against time t at domain $t \in [0, \infty)$ yields in:

$$\varepsilon_v(x,z,t) = m_1^s\left(\frac{1+K}{2}\right)[\sigma_z(t) - \sigma_z(0)] + (m_2^s - m_1^s)[u_a(x,z,t) - u_a(x,z,0)] - m_2^s[u_w(x,z,t) - u_w(x,z,0)] \qquad [7\text{-}27]$$

The normalised settlement, denoted as S^*, can be determined based on the volumetric strain ε_v provided in Equation [7-27]:

$$S^* = \frac{S(t)}{S_{max}} = \frac{\int_0^H\int_0^L \varepsilon_v(x,z,t)dxdz}{m_1^s\left(\frac{1+K}{2}\right)(q_z)_{max}HL} \qquad [7\text{-}28]$$

where $S(t)$ is the ground surface settlement corresponding to time t; and S_{max} is the maximum ground surface settlement. In Equation [7-28], the normalised settlement S^*, which is a function of time t, indicates the settlement response under different types of loadings at a particular time.

7.5. Worked examples

In this study, four different types of time-dependent loadings, namely ramping, asymptotic, sinusoid, and damped sine wave, are simulated and presented in separate examples. The analytical procedure accommodates the simulated loading functions to obtain a closed-form solution for 2D plane strain consolidation. Based on the proposed solution, the study further investigates the effects of air to water permeability ratio (k_a/k_w) on the change of normalised excess pore pressures (i.e. u_a/u_{atm} and u_w/u_{atm}) and normalised settlement (S^*) of the homogeneous soil stratum under the applied loads. In addition, parametric studies are conducted by investigating effects of loading parameters on the changes of the normalised pore pressures and the settlement. The soil properties adopted in this study are as follows:

- Material properties: $n = 0.50$; $S_r = 80\%$; $k_w = 10^{-10}\text{ms}^{-1}$;
  $L = 2\text{m}$; $H = 5\text{m}$; $u_{atm} = 100\text{kPa}$;
  $u_a^0 = 20\text{kPa}$; $u_w^0 = 40\text{kPa}$; $q_0 = 100\text{kPa}$;
  $m_1^s = -5 \times 10^{-4}\text{kPa}^{-1}$; $m_2^s = 0.2m_1^s$;
  $m_1^w = 0.1m_1^s$; $m_2^w = 4m_1^w$. [7-29]

- Physical properties: $R = 8.314\text{J.mol}^{-1}\text{K}^{-1}$; $M = 0.029\text{kg.mol}^{-1}$;
  $\Theta = (\theta° + 273.16)\text{K}$; $\theta° = 20℃$. [7-30]

An external loading exerted on the ground surface of unsaturated soil causes immediate undrained compression and induces initial excess pore-air and pore-water pressures. Based on the existing equations for initial pore pressures proposed by Fredlund & Hasan (1979), it is estimated that, under the isotropic condition, an initial loading $q_0 = 100\text{kPa}$ will result in the immediate increases of pore-air pressure $u_a^0 = 20\text{kPa}$ and pore-water pressure $u_w^0 = 40\text{kPa}$. When time elapses, the excess pore pressures begin to change correspondingly depending on the applied loads. The evaluations of the initial excess pore pressures are provided in Appendix D. For the permeability ratio k_a/k_w, the air permeability k_a is varying from 10^{-12} to 10^{-8}m/s whilst the water permeability k_w is kept constant as 10^{-10}m/s. Furthermore, the properties provided in Equations [7-29] and [7-30] will be employed to determine the consolidation coefficients with respect to the air phase (C_a, c_v^a and c_σ^a) and the water

phase (C_w, c_v^w and c_σ^w). For the sake of generality, the point of investigation, where excess pore-air and pore-water pressure dissipation rates are estimated, is considered to be at $x = 0.5L$ and $z = 0.8H$ for each case of loading. Considering the isotropic loading condition, the term $K = 1$ is adopted in the worked examples.

7.5.1. Consolidation under ramped loading

An external ramped loading can be used to simulate the linearly imposed surcharge during construction. A general ramped function can be presented in Equation [7-31]:

$$q_z(t) = q_0 + at \qquad [7\text{-}31]$$

where q_0 is the initial surcharge (kPa) and 'a' is the linear loading rate (kPa/s). Equation [7-31] can be substituted back into the inverse Laplace transformed $\mathcal{L}^{-1}\{\mathbf{A}^{-1}.\mathbf{C}\}$ as presented in Equation [7-24]. The complete analytical solutions are presented in Equations [E-1] and [E-2] in Appendix E. Figure 7.2 depicts the loading varying linearly with an initial surcharge $q_0 = 100$ kPa and a linear loading rate $a = 10^{-5}$ kPa/s, which are adopted in this study.

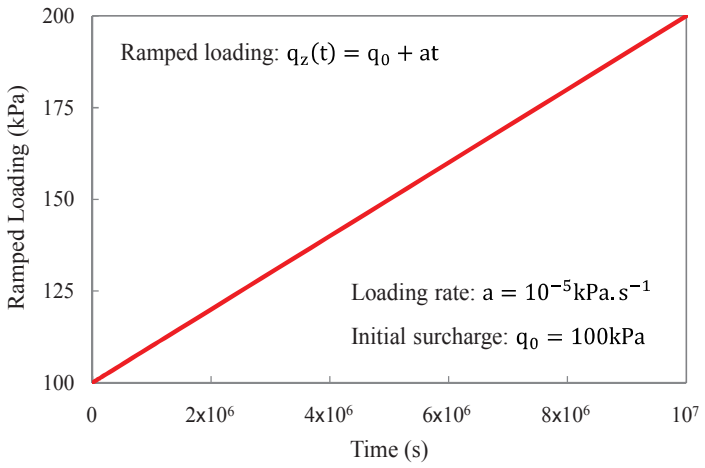

Figure 7.2. Load varying linearly with time

Based on Equation [E-1], Figures 7.3(a) and 7.3(b) illustrate the excess pore-air and pore-water pressure dissipation patterns varying with k_a/k_w, respectively. Considering a logarithmic time-scale, when the loading time is short, the dissipation of excess pore pressures induced by ramped loading is similar to that induced by constant loading (Qin

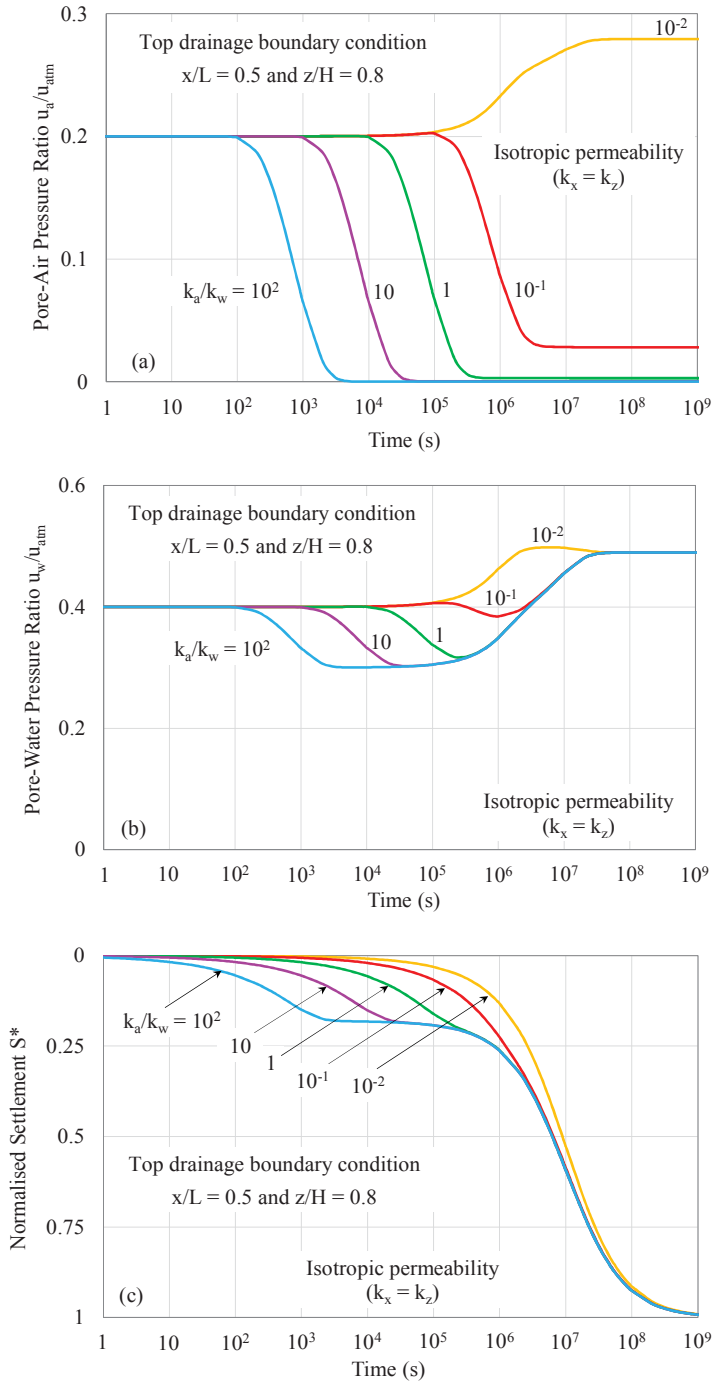

Figure 7.3. Variations in (a) excess pore-air pressure; (b) excess pore-water pressure; and (c) settlement with different k_a/k_w due to ramped loading

et al. 2008; Shan et al. 2012; Zhou et al. 2014). After a considerable duration (i.e., 10^5 s), when $k_a/k_w > 1$, the excess pore-air pressure has almost diminished (Figure 7.3(a)). In contrast, for all values of k_a/k_w, the excess pore-water pressure patterns start

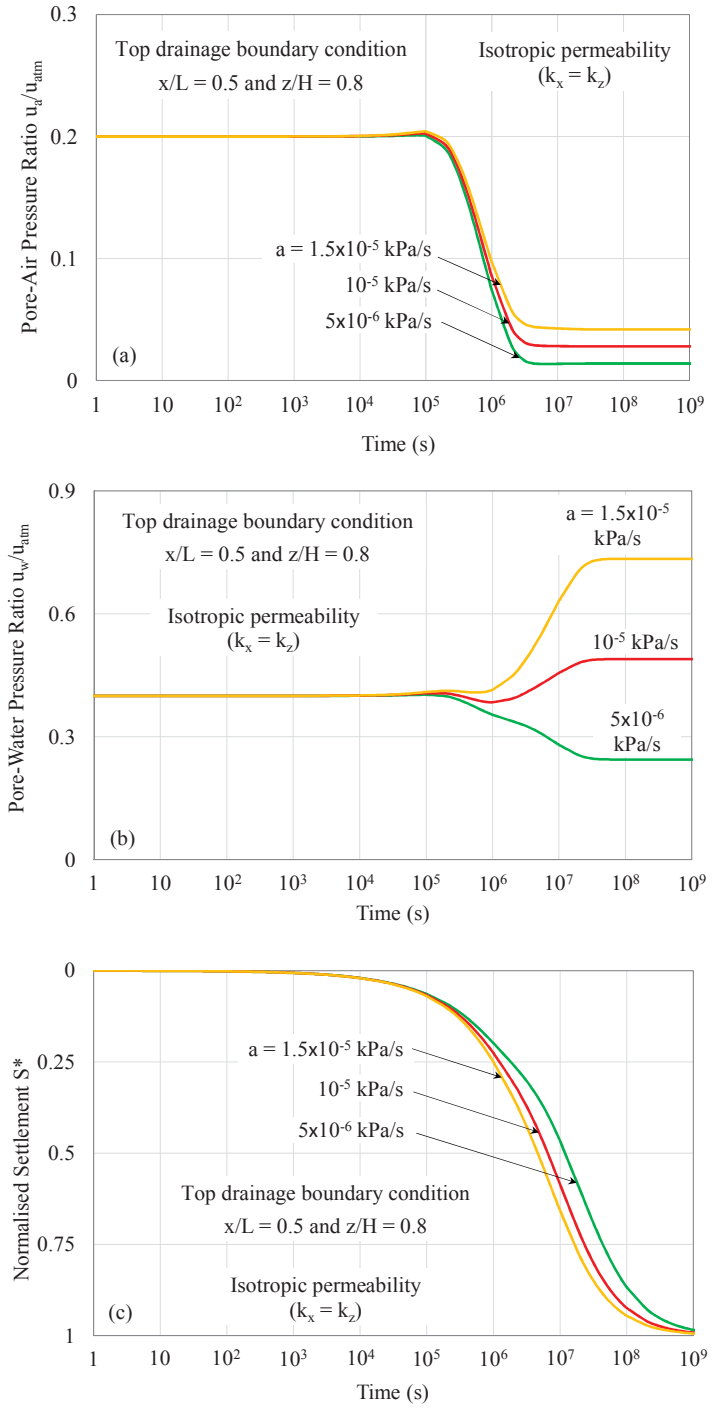

Figure 7.4. Influence of linear loading rate 'a' on (a) excess pore-air pressure; (b) excess pore-water pressure; and (c) settlement with $k_a/k_w = 0.1$

to increase significantly after 10^5 s due to the slow dissipation rate of the excess pore-water pressure (Figure 7.3(b)).

On the other hand, variations in the normalised settlement S^* for ramped loading, which can be obtained from Equation [7-28], are presented in a semi-logarithmic plot (Figure 7.3(c)). There is a noticeable variation in S^* with different values of k_a/k_w in the early stages of compression. During this stage, it can be observed that settlement tends to proceed more quickly as k_a/k_w increases. These patterns later converge into almost a single curve and continue to increase until they become constant after a long time. Before 10^5 s, the normalised settlement is similar to that induced by constant loading. This is due to the insignificant increase in the ramped loading during this time. However, the compression patterns begin to increase drastically due to the significantly increasing load after 10^5 s.

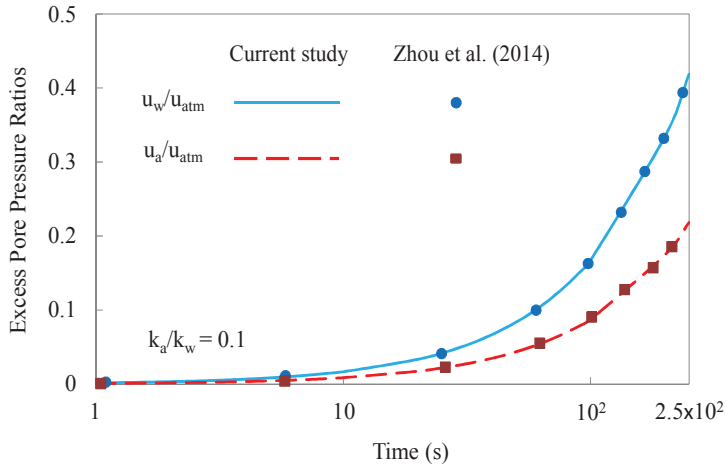

Figure 7.5. Variations in excess pore-air and pore-water pressures due to ramped loading in 1D consolidation

For the parametric study, significant effects of the linear loading rate 'a', ranging from 5×10^{-6} to 1.5×10^{-5} kPa/s, on predictions of the 2D consolidation can be demonstrated in Figure 7.4. The permeability ratio $k_a/k_w = 0.1$ is adopted in this case. Note that the increasing load rate 'a' may result in a quicker increase in the ramped loading, which in turn induces higher excess pore pressures after 10^5 s (Figures 7.4(a) and 7.4(b)). Likewise, the higher loading rate 'a' (e.g., 1.5×10^{-5} kPa/s) increases the rate of settlement during the later stages of consolidation compared to a smaller rate 'a' (e.g., 5×10^{-6} kPa/s) (Figure 7.4(c)).

When the horizontal length is infinite, the coefficient of permeability for both air and water phases in the x-direction (k_{a_x} and k_{w_x}) can be neglected and the K value is considered to be 0. Thus, the solutions for 2D plane strain consolidation (i.e., Equations [E-1] and [E-2]) convert to the solution for 1D consolidation, as provided in Equation [E-4] in Appendix E. As reported in Figure 7.5, the validation is conducted against the existing analytical solution adapted for ramped loading given by Zhou et al. (2014). In this comparison, the parameters $q_0 = 0$ and $a = 0.41\ \mathrm{kPa/s}$ are adopted as equivalent to the normalised loading parameters demonstrated by Zhou et al. (2014). As observed, the analytical predictions obtained from Equation [E-4] show good agreement with the existing results in literature, suggesting that the proposed solution is reliable (Figure 7.5).

7.5.2. Consolidation under asymptotic loading

During construction, the ground surface of the unsaturated soil deposit may be subjected to asymptotic loading as mathematically simulated in Equation [7-32]:

$$q_z(t) = q_0 + A \times q_0\left(1 - e^{-bt}\right) \qquad [7\text{-}32]$$

where 'A' is the parameter influencing the load magnitude and 'b' is the loading parameter controlling the rate of asymptotic loading. Equation [7-32] can be substituted back into the inverse Laplace transformed $\mathcal{L}^{-1}\{\mathbf{A}^{-1}.\mathbf{C}\}$ as presented in Equation [7-24].

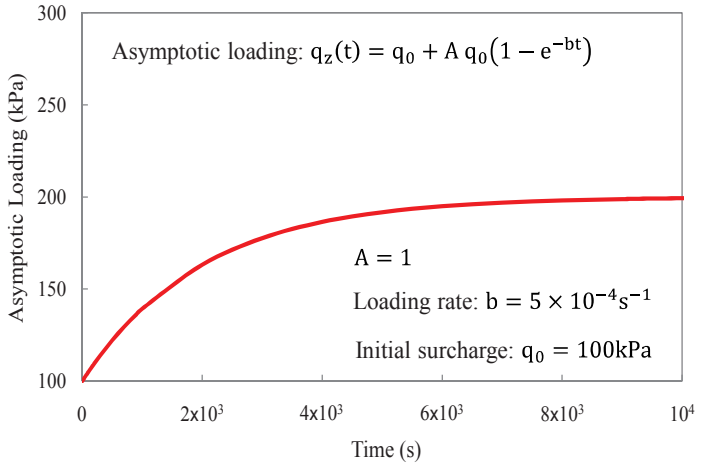

Figure 7.6. Load varying exponentially with time

The complete analytical solutions are presented in Equations [E-6] and [E-7] in Appendix E. Figure 7.6 shows that the loading varies exponentially with time when adopting the parameters $b = 5 \times 10^{-4}/s$ and $A = 1$.

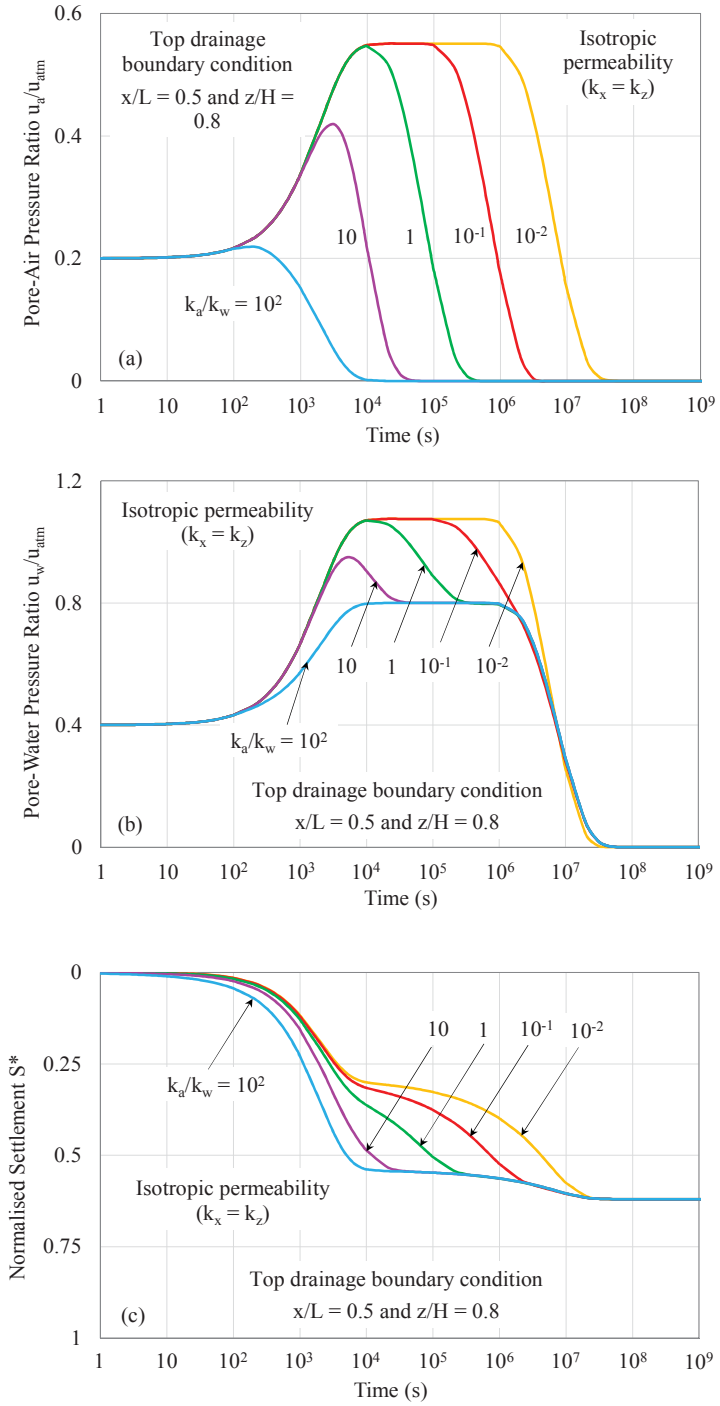

Figure 7.7. Variations in (a) excess pore-air pressure; (b) excess pore-water pressure; and (c) settlement with different k_a/k_w due to asymptotic loading

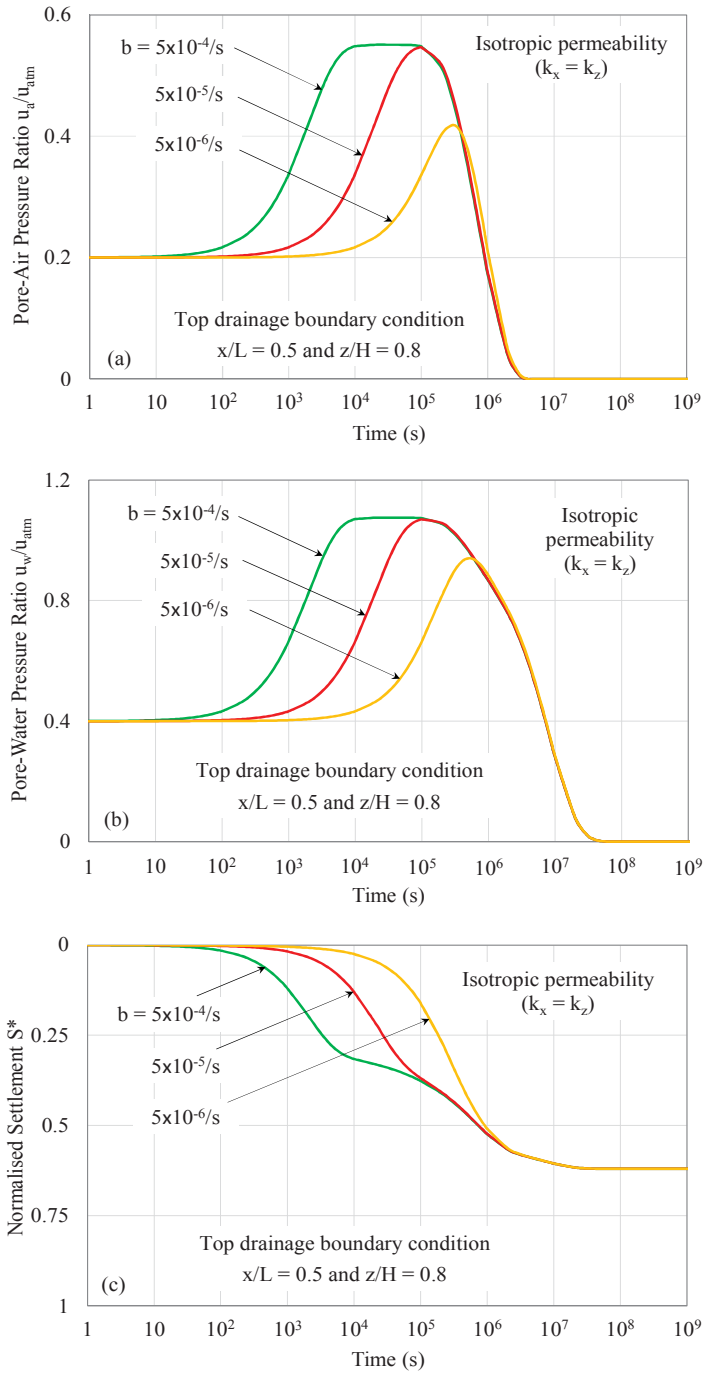

Figure 7.8. Influence of exponential loading rate 'b' on (a) excess pore-air pressure; (b) excess pore-water pressure; and (c) settlement with $k_a/k_w = 0.1$

Based on Equation [E-6], Figures 7.7(a) and 7.7(b) illustrate the changes in the excess pore-air and pore-water pressures induced by the asymptotic loading, respectively. At the beginning of the loading process, there is no significant change in both the excess pore-air and pore-water pressures, similar to the case of ramped loading

shown in Section 5.1. Because the loading accelerates, the excess pore-air and pore-water pressures with $k_a/k_w < 1$ increase exponentially and reach their highest value at about 10^4 s. In comparison, the excess pore pressures with $k_a/k_w \geq 1$ tend to dissipate more quickly; as a result, the excess pore pressures reach the highest value before 10^4 s.

Figure 7.7(c) presents the normalised settlement S^* varying with different values of k_a/k_w due to the asymptotic loading, which can be obtained based on Equation [7-28]. It can be observed that the settlement patterns drastically increase during the early stages of compression as the loading begins to accelerate. When the loading approaches the asymptote, the settlement continues to increase at a slow rate while forming inverse S-shaped curves. It can be observed that there is a noticeable variation in the settlement during the later stages, in which the increasing k_a/k_w may result in a faster reduction of the soil volume. The soil eventually experiences no further volume reduction after 10^8 s. It is worth mentioning that S^* in this case is less than 1 as the average load intensity is less than $(q_z)_{max}$.

The effects of the exponential loading rate 'b', ranging from 5×10^{-6} to 5×10^{-4}/ s, on the 2D consolidation are illustrated in Figure 7.8. Considering the permeability ratio $k_a/k_w = 0.1$, the excess pore-air and pore-water pressures take a shorter time to achieve their highest values when the loading rate 'b' increases (Figures 7.8(a) and 7.8(b)). It can also be predicted that the highest value of the excess pore pressure is prone to increase with the 'b' value. As observed in Figures 7.8(a) and 7.8(b), prior to significant dissipation, the excess pore-air and pore-water pressures tend to increase faster as the loading parameter 'b' increases. Moreover, as evident in Figures 7.8(a) and 7.8(b), when the dissipated excess pore pressures are counter-balanced by the increasing external loading, the excess pore pressures stay rather constant. In Figure 7.8(c), the settlement of the soil stratum with a higher 'b' value (e.g., 5×10^{-4}/s) proceeds faster than that with a smaller 'b' value (e.g., 5×10^{-6}/s) during the early stages of the consolidation process.

7.5.3. Consolidation under sinusoidal loading

A sinusoidal loading may present the road traffic loading or heavy train imposed on the unsaturated ground and can be formulated in Equation [7-33] as follows:

$$q_z(t) = q_0[B \times \sin(\theta t) + 1] \qquad [7\text{-}33]$$

where 'B' is the parameter influencing the loading amplitude; and 'θ' is the angular frequency (rad/s) for sinusoidal loading function. Equation [7-33] is substituted into the inverse Laplace transformed $\mathcal{L}^{-1}\{\mathbf{A}^{-1}.\mathbf{C}\}$ as presented in Equation [7-24]. The complete analytical solutions are presented in Equations [E-9] and [E-10] in Appendix E. Figure 7.9 shows the external loading varying periodically with an angular frequency $\theta = 2\pi \times 10^{-7}\text{rad/s}$ and parameter $B = 1$.

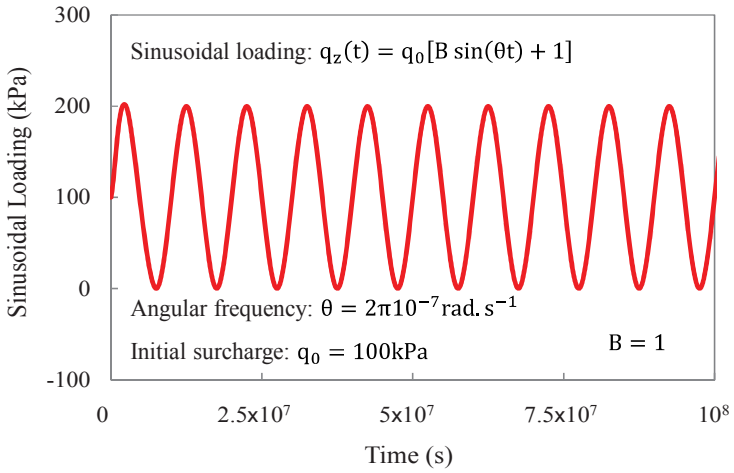

Figure 7.9. Load varying periodically with time

Figures 7.10(a) and 7.10(b) respectively illustrate the change in excess pore-air and pore-water pressures based on Equations [E-9]. Under the sinusoidal loading, after a long period of time, the excess pore pressures do not fully dissipate but rather oscillate continuously with constant amplitudes depending on the dissipation rate of excess pore pressures. This phenomenon is due to the fact that the simulated load function consists of loading-unloading curves, which influence the change in excess pore pressures. Referring to the logarithmic time-scale, it can be observed that, when $k_a/k_w \geq 10$, the excess pore-air pressure has already diminished before 10^6s due to the high dissipation rate. This results in no oscillation of excess pore-air pressure during the later stages (Figure 7.10(a)). However, for any value of k_a/k_w, the excess pore-water pressure continues oscillating indefinitely because of the slow dissipation rate (Figure 7.10(b)).

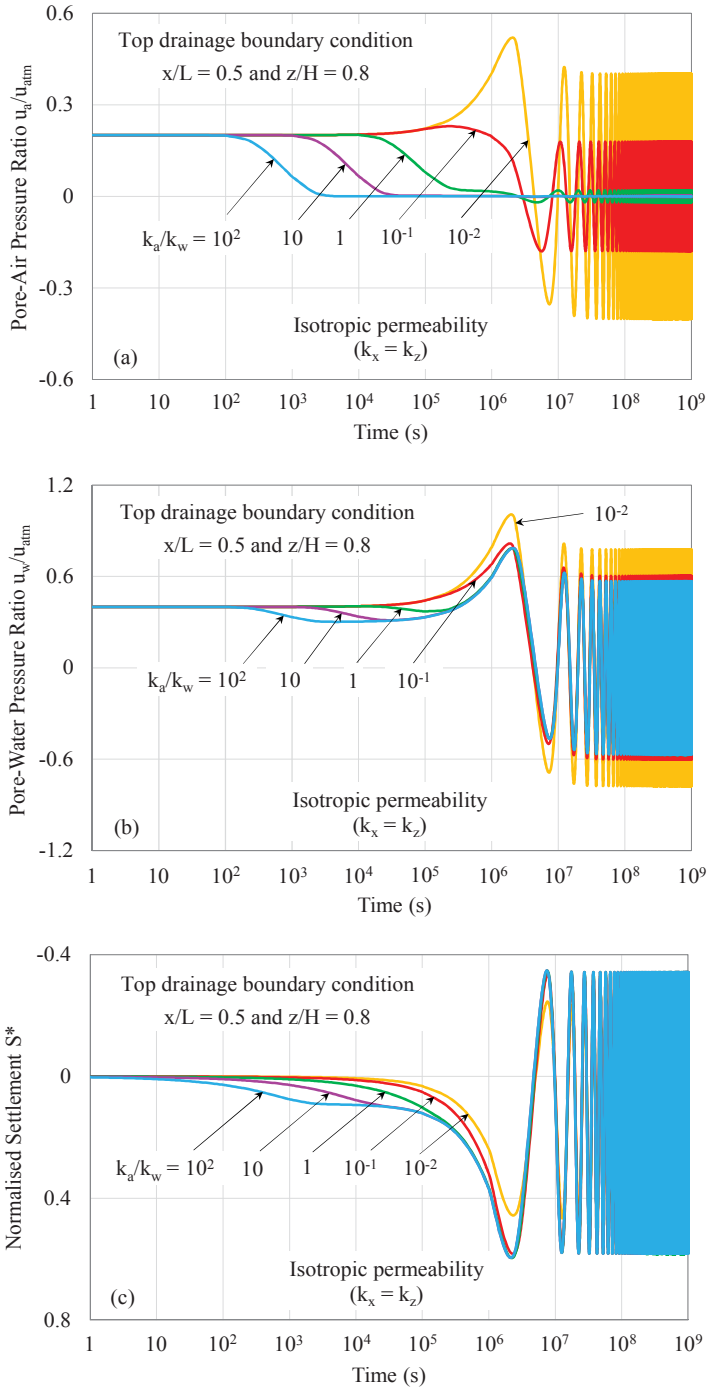

Figure 7.10. Variations in (a) excess pore-air pressure; (b) excess pore-water pressure; and (c) settlement with different k_a/k_w due to sinusoidal loading

Figure 7.10(c) depicts the change in the normalised settlement S^* for the sinusoidal loading, as defined by Equation [7-28]. The settlement patterns initially form inverse S curves when $k_a/k_w > 1$ at a relatively slow rate and then oscillate indefinitely after

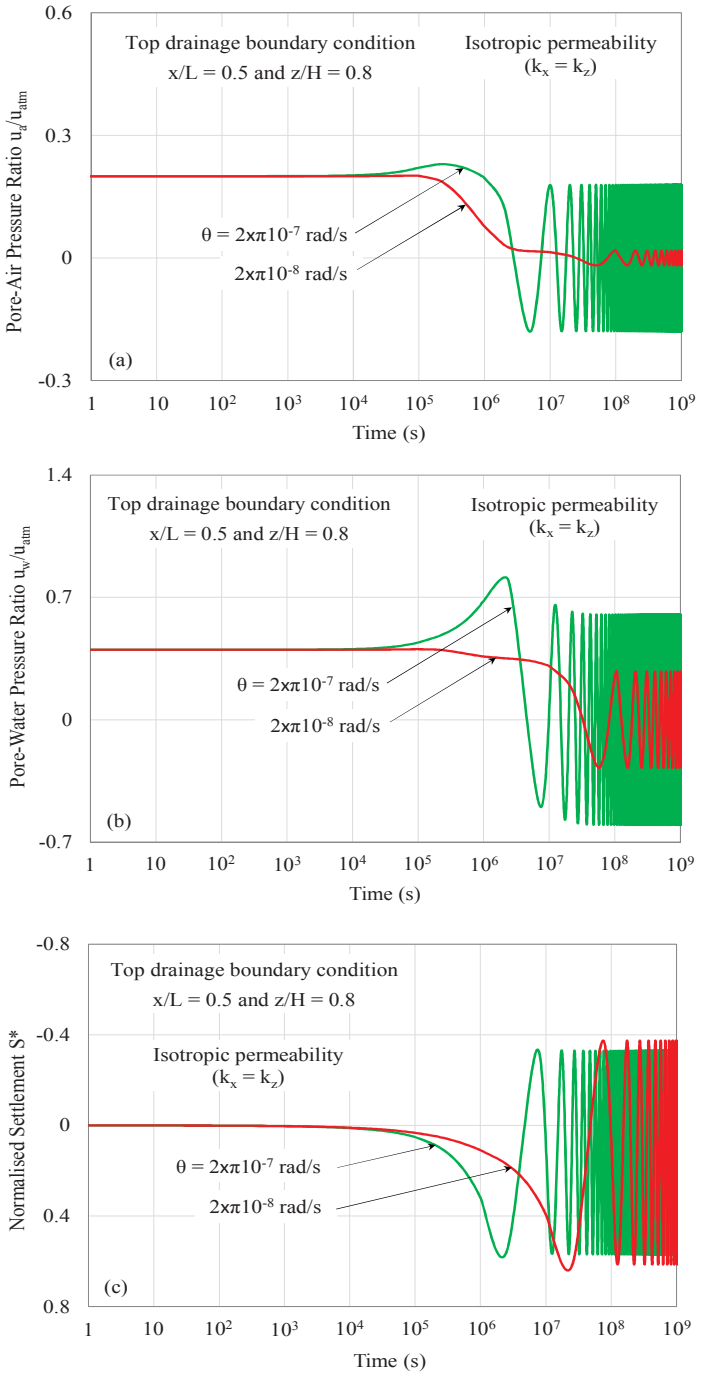

Figure 7.11. Influence of angular frequency 'θ' on (a) excess pore-air pressure; (b) excess pore-water pressure; and (c) settlement with $k_a/k_w = 0.1$

10^6s. Such phenomenon indicates that the air and water are squeezed out during the loading process and then absorbed in during the unloading process. This may lead to the continuous changes in the soil volume with time.

The effects of the angular frequency 'θ', including $2\pi \times 10^{-8}$ and $2\pi \times 10^{-7}\mathrm{rad/s}$, on the excess pore pressures and the consolidation settlement are demonstrated in Figure 7.11. Taking $k_a/k_w = 0.1$ for the analysis, it can be observed that the smaller angular frequency 'θ' (e.g. $2\pi \times 10^{-8}\mathrm{rad/s}$) leads to a slow loading rate and thus, allowing sufficient time for excess pore-air and pore-water pressures to dissipate (Figures 7.11(a) and 7.11(b)). This eventually results in insignificant oscillations (due to the small amplitude) in the excess pore pressures. In contrary, the higher angular frequency 'θ' (e.g. $2\pi \times 10^{-7}\mathrm{rad/s}$) produces more significant oscillations (due to the big amplitude) whilst increases the vibration frequency for excess pore pressures. It can also be observed that, in the later stages, the increasing-decreasing (due to loading-unloading process) patterns of normalised settlement with higher 'θ' tends to proceed more quickly than that with smaller 'θ' (Figure 7.11(c)).

7.5.4. Consolidation under damped sine wave loading

Another road traffic loading such as a damped sine wave loading is mathematically simulated in Equation [7-34] as follows:

$$q_z(t) = q_0[C \times e^{-ct}\sin(\vartheta t) + 1] \qquad [7\text{-}34]$$

where 'C' is the parameter influencing the loading amplitude; 'c' is the loading parameter controlling damping rate; and 'ϑ' is the angular frequency $(\mathrm{rad/s})$ for damped loading function. Equation [7-34] can be substituted into the inverse Laplace transformed $\mathcal{L}^{-1}\{\mathbf{A}^{-1}.\mathbf{C}\}$ as presented in Equation [7-24]. The complete analytical solutions are presented in Equations [E-12] and [E-13] in Appendix E. In this study, Figure 7.12 shows a typical damped sine wave loading with an angular frequency $\vartheta = 2\pi \times 10^{-2}\mathrm{rad/s}$, loading parameters $c = 5 \times 10^{-4}\mathrm{s}^{-1}$ and $C = 1$.

As obtained in Equation [E-12], Figures 7.13(a) and 7.13(b) depict the excess pore-air and pore-water pressure dissipation rates varying with k_a/k_w, respectively. A typical damped sine wave presented in Figure 7.12 consists of vibrations with the highest peak to peak amplitude at the very beginning. However, as time passes, the amplitude exponentially approaches zero and the loading will stabilise at a constant value q_0. Correspondingly, the excess pore pressures appear to vibrate continuously at the early stages and then gradually dissipate after $10^4\mathrm{s}$. It can be observed that the

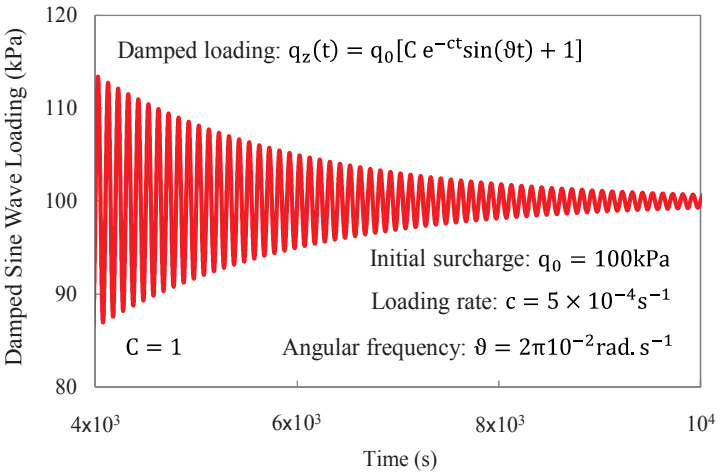

Figure 7.12. Damped sine wave load varying with time

change in the excess pore pressures after 10^4s is similar to that induced by the constant loading (Qin et al. 2008; Shan et al. 2012; Zhou et al. 2014).

Figure 7.13(c) depicts the change in the normalised settlement S^* due to the damped sine wave loading, defined by Equation [7-28]. The normalised settlement initially oscillates corresponding to the loading-unloading process. As the damped sine wave loading stabilises after 10^4s, the soil volume gradually decreases resembling to the patterns proposed for the constant loading. The soil volume is subjected to no further deformation after 10^8s.

The significant effects of the damping parameter 'c' (5×10^{-4} and 5×10^{-3}/s) and the angular frequency 'ϑ' ($2\pi \times 10^{-3}$ and $2\pi \times 10^{-2}$rad/s) on the 2D consolidation are presented in Figures 7.14 and 7.15, respectively. Considering $k_a/k_w = 0.1$ and $\vartheta = 2\pi \times 10^{-2}$rad/s, the higher value of the parameter 'c' (e.g. 5×10^{-3}/s) will accelerate the damping process, in which the amplitude approaches zero faster than that with smaller 'c' (e.g. 5×10^{-4}/s); and as the result, the excess pore-air and pore-water pressures (Figures 7.14(a) and 7.14(b), respectively) and the normalised settlement (Figure 7.14(c)) stabilise more quickly. It is noticed that both adopted 'c' values induce the same dissipation rate for excess pore pressures after 10^4s. Likewise, the change in parameter 'c' no longer influences the settlement rate after this time.

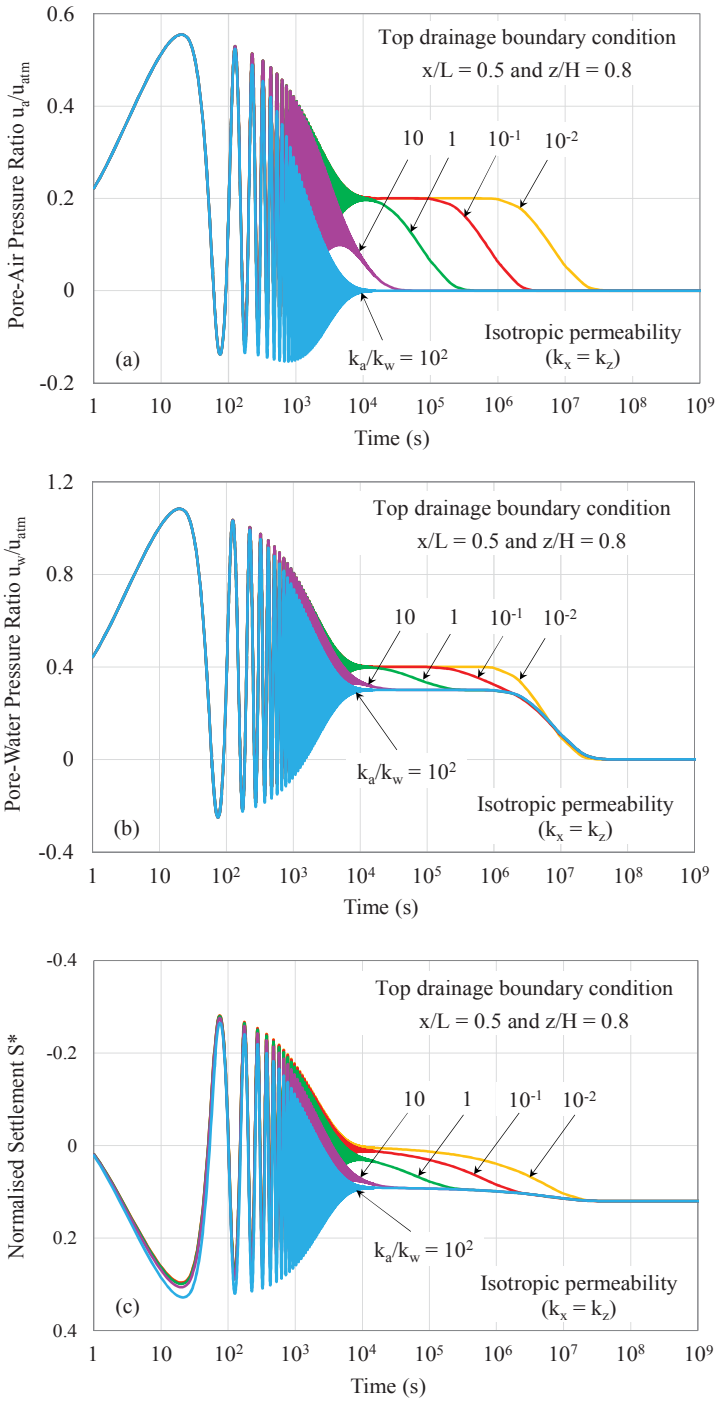

Figure 7.13. Variations in (a) excess pore-air pressure; (b) excess pore-water pressure; and (c) settlement with different k_a/k_w due to damped sine wave loading

In a case when 'ϑ' is varying whilst 'c' remains unchanged ($c = 5 \times 10^{-3}/s$), at the beginning of consolidation, the higher angular frequency 'ϑ' (e.g. $2\pi \times 10^{-2} rad/s$) will shorten the wavelength and induce more oscillations in excess pore pressures (Figures

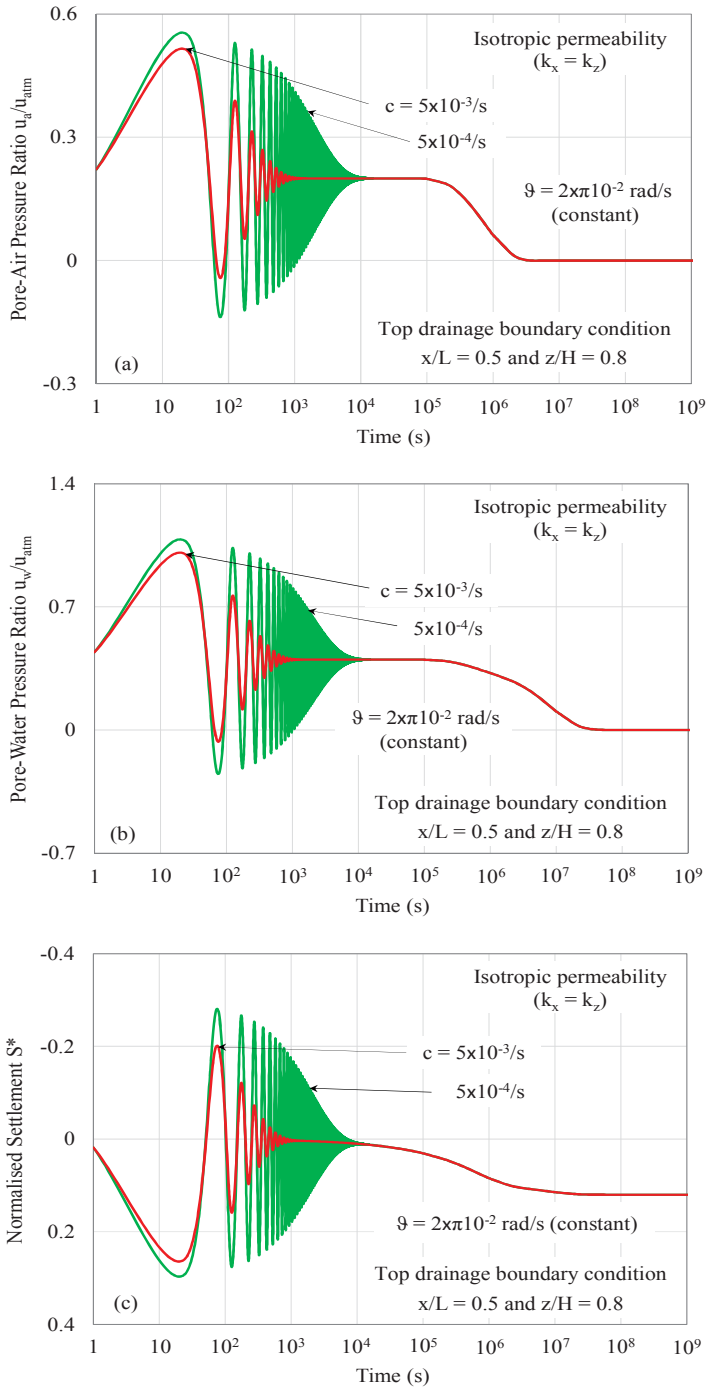

Figure 7.14. Influence of exponential loading rate 'c' on (a) excess pore-air pressure; (b) excess pore-water pressure; and (c) settlement with $k_a/k_w = 0.1$

7.15(a) and 7.15(b)) and normalised settlement (Figure 7.15(c)), compared to that with the smaller angular frequency 'ϑ' (e.g. $2\pi \times 10^{-3}\text{rad/s}$). As expected, once the damped loading stabilises, the consolidation of unsaturated soil is no longer influenced

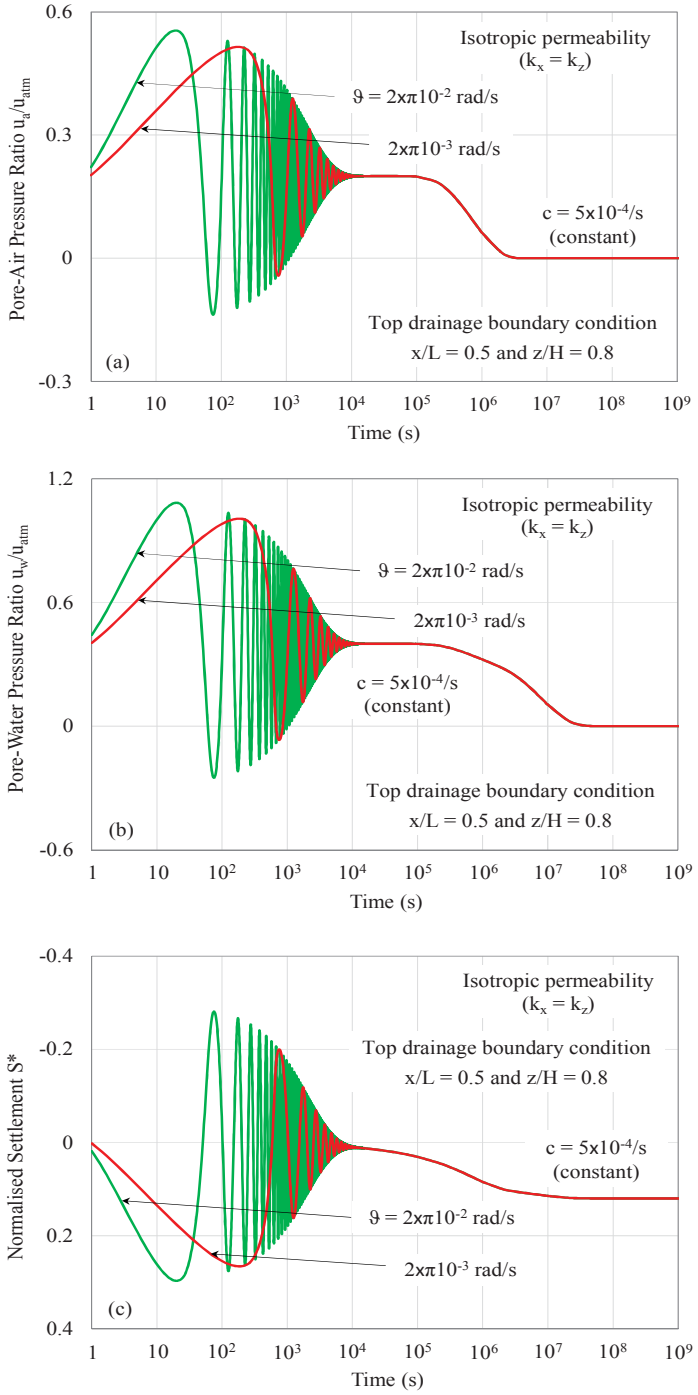

Figure 7.15. Influence of angular frequency 'ϑ' on (a) excess pore-air pressure; (b) excess pore-water pressure; and (c) settlement with $k_a/k_w = 0.1$

by the parameter 'ϑ'. This indicates that, for any value of 'ϑ', the similar excess pore pressure dissipation rate as well as similar settlement rate can be observed after 10^4s.

7.5.5. Parametric study on pore pressure isochrones

The effects of parameter 'a', ranging from 5×10^{-6} to 1.5×10^{-5}kPa/s, on the distribution of excess pore pressures along x- and z-domains can be depicted in Figures 7.16(a) and 7.16(b), respectively. A set of normalised excess pore-air (u_a/u_a^0) and pore-water (u_w/u_w^0) pressure isochrones against the time factor T can be predicted under the ramped loading with different values of 'a'. The time factor T in this study is defined as $T = k_w t/(m_1^s \gamma_w H^2)$ and $k_a/k_w = 0.1$ is adopted for the analysis. At $T = 2 \times 10^{-2}$ (e.g. $t = 1.25 \times 10^7$s), it can be noticed that the isochrones (along both x- and z-directions) with higher 'a' (e.g. 1.5×10^{-5}kPa/s) represents higher excess pore pressures due to the higher applied loads. In other words, these isochrones confirm that the excess pore pressures increase with increasing 'a'. As expected, the excess pore-air and pore-water pressures increase with distance from the permeable boundaries.

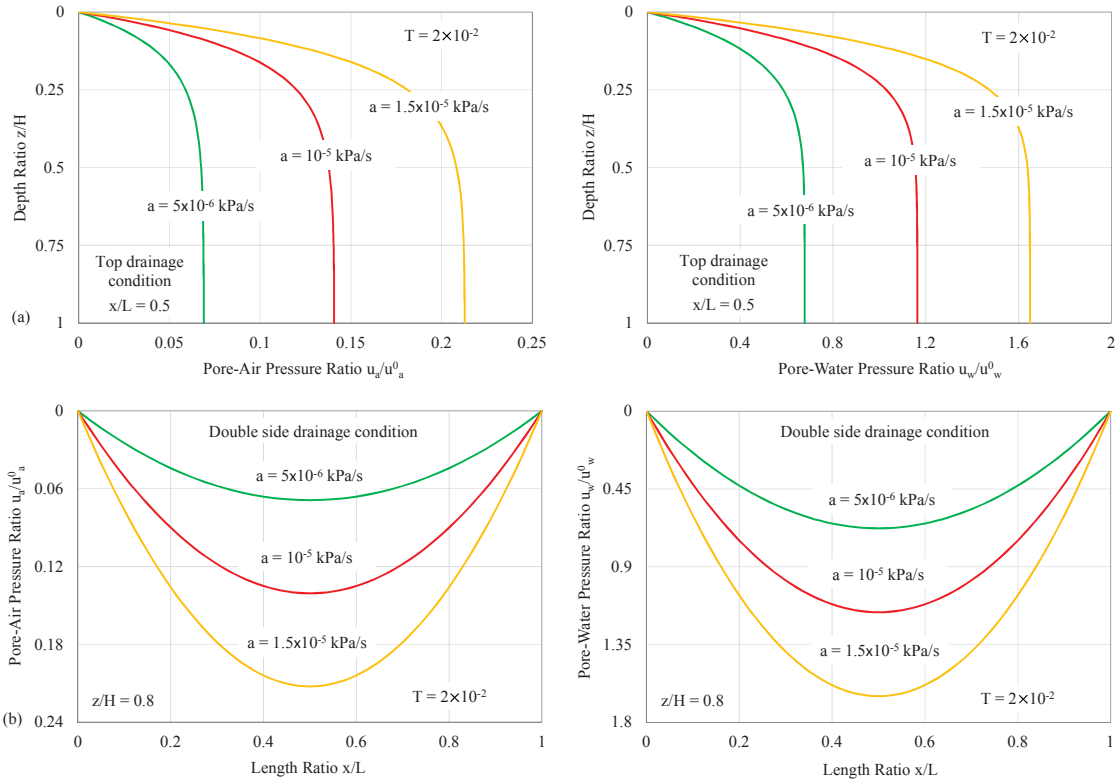

Figure 7.16. Excess pore pressure isochrones against (a) depth ratio and (b) length ratio due to effects of linear loading rate 'a' under top drainage boundary condition (at $T = 2 \times 10^{-2}$)

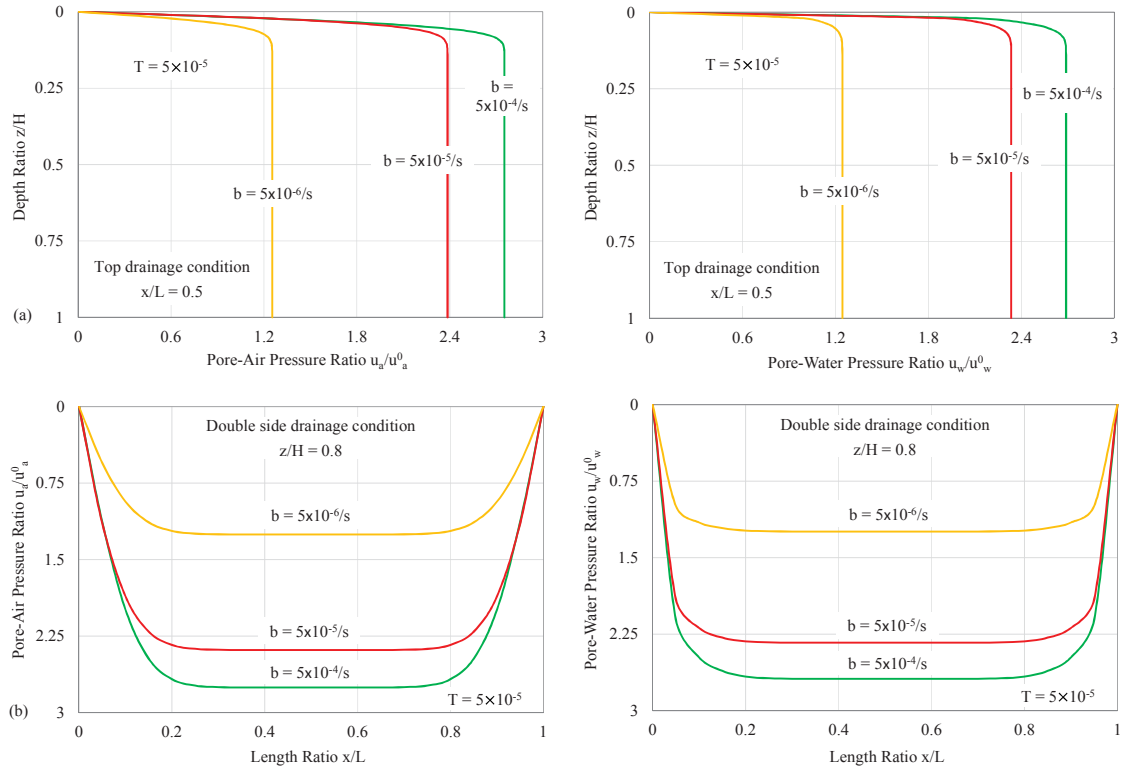

Figure 7.17. Excess pore pressure isochrones against (a) depth ratio and (b) length ratio due to effects of exponential loading rate 'b' under top drainage boundary condition (at $T = 5 \times 10^{-5}$)

The effects of exponential parameter 'b', ranging from 5×10^{-6} to 5×10^{-4}/s, on the distribution of excess pore pressures along x- and z-domains are depicted in Figures 7.17(a) and 7.17(b), respectively. These pressure isochrones describe the change in excess pore-air (u_a/u_a^0) and pore-water (u_w/u_w^0) pressures against the time factor T due to the asymptotic loading with different values of 'b'. The permeability ratio $k_a/k_w = 0.1$ is adopted for the analysis. When the asymptotic loading starts to increase significantly at $T = 5 \times 10^{-5}$ (e.g. $t = 3.125 \times 10^4$s), it can be observed that the isochrones (along both x- and z-directions) with higher 'b' (e.g. 5×10^{-4}/s) represent higher excess pore pressures, induced by the higher applied loads. However, at the later stages, when T increases, it is predicted that the excess pore pressures will be similar regardless of different values of 'b'. Similar to the case of ramped loading, excess pore pressures induced by the asymptotic loading increase with distance from the permeable boundaries.

7.6. Summary

This chapter has investigated the 2D plane strain consolidation behaviour, in terms of changes in excess pore-air and pore-water pressures as well as the ground surface settlement, of the unsaturated soil stratum subjected to different time-dependent loadings. The proposed analytical solution adopts the eigenfunction expansion and Laplace transformation techniques. For the mathematical procedure, the general solution consisting of the eigenfunctions is first obtained and substituted into the governing equations. The derived governing equations then are truncated into ordinary differential equations using term by term differentiation and orthogonality of sine functions. When the Laplace complex variables are all converted, the inverse Laplace technique is used to obtain the final solution. The verification for ramped loading conducted in this chapter shows a good agreement with the analytical results in the literature.

Time-dependent ramped, asymptotic, sinusoidal, and damped sine wave loadings have been mathematically simulated and incorporated in the solution. Considering logarithmic time-scale, when k_a/k_w increases, the excess pore-air pressure induced by the adopted loads may be dissipated significantly whilst the load is being applied. However, for any value of k_a/k_w, the change in excess pore-water pressure correspondingly reflects the loading pattern due to the slow dissipation rate. For parametric studies, the effects of loading parameters ‘a’, ‘b’, ‘c’, ‘θ’ and ‘ϑ’ in the mentioned loading functions have been also investigated. Results of these studies reveal that, for the ramped and asymptotic loadings, excess pore pressure dissipation rates generally increase with increasing loading rates ‘a’ and ‘b’; whilst higher angular frequencies ‘θ’ and ‘ϑ’, as presented in the sinusoidal and damped sine wave loadings, may shorten the wavelength and increase more oscillations for excess pore pressures and the ground surface settlement. Additionally, higher damping parameter ‘c’, shown in the damped loading, accelerates the damping process for the excess pore pressures and settlement. Moreover, under the ramped and asymptotic loadings, excess pore pressure isochrones in both vertical and horizontal directions have been analysed to confirm the validity for the parametric studies. It can be found that the isochrones with higher loading parameters (i.e. ‘a’ and ‘b’) will present higher excess pore pressures. As

expected, the excess pore pressures in both cases increase with distance from the vertical drainage boundaries.

CHAPTER 8

ANALYTICAL SOLUTION TO AXISYMMETRIC CONSOLIDATION IN UNSATURATED SOILS WITH LINEARLY DEPTH-DEPENDENT INITIAL CONDITIONS

8.1. Introduction

This chapter proposes an analytical solution to predict the consolidation of unsaturated soils considering both radial and vertical flows. In addition, both uniformly and linearly distributed initial excess pore-air and pore-water pressures along the depth will be captured in this study. The uncoupled polar governing equations of flow with respect to air and water phases are first derived from the 3D Cartesian equations given by Fredlund et al. (2012). Based on an assumption of the free strain case, separation of variables and Laplace transformation techniques are used in this study to obtain the final solution. Graphical presentations are provided to demonstrate the effects of the air to water permeability ratio, different radii, and depth-dependent initial conditions on the changes in excess pore-air and pore-water pressures. Additionally, the matric suction change, the degree of consolidation and the excess pore pressure isochrones against time are graphically presented.

8.2. Polar governing equations of flow

The installation of vertical drain wells can be categorized in square and triangular patterns. According to Barron (1948), most drain well systems are installed in triangular patterns due to economic reasons. Figure 8.1(a) presents the plan of the drain well pattern and the influence zone of each well. Figure 8.1(b) depicts the details of the typical well within an unsaturated soil stratum. Dimensions of the soil system include a depth H and a radius of the influence zone r_e. The vertical drain well with the radius r_w is located at the centre of the influence zone. When a constant loading is applied to the

soil, the air and water phases will dissipate through the boundary of the drain well and through the permeable top boundary only or permeable top and base boundaries of the soil simultaneously.

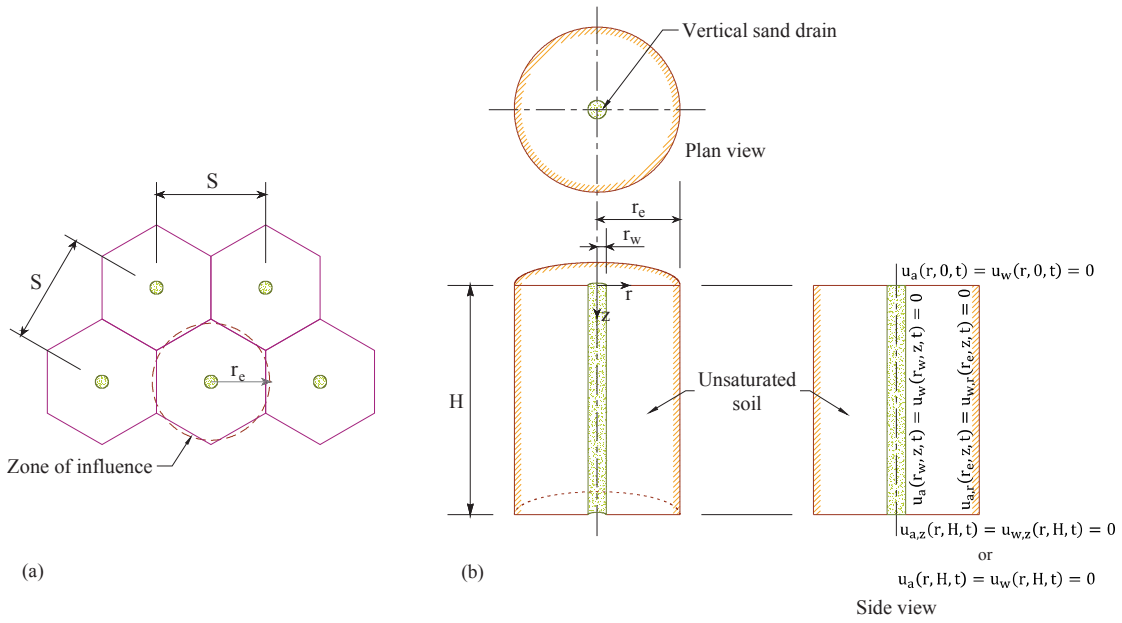

Figure 8.1. Vertical drain system: (a) triangular drain well pattern and (b) details of a typical well

In the literature for consolidation theory of unsaturated soils, the flows of air and water phases within the soil are assumed to be independent and continuous (Fredlund & Hasan 1979; Dakshanamurthy & Fredlund 1980; Darkshanamurthy et al. 1984). Particularly, the air flow follows Fick's law, whereas Darcy's law is employed to describe the flow of water. Both air and water flows are usually simulated under the Cartesian governing equations for unsaturated soils (Fredlund & Hasan 1979; Dakshanamurthy & Fredlund 1980; Darkshanamurthy et al. 1984). Prior to the evaluation of the axisymmetric consolidation, the Cartesian equations should be transformed into the polar forms. The detailed polar transformation of governing equations is provided in Appendix F. Through mathematical derivations obtained from the net flux of the air and water phases per unit volume and constitutive equations for soil deformation, a set of uncoupled governing flow equations can be presented as follows:

(a) Polar governing equations considering the radial flow only:

$$u_{a,t} + C_a\, u_{w,t} + c_{v_r}^{a}\left(u_{a,rr} + \frac{1}{r}u_{a,r}\right) = 0 \qquad [8\text{-}1a]$$

$$u_{w,t} + C_w\, u_{a,t} + c_{v_r}^{w}\left(u_{w,rr} + \frac{1}{r}u_{w,r}\right) = 0 \qquad [8\text{-}1b]$$

(b) Polar governing equations considering both radial and vertical flows:

$$u_{a,t} + C_a\, u_{w,t} + c_{v_r}^{a}\left(u_{a,rr} + \frac{1}{r}u_{a,r}\right) + c_{v_z}^{a}u_{a,zz} = 0 \qquad [8\text{-}2a]$$

$$u_{w,t} + C_w\, u_{a,t} + c_{v_r}^{w}\left(u_{w,rr} + \frac{1}{r}u_{w,r}\right) + c_{v_z}^{w}u_{w,zz} = 0 \qquad [8\text{-}2b]$$

where u_a and u_w are the excess pore-air and pore-water pressures (kPa), respectively; $u_{a,t}$ and $u_{w,t}$ are the first order derivatives against time for excess pore-air and pore-water pressure functions, respectively; $u_{a,r}$ and $u_{w,r}$ are the first order derivatives against radius for excess pore-air and pore-water pressure functions, respectively; $u_{a,rr}$ and $u_{w,rr}$ are the second order derivatives against radius for excess pore-air and pore-water pressure functions, respectively; $u_{a,zz}$ and $u_{w,zz}$ are the second order derivatives against depth for excess pore-air and pore-water pressure functions, respectively. Additionally, the consolidation coefficients are:

$$C_a = \frac{1}{\left[\left(\frac{m_1^a}{m_2^a}-1\right)-\frac{n(1-S_r)}{m_2^a(u_a^0+u_{atm})}\right]} \qquad [8\text{-}3a]$$

$$c_{v_r}^{a} = \frac{k_{a_r}R\Theta}{gM}\frac{1}{\left[m_2^a(u_a^0+u_{atm})\left(\frac{m_1^a}{m_2^a}-1\right)-n(1-S_r)\right]} \qquad [8\text{-}3b]$$

$$c_{v_z}^{a} = \frac{k_{a_z}R\Theta}{gM}\frac{1}{\left[m_2^a(u_a^0+u_{atm})\left(\frac{m_1^a}{m_2^a}-1\right)-n(1-S_r)\right]} \qquad [8\text{-}3c]$$

$$C_w = \frac{m_1^w}{m_2^w} - 1 \qquad [8\text{-}3d]$$

$$c_{v_r}^{w} = \frac{1}{m_2^w}\left(\frac{k_{w_r}}{\gamma_w}\right) \qquad [8\text{-}3e]$$

$$c_{v_z}^{w} = \frac{1}{m_2^w}\left(\frac{k_{w_z}}{\gamma_w}\right) \qquad [8\text{-}3d]$$

where k_{a_r} and k_{w_r} are the coefficients of air and water permeability in the radial domain (m/s), respectively; k_{a_z} and k_{w_z} are the coefficients of air and water permeability in the vertical domain (m/s), respectively; m_1^a and m_1^w are the coefficients

of air and water volume change with respect to the change of net stress ($1/\mathrm{kPa}$), respectively; m_2^a and m_2^w are the coefficients of air and water volume change with respect to the change of suction ($1/\mathrm{kPa}$), respectively; g is the gravitational constant (i.e. $9.81\ \mathrm{m/s^2}$); u_a^0 is the initial pore-air pressure at the soil surface (kPa); u_{atm} is the atmospheric pressure (i.e. 100 kPa); R is the universal air constant (i.e. $8.314\ \mathrm{J/mol.K}$); $\Theta = (\theta^\circ + 273)$, is the absolute temperature (K); θ° is the temperature in degree Celsius; M is the molecular mass of air (i.e. $0.029\ \mathrm{kg/mol}$); n is the porosity during consolidation process; S_r is the degree of saturation during consolidation process; and γ_w is the water unit weight ($9.81\ \mathrm{kN/m^3}$).

8.3. Analytical solution

8.3.1. Boundary and initial conditions

It is assumed that the boundary of the influence zone of the soil (i.e. $r = r_e$) is impermeable whereas the surface of the drain cylinder (i.e. $r = r_w$) is permeable, thus,

$$u_a(r_w, z, t) = u_w(r_w, z, t) = u_{a,r}(r_e, z, t) = u_{w,r}(r_e, z, t) = 0 \quad [8\text{-}4]$$

In addition, the pervious top – impervious base (PTIB) and pervious top – pervious base (PTPB) boundary conditions can be presented as below:

(a) The PTIB condition:

$$u_a(r, 0, t) = u_w(r, 0, t) = u_{a,z}(r, H, t) = u_{w,z}(r, H, t) = 0 \quad [8\text{-}5a]$$

(b) The PTPB condition:

$$u_a(r, 0, t) = u_w(r, 0, t) = u_a(r, H, t) = u_w(r, H, t) = 0 \quad [8\text{-}5b]$$

Most literature and laboratory experiments have assumed that, immediately after loading, the initial excess pore pressures are distributed uniformly throughout depth (Craig 2004; Venkatramaiah 2006; Coduto et al. 2011). However, this uniform initial condition may be only applicable when the external applied loading is indefinite and uniformly applied on the surface of the soil. In a case when footings built on the ground are small or the soil stratum is thick, the initial excess pore pressures generated by

loading may decrease with depth. A simplified simulation for such initial condition can be presented adopting a linear distribution of excess pore pressures (Rowe 2001; Aysen 2002; Venkatramaiah 2006; Fang 2013). In this study, simulations for the linear distribution of initial excess pore pressures at $r \in (r_w, r_e)$ and $z \in (0, H)$, are adopted as follows:

$$u_a(r, z, 0) = u_a^0 \left(1 - \zeta_a \frac{z}{H}\right) \quad [8\text{-}6a]$$

$$u_w(r, z, 0) = u_w^0 \left(1 - \zeta_w \frac{z}{H}\right) \quad [8\text{-}6b]$$

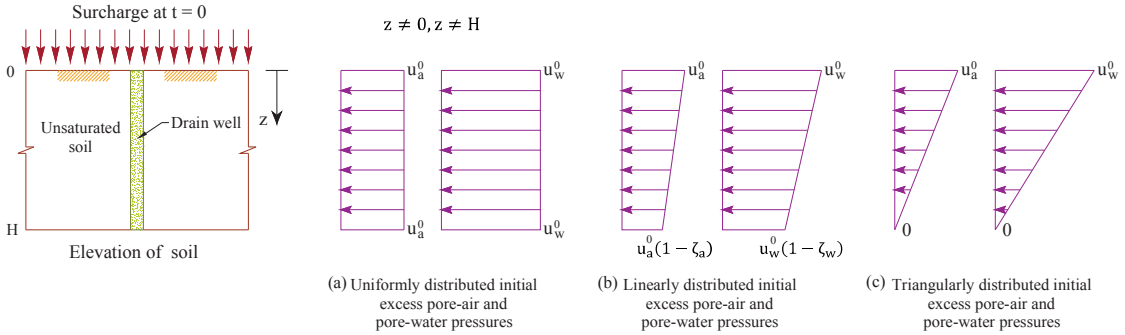

Figure 8.2. Initial conditions: (a) uniform, (b) trapezoidal and (c) triangular distributions of initial excess pore pressures

where u_a^0 and u_w^0 are the initial pore-air and pore-water pressures at the soil surface, respectively; and ζ_a and ζ_w are the dimensionless parameters controlling the gradients of initial pore-air and pore-water pressure distributions. Note that the proposed parameters ζ_a and ζ_w would range from 0 to 1. Figure 8.2 shows the distribution of initial pore pressures in response of changes of ζ_a and ζ_w. When $\zeta_a = \zeta_w = 0$, the initial excess pore pressures are distributed uniformly along z-direction (Figure 8.2(a)); when ζ_a and ζ_w parameters are between 0 and 1, the initial condition presents trapezoidal distribution (Figure 8.2(b)); and when $\zeta_a = \zeta_w = 1$, the triangular distribution of initial excess pore pressures is produced (Figure 8.2(c)).

8.3.2. Excess pore pressure dissipation

A natural soil usually consists of nonlinear properties which may further require arduous numerical approaches to estimate the soil compression. In order to achieve an analytical solution, the following assumptions have been made in this study:

(1) The soil stratum is homogeneous;
(2) The air and water flows are continuous and independent;
(3) The soil grain and pore-water are incompressible;
(4) Environmental factors (e.g. air diffusion, temperature change) are neglected;
(5) Well resistance and smear effects are discarded;
(6) Consolidation parameters for air phase (C_a, $c_{v_r}^a$ and $c_{v_z}^a$) and water phase (C_w, $c_{v_r}^w$ and $c_{v_z}^w$) are constant for the applied stress increment;

It should be noted that the unit weight of water (γ_w) is assumed to remain constant, implying that pore-water is incompressible, as mentioned in Assumption (3). On the other hand, Assumption (6) may not be completely accurate for some cases. In particular, the soil properties such as permeability (k_a and k_w), degree of saturation (S_r), and porosity (n) in a soil stratum vary during the consolidation induced by a constant load, thus the consolidation parameters would eventually change. However, it may be acceptable to assume that these parameters are constant during the transient process for a particular stress increment.

For the sake of generality, Equations [8-2a] and [8-2b] are considered for the analytical procedure. Firstly, general solutions for u_a and u_w can be written as products of functions with respect to dimensions r and z and time t. In addition, based on the homogeneous boundary conditions for the depth given in Equations [8-5a] and [8-5b], Fourier sine series can represent functions of the depth z. Hence,

$$u_a(r,z,t) = R_a(r).Z_a(z).T_a(t) = \sum_{j=0}^{\infty} U_a(r,t)\sin\left(\frac{\sqrt{\mu^j}}{H}z\right) \quad [8\text{-}7a]$$

$$u_w(r,z,t) = R_w(r).Z_w(z).T_w(t) = \sum_{j=0}^{\infty} U_w(r,t)\sin\left(\frac{\sqrt{\mu^j}}{H}z\right) \quad [8\text{-}7b]$$

where $R_a(r) = R_w(r) = R(r)$, are the eigenfunctions for the domain r; $Z_a(z) = Z_w(z) = \sin\left(z\sqrt{\mu^j}/H\right)$, are the eigenfunctions for the domain z; $T_a(t)$ and $T_w(t)$ are the generalized Fourier coefficients with respect to air and water phases, respectively; $U_a(r,t) = R(r)\,T_a(t)$ and $U_w(r,t) = R(r)\,T_w(t)$. Note that $R_a(r)$ resembles to $R_w(r)$, and $Z_a(z)$ resembles to $Z_w(z)$ due to similar boundary conditions, as provided in Equations [8-4] and [8-5]. Under the PTIB boundary condition, the term μ^j can be defined as:

$$\mu^j = [(2j+1)\pi/2]^2, \qquad (j = 0, 1, 2, ...) \qquad [8\text{-}8a]$$

or μ^j for the PTPB boundary condition is given by:

$$\mu^j = (j\pi)^2, \qquad (j = 0, 1, 2, ...) \qquad [8\text{-}8b]$$

Then substituting Equations [8-7a] and [8-7b] into Equations [8-2a] and [8-2b], respectively, results in:

$$U_{a,t}(r,t) + C_a\,U_{w,t}(r,t) + c_{v_r}^a\left[U_{a,rr}(r,t) + \frac{1}{r}U_{a,r}(r,t)\right] - c_{v_z}^a\frac{\mu^j}{H^2}\,U_a(r,t) = 0 \qquad [8\text{-}9a]$$

$$U_{w,t}(r,t) + C_w\,U_{a,t}(r,t) + c_{v_r}^w\left[U_{w,rr}(r,t) + \frac{1}{r}U_{w,r}(r,t)\right] - c_{v_z}^w\frac{\mu^j}{H^2}\,U_w(r,t) = 0 \qquad [8\text{-}9b]$$

Applying the separation of variables to Equations [8-9a] and [8-9b] gives:

$$k_{a_r}\left[\frac{R_{,rr}(r)}{R(r)} + \frac{1}{r}\frac{R_{,r}(r)}{R(r)}\right] - k_{a_z}\frac{\mu^j}{H^2} = -\frac{1}{c_v^a}\left[\frac{T_{a,t}(t)}{T_a(t)} + C_a\frac{T_{w,t}(t)}{T_a(t)}\right] = -\lambda_a^{ij} \qquad [8\text{-}10a]$$

$$k_{w_r}\left[\frac{R_{,rr}(r)}{R(r)} + \frac{1}{r}\frac{R_{,r}(r)}{R(r)}\right] - k_{w_z}\frac{\mu^j}{H^2} = -\frac{1}{c_v^w}\left[\frac{T_{w,t}(t)}{T_w(t)} + C_w\frac{T_{a,t}(t)}{T_w(t)}\right] = -\lambda_w^{ij} \qquad [8\text{-}10b]$$

where $c_v^a = \frac{R\Theta}{gM}\frac{1}{\left[m_2^a(u_a^0+u_{atm})\left(\frac{m_1^a}{m_2^a}-1\right)-n(1-S_r)\right]}$; and $c_v^w = \frac{1}{m_2^w}\left(\frac{1}{\gamma_w}\right)$. [8-11]

Then, two sets of ordinary differential equations (ODEs) can be obtained as below:

$$\begin{cases} R_{,rr}(r) + \frac{1}{r}R_{,r}(r) + \frac{\xi^i}{(r_w)^2}\,R(r) = 0 \\ T_{a,t}(t) + C_a\,T_{w,t}(t) - c_v^a\left(\lambda_a^{ij}\right)T_a(t) = 0 \end{cases}, \qquad (i = 0, 1, 2, ...;\ j = 0, 1, 2, ...) \qquad [8\text{-}12a]$$

$$\begin{cases} R_{,rr}(r) + \frac{1}{r} R_{,r}(r) + \frac{\xi^i}{(r_w)^2} R(r) = 0 \\ T_{w,t}(t) + C_w T_{a,t}(t) - c_v^w\left(\lambda_w^{ij}\right) T_w(t) = 0 \end{cases}, \quad (i = 0, 1, 2, ...; j = 0, 1, 2, ...) \qquad [8\text{-}12b]$$

owing to the fact that

$$\begin{cases} \lambda_a^{ij} = k_{a_r} \frac{\xi^i}{(r_w)^2} + k_{a_z} \frac{\mu^j}{H^2} \\ \lambda_w^{ij} = k_{w_r} \frac{\xi^i}{(r_w)^2} + k_{w_z} \frac{\mu^j}{H^2} \end{cases}, \quad (i = 0, 1, 2, ...; j = 0, 1, 2, ...) \qquad [8\text{-}13]$$

Note that ξ^i and μ^j are eigenvalues while λ_a^{ij} and λ_w^{ij} are constant values ($i = 0, 1, 2, ...; j = 0, 1, 2, ...$). Based on Equation [8-12], Fourier Bessel series are taken as the solution for the radial function $R^i(r)$ ($i = 0, 1, 2, ...$), resulting in:

$$R^i(r) = A J_0\left(\frac{\sqrt{\xi^i}}{r_w} r\right) + B Y_0\left(\frac{\sqrt{\xi^i}}{r_w} r\right) \qquad [8\text{-}14]$$

where A and B are the Bessel constants; and $J_0\left(r\sqrt{\xi^i}/r_w\right)$ and $Y_0\left(r\sqrt{\xi^i}/r_w\right)$ are the Bessel functions of the first kind and the second kind of order zero, respectively. Incorporating the radial boundary condition in Equation [8-4] into Equation [8-14] yields in:

$$\begin{cases} A J_0\left(\sqrt{\xi^i}\right) + B Y_0\left(\sqrt{\xi^i}\right) = 0 \\ A J_1\left(\varrho\sqrt{\xi^i}\right) + B Y_1\left(\varrho\sqrt{\xi^i}\right) = 0 \end{cases} \qquad [8\text{-}15]$$

where $\varrho = r_e/r_w$; and $J_1\left(\varrho\sqrt{\xi^i}\right)$ and $Y_1\left(\varrho\sqrt{\xi^i}\right)$ are the Bessel functions of the first kind and the second kind of order one at $r = r_e$. To assure $A \neq 0$ as well as $B \neq 0$, the following condition must be satisfied:

$$J_0\left(\sqrt{\xi^i}\right) Y_1\left(\varrho\sqrt{\xi^i}\right) - J_1\left(\varrho\sqrt{\xi^i}\right) Y_0\left(\sqrt{\xi^i}\right) = 0 \qquad [8\text{-}16]$$

Note that the eigenvalue ξ^i ($i = 0, 1, 2, ...$) is the i^{th} root of Equation [8-16]. Besides, the relationship between constants A and B in Equation [8-15] can be obtained as follows:

$$B = -A\,\frac{J_1\left(\varrho\sqrt{\xi^i}\right)}{Y_1\left(\varrho\sqrt{\xi^i}\right)} \qquad [8\text{-}17]$$

Combining Equations [8-14] and [8-17], the radial function $R^i(r)$ $(i = 0, 1, 2, ...)$ becomes:

$$R^i(r) = \frac{A}{Y_1\left(\varrho\sqrt{\xi^i}\right)}\,D^i\left(\frac{\sqrt{\xi^i}}{r_w}r\right) \qquad [8\text{-}18]$$

$$\text{where } D^i\left(\frac{\sqrt{\xi^i}}{r_w}r\right) = J_0\left(\frac{\sqrt{\xi^i}}{r_w}r\right)\,Y_1\left(\varrho\sqrt{\xi^i}\right) - J_1\left(\varrho\sqrt{\xi^i}\right)\,Y_0\left(\frac{\sqrt{\xi^i}}{r_w}r\right). \qquad [8\text{-}19]$$

To obtain the generalized Fourier coefficients $T_a^{ij}(t)$ and $T_w^{ij}(t)$ $(i = 0, 1, 2, ...;$ $j = 0, 1, 2, ...)$, the Laplace transformation should be first applied to the function of time in Equations [8-12a] and [8-12b], thus,

$$\left[s - c_v^a\left(\lambda_a^{ij}\right)\right]\overline{T}_a^{ij}(s) + sC_a\,\overline{T}_w^{ij}(s) - \left[T_a^{ij}(0) + C_a\,T_w^{ij}(0)\right] = 0 \qquad [8\text{-}20a]$$

$$\left[s - c_v^w\left(\lambda_w^{ij}\right)\right]\overline{T}_w^{ij}(s) + sC_w\,\overline{T}_a^{ij}(s) - \left[T_w^{ij}(0) + C_w\,T_a^{ij}(0)\right] = 0 \qquad [8\text{-}20b]$$

where $\overline{T}_a^{ij}(s)$ and $\overline{T}_w^{ij}(s)$ $(i = 0, 1, 2, ...;\ j = 0, 1, 2, ...)$ are the Laplace transformed equations with complex subjugate s. Solving simultaneously for $\overline{T}_a^{ij}(s)$ and $\overline{T}_w^{ij}(s)$ $(i = 0, 1, 2, ...; j = 0, 1, 2, ...)$ gives:

$$\overline{T}_a^{ij}(s) = \frac{T_a^{ij}(0)(C_wC_a-1)s + c_v^w\left[T_a^{ij}(0) + C_a\,T_w^{ij}(0)\right]\lambda_w^{ij}}{(C_wC_a-1)s^2 + \left(\lambda_w^{ij}c_v^w + \lambda_a^{ij}c_v^a\right)s - c_v^wc_v^a\lambda_w^{ij}\lambda_a^{ij}} \qquad [8\text{-}21a]$$

$$\overline{T}_w^{ij}(s) = \frac{T_w^{ij}(0)(C_wC_a-1)s + c_v^a\left[T_w^{ij}(0) + C_w\,T_a^{ij}(0)\right]\lambda_a^{ij}}{(C_wC_a-1)s^2 + \left(\lambda_w^{ij}c_v^w + \lambda_a^{ij}c_v^a\right)s - c_v^wc_v^a\lambda_w^{ij}\lambda_a^{ij}} \qquad [8\text{-}21b]$$

Constant terms $T_a^{ij}(0)$ and $T_w^{ij}(0)$ $(i = 0, 1, 2, ...; j = 0, 1, 2, ...)$ in Equation [8-21] can be obtained using the orthogonalities of Bessel and sine functions, as shown below:

$$T_a^{ij}(0) = \frac{Y_1\left(\varrho\sqrt{\xi^i}\right)}{A} \frac{\int_0^H \int_{r_w}^{r_e} u_a(r,z,0)\, D^i\left(\frac{\sqrt{\xi^i}}{r_w}r\right) \sin\left(\frac{\sqrt{\mu^j}}{H}z\right) rdrdz}{\int_0^H \int_{r_w}^{r_e} \left[D^i\left(\frac{\sqrt{\xi^i}}{r_w}r\right)\sin\left(\frac{\sqrt{\mu^j}}{H}z\right)\right]^2 rdrdz} = \frac{Y_1\left(\varrho\sqrt{\xi^i}\right)}{A}\, \Xi_a \qquad [8\text{-}22a]$$

$$T_w^{ij}(0) = \frac{Y_1\left(\varrho\sqrt{\xi^i}\right)}{A} \frac{\int_0^H \int_{r_w}^{r_e} u_w(r,z,0)\, D^i\left(\frac{\sqrt{\xi^i}}{r_w}r\right) \sin\left(\frac{\sqrt{\mu^j}}{H}z\right) rdrdz}{\int_0^H \int_{r_w}^{r_e} \left[D^i\left(\frac{\sqrt{\xi^i}}{r_w}r\right)\sin\left(\frac{\sqrt{\mu^j}}{H}z\right)\right]^2 rdrdz} = \frac{Y_1\left(\varrho\sqrt{\xi^i}\right)}{A}\, \Xi_w \qquad [8\text{-}22b]$$

where $\Xi_a = \frac{X^i}{\Upsilon^i\sqrt{\xi^i}} \frac{4}{H}\int_0^H \left[u_a(r,z,0)\, \sin\left(\frac{\sqrt{\mu^j}}{H}z\right)\right] dz;$

$\Xi_w = \frac{X^i}{\Upsilon^i\sqrt{\xi^i}} \frac{4}{H}\int_0^H \left[u_w(r,z,0)\, \sin\left(\frac{\sqrt{\mu^j}}{H}z\right)\right] dz;$

$X^i = (r_w)^2 \left[J_1\left(\varrho\sqrt{\xi^i}\right) Y_1\left(\sqrt{\xi^i}\right) - J_1\left(\sqrt{\xi^i}\right) Y_1\left(\varrho\sqrt{\xi^i}\right)\right]$; and

$\Upsilon^i =$

$$(r_e)^2 \left[J_0\left(\varrho\sqrt{\xi^i}\right) Y_1\left(\varrho\sqrt{\xi^i}\right) - J_1\left(\varrho\sqrt{\xi^i}\right) Y_0\left(\varrho\sqrt{\xi^i}\right)\right]^2 -$$

$$(r_w)^2 \left[J_0\left(\sqrt{\xi^i}\right) Y_1\left(\varrho\sqrt{\xi^i}\right) - J_1\left(\varrho\sqrt{\xi^i}\right) Y_0\left(\sqrt{\xi^i}\right)\right]^2 - \left(\frac{X^i}{r_w}\right)^2. \qquad [8\text{-}23]$$

Combining Equations [8-21] – [8-23] and then taking the Laplace inverse to obtain the generalized Fourier coefficients $T_a^{ij}(t)$ and $T_w^{ij}(t)$ ($i = 0, 1, 2, ...$; $j = 0, 1, 2, ...$):

$$T_a^{ij}(t) = \frac{Y_1\left(\varrho\sqrt{\xi^i}\right)}{A} \frac{\Omega\left(e^{\alpha_1^{ij}t} - e^{\alpha_2^{ij}t}\right) + \Psi\left(e^{\alpha_1^{ij}t} + e^{\alpha_2^{ij}t}\right)}{2\eta^{ij}} \qquad [8\text{-}24a]$$

$$T_w^{ij}(t) = \frac{Y_1\left(\varrho\sqrt{\xi^i}\right)}{A} \frac{\Omega'\left(e^{\alpha_1^{ij}t} - e^{\alpha_2^{ij}t}\right) + \Psi'\left(e^{\alpha_1^{ij}t} + e^{\alpha_2^{ij}t}\right)}{2\eta^{ij}} \qquad [8\text{-}24b]$$

where $\eta^{ij} = \left[\left(c_v^a\lambda_a^{ij} - c_v^w\lambda_w^{ij}\right)^2 + 4c_v^a c_v^w C_w C_a \lambda_a^{ij}\lambda_w^{ij}\right]^{\frac{1}{2}};$

$\alpha_1^{ij} = \frac{1}{2}\left(\frac{c_v^a\lambda_a^{ij} + c_v^w\lambda_w^{ij} + \eta^{ij}}{1 - C_w C_a}\right);$ $\alpha_2^{ij} = \frac{1}{2}\left(\frac{c_v^a\lambda_a^{ij} + c_v^w\lambda_w^{ij} - \eta^{ij}}{1 - C_w C_a}\right);$

$\Omega = \left(c_v^a\lambda_a^{ij} - c_v^w\lambda_w^{ij}\right)\Xi_a - 2c_v^w C_a \lambda_w^{ij}\, \Xi_w;$ $\Psi = \eta^{ij}\, \Xi_a;$

$\Omega' = \left(c_v^w\lambda_w^{ij} - c_v^a\lambda_a^{ij}\right)\Xi_w - 2c_v^a C_w \lambda_a^{ij}\, \Xi_a$; and $\Psi' = \eta^{ij}\, \Xi_w.$ [8-25]

Substituting Equations [8-18] and [8-24] into Equation [8-7] gives the solutions as shown below:

$$u_a(r,z,t) = \sum_{j=0}^{\infty} D^i \left(\frac{\sqrt{\xi^i}}{r_w} r\right) \sin\left(\frac{\sqrt{\mu^j}}{H} z\right) \left[\frac{\Omega\left(e^{\alpha_1^{ij} t} - e^{\alpha_2^{ij} t}\right) + \Psi\left(e^{\alpha_1^{ij} t} + e^{\alpha_2^{ij} t}\right)}{2\eta^{ij}}\right] \quad [8\text{-}26a]$$

$$u_w(r,z,t) = \sum_{j=0}^{\infty} D^i \left(\frac{\sqrt{\xi^i}}{r_w} r\right) \sin\left(\frac{\sqrt{\mu^j}}{H} z\right) \left[\frac{\Omega'\left(e^{\alpha_1^{ij} t} - e^{\alpha_2^{ij} t}\right) + \Psi'\left(e^{\alpha_1^{ij} t} + e^{\alpha_2^{ij} t}\right)}{2\eta^{ij}}\right] \quad [8\text{-}26b]$$

Note that the Bessel constant A presented in Equations [8-18] and [8-24] is cancelled out when the solutions are formed. The proposed equations provided in Equations [8-26a] and [8-26b] present the time-dependent changes in the excess pore-air and pore-water pressures, respectively, along dimensions r and z. Similar approach can be conducted to obtain solutions for Equations [8-1a] and [8-1b], in which the vertical permeability coefficient (k_z) is discarded and both top and base boundaries of the soil are considered to be undrained. Complete set of analytical solutions for axisymmetric consolidation with or without the vertical flow are presented in Appendix G. In addition, for the consolidation with the vertical flow, both cases of uniform and linear distributions of initial excess pore pressures along the soil depth are also captured in the solutions presented in Appendix G.

8.3.3. Average degree of consolidation

The average excess pore-air and pore-water pressures (i.e. $\bar{u}_a$ and $\bar{u}_w$, respectively) can be obtained by averaging the pore pressures in both r- and z-directions as follows:

$$\bar{u}_a(t) = \frac{1}{\pi[(r_e)^2 - (r_w)^2]} \frac{1}{H} \int_0^H \int_{r_w}^{r_e} 2\pi\, u_a(r,z,t)\, r dr dz \quad [8\text{-}27a]$$

$$\bar{u}_w(t) = \frac{1}{\pi[(r_e)^2 - (r_w)^2]} \frac{1}{H} \int_0^H \int_{r_w}^{r_e} 2\pi\, u_w(r,z,t)\, r dr dz \quad [8\text{-}27b]$$

The constitutive model for the soil skeleton can be adopted from Fredlund et al. (2012). It is assumed that the volume change coefficients with respect to air and water phases are constant during the consolidation process at a particular stress increment. When $\partial\sigma_r/\partial t = \partial\sigma_\theta/\partial t = \partial\sigma_z/\partial t = 0$, the constitutive relationship under the 3D loading condition is presented as below:

$$\frac{\partial\left(\frac{\Delta V}{V_0}\right)}{\partial t} = (m_2^s - m_1^s)\frac{\partial \bar{u}_a}{\partial t} - m_2^s \frac{\partial \bar{u}_w}{\partial t} \quad [8\text{-}28]$$

where m_1^s and m_2^s are the coefficients of volume change of the soil element with respect to the change in the net stress and change in suction ($1/\text{kPa}$), respectively. It is worth noting that $m_1^s = m_1^a + m_1^w$ and $m_2^s = m_2^a + m_2^w$. By integrating Equation [8-28] against the time variable t, the average volumetric strain $\bar{\varepsilon}_v$ is presented as follows:

$$\bar{\varepsilon}_v(t) = (m_2^s - m_1^s)[\bar{u}_a(t) - \bar{u}_a(0)] - m_2^s[\bar{u}_w(t) - \bar{u}_w(0)] \quad [8\text{-}29]$$

The average degree of consolidation, $\bar{U}$, based on the volumetric strain $\bar{\varepsilon}_v$, can be derived as follows:

$$\bar{U} = \left|\frac{\bar{\varepsilon}_v(t)}{\bar{\varepsilon}_v(\infty)}\right| \quad [8\text{-}30]$$

where $\bar{\varepsilon}_v(\infty)$ is the final average volumetric strain when time t approaches infinity. Equation [8-30] describes the time-dependent response of consolidation settlement of the unsaturated soil due to a constant load at a particular time. Complete equations presenting the average degree of consolidation $\bar{U}$ are provided in Appendix G.

8.4. Examples

In this study, the axisymmetric consolidation with and without the vertical flows of air and water phases are investigated in two examples. The uniformly and linearly distributed initial excess pore pressures, simulated by the parameters ζ_a and ζ_w, are highlighted in the axisymmetric consolidation considering both radial and vertical flows. Following Conte (2004, 2006) and Fredlund et al. (2012), this study adopts:

- Volume change coefficients $m_1^s = -5.64 \times 10^{-4}\ \text{kPa}^{-1}$, $m_2^s = 0.2m_1^s$, $m_1^w = -1.13 \times 10^{-4}\ \text{kPa}^{-1}$, $m_2^w = 1.8m_1^w$;
- Material properties $n = 0.50$, $S_r = 80\%$;
- Physical properties $\Theta = (\theta° + 273.16)\ \text{K}$, $\theta° = 20℃$, $R = 8.314\ \text{J/mol. K}$, $M = 0.029\ \text{kg/mol}$, $u_{atm} = 100\ \text{kPa}$;
- Dimensions $r_w = 0.2\ \text{m}$, $r_e = 1.8\ \text{m}$, $H = 5\ \text{m}$;

- Other properties $k_w = 10^{-10}$ m/s, $q_0 = 100$ kPa, $u_a^0 = 20$ kPa, $u_w^0 = 40$ kPa. [8-31]

The above soil properties are assumed to be constant during the consolidation process. An instantaneous compression induced by the external applied load q_0 generates initial excess pore-air and pore-water pressures (i.e., u_a^0 and u_w^0, respectively). Considering that the soil is loaded three-dimensionally under isotropic conditions, changes in excess pore pressures can be determined using a method given by Fredlund & Hasan (1979), and Fredlund et al. (2012). Detailed evaluations for the initial excess pore-air and pore-water pressures are provided in Appendix H. On the other hand, when considering the triangular vertical drain system, both adopted values of radii of influence zone r_e and sand drain r_w are realistic and practical for evaluations of axisymmetric consolidation. In particular, the centre to centre spacing (S) for the adopted $r_e = 1.8$ m is determined to be 3.4 m (i.e. $r_e = 0.525S$), which is in the desirable range of spacing (1.2 – 3.6 m) recommended by Holtz (1987). Additionally, the adopted $r_w = 0.2$ m is also in the design range (0.075 – 0.3 m) given by Holtz et al. (1991) and Smoltczyk (2003).

For the sake of simplicity, the diagonal permeability k_{rz} is discarded and only isotropic permeability condition (i.e. $k_{a_r} = k_{a_z} = k_a$ and $k_{w_r} = k_{w_z} = k_w = 10^{-10}$ m/s) is considered in this study. Thus, the coefficients of consolidation can be obtained based on given properties presented in Equation [8-31]:

$$C_a = -6.53 \times 10^{-2}, \qquad c_{v_r}^a = c_{v_z}^a = -52 \times 10^3 k_a \text{ m}^2/\text{s}$$
$$C_w = 44.32 \times 10^{-2}, \qquad c_{v_r}^w = c_{v_z}^w = -5.03 \times 10^{-8} \text{ m}^2/\text{s} \qquad [8\text{-}32]$$

Example 1 demonstrates changes in excess pore pressure dissipation and settlement due to the only radial flows of air and water. These changes are examined against the permeability ratio (k_a/k_w) and radial distances from the well (r). Example 2, on the other hand, presents the consolidation process including both radial and vertical flows, and captures: (a) uniform initial condition (i.e. $\zeta_a = \zeta_w = 0$); and (b) linear initial condition (i.e. $\zeta_a, \zeta_w > 0$). The effects of k_a/k_w on the axisymmetric consolidation behavior under the PTIB and PTPB boundary conditions are investigated in Example 2(a) whereas significant effects of ζ_a and ζ_w are highlighted in Example 2(b).

Additionally, the excess pore pressure isochrones and the matric suction changes (Δs) are presented in both examples.

8.4.1. Example 1 – Axisymmetric consolidation with radial flow only

Since only radial flow is considered in this example, the uniform initial excess pore pressures over the radial domain, u_a^0 and u_w^0, may be adopted. The changes in the normalised pore-air (u_a/u_a^0) and pore-water (u_w/u_w^0) pressures, and the degree of consolidation ($\bar{U}$) are analysed in this section.

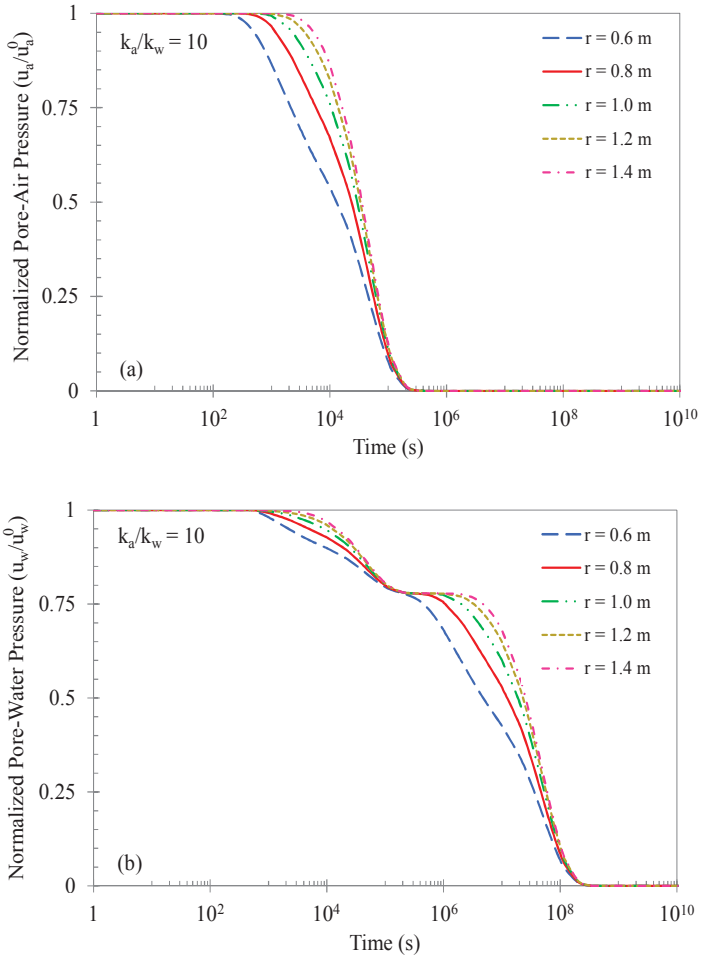

Figure 8.3. Dissipation of (a) excess pore-air and (b) excess pore-water pressures varying with different radii (for radial flow only)

Adopting Equation [G-3] in Appendix G, Figure 8.3 illustrates dissipation curves of the excess pore pressures at different radii, while adopting $k_a/k_w = 10$. In general, it

can be observed that the excess pore-air (Figure 8.3(a)) and pore-water (Figure 8.3(b)) pressures dissipate more quickly for the points closer to the drain well. When the radius considerably increases (i.e. $r \geq 1$ m), the effects of radial distance on the dissipation rate become insignificant. While the excess pore-air pressure is fully dissipated, there is a delay period in the excess pore-water pressure curve, known as plateau (Figure 8.3(b)). It can be observed that the increase in the radius of the point of interest results in longer plateau and thus a clear double S-shaped pattern for the excess pore-water pressure dissipation.

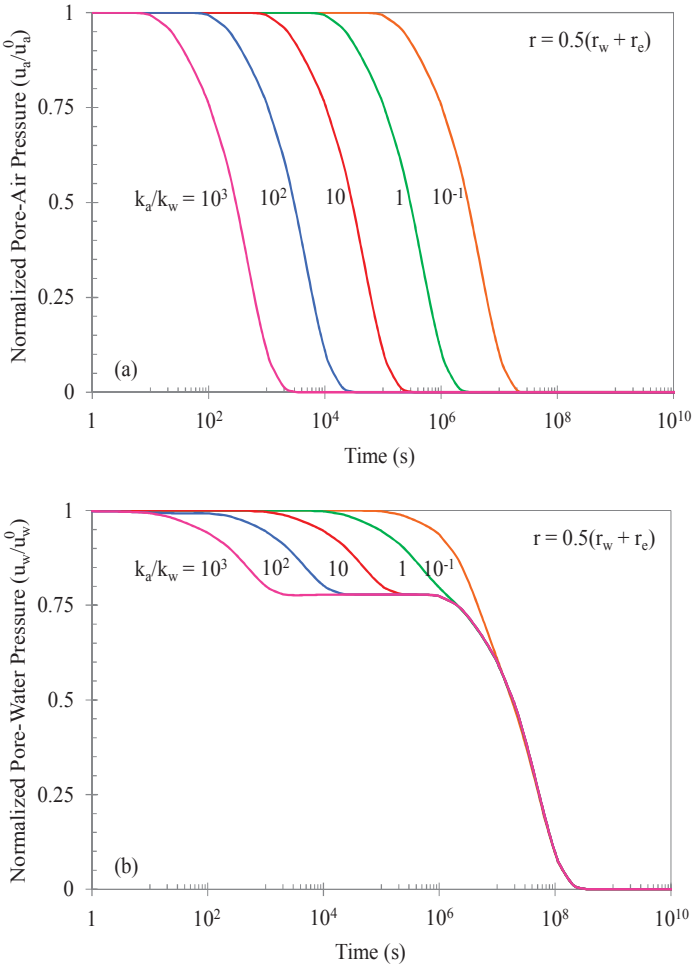

Figure 8.4. Dissipation of (a) excess pore-air and (b) excess pore-water pressures varying with different k_a/k_w values (for radial flow only)

Figure 8.4 demonstrates changes in excess pore pressures with different k_a/k_w values. It is worth noting that the air permeability k_a is varying while the water

permeability k_w is kept constant at 10^{-10} m/s. In addition, the radius $r = 0.5(r_w + r_e)$ is taken for the investigation. Figure 8.4(a) illustrates parallel curves of excess pore-air pressure due to different k_a/k_w values. It can be noted that, when k_a/k_w increases, the excess pore-air pressure is prone to dissipate faster. When k_a/k_w is very high, for instance $k_a/k_w \geq 10^3$, the excess pore-air pressure may dissipate instantaneously. This observation was also reported by Conte (2004). Figure 8.4(b) shows the typical excess pore-water pressure dissipation varying with k_a/k_w when time elapses. It can be observed that the dissipation at the early stages of consolidation proceeds more quickly as the result of increasing k_a/k_w. After the excess pore-air pressure completely diminishes, a plateau may occur in the excess pore-water pressure patterns when $k_a/k_w > 1$. It should be noted that the plateau gets longer as k_a/k_w increases. Afterwards, the curves of excess pore-water pressure dissipation converge to a single curve and complete dissipation occurs at approximately the same time (i.e. after $t = 10^8$ s).

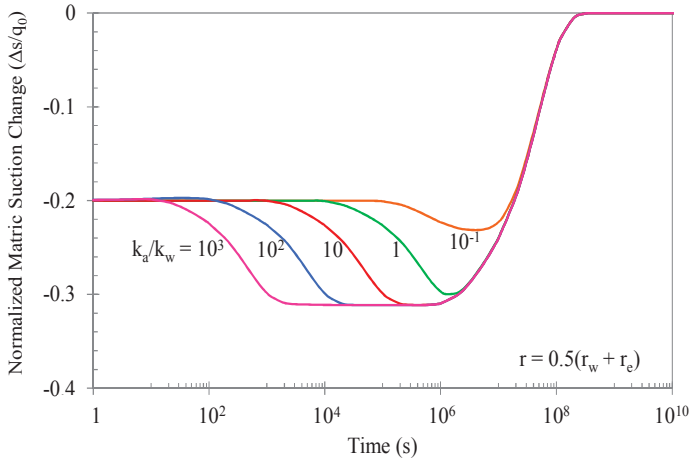

Figure 8.5. Matric suction change varying with different k_a/k_w values (for radial flow only)

Figure 8.5 shows the normalised matric suction change ($\Delta s/q_0$) varying with k_a/k_w values at $r = 0.5(r_w + r_e)$. Initially, the matric suction decreases and attains the lowest value due to the excess pore-air pressure dissipation. It can be observed that the decrease in the suction proceeds faster as the result of increasing k_a/k_w. After the plateau period, the suction gradually increases as the excess pore-water pressure

dissipates while the excess pore-air pressure diminished completely. As observed, there is no further change in the matric suction after $t = 10^8$ s.

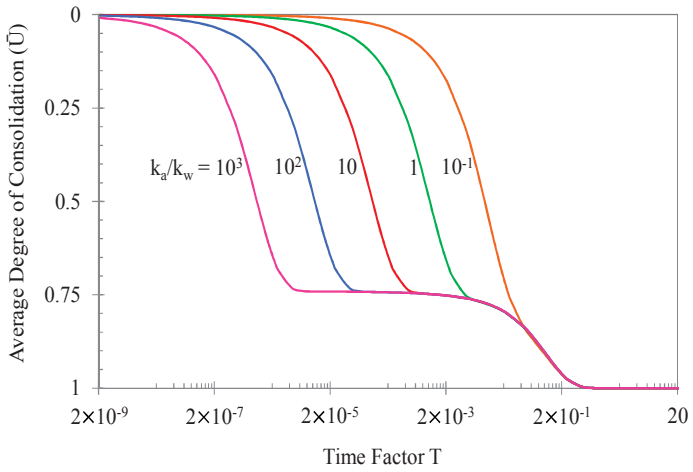

Figure 8.6. Average degree of consolidation varying with different k_a/k_w values (for radial flow only)

Based on Equation [G-5] in Appendix G, Figure 8.6 illustrates the variations of the average degree of consolidation ($\bar{U}$) against time factor T (i.e. $T = k_w t/(m_1^s \gamma_w H^2)$) with different k_a/k_w values. It is obvious that $\bar{U}$ patterns consist of double inverse S curves when $k_a/k_w \geq 0.1$, similar to the excess pore-water pressure dissipation process. The early stages of consolidation are governed by the simultaneous dissipation of both excess pore-air and pore-water pressures; and once the excess pore-air pressure is fully dissipated in the soil system, $\bar{U}$ patterns converge to only one curve and gradually approach 1 at the later stages. It is worth noting that the later stages of consolidation of unsaturated soils resembles to the classical consolidation introduced by Terzaghi (1943) since the process during this time is excess pore-air pressure-free. On the other hand, the soil stratum tends to settle more quickly at the beginning of the consolidation as k_a/k_w increases.

Figure 8.7 represents groups of excess pore pressure isochrones along the radius varying with T while $k_a/k_w = 0.1$ is adopted in this analysis. The results in this study generally demonstrate expected dissipation characteristics comparable to the given boundary condition (i.e. Equation [8-4]), in which excess pore pressures are zero at

$r = r_w$ and approach highest values at $r = r_e$. It is also noted that the dissipation rate of the excess pore-air pressure is faster than that of the excess pore-water pressure.

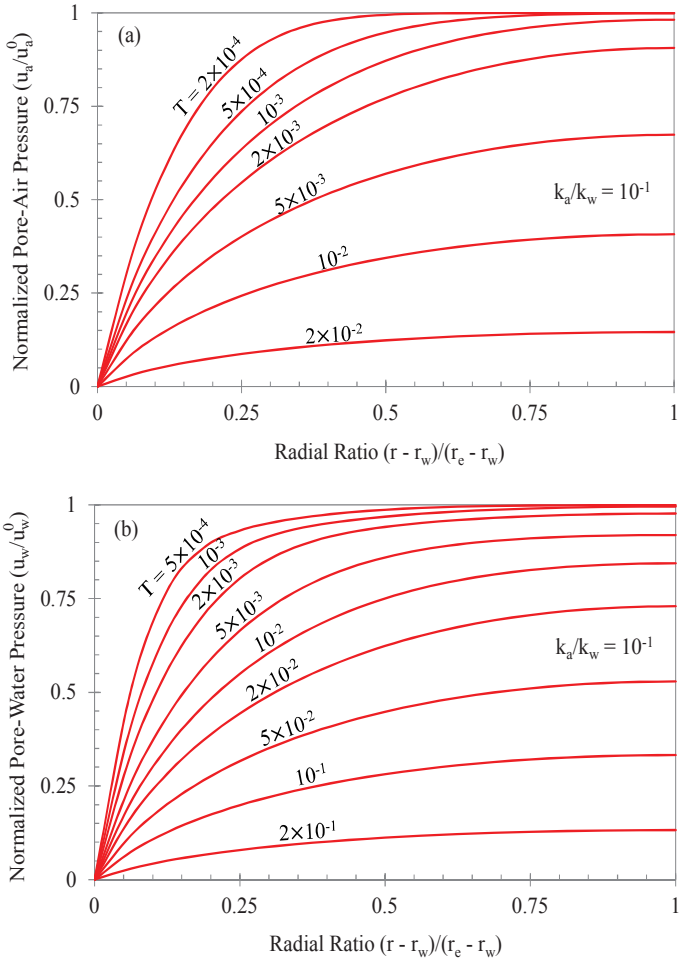

Figure 8.7. Distribution of (a) excess pore-air and (b) pore-water pressures along the radial domain (for radial flow only)

8.4.2. Example 2 – Axisymmetric consolidation with both radial and vertical flows

8.4.2.1. Uniform initial condition ($\zeta_a = \zeta_w = 0$)

The condition $\zeta_a = \zeta_w = 0$ indicates that, under the undrained compression, the initial excess pore pressures u_a^0 and u_w^0 are ubiquitously distributed throughout the soil depth. Variations of normalised pore pressures, u_a/u_a^0 and u_w/u_w^0, and degree of consolidation, $\bar{U}$, will be investigated in this section. Throughout the analysis, the point of investigation is located at $r = 0.5(r_w + r_e)$ and $z = 0.5H$.

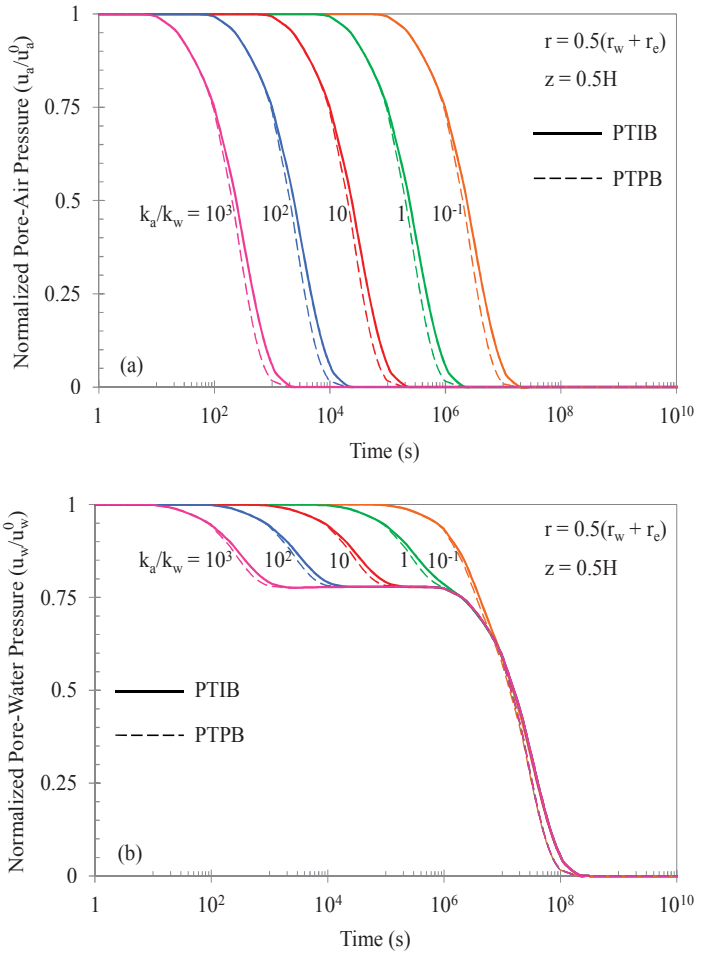

Figure 8.8. Dissipation of (a) excess pore-air and (b) pore-water pressures varying with different k_a/k_w values under the PTIB and PTPB boundary conditions (for radial and vertical flows, uniform initial condition)

Considering Equations [G-9] and [G-10] in Appendix G, Figure 8.8 depicts the dissipation rate of excess pore pressures varying with k_a/k_w under the PTIB and PTPB boundaries, along with the radial drainage boundary. As expected, variations of k_a/k_w result in single inverse S curves for the excess pore-air pressure (Figure 8.8(a)) and typical double inverse S curves for the excess pore-water pressure (Figure 8.8(b)). It can be also observed that the excess pore pressure dissipations assisted by the PTIB boundaries of the soil have comparable rates with those in PTPB boundaries. This result indicates that the radial flow, induced by drain wells, controls the dissipation while the

effects of the vertical flow on the dissipation process are less significant. It should be noted that the dissipation rate under the PTIB boundary condition comparatively resembles to that presented in Figure 8.4. Besides, the Mandel-Cryer effect during the compression (Mandel 1953; Cryer 1963), which has been widely known as the phenomenon being characterized by the Poisson's ratio and leading to increases in the excess pore-water pressure prior to the dissipation, can be discarded in this analysis. Rigorous numerical studies conducted by Conte (2004) and Wong et al. (1998) elucidate that the mentioned effect plays a minor role in the consolidation of unsaturated soils. Moreover, Fredlund et al. (2012) also confirms that the consideration of Mandel-Cryer effect in the computation may be unnecessary since the uncoupled theory of consolidation provides a decent approximation to the fully coupled approach.

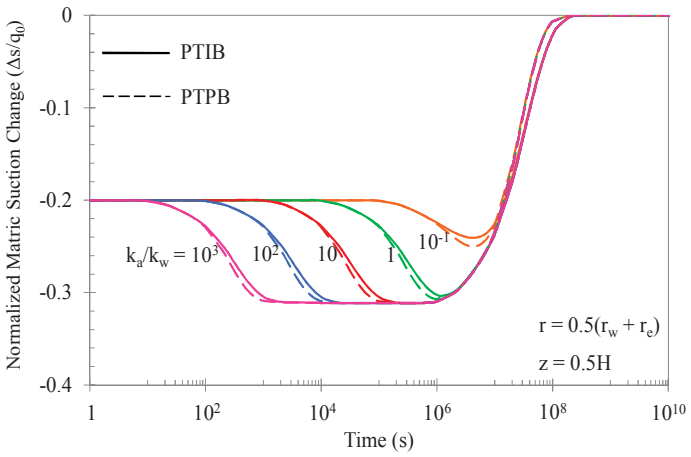

Figure 8.9. Matric suction change varying with different k_a/k_w values under the the PTIB and PTPB boundary conditions (for radial and vertical flows, uniform initial condition)

On the other hand, Figure 8.9 shows the normalised matric suction change ($\Delta s/q_0$) varying with time while adopting the PTIB and PTPB boundary conditions. As observed, although the matric suction in the PTPB boundary system tends to initially decrease and then increase slightly faster than that in the PTIB boundary system, the matric suctions in both boundary conditions eventually become constant at about the same time (i.e. after $t = 10^8$ s). It is worth noting that, while the total stresses remain unchanged due to the constant external loading, the consolidation process may be

attributed initially to the increase in the net stress ($\overline{\sigma}$), and subsequently to the increase in the matric suction (s) during the later stages of consolidation.

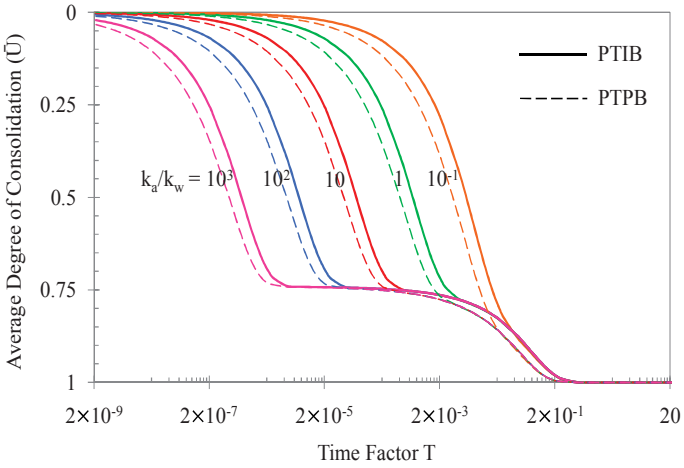

Figure 8.10. Average degree of consolidation varying with different k_a/k_w values under the the PTIB and PTPB boundary conditions (for radial and vertical flows, uniform initial condition)

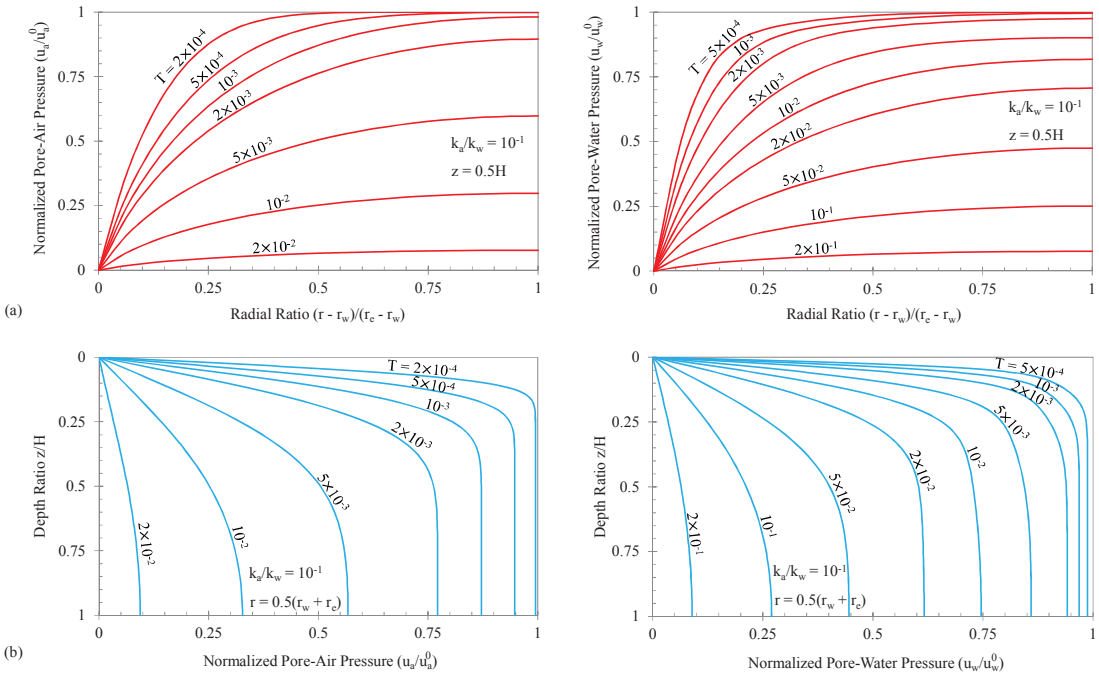

Figure 8.11. Distribution of excess pore-air and pore-water pressures along (a) radial and (b) vertical domains under the PTIB boundary condition (for radial and vertical flows, uniform initial condition)

Figure 8.10 presents changes in the average degree of consolidation ($\overline{U}$) against time factor T (i.e. $T = k_w t/(m_1^s \gamma_w H^2)$) under the PTIB and PTPB boundary conditions, as referred to Equation [G-12] in Appendix G. Similar to Figure 8.6, the results of $\overline{U}$ show the expected double inverse S curves, when $k_a/k_w \geq 0.1$. It can be observed that, although there are clear differences in $\overline{U}$ for the PTIB and PTPB boundary systems at the early stages, the consolidation process ends almost at the same time (i.e. after $T = 0.2$ or after $t = 10^8$ s).

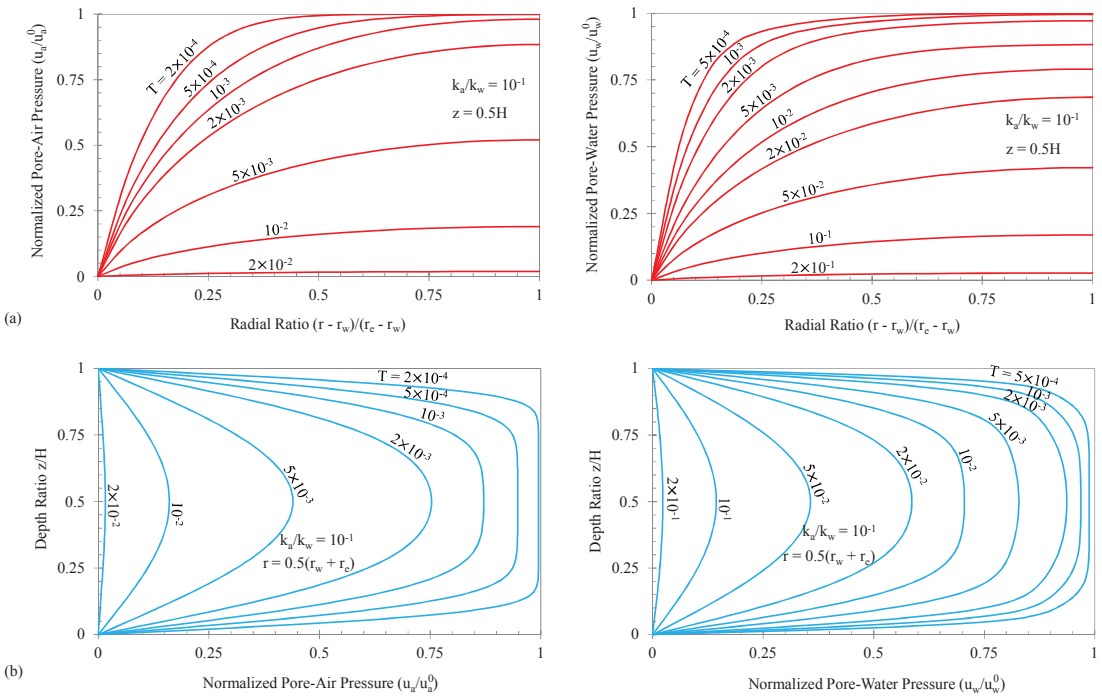

Figure 8.12. Distribution of excess pore-air and pore-water pressures along (a) radial and (b) vertical domains under the PTPB boundary condition (for radial and vertical flows, uniform initial condition)

Figures 8.11 and 8.12 represent groups of excess pore pressure isochrones varying with T (along the r- and z-directions) under the PTIB and PTPB boundary systems, respectively. The ratio $k_a/k_w = 0.1$ is taken for this investigation. As observed, the isochrones in Figures 8.11(a) and 8.12(a) satisfy the radial boundary condition given in Equation [8-4], and also those in Figures 8.11(b) and 8.12(b) satisfy the vertical boundary condition, as provided in Equations [8-5a] and [8-5b], respectively. It can be found that the excess pore pressures in the PTPB boundary system dissipate just slightly

faster than those in the PTIB boundary system. This suggests that the effects of the vertical flow may be less significant as the soil thickness increases.

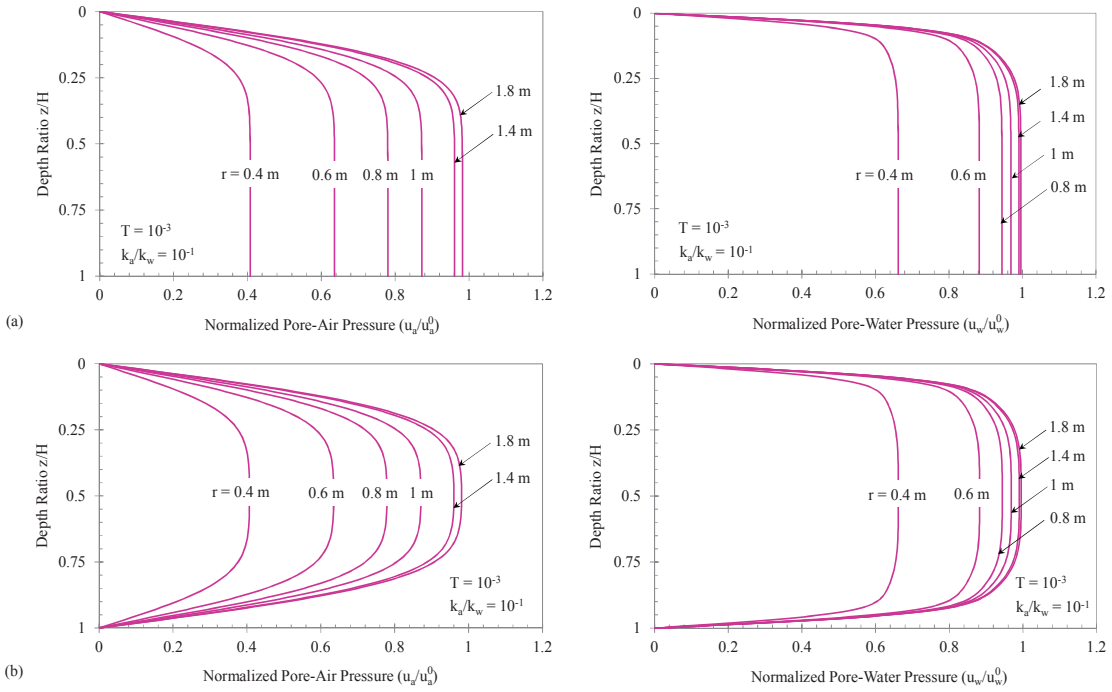

Figure 8.13. Distribution of excess pore pressures along the vertical domain at T = 10^{-3} at different radii under (a) PTIB and (b) PTPB boundary conditions (for radial and vertical flows, uniform initial condition)

Figure 8.13 depicts excess pore pressure isochrones at a particular time $T = 10^{-3}$ at various radii while adopting $k_a/k_w = 0.1$. It can be observed that the excess pore-air and pore-water pressures tend to increase when the point of interest is farther away from the drain well. In contrast, the excess pore pressures reduce as the radius decreases. This is due to the fact that a considerable portion of pressures preferably dissipate through the permeable boundary. When the radius considerably increases (i.e. $r \geq 1$ m), the effects of radial distance on the pore pressure isochrones will be less pronounced.

8.4.2.2. Linear initial condition ($\zeta_a, \zeta_w > 0$)

This section highlights the effects of the proposed parameters ζ_a and ζ_w on the axisymmetric consolidation, as presented in Equations [8-6a] and [8-6b], respectively. Since $\zeta_a, \zeta_w > 0$, the initial excess pore pressures are linearly distributed along the soil

depth. In this study, the normalised pore-air (u_a/u_a^0) and pore-water (u_w/u_w^0) pressures are presented and discussed. Additionally, the point at $r = 0.5(r_w + r_e)$ and $z = 0.5H$ is selected for further analysis.

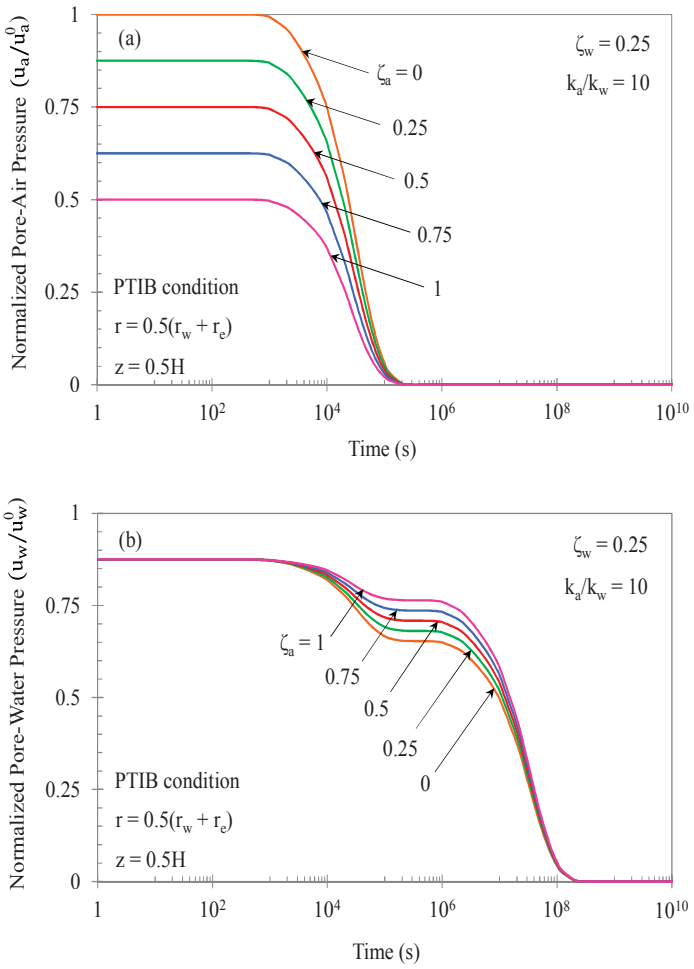

Figure 8.14. Dissipation of (a) excess pore-air and (b) pore-water pressures varying with ζ_a (while ζ_w is constant) under the PTIB boundary condition (for radial and vertical flows, linear initial condition)

Based on Equation [G-17] in Appendix G, Figure 8.14 shows the effects of ζ_a on the excess pore pressure dissipation rates when $k_a/k_w = 10$ and PTIB boundary condition are adopted. In this analysis, the parameter ζ_a varies from 0 to 1 while ζ_w remains constant equal to 0.25. As demonstrated in Figure 8.14(a), the increasing ζ_a values lead to a reduction in the average initial excess pore-air pressure at the beginning of consolidation. The excess pore-air pressures (with different ζ_a values) begin to dissipate significantly at about $t = 10^3$ s and are then fully dissipated at almost the same time

(i.e. after $t = 10^5$ s). In Figure 8.14(b), it is observed that the increasing ζ_a values result in a slower rate of the excess pore-water pressure dissipation during the plateau period. However, at the later stages of consolidation, excess pore-water pressures (with different ζ_a values) fully dissipate with approximately the same rate.

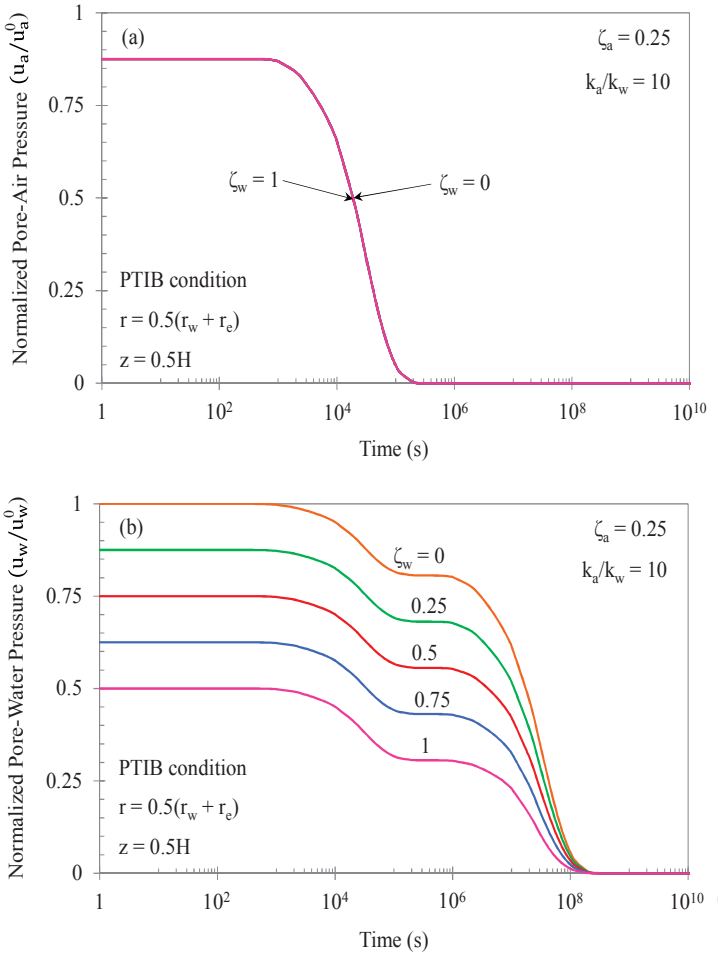

Figure 8.15. Dissipation of (a) excess pore-air and (b) pore-water pressures varying with ζ_w (while ζ_a is constant) under the PTIB boundary condition (for radial and vertical flows, linear initial condition)

Figure 8.15, on the other hand, investigates the influence of ζ_w on the dissipation rates while considering $k_a/k_w = 10$ and PTIB boundary condition. The parameter ζ_w is varying from 0 to 1 whereas ζ_a is kept constant equal to 0.25 in this case. As observed, there is no variation in the excess pore-air pressure dissipation despite different ζ_w values (Figure 8.15(a)). When ζ_w increases, the average initial excess pore-water

pressure decreases at the beginning of consolidation (Figure 8.15(b)). Nevertheless, at the later stages of consolidation, all excess pore-water pressures (with different ζ_w values) diminish at almost the same time (i.e. after $t = 10^8$ s).

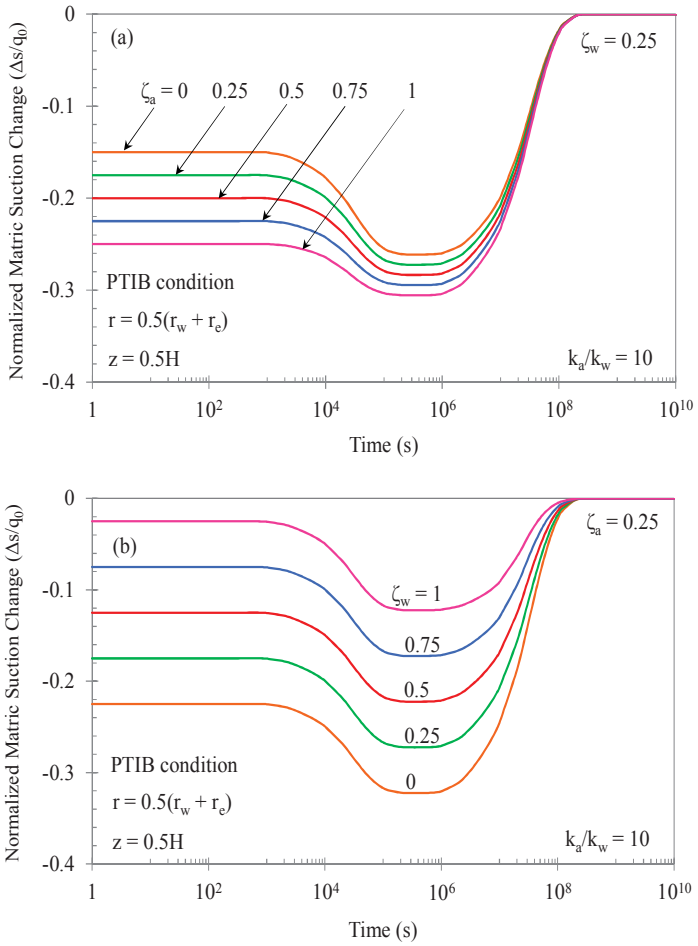

Figure 8.16. Matric suction change due to variations of (a) ζ_a and (b) ζ_w under the PTIB boundary condition (for radial and vertical flows, linear initial condition)

Figure 8.16 demonstrates changes in the matric suction due to variations of ζ_a and ζ_w when adopting $k_a/k_w = 10$ and PTIB boundary condition. As shown in Figure 8.16(a), increasing ζ_a leads to smaller suction at the beginning of consolidation since the average initial excess pore-air pressure reduces while the initial pore-water pressure remains unchanged. This observation is contrary to the effects of ζ_w, in which the increasing ζ_w leads to higher suction at the beginning of consolidation due to a considerable reduction in the average initial excess pore-water pressure, as presented in Figure 8.16(b). At the

later stages, in both cases, matric suctions will increase gradually and approach a constant value at approximately the same time (i.e. after $t = 10^8$ s).

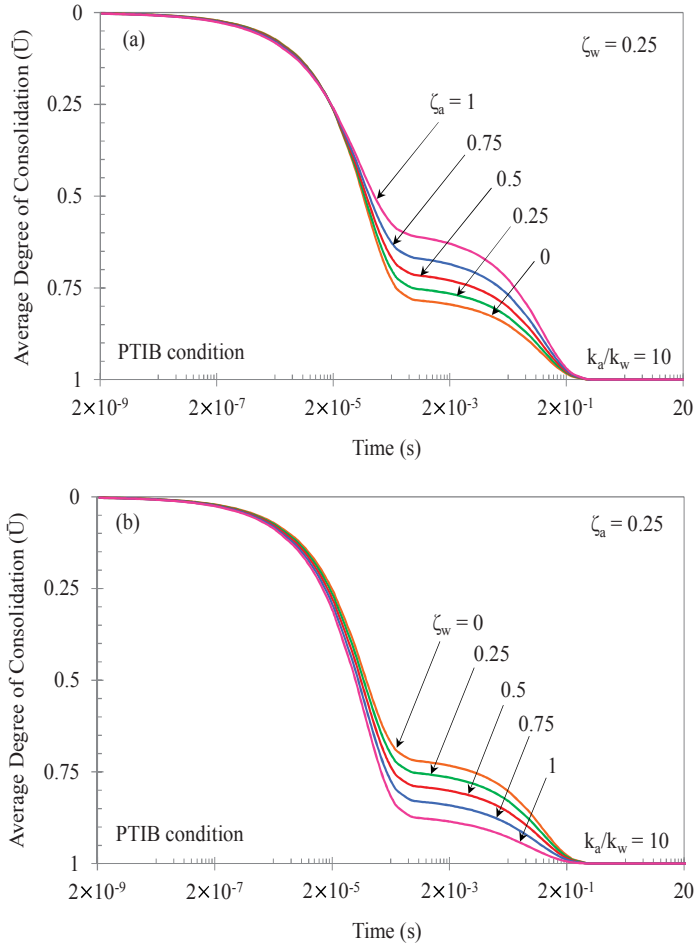

Figure 8.17. Average degree of consolidation due to variations of (a) ζ_a and (b) ζ_w under the PTIB boundary condition (for radial and vertical flows, linear initial condition)

Figure 8.17, referred to Equation [G-20] in Appendix G, illustrates the changes in the average degree of consolidation ($\bar{U}$) against time factor T (i.e. $T = k_w t/(m_1^s \gamma_w H^2)$) due to the effects of ζ_a and ζ_w, while $k_a/k_w = 10$ and PTIB condition are considered. As observed, $\bar{U}$ patterns initially increase with almost similar rates and then begin to vary during the later stages of consolidation, at which the increasing ζ_a decelerates the consolidation (Figure 8.17(a)) whereas the increasing ζ_w accelerates the consolidation process (Figure 8.17(b)). This is due to the fact that $\bar{U}$ curves are dependent on the dissipation rate of excess pore-water pressure, particularly a faster rate of excess pore-

water pressure dissipation leads to faster consolidation rate and vice versa. It can be observed that consolidation completes almost at the same time regardless of values of ζ_a and ζ_w (i.e. after $t = 10^8$ s).

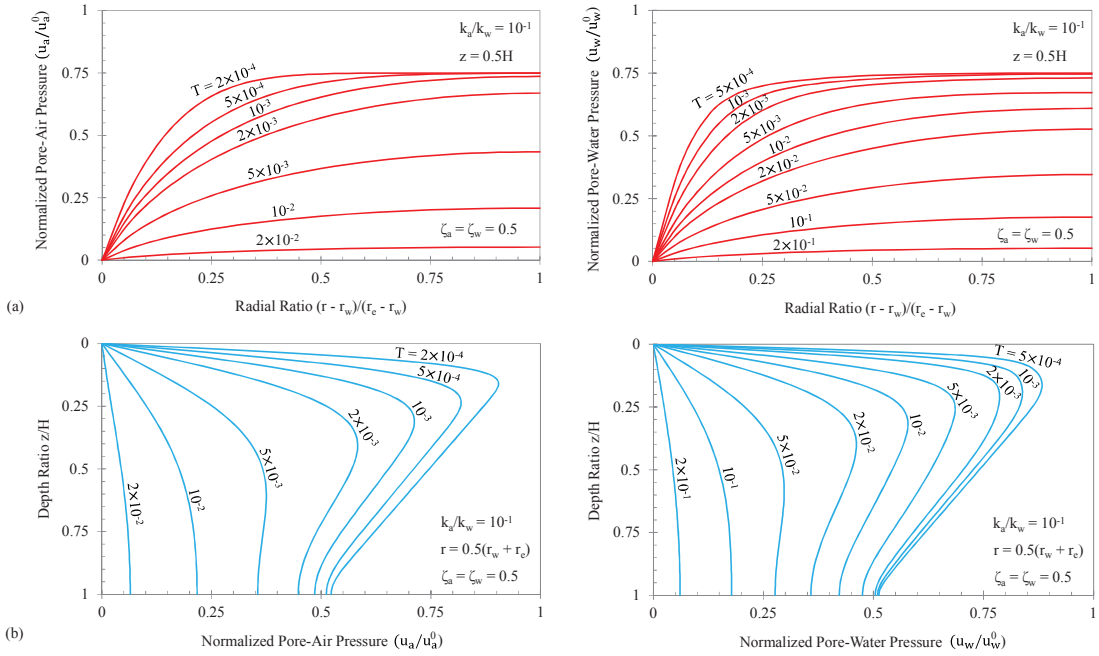

Figure 8.18. Distribution of excess pore pressures along (a) radial and (b) vertical domains under PTIB boundary condition while adopting $\zeta_a = \zeta_w = 0.5$ (for radial and vertical flows, linear initial condition)

Figures 8.18 and 8.19 demonstrate the excess pore pressure isochrones varying with T (along r- and z-directions) considering the PTIB and PTPB boundary systems, respectively, while adopting $\zeta_a = \zeta_w = 0.5$ and the ratio $k_a/k_w = 0.1$. The pressure isochrones in Figures 8.18(a) and 8.19(a) satisfy the radial boundary condition presented in Equations [8-4]. Under an undrained compression, linearly distributed initial excess pore pressures generated by the applied constant load (q_0) are clearly captured in Figures 8.18(b) and 8.19(b). It is observed that the excess pore pressures under the PTIB boundary conditions undergo the pressure redistribution process, in which some pressures dissipate through the permeable top surface while the rest is transferred toward the base of the soil (i.e. at $z = H$). This phenomenon results in notable increases in both excess pore-air and pore-water pressures with time towards the bottom of the soil deposit (Figure 8.18(b)). Considering the PTPB boundary condition,

the redistribution of excess pore pressures also occurs to achieve the pressure equilibrium. Evidently, the maximum values of excess pore pressures at a particular time no longer occur consistently at the mid-depth but move toward the base of the soil due to the pressure redistribution (Figure 8.19(b)).

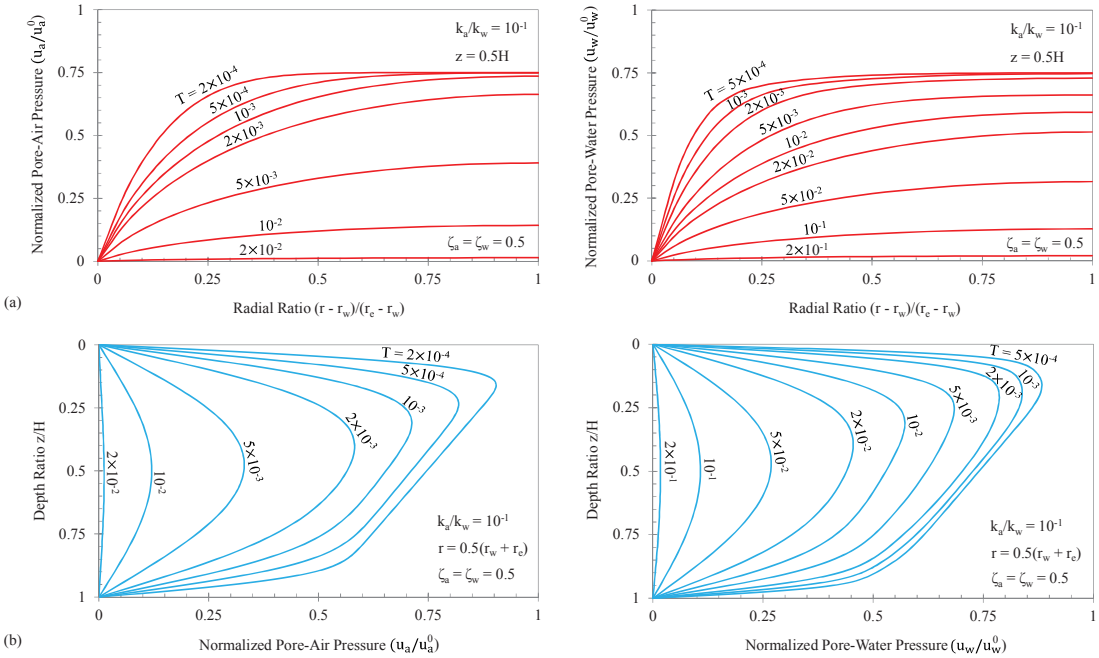

Figure 8.19. Distribution of excess pore pressures along (a) radial and (b) vertical domains under the PTPB boundary condition while adopting $\zeta_a = \zeta_w = 0.5$ (for radial and vertical flows, linear initial condition)

Figure 8.20 shows excess pore pressure isochrones at $T = 10^{-3}$ at various radii while adopting $\zeta_a = \zeta_w = 0.5$ and $k_a/k_w = 0.1$. Similar to the result presented in Figure 8.13, the excess pore-air and pore-water pressures increase when the point is farther away from the drain well. The effects of radial distance on the pressure isochrones become less significant when the radius considerably increases (i.e. $r \geq 1$ m).

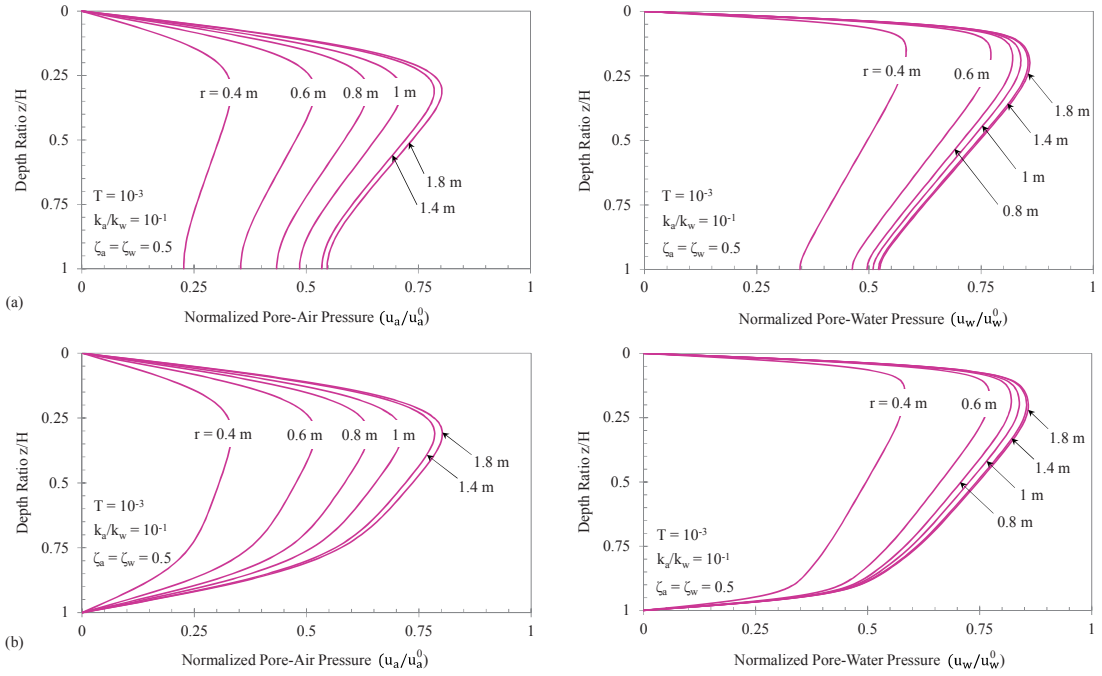

Figure 8.20. Distribution of excess pore pressures along the vertical domain at T = 10^{-3} at different radii under (a) PTIB and (b) PTPB boundary conditions while adopting $\zeta_a = \zeta_w = 0.5$ (for radial and vertical flows, linear initial condition)

8.5. Summary

This chapter has provided an analytical solution to predict the axisymmetric consolidation of unsaturated soils using variables separation and Laplace transformation techniques. The mathematical method captures the uniformly and linearly distributed excess pore pressures as initial conditions. The 3D Cartesian governing equations were first transformed into the polar equations. Subsequently, final solutions predicting excess pore pressure dissipation rates were obtained using Fourier Bessel and sine series, and Laplace transforms.

In this study, two examples have been presented to illustrate the capabilities of the proposed analytical approach. The axisymmetric consolidation with only radial flow has been presented in Example 1, whereas the case considering both radial and vertical flows has been investigated in Example 2. Overall, both examples show the significant effects of the air to water permeability ratio (k_a/k_w) on the dissipation process, in which changes in the ratio result in a single inverse S curves for the excess pore-air

pressure, and double inverse S curves for the excess pore-water pressures and degree of consolidation. Besides, the excess pore pressures tend to dissipate faster for the points closer to the drain well. In Example 2, considering the uniform distribution of initial excess pore pressures, it can be concluded that the radial flow governs the axisymmetric consolidation while effects of vertical flow are less notable. It should also be noted that the compression process is ascribed to the increase in matric suction at the later stages of consolidation. On the other hand, the linear distribution of initial excess pore pressures with depth has considerable impacts on the dissipation process. In particular, the rapid reduction in both initial excess pore pressures with depth would lead to reduced average excess pore-air and pore-water pressures at the beginning of consolidation. Furthermore, the effects of initial pore pressures cause the pressure redistribution phenomenon in which, under the applied loads, some excess pore pressures are transferred toward the base of the soil, resulting in notable increases in the excess pore pressures.

CHAPTER 9

AXISYMMETRIC CONSOLIDATION IN UNSATURATED SOIL DEPOSIT SUBJECTED TO TIME-DEPENDENT LOADINGS

9.1. Introduction

This chapter provides an analytical solution to axisymmetric consolidation while capturing the radial and vertical flows of air and water phases. Polar governing flow equations are derived and coupled with simulated time-dependent applied loads, namely ramping, asymptotic, sinusoid and damped sine wave. Uniformly distributed initial excess pore-air and pore-water pressures are adopted in the analytical procedure. Standard approaches such as the separation of variables and Laplace transformation are used to obtain the final solutions. The permeability ratio and loading parameters against the dissipation of excess pore pressures and consolidation settlement are demonstrated graphically. In those cases of ramped and asymptotic loadings, the matric suction and net stress varying with time are discussed in the worked examples.

9.2. Polar governing equations of flow

For simplification the existing literature (Fredlund & Hasan 1979; Dakshanamurthy & Fredlund 1980; Darkshanamurthy et al. 1984) assumed that the flows of air and water phases are independent and continuous during consolidation. The flows are empirically derived to form a set of 3D Cartesian equations that describe the air and water flux per unit volume in a soil element as shown below:

$$\frac{\partial\left(\frac{\Delta V_a}{V_0}\right)}{\partial t} = \frac{R\Theta}{gM\left(u_a^0+u_{atm}\right)}\left[k_{a_x}\left(\frac{\partial^2 u_a}{\partial x^2}\right) + k_{a_y}\left(\frac{\partial^2 u_a}{\partial y^2}\right) + k_{a_z}\left(\frac{\partial^2 u_a}{\partial z^2}\right)\right] - \frac{n(1-S_r)}{\left(u_a^0+u_{atm}\right)}\left(\frac{\partial u_a}{\partial t}\right) \quad [9\text{-}1a]$$

$$\frac{\partial\left(\frac{\Delta V_w}{V_0}\right)}{\partial t} = \frac{1}{\gamma_w}\left[k_{w_x}\left(\frac{\partial^2 u_w}{\partial x^2}\right) + k_{w_y}\left(\frac{\partial^2 u_w}{\partial y^2}\right) + k_{w_z}\left(\frac{\partial^2 u_w}{\partial z^2}\right)\right] \quad [9\text{-}1b]$$

where k_{a_x}, k_{a_y} and k_{a_z} are the coefficients of air permeability in the x-, y- and z-domain (m/s), respectively; k_{w_x}, k_{w_y} and k_{w_z} are the coefficients of water permeability in the x-, y- and z-domain (m/s), respectively; u_a and u_w are excess pore-air and pore-water pressures, respectively; u_a^0 is the initial pore-air pressure (kPa); u_{atm} is the atmospheric pressure (kPa); R is the universal air constant $(J/mol.K)$; $\Theta = (\theta^\circ + 273)$, is the absolute temperature (K); θ° is the temperature (℃); M is the molecular mass of air phase (kg/mol); n is the porosity during consolidation process; S_r is the degree of saturation during consolidation process; g is the gravitational constant $(9.81\ m/s^2)$; and γ_w is the water unit weight $(9.81\ kN/m^3)$. Cartesian coordinates (x, y, z) presented in Equation [9-1] can be expressed in polar coordinates as follows:

$$x = r\cos\theta \qquad [9\text{-}2a]$$

$$y = r\sin\theta \qquad [9\text{-}2b]$$

$$z = z \qquad [9\text{-}2c]$$

hence,

$$r = (x^2 + y^2)^{1/2} \qquad [9\text{-}3a]$$

$$\theta = \tan^{-1}\left(\frac{y}{x}\right) \qquad [9\text{-}3b]$$

Assuming $k_{a_x} = k_{a_y} = k_{a_r}$ and $k_{w_x} = k_{w_y} = k_{w_r}$, the polar transformation can be conducted by combining Equations [9-1], [9-2] and [9-3], thus,

$$\frac{\partial\left(\frac{\Delta V_a}{V_0}\right)}{\partial t} = \frac{R\Theta}{gM(u_a^0+u_{atm})}\left[k_{a_r}\left(\frac{\partial^2 u_a}{\partial r^2} + \frac{1}{r}\frac{\partial u_a}{\partial r}\right) + k_{a_z}\left(\frac{\partial^2 u_a}{\partial z^2}\right)\right] - \frac{n(1-S_r)}{(u_a^0+u_{atm})}\left(\frac{\partial u_a}{\partial t}\right) \qquad [9\text{-}4a]$$

$$\frac{\partial\left(\frac{\Delta V_w}{V_0}\right)}{\partial t} = \frac{1}{\gamma_w}\left[k_{w_r}\left(\frac{\partial^2 u_w}{\partial r^2} + \frac{1}{r}\frac{\partial u_w}{\partial r}\right) + k_{w_z}\left(\frac{\partial^2 u_w}{\partial z^2}\right)\right] \qquad [9\text{-}4b]$$

where k_{a_r} and k_{w_r} are the coefficients of air and water permeability in the r-domain (m/s), respectively. Note that the pore pressures within a soil element are independent of θ under the axially symmetric case. The constitutive relationship between soil deformation and stress state variables under the 3D loading condition can be adopted as:

$$\frac{\partial\left(\frac{\Delta V_a}{V_0}\right)}{\partial t} = m_1^a\frac{\partial}{\partial t}\left(\frac{\sigma_r+\sigma_\theta+\sigma_z}{3}\right) + (m_2^a - m_1^a)\frac{\partial u_a}{\partial t} - m_2^a\frac{\partial u_w}{\partial t} \qquad [9\text{-}5a]$$

$$\frac{\partial\left(\frac{\Delta V_w}{V_0}\right)}{\partial t} = m_1^w \frac{\partial}{\partial t}\left(\frac{\sigma_r+\sigma_\theta+\sigma_z}{3}\right) + (m_2^w - m_1^w)\frac{\partial u_a}{\partial t} - m_2^w \frac{\partial u_w}{\partial t} \quad [9\text{-}5b]$$

where m_1^a and m_1^w are the coefficients of volume change of air and water with respect to the change of net stress (1/kPa), respectively; m_2^a and m_2^w are the coefficients of volume change of air and water with respect to the change of suction (1/kPa), respectively; σ_r, σ_θ and σ_z are the total stresses in the r-, θ- and z-domains (kPa), respectively. By equating Equations [9-4a] and [9-4b] to Equations [9-5a] and [9-5b], respectively, the results would provide the governing flow equations including time-dependent loadings as follows:

$$u_{a,t} + C_a u_{w,t} + c_{v_r}^a\left(u_{a,rr} + \frac{1}{r}u_{a,r}\right) + c_{v_z}^a u_{a,zz} - c_\sigma^a\left(\sigma_{r,t} + \sigma_{\theta,t} + \sigma_{z,t}\right) = 0 \quad [9\text{-}6a]$$

$$u_{w,t} + C_w u_{a,t} + c_{v_r}^w\left(u_{w,rr} + \frac{1}{r}u_{w,r}\right) + c_{v_z}^w u_{w,zz} - c_\sigma^w\left(\sigma_{r,t} + \sigma_{\theta,t} + \sigma_{z,t}\right) = 0 \quad [9\text{-}6b]$$

where $u_{a,t}$ and $u_{w,t}$ are the first order partial differential equations (PDEs) of excess pore-air and pore-water pressures with respect to time, respectively; $u_{a,r}$ and $u_{w,r}$ are the first order PDEs of excess pore-air and pore-water pressures with respect to the r-domain, respectively; $u_{a,rr}$ and $u_{w,rr}$ are the second order PDEs of excess pore-air and pore-water pressures with respect to the r-domain, respectively; $u_{a,zz}$ and $u_{w,zz}$ are the second order PDEs of excess pore-air and pore-water pressures with respect to the z-domain, respectively; and $\sigma_{r,t}$, $\sigma_{\theta,t}$ and $\sigma_{z,t}$ are the first order PDEs with respect to time of loadings in the r-, θ- and z-domains, respectively. In addition,

$$C_a = \frac{1}{\left[\left(\frac{m_1^a}{m_2^a}-1\right) - \frac{n(1-S_r)}{m_2^a(u_a^0+u_{atm})}\right]} \quad [9\text{-}7a]$$

$$c_{v_r}^a = \frac{k_{a_r}R\Theta}{gM}\frac{1}{\left[m_2^a(u_a^0+u_{atm})\left(\frac{m_1^a}{m_2^a}-1\right) - n(1-S_r)\right]} \quad [9\text{-}7b]$$

$$c_{v_z}^a = \frac{k_{a_z}R\Theta}{gM}\frac{1}{\left[m_2^a(u_a^0+u_{atm})\left(\frac{m_1^a}{m_2^a}-1\right) - n(1-S_r)\right]} \quad [9\text{-}7c]$$

$$c_\sigma^a = \frac{1}{3\left[\left(1-\frac{m_2^a}{m_1^a}\right) - \frac{n(1-S_r)}{m_1^a(u_a^0+u_{atm})}\right]} \quad [9\text{-}7d]$$

$$C_w = \left(\frac{m_1^w}{m_2^w} - 1\right) \quad [9\text{-}7e]$$

$$c_{v_r}^w = \frac{1}{m_2^w}\left(\frac{k_{w_r}}{\gamma_w}\right) \quad [9\text{-}7f]$$

$$c_{v_z}^{w} = \frac{1}{m_2^w}\left(\frac{k_{w_z}}{\gamma_w}\right) \quad [9\text{-}7g]$$

$$c_{\sigma}^{w} = \frac{m_1^w}{3m_2^w} \quad [9\text{-}7h]$$

The detailed polar transformation of the governing flow equations is clearly presented by Ho et al. (2016). It should be noted that the solutions for u_a and u_w in Equation [9-6] would consist of functions of radial and vertical coordinates, and time.

9.3. Analytical solution

9.3.1. Boundary and initial conditions

A simplified elevation of the drain well system is depicted in Figure 9.1. The system consists of the radius r_e of the influence zone and finite depth H. A typical drain well, of which the radius is denoted as r_w, is installed at the middle of the influence zone. Under undrained conditions, an application of external loads would generate excess pore-air and pore-water pressures, but after a certain time these excess pore pressures would gradually dissipate towards the drain wells and permeable vertical boundaries. Figure 9.1(a) presents a pervious top – impervious base (PTIB) boundary condition,

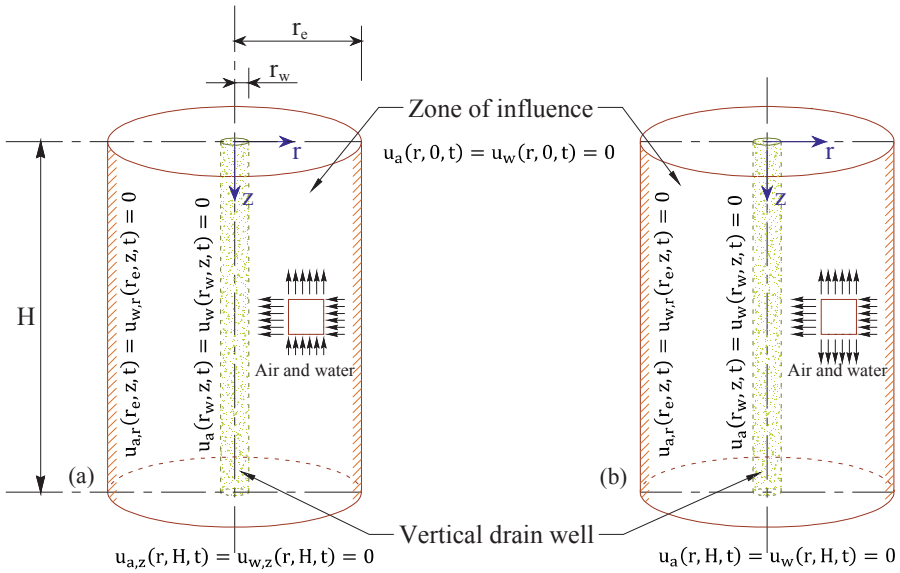

Figure 9.1. Simplified elevation of the vertical drain well system under (a) PTIB and (b) PTPB boundary conditions

indicating upward flows of air and water during the loading process. Figure 9.1(b) shows a pervious top – pervious base (PTPB) boundary condition that describes free drainage at both ends of the soil deposit.

Following Barron (1948), the surface of a sand drain cylinder is considered to be permeable to air and water whereas the boundary of the influence zone is assumed to be impermeable, so the radial boundary conditions when $r \in [r_w, r_e]$ are:

$$u_a(r_w, z, t) = u_w(r_w, z, t) = 0 \quad [9\text{-}8a]$$

$$u_{a,r}(r_e, z, t) = u_{w,r}(r_e, z, t) = 0 \quad [9\text{-}8b]$$

Drainage also takes place towards the permeable vertical boundaries, as shown below:

(a) The PTIB boundary condition when $z \in [0, H]$:

$$u_a(r, 0, t) = u_w(r, 0, t) = 0 \quad [9\text{-}9a]$$

$$u_{a,z}(r, H, t) = u_{w,z}(r, H, t) = 0 \quad [9\text{-}9b]$$

(b) The PTPB boundary condition when $z \in [0, H]$:

$$u_a(r, 0, t) = u_w(r, 0, t) = 0 \quad [9\text{-}10a]$$

$$u_a(r, H, t) = u_w(r, H, t) = 0 \quad [9\text{-}10b]$$

The initial conditions at $r \in (r_w, r_e)$ and $z \in (0, H)$ are:

$$u_a(r, z, 0) = u_a^0 \quad [9\text{-}11a]$$

$$u_w(r, z, 0) = u_w^0 \quad [9\text{-}11b]$$

As soon as loads are applied onto the ground surface, it is assumed that initial excess pore pressures u_a^0 and u_w^0, are distributed ubiquitously into the soil, except for the permeable boundaries.

9.3.2. Excess pore-air and pore-water pressures

Before presenting the analytical procedure, it is worth mentioning the conventional assumptions from existing literature (Fredlund & Hasan 1979; Dakshanamurthy &

Fredlund 1980; Darkshanamurthy et al. 1984; Fredlund et al. 2012) and some additional assumptions that satisfy the polar governing flow equations for unsaturated soils adopted in this study:

(1) The soil stratum is homogeneous;
(2) The flows of air and water are continuous and independent;
(3) Solid grain and pore-water are incompressible;
(4) Air diffusion is neglected;
(5) Isothermal condition is considered;
(6) Well resistance and smear effects are ignored;
(7) The loaded area is very large and the external load is uniform, thus the soil stratum only deforms along the z-direction;
(8) The consolidation coefficients for air (C_a, $c_{v_r}^a$, $c_{v_z}^a$ and c_σ^a) and water (C_w, $c_{v_r}^w$, $c_{v_z}^w$ and c_σ^w) are assumed to be constant during the loading process.

The above assumptions, especially Assumption (8), may not be strictly accurate for some applications. In particular, the consolidation coefficients with respect to air and water phases may vary during the loading process due to variable soil properties such as permeability coefficients, porosity, degree of saturation, and volume change coefficients to name but a few. To successfully obtain the analytical solution, these properties must be kept constant throughout consolidation, although the soil properties for each stress increment can be revised and updated under the transient process.

The following general solutions are adopted for the PDEs presented in Equation [9-6]:

$$u_a(r,z,t) = \sum_{i=0}^{\infty}\sum_{j=0}^{\infty} R_a(r)\, Z_a(z)\, T_a(t) \qquad [9\text{-}12a]$$

$$u_w(r,z,t) = \sum_{i=0}^{\infty}\sum_{j=0}^{\infty} R_w(r)\, Z_w(z)\, T_w(t) \qquad [9\text{-}12b]$$

where $R_a(r) = R_w(r) = R(r)$, are the eigenfunction of radial domain;
$Z_a(z) = Z_w(z) = Z(z)$, are the eigenfunction of vertical domain; and
$T_a(t)$ and $T_w(t)$ are the generalized Fourier coefficients with respect to air and water phases, respectively.

Note that $R_a(r) = R_w(r) = R(r)$ and $Z_a(z) = Z_w(z) = Z(z)$ due to similar boundary drainage conditions. Employing the Fourier sine series as a solution of the eigenfunction $Z(z)$, Equations [9-12a] and [9-12b] become:

$$u_a(r,z,t) = \sum_{i=0}^{\infty}\sum_{j=0}^{\infty} R(r)\, T_a(t) \sin\left(\frac{z\sqrt{\mu^j}}{H}\right) \qquad [9\text{-}13a]$$

$$u_w(r,z,t) = \sum_{i=0}^{\infty}\sum_{j=0}^{\infty} R(r)\, T_w(t) \sin\left(\frac{z\sqrt{\mu^j}}{H}\right) \qquad [9\text{-}13b]$$

where $\sqrt{\mu^j} = (2j+1)\pi/2$ for the PTIB boundary condition; or
$= j\pi$ for the PTPB boundary condition ($j = 0, 1, 2, ...$). [9-14]

Under an axisymmetric condition the entire drain well system can be treated as a unit mass of the soil, hence $\partial\sigma_r/\partial t = \partial\sigma_\theta/\partial t$ can be adopted, while combining Equations [9-6], [9-13] and [9-14] and then separating the variables by introducing constants λ_a^{ij} and λ_w^{ij} ($i = 0, 1, 2, ...$; $j = 0, 1, 2, ...$) would yield:

$$k_{a_r}\left[\frac{R_{,rr}(r)}{R(r)} + \frac{1}{r}\frac{R_{,r}(r)}{R(r)}\right] + k_{a_z}\left(\frac{\sqrt{\mu^j}}{H}\right)^2 = -\frac{1}{c_v^a}\left[\frac{T_{a,t}(t)}{T_a(t)} + C_a\frac{T_{w,t}(t)}{T_a(t)} - a^i\,\frac{2\,b^j}{\sqrt{\mu^j}}\,c_\sigma^a(1 + 2K)\frac{\sigma_{z,t}(t)}{T_a(t)}\right] = -\lambda_a^{ij} \qquad [9\text{-}15a]$$

$$k_{w_r}\left[\frac{R_{,rr}(r)}{R(r)} + \frac{1}{r}\frac{R_{,r}(r)}{R(r)}\right] + k_{w_z}\left(\frac{\sqrt{\mu^j}}{H}\right)^2 = -\frac{1}{c_v^w}\left[\frac{T_{w,t}(t)}{T_w(t)} + C_w\frac{T_{a,t}(t)}{T_w(t)} - a^i\,\frac{2\,b^j}{\sqrt{\mu^j}}\,c_\sigma^w(1 + 2K)\frac{\sigma_{z,t}(t)}{T_w(t)}\right] = -\lambda_w^{ij} \qquad [9\text{-}15b]$$

where $c_v^a = \frac{R\Theta}{gM}\frac{1}{\left[m_2^a(u_a^0+u_{atm})\left(\frac{m_1^a}{m_2^a}-1\right)-n(1-S_r)\right]}$; $c_v^w = \frac{1}{m_2^w}\left(\frac{1}{\gamma_w}\right)$;

$K = \frac{\partial\sigma_r}{\partial\sigma_z} = \frac{\partial\sigma_\theta}{\partial\sigma_z}$; $a^i = \frac{\int_{r_w}^{r_e} R(r)\,r\,dr}{\int_{r_w}^{r_e}[R(r)]^2\,r\,dr}$; and

$b^j = 1$ for the PTIB boundary condition; or
$= 1-(-1)^j$ for the PTPB boundary condition. [9-16]

The parameter K in Equation [9-15] depends on the loaded area and dimensions of the footing built on top of deposits of unsaturated soil, referred to the elastic theory by Jumikis (1969). It should be noted that for free strain consolidation, when the loaded area is very large and the applied load is uniform, K can be considered as being constant

during the loading stage. For non-uniform loads, K may vary as the soil deforms laterally. It can be noted that only large and uniformly distributed loads are considered in this study.

After separating the variables, two sets of ordinary differential equations (ODEs) are obtained as follows:

$$\begin{cases} R^{i}_{,rr}(r) + R^{i}_{,r}(r) + \left(\frac{\sqrt{\xi^{i}}}{r_w}\right)^2 R^{i}(r) = 0 \\ T^{ij}_{a,t}(t) + C_a\, T^{ij}_{w,t}(t) - c^{a}_{v}\left(\lambda^{ij}_{a}\right) T^{ij}_{a}(t) - a^{i}\, \frac{2\, b^{j}}{\sqrt{\mu^{j}}}\, c^{a}_{\sigma}(1+2K)\sigma_{z,t}(t) = 0 \end{cases} \quad [9\text{-}17a]$$

$$\begin{cases} R^{i}_{,rr}(r) + R^{i}_{,r}(r) + \left(\frac{\sqrt{\xi^{i}}}{r_w}\right)^2 R^{i}(r) = 0 \\ T^{ij}_{w,t}(t) + C_w\, T^{ij}_{a,t}(t) - c^{w}_{v}\left(\lambda^{ij}_{w}\right) T^{ij}_{w}(t) - a^{i}\, \frac{2\, b^{j}}{\sqrt{\mu^{j}}}\, c^{w}_{\sigma}(1+2K)\sigma_{z,t}(t) = 0 \end{cases} \quad [9\text{-}17b]$$

In relation to Equation [9-17], the separation constants λ^{ij}_{a} and λ^{ij}_{w} ($i = 0, 1, 2, ...$; $j = 0, 1, 2, ...$) can be expressed as:

$$\lambda^{ij}_{a} = k_{a_r}\left(\frac{\sqrt{\xi^{i}}}{r_w}\right)^2 + k_{a_z}\left(\frac{\sqrt{\mu^{j}}}{H}\right)^2 \quad [9\text{-}18a]$$

$$\lambda^{ij}_{w} = k_{w_r}\left(\frac{\sqrt{\xi^{i}}}{r_w}\right)^2 + k_{w_z}\left(\frac{\sqrt{\mu^{j}}}{H}\right)^2 \quad [9\text{-}18b]$$

Fourier Bessel series is adopted as the solution for the eigenfunction $R(r)$, giving:

$$R^{i}(r) = c^{i}\, J_0\left(\frac{r\sqrt{\xi^{i}}}{r_w}\right) + d^{i}\, Y_0\left(\frac{r\sqrt{\xi^{i}}}{r_w}\right) \quad [9\text{-}19]$$

where c^{i} and d^{i} ($i = 0, 1, 2, ...$) are the Bessel constants; and $J_0\left(r\sqrt{\xi^{i}}/r_w\right)$ and $Y_0\left(r\sqrt{\xi^{i}}/r_w\right)$ are the Bessel functions of the first kind and the second kind of order zero, respectively. By referring to the radial boundary condition in Equation [9-8],

$$c^i J_0\left(\sqrt{\xi^i}\right) + d^i Y_0\left(\sqrt{\xi^i}\right) = 0 \quad [9\text{-}20a]$$

$$c^i J_1\left(\varrho\sqrt{\xi^i}\right) + d^i Y_1\left(\varrho\sqrt{\xi^i}\right) = 0 \quad [9\text{-}20b]$$

where $\varrho = r_e/r_w$; and $J_1\left(\varrho\sqrt{\xi^i}\right)$ and $Y_1\left(\varrho\sqrt{\xi^i}\right)$ are the Bessel functions of the first kind and the second kind of order at $r = r_e$. To avoid constants c^i and d^i equal to zero, the following condition must be satisfied:

$$\begin{vmatrix} J_0\left(\sqrt{\xi^i}\right) & Y_0\left(\sqrt{\xi^i}\right) \\ J_1\left(\varrho\sqrt{\xi^i}\right) & Y_1\left(\varrho\sqrt{\xi^i}\right) \end{vmatrix} = 0 \quad [9\text{-}21]$$

which results in:

$$J_0\left(\sqrt{\xi^i}\right) Y_1\left(\varrho\sqrt{\xi^i}\right) - J_1\left(\varrho\sqrt{\xi^i}\right) Y_0\left(\sqrt{\xi^i}\right) = 0 \quad [9\text{-}22]$$

It should be noted that the eigenvalue ξ^i $(i = 0, 1, 2, ...)$ is the i^{th} root of Equation [9-22]. Adopting Equation [9-20b], the constant d^i can be expressed as a function of c^i, as shown in Equation [9-23]:

$$d^i = -c^i \frac{J_1\left(\varrho\sqrt{\xi^i}\right)}{Y_1\left(\varrho\sqrt{\xi^i}\right)} \quad [9\text{-}23]$$

Then substituting Equation [9-23] into Equation [9-19] leads to:

$$R^i(r) = \frac{c^i}{Y_1\left(\varrho\sqrt{\xi^i}\right)} D^i\left(\frac{r\sqrt{\xi^i}}{r_w}\right) \quad [9\text{-}24]$$

$$\text{where } D^i\left(\frac{r\sqrt{\xi^i}}{r_w}\right) = J_0\left(\frac{r\sqrt{\xi^i}}{r_w}\right) Y_1\left(\varrho\sqrt{\xi^i}\right) - J_1\left(\varrho\sqrt{\xi^i}\right) Y_0\left(\frac{r\sqrt{\xi^i}}{r_w}\right). \quad [9\text{-}25]$$

The constant a^i presented in Equation [9-16] can now be determined using the orthogonality of the Fourier Bessel series:

$$a^i = \frac{Y_1\left(\varrho\sqrt{\xi^i}\right)}{c^i}\frac{\int_{r_w}^{r_e} D^i\left(\frac{r\sqrt{\xi^i}}{r_w}\right)rdr}{\int_{r_w}^{r_e}\left[D^i\left(\frac{r\sqrt{\xi^i}}{r_w}\right)\right]^2 rdr} = \frac{2\,Y_1\left(\varrho\sqrt{\xi^i}\right)}{c^i}\frac{X^i}{\Upsilon^i\sqrt{\xi^i}} \qquad [9\text{-}26]$$

where $X^i = (r_w)^2\left[J_1\left(\varrho\sqrt{\xi^i}\right)Y_1\left(\sqrt{\xi^i}\right) - J_1\left(\sqrt{\xi^i}\right)Y_1\left(\varrho\sqrt{\xi^i}\right)\right]$; and

$$\Upsilon^i = (r_e)^2\left[J_0\left(\varrho\sqrt{\xi^i}\right)Y_1\left(\varrho\sqrt{\xi^i}\right) - J_1\left(\varrho\sqrt{\xi^i}\right)Y_0\left(\varrho\sqrt{\xi^i}\right)\right]^2 -$$
$$(r_w)^2\left[J_0\left(\sqrt{\xi^i}\right)Y_1\left(\varrho\sqrt{\xi^i}\right) - J_1\left(\varrho\sqrt{\xi^i}\right)Y_0\left(\sqrt{\xi^i}\right)\right]^2 - \left(\frac{X^i}{r_w}\right)^2. \qquad [9\text{-}27]$$

Incorporating Equations [9-17], [9-26] and [9-27] yields:

$$T_{a,t}^{ij}(t) + C_a\,T_{w,t}^{ij}(t) - c_v^a\left(\lambda_a^{ij}\right)T_a^{ij}(t) - \frac{Y_1\left(\varrho\sqrt{\xi^i}\right)}{c^i}\varpi^{ij}\,c_\sigma^a(1+2K)\sigma_{z,t}(t) = 0 \qquad [9\text{-}28a]$$

$$T_{w,t}^{ij}(t) + C_w\,T_{a,t}^{ij}(t) - c_v^w\left(\lambda_w^{ij}\right)T_w^{ij}(t) - \frac{Y_1\left(\varrho\sqrt{\xi^i}\right)}{c^i}\varpi^{ij}\,c_\sigma^w(1+2K)\sigma_{z,t}(t) = 0 \qquad [9\text{-}28b]$$

where $\varpi^{ij} = \frac{4\,X^i}{\Upsilon^i\sqrt{\xi^i}}\frac{1}{\sqrt{\mu^j}}$ for PTIB boundary condition; or

$= \frac{4\,X^i}{\Upsilon^i\sqrt{\xi^i}}\frac{1-(-1)^j}{\sqrt{\mu^j}}$ for PTPB boundary condition. [9-29]

Laplace transforming Equation [9-28] gives:

$$\left[s - c_v^a\left(\lambda_a^{ij}\right)\right]\overline{T}_a^{ij}(s) + s\,C_a\,\overline{T}_w^{ij}(s) = \left[T_a^{ij}(0) + C_a\,T_w^{ij}(0)\right] + \frac{Y_1\left(\varrho\sqrt{\xi^i}\right)}{c^i}\varpi^{ij}\,c_\sigma^a(1+2K)\left[s\overline{\sigma}_z(s) - \sigma(0)\right] \qquad [9\text{-}30a]$$

$$\left[s - c_v^w\left(\lambda_w^{ij}\right)\right]\overline{T}_w^{ij}(s) + s\,C_w\,\overline{T}_a^{ij}(s) = \left[T_w^{ij}(0) + C_w\,T_a^{ij}(0)\right] + \frac{Y_1\left(\varrho\sqrt{\xi^i}\right)}{c^i}\varpi^{ij}\,c_\sigma^w(1+2K)\left[s\overline{\sigma}_z(s) - \sigma(0)\right] \qquad [9\text{-}30b]$$

In addition, the terms $T_a^{ij}(0)$ and $T_w^{ij}(0)$ ($i = 0, 1, 2, ...$; $j = 0, 1, 2, ...$) are constant and can be obtained using orthogonalities of Bessel and sine functions:

$$T_a^{ij}(0) = \frac{Y_1\left(\varrho\sqrt{\xi^i}\right)}{c^i} \frac{\int_0^H \int_{r_w}^{r_e} u_a(r,z,0)\, D^i\left(\frac{r\sqrt{\xi^i}}{r_w}\right) \sin\left(\frac{z\sqrt{\mu^j}}{H}\right) rdrdz}{\int_0^H \int_{r_w}^{r_e} \left[D^i\left(\frac{r\sqrt{\xi^i}}{r_w}\right)\sin\left(\frac{z\sqrt{\mu^j}}{H}\right)\right]^2 rdrdz} = \varpi^{ij} u_a^0 \quad [9\text{-}31a]$$

$$T_w^{ij}(0) = \frac{Y_1\left(\varrho\sqrt{\xi^i}\right)}{c^i} \frac{\int_0^H \int_{r_w}^{r_e} u_w(r,z,0)\, D^i\left(\frac{r\sqrt{\xi^i}}{r_w}\right) \sin\left(\frac{z\sqrt{\mu^j}}{H}\right) rdrdz}{\int_0^H \int_{r_w}^{r_e} \left[D^i\left(\frac{r\sqrt{\xi^i}}{r_w}\right)\sin\left(\frac{z\sqrt{\mu^j}}{H}\right)\right]^2 rdrdz} = \varpi^{ij} u_w^0 \quad [9\text{-}31b]$$

Combining Equations [9-30] and [9-31] and then rewriting the derived equations into a simplified matrix form result in:

$$\mathbf{A}.\mathbf{T} = \frac{Y_1\left(\varrho\sqrt{\xi^i}\right)}{c^i}\, \varpi^{ij}\, (\mathbf{B} + \mathbf{C}) \quad [9\text{-}32]$$

where $\mathbf{A} = \begin{bmatrix} s - c_v^a \lambda_a^{ij} & sC_a \\ sC_w & s - c_v^w \lambda_w^{ij} \end{bmatrix}$; $\mathbf{B} = \begin{Bmatrix} u_a^0 + C_a\, u_w^0 \\ C_w\, u_a^0 + u_w^0 \end{Bmatrix}$;

$\mathbf{C} = \begin{Bmatrix} c_\sigma^a \\ c_\sigma^w \end{Bmatrix} (1 + 2K)\, [s\bar{\sigma}_z(s) - \sigma(0)]$; and $\mathbf{T} = \begin{Bmatrix} \overline{T}_a^{ij}(s) \\ \overline{T}_w^{ij}(s) \end{Bmatrix}$. [9-33]

Solving for $\overline{T}_a^{ij}(s)$ and $\overline{T}_w^{ij}(s)$ $(i = 0, 1, 2, ...; j = 0, 1, 2, ...)$ gives:

$$\mathbf{T} = \frac{Y_1\left(\varrho\sqrt{\xi^i}\right)}{c^i}\, \varpi^{ij}\, (\mathbf{A}^{-1}.\mathbf{B} + \mathbf{A}^{-1}.\mathbf{C}) \quad [9\text{-}34]$$

where $\mathbf{A}^{-1}.\mathbf{B} = \begin{Bmatrix} \frac{u_a^0(C_wC_a-1)s + c_v^w\left[u_a^0 + C_a\, T_w^{ij}(0)\right]\lambda_w^{ij}}{(C_wC_a-1)s^2 + \left(\lambda_w^{ij}c_v^w + \lambda_a^{ij}c_v^a\right)s - c_v^w c_v^a \lambda_w^{ij}\lambda_a^{ij}} \\ \frac{u_w^0(C_wC_a-1)s + c_v^a\left[u_w^0 + C_w\, u_a^0\right]\lambda_a^{ij}}{(C_wC_a-1)s^2 + \left(\lambda_w^{ij}c_v^w + \lambda_a^{ij}c_v^a\right)s - c_v^w c_v^a \lambda_w^{ij}\lambda_a^{ij}} \end{Bmatrix}$; and

$$\mathbf{A}^{-1}.\mathbf{C} = \begin{Bmatrix} \frac{(1+2K)\left[(C_a c_\sigma^w - c_\sigma^a)s + c_v^w c_\sigma^a \lambda_w^{ij}\right][s\bar{\sigma}_z(s) - \sigma(0)]}{(C_wC_a-1)s^2 + \left(c_v^a\lambda_a^{ij} + c_v^w\lambda_w^{ij}\right)s - c_v^a c_v^w \lambda_a^{ij}\lambda_w^{ij}} \\ \frac{(1+2K)\left[(C_w c_\sigma^a - c_\sigma^w)s + c_v^a c_\sigma^w \lambda_a^{ij}\right][s\bar{\sigma}_z(s) - \sigma(0)]}{(C_wC_a-1)s^2 + \left(c_v^a\lambda_a^{ij} + c_v^w\lambda_w^{ij}\right)s - c_v^a c_v^w \lambda_a^{ij}\lambda_w^{ij}} \end{Bmatrix}. \quad [9\text{-}35]$$

The generalized Fourier coefficients for air and water can be obtained by taking the Laplace inverse of Equation [9-34], leading to:

$$\mathcal{L}^{-1}\{\mathbf{T}\} = \frac{Y_1\left(\varrho\sqrt{\xi^i}\right)}{c^i}\,\varpi^{ij}\left\{\mathcal{L}^{-1}\{\mathbf{A}^{-1}.\mathbf{B}\} + \mathcal{L}^{-1}\{\mathbf{A}^{-1}.\mathbf{C}\}\right\} \qquad [9\text{-}36]$$

where $\mathcal{L}^{-1}\{\mathbf{T}\} = \begin{Bmatrix} T_a^{ij}(t) \\ T_w^{ij}(t) \end{Bmatrix}$;

$$\mathcal{L}^{-1}\{\mathbf{A}^{-1}.\mathbf{B}\} = \begin{Bmatrix} \frac{\Omega\left(e^{\alpha_1^{ij}t} - e^{\alpha_2^{ij}t}\right) + \Psi\left(e^{\alpha_1^{ij}t} + e^{\alpha_2^{ij}t}\right)}{2\eta^{ij}} \\ \frac{\Omega'\left(e^{\alpha_1^{ij}t} - e^{\alpha_2^{ij}t}\right) + \Psi'\left(e^{\alpha_1^{ij}t} + e^{\alpha_2^{ij}t}\right)}{2\eta^{ij}} \end{Bmatrix};$$

$$\eta^{ij} = \left[\left(c_v^a\lambda_a^{ij} - c_v^w\lambda_w^{ij}\right)^2 + 4c_v^a c_v^w C_w C_a \lambda_a^{ij}\lambda_w^{ij}\right]^{\frac{1}{2}};$$

$$\alpha_1^{ij} = \frac{1}{2}\left(\frac{c_v^a\lambda_a^{ij} + c_v^w\lambda_w^{ij} + \eta^{ij}}{1 - C_w C_a}\right); \qquad \alpha_2^{ij} = \frac{1}{2}\left(\frac{c_v^a\lambda_a^{ij} + c_v^w\lambda_w^{ij} - \eta^{ij}}{1 - C_w C_a}\right);$$

$$\Omega = \left(c_v^a\lambda_a^{ij} - c_v^w\lambda_w^{ij}\right)u_a^0 - 2c_v^w C_a\lambda_w^{ij}u_w^0; \qquad \Psi = \eta^{ij}u_a^0;$$

$$\Omega' = \left(c_v^w\lambda_w^{ij} - c_v^a\lambda_a^{ij}\right)u_w^0 - 2c_v^a C_w\lambda_a^{ij}u_a^0; \text{ and} \qquad \Psi' = \eta^{ij}u_w^0. \qquad [9\text{-}37]$$

In Equation [9-36], the term $\mathcal{L}^{-1}\{\mathbf{A}^{-1}.\mathbf{C}\}$ may change depending on different loading functions. Note that the exclusion of the term $\mathcal{L}^{-1}\{\mathbf{A}^{-1}.\mathbf{C}\}$ in the analytical model would lead to a case of soil deformation induced by a constant loading. The final solutions for predicting the dissipation rates of excess pore pressures can be deduced as follows:

$$\mathbf{U} = \sum_{j=0}^{\infty}\varpi^{ij}\,D^i\left(\frac{r\sqrt{\xi^i}}{r_w}\right)\sin\left(\frac{z\sqrt{\mu^j}}{H}\right)\left\{\mathcal{L}^{-1}\{\mathbf{A}^{-1}.\mathbf{B}\} + \mathcal{L}^{-1}\{\mathbf{A}^{-1}.\mathbf{C}\}\right\} \qquad [9\text{-}38]$$

where $\mathbf{U} = \begin{Bmatrix} u_a(r,z,t) \\ u_w(r,z,t) \end{Bmatrix}$. [9-39]

Note that the constant term c^i in the eigenfunction $R^i(r)$ is cancelled out when the final solution is formed. Equation [9-38] predicts the dissipation rates of excess pore-air and pore-pressures induced by a particular loading. A full set of analytical solutions for the consolidation of deposits of unsaturated soil under various types of external loadings are presented in Appendix I.

9.3.3. Normalised settlement

By assuming that the coefficients of volume change of the soil are constant during consolidation, the constitutive model for the soil structure can be presented as:

$$\frac{\partial\left(\frac{\Delta V}{V_0}\right)}{\partial t} = m_1^s\left(\frac{1+2K}{3}\right)\frac{\partial\sigma_z}{\partial t} + (m_2^s - m_1^s)\frac{\partial u_a}{\partial t} - m_2^s\frac{\partial u_w}{\partial t} \quad [9\text{-}40]$$

where m_1^s and m_2^s are the coefficients of volume change of the soil element with respect to changes in the net stress and suction $(1/\text{kPa})$, respectively. Integrating Equation [9-40] against time leads to:

$$\varepsilon_v(r,z,t) = m_1^s\left(\frac{1+2K}{3}\right)[\sigma_z(t) - \sigma_z(0)] + (m_2^s - m_1^s)[u_a(r,z,t) - u_a(r,z,0)] - m_2^s[u_w(r,z,t) - u_w(r,z,0)] \quad [9\text{-}41]$$

where ε_v is the volumetric strain of the soil. Consolidation settlement occurs due to the dissipation of excess pore pressure, so for the sake of simplicity, settlement can be normalised as set out below:

$$S^* = \frac{S(t)}{S_{max}} = \frac{1}{\pi[(r_e)^2 - (r_w)^2]}\frac{1}{H}\frac{\int_0^H\int_{r_w}^{r_e} 2\pi\,\varepsilon_v(r,z,t)\,r\,dr\,dz}{m_1^s\left(\frac{1+2K}{3}\right)(q_z)_{max}} \quad [9\text{-}42]$$

where S^* and S_{max} are the normalised and maximum settlement, respectively. Equation [9-42] is a function of time t describing the settlement response of the unsaturated soil due to an external applied load at a particular time. Recent studies report that soil cementation and visco-plastic behaviour of soft soils also have considerable impacts on the time-dependent deformation (Nguyen et al. 2014; Le et al. 2015). However, these factors are not included in this study.

9.4. Worked Examples

In this study, unsaturated soil consolidation induced by time-dependent loadings is predicted against variations of air to water permeability ratio (k_a/k_w) and loading parameters. The normalised excess pore-air (u_a/u_{atm}) and pore-water pressures (u_w/u_{atm}) and consolidation settlement (S^*) are analysed further. Moreover, the external loadings used in this study such as ramping, asymptotic, sinusoid and damped

sine wave are the four primary loadings available in engineering practice and they are good representatives for practical simulations (construction, road traffic etc.). Figure 9.2 presents four types of time-dependent loads with various loading parameters exerted on the unsaturated soil deposit. The loadings are simulated mathematically as follows:

Ramping: $$q_z(t) = q_0 + at \quad [9\text{-}43a]$$

Asymptotic: $$q_z(t) = q_0 + A\,q_0\left(1 - e^{-bt}\right) \quad [9\text{-}43b]$$

Sinusoid: $$q_z(t) = q_0[B\ \sin(\phi t) + 1] \quad [9\text{-}43c]$$

Damped sine wave: $$q_z(t) = q_0[C\,e^{-ct}\sin(\varphi t) + 1] \quad [9\text{-}43d]$$

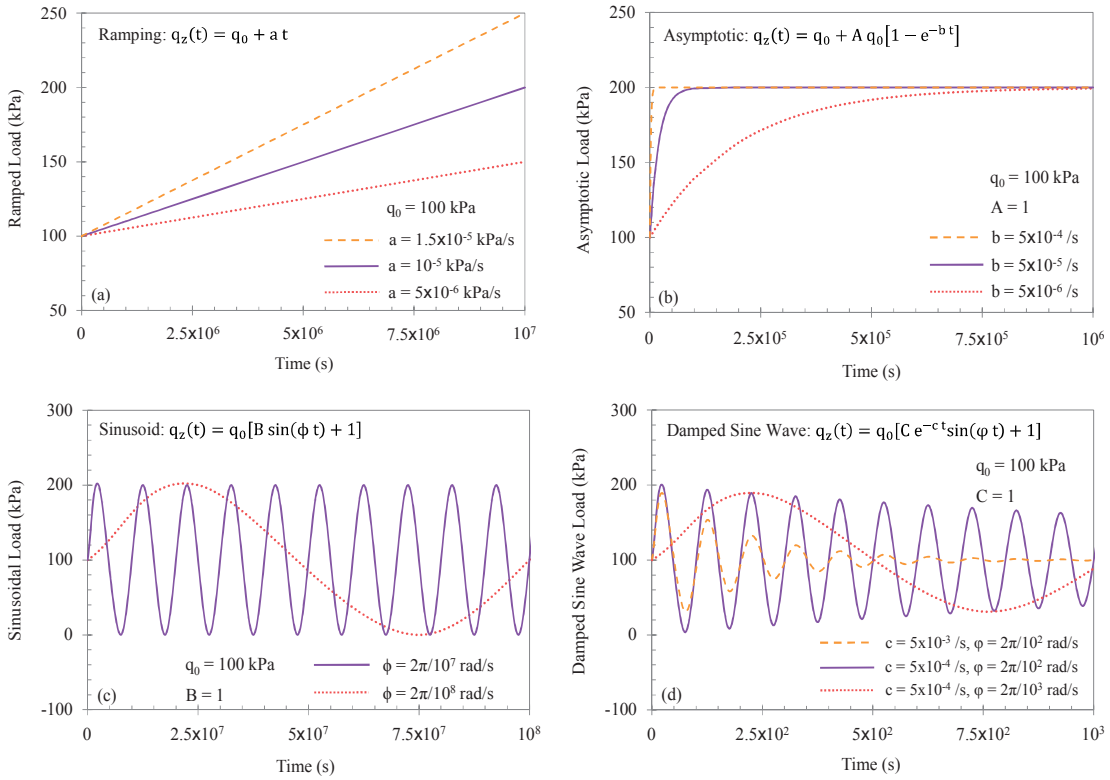

Figure 9.2. Four primary time-dependent loadings: (a) ramping, (b) asymptotic, (c) sinusoid and (d) damped sine wave

where q_0 is the initial surcharge (kPa); 'a' is the linear loading rate (kPa/s); 'b' and 'c' are the exponential loading rates of the asymptotic and damped sine wave functions (/s), respectively; 'ϕ' and 'φ' are the angular frequencies of the sinusoidal and damped sine wave functions (rad/s), respectively; A, B and C are the loading constants. On the other hand, the unsaturated soil properties adopted in the worked examples are as follows:

- Soil properties: $m_1^s = -5.64 \times 10^{-4}\ kPa^{-1}$, $m_2^s = 0.2m_1^s$, $m_1^w = -1.13 \times 10^{-4}\ kPa^{-1}$, $m_2^w = 1.8m_1^w$, $m_1^a = m_1^s - m_1^w$, $m_2^a = m_1^s - m_1^w$, $n = 0.50$, $S_r = 80\%$;
- Physical properties: $\Theta = (\theta° + 273.16)\ K$, $\theta° = 20℃$, $R = 8.31\ J/mol.K$, $M = 0.03\ kg/mol$;
- Other properties: $k_w = 10^{-10}\ m/s$, $u_{atm} = 100\ kPa$, $u_a^0 = 20\ kPa$, $u_w^0 = 40\ kPa$;
- Soil dimensions: $r_w = 0.2\ m$, $r_e = 1.8\ m$, $H = 5\ m$;
- Loading constants: $q_0 = 100\ kPa$, $A = B = C = 1$.

By referring to Fredlund et al. (2012), under an instantaneous condition, an application of initial surcharge q_0 (i.e., 100 kPa) results in an initial excess pore-air pressure u_a^0 and pore-water pressure u_w^0 of 20 kPa and 40 kPa, respectively, but after a certain time the excess pore pressures vary with time, depending on the applied loads. On the other hand, variations of k_a/k_w (i.e., from 10^{-2} to 10^3) are mainly based on changes in the air permeability coefficient while the water permeability coefficient is kept constant (i.e., 10^{-10} m/s). For the purpose of generalization, consolidation will be examined under PTIB boundary conditions at $r = 0.5(r_w + r_e)$ and $z = 0.5H$, and the stress ratio $K = 1$ and the isotropic permeability condition (i.e., $k_r = k_z$) are used in the worked examples.

9.4.1. Ramped loading

The ramped loading function (e.g., construction surcharge) in Equation [9-43a] is incorporated into the inverse Laplace transformed $\mathcal{L}^{-1}\{\mathbf{A}^{-1}.\mathbf{C}\}$ to produce the final solution. Complete analytical solutions for the case of ramped loading are presented in Equations [I-1] and [I-2], in Appendix I.

Figure 9.3 shows the dissipation rates of excess pore-air and pore-water pressures induced by ramped loading under the PTIB condition. The loading rate $a = 10^{-5}\ kPa/s$ is adopted for this analysis. As Figure 9.3(a) shows, in a semi-logarithmic plot there appears to be a pronounced increase in the dissipation of excess pore-air pressure at

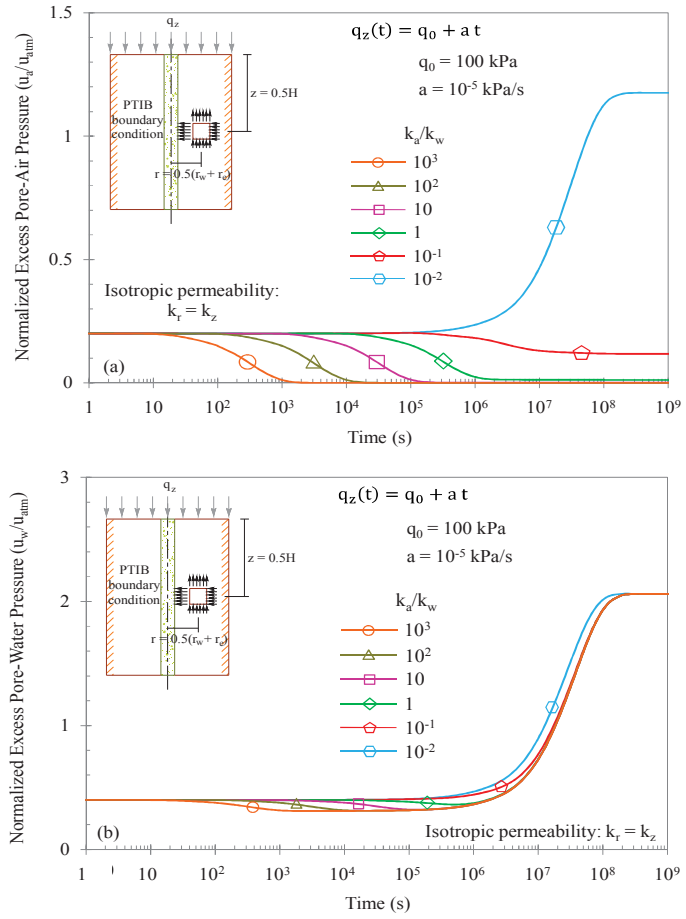

Figure 9.3. Dissipation rates of (a) excess pore-air and (b) excess pore-water pressures varying with k_a/k_w under the ramped loading

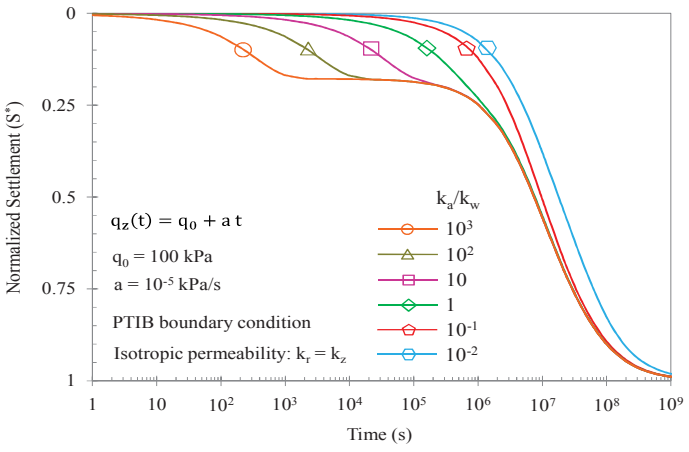

Figure 9.4. Normalised settlement varying with k_a/k_w under the ramped loading

latter stages of consolidation (i.e., after about 10^6 s) when $k_a/k_w < 1$, but as k_a/k_w increases the ramped loading may have insignificant impacts on the dissipation rate.

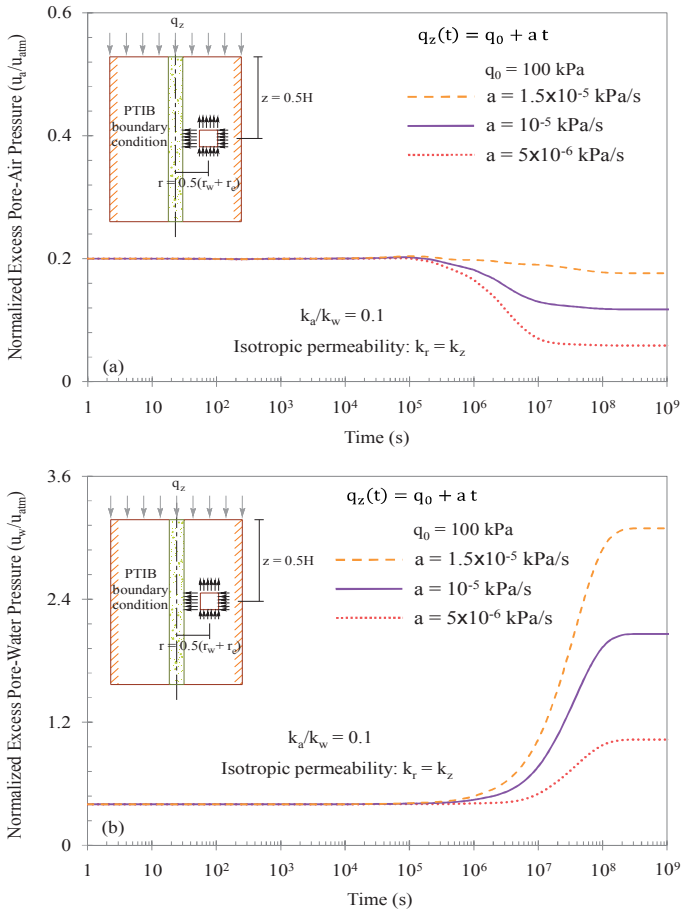

Figure 9.5. Effects of the linear loading parameter 'a' on the dissipation rates of (a) excess pore-air and (b) excess pore-water pressures

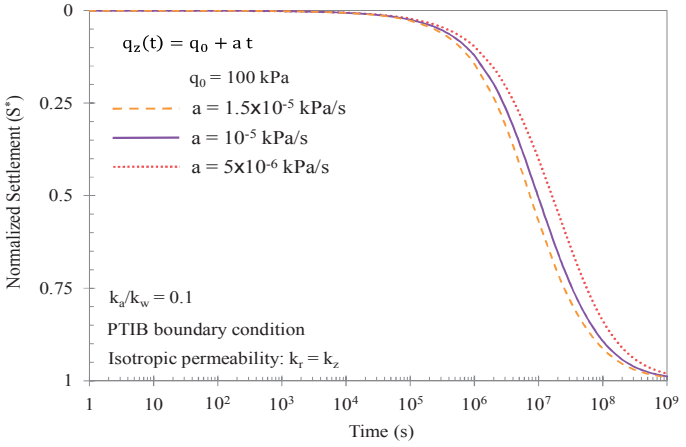

Figure 9.6. Effects of the linear loading parameter 'a' on the normalised settlement

This indicates that the dissipation of excess pore-air pressure has almost been completed before 10^6 s. In Figure 9.3(b), for all k_a/k_w values, the excess pore-water pressure

begins to increase dramatically during the latter stages because the dissipation rate of excess pore-water pressure is relatively slow compared to the loading rate. However, it is observed that the excess pore-water pressure approaches a constant value after about 10^8 s. This indicates that, considering the selected material properties, the dissipation rate of the excess pore-water pressure is counterbalanced with the loading rate (or excess pore-water pressure generation rate).

Variations of the normalised settlement S^* due to the ramped loading are illustrated in Figure 9.4. As observed, the settlement curves are similar to those induced by a constant loading at the beginning of consolidation, in which the settlement generally proceeds faster as k_a/k_w increases, thus characterizing inverse sigmoid shapes. However, for all the k_a/k_w values, the settlement curves increase dramatically after 10^6 s as a result of a significantly increasing load.

For the parametric study, the significant effects of the linear loading rate 'a' (i.e., ranging from 5×10^{-6} to 1.5×10^{-5} kPa/s) on the dissipation of excess pore pressure under PTIB condition are depicted in Figure 9.5. It should be noted that the permeability ratio $k_a/k_w = 0.1$ is used for this analysis. As observed, increasing 'a' leads to a noticeable increase in the ramped loading after 10^6 s, which then induces larger excess pore-air and pore-water pressures at latter stages of consolidation. Moreover, the ramped loading with higher 'a' (i.e., 1.5×10^{-5} kPa/s) causes the unsaturated soil deposit to consolidate faster, as shown in Figure 9.6.

9.4.2. Asymptotic loading

The asymptotic loading function (e.g., construction surcharge, embankment) in Equation [9-43b] is incorporated into the inverse Laplace term $\mathcal{L}^{-1}\{\mathbf{A}^{-1}.\mathbf{C}\}$. Complete analytical solutions for axisymmetric consolidation induced by the asymptotic loading are presented in Equations [I-3] and [I-4], in Appendix I.

Figure 9.7 shows the dissipation rates of excess pore-air and pore-water pressures due to the asymptotic loading while considering the PTIB condition. The loading rate $b = 5 \times 10^{-4}$ /s is adopted for this analysis. Note that an increase in the applied load begins to accelerate as time elapses, until it reaches the asymptote of $2q_0$ at about 10^4 s. As with the load, under a semi-logarithmic scale, patterns of excess pore-air and pore-

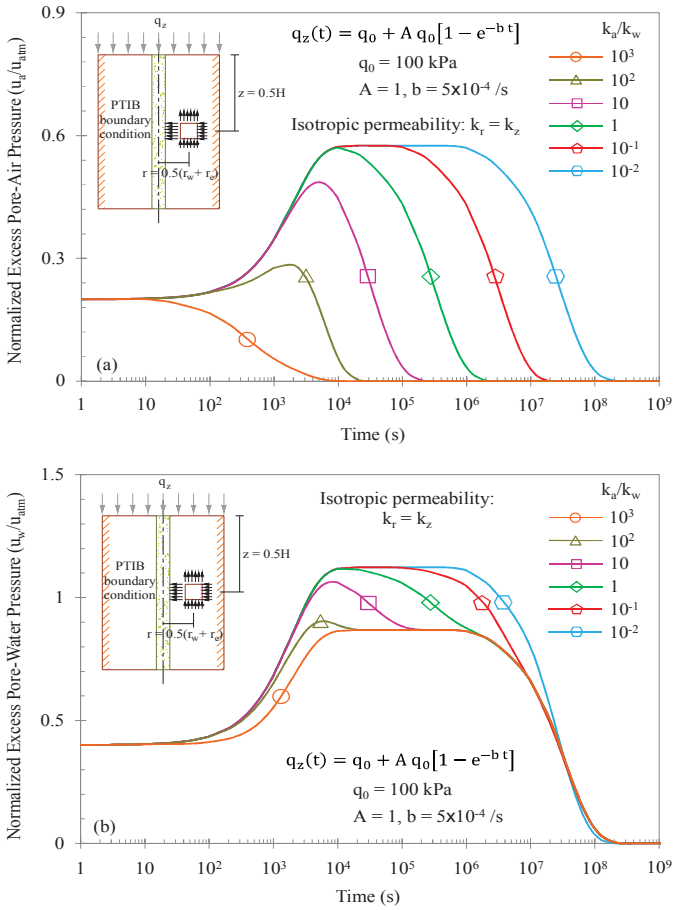

Figure 9.7. Dissipation rates of (a) excess pore-air and (b) excess pore-water pressures varying with k_a/k_w under the asymptotic loading

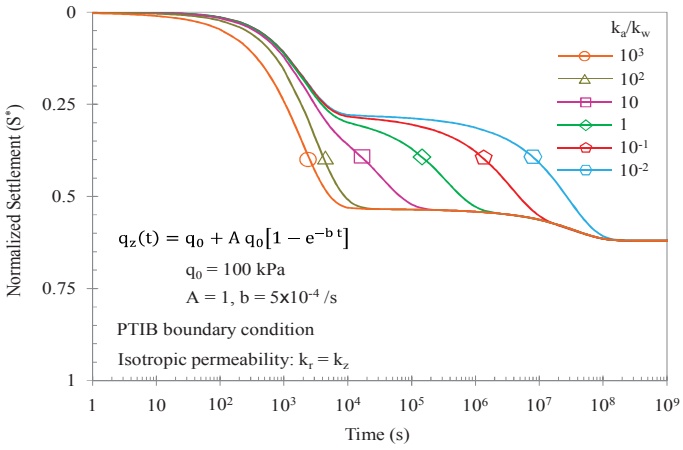

Figure 9.8. Normalised settlement varying with k_a/k_w under the asymptotic loading

water pressure having $k_a/k_w \leq 10$ would increase exponentially until they attain the highest value at about 10^4 s. For $k_a/k_w > 10$, both excess pore pressures may

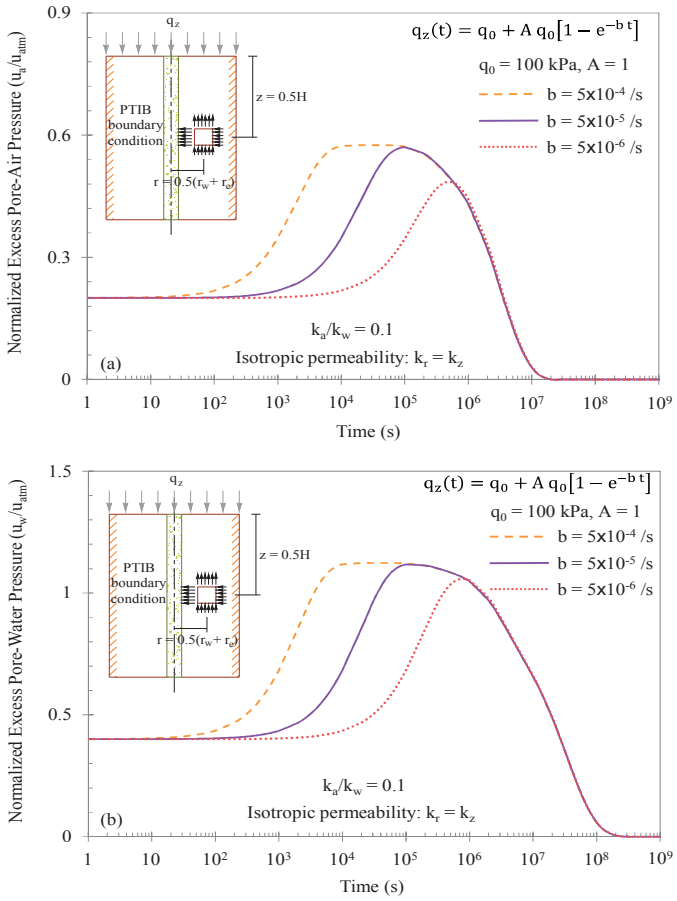

Figure 9.9. Effects of the exponential loading parameter 'b' on the dissipation rates of (a) excess pore-air and (b) excess pore-water pressures

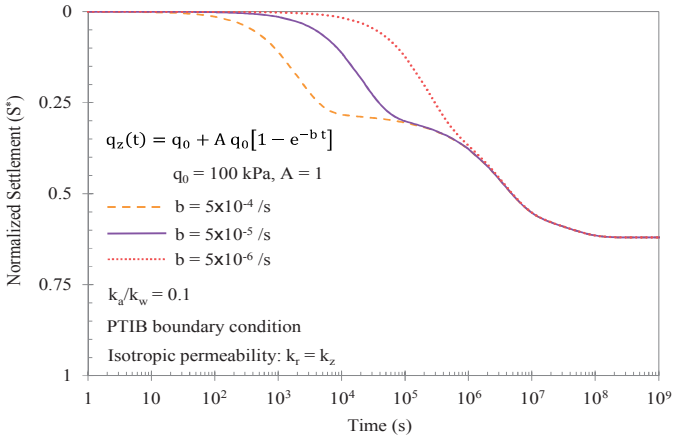

Figure 9.10. Effects of the exponential loading parameter 'b' on the normalised settlement

approach their highest value before 10^4 s. Note that the highest value of excess pore pressures tends to decrease when k_a/k_w increases noticeably.

The normalised settlement S^* of unsaturated soil subjected to asymptotic loading is presented in Figure 9.8. Unlike the impact of ramped loading, the settlement curves increase dramatically during the early stages of consolidation, but then settlement begins to decelerate when the applied load approaches the asymptote. At latter stages of consolidation, the settlement of unsaturated soil deposit proceeds faster as k_a/k_w increases. The volume of soil continues to decrease at a slow rate until no further reduction in volume is observed after 10^8 s.

Figures 9.9 and 9.10, on the other hand, demonstrate the effects of the loading parameter 'b' (i.e., ranging from 5×10^{-6} to 5×10^{-4} /s) on the dissipation and settlement under the PTIB condition, respectively, while considering $k_a/k_w = 0.1$. In Figure 9.9, the excess pore-air and pore-water pressures attain their highest value at a slower rate when 'b' decreases. It should be noted that the highest value of excess pore pressures may reduce as 'b' decreases because a large amount of excess pore pressures already dissipated before the loading approaches the asymptote. As reported in Figure 9.10, the settlement curves with a higher 'b' are prone to proceed faster during the early stages of consolidation, then they converge into a single curve and continue to increase at a very slow rate until no further reduction in volume is observed after 10^8 s.

9.4.3. Sinusoidal loading

The sinusoidal loading function (e.g., road traffic or heavy train loadings) in Equation [9-43c] can be substituted into the term $\mathcal{L}^{-1}\{\mathbf{A}^{-1}.\mathbf{C}\}$ to obtain the final solution. Complete analytical solutions for axisymmetric consolidation due to sinusoidal loading are presented in Equations [I-5] and [I-6], in Appendix I.

Figure 9.11 depicts the changes in excess pore-air and pore-water pressures induced by sinusoidal loading under the PTIB boundary condition. The angular frequency $\phi = 2\pi \times 10^{-7}$ rad/s is adopted for the analysis. Both excess pore pressure curves consist of harmonic oscillations that correspond to the external loading-unloading process. It should be noted that the stiffness of unsaturated soils, particularly compacted clays, may be different depending on the loading-unloading cycles and suction variations (Mendoza et al. 2005). However, as a simplifying assumption to solve the governing equations, the stiffness is assumed constant under the sinusoidal loading. It

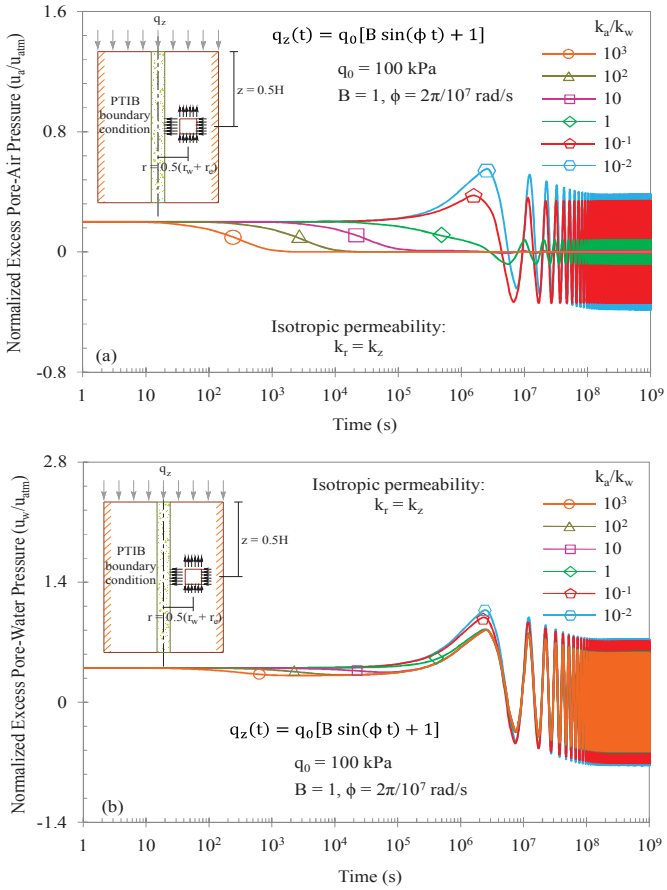

Figure 9.11. Dissipation rates of (a) excess pore-air and (b) excess pore-water pressures varying with k_a/k_w under the sinusoidal loading

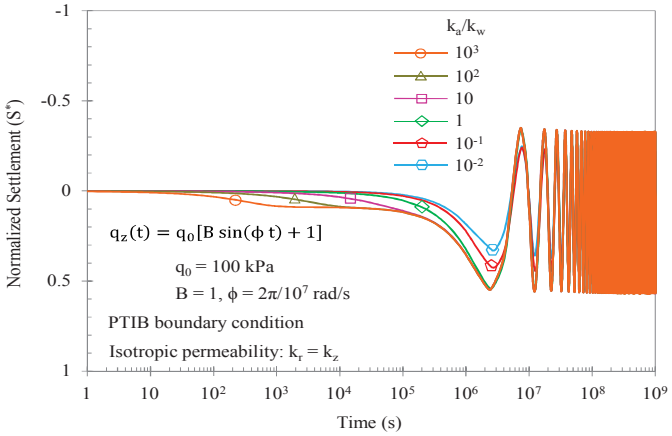

Figure 9.12. Normalised settlement varying with k_a/k_w under the sinusoidal loading

should be noted that for small stress increments, the stiffness may be reasonably assumed constant for practical applications. Unlike other loading functions, the

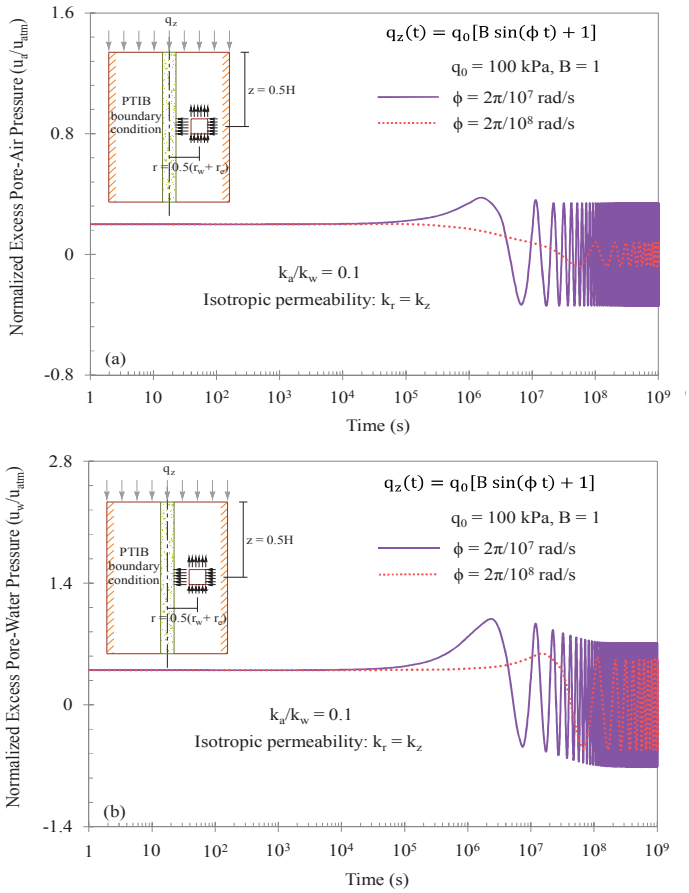

Figure 9.13. Effects of the angular frequency 'ϕ' on the dissipation rates of (a) excess pore-air and (b) excess pore-water pressures

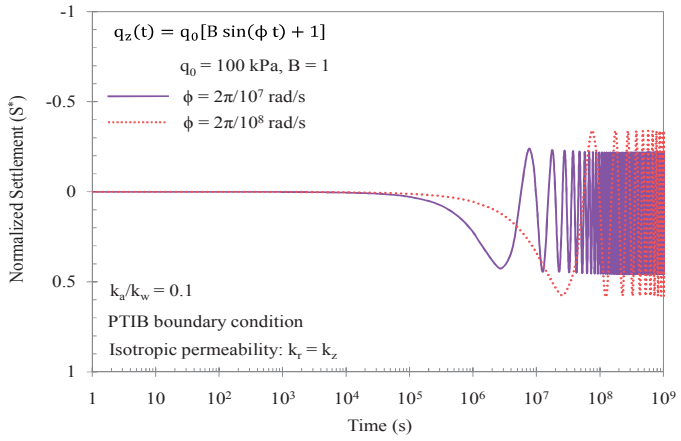

Figure 9.14. Effects of the angular frequency 'ϕ' on the normalised settlement

sinusoidal load results in permanent oscillations in excess pore pressures after a long period of time. Figure 9.11(a) shows that the sinusoidal amplitude of excess pore-air

pressure curve is attenuated significantly when k_a/k_w increases. This result indicates that the excess pore-air pressure with higher values of k_a/k_w, particularly $k_a/k_w \geq 1$, is almost fully dissipated at the latter stages of consolidation, so the applied load only has minor impacts on the dissipation process. However, the amplitudes of excess pore-water pressures, except for $k_a/k_w < 1$, are almost identical after a long time, as shown in Figure 9.11(b).

The normalised settlement S^* of unsaturated soils subjected to sinusoidal loading is presented in Figure 9.12. As with the dissipation process, the pattern of settlement includes indefinite oscillations in response to the unloading-loading process of a typical sinusoidal loading. During the early stages, the patterns of settlement form inverse sigmoid curves at a slow rate when $k_a/k_w > 10$. These patterns begin to oscillate indefinitely after 10^6 s because the air and water are squeezed out of the soil stratum during the loading process and then absorbed back in during the unloading process. This repetitive process leads to continuous changes in the volume of the soil over time.

The significant impact of the angular frequency 'ϕ' (i.e., $2\pi \times 10^{-8}$ and $2\pi \times 10^{-7}$ rad/s) on axisymmetric consolidation can be seen in Figures 9.13 and 9.14. The parametric study uses $k_a/k_w = 0.1$ for the analysis. Figure 9.13 shows that, as expected, loading with a smaller 'ϕ' reduces the number of oscillations in both excess pore pressures. Furthermore, a decrease in the frequency 'ϕ' may allow sufficient time for excess pore pressures to dissipate and therefore the amplitudes of pore pressure oscillation would attenuate significantly at the latter stages of consolidation. However, loading with a smaller 'ϕ' causes a noticeable increase in the amplitude of settlement curve due to the slow loading-unloading process, as shown in Figure 9.14. Moreover, the soil subjected to sinusoidal loading with a smaller 'ϕ' tends to proceed at a slower rate at the latter stages compared to that with a higher 'ϕ'.

9.4.4. Damped sine wave loading

The damped loading function (e.g., road traffic loadings) in Equation [9-43d] can be substituted back into the inverse Laplace term $\mathcal{L}^{-1}\{\mathbf{A}^{-1}.\mathbf{C}\}$ to obtain the final solution. Complete analytical solutions for the case of damped sine wave loading are presented in Equations [I-7] and [I-8] in Appendix I.

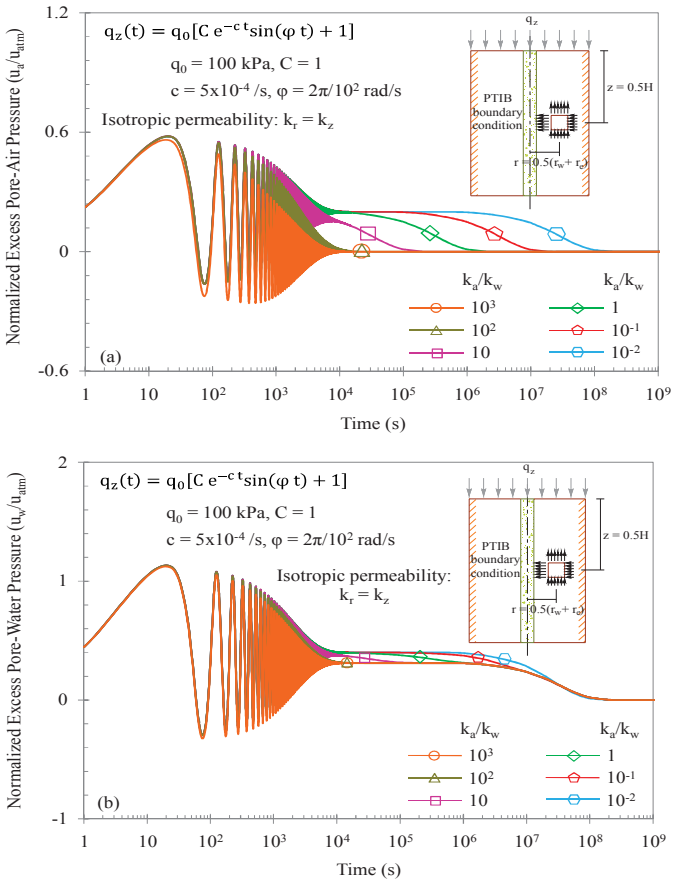

Figure 9.15. Dissipation rates of (a) excess pore-air and (b) excess pore-water pressures varying with k_a/k_w under the damped sine wave loading

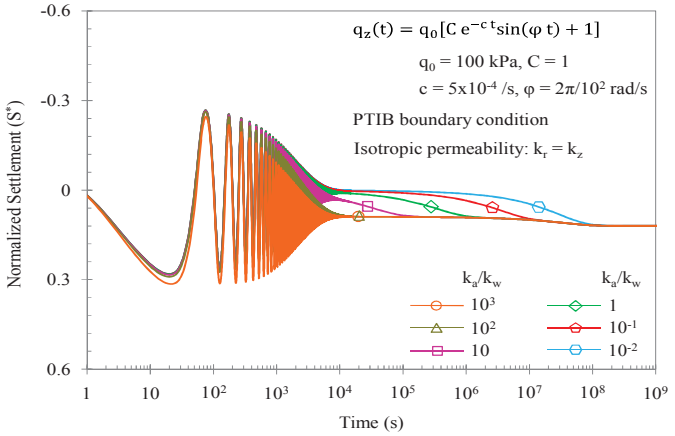

Figure 9.16. Normalised settlement varying with k_a/k_w under the damped sine wave loading

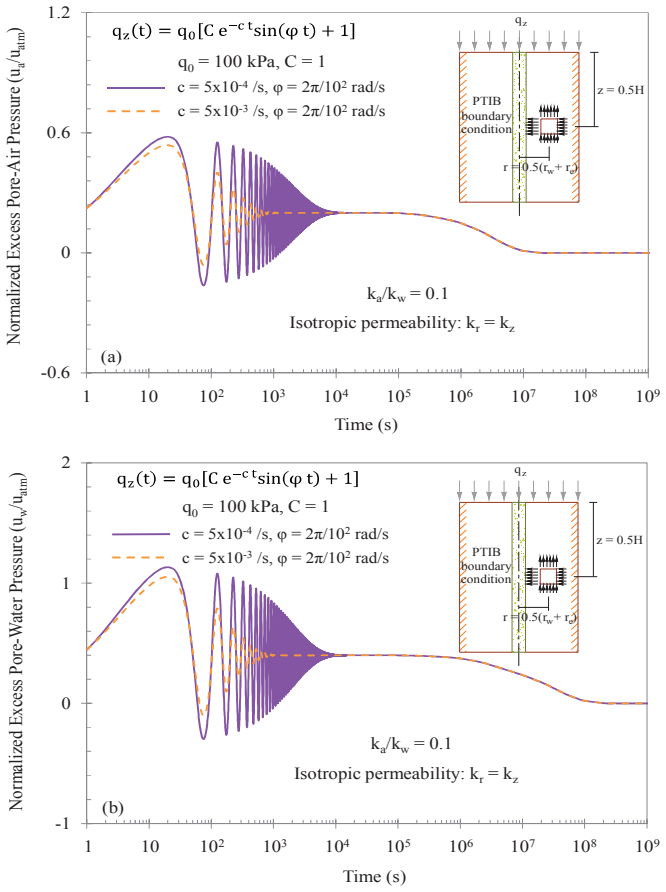

Figure 9.17. Effects of the exponential loading parameter 'c' on the dissipation rates of (a) excess pore-air and (b) excess pore-water pressures while keeping the angular frequency 'φ' constant

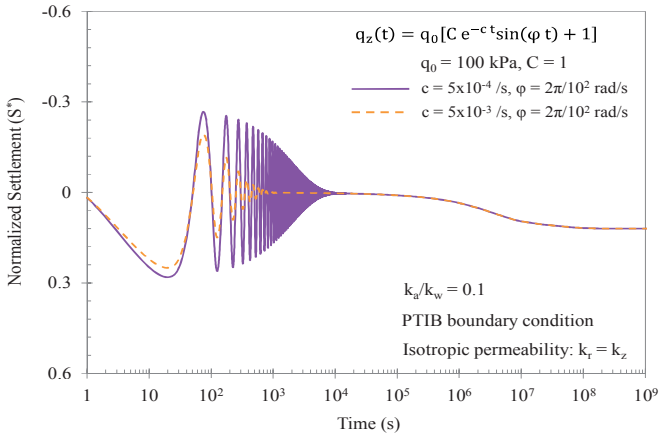

Figure 9.18. Effects of the exponential loading parameter 'c' on the normalised settlement while keeping the angular frequency 'φ' constant

Figure 9.15 shows the dissipation rates of excess pore-air and pore-water pressures induced by the damped sine wave loading under the PTIB boundary condition. The loading rate $c = 5 \times 10^{-4}$ /s and the angular frequency $\varphi = 2\pi \times 10^{-2}$ rad/s are used for this analysis. In the semi-logarithmic graph, both excess pore pressure curves oscillate with exponentially decreasing amplitudes in response to the applied damped loading. The excess pore pressures eventually stabilize as the amplitude approaches zero (i.e., at about 10^4 s). Note that the patterns of dissipation after 10^4 s are very similar to those induced by a constant loading. During this time the increasing k_a/k_w causes the excess pore-air pressure (Figure 9.15(a)) to dissipate faster, whereas the excess pore-water pressure, for all k_a/k_w values, converge to a single curve and then dissipate at a relatively slow rate (Figure 9.15(b)).

Similarly, the normalised settlement curves initially oscillate in response to the loading-unloading process, as shown in Figure 9.16. Once the loading amplitude approaches zero the settlement patterns stabilize and continue to increase at a very slow rate. The soil experiences no further deformation after 10^8s.

Figures 9.17 and 9.18 demonstrate effects of the loading parameter 'c' (i.e., 5×10^{-4} and 5×10^{-3} /s) on the dissipation of excess pore pressures and consolidation settlement, respectively, while adopting $k_a/k_w = 0.1$ and $\varphi = 2\pi \times 10^{-2}$ rad/s. As noted, the smaller 'c' accelerates the damping process and significantly reduces the number of oscillations. This result indicates that the amplitudes of excess pore-air and pore-water pressure dissipation and settlement patterns with smaller 'c' approach zero faster than those with higher 'c', but after 10^4 s the 'c' value no longer influences the dissipation and settlement rates.

Figures 9.19 and 9.20, on the other hand, investigate the effects of 'φ' (i.e., $2\pi \times 10^{-3}$ and $2\pi \times 10^{-2}$ rad/s) on the dissipation of excess pore pressure and consolidation settlement, respectively, while considering $k_a/k_w = 0.1$ and $c = 5 \times 10^{-4}$ /s. When predicting both dissipation and settlement, a smaller angular frequency 'φ' would reduce the number of oscillations while increasing the wavelength. Similar to the effects of 'c', when the damped loading stabilizes after 10^4s, the parameter 'φ' would have no impact on the dissipation and settlement rates of the unsaturated soil.

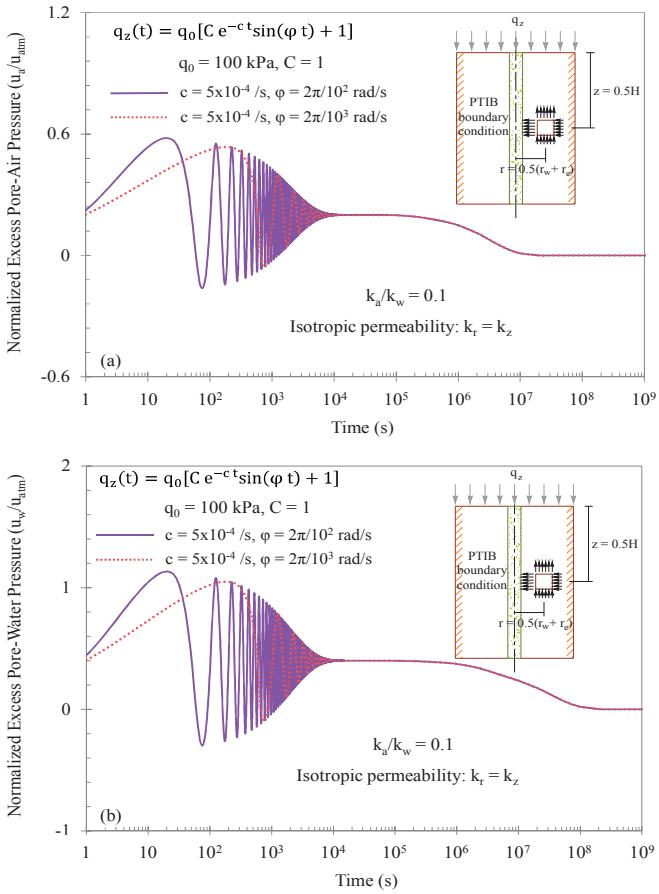

Figure 9.19. Effects of the angular frequency 'φ' on the dissipation rates of (a) excess pore-air and (b) excess pore-water pressures while keeping the exponential loading parameter 'c' constant

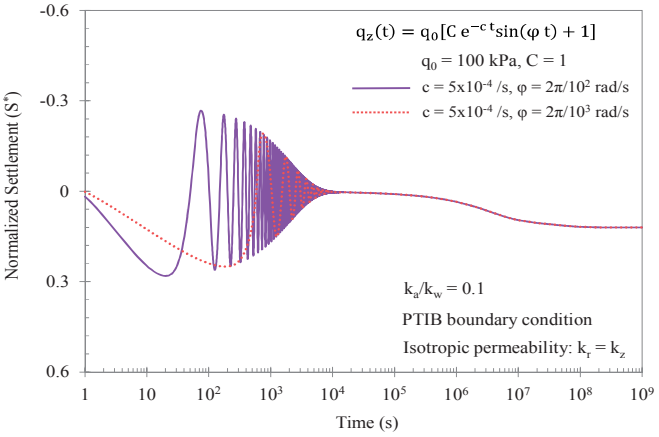

Figure 9.20. Effects of the angular frequency 'φ' on the normalised settlement while keeping the exponential loading parameter 'c' constant

9.4.5. Variations in matric suction and net stress

This section investigates the variations in matric suction and net stress induced by the ramped and asymptotic loadings. Changes in matric suction (Δs) and net stress ($\Delta\bar{\sigma}$) are mainly attributed to time-dependent variations of excess pore-air and pore-water pressures, and external applied stresses. Effects of the permeability ratio k_a/k_w and loading parameters 'a' and 'b' on the normalised suction change ($\Delta s/q_0$) and normalised net stress change ($\Delta\bar{\sigma}/q_z(t)$) are analysed.

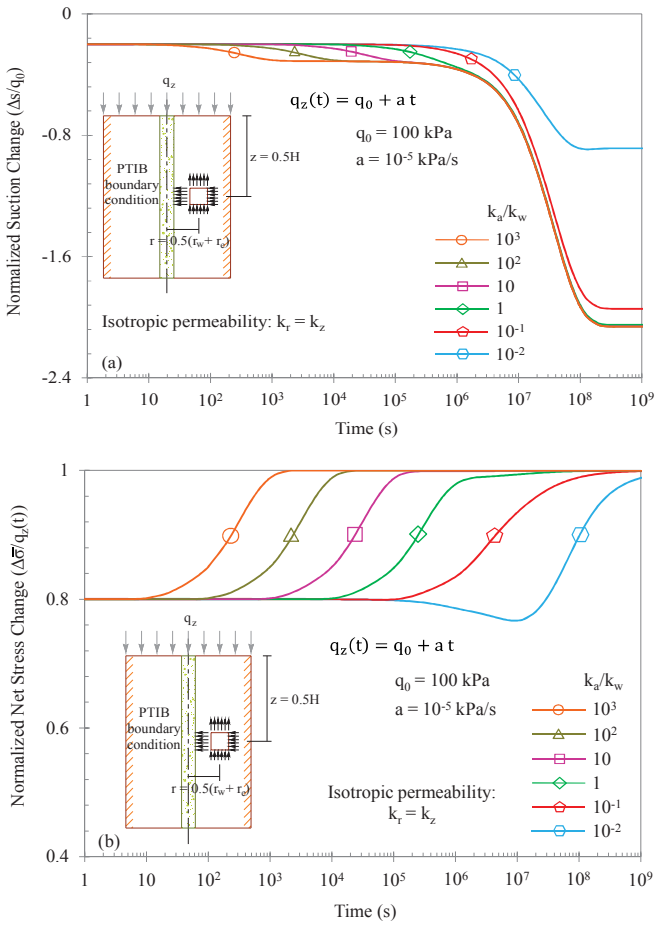

Figure 9.21. Effects of the permeability ratio k_a/k_w on the (a) normalised matric suction and (b) normalised net stress under the ramped loading

Figure 9.21 presents changes in the matric suction and net stress induced by the ramped loading under the PTIB condition. At the beginning of consolidation, the suction decreases at a very slow rate when $k_a/k_w \geq 1$. Figure 9.21(a) shows that a plateau occurs after the initial reduction of matric suction, and it increases in length as

k_a/k_w increases. A long time after loading, the suction decreases dramatically since the excess pore-water pressures increase significantly compared to the excess pore-air pressures. Particularly, when $k_a/k_w > 1$, the excess pore-air pressures are almost fully dissipated while excess pore-water pressures continue to increase with load. Figure 9.21(b) shows that the net stress increases much faster as k_a/k_w increases.

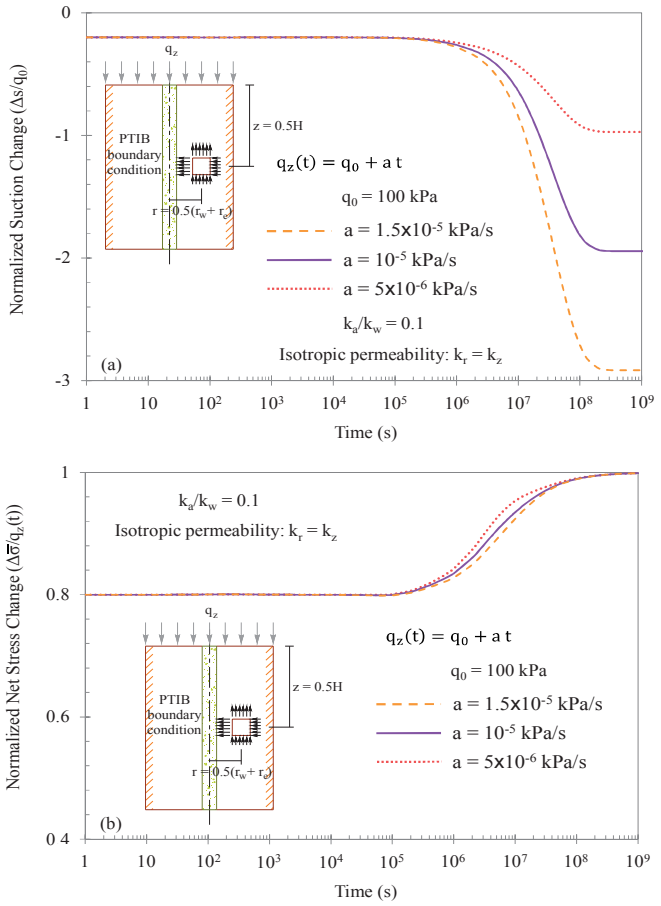

Figure 9.22. Effects of the linear loading parameter 'a' on the (a) normalised matric suction and (b) normalised net stress

By considering the PTIB boundaries, the effects of the linear loading rate 'a' (i.e., ranging from 5×10^{-6} to 1.5×10^{-5} kPa/s) on changes of matric suction and net stress are also investigated in Figure 9.22. As Figure 9.22(a) illustrates, increasing 'a' results in a greater reduction in the suction due to a significant increase in the excess pore-water pressure induced by the ramped loading. The net stress, as shown in Figure 9.22(b), tends to increase more slowly as 'a' increases because the excess pore-air pressure increases with 'a'.

Figure 9.23 demonstrates changes in the matric suction and net stress induced by the asymptotic loading under the PTIB condition. Figure 9.23(a) shows that the matric suction initially decreases and then attains the lowest value due to the full dissipation of excess pore-air pressure. After the plateau period, most of suction patterns, except for $k_a/k_w = 0.1$, significantly increase and approach zero at the same time (i.e., after 10^8 s). In Figure 9.23(b), for $k_a/k_w \leq 10$, the net stress patterns decrease moderately at the early stages as a result of a noticeable increase in the excess pore-air pressure, but they eventually increases and remains constant once the excess pore-air pressure has diminished. It can be observed that the net stress increases more quickly with higher k_a/k_w values.

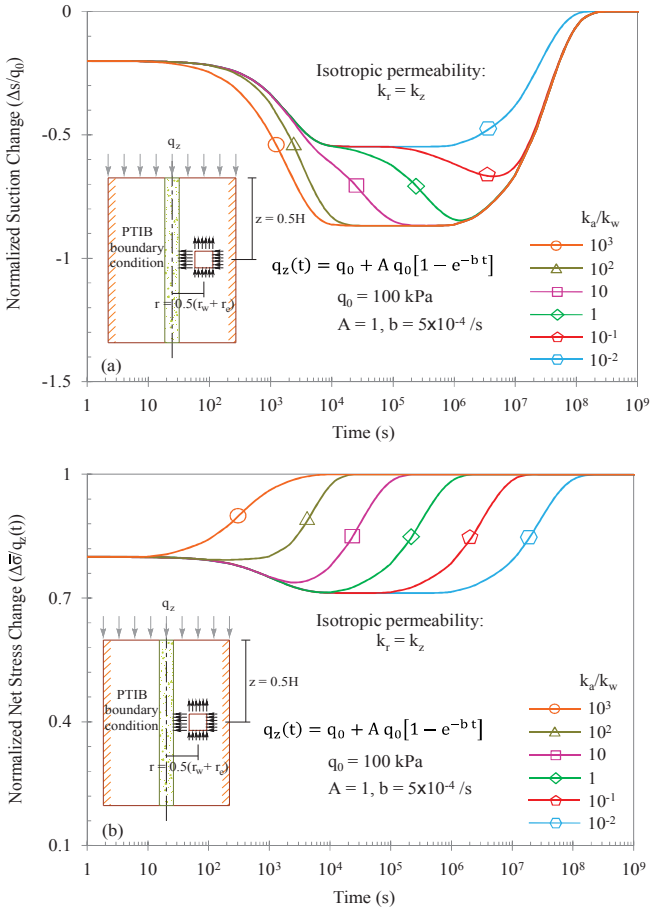

Figure 9.23. Effects of the permeability ratio k_a/k_w on the (a) normalised matric suction and (b) normalised net stress under the asymptotic loading

Figure 9.24 illustrates the effects of the asymptotic loading parameter 'b' (i.e., ranging from 5×10^{-6} to 5×10^{-4} /s) on changes in the matric suction and net stress

while considering the PTIB condition. Here, an increase in 'b' reduces the matric suction faster at the beginning of consolidation, characterizing a clear inverse sigmoid shape, as documented in Figure 9.24(a). After this initial reduction, a plateau appears and may increase in length if 'b' increases. The emergence of plateau period indicates that both excess pore pressures have already approached the highest values and remained constant temporarily prior to dissipation. When 'b' decreases, the plateau in the suctions becomes less obvious. Eventually, the suctions begin to increase at the same rate regardless of the 'b' values until they approach a constant value after 10^8 s. In Figure 9.24(b), there is a slight reduction in the net stress at the beginning of consolidation due to an increase in the excess pore-air pressure, but note that the net stresses decreases faster as 'b' increases. The curves subsequently increase at an almost similar rate until they attain a constant value after 10^8 s.

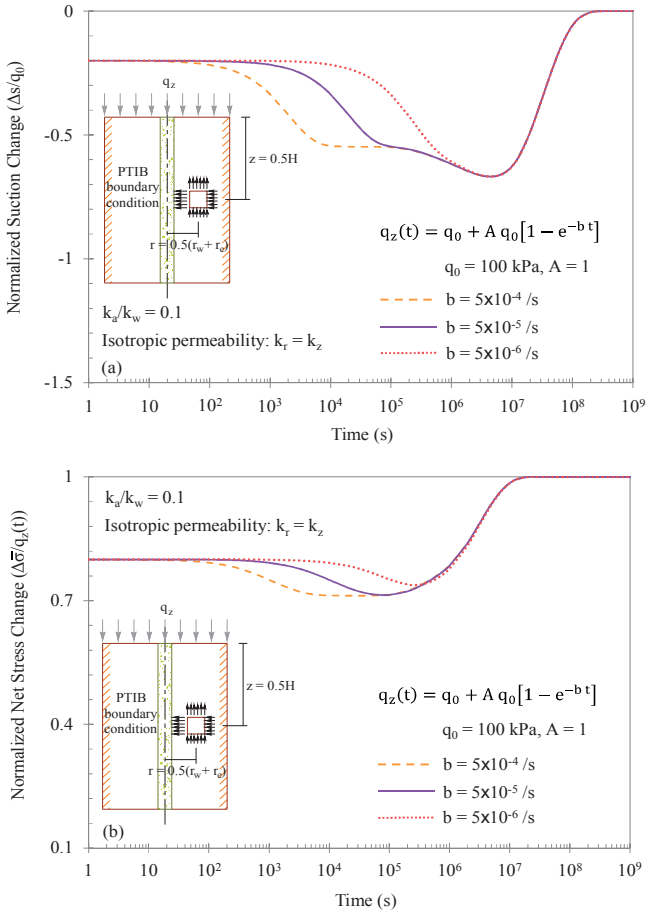

Figure 9.24. Effects of the exponential loading parameter 'b' on the (a) normalised matric suction and (b) normalised net stress

9.5. Summary

The chapter has proposed an analytical method to predict the axisymmetric consolidation of deposits of unsaturated soil subjected to various time-dependent loadings. To obtain the analytical solutions, the mathematical procedure used the separation of variables and Laplace transformation techniques. The polar governing equations for air and water flows were first determined and presented as a set of PDEs, and then general solutions were introduced for those equations. Fourier Bessel and sine series were used to present the functions of radial and vertical flows, respectively. Later, the Laplace and inverse Laplace transformations were applied to obtain the generalized Fourier coefficients and the analytical solutions capturing effects of time-dependent loadings were eventually attained.

The analytical solutions incorporated four time-dependent loading functions, namely ramping, asymptotic, sinusoid, and damped sine wave, and the results were presented through semi-logarithmic graphs. Investigating the effects of permeability ratio k_a/k_w and loading parameters 'a', 'b', 'c', 'ϕ' and 'φ' on the axisymmetric consolidation of unsaturated soils has been the primary purpose of this study. In general, it is concluded that applied loads have minor impacts on changes in excess pore-air pressure for greater k_a/k_w values, but they significantly influence changes in excess pore-water pressure for all k_a/k_w values. The parametric studies show that increasing the loading rates 'a' and 'b', as proposed in the ramped and asymptotic loadings respectively, would result in larger excess pore pressures, whereas the smaller angular frequencies 'ϕ' and 'φ' presented in the sinusoidal and damped sine wave loadings respectively, would expectedly lead to a reduced number of oscillations in both dissipation and settlement. Moreover, the parameter 'c' would help to accelerate the damping process for the dissipation and settlement. The effects of the ratio k_a/k_w and loading parameters 'a' and 'b' on the changes of normalised matric suction and normalised net stress have been also investigated in this study. It is predicted, for both ramped and asymptotic loading cases, that increasing k_a/k_w would lead to a faster initial reduction in suction and increase in net stress. A larger value of 'a' results in a greater reduction in suction and a slower increase in net stress, whereas a larger value of 'b' accelerates the initial reduction of matric suction and net stress.

CHAPTER 10

CONCLUSIONS AND RECOMMENDATIONS

10.1. Summary

Most engineered structures have been built in the arid and semi-arid regions, where the flux boundary problems frequently take place. In these areas, the strata that lie above the water table are generally in an unsaturated state. Humans live in direct contact with the unsaturated zone, known as the vadose zone, and induce significant impacts on the upper ground. These impacts result in a greater need to include unsaturated soil mechanics in geotechnical studies, especially consolidation theory, for the sake of proper structural development. The main objective of this study is to develop novel analytical models to evaluate the time-dependent settlement of an unsaturated soil stratum.

Chapter 1 generally provided an overview of unsaturated soil studies, particularly the consolidation theory and existing predictive models. In addition, the outline and structure of the thesis were also highlighted. Chapter 2, on the other hand, presented a comprehensive literature reviews in regards to development of consolidation theory. In this chapter, definition of unsaturated soils along with important properties was first introduced. This section was then followed by some relevant studies associated with problematic soils, such as collapsible and expansive soils, in arid climatic regions. Chapter 2 also sufficiently discussed the selection of independent stress state variables for constitutive formulations. In particular, combinations of stress variables could be determined on the basis of equilibrium analyses for the unsaturated soil structure. Chapter 2 further showed the volume-mass constitutive equations proposed by Fredlund and his co-workers, describing the volume change of unsaturated soils. Moreover, the proposed models were proven to be valid through rigorous experiments (i.e., triaxial and oedometer tests) conducted by various researchers. Alternative frameworks such as

elastoplastic (EP) models for the volume change prediction were also highlighted in this chapter. Finally, literature review regarding consolidation studies of fully saturated and unsaturated soils was presented. Likewise, several existing models predicting consolidation for both cases were sufficiently discussed in Chapter 2.

Chapter 3 presented a novel analytical solution for the one-dimensional (1D) consolidation of a single-layer unsaturated soil using eigenfunction expansion and Laplace transformation methods. Homogeneous boundary conditions, namely one-way and two-way drainage systems, and two typical cases of initial conditions, including uniform and linear distributions of the initial excess pore pressures, were adopted for the mathematical derivation. Fourier sine series was used to describe the flow patterns whereas the application of Laplace transformation produced a generalised Fourier coefficient (function of time). Consolidation behaviour, in terms of excess pore pressures and settlement, were mainly investigated against the permeability ratio (k_a/k_w). Furthermore, pore pressure isochrones along the vertical direction were graphically presented and discussed. For the verification, the analytical solution showed a good agreement with results obtained from literature, indicating that proposed equations are valid for use.

In Chapter 4, the analytical solution for the 1D consolidation of unsaturated soils was further extended capturing the effects of time-dependent loadings. Four external loads available in engineering practice, such as ramping, asymptotic, sinusoid and damped sine wave, were mathematically simulated and incorporated in the proposed equations. Changes in excess pore-air and pore-water pressure and consolidation settlement were predicted against the permeability ratio, k_a/k_w. Verification for the case of asymptotic loading confirmed the validity of the obtained solutions. Chapter 5, on the other hand, provided an analytical model to predict the soil deformation induced by temperature varying with depth and time. Thermal functions were simulated such that temperature would decrease with depth and vary linearly, exponentially and diurnally with time. Combined effects of temperature variations and constant loading on the excess pore pressure dissipation rates at different depths were highlighted. Soil settlement induced by the temperature changes only and by combined temperature and loading effects was also predicted and discussed.

Chapters 6 and 7 provided analytical solutions for the 2D plane strain consolidation of unsaturated soils subjected to the constant loading and time-dependent loadings (i.e. ramping, asymptotic, sinusoid and damped sine wave), respectively. The studies used Fourier sine series to describe the horizontal and vertical flows (in x- and z-directions, respectively) while Laplace transformation was applied to obtain the function of time. In Chapter 6, uniform and linearly depth dependent initial conditions were adopted for the mathematical derivation. Both chapters analysed the 2D plane strain consolidation against the permeability ratio k_a/k_w. In addition, influences of isotropic and anisotropic permeability conditions on the consolidation were clearly addressed, particularly in Chapter 6. Pore pressure isochrones over flow domains were graphically presented in both chapters. For Chapter 7, effects of loading parameters were analysed through excess pore pressures, settlement and pressure isochrones. Transition exercise from the 2D consolidation equation for the ramped loading to the 1D equation was conducted for verification purposes. A good agreement between the analytical predictions and results available in literature indicates that the proposed solutions are valid.

Lastly, Chapters 8 and 9 provided analytical solutions to predict the axisymmetric consolidation of unsaturated soils subjected to the constant loading and various time-dependent loadings (i.e. ramping, asymptotic, sinusoid and damped sine wave), respectively, under the free strain condition. The vertical drain assisted consolidation could be modelled assuming axisymmetric condition around the drain well. Fourier Bessel series and Laplace transformation were adopted to obtain final solutions. Time-dependent changes in excess pore pressures and settlement varying with k_a/k_w were investigated in both chapters. Chapter 8 demonstrates effects of radial distance from the drain well on the dissipation rate. Besides, variations of suction change were investigated based on different values of k_a/k_w. Likewise, Chapter 9 graphically presented changes in suction and net stress for each loading case.

10.2. Conclusions

In late 1970s, the consolidation studies for unsaturated soils became more prevalent as Fredlund & Hasan (1979) successfully proposed the governing equations describing independent flows of air and water within a soil element. Later, Dakshanamurthy & Fredlund (1980), and Dakshanamurthy et al. (1984) accomplished the consolidation

theories by expanding the existing equations to two-dimensional (2D) and three-dimensional (3D) consolidation equations, respectively. Unlike saturated soil mechanics, the consideration of the air phase in these theories has been a major challenge in estimating the dissipation of excess pore pressures and settlement.

Past decades have seen a notable growth in numerical models to predict the time-dependent deformation of unsaturated soils. Evidently, some well-recognised solutions were obtained using the finite element method for coupled 3D consolidation (e.g. Wong et al. 1998), the finite element approximation for coupled and uncoupled 2D plane strain consolidation (e.g. Conte 2004), and the differential quadrature method (DQM) for axisymmetric consolidation (e.g. Zhou 2013). On the other hand, there has been limited analytical research due to the complexity of consolidation problems. Most analytical procedure have been conducted adopting consolidation theory proposed by Fredlund & Hasan (1979). Among initial studies, Qin et al. (2008) provided an analytical solution for the 1D consolidation employing Cayley-Hamilton and Laplace transformation techniques. Although the verification exercise demonstrates the validity of the analytical prediction, the adopted procedure exhibits some cumbersome evaluations associated with complex arguments. The solution proposed by Qin et al. (2008) therefore may offer limited application. Shan et al. (2012) and Zhou et al. (2014) dealt with unsaturated consolidation problems using alternative solutions, ψ_i and ϕ_i, respectively, such that the nonhomogeneous partial differential equations (PDEs) would be converted to the homogeneous forms to handle final solutions easily. Final equations in these studies, however, are not properly presented, leading to uncertainty in verification. Furthermore, final solution provided by Zhou et al. (2014) may be mathematically undefined when the soil becomes fully saturated.

In an attempt to propose a simple yet effective solution for the consolidation of unsaturated soil deposits, eigenfunction expansion and Laplace transformation techniques have been adopted for the analytical development. The selection of the above mentioned techniques would allow the general solution to be expressed in a series of the eigenfunction of the related homogeneous problem. This indicates that the nonhomogeneous equations for unsaturated consolidation can be solved directly without an intermediate step of converting the nonhomogeneous PDEs to the homogeneous PDEs as performed by Shan et al. (2012). Furthermore, these techniques would also

produce a closed-form solution that can smoothly convert to the classical solution for saturated soils given by Terzaghi (1925). Governing equations proposed by Fredlund and his co-workers (e.g. Fredlund & Hasan 1979; Dakshanamurthy & Fredlund 1980, 1981; Darkshanamurthy et al. 1984) were adopted for mathematical formulations.

The development of analytical solutions for the unsaturated consolidation would provide fundamental understandings of time-dependent deformation of unsaturated soils and influencing factors (e.g. external loads, temperature variations etc.). For the study of the 1D consolidation of unsaturated soils, the permeability ratio k_a/k_w has significant impacts on the rates of excess pore-air and pore-water pressure dissipation and consolidation settlement. In particular, when considering a uniform initial condition, increasing k_a/k_w values characterise a double inverse sigmoid in both excess pore-water and settlement curves, and a single inverse sigmoid in excess-air pressure curves. It is also found that the excess pore-air pressure tends to dissipate more quickly as k_a/k_w increases. Furthermore, the complete dissipation of excess-pore air pressure would result in delay period in the excess pore-water pressure curve. On the other hand, the study demonstrates that the consolidation in the two-way drainage system proceeds faster than that in the one-way drainage system. For the case of linear initial condition, the rapid reduction in distributions of initial pore pressures with depth would lead to reduced average excess pore-air and pore-water pressures at the beginning of consolidation. During the dissipation process, both excess pore pressure patterns (with the similar k_a/k_w value) vary due to different initial conditions. However, these pressures would later diminish at the same time. Validation exercise of this study was implemented by comparing results with an existing model (Shan et al. 2012), suggesting that the proposed equations are valid for practical use.

On the other hand, effects of time-dependent loadings, namely ramping, asymptotic, sinusoid and damped sine wave, on the 1D consolidation of unsaturated soils were sufficiently investigated. Changes in excess pore-water pressure (for any value of k_a/k_w) correspondingly reflect the above mentioned loading patterns due to the slow dissipation process. However, as k_a/k_w increases, the excess pore-air pressure, induced by adopted loads, may dissipate significantly while the load is being applied. Thus, external loadings, except for the damped sine wave, may have less pronounced impacts on the excess pore-air pressure dissipation with large k_a/k_w values. Verification

exercise shows a good agreement between the proposed model and existing results given by Shan et al. (2012).

In addition, significant influences of time-dependent temperature variations on the 1D deformation of unsaturated soils were rigorously studied. Changes in temperature were simulated under the time-dependent linear, exponential and diurnal functions, and then were incorporated in the general solution. For the time-dependent linear temperature variations, excess pore-air pressure attains a constant value whereas the excess pore-water pressure diminishes a very long time after the heat begins to increase. Besides, when the temperature increases exponentially, it is predicted that excess pore pressures near the ground surface would increase faster than those at lower depths. Once the temperature approaches the maximum value, both excess pore-air and pore-water pressures would be fully dissipated. For the case of diurnal temperature wave, oscillations in the excess pore pressure curves can be observed. These oscillations are characterised by heat generated on the basis of regular succession of days and nights. Since heat is transmitted through the soil profile very slowly, the excess pore pressure curves would experience the damping and retarding effects.

For the study of the 2D plane strain consolidation, the isotropic permeability (i.e., $k_x/k_z = 1$) and anisotropic permeability (i.e., $k_x/k_z \neq 1$) conditions were highlighted. Under the constant loading, it is predicted that increases in the horizontal to vertical permeability ratio (k_x/k_z) lead to faster dissipation rate of excess pore pressures, and thus faster consolidation rate. Indeed, effects of vertical drainage boundaries on the dissipation process are much attenuated with increasing k_x/k_z. It was also concluded that the rate of consolidation under the one-way drainage system would be very similar to that under the two-way drainage system because the vertical drains installed in the soil stratum allows a large amount of excess pore pressures to be dissipated horizontally. It is worth mentioning that the proposed equations for 2D consolidation of unsaturated soils subjected to the constant loading can convert back to the classical consolidation equation presented by Terzaghi (1925). Considering the soil compression under the time-dependent loadings (i.e. ramping, asymptotic, sinusoid and damped sine wave), the excess pore-water pressures and settlement would change corresponding to a particular loading function, similar to the 1D consolidation study. Excess pore-air pressure with large k_a/k_w, on the other hand, is insignificantly affected by the external

applied loads, except for the case of damped sine wave. With the adopted loading parameters, the damped loading results in significant oscillations in excess pore pressures and settlement at the beginning of consolidation regardless of k_a/k_w values.

For the study of axisymmetric consolidation of unsaturated soils induced by the radial flows of air and water only, the excess pore-air and pore-water pressures are prone to dissipate more quickly for the point of investigation closer to the drain well. For the consolidation induced by both radial and vertical flows, it is predicted that the excess pore pressure dissipations assisted by the pervious top – impervious base (PTIB) boundaries of the soil have comparable rates with those in the pervious top – pervious base (PTPB) boundaries. This finding implies that the radial flow, as induced by the drains, governs the dissipation process. The study also shows that the consolidation of unsaturated soil deposits is ascribed initially to the increase in the net stress and subsequently to the increase in the matric suction. On the other hand, significant effects of radial distance on the pore pressure isochrones were highlighted. More specifically, excess pore-air and pore-water pressures tend to increase when the point of investigation is farther away from the drain well. However, if the point of interest is very close to the boundary of influence zone (r_e), the effects of radial distance will be insignificant.

This research has established a comprehensive catalogue of analytical models for the consolidation of unsaturated soils capturing various initial and loading conditions. The research areas are systematically provided in three categories: (1) 1D consolidation, (2) 2D plane strain consolidation, and (3) free strain axisymmetric consolidation. The proposed solutions, which predict excess pore pressure dissipation and settlement, can smoothly convert back to the traditional equation given by Terzaghi (1925) when the soil is fully saturated. Additionally, verification exercises indicate that these solutions are valid for practical use. In particular, practicing engineers may adopt some programmable methods such as Microsoft Excel and MATLAB software to generate results from these proposed equations and predict time-dependent deformation of unsaturated soil deposits.

10.3. Recommendations for future studies

Although the unsaturated consolidation studies have been systematically presented in this thesis, the research areas can be further expanded to conduct the following aspects:

- The proposed analytical models were determined based on the assumption of constant stiffness parameters for unsaturated soils. This indicates that the coefficients of volume change (i.e., m_1^s, m_2^s, m_1^w and m_2^w) are considered to be constant within a very small stress increment. This assumption is acceptable for predicting soil deformation during a transient process at a particular stress increment. Furthermore, it is also necessary to adopt this assumption in order to achieve the analytical procedure. To improve the reliability of the model, volume change coefficients can be expressed as nonlinear functions capturing complex rheological effects such as viscoelastic behaviour.
- Current research emphasises the consolidation analyses for the homogeneous single-layer soil only. In order to conduct a more rigorous and reliable analysis, multi-layered unsaturated soils, whose properties may vary in each layer, are recommended for the future work.
- For the sake of simple evaluations, the coefficients of permeability with respect to the air phase (k_a) and water phase (k_w) were assumed constant during the consolidation. They are, however, functions of the porosity and the degree of saturation of soil and change with time. These coefficients have been reported as nonlinear properties in many existing literature. Thus, for the future work, it is recommended that these permeability coefficients can be simulated as functions of void ratio (volumetric strain), and included in the solution.
- For the sake of simplicity purposes, the proposed analytical solutions were obtained capturing the typical homogeneous boundary conditions. The future study may include the time-dependent boundary conditions to derive more rigorous equations.
- In the study of axisymmetric consolidation, the analytical procedure was conducted on the basis of free strain analysis only. There have been some theoretical uncertainties when dealing with the equal strain consolidation of unsaturated soils. Future research may invest more on the equal strain hypothesis for the sake of proper estimation. Besides, the effects of smear zone properties and well resistance are essential for the axisymmetric consolidation studies.

- There has been hitherto limited research on the elastic visco-plastic (EVP) to evaluate creep behaviour of unsaturated soils. Theoretically, when the excess pore pressures have diminished, the soil stratum may continue to settle due to the rearrangement of soil structure under loading. The future study can develop the EVP theory for unsaturated soils employing the proposed consolidation equations.

REFERENCES

Aitchison, G 1961, 'Relationships of moisture stress and effective stress functions in unsaturated soils', *Conference of the British National Society of The International Society for Soil Mechanics and Foundation Engineering*, London, United Kingdom, pp. 47-52.

Al-Homoud, A, Basma, A, Husein Malkawi, A & Al Bashabsheh, M 1995, 'Cyclic swelling behavior of clays', *Journal of Geotechnical Engineering*, vol. 121, no. 7, pp. 562-565.

Alonso, EE, Gens, A & Hight, D 1987, 'Special problem soils. General report', *Proceedings of the 9th European Conference on Soil Mechanics and Foundation Engineering*, Dublin, vol. 3, pp. 1087-1146.

Alonso, EE, Gens, A & Josa, A 1990, 'A constitutive model for partially saturated soils', *Géotechnique*, vol. 40, no. 3, pp. 405-430.

Alonso, EE, Pereira, JM, Vaunat, J & Olivella, S 2010, 'A microstructurally based effective stress for unsaturated soils', *Géotechnique*, vol. 60, no. 12, pp. 913-925.

Alsherif, NA & McCartney, JS 2015, 'Thermal behaviour of unsaturated silt at high suction magnitudes', *Géotechnique*, vol. 65, no. 9, pp. 703-716.

Anayev, V & Volyanick, N 1986, 'Engineering geologic peculiarities of construction work on loessial soils', *Proceedings of the 5th International Congress of the Association of Engineering Geologists*, vol. 2, pp. 659-665.

Aysen, A 2002, *Soil mechanics: basic concepts and engineering applications*, CRC Press, Lisse, Netherlands.

Barden, L 1965, 'Consolidation of compacted and unsaturated clays', *Géotechnique*, vol. 15, no. 3, pp. 267-286.

Barden, L 1974, 'Consolidation of clays compacted 'dry'and 'wet'of optimum water content', *Géotechnique*, vol. 24, no. 4, pp. 605-625.

Barden, L, Madedor, AO & Sides, GR 1969, 'Volume change characteristics of unsaturated clay', *Journal of Soil Mechanics and Foundations Division*, vol. 95, pp. 32-52.

Barron, RA 1948, 'Consolidation of fine-grained soils by drain wells', *Transaction of ASCE*, vol. 113, pp. 718-742.

Basu, D & Prezzi, M 2007, 'Effect of the smear and transition zones around prefabricated vertical drains installed in a triangular pattern on the rate of soil consolidation', *International Journal of Geomechanics*, vol. 7, no. 1, pp. 34-43.

Bell, F & Culshaw, M 2001, 'Problem soils: a review from a British perspective', *Proceedings of Problematic Soils Conference*, Nottingham, pp. 1-37.

Bell, F & Maud, R 1995, 'Expansive clays and construction, especially of low-rise structures: a viewpoint from Natal, South Africa', *Environmental & Engineering Geoscience*, vol. 1, no. 1, pp. 41-59.

Biot, MA 1941, 'General theory of three-dimensional consolidation', *Journal of Applied Physics*, vol. 12, no. 2, pp. 155-164.

Bishop, AW 1959, *The principles of effective stress*, Lecture delivered in Oslo, Norway, Technisk Ukeblad, vol. 106, no. 39, pp. 859-863.

Bishop, AW & Blight, G 1963, 'Some aspects of effective stress in saturated and partly saturated soils', *Géotechnique*, vol. 13, no. 3, pp. 177-197.

Bishop, AW & Eldin, G 1950, 'Undrained triaxial tests on saturated sands and their significance in the general theory of shear strength', *Géotechnique*, vol. 2, no. 1, pp. 13-32.

Blight, G 1965, 'A study of effective stresses for volume change', *Moisture Equilibria and Moisture Changes in Soils Beneath Covered Areas*, Butterworth, Sydney, Australia, pp. 259-269.

Blight, G 1984, 'Uplift forces measured in piles in expansive clay', *Proceedings of the 5th International Conference on Expansive Soils*, Adelaide, pp. 240-244.

Blight, GE 1961, *Strength and consolidation characteristics of compacted soils*, PhD thesis, University of London, London, England, 217 pp.

Blight, GE 1971, 'Flow of air through soils', *Journal of Soil Mechanics and Foundations Division*, vol. 97, no. SM4, pp. 607-624.

Bolzon, G, Schrefler, B & Zienkiewicz, O 1996, 'Elastoplastic soil constitutive laws generalized to partially saturated states', *Géotechnique*, vol. 46, no. 2, pp. 279-289.

Bouwer, H 1978, *Groundwater hydrology*, vol. 480, McGraw-Hill, New York.

Brackley, I 1971, 'Partial collapse in unsaturated expansive clay', *Proceedings of the 5th Regional Conference for Africa Soil Mechanics and Foundation Engineering*, pp. 23-30.

Budhu, M 2008, *Soil mechanics and foundations,* John Wiley and Sons, Hoboken.

Building Research Establishment 1993, *Low-rise buildings on shrinkable clay soils: BRE Digest*, vols. 240, 241 & 242, CRC, London.

Burland, J 1964, 'Effective stresses in partly saturated soils', *Géotechnique*, vol. 14, no. 1, pp. 64-68.

Buscarnera, G & Nova, R 2009, 'An elastoplastic strainhardening model for soil allowing for hydraulic bonding–debonding effects', *International Journal for Numerical and Analytical Methods in Geomechanics*, vol. 33, no. 8, pp. 1055-1086.

Cameron, D 2001, 'The extent of soil desiccation near trees in a semi-arid environment', *Geotechnical and Geological Engineering*, vol. 19, pp. 357-370.

Cameron, D & Mills, K 2009, 'Tree water use, soil suctions and reference evapotranspiration in a semi-arid climate', *Proceedings of the 4th Asia-Pacific Conference Unsaturated Soils*, vol. 1, pp. 295-300.

Chai, JC & Miura, N 1999, 'Investigation of factors affecting vertical drain behavior', *Journal of Geotechnical and Geoenvironmental Engineering*, vol. 125, no. 3, pp. 216-226.

Chen, FH 2012, *Foundations on expansive soils*, vol. 12, Elsevier, Denver.

Childs, EC & Collis-George, N 1950, 'The permeability of porous materials', *Proceedings of the Royal Society of London. Series A. Mathematical and Physical Sciences*, vol. 201, no. 1066, pp. 392-405.

Chiu, C & Ng, C 2003, 'A state-dependent elasto-plastic model for saturated and unsaturated soils', *Géotechnique*, vol. 53, no. 9, pp. 809-829.

Clevenger, WA 1956, 'Experiences with Loess as Foundation Materials', *Journal of the Soil Mechanics and Foundations Division*, vol. 82, no. 3, pp. 1-26.

Coduto, DP & Huitric, R 1990, 'Monitoring landfill movements using precise instruments', *ASTM Special Technical Publication*, no. 1070, pp. 358-370.

Coduto, DP, Yeung, MR & Kitch, WA 2011, *Geotechnical engineering: principles and practices*, Pearson Higher Education, Upper Saddle River.

Coleman, J 1962, 'Correspondence', *Géotechnique*, vol. 12, no. 4, pp. 348-350.

Conte, E 2004, 'Consolidation analysis for unsaturated soils', *Canadian Geotechnical Journal*, vol. 41, no. 4, pp. 599-612.

Conte, E 2006, 'Plane strain and axially symmetric consolidation in unsaturated soils', *International Journal of Geomechanics*, vol. 6, no. 2, pp. 131-135.

Conte, E & Troncone, A 2009, 'Radial consolidation with vertical drains and general time-dependent loading', *Canadian Geotechnical Journal*, vol. 46, no. 1, pp. 25-36.

Craig, RF 2004, *Craig's soil mechanics*, Spon Press, Taylor and Francis Group, New York.

Croney, D, Coleman, JD & Black, WPM 1958, 'Movement and distribution of water in soil in relation to highway design and performance', *Water and Its Conduction in Soils*, Washington DC, no. 40, pp. 226-252.

Crump, KS 1976, 'Numerical inversion of Laplace transforms using a Fourier series approximation', *Journal of the ACM (JACM)*, vol. 23, no. 1, pp. 89-96.

Cryer, C 1963, 'A comparison of the three-dimensional consolidation theories of Biot and Terzaghi', *The Quarterly Journal of Mechanics and Applied Mathematics*, vol. 16, no. 4, pp. 401-412.

Cui, Y & Delage, P 1996, 'Yielding and plastic behaviour of an unsaturated compacted silt', *Géotechnique*, vol. 46, no. 2, pp. 291-311.

Cuisinier, O & Laloui, L 2004, 'Fabric evolution during hydro-mechanical loading of a compacted silt', *International Journal for Numerical and Analytical Methods in Geomechanics*, vol. 28, no. 6, pp. 483-499.

Dakshanamurthy, V & Fredlund, D 1980, 'Moisture and air flow in an unsaturated soil', *Proceedings of the 4th International Conference on Expansive Soils*, ASCE, pp. 514-532.

Dakshanamurthy, V & Fredlund, D 1981, 'A mathematical model for predicting moisture flow in an unsaturated soil under hydraulic and temperature gradients', *Water Resources Research*, vol. 17, no. 3, pp. 714-722.

Darkshanamurthy, V, Fredlund, D & Rahardjo, H 1984, 'Coupled three-dimensional consolidation theory of unsaturated porous media', *Proceedings of the 5th International Conference on Expansive Soils*, pp. 99-103.

Das, BM & Sobhan, K 2013, *Principles of geotechnical engineering*, Cengage Learning, Stamford.

Day, RW 1994, 'Swell-shrink behaviour of compacted clay', *Journal of Geotechnical Engineering*, vol. 120, no. 3, pp. 618-623.

Delage, P, Audiguier, M, Cui, YJ & Howat, MD 1996, 'Microstructure of a compacted silt', *Canadian Geotechnical Journal*, vol. 33, no. 1, pp. 150-158.

Delage, P & Graham, J 1995, 'Understanding the behaviour of unsaturated soils requires reliable conceptual models: state of the art report', *Proceedings of the 1st International Conference on Unsaturated Soils*, Balkema, Rotterdam, vol. 3, pp. 1223-1256.

Delage, P & Lefebvre, G 1984, 'Study of the structure of a sensitive Champlain clay and of its evolution during consolidation', *Canadian Geotechnical Journal*, vol. 21, no. 1, pp. 21-35.

Deng, YB, Xie, KH & Lu, MM 2013, 'Consolidation by vertical drains when the discharge capacity varies with depth and time', *Computers and Geotechnics*, vol. 48, pp. 1-8.

Dregne, HE 2011, *Soils of arid regions*, vol. 6, Elsevier Scientific Publishing Company, Amsterdam.

Dunn, IS, Anderson, LR & Kiefer, FW 1980, *Fundamentals of geotechnical analysis*, John Wiley and Sons, New York.

Edlefsen, NE & Anderson, AB 1943, 'Thermodynamics of soil moisture', *Hilgardia: A Journal of Agricultural Science Published by the California Agricultural Experiment Station*, vol. 15, no. 2, pp. 31-298.

Fang, HY 2013, *Foundation engineering handbook*, Springer Science and Business Media, New York.

Feng, G, Meiri, A & Letey, J 2003, 'Evaluation of a model for irrigation management under saline conditions', *Soil Science Society of America Journal*, vol. 67, no. 1, pp. 71-76.

Fookes, PG & Parry, RHG 1994, *Engineering characteristics of arid soils*, International Symposium on Engineering Characteristics of Arid Soils, AA Balkema.

Fredlund, DG 1984, 'Consolidation of unsaturated porous media', *Fundamentals of Transport Phenomena in Porous Media*, pp. 525-578.

Fredlund, DG 1987, 'The stress state for expansive soils', *Proceedings of the 6th International Conference on Expansive Soils*, Centre Board of Irrigation and Power, New Delhi, India, pp. 1-9.

Fredlund, DG 1996, 'The scope of unsaturated soil mechanics: An overview', *Proceedings of the 1st International Conference on Unsaturated Soils*, Paris, vol. 3, pp. 1155-1177.

Fredlund, DG 2014, 'The emergence of unsaturated soil mechanics', *Canadian Geotechnical Journal*, vol. 51, no. 12, pp. 9-10.

Fredlund, DG & Hasan, JU 1979, 'One-dimensional consolidation theory: unsaturated soils', *Canadian Geotechnical Journal*, vol. 16, no. 3, pp. 521-531.

Fredlund, DG & Morgenstern, NR 1977, 'Stress state variables for unsaturated soils', *Journal of Geotechnical and Geoenvironmental Engineering*, vol. 103, no. ASCE 12919, pp. 447-466.

Fredlund, DG & Rahardjo, H 1986, 'Unsaturated soil consolidation theory and laboratory experimental data', *Canadian Geotechnical Journal*, pp. 450-456.

Fredlund, DG & Rahardjo, H 1993, *Soil mechanics for unsaturated soils*, John Wiley and Sons, New York.

Fredlund, DG, Rahardjo, H & Fredlund, MD 2012, *Unsaturated soil mechanics in engineering practice*, John Wiley and Sons, New Jersey.

Fritz, SJ & Marine, IW 1983, 'Experimental support for a predictive osmotic model of clay membranes', *Geochimica et Cosmochimica Acta*, vol. 47, no. 8, pp. 1515-1522.

Fung, Y 1965, *Foundations of solid mechanics*, Prentice Hall, New Jersey.

Gallipoli, D, Gens, A, Sharma, R & Vaunat, J 2003, 'An elasto-plastic model for unsaturated soil incorporating the effects of suction and degree of saturation on mechanical behaviour', *Géotechnique*, vol. 53, no. 1, pp. 123-136.

Gao, GY, Peng, ZG, Jiang, JP & Gu, BH 2007, 'Vertical bearing behavior of belled pier in thick loess-like soil', *Rock and Soil Mechanics*, vol. 28, no. 6, pp. 1167-1171.

Geng, X, Indraratna, B & Rujikiatkamjorn, C 2010, 'Analytical solutions for a single vertical drain with vacuum and time-dependent surcharge preloading in membrane and membraneless systems', *International Journal of Geomechanics*, vol. 12, no. 1, pp. 27-42.

Georgiadis, K, Potts, DM & Zdravkovic, L 2005, 'Three-dimensional constitutive model for partially and fully saturated soils', *International Journal of Geomechanics*, vol. 5, no. 3, pp. 244-255.

Gibbs, HJ & Bara, JP 1962, *Predicting surface subsidence from basic soil tests*, ASTM Special Technical Publication, pp. 231-246.

Gibson, R, Schiffman, R & Pu, S 1970, 'Plane strain and axially symmetric consolidation of a clay layer on a smooth impervious base', *The Quarterly Journal of Mechanics and Applied Mathematics*, vol. 23, no. 4, pp. 505-520.

Graham, J, Oswell, J & Gray, M 1992, 'The effective stress concept in saturated sand-clay buffer', *Canadian Geotechnical Journal*, vol. 29, no. 6, pp. 1033-1043.

Haberman, R 2012, *Applied partial differential equations: with Fourier series and boundary value problems*, Pearson Higher Education, Massachusetts.

Handy, RL 1973, 'Collapsible loess in Iowa', *Soil Science Society of America Journal*, vol. 37, no. 2, pp. 281-284.

Hansbo, S 1981, 'Consolidation of fine-grained soils by prefabricated drains', *Proceedings of the 10th International Conference on Soil Mechanics and Foundation Engineering*, Stockholm, vol. 3, pp. 677-682.

Hansbo, S 1986, 'Preconsolidation of soft compressible subsoil by the use of prefabricated vertical drains', *Annales des Travaux Publics de Belgique*, vol. 6, pp. 553-563.

Hansbo, S 1987, 'Design aspects of vertical drains and lime column installations', *Southeast Asian Geotechnical Conference*, vol. 9, pp. 1-12.

Hillel, D 2003, *Introduction to environmental soil physics*, Elsevier Academic Press, California.

Hird, C & Moseley, V 2000, 'Model study of seepage in smear zones around vertical drains in layered soil', *Géotechnique*, vol. 50, no. 1, pp. 89-97.

Ho, L, Fatahi, B & Khabbaz, H 2014, 'Analytical solution for one-dimensional consolidation of unsaturated soils using eigenfunction expansion method', *International Journal for Numerical and Analytical Methods in Geomechanics*, vol. 38, no. 10, pp. 1058-1077.

Ho, L, Fatahi, B & Khabbaz, H 2016, 'Analytical solution to axisymmetric consolidation in unsaturated soils with linearly depth-dependent initial conditions', *Computers and Geotechnics*, vol. 74, pp. 102-121.

Holtz, RD 1987, 'Preloading with prefabricated vertical strip drains', *Geotextiles and Geomembranes*, vol. 6, no. 1, pp. 109-131.

Holtz, RD & Holm, B 1973, 'Excavation and sampling around some sand drains at Ska-Edeby, Sweden', *Proceedings of Specialty Conference on Performance on Earth and Earth Supported Structure*, Purdue University, vol. 1, pp. 435-464.

Holtz, RD, Jamiolkowski, M, Lancellotta, R & Pedroni, R 1991, *Prefabricated vertical drains: design and performance*, Construction Industry Research and Information, London.

Holtz, RD & Kovacs, WD 1981, *An introduction to geotechnical engineering*, Prentice Hall, New Jersey.

Horne, M 1964, 'The consolidation of a stratified soil with vertical and horizontal drainage', *International Journal of Mechanical Sciences*, vol. 6, no. 2, pp. 187-197.

Houston, S 1996, 'Foundations and pavements on unsaturated soils. Part one: Collapsible soils', *Proceedings of the 1st International Conference on Unsaturated Soils*, Paris, vol. 3, pp. 1421-1439.

Houston, SL, Houston, WN & Spadola, DJ 1988, 'Prediction of field collapse of soils due to wetting', *Journal of Geotechnical Engineering*, vol. 114, no. 1, pp. 40-58.

Houston, SL, Houston, WN, Zapata, CE & Lawrence, C 2001, 'Geotechnical engineering practice for collapsible soils', *Geotechnical and Geological Engineering*, vol. 19, pp. 333-355.

Hung, VQ 2002, *Uncoupled and coupled solutions of volume change problems in expansive soils*, PhD thesis, University of Saskatchewan, Saskatoon.

Indraratna, B & Bamunawita, C 2002, 'Soft clay stabilisation by mandrel driven geosynthetic vertical drains', *Australian Geomechanics*, vol. 37, no. 5, pp. 57-86.

Indraratna, B, Perera, D, Rujikiatkamjorn, C & Kelly, R 2014, 'Soil disturbance analysis due to vertical drain installation', *Proceedings of the Institution of Civil Engineering-Geotechnical Engineering*, vol. 168, no. 3, pp. 236-246.

Indraratna, B & Redana, I 1997, 'Plane-strain modelling of smear effects associated with vertical drains', *Journal of Geotechnical and Geoenvironmental Engineering*, vol. 123, no. 5, pp. 474-478.

Indraratna, B, Rujikiatkamjorn, C & Sathananthan, I 2005a, 'Radial consolidation of clay using compressibility indices and varying horizontal permeability', *Canadian Geotechnical Journal*, vol. 42, no. 5, pp. 1330-1341.

Indraratna, B, Sathananthan, I, Rujikiatkamjorn, C & Balasubramaniam, A 2005b, 'Analytical and numerical modeling of soft soil stabilized by prefabricated vertical drains incorporating vacuum preloading', *International Journal of Geomechanics*, vol. 5, no. 2, pp. 114-124.

Indraratna, B, Rujikiatkamjorn, C & Sathananthan, I 2005c, 'Analytical and numerical solutions for a single vertical drain including the effects of vacuum preloading', *Canadian Geotechnical Journal*, vol. 42, no. 4, pp. 994-1014.

Jamiolkowski, M, Lancellotta, R & Wolski, W 1983, 'Precompression and speeding up consolidation', *Proceedings of the 8th International Conference on Soil Mechanics and Foundation Engineering*, vol. 3, pp. 1201-1206.

Jennings, J 1960, 'A revised effective stress law for use in the prediction of the behaviour of unsaturated soils', in *Pore Pressure and Suction in Soils*, London, pp. 26-30.

Jennings, J & Burland, J 1962, 'Limitations to the use of effective stresses in partly saturated soils', *Géotechnique*, vol. 12, no. 2, pp. 125-144.

Jones, LD & Jefferson, I 2012, 'Expansive soils' in *Institution of Civil Engineers Manual Series*, ICE Publishing, London, pp. 413-441.

Jumikis, AR 1969, *Theoretical soil mechanics*, Van Nostrand Reinhold, Princeton, New York.

Katti, RK & Katti, AR 1994, *Behaviour of saturated expansive soil and control methods*, CRC Press, AA Balkema.

Kaye, GWC & Laby, TH 1921, 'Tables of physical and chemical constants', *Journal of the Rontgen Society*, vol. 17, no. 67, pp. 92-93.

Khalili, N & Khabbaz, H 1998, 'A unique relationship of chi for the determination of the shear strength of unsaturated soils', *Géotechnique*, vol. 48, no. 5, pp. 681-687.

Kohgo, Y, Nakano, M & Miyazaki, T 1993, 'Theoretical aspects of constitutive modelling for unsaturated soils', *Soils and Foundations*, vol. 33, no. 4, pp. 49-63.

Koliji, A, Laloui, L, Cuisinier, O & Vulliet, L 2006, 'Suction induced effects on the fabric of a structured soil', *Transport in Porous Media*, vol. 64, no. 2, pp. 261-278.

Koliji, A, Vulliet, L & Laloui, L 2010, 'Structural characterisation of unsaturated aggregated soil', *Canadian Geotechnical Journal*, vol. 47, no. 3, pp. 297-311.

Krahn, J & Fredlund, DG 1972, 'On total, matric and osmotic suction', *Journal of Soil Science*, vol. 114, no. 5, pp. 339-348.

Lambe, TW & Whitman, RV 2008, *Soil mechanics SI version*, John Wiley and Sons, Delhi.

Le, TM, Fatahi, B & Khabbaz, H 2015, 'Numerical optimisation to obtain elastic viscoplastic model parameters for soft clay', *International Journal of Plasticity*, vol. 65, pp. 1-21.

Lei, GH, Zheng, Q, Ng, CWW, Chiu, ACF & Xu, B 2015, 'An analytical solution for consolidation with vertical drains under multi-ramp loading', *Géotechnique*, vol. 65, no. 7, pp. 531-547.

Leo, CJ 2004, 'Equal Strain Consolidation by Vertical Drains', *Journal of Geotechnical and Geoenvironmental Engineering*, vol. 130, no. 3, pp. 316-327.

Lloret, A & Alonso, E 1980, 'Consolidation of unsaturated soils including swelling and collapse behaviour', *Géotechnique*, vol. 30, no. 4, pp. 449-477.

Loret, B & Khalili, N 2000, 'A three-phase model for unsaturated soils', *International Journal for Numerical and Analytical Methods in Geomechanics*, vol. 24, no. 11, pp. 893-927.

Loret, B & Khalili, N 2002, 'An effective stress elastic–plastic model for unsaturated porous media', *Mechanics of Materials*, vol. 34, no. 2, pp. 97-116.

Lu, MM, Wang, SY, Sloan, SW, Indraratna, B & Xie, KH 2015, 'Nonlinear radial consolidation of vertical drains under a general time-variable loading', *International Journal for Numerical and Analytical Methods in Geomechanics*, vol. 39, no. 1, pp. 51-62.

Lutenegger, AJ 1986, 'Dynamic compaction in friable loess', *Journal of Geotechnical Engineering*, vol. 112, no. 6, pp. 663-667.

Mandel, J 1953, 'Consolidation Des Sols', *Géotechnique*, vol. 3, no. 7, pp. 287-299.

Marshall, TJ, Holmes, JW & Rose, CW 1996, *Soil physics*, Cambridge University Press, Cambridge.

Matyas, EL & Radhakrishna, H 1968, 'Volume change characteristics of partially saturated soils', *Géotechnique*, vol. 18, no. 4, pp. 432-448.

Means, RE & Parcher, JV 1963, *Physical properties of soils*, Charles E. Merrill Books, Ohio.

Mendoza, C, Colmenares, J & Merchan, V 2005, 'Stiffness of an unsaturated compacted clayey soil at very small strains', in *Conference on Advanced Experimental Unsaturated Soil Mechanics*, Trento, pp. 199-204.

Mesri, G, Lo, DOK & Feng, TW 1994, 'Settlement of embankments on soft clays', *Vertical and Horizontal Deformations of Foundations and Embankments*, ASCE, pp. 8-56.

Nelson, JD & Miller, DJ 1997, *Expansive soils: problems and practice in foundation and pavement engineering*, John Wiley and Sons, New York.

Morgenstern, N 1979, 'Properties of compacted soils', *Proceedings of 6th Panamerican Conference on Soil Mechanics and Foundation Engineering*, Lima, vol. 3, pp. 349-354.

Morris, P 2002, 'Analytical solutions of linear finite-strain one-dimensional consolidation', *Journal of Geotechnical and Geoenvironmental Engineering*, vol. 128, no. 4, pp. 319-326.

Morris, P 2005, 'Analytical solutions of linear finite-and small-strain one-dimensional consolidation', *International Journal for Numerical and Analytical Methods in Geomechanics*, vol. 29, no. 2, pp. 127-140.

Murray, EJ & Sivakumar, V 2010, *Unsaturated soils: a fundamental interpretation of soil behaviour*, John Wiley and Sons, Chichester, West Sussex.

Yoshikuni, H & Nakanodo, H 1974, 'Consolidation of soils by vertical drain wells with finite permeability', *Soils and Foundations*, vol. 14, pp. 35-46.

Neville, AM & Kennedy, JB 1964, 'Basic statistical methods for engineers and scientists', *Basic Statistical Methods for Engineers and Scientists*, International Textbook, Pennsylvania.

Ng, CW & Menzies, B 2007, *Advanced unsaturated soil mechanics and engineering*, Taylor and Francis Group, New York.

Nguyen, LD, Fatahi, B & Khabbaz, H 2014, 'A constitutive model for cemented clays capturing cementation degradation', *International Journal of Plasticity*, vol. 56, pp. 1-18.

Northmore, K, Bell, F & Culshaw, M 1996, 'The engineering properties and behaviour of the brickearth of south Essex', *Quarterly Journal of Engineering Geology and Hydrogeology*, vol. 29, no. 2, pp. 147-161.

Nuth, M & Laloui, L 2008, 'Effective stress concept in unsaturated soils: Clarification and validation of a unified framework', *International Journal for Numerical and Analytical Methods in Geomechanics*, vol. 32, no. 7, pp. 771-801.

O'Neill, MW & Poormoayed, M 1980, 'Methodology for foundations on expansive clays', *Journal of Geotechnical and Geoenvironmental Engineering*, vol. 106, no. ASCE 15949, pp. 1345-1367.

Olson, RE 1977, 'Consolidation under time-dependent loading', *Journal of the Geotechnical Engineering Division*, vol. 103, no. 1, pp. 55-60.

Onoue, A 1988, 'Consolidation of multilayered anisotropic soils by vertical drains with well resistance', *Soils and Foundations*, vol. 28, no. 3, pp. 75-90.

Pells, P, Robertson, A, Jennings, J & Knight, K 1975, 'A guide to construction on or with materials exhibiting additional settlement due to "collapse" of grain structure', *Proceedings of the 6th Regional Conference for Africa Soil Mechanics and Foundation Engineering*, pp. 99-105.

Pereira, JM, Wong, H, Dubujet, P & Dangla, P 2005, 'Adaptation of existing behaviour models to unsaturated states: Application to CJS model', *International Journal for Numerical and Analytical Methods in Geomechanics*, vol. 29, no. 11, pp. 1127-1155.

Perera, D, Indraratna, B & Rujikiatkamjorn, C 2014, 'Soil disturbance associated with mandrel-driven prefabricated vertical drains: field experience', *Southeast Asia Conference on Soft Soils Engineering and Ground Improvement*, pp. F5-1-F5-6.

Pham, HQ, Fredlund, DG & Barbour, SL 2005, 'A study of hysteresis models for soil-water characteristic curves', *Canadian Geotechnical Journal*, vol. 42, no. 6, pp. 1548-1568.

Punmia, B & Jain, AK 2005, *Soil mechanics and foundations*, Laxmi Publications, New Delhi.

Qin, AF, Chen, GJ, Tan, YW & Sun, DA 2008, 'Analytical solution to one-dimensional consolidation in unsaturated soils', *Applied Mathematics and Mechanics*, vol. 29, pp. 1329-1340.

Qin, AF, Sun, DA & Tan, YW 2010a, 'Semi-analytical solution to one-dimensional consolidation in unsaturated soils', *Applied Mathematics and Mechanics*, vol. 31, pp. 215-226.

Qin, AF, Sun, DA. & Tan, YW 2010b, 'Analytical solution to one-dimensional consolidation in unsaturated soils under loading varying exponentially with time', *Computers and Geotechnics*, vol. 37, no. 1, pp. 233-238.

Qin, AF, Sun, DA, Yang, LP & Weng, YF 2010c, 'A semi-analytical solution to consolidation of unsaturated soils with the free drainage well', *Computers and Geotechnics*, vol. 37, no. 7, pp. 867-875.

Qin, AF, Sun, DA & Zhang, JL 2014, 'Semi-analytical solution to one-dimensional consolidation for viscoelastic unsaturated soils', *Computers and Geotechnics*, vol. 62, pp. 110-117.

Rahardjo, H & Fredlund, DG 1995, 'Experimental verification of the theory of consolidation for unsaturated soils', *Canadian Geotechnical Journal*, vol. 32, no. 5, pp. 749-766.

Rao, KS & Satyadas, G 1987, 'Swelling potential with cycles of swelling and partial shrinkage', *Proceedings of the 6th International Conference on Expansive Soils*, pp. 137-142.

Rendulic, L 1936, 'Relation between void ratio and effective principal stresses for a remoulded silty clay', *Proceedings of 1st International Conference on Soil Mechanics and Foundation Engineering*, vol. 3, pp. 48-51.

Rezaei, M, Ajalloeian, R & Ghafoori, M 2012, 'Geotechnical Properties of Problematic Soils Emphasis on Collapsible Cases', *International Journal of Geosciences*, vol. 3, no. 1, pp. 105-110.

Richards, B 1966, 'The significance of moisture flow and equilibria in unsaturated soils in relation to the design of engineering structures built on shallow foundations in Australia', *Symposium on Permeability and Capillarity*, American Society for Testing and Materials, New Jersey.

Romero, E & Simms, PH 2008, 'Microstructure investigation in unsaturated soils: a review with special attention to contribution of mercury intrusion porosimetry and environmental scanning electron microscopy', *Geotechnical and Geological Engineering*, vol. 26, no. 6, pp. 705-727.

Rosenhaupt, S & Mueller, G 1963, 'Openings in Masonry Walls on Settling Supports', *Journal of the Structural Division*, vol. 89, no. 3, pp. 107-134.

Rowe, RK 2001, *Geotechnical and geoenvironmental engineering handbook*, Springer Science and Business Media, New York.

Santagiuliana, R & Schrefler, B 2006, 'Enhancing the Bolzon–Schrefler–Zienkiewicz constitutive model for partially saturated soil', *Transport in Porous Media*, vol. 65, no. 1, pp. 1-30.

Scott, RF 1963, *Principles of soil mechanics*, Addison-Wesley Publishing Company, Massachusetts.

Shan, ZD, Ling, DS & Ding, HJ 2012, 'Exact solutions for one-dimensional consolidation of single-layer unsaturated soil', *International Journal for Numerical and Analytical Methods in Geomechanics*, vol. 36, no. 6, pp. 708-722.

Shan, ZD, Ling, DS & Ding, HJ 2013, 'Analytical solution for 1D consolidation of unsaturated soil with mixed boundary condition', *Applied Physics and Engineering*, vol. 14, no. 1, pp. 61-70.

Shan, ZD, Ling, DS & Ding, HJ 2014, 'Analytical solution for the 1D consolidation of unsaturated multi-layered soil', *Computers and Geotechnics*, vol. 57, pp. 17-23.

Sheng, DC 2011, 'Constitutive modelling of unsaturated soils: Discussion of fundamental principles', *Unsaturated soils*, vol. 1, pp. 91-112.

Sheng, DC, Fredlund, DG & Gens, A 2008, 'A new modelling approach for unsaturated soils using independent stress variables', *Canadian Geotechnical Journal*, vol. 45, no. 4, pp. 511-534.

Sheng, DC, Sloan, SW & Gens, A 2004, 'A constitutive model for unsaturated soils: thermomechanical and computational aspects', *Computational Mechanics*, vol. 33, no. 6, pp. 453-465.

Simms, PH & Yanful, EK 2001, 'Measurement and estimation of pore shrinkage and pore distribution in a clayey till during soil-water characteristic curve tests', *Canadian Geotechnical Journal*, vol. 38, no. 4, pp. 741-754.

Simms, PH & Yanful, EK 2002, 'Predicting soil-water characteristic curves of compacted plastic soils from measured pore-size distributions', *Géotechnique*, vol. 52, no. 4, pp. 269-278.

Skempton, A 1984, 'Effective stress in soils, concrete and rocks', *Pore Pressure and Suction in Soils*, vol. 1032, pp. 4-16.

Smoltczyk, U 2003, *Geotechnical engineering handbook*, Ernst and Sohn, Berlin.

Sokolovich, V & Semkin, V 1984, 'Chemical stabilization of loess soils', *Soil Mechanics and Foundation Engineering*, vol. 21, no. 4, pp. 149-154.

Songyu, L, Heyuan, L, Peng, J & Yanjun, D 1998, 'Approach to cyclic swelling behaviour of compacted clays', *Proceedings of the 2nd International Conference on Unsaturated Soils*, Beijing, vol. 2, pp. 219-225.

Souza, A, Cintra, J, Vilar, O, Alonso, E & Delage, P 1995, 'Shallow foundations on collapsible soil improved by compaction', *Unsaturated Soils*, vols. 1 and 2, pp. 1017-1021.

Sowers, GB & Sowers, GF 1951, 'Introductory Soil Mechanics and Foundations', *Soil Science*, vol. 72, no. 5, p. 405.

Sposito, G 1981, *The thermodynamics of soil solutions*, Oxford University Press, Oxford.

Sreedeep, S & Singh, DN 2006, 'Methodology for determination of osmotic suction of soils', *Geotechnical and Geological Engineering*, vol. 24, no. 5, pp. 1469-1479.

Sun, DA, Cui, HB, Matsuoka, H & Sheng, DC 2007, 'A three-dimensional elastoplastic model for unsaturated compacted soils with hydraulic hysteresis', *Soils and Foundations*, vol. 47, no. 2, pp. 253-264.

Tang, GX, Graham, J, Blatz, J, Gray, M & Rajapakse, RKND 2002, 'Suctions, stresses and strengths in unsaturated sand-bentonite', *Engineering Geology*, vol. 64, no. 2, pp. 147-156.

Tang, XW & Onitsuka, K 2000, 'Consolidation by vertical drains under time-dependent loading', *International Journal for Numerical and Analytical Methods in Geomechanics*, vol. 24, no. 9, pp. 739-751.

Taylor, DW 1948, *Fundamentals of soil mechanics*, John Wiley and Sons, vol. 66, New York.

Terzaghi, K 1925, *Erdbaumechanik auf bodenphysikalischer grundlag* (in German), Franz Deuticke, Vienna.

Terzaghi, K 1943, *Theoretical soil mechanics*, John Wiley and Sons, New York.

Thornthwaite, CW 1948, 'An approach toward a rational classification of climate', *Geographical Review*, vol. 38, no. 1, pp. 55-94.

Thu, TM, Rahardjo, H & Leong, EC 2007, 'Elastoplastic model for unsaturated soil with incorporation of the soil-water characteristic curve', *Canadian Geotechnical Journal*, vol. 44, no. 1, pp. 67-77.

Toll, D & Ong, B 2003, 'Critical-state parameters for an unsaturated residual sandy clay', *Géotechnique.*, vol. 53, no. 1, pp. 93-103.

Tripathy, S, Rao, KS & Fredlund, DG 2002, 'Water content-void ratio swell-shrink paths of compacted expansive soils', *Canadian Geotechnical Journal*, vol. 39, no. 4, pp. 938-959.

Valliappan, S & Khalili-Naghadeh, N 1990, 'Flow through fissured porous media with deformable matrix', *International Journal for Numerical Methods in Engineering*, vol. 29, no. 5, pp. 1079-1094.

Venkatramaiah, C 2006, *Geotechnical engineering*, New Age International Publishers, New Delhi.

Verruijt, A & van Baars, S 2007, *Soil mechanics*, Dreft University of Technology.

Vu, H & Fredlund, DG 2003, 'Uncoupled and coupled solutions of two-dimensional swelling in expansive soils', *Proceedings of the 2nd Asian Conference on Unsaturated Soils*, pp. 53-58.

Walker, R & Indraratna, B 2006, 'Vertical drain consolidation with parabolic distribution of permeability in smear zone', *Journal of Geotechnical and Geoenvironmental Engineering*, vol. 132, no. 7, pp. 937-941.

Walker, R & Indraratna, B 2007, 'Vertical drain consolidation with overlapping smear zones', *Géotechnique*, vol. 57, no. 5, pp. 463-467.

Walker, R & Indraratna, B 2009, 'Consolidation analysis of a stratified soil with vertical and horizontal drainage using the spectral method', *Géotechnique*, vol. 59, no. 5, pp. 439-449.

Wang, XS & Jiao, JJ 2004, 'Analysis of soil consolidation by vertical drains with double porosity model', *International Journal for Numerical and Analytical Methods in Geomechanics*, vol. 28, no. 14, pp. 1385-1400.

Wheeler, SJ & Karube, D 1996, 'Constitutive modelling. State of the art report', *Unsaturated Soils*, pp. 1179-1200.

Wheeler, SJ & Sivakumar, V 1995, 'An elasto-plastic critical state framework for unsaturated soil', *Géotechnique*, vol. 45, no. 1, pp. 35-53.

Wong, TT, Fredlund, DG & Krahn, J 1998, 'A numerical study of coupled consolidation in unsaturated soils', *Canadian Geotechnical Journal*, vol. 35, no. 6, pp. 926-937.

Wu, H & Hu, L 2013, 'Analytical solution for axisymmetric electro-osmotic consolidation', *Géotechnique*, vol. 63, no. 12, pp. 1074-1079.

Wu, JQ & Nofziger, DL 1999, 'Incorporating temperature effects on pesticide degradation into a management model', *Journal of Environmental Quality*, vol. 28, no. 1, pp. 92-100.

Xie, KH, Xie, XY & Jiang, W 2002, 'A study on one-dimensional nonlinear consolidation of double-layered soil', *Computers and Geotechnics*, vol. 29, no. 2, pp. 151-168.

Xie, KH & Leo, CJ 2004, 'Analytical solutions of one-dimensional large strain consolidation of saturated and homogeneous clays', *Computers and Geotechnics*, vol. 31, no. 4, pp. 301-314.

Zhang, X & Lytton, RL 2008, 'Discussion of "A new modelling approach for unsaturated soils using independent stress variables" Appears in Canadian Geotechnical Journal, 45 (4): 511-534', *Canadian Geotechnical Journal*, vol. 45, no. 12, pp. 1784-1787.

Zhou, WH 2013, 'Axisymmetric consolidation of unsaturated soils by differential quadrature method', *Mathematical Problems in Engineering*, vol. 2013, pp. 1-4.

Zhou, WH & Tu, S 2012, 'Unsaturated consolidation in a sand drain foundation by differential quadrature method', *Procedia Earth and Planetary Science*, vol. 5, pp. 52-57.

Zhou, WH & Zhao, LS 2014, 'One-dimensional consolidation of unsaturated soil subjected to time-dependent loading with various initial and boundary conditions', *International Journal of Geomechanics*, vol. 14, no. 2, pp. 291-301.

Zhou, WH, Zhao, LS & Li, XB 2014, 'A simple analytical solution to one-dimensional consolidation for unsaturated soils', *International Journal for Numerical and Analytical Methods in Geomechanics*, vol. 38, no. 8, pp. 794-810.

Zhu, GF & Yin, JH 1998, 'Consolidation of soil under depth-dependent ramp load', *Canadian Geotechnical Journal*, vol. 35, no. 2, pp. 344-350.

Zhu, GF & Yin, JH 2004, 'Consolidation analysis of soil with vertical and horizontal drainage under ramp loading considering smear effects', *Geotextiles and Geomembranes*, vol. 22, no. 1, pp. 63-74.

APPENDIX A – Dissipation rates of excess pore pressures induced by time-dependent loadings in the 1D consolidation

Substituting Equation [4-30] into Equation [4-21] results in the closed-form solution for excess pore-air and pore-water pressures as follows:

$$u_a(z,t) = \sum_{k=0}^{\infty} D_k \sin(K z) \left\{ \frac{\omega \left[e^{\alpha_1 (K)^2 t} - e^{\alpha_2 (K)^2 t} \right] + \psi \left[e^{\alpha_1 (K)^2 t} + e^{\alpha_2 (K)^2 t} \right]}{2\eta} + \frac{X_1}{(K)^2} \left[\frac{e^{\alpha_1 (K)^2 t} (\alpha_1 + \beta)}{\alpha_1 (\alpha_1 - \alpha_2)} + \frac{e^{\alpha_2 (K)^2 t} (\alpha_2 + \beta)}{\alpha_2 (\alpha_2 - \alpha_1)} + \frac{\beta}{\alpha_1 \alpha_2} \right] \right\} \quad [A\text{-}1a]$$

$$u_w(z,t) = \sum_{k=0}^{\infty} D_k \sin(K z) \left\{ \frac{\omega' \left[e^{\alpha_1 (K)^2 t} - e^{\alpha_2 (K)^2 t} \right] + \psi' \left[e^{\alpha_1 (K)^2 t} + e^{\alpha_2 (K)^2 t} \right]}{2\eta} + \frac{X_1'}{(K)^2} \left[\frac{e^{\alpha_1 (K)^2 t} (\alpha_1 + \beta')}{\alpha_1 (\alpha_1 - \alpha_2)} + \frac{e^{\alpha_2 (K)^2 t} (\alpha_2 + \beta')}{\alpha_2 (\alpha_2 - \alpha_1)} + \frac{\beta'}{\alpha_1 \alpha_2} \right] \right\} \quad [A\text{-}1b]$$

Substituting Equation [4-33] into Equation [4-21] results in the closed-form solution for excess pore-air and pore-water pressures as follows:

$$u_a(z,t) = \sum_{k=0}^{\infty} D_k \sin(K z) \left\{ \frac{\omega \left[e^{\alpha_1 (K)^2 t} - e^{\alpha_2 (K)^2 t} \right] + \psi \left[e^{\alpha_1 (K)^2 t} + e^{\alpha_2 (K)^2 t} \right]}{2\eta} + X_2 \left\{ \frac{e^{-bt} [\beta (K)^2 - b]}{[b + \alpha_1 (K)^2] [b + \alpha_2 (K)^2]} + \frac{e^{\alpha_1 (K)^2 t} (\alpha_1 + \beta)}{[b + \alpha_1 (K)^2] (\alpha_1 - \alpha_2)} + \frac{e^{\alpha_2 (K)^2 t} (\alpha_2 + \beta)}{[b + \alpha_2 (K)^2] (\alpha_2 - \alpha_1)} \right\} \right\} \quad [A\text{-}2a]$$

$$u_w(z,t) = \sum_{k=0}^{\infty} D_k \sin(K z) \left\{ \frac{\omega' \left[e^{\alpha_1 (K)^2 t} - e^{\alpha_2 (K)^2 t} \right] + \psi' \left[e^{\alpha_1 (K)^2 t} + e^{\alpha_2 (K)^2 t} \right]}{2\eta} + X_2' \left\{ \frac{e^{-bt} [\beta' (K)^2 - b]}{[b + \alpha_1 (K)^2] [b + \alpha_2 (K)^2]} + \frac{e^{\alpha_1 (K)^2 t} (\alpha_1 + \beta')}{[b + \alpha_1 (K)^2] (\alpha_1 - \alpha_2)} + \frac{e^{\alpha_2 (K)^2 t} (\alpha_2 + \beta')}{[b + \alpha_2 (K)^2] (\alpha_2 - \alpha_1)} \right\} \right\} \quad [A\text{-}2b]$$

Substituting Equation [4-36] into Equation [4-21] results in the closed-form solution for excess pore-air and pore-water pressures as follows:

$$u_a(z,t) = \sum_{k=0}^{\infty} D_k \sin(K z) \left\{ \frac{\omega \left[e^{\alpha_1 (K)^2 t} - e^{\alpha_2 (K)^2 t} \right] + \psi \left[e^{\alpha_1 (K)^2 t} + e^{\alpha_2 (K)^2 t} \right]}{2\eta} + X_3 \left\{ \frac{e^{\alpha_1 (K)^2 t} \alpha_1 (K)^2 (\alpha_1 + \beta)}{\{[\alpha_1 (K)^2]^2 + \phi^2\}(\alpha_1 - \alpha_2)} + \frac{e^{\alpha_2 (K)^2 t} \alpha_2 (K)^2 (\alpha_2 + \beta)}{\{[\alpha_2 (K)^2]^2 + \phi^2\}(\alpha_2 - \alpha_1)} + \frac{\zeta_1^k \cos(\phi t) + \zeta_2^k \sin(\phi t)}{\{[\alpha_1 (K)^2]^2 + \phi^2\}\{[\alpha_2 (K)^2]^2 + \phi^2\}} \right\} \right\} \quad [A\text{-}3a]$$

$$u_w(z,t) = \sum_{k=0}^{\infty} D_k \sin(K z) \left\{ \frac{\omega' \left[e^{\alpha_1 (K)^2 t} - e^{\alpha_2 (K)^2 t} \right] + \psi' \left[e^{\alpha_1 (K)^2 t} + e^{\alpha_2 (K)^2 t} \right]}{2\eta} + X_3' \left\{ \frac{e^{\alpha_1 (K)^2 t} \alpha_1 (K)^2 (\alpha_1 + \beta')}{\{[\alpha_1 (K)^2]^2 + \phi^2\}(\alpha_1 - \alpha_2)} + \frac{e^{\alpha_2 (K)^2 t} \alpha_2 (K)^2 (\alpha_2 + \beta')}{\{[\alpha_2 (K)^2]^2 + \phi^2\}(\alpha_2 - \alpha_1)} + \frac{\zeta_1'^k \cos(\phi t) + \zeta_2'^k \sin(\phi t)}{\{[\alpha_1 (K)^2]^2 + \phi^2\}\{[\alpha_2 (K)^2]^2 + \phi^2\}} \right\} \right\} \quad [A\text{-}3b]$$

Substituting Equation [4-39] into Equation [4-21] results in the closed-form solution for excess pore-air and pore-water pressures as follows:

$$u_a(z,t) = \sum_{k=0}^{\infty} D_k \sin(K z) \left\{ \frac{\omega \left[e^{\alpha_1 (K)^2 t} - e^{\alpha_2 (K)^2 t} \right] + \psi \left[e^{\alpha_1 (K)^2 t} + e^{\alpha_2 (K)^2 t} \right]}{2\eta} + X_4 \left\{ \frac{e^{\alpha_1 (K)^2 t} \alpha_1 (K)^2 (\alpha_1 + \beta)}{\{[\alpha_1 (K)^2 + c]^2 + \varphi^2\}(\alpha_1 - \alpha_2)} + \frac{e^{\alpha_2 (K)^2 t} \alpha_2 (K)^2 (\alpha_2 + \beta)}{\{[\alpha_2 (K)^2 + c]^2 + \varphi^2\}(\alpha_2 - \alpha_1)} + \frac{e^{-ct}[\xi_1^k \cos(\varphi t) + \xi_2^k \sin(\varphi t)]}{\varphi \{[\alpha_1 (K)^2 + c]^2 + \varphi^2\}\{[\alpha_2 (K)^2 + c]^2 + \varphi^2\}} \right\} \right\} \quad [A\text{-}4a]$$

$$u_w(z,t) = \sum_{k=0}^{\infty} D_k \sin(K z) \left\{ \frac{\omega' \left[e^{\alpha_1 (K)^2 t} - e^{\alpha_2 (K)^2 t} \right] + \psi' \left[e^{\alpha_1 (K)^2 t} + e^{\alpha_2 (K)^2 t} \right]}{2\eta} + X_4' \left\{ \frac{e^{\alpha_1 (K)^2 t} \alpha_1 (K)^2 (\alpha_1 + \beta')}{\{[\alpha_1 (K)^2 + c]^2 + \varphi^2\}(\alpha_1 - \alpha_2)} + \frac{e^{\alpha_2 (K)^2 t} \alpha_2 (K)^2 (\alpha_2 + \beta')}{\{[\alpha_2 (K)^2 + c]^2 + \varphi^2\}(\alpha_2 - \alpha_1)} + \frac{e^{-ct}[\xi_1'^k \cos(\varphi t) + \xi_2'^k \sin(\varphi t)]}{\varphi \{[\alpha_1 (K)^2 + c]^2 + \varphi^2\}\{[\alpha_2 (K)^2 + c]^2 + \varphi^2\}} \right\} \right\} \quad [A\text{-}4b]$$

APPENDIX B – Predicted excess pore pressures due to temperature variations in the 1D consolidation

Following Equations [5-9] – [5-22] while incorporating Equation [5-27a], the excess pore-air and pore-water pressures induced by the time-dependent linear temperature and constant loading can be determined as follows:

$$u_a(z,t) = \sum_{k=0}^{\infty}\left\{\frac{\varpi^k\left[\Omega\left(e^{\alpha_1^k t}-e^{\alpha_2^k t}\right)+\Psi\left(e^{\alpha_1^k t}+e^{\alpha_2^k t}\right)\right]}{2\eta}+\Upsilon^k\left[\frac{e^{\alpha_1^k t}\,\beta_1^k}{\alpha_1^k(\alpha_1^k-\alpha_2^k)}+\frac{e^{\alpha_2^k t}\,\beta_2^k}{\alpha_2^k(\alpha_2^k-\alpha_1^k)}+\right.\right.$$

$$\left.\left.\frac{\beta_1^k-\alpha_1^k}{\alpha_1^k\alpha_2^k}\right]\right\}\sin(K\,z) \qquad [B\text{-}1a]$$

$$u_w(z,t) = \sum_{k=0}^{\infty}\left\{\frac{\varpi^k\left[\Omega'\left(e^{\alpha_1^k t}-e^{\alpha_2^k t}\right)+\Psi'\left(e^{\alpha_1^k t}+e^{\alpha_2^k t}\right)\right]}{2\eta}+\Upsilon'^k\left(\frac{e^{\alpha_2^k t}-e^{\alpha_1^k t}}{\alpha_1^k-\alpha_2^k}\right)\right\}\sin(K\,z) \qquad [B\text{-}1b]$$

where $\Upsilon^k = \frac{aC_\Theta \iota^k}{C_w C_a - 1}$; $\Upsilon'^k = \frac{aC_w C_\Theta \iota^k}{C_w C_a - 1}$;

$\alpha_1^k = \frac{1}{2}\left(\frac{c_v^w + c_v^a + \eta}{1 - C_w C_a}\right)(K)^2$; $\alpha_2^k = \frac{1}{2}\left(\frac{c_v^w + c_v^a - \eta}{1 - C_w C_a}\right)(K)^2$;

$\beta_1^k = \left[\frac{1}{2}\left(\frac{c_v^w + c_v^a + \eta}{1 - C_w C_a}\right) - c_v^w\right](K)^2$; $\beta_2^k = \left[\frac{1}{2}\left(\frac{c_v^w + c_v^a - \eta}{1 - C_w C_a}\right) - c_v^w\right](K)^2$; and

$\iota^k = \frac{2\left[HK - \xi\,(-1)^k\right]}{(HK)^2}$, for the one-way drainage condition ($k = 0, 1, 2, ...$); or

$= \frac{2\left[1 + (\xi - 1)(-1)^k\right]}{HK}$, for the two-way drainage condition ($k = 0, 1, 2, ...$). [B-2]

Following Equations [5-9] – [5-22] while incorporating Equation [5-27b], the excess pore-air and pore-water pressures induced by the time-dependent exponential temperature and constant loading can be predicted as follows:

$$u_a(z,t) = \sum_{k=0}^{\infty}\left\{\frac{\varpi^k\left[\Omega\left(e^{\alpha_1^k t}-e^{\alpha_2^k t}\right)+\Psi\left(e^{\alpha_1^k t}+e^{\alpha_2^k t}\right)\right]}{2\eta}+\Upsilon^k\left\{\frac{e^{\alpha_1^k t}\,\beta_1^k}{(\alpha_1^k+b)(\alpha_1^k-\alpha_2^k)}+\frac{e^{\alpha_2^k t}\,\beta_2^k}{(\alpha_2^k+b)(\alpha_2^k-\alpha_1^k)}+\right.\right.$$

$$\left.\left.\frac{e^{-bt}\left[(\beta_1^k-\alpha_1^k)-b\right]}{(\alpha_1^k+b)(\alpha_2^k+b)}\right\}\right\}\sin(K\,z) \qquad [B\text{-}3a]$$

$$u_w(z,t) = \sum_{k=0}^{\infty}\left\{\frac{\varpi^k\left[\Omega'\left(e^{\alpha_1^k t}-e^{\alpha_2^k t}\right)+\Psi'\left(e^{\alpha_1^k t}+e^{\alpha_2^k t}\right)\right]}{2\eta} + \Upsilon'^k\left\{\frac{e^{\alpha_1^k t}\,\alpha_1^k}{(\alpha_1^k+b)(\alpha_2^k-\alpha_1^k)} + \frac{e^{\alpha_2^k t}\,\alpha_2^k}{(\alpha_2^k+b)(\alpha_1^k-\alpha_2^k)} + \frac{be^{-bt}}{(\alpha_1^k+b)(\alpha_2^k+b)}\right\}\right\}\sin(K\,z) \quad \text{[B-3b]}$$

where $\Upsilon^k = \frac{bAC_\Theta \iota^k}{C_w C_a - 1}$; $\quad \Upsilon'^k = \frac{bAC_w C_\Theta \iota^k}{C_w C_a - 1}$;

$\alpha_1^k = \frac{1}{2}\left(\frac{c_v^w + c_v^a + \eta}{1 - C_w C_a}\right)(K)^2$; $\quad \alpha_2^k = \frac{1}{2}\left(\frac{c_v^w + c_v^a - \eta}{1 - C_w C_a}\right)(K)^2$;

$\beta_1^k = \left[\frac{1}{2}\left(\frac{c_v^w + c_v^a + \eta}{1 - C_w C_a}\right) - c_v^w\right](K)^2$; $\quad \beta_2^k = \left[\frac{1}{2}\left(\frac{c_v^w + c_v^a - \eta}{1 - C_w C_a}\right) - c_v^w\right](K)^2$; and

$\iota^k = \frac{2\left[HK - \xi(-1)^k\right]}{(HK)^2}$, for the one-way drainage condition ($k = 0, 1, 2, ...$); or

$= \frac{2\left[1 + (\xi - 1)(-1)^k\right]}{HK}$, for the two-way drainage condition ($k = 0, 1, 2, ...$). [B-4]

Following in Equations [5-9] – [5-22] while incorporating Equation [5-27c], the excess pore-air and pore-water pressures induced by the time-dependent diurnal temperature wave and constant loading can be estimated as follows:

$$u_a(z,t) = \sum_{k=0}^{\infty}\left\{\frac{\varpi^k\left[\Omega\left(e^{\alpha_1^k t}-e^{\alpha_2^k t}\right)+\Psi\left(e^{\alpha_1^k t}+e^{\alpha_2^k t}\right)\right]}{2\eta} + \Upsilon_d^k\left\{\frac{e^{\alpha_1^k t}\left[(\alpha_1^k)^2+\zeta_d^k\right]\beta_1^k}{\left[(\alpha_1^k)^2+(\omega_d)^2\right](\alpha_2^k-\alpha_1^k)} + \frac{e^{\alpha_2^k t}\left[(\alpha_2^k)^2+\zeta_d^k\right]\beta_2^k}{\left[(\alpha_2^k)^2+(\omega_d)^2\right](\alpha_1^k-\alpha_2^k)} + \frac{A_d^k\sin(\omega_d t)+B_d^k\cos(\omega_d t)}{\omega_d\left[(\alpha_1^k)^2+(\omega_d)^2\right]\left[(\alpha_2^k)^2+(\omega_d)^2\right]}\right\}\right\}\sin(K\,z) \quad \text{[B-5a]}$$

$$u_w(z,t) = \sum_{k=0}^{\infty}\left\{\frac{\varpi^k\left[\Omega'\left(e^{\alpha_1^k t}-e^{\alpha_2^k t}\right)+\Psi'\left(e^{\alpha_1^k t}+e^{\alpha_2^k t}\right)\right]}{2\eta} + \Upsilon_d'^k\left\{\frac{e^{\alpha_1^k t}\left[(\alpha_1^k)^2+\zeta_d^k\right]\alpha_1^k}{\left[(\alpha_1^k)^2+(\omega_d)^2\right](\alpha_1^k-\alpha_2^k)} + \frac{e^{\alpha_2^k t}\left[(\alpha_2^k)^2+\zeta_d^k\right]\alpha_2^k}{\left[(\alpha_2^k)^2+(\omega_d)^2\right](\alpha_2^k-\alpha_1^k)} + \frac{A_d'^k\sin(\omega_d t)+B_d'^k\cos(\omega_d t)}{\left[(\alpha_1^k)^2+(\omega_d)^2\right]\left[(\alpha_2^k)^2+(\omega_d)^2\right]}\right\}\right\}\sin(K\,z) \quad \text{[B-5b]}$$

where $\Upsilon_d^k = \frac{C_\Theta C_d^k A_d d_d \omega_d}{C_w C_a - 1}$; $\quad \Upsilon_d'^k = \frac{C_w C_\Theta C_d^k A_d d_d \omega_d}{C_w C_a - 1}$; $\quad \zeta_d^k = \frac{D_d^k \omega_d}{C_d^k}$;

$\alpha_1^k = \frac{1}{2}\left(\frac{c_v^w + c_v^a + \eta}{1 - C_w C_a}\right)(K)^2$; $\quad \alpha_2^k = \frac{1}{2}\left(\frac{c_v^w + c_v^a - \eta}{1 - C_w C_a}\right)(K)^2$;

$$\beta_1^k = \left[\frac{1}{2}\left(\frac{c_v^w + c_v^a + \eta}{1 - C_w C_a}\right) - c_v^w\right](K)^2; \qquad \beta_2^k = \left[\frac{1}{2}\left(\frac{c_v^w + c_v^a - \eta}{1 - C_w C_a}\right) - c_v^w\right](K)^2;$$

$$A_d^k = \left[\alpha_1^k \alpha_2^k - (\omega_d)^2\right]\left[\left(\alpha_1^k - \beta_1^k\right)\zeta_d^k + (\omega_d)^2\right] + \left(\alpha_1^k + \alpha_2^k\right)(\omega_d)^2\left[\zeta_d^k - \left(\alpha_1^k - \beta_1^k\right)\right];$$

$$A_d'^k = \omega_d\left[(\omega_d)^2 - \left(\alpha_1^k + \alpha_2^k\right)\zeta_d^k - \alpha_1^k \alpha_2^k\right];$$

$$B_d^k = \omega_d\left\{\left(\alpha_1^k + \alpha_2^k\right)\left[\left(\alpha_1^k - \beta_1^k\right)\zeta_d^k + (\omega_d)^2\right] + \left[\alpha_1^k \alpha_2^k - (\omega_d)^2\right]\left[\left(\alpha_1^k - \beta_1^k\right) - \zeta_d^k\right]\right\};$$

$$B_d'^k = \zeta_d^k\left[\alpha_1^k \alpha_2^k - (\omega_d)^2\right] - \left(\alpha_1^k + \alpha_2^k\right)(\omega_d)^2;$$

$$C_d^k = E_d^k \cos(\omega_d t_0) + F_d^k \sin(\omega_d t_0);$$

$$D_d^k = E_d^k \sin(\omega_d t_0) - F_d^k \cos(\omega_d t_0); \qquad \text{[B-6]}$$

in which

i. One-way drainage condition:

$$E_d^k = \frac{2}{H}\frac{2d_d K - e^{-\frac{H}{d_d}}\left\{\sin\left(\frac{H}{d_d}\right)\left[(d_d K)^2 + 2\right](-1)^k - \cos\left(\frac{H}{d_d}\right)\left[(d_d K)^2 - 2\right](-1)^k\right\}}{(d_d K)^4 + 4};$$

$$F_d^k = \frac{2}{H}\frac{(d_d K)^3 - e^{-\frac{H}{d_d}}\left\{\sin\left(\frac{H}{d_d}\right)\left[(d_d K)^2 - 2\right](-1)^k + \cos\left(\frac{H}{d_d}\right)\left[(d_d K)^2 + 2\right](-1)^k\right\}}{(d_d K)^4 + 4}; \text{ or}$$

ii. Two-way drainage condition:

$$E_d^k = \frac{2}{H}\frac{2d_d K - e^{-\frac{H}{d_d}}\left\{\sin\left(\frac{H}{d_d}\right)(d_d K)^3(-1)^k + 2\cos\left(\frac{H}{d_d}\right)(d_d K)(-1)^k\right\}}{(d_d K)^4 + 4}; \text{ and}$$

$$F_d^k = \frac{2}{H}\frac{(d_d K)^3 - e^{-\frac{H}{d_d}}\left[\cos\left(\frac{H}{d_d}\right)(d_d K)^3(-1)^k - 2\sin\left(\frac{H}{d_d}\right)(d_d K)(-1)^k\right]}{(d_d K)^4 + 4}. \qquad \text{[B-7]}$$

APPENDIX C – Dissipation rates of excess pore pressures and average degree of consolidation in the 2D plane strain consolidation

Worked example 1

By combining Equations [6-24], [6-25] and [6-32], the closed-form solutions describing the dissipation of excess pore pressures adopting isotropic and anisotropic permeability conditions are presented as follows:

(a) Isotropic permeability condition ($k_x = k_z$):

$$u_a(x,z,t) = \sum_{i=0}^{\infty}\sum_{j=0}^{\infty} \varpi_{ij}\sin(Ix)\sin(Jz)\left[\frac{\Omega_1\left(e^{\alpha_1\Lambda^{ij}t}-e^{\alpha_2\Lambda^{ij}t}\right)+\Psi_1\left(e^{\alpha_1\Lambda^{ij}t}+e^{\alpha_2\Lambda^{ij}t}\right)}{\eta}\right] \quad [C\text{-}1a]$$

$$u_w(x,z,t) = \sum_{i=0}^{\infty}\sum_{j=0}^{\infty} \varpi_{ij}\sin(Ix)\sin(Jz)\left[\frac{\Omega_1'\left(e^{\alpha_1\Lambda^{ij}t}-e^{\alpha_2\Lambda^{ij}t}\right)+\Psi_1'\left(e^{\alpha_1\Lambda^{ij}t}+e^{\alpha_2\Lambda^{ij}t}\right)}{\eta}\right] \quad [C\text{-}1b]$$

(b) Anisotropic permeability condition ($k_x \neq k_z$):

$$u_a(x,z,t) = \sum_{i=0}^{\infty}\sum_{j=0}^{\infty} \varpi_{ij}\sin(Ix)\sin(Jz)\left[\frac{\omega_1\left(e^{\alpha_1^{ij}t}-e^{\alpha_2^{ij}t}\right)+\psi_1\left(e^{\alpha_1^{ij}t}+e^{\alpha_2^{ij}t}\right)}{\eta^{ij}}\right] \quad [C\text{-}2a]$$

$$u_w(x,z,t) = \sum_{i=0}^{\infty}\sum_{j=0}^{\infty} \varpi_{ij}\sin(Ix)\sin(Jz)\left[\frac{\omega_1'\left(e^{\alpha_1^{ij}t}-e^{\alpha_2^{ij}t}\right)+\psi_1'\left(e^{\alpha_1^{ij}t}+e^{\alpha_2^{ij}t}\right)}{\eta^{ij}}\right] \quad [C\text{-}2b]$$

where $\varpi_{ij} = \frac{2[1-(-1)^i]}{LHIJ}$ for top drainage boundary system;

$= \frac{2[1-(-1)^i][1-(-1)^j]}{LHIJ}$ for top-base drainage boundary system;

$$\Omega_1 = \left(c_{v_1}^a - c_{v_1}^w\right)u_a^0 - 2c_{v_1}^w C_a u_w^0; \qquad \Psi_1 = \eta u_a^0;$$

$$\Omega_1' = \left(c_{v_1}^w - c_{v_1}^a\right)u_w^0 - 2c_{v_1}^a C_w u_a^0; \qquad \Psi_1' = \eta u_w^0;$$

$$\omega_1 = \left(c_{v_2}^a \lambda_a^{ij} - c_{v_2}^w \lambda_w^{ij}\right)u_a^0 - 2c_{v_2}^w C_a \lambda_w^{ij} u_w^0; \qquad \psi_1 = \eta^{ij} u_a^0;$$

$$\omega_1' = \left(c_{v_2}^w \lambda_w^{ij} - c_{v_2}^a \lambda_a^{ij}\right)u_w^0 - 2c_{v_2}^a C_w \lambda_a^{ij} u_a^0; \text{ and} \qquad \psi_1' = \eta^{ij} u_w^0. \quad [C\text{-}3]$$

The average degree of consolidation can be obtained capturing the constant initial condition:

$$\overline{U} = \left| \frac{\int_0^H \int_0^L \varepsilon_{v_1}(x,z,t)dxdz}{\int_0^H \int_0^L \varepsilon_{v_1}(x,z,\infty)dxdz} \right| \qquad [C\text{-}4]$$

where $\int_0^H \int_0^L \varepsilon_{v_1}(x,z,t)dxdz = (m_2^s - m_1^s)\left\{\int_0^H \int_0^L [u_a(x,z,t)]dxdz - LHu_a^0\right\} -$

$m_2^s\left\{\int_0^H \int_0^L [u_a(x,z,t)]dxdz - LHu_w^0\right\}$;

$$\int_0^H \int_0^L \varepsilon_{v_1}(x,z,\infty)dxdz = (m_1^s - m_2^s)LHu_a^0 + (m_2^s)LHu_w^0; \qquad [C\text{-}5]$$

with $\varpi'_{ij} = \frac{2[1-(-1)^i]^2}{LH(IJ)^2}$ for top drainage boundary system; or

$= \frac{2[1-(-1)^i]^2[1-(-1)^j]^2}{LH(IJ)^2}$ for top-base drainage boundary system; [C-6]

(a) Isotropic permeability condition ($k_x = k_z$):

$$\int_0^H \int_0^L u_a(x,z,t)dxdz = \sum_{i=0}^{\infty}\sum_{j=0}^{\infty} \varpi'_{ij}\left[\frac{\Omega_1\left(e^{\alpha_1\Lambda^{ij}t} - e^{\alpha_2\Lambda^{ij}t}\right) + \Psi_1\left(e^{\alpha_1\Lambda^{ij}t} + e^{\alpha_2\Lambda^{ij}t}\right)}{\eta}\right] \qquad [C\text{-}7a]$$

$$\int_0^H \int_0^L u_w(x,z,t)dxdz = \sum_{i=0}^{\infty}\sum_{j=0}^{\infty} \varpi'_{ij}\left[\frac{\Omega'_1\left(e^{\alpha_1\Lambda^{ij}t} - e^{\alpha_2\Lambda^{ij}t}\right) + \Psi'_1\left(e^{\alpha_1\Lambda^{ij}t} + e^{\alpha_2\Lambda^{ij}t}\right)}{\eta}\right] \qquad [C\text{-}7b]$$

(b) Anisotropic permeability condition ($k_x \neq k_z$):

$$\int_0^H \int_0^L u_a(x,z,t)dxdz = \sum_{i=0}^{\infty}\sum_{j=0}^{\infty} \varpi'_{ij}\left[\frac{\omega_1\left(e^{\alpha_1^{ij}t} - e^{\alpha_2^{ij}t}\right) + \psi_1\left(e^{\alpha_1^{ij}t} + e^{\alpha_2^{ij}t}\right)}{\eta^{ij}}\right] \qquad [C\text{-}8a]$$

$$\int_0^H \int_0^L u_w(x,z,t)dxdz = \sum_{i=0}^{\infty}\sum_{j=0}^{\infty} \varpi'_{ij}\left[\frac{\omega'_1\left(e^{\alpha_1^{ij}t} - e^{\alpha_2^{ij}t}\right) + \psi'_1\left(e^{\alpha_1^{ij}t} + e^{\alpha_2^{ij}t}\right)}{\eta^{ij}}\right] \qquad [C\text{-}8b]$$

Worked example 2

By introducing the initial condition provided in Equation [6-7] to Equations [6-24] and [6-25], the exact solutions predicting the dissipation of excess pore pressures are as below:

(a) Isotropic permeability condition ($k_x = k_z$):

$$u_a(x,z,t) = \sum_{i=0}^{\infty}\sum_{j=0}^{\infty} \varrho_{ij}\sin(Ix)\sin(Jz)\left[\frac{\Omega_2\left(e^{\alpha_1\Lambda^{ij}t}-e^{\alpha_2\Lambda^{ij}t}\right)+\Psi_2\left(e^{\alpha_1\Lambda^{ij}t}+e^{\alpha_2\Lambda^{ij}t}\right)}{\eta}\right] \quad \text{[C-9a]}$$

$$u_w(x,z,t) = \sum_{i=0}^{\infty}\sum_{j=0}^{\infty} \varrho_{ij}\sin(Ix)\sin(Jz)\left[\frac{\Omega_2'\left(e^{\alpha_1\Lambda^{ij}t}-e^{\alpha_2\Lambda^{ij}t}\right)+\Psi_2'\left(e^{\alpha_1\Lambda^{ij}t}+e^{\alpha_2\Lambda^{ij}t}\right)}{\eta}\right] \quad \text{[C-9b]}$$

(b) Anisotropic permeability condition ($k_x \neq k_z$):

$$u_a(x,z,t) = \sum_{i=0}^{\infty}\sum_{j=0}^{\infty} \varrho_{ij}\sin(Ix)\sin(Jz)\left[\frac{\omega_2\left(e^{\alpha_1^{ij}t}-e^{\alpha_2^{ij}t}\right)+\psi_2\left(e^{\alpha_1^{ij}t}+e^{\alpha_2^{ij}t}\right)}{\eta^{ij}}\right] \quad \text{[C-10a]}$$

$$u_w(x,z,t) = \sum_{i=0}^{\infty}\sum_{j=0}^{\infty} \varrho_{ij}\sin(Ix)\sin(Jz)\left[\frac{\omega_2'\left(e^{\alpha_1^{ij}t}-e^{\alpha_2^{ij}t}\right)+\psi_2'\left(e^{\alpha_1^{ij}t}+e^{\alpha_2^{ij}t}\right)}{\eta^{ij}}\right] \quad \text{[C-10b]}$$

where

(i) Top drainage boundary condition:

$$\varrho_{ij} = \frac{2[1-(-1)^i]}{LI(HJ)^2};$$
$$\Omega_2 = \left(c_{v_1}^a - c_{v_1}^w\right)\left[HJ-(-1)^j\zeta_a\right]u_a^0 - 2c_{v_1}^w C_a\left[HJ-(-1)^j\zeta_w\right]u_w^0;$$
$$\Psi_2 = \eta\left[HJ-(-1)^j\zeta_a\right]u_a^0;$$
$$\Omega_2' = \left(c_{v_1}^w - c_{v_1}^a\right)\left[HJ-(-1)^j\zeta_w\right]u_w^0 - 2c_{v_1}^a C_w\left[HJ-(-1)^j\zeta_a\right]u_a^0;$$
$$\Psi_2' = \eta\left[HJ-(-1)^j\zeta_w\right]u_w^0;$$
$$\omega_2 = \left(c_{v_2}^a\lambda_a^{ij} - c_{v_2}^w\lambda_w^{ij}\right)\left[HJ-(-1)^j\zeta_a\right]u_a^0 - 2c_{v_2}^w C_a\lambda_w^{ij}\left[HJ-(-1)^j\zeta_w\right]u_w^0;$$
$$\psi_2 = \eta^{ij}\left[HJ-(-1)^j\zeta_a\right]u_a^0;$$
$$\omega_2' = \left(c_{v_2}^w\lambda_w^{ij} - c_{v_2}^a\lambda_a^{ij}\right)\left[HJ-(-1)^j\zeta_w\right]u_w^0 - 2c_{v_2}^a C_w\lambda_a^{ij}\left[HJ-(-1)^j\zeta_a\right]u_a^0; \text{ and}$$
$$\psi_2' = \eta^{ij}\left[HJ-(-1)^j\zeta_w\right]u_w^0; \quad \text{[C-11]}$$

(ii) Top-base drainage boundary condition:

$$\varrho_{ij} = \frac{2[1-(-1)^i]}{LHIJ};$$
$$\Omega_2 = \left(c_{v_1}^a - c_{v_1}^w\right)\left[1+(-1)^j(\zeta_a-1)\right]u_a^0 - 2c_{v_1}^w C_a\left[1+(-1)^j(\zeta_w-1)\right]u_w^0;$$
$$\Psi_2 = \eta\left[1+(-1)^j(\zeta_a-1)\right]u_a^0;$$

$$\Omega_2' = \left(c_{v_1}^w - c_{v_1}^a\right)\left[1 + (-1)^j(\zeta_w - 1)\right]u_w^0 - 2c_{v_1}^a C_w\left[1 + (-1)^j(\zeta_a - 1)\right]u_a^0;$$

$$\Psi_2' = \eta\left[1 + (-1)^j(\zeta_w - 1)\right]u_w^0;$$

$$\omega_2 = \left(c_{v_2}^a\lambda_a^{ij} - c_{v_2}^w\lambda_w^{ij}\right)\left[1 + (-1)^j(\zeta_a - 1)\right]u_a^0 - 2c_{v_2}^w C_a\lambda_w^{ij}\left[1 + (-1)^j(\zeta_w - 1)\right]u_w^0;$$

$$\psi_2 = \eta^{ij}\left[1 + (-1)^j(\zeta_a - 1)\right]u_a^0;$$

$$\omega_2' = \left(c_{v_2}^w\lambda_w^{ij} - c_{v_2}^a\lambda_a^{ij}\right)\left[1 + (-1)^j(\zeta_w - 1)\right]u_w^0 - 2c_{v_2}^a C_w\lambda_a^{ij}\left[1 + (-1)^j(\zeta_a - 1)\right]u_a^0; \text{ and}$$

$$\psi_2' = \eta^{ij}\left[1 + (-1)^j(\zeta_w - 1)\right]u_w^0. \qquad \text{[C-12]}$$

The average degree of consolidation can be obtained capturing the linear initial condition:

$$\overline{U} = \left|\frac{\int_0^H\int_0^L \varepsilon_{v_2}(x,z,t)dxdz}{\int_0^H\int_0^L \varepsilon_{v_2}(x,z,\infty)dxdz}\right| \qquad \text{[C-13]}$$

where $\int_0^H\int_0^L \varepsilon_{v_2}(x,z,t)dxdz = (m_2^s - m_1^s)\left\{\int_0^H\int_0^L[u_a(x,z,t)]dxdz - LHu_a^0\left(1 - \frac{\zeta_a}{2}\right)\right\} - m_2^s\left\{\int_0^H\int_0^L[u_a(x,z,t)]dxdz - LHu_w^0\left(1 - \frac{\zeta_w}{2}\right)\right\};$

$$\int_0^H\int_0^L \varepsilon_{v_2}(x,z,\infty)dxdz = (m_1^s - m_2^s)LHu_a^0\left(1 - \frac{\zeta_a}{2}\right) + (m_2^s)LHu_w^0\left(1 - \frac{\zeta_w}{2}\right); \qquad \text{[C-14]}$$

with $\varrho_{ij}' = \frac{2\left[1-(-1)^i\right]^2}{L(HI)^2J^3}$ for top drainage boundary system; or

$= \frac{2\left[1-(-1)^i\right]^2\left[1-(-1)^j\right]}{LH(IJ)^2}$ for top-base drainage boundary system; [C-15]

(a) Isotropic permeability condition ($k_x = k_z$):

$$\int_0^H\int_0^L u_a(x,z,t)dxdz = \sum_{i=0}^{\infty}\sum_{j=0}^{\infty}\varrho_{ij}'\left[\frac{\Omega_2\left(e^{\alpha_1\Lambda^{ij}t} - e^{\alpha_2\Lambda^{ij}t}\right) + \Psi_2\left(e^{\alpha_1\Lambda^{ij}t} + e^{\alpha_2\Lambda^{ij}t}\right)}{\eta}\right] \qquad \text{[C-16a]}$$

$$\int_0^H\int_0^L u_w(x,z,t)dxdz = \sum_{i=0}^{\infty}\sum_{j=0}^{\infty}\varrho_{ij}'\left[\frac{\Omega_2'\left(e^{\alpha_1\Lambda^{ij}t} - e^{\alpha_2\Lambda^{ij}t}\right) + \Psi_2'\left(e^{\alpha_1\Lambda^{ij}t} + e^{\alpha_2\Lambda^{ij}t}\right)}{\eta}\right] \qquad \text{[C-16b]}$$

(b) Anisotropic permeability condition ($k_x \neq k_z$):

$$\int_0^H \int_0^L u_a(x,z,t)dxdz = \sum_{i=0}^{\infty}\sum_{j=0}^{\infty} \varrho'_{ij}\left[\frac{\omega_2\left(e^{\alpha_1^{ij}t}-e^{\alpha_2^{ij}t}\right)+\psi_2\left(e^{\alpha_1^{ij}t}+e^{\alpha_2^{ij}t}\right)}{\eta^{ij}}\right] \qquad [C\text{-}17a]$$

$$\int_0^H \int_0^L u_w(x,z,t)dxdz = \sum_{i=0}^{\infty}\sum_{j=0}^{\infty} \varrho'_{ij}\left[\frac{\omega'_2\left(e^{\alpha_1^{ij}t}-e^{\alpha_2^{ij}t}\right)+\psi'_2\left(e^{\alpha_1^{ij}t}+e^{\alpha_2^{ij}t}\right)}{\eta^{ij}}\right] \qquad [C\text{-}17b]$$

APPENDIX D – Evaluation of initial excess pore pressures due to a change in total stress in the 2D plane strain consolidation

Considering the isotropic loading condition, the changes in excess pore-air and pore-water pressures in response to the applied total loads can be expressed in terms of change in the total minor principal stress (Fredlund & Hasan 1979; Fredlund et al. 2012):

$$\Delta u_a = B_a \, \Delta\sigma_3 \qquad \text{[D-1a]}$$

$$\Delta u_w = B_w \, \Delta\sigma_3 \qquad \text{[D-1b]}$$

where Δu_a and Δu_w are changes in excess pore-air and pore-water pressures due to applied loads, respectively; $\Delta\sigma_3$ is the change in the minor principal stresses; B_a and B_w are tangent pore pressure parameters with respect to air and water phases under an undrained compression, respectively. The parameters of interest B_a and B_w can be further developed as follows (Fredlund & Hasan 1979; Fredlund et al. 2012):

$$B_a = \frac{R_2^s R_1^a - R_2^a}{1 - R_1^s R_1^a} \qquad \text{[D-2a]}$$

$$B_w = \frac{R_2^s - R_1^s R_2^a}{1 - R_1^s R_1^a} \qquad \text{[D-2b]}$$

where $R_1^s = \frac{(m_2^s - m_1^s) - \frac{(1 - S_r + hS_r)\, n}{(u_a + u_{atm})}}{m_2^s + nS_r\beta_w}$; $\quad R_2^s = \frac{m_1^s}{m_2^s + nS_r\beta_w}$;

$R_1^a = \frac{m_2^a}{(m_2^a - m_1^a) - \frac{(1 - S_r + hS_r)\, n}{(u_a + u_{atm})}}$; $\quad R_2^a = \frac{m_1^a}{(m_2^a - m_1^a) - \frac{(1 - S_r + hS_r)\, n}{(u_a + u_{atm})}}$; and

$\beta_w = -\frac{1}{V_w}\frac{dV_w}{du_w}$. [D-3]

The term h in Equation [D-3] is the volumetric coefficient of solubility. On the other hand, the solutions for parameters B_a and B_w require an iterative procedure as they contain the absolute pore-air pressure. It should be noted that, in the undrained loading condition, the increase in the total stress applied on a soil may result in the reduction of matric suction. When the total stress becomes appreciably large, all air bubbles dissolve in water and the pore-air and pore-water pressures approach a single value, indicating the matric suction equals to zero (Lloret & Alonso 1980; Fredlund et al. 2012). In this

situation, the tangent parameters B_a and B_w will approach 1 as the change in the total stress is almost similar to the change in the pore-water pressure.

APPENDIX E – Solutions predicting excess pore pressure dissipation rates induced by time-dependent loadings in the 2D consolidation

i. Consolidation under ramped loading

The dissipation of excess pore-air and pore-water pressures can be estimated by substituting Equation [7-31] into Equation [7-24]:

(a) Isotropic permeability condition ($k_x = k_z$):

$$u_a(x,z,t) = \sum_{i=0}^{\infty}\sum_{j=0}^{\infty} \varpi_{ij}\sin(Ix)\sin(Jz)\left\{\frac{\Omega\left(e^{\alpha_1\Lambda^{ij}t}-e^{\alpha_2\Lambda^{ij}t}\right)+\Psi\left(e^{\alpha_1\Lambda^{ij}t}+e^{\alpha_2\Lambda^{ij}t}\right)}{2\eta}+ X_1(1+K)\left[\frac{e^{\alpha_1\Lambda^{ij}t}(\alpha_1+\beta_1)}{\alpha_1(\alpha_1-\alpha_2)\Lambda^{ij}}+\frac{e^{\alpha_2\Lambda^{ij}t}(\alpha_2+\beta_1)}{\alpha_2(\alpha_2-\alpha_1)\Lambda^{ij}}+\frac{\beta_1}{\alpha_1\alpha_2\Lambda^{ij}}\right]\right\} \quad [E\text{-}1a]$$

$$u_w(x,z,t) = \sum_{i=0}^{\infty}\sum_{j=0}^{\infty} \varpi_{ij}\sin(Ix)\sin(Jz)\left\{\frac{\Omega'\left(e^{\alpha_1\Lambda^{ij}t}-e^{\alpha_2\Lambda^{ij}t}\right)+\Psi'\left(e^{\alpha_1\Lambda^{ij}t}+e^{\alpha_2\Lambda^{ij}t}\right)}{2\eta}+ X_1'(1+K)\left[\frac{e^{\alpha_1\Lambda^{ij}t}(\alpha_1+\beta_1')}{\alpha_1(\alpha_1-\alpha_2)\Lambda^{ij}}+\frac{e^{\alpha_2\Lambda^{ij}t}(\alpha_2+\beta_1')}{\alpha_2(\alpha_2-\alpha_1)\Lambda^{ij}}+\frac{\beta_1'}{\alpha_1\alpha_2\Lambda^{ij}}\right]\right\} \quad [E\text{-}1b]$$

(b) Anisotropic permeability condition ($k_x \neq k_z$):

$$u_a(x,z,t) = \sum_{i=0}^{\infty}\sum_{j=0}^{\infty} \varpi_{ij}\sin(Ix)\sin(Jz)\left\{\frac{\omega\left(e^{\alpha_1^{ij}t}-e^{\alpha_2^{ij}t}\right)+\psi\left(e^{\alpha_1^{ij}t}+e^{\alpha_2^{ij}t}\right)}{2\eta^{ij}}+X_1(1+ K)\left[\frac{e^{\alpha_1^{ij}t}\left(\alpha_1^{ij}+\beta_2\lambda_w^{ij}\right)}{\alpha_1^{ij}\left(\alpha_1^{ij}-\alpha_2^{ij}\right)}+\frac{e^{\alpha_2^{ij}t}\left(\alpha_2^{ij}+\beta_2\lambda_w^{ij}\right)}{\alpha_2^{ij}\left(\alpha_2^{ij}-\alpha_1^{ij}\right)}+\frac{\beta_2\lambda_w^{ij}}{\alpha_1^{ij}\alpha_2^{ij}}\right]\right\} \quad [E\text{-}2a]$$

$$u_w(x,z,t) = \sum_{i=0}^{\infty}\sum_{j=0}^{\infty} \varpi_{ij}\sin(Ix)\sin(Jz)\left\{\frac{\omega'\left(e^{\alpha_1^{ij}t}-e^{\alpha_2^{ij}t}\right)+\psi'\left(e^{\alpha_1^{ij}t}+e^{\alpha_2^{ij}t}\right)}{2\eta^{ij}}+X_1'(1+ K)\left[\frac{e^{\alpha_1^{ij}t}\left(\alpha_1^{ij}+\beta_2'\lambda_a^{ij}\right)}{\alpha_1^{ij}\left(\alpha_1^{ij}-\alpha_2^{ij}\right)}+\frac{e^{\alpha_2^{ij}t}\left(\alpha_2^{ij}+\beta_2'\lambda_a^{ij}\right)}{\alpha_2^{ij}\left(\alpha_2^{ij}-\alpha_1^{ij}\right)}+\frac{\beta_2'\lambda_a^{ij}}{\alpha_1^{ij}\alpha_2^{ij}}\right]\right\} \quad [E\text{-}2b]$$

where $X_1 = \frac{a(C_a c_\sigma^w - c_\sigma^a)}{C_a C_w - 1}$; $X_1' = \frac{a(C_w c_\sigma^a - c_\sigma^w)}{C_a C_w - 1}$;

$$\beta_1 = \frac{c_\sigma^a c_{v_1}^w}{C_a c_\sigma^w - c_\sigma^a}; \qquad \beta_1' = \frac{c_\sigma^w c_{v_1}^a}{C_w c_\sigma^a - c_\sigma^w};$$

$$\beta_2 = \frac{c_\sigma^a c_{v_2}^w}{C_a c_\sigma^w - c_\sigma^a}; \text{ and} \qquad \beta_2' = \frac{c_\sigma^w c_{v_2}^a}{C_w c_\sigma^a - c_\sigma^w}. \qquad \text{[E-3]}$$

When the coefficient of permeability in x-direction for both air and water phases are neglected, Equations [E-1] and [E-2] become:

$$u_a(z,t) = \sum_{j=0}^{\infty} \upsilon_j \sin(Jz) \left\{ \frac{\Omega\left(e^{\alpha_1 J^2 t} - e^{\alpha_2 J^2 t}\right) + \Psi\left(e^{\alpha_1 J^2 t} + e^{\alpha_2 J^2 t}\right)}{2\eta} + \frac{X_1}{J^2} \left[\frac{e^{\alpha_1 J^2 t}(\alpha_1 + \beta_1)}{\alpha_1(\alpha_1 - \alpha_2)} + \frac{e^{\alpha_2 J^2 t}(\alpha_2 + \beta_1)}{\alpha_2(\alpha_2 - \alpha_1)} + \frac{\beta_1}{\alpha_1 \alpha_2} \right] \right\} \qquad \text{[E-4a]}$$

$$u_w(z,t) = \sum_{j=0}^{\infty} \upsilon_j \sin(Jz) \left\{ \frac{\Omega'\left(e^{\alpha_1 J^2 t} - e^{\alpha_2 J^2 t}\right) + \Psi'\left(e^{\alpha_1 J^2 t} + e^{\alpha_2 J^2 t}\right)}{2\eta} + \frac{X_1'}{J^2} \left[\frac{e^{\alpha_1 J^2 t}(\alpha_1 + \beta_1')}{\alpha_1(\alpha_1 - \alpha_2)} + \frac{e^{\alpha_2 J^2 t}(\alpha_2 + \beta_1')}{\alpha_2(\alpha_2 - \alpha_1)} + \frac{\beta_1'}{\alpha_1 \alpha_2} \right] \right\} \qquad \text{[E-4b]}$$

where $\upsilon_j = \frac{2}{HJ}$, for the top drainage condition; or

$= \frac{2[1-(-1)^j]}{HJ}$, for the top and base drainage condition. [E-5]

ii. Consolidation under asymptotic loading

The dissipation of excess pore-air and pore-water pressures can be estimated by substituting Equation [7-32] into Equation [7-24]:

(a) Isotropic permeability condition ($k_x = k_z$):

$$u_a(x,z,t) = \sum_{i=0}^{\infty} \sum_{j=0}^{\infty} \varpi_{ij} \sin(Ix) \sin(Jz) \left\{ \frac{\Omega\left(e^{\alpha_1 \Lambda^{ij} t} - e^{\alpha_2 \Lambda^{ij} t}\right) + \Psi\left(e^{\alpha_1 \Lambda^{ij} t} + e^{\alpha_2 \Lambda^{ij} t}\right)}{2\eta} + X_2(1+K) \left[\frac{e^{-bt}(\beta_1 \Lambda^{ij} - b)}{(b+\alpha_1 \Lambda^{ij})(b+\alpha_2 \Lambda^{ij})} + \frac{e^{\alpha_1 \Lambda^{ij} t}(\alpha_1 + \beta_1)}{(b+\alpha_1 \Lambda^{ij})(\alpha_1 - \alpha_2)} + \frac{e^{\alpha_2 \Lambda^{ij} t}(\alpha_2 + \beta_1)}{(b+\alpha_2 \Lambda^{ij})(\alpha_2 - \alpha_1)} \right] \right\} \qquad \text{[E-6a]}$$

$$u_w(x,z,t) = \sum_{i=0}^{\infty} \sum_{j=0}^{\infty} \varpi_{ij} \sin(Ix) \sin(Jz) \left\{ \frac{\Omega'\left(e^{\alpha_1 \Lambda^{ij} t} - e^{\alpha_2 \Lambda^{ij} t}\right) + \Psi'\left(e^{\alpha_1 \Lambda^{ij} t} + e^{\alpha_2 \Lambda^{ij} t}\right)}{2\eta} + X_2'(1+K) \left[\frac{e^{-bt}(\beta_1' \Lambda^{ij} - b)}{(b+\alpha_1 \Lambda^{ij})(b+\alpha_2 \Lambda^{ij})} + \frac{e^{\alpha_1 \Lambda^{ij} t}(\alpha_1 + \beta_1')}{(b+\alpha_1 \Lambda^{ij})(\alpha_1 - \alpha_2)} + \frac{e^{\alpha_2 \Lambda^{ij} t}(\alpha_2 + \beta_1')}{(b+\alpha_2 \Lambda^{ij})(\alpha_2 - \alpha_1)} \right] \right\} \qquad \text{[E-6b]}$$

(b) Anisotropic permeability condition ($k_x \neq k_z$):

$$u_a(x,z,t) = \sum_{i=0}^{\infty}\sum_{j=0}^{\infty} \varpi_{ij}\sin(Ix)\sin(Jz)\left\{\frac{\omega\left(e^{\alpha_1^{ij}t}-e^{\alpha_2^{ij}t}\right)+\psi\left(e^{\alpha_1^{ij}t}+e^{\alpha_2^{ij}t}\right)}{2\eta^{ij}} + X_2(1+ K)\left[\frac{e^{-bt}\left(\beta_2\lambda_w^{ij}-b\right)}{\left(b+\alpha_1^{ij}\right)\left(b+\alpha_2^{ij}\right)} + \frac{e^{\alpha_1^{ij}t}\left(\alpha_1^{ij}+\beta_2\lambda_w^{ij}\right)}{\left(b+\alpha_1^{ij}\right)\left(\alpha_1^{ij}-\alpha_2^{ij}\right)} + \frac{e^{\alpha_2^{ij}t}\left(\alpha_2^{ij}+\beta_2\lambda_w^{ij}\right)}{\left(b+\alpha_2^{ij}\right)\left(\alpha_2^{ij}-\alpha_1^{ij}\right)}\right]\right\} \quad [E\text{-}7a]$$

$$u_w(x,z,t) = \sum_{i=0}^{\infty}\sum_{j=0}^{\infty} \varpi_{ij}\sin(Ix)\sin(Jz)\left\{\frac{\omega'\left(e^{\alpha_1^{ij}t}-e^{\alpha_2^{ij}t}\right)+\psi'\left(e^{\alpha_1^{ij}t}+e^{\alpha_2^{ij}t}\right)}{2\eta^{ij}} + X_2'(1+ K)\left[\frac{e^{-bt}\left(\beta_2'\lambda_a^{ij}-b\right)}{\left(b+\alpha_1^{ij}\right)\left(b+\alpha_2^{ij}\right)} + \frac{e^{\alpha_1^{ij}t}\left(\alpha_1^{ij}+\beta_2'\lambda_a^{ij}\right)}{\left(b+\alpha_1^{ij}\right)\left(\alpha_1^{ij}-\alpha_2^{ij}\right)} + \frac{e^{\alpha_2^{ij}t}\left(\alpha_2^{ij}+\beta_2'\lambda_a^{ij}\right)}{\left(b+\alpha_2^{ij}\right)\left(\alpha_2^{ij}-\alpha_1^{ij}\right)}\right]\right\} \quad [E\text{-}7b]$$

where $X_2 = \frac{Abq_0(C_a c_\sigma^w - c_\sigma^a)}{C_a C_w - 1}$; and $X_2' = \frac{Abq_0(C_w c_\sigma^a - c_\sigma^w)}{C_a C_w - 1}$. [E-8]

iii. Consolidation under sinusoidal loading

The dissipation of excess pore-air and pore-water pressures can be estimated by substituting Equation [7-33] into Equation [7-24]:

(a) Isotropic permeability condition ($k_x = k_z$):

$$u_a(x,z,t) = \sum_{i=0}^{\infty}\sum_{j=0}^{\infty} \varpi_{ij}\sin(Ix)\sin(Jz)\left\{\frac{\Omega\left(e^{\alpha_1\Lambda^{ij}t}-e^{\alpha_2\Lambda^{ij}t}\right)+\Psi\left(e^{\alpha_1\Lambda^{ij}t}+e^{\alpha_2\Lambda^{ij}t}\right)}{2\eta} + X_3(1+K)\left[\frac{e^{\alpha_1\Lambda^{ij}t}\alpha_1\Lambda^{ij}(\alpha_1+\beta_1)}{\left[\left(\alpha_1\Lambda^{ij}\right)^2+\theta^2\right](\alpha_1-\alpha_2)} + \frac{e^{\alpha_2\Lambda^{ij}t}\alpha_2\Lambda^{ij}(\alpha_2+\beta_1)}{\left[\left(\alpha_2\Lambda^{ij}\right)^2+\theta^2\right](\alpha_2-\alpha_1)} + \frac{\zeta_1\cos(\theta t)+\xi_1\sin(\theta t)}{\left[\left(\alpha_1\Lambda^{ij}\right)^2+\theta^2\right]\left[\left(\alpha_2\Lambda^{ij}\right)^2+\theta^2\right]}\right]\right\} \quad [E\text{-}9a]$$

$$u_w(x,z,t) = \sum_{i=0}^{\infty}\sum_{j=0}^{\infty} \varpi_{ij}\sin(Ix)\sin(Jz)\left\{\frac{\Omega'\left(e^{\alpha_1\Lambda^{ij}t}-e^{\alpha_2\Lambda^{ij}t}\right)+\Psi'\left(e^{\alpha_1\Lambda^{ij}t}+e^{\alpha_2\Lambda^{ij}t}\right)}{2\eta} + X_3'(1+K)\left[\frac{e^{\alpha_1\Lambda^{ij}t}\alpha_1\Lambda^{ij}(\alpha_1+\beta_1')}{\left[\left(\alpha_1\Lambda^{ij}\right)^2+\theta^2\right](\alpha_1-\alpha_2)} + \frac{e^{\alpha_2\Lambda^{ij}t}\alpha_2\Lambda^{ij}(\alpha_2+\beta_1')}{\left[\left(\alpha_2\Lambda^{ij}\right)^2+\theta^2\right](\alpha_2-\alpha_1)} + \frac{\zeta_1'\cos(\theta t)+\xi_1'\sin(\theta t)}{\left[\left(\alpha_1\Lambda^{ij}\right)^2+\theta^2\right]\left[\left(\alpha_2\Lambda^{ij}\right)^2+\theta^2\right]}\right]\right\} \quad [E\text{-}9b]$$

(b) Anisotropic permeability condition ($k_x \neq k_z$):

$$u_a(x,z,t) = \sum_{i=0}^{\infty}\sum_{j=0}^{\infty} \varpi_{ij}\sin(Ix)\sin(Jz)\left\{\frac{\omega\left(e^{\alpha_1^{ij}t}-e^{\alpha_2^{ij}t}\right)+\psi\left(e^{\alpha_1^{ij}t}+e^{\alpha_2^{ij}t}\right)}{2\eta^{ij}} + X_3(1 + K)\left[\frac{e^{\alpha_1^{ij}t}\alpha_1^{ij}\left(\alpha_1^{ij}+\beta_2\lambda_w^{ij}\right)}{\left[\left(\alpha_1^{ij}\right)^2+\theta^2\right]\left(\alpha_1^{ij}-\alpha_2^{ij}\right)} + \frac{e^{\alpha_2^{ij}t}\alpha_2^{ij}\left(\alpha_2^{ij}+\beta_2\lambda_w^{ij}\right)}{\left[\left(\alpha_2^{ij}\right)^2+\theta^2\right]\left(\alpha_2^{ij}-\alpha_1^{ij}\right)} + \frac{\zeta_2\cos(\theta t)+\xi_2\sin(\theta t)}{\left[\left(\alpha_1^{ij}\right)^2+\theta^2\right]\left[\left(\alpha_2^{ij}\right)^2+\theta^2\right]}\right]\right\} \quad \text{[E-10a]}$$

$$u_w(x,z,t) = \sum_{i=0}^{\infty}\sum_{j=0}^{\infty} \varpi_{ij}\sin(Ix)\sin(Jz)\left\{\frac{\omega'\left(e^{\alpha_1^{ij}t}-e^{\alpha_2^{ij}t}\right)+\psi'\left(e^{\alpha_1^{ij}t}+e^{\alpha_2^{ij}t}\right)}{2\eta^{ij}} + X_3'(1 + K)\left[\frac{e^{\alpha_1^{ij}t}\alpha_1^{ij}\left(\alpha_1^{ij}+\beta_2'\lambda_a^{ij}\right)}{\left[\left(\alpha_1^{ij}\right)^2+\theta^2\right]\left(\alpha_1^{ij}-\alpha_2^{ij}\right)} + \frac{e^{\alpha_2^{ij}t}\alpha_2^{ij}\left(\alpha_2^{ij}+\beta_2'\lambda_a^{ij}\right)}{\left[\left(\alpha_2^{ij}\right)^2+\theta^2\right]\left(\alpha_2^{ij}-\alpha_1^{ij}\right)} + \frac{\zeta_2'\cos(\theta t)+\xi_2'\sin(\theta t)}{\left[\left(\alpha_1^{ij}\right)^2+\theta^2\right]\left[\left(\alpha_2^{ij}\right)^2+\theta^2\right]}\right]\right\} \quad \text{[E-10b]}$$

where $X_3 = \frac{Bq_0\theta(C_a c_\sigma^w - c_\sigma^a)}{C_a C_w - 1}$; $X_3' = \frac{Bq_0\theta(C_w c_\sigma^a - c_\sigma^w)}{C_a C_w - 1}$;

$$\zeta_1 = \Lambda^{ij}\left[\alpha_1\alpha_2\beta_1\left(\Lambda^{ij}\right)^2 - (\alpha_1+\alpha_2+\beta_1)\theta^2\right];$$

$$\zeta_1' = \Lambda^{ij}\left[\alpha_1\alpha_2\beta_1'\left(\Lambda^{ij}\right)^2 - (\alpha_1+\alpha_2+\beta_1')\theta^2\right];$$

$$\zeta_2 = \alpha_1^{ij}\alpha_2^{ij}\beta_2\lambda_w^{ij} - \left(\alpha_1^{ij}+\alpha_2^{ij}+\beta_2\lambda_w^{ij}\right)\theta^2;$$

$$\zeta_2' = \alpha_1^{ij}\alpha_2^{ij}\beta_2'\lambda_a^{ij} - \left(\alpha_1^{ij}+\alpha_2^{ij}+\beta_2'\lambda_a^{ij}\right)\theta^2;$$

$$\xi_1 = \theta\left\{\theta^2 - [\beta_1(\alpha_1+\alpha_2)+\alpha_1\alpha_2]\left(\Lambda^{ij}\right)^2\right\};$$

$$\xi_1' = \theta\left\{\theta^2 - [\beta_1'(\alpha_1+\alpha_2)+\alpha_1\alpha_2]\left(\Lambda^{ij}\right)^2\right\};$$

$$\xi_2 = \theta\left\{\theta^2 - \left[\beta_2\lambda_w^{ij}\left(\alpha_1^{ij}+\alpha_2^{ij}\right)+\alpha_1^{ij}\alpha_2^{ij}\right]\right\}; \text{ and}$$

$$\xi_2' = \theta\left\{\theta^2 - \left[\beta_2'\lambda_a^{ij}\left(\alpha_1^{ij}+\alpha_2^{ij}\right)+\alpha_1^{ij}\alpha_2^{ij}\right]\right\}. \quad \text{[E-11]}$$

iv. Consolidation under damped sine wave loading

The dissipation of excess pore-air and pore-water pressures can be estimated by substituting Equation [7-34] into Equation [7-24]:

(a) Isotropic permeability condition ($k_x = k_z$):

$$u_a(x,z,t) = \sum_{i=0}^{\infty}\sum_{j=0}^{\infty} \varpi_{ij}\sin(Ix)\sin(Jz)\left\{\frac{\Omega\left(e^{\alpha_1\Lambda^{ij}t}-e^{\alpha_2\Lambda^{ij}t}\right)+\Psi\left(e^{\alpha_1\Lambda^{ij}t}+e^{\alpha_2\Lambda^{ij}t}\right)}{2\eta}+\right.$$

$$X_4(1+K)\left[\frac{e^{\alpha_1\Lambda^{ij}t}\alpha_1\Lambda^{ij}(\alpha_1+\beta_1)}{\left[(\alpha_1\Lambda^{ij}+c)^2+\vartheta^2\right](\alpha_1-\alpha_2)}+\frac{e^{\alpha_2\Lambda^{ij}t}\alpha_2\Lambda^{ij}(\alpha_2+\beta_1)}{\left[(\alpha_2\Lambda^{ij}+c)^2+\vartheta^2\right](\alpha_2-\alpha_1)}+\right.$$

$$\left.\left.\frac{e^{-ct}[\varrho_1\cos(\vartheta t)+\varsigma_1\sin(\vartheta t)]}{\vartheta\left[(\alpha_1\Lambda^{ij}+c)^2+\vartheta^2\right]\left[(\alpha_2\Lambda^{ij}+c)^2+\vartheta^2\right]}\right]\right\} \qquad \text{[E-12a]}$$

$$u_w(x,z,t) = \sum_{i=0}^{\infty}\sum_{j=0}^{\infty} \varpi_{ij}\sin(Ix)\sin(Jz)\left\{\frac{\Omega'\left(e^{\alpha_1\Lambda^{ij}t}-e^{\alpha_2\Lambda^{ij}t}\right)+\Psi'\left(e^{\alpha_1\Lambda^{ij}t}+e^{\alpha_2\Lambda^{ij}t}\right)}{2\eta}+\right.$$

$$X_4'(1+K)\left[\frac{e^{\alpha_1\Lambda^{ij}t}\alpha_1\Lambda^{ij}(\alpha_1+\beta_1')}{\left[(\alpha_1\Lambda^{ij}+c)^2+\vartheta^2\right](\alpha_1-\alpha_2)}+\frac{e^{\alpha_2\Lambda^{ij}t}\alpha_2\Lambda^{ij}(\alpha_2+\beta_1')}{\left[(\alpha_2\Lambda^{ij}+c)^2+\vartheta^2\right](\alpha_2-\alpha_1)}+\right.$$

$$\left.\left.\frac{e^{-ct}[\varrho_1'\cos(\vartheta t)+\varsigma_1'\sin(\vartheta t)]}{\vartheta\left[(\alpha_1\Lambda^{ij}+c)^2+\vartheta^2\right]\left[(\alpha_2\Lambda^{ij}+c)^2+\vartheta^2\right]}\right]\right\} \qquad \text{[E-12b]}$$

(b) Anisotropic permeability condition ($k_x \neq k_z$):

$$u_a(x,z,t) = \sum_{i=0}^{\infty}\sum_{j=0}^{\infty} \varpi_{ij}\sin(Ix)\sin(Jz)\left\{\frac{\omega\left(e^{\alpha_1^{ij}t}-e^{\alpha_2^{ij}t}\right)+\psi\left(e^{\alpha_1^{ij}t}+e^{\alpha_2^{ij}t}\right)}{2\eta^{ij}}+X_4(1+\right.$$

$$K)\left[\frac{e^{\alpha_1^{ij}t}\alpha_1^{ij}\left(\alpha_1^{ij}+\beta_2\lambda_w^{ij}\right)}{\left[\left(\alpha_1^{ij}+c\right)^2+\vartheta^2\right]\left(\alpha_1^{ij}-\alpha_2^{ij}\right)}+\frac{e^{\alpha_2^{ij}t}\alpha_2^{ij}\left(\alpha_2^{ij}+\beta_2\lambda_w^{ij}\right)}{\left[\left(\alpha_2^{ij}+c\right)^2+\vartheta^2\right]\left(\alpha_2^{ij}-\alpha_1^{ij}\right)}+\right.$$

$$\left.\left.\frac{e^{-ct}[\varrho_2\cos(\vartheta t)+\varsigma_2\sin(\vartheta t)]}{\vartheta\left[\left(\alpha_1^{ij}+c\right)^2+\vartheta^2\right]\left[\left(\alpha_2^{ij}+c\right)^2+\vartheta^2\right]}\right]\right\} \qquad \text{[E-13a]}$$

$$u_w(x,z,t) = \sum_{i=0}^{\infty}\sum_{j=0}^{\infty} \varpi_{ij}\sin(Ix)\sin(Jz)\left\{\frac{\omega'\left(e^{\alpha_1^{ij}t}-e^{\alpha_2^{ij}t}\right)+\psi'\left(e^{\alpha_1^{ij}t}+e^{\alpha_2^{ij}t}\right)}{2\eta^{ij}}+X_4'(1+\right.$$

$$K)\left[\frac{e^{\alpha_1^{ij}t}\alpha_1^{ij}\left(\alpha_1^{ij}+\beta_2'\lambda_a^{ij}\right)}{\left[\left(\alpha_1^{ij}+c\right)^2+\vartheta^2\right]\left(\alpha_1^{ij}-\alpha_2^{ij}\right)}+\frac{e^{\alpha_2\Lambda^{ij}t}\alpha_2\Lambda^{ij}\left(\alpha_2+\beta_2'\lambda_a^{ij}\right)}{\left[\left(\alpha_2^{ij}+c\right)^2+\vartheta^2\right]\left(\alpha_2^{ij}-\alpha_1^{ij}\right)}+\right.$$

$$\left.\left.\frac{e^{-ct}[\varrho_2'\cos(\vartheta t)+\varsigma_2'\sin(\vartheta t)]}{\vartheta\left[\left(\alpha_1^{ij}+c\right)^2+\vartheta^2\right]\left[\left(\alpha_2^{ij}+c\right)^2+\vartheta^2\right]}\right]\right\} \qquad \text{[E-13b]}$$

where $X_4 = \frac{Cq_0\vartheta(C_a c_\sigma^w - c_\sigma^a)}{C_a C_w - 1}$; $\quad X_4' = \frac{Cq_0\vartheta(C_w c_\sigma^a - c_\sigma^w)}{C_a C_w - 1}$;

$$\varrho_1 = \vartheta\Lambda^{ij}\left[\alpha_1\alpha_2\beta_1\left(\Lambda^{ij}\right)^2 - 2c\alpha_1\alpha_2\Lambda^{ij} - (c^2+\vartheta^2)(\alpha_1+\alpha_2+\beta_1)\right];$$

$$\varrho_1' = \vartheta\Lambda^{ij}\left[\alpha_1\alpha_2\beta_1'\left(\Lambda^{ij}\right)^2 - 2c\alpha_1\alpha_2\Lambda^{ij} - (c^2+\vartheta^2)(\alpha_1+\alpha_2+\beta_1')\right];$$

$$\varrho_2 = \vartheta\left[\alpha_1^{ij}\alpha_2^{ij}\beta_2\lambda_w^{ij} - 2c\alpha_1^{ij}\alpha_2^{ij} - (c^2+\vartheta^2)\left(\alpha_1^{ij}+\alpha_2^{ij}+\beta_2\lambda_w^{ij}\right)\right];$$

$$\varrho_2' = \vartheta\left[\alpha_1^{ij}\alpha_2^{ij}\beta_2'\lambda_a^{ij} - 2c\alpha_1^{ij}\alpha_2^{ij} - (c^2+\vartheta^2)\left(\alpha_1^{ij}+\alpha_2^{ij}+\beta_2'\lambda_a^{ij}\right)\right];$$

$$\varsigma_1 = (c^2+\vartheta^2)^2 + c(\alpha_1+\alpha_2-\beta_1)(c^2+\vartheta^2)\Lambda^{ij} + [(c^2-\vartheta^2)\alpha_1\alpha_2 - \beta_1(\alpha_1+\alpha_2)(c^2+\vartheta^2)]\left(\Lambda^{ij}\right)^2 - c\alpha_1\alpha_2\beta_1\left(\Lambda^{ij}\right)^3;$$

$$\varsigma_1' = (c^2+\vartheta^2)^2 + c(\alpha_1+\alpha_2-\beta_1')(c^2+\vartheta^2)\Lambda^{ij} + [(c^2-\vartheta^2)\alpha_1\alpha_2 - \beta_1'(\alpha_1+\alpha_2)(c^2+\vartheta^2)]\left(\Lambda^{ij}\right)^2 - c\alpha_1\alpha_2\beta_1'\left(\Lambda^{ij}\right)^3;$$

$$\varsigma_2 = (c^2+\vartheta^2)^2 + c\left(\alpha_1^{ij}+\alpha_2^{ij}-\beta_2\lambda_w^{ij}\right)(c^2+\vartheta^2) + \left[(c^2-\vartheta^2)\alpha_1^{ij}\alpha_2^{ij} - \beta_2\lambda_w^{ij}\left(\alpha_1^{ij}+\alpha_2^{ij}\right)(c^2+\vartheta^2)\right] - c\alpha_1^{ij}\alpha_2^{ij}\beta_2\lambda_w^{ij}; \text{ and}$$

$$\varsigma_2' = (c^2+\vartheta^2)^2 + c\left(\alpha_1^{ij}+\alpha_2^{ij}-\beta_2'\lambda_a^{ij}\right)(c^2+\vartheta^2) + \left[(c^2-\vartheta^2)\alpha_1^{ij}\alpha_2^{ij} - \beta_2'\lambda_a^{ij}\left(\alpha_1^{ij}+\alpha_2^{ij}\right)(c^2+\vartheta^2)\right] - c\alpha_1^{ij}\alpha_2^{ij}\beta_2'\lambda_a^{ij}. \qquad \text{[E-14]}$$

APPENDIX F – Polar transformation for x- and y-coordinates

The net flux of air and water per unit volume of the element in Cartesian coordinates (x, y, z) can be presented as follows:

(a) Volume change in the 2D Cartesian system:

$$\frac{\partial\left(\frac{\Delta V_a}{V_0}\right)}{\partial t} = \frac{R\Theta}{gM\left(u_a^0+u_{atm}\right)}\left[k_{a_x}\left(\frac{\partial^2 u_a}{\partial x^2}\right) + k_{a_y}\left(\frac{\partial^2 u_a}{\partial y^2}\right)\right] - \frac{n(1-S_r)}{\left(u_a^0+u_{atm}\right)}\left(\frac{\partial u_a}{\partial t}\right) \quad [F\text{-}1a]$$

$$\frac{\partial\left(\frac{\Delta V_w}{V_0}\right)}{\partial t} = \frac{1}{\gamma_w}\left[k_{w_x}\left(\frac{\partial^2 u_w}{\partial x^2}\right) + k_{w_y}\left(\frac{\partial^2 u_w}{\partial y^2}\right)\right] \quad [F\text{-}1b]$$

(b) Volume change in the 3D Cartesian system:

$$\frac{\partial\left(\frac{\Delta V_a}{V_0}\right)}{\partial t} = \frac{R\Theta}{gM\left(u_a^0+u_{atm}\right)}\left[k_{a_x}\left(\frac{\partial^2 u_a}{\partial x^2}\right) + k_{a_y}\left(\frac{\partial^2 u_a}{\partial y^2}\right) + k_{a_z}\left(\frac{\partial^2 u_a}{\partial z^2}\right)\right] - \frac{n(1-S_r)}{\left(u_a^0+u_{atm}\right)}\left(\frac{\partial u_a}{\partial t}\right) \quad [F\text{-}2a]$$

$$\frac{\partial\left(\frac{\Delta V_w}{V_0}\right)}{\partial t} = \frac{1}{\gamma_w}\left[k_{w_x}\left(\frac{\partial^2 u_w}{\partial x^2}\right) + k_{w_y}\left(\frac{\partial^2 u_w}{\partial y^2}\right) + k_{w_z}\left(\frac{\partial^2 u_w}{\partial z^2}\right)\right] \quad [F\text{-}2b]$$

Cartesian coordinates (x, y) can be transformed into the following set of polar coordinates (r, θ):

$$\begin{cases} r = \sqrt{x^2 + y^2} \\ \theta = \tan^{-1}\left(\frac{y}{x}\right) \end{cases} \quad [F\text{-}3]$$

Also,

$$\begin{cases} x = r\cos\theta \\ y = r\sin\theta \end{cases} \quad [F\text{-}4]$$

Differentiating the equation of the radius r in Equation [F-3] with respect to x and y results in:

$$\frac{\partial r}{\partial x} = \frac{x}{\sqrt{x^2+y^2}} = \frac{x}{r} = \cos\theta \quad [F\text{-}5a]$$

$$\frac{\partial r}{\partial y} = \frac{y}{\sqrt{x^2+y^2}} = \frac{y}{r} = \sin\theta \quad [F\text{-}5b]$$

Then, differentiating the equation of the polar angle θ in Equation [F-4] with respect to x and y gives:

$$\frac{\partial\theta}{\partial x} = \frac{\partial}{\partial x}\left[\cos^{-1}\left(\frac{x}{\sqrt{x^2+y^2}}\right)\right] = -\frac{y}{x^2+y^2} = -\frac{y}{r^2} = -\frac{\sin\theta}{r} \quad \text{[F-6a]}$$

$$\frac{\partial\theta}{\partial y} = \frac{\partial}{\partial y}\left[\sin^{-1}\left(\frac{y}{\sqrt{x^2+y^2}}\right)\right] = \frac{x}{x^2+y^2} = \frac{x}{r^2} = \frac{\cos\theta}{r} \quad \text{[F-6b]}$$

Considering excess pore pressures u_a and u_w as functions of both r and θ:

(a) In the x-direction:

$$\frac{\partial u_a}{\partial x} = \frac{\partial u_a}{\partial r}\frac{\partial r}{\partial x} + \frac{\partial u_a}{\partial \theta}\frac{\partial \theta}{\partial x} = \frac{\partial u_a}{\partial r}\cos\theta - \frac{1}{r}\frac{\partial u_a}{\partial \theta}\sin\theta \quad \text{[F-7a]}$$

$$\frac{\partial u_w}{\partial x} = \frac{\partial u_w}{\partial r}\frac{\partial r}{\partial x} + \frac{\partial u_w}{\partial \theta}\frac{\partial \theta}{\partial x} = \frac{\partial u_w}{\partial r}\cos\theta - \frac{1}{r}\frac{\partial u_w}{\partial \theta}\sin\theta \quad \text{[F-7b]}$$

(b) In the y-direction:

$$\frac{\partial u_a}{\partial y} = \frac{\partial u_a}{\partial r}\frac{\partial r}{\partial y} + \frac{\partial u_a}{\partial \theta}\frac{\partial \theta}{\partial y} = \frac{\partial u_a}{\partial r}\sin\theta + \frac{1}{r}\frac{\partial u_a}{\partial \theta}\cos\theta \quad \text{[F-8a]}$$

$$\frac{\partial u_w}{\partial y} = \frac{\partial u_w}{\partial r}\frac{\partial r}{\partial y} + \frac{\partial u_w}{\partial \theta}\frac{\partial \theta}{\partial y} = \frac{\partial u_w}{\partial r}\sin\theta + \frac{1}{r}\frac{\partial u_w}{\partial \theta}\cos\theta \quad \text{[F-8b]}$$

Taking the second derivatives of Equations [F-7] and [F-8] with respect to x and y, respectively, gives:

(a) In the x-direction:

$$\frac{\partial^2 u_a}{\partial x^2} = \left(\cos\theta\frac{\partial}{\partial r} - \frac{1}{r}\sin\theta\frac{\partial}{\partial \theta}\right)\left(\frac{\partial u_a}{\partial r}\cos\theta - \frac{1}{r}\frac{\partial u_a}{\partial \theta}\sin\theta\right) \quad \text{[F-9a]}$$

$$\frac{\partial^2 u_w}{\partial x^2} = \left(\cos\theta\frac{\partial}{\partial r} - \frac{1}{r}\sin\theta\frac{\partial}{\partial \theta}\right)\left(\frac{\partial u_w}{\partial r}\cos\theta - \frac{1}{r}\frac{\partial u_w}{\partial \theta}\sin\theta\right) \quad \text{[F-9b]}$$

(b) In the y-direction:

$$\frac{\partial^2 u_a}{\partial y^2} = \left(\sin\theta\frac{\partial}{\partial r} + \frac{1}{r}\cos\theta\frac{\partial}{\partial \theta}\right)\left(\frac{\partial u_a}{\partial r}\sin\theta + \frac{1}{r}\frac{\partial u_a}{\partial \theta}\cos\theta\right) \quad \text{[F-10a]}$$

$$\frac{\partial^2 u_w}{\partial y^2} = \left(\sin\theta\frac{\partial}{\partial r} + \frac{1}{r}\cos\theta\frac{\partial}{\partial \theta}\right)\left(\frac{\partial u_w}{\partial r}\sin\theta + \frac{1}{r}\frac{\partial u_w}{\partial \theta}\cos\theta\right) \quad \text{[F-10b]}$$

Thus,

$$\frac{\partial^2 u_a}{\partial x^2} = \frac{\partial^2 u_a}{\partial r^2}\cos^2\theta - 2\left(\frac{\partial^2 u_a}{\partial\theta\ \partial r}\frac{\sin\theta\cos\theta}{r} - \frac{\partial u_a}{\partial\theta}\frac{\sin\theta\cos\theta}{r}\right) + \frac{\partial u_a}{\partial r}\frac{\sin^2\theta}{r} + \frac{\partial^2 u_a}{\partial\theta^2}\frac{\sin^2\theta}{r^2} \quad [F\text{-}11a]$$

$$\frac{\partial^2 u_w}{\partial x^2} = \frac{\partial^2 u_w}{\partial r^2}\cos^2\theta - 2\left(\frac{\partial^2 u_w}{\partial\theta\ \partial r}\frac{\sin\theta\cos\theta}{r} - \frac{\partial u_w}{\partial\theta}\frac{\sin\theta\cos\theta}{r}\right) + \frac{\partial u_w}{\partial r}\frac{\sin^2\theta}{r} + \frac{\partial^2 u_w}{\partial\theta^2}\frac{\sin^2\theta}{r^2} \quad [F\text{-}11b]$$

and

$$\frac{\partial^2 u_a}{\partial y^2} = \frac{\partial^2 u_a}{\partial r^2}\sin^2\theta + 2\left(\frac{\partial^2 u_a}{\partial\theta\ \partial r}\frac{\sin\theta\cos\theta}{r} - \frac{\partial u_a}{\partial\theta}\frac{\sin\theta\cos\theta}{r}\right) + \frac{\partial u_a}{\partial r}\frac{\cos^2\theta}{r} + \frac{\partial^2 u_a}{\partial\theta^2}\frac{\cos^2\theta}{r^2} \quad [F\text{-}12a]$$

$$\frac{\partial^2 u_w}{\partial y^2} = \frac{\partial^2 u_w}{\partial r^2}\sin^2\theta + 2\left(\frac{\partial^2 u_w}{\partial\theta\ \partial r}\frac{\sin\theta\cos\theta}{r} - \frac{\partial u_w}{\partial\theta}\frac{\sin\theta\cos\theta}{r}\right) + \frac{\partial u_w}{\partial r}\frac{\cos^2\theta}{r} + \frac{\partial^2 u_w}{\partial\theta^2}\frac{\cos^2\theta}{r^2} \quad [F\text{-}12b]$$

Adding Equations [F-11a] and [F-12a] as well as Equations [F-11b] and [F-12b] yields:

$$\frac{\partial^2 u_a}{\partial x^2} + \frac{\partial^2 u_a}{\partial y^2} = \frac{\partial^2 u_a}{\partial r^2} + \frac{1}{r}\frac{\partial u_a}{\partial r} + \frac{1}{r^2}\frac{\partial^2 u_a}{\partial\theta^2} \quad [F\text{-}13a]$$

$$\frac{\partial^2 u_w}{\partial x^2} + \frac{\partial^2 u_w}{\partial y^2} = \frac{\partial^2 u_w}{\partial r^2} + \frac{1}{r}\frac{\partial u_w}{\partial r} + \frac{1}{r^2}\frac{\partial^2 u_w}{\partial\theta^2} \quad [F\text{-}13b]$$

For the case of axial symmetry, the pore pressures u_a and u_w are independent of θ, thus,

$$\frac{\partial^2 u_a}{\partial x^2} + \frac{\partial^2 u_a}{\partial y^2} = \frac{\partial^2 u_a}{\partial r^2} + \frac{1}{r}\frac{\partial u_a}{\partial r} \quad [F\text{-}14a]$$

$$\frac{\partial^2 u_w}{\partial x^2} + \frac{\partial^2 u_w}{\partial y^2} = \frac{\partial^2 u_w}{\partial r^2} + \frac{1}{r}\frac{\partial u_w}{\partial r} \quad [F\text{-}14b]$$

Assuming $k_{a_x} = k_{a_y} = k_{a_r}$ and $k_{w_x} = k_{w_y} = k_{w_r}$, Equation [F-14] can be substituted into Equations [F-1] and [F-2]:

(a) Volume change in radial direction only:

$$\frac{\partial\left(\frac{\Delta V_a}{V_0}\right)}{\partial t} = \frac{k_{a_r} R\Theta}{gM\left(u_a^0 + u_{atm}\right)}\left(\frac{\partial^2 u_a}{\partial r^2} + \frac{1}{r}\frac{\partial u_a}{\partial r}\right) - \frac{n(1-S_r)}{\left(u_a^0 + u_{atm}\right)}\left(\frac{\partial u_a}{\partial t}\right) \quad [F\text{-}15a]$$

$$\frac{\partial\left(\frac{\Delta V_w}{V_0}\right)}{\partial t} = \frac{k_{w_r}}{\gamma_w}\left(\frac{\partial^2 u_w}{\partial r^2} + \frac{1}{r}\frac{\partial u_w}{\partial r}\right) \quad [F\text{-}15b]$$

(b) Volume change in radial and vertical directions:

$$\frac{\partial\left(\frac{\Delta V_a}{V_0}\right)}{\partial t} = \frac{R\Theta}{gM\left(u_a^0+u_{atm}\right)}\left[k_{a_r}\left(\frac{\partial^2 u_a}{\partial r^2}+\frac{1}{r}\frac{\partial u_a}{\partial r}\right)+k_{a_z}\left(\frac{\partial^2 u_a}{\partial z^2}\right)\right]-\frac{n(1-S_r)}{\left(u_a^0+u_{atm}\right)}\left(\frac{\partial u_a}{\partial t}\right) \quad [F\text{-}16a]$$

$$\frac{\partial\left(\frac{\Delta V_w}{V_0}\right)}{\partial t} = \frac{1}{\gamma_w}\left[k_{w_r}\left(\frac{\partial^2 u_w}{\partial r^2}+\frac{1}{r}\frac{\partial u_w}{\partial r}\right)+k_{w_z}\left(\frac{\partial^2 u_w}{\partial z^2}\right)\right] \quad [F\text{-}16b]$$

Following Fredlund et al. (2012), the 3D constitutive equations linking the soil deformation and stress state variables can be expressed in the polar coordinates (r, θ, z), as presented below:

$$\frac{\partial\left(\frac{\Delta V_a}{V_0}\right)}{\partial t} = m_1^a\frac{\partial}{\partial t}\left(\frac{\sigma_r+\sigma_\theta+\sigma_z}{3}-u_a\right)+m_2^a\frac{\partial(u_a-u_w)}{\partial t} \quad [F\text{-}17a]$$

$$\frac{\partial\left(\frac{\Delta V_w}{V_0}\right)}{\partial t} = m_1^w\frac{\partial}{\partial t}\left(\frac{\sigma_r+\sigma_\theta+\sigma_z}{3}-u_a\right)+m_2^w\frac{\partial(u_a-u_w)}{\partial t} \quad [F\text{-}17b]$$

where σ_r, σ_θ and σ_z are the total stress in r-, θ- and z-directions, respectively. Under the constant loading condition, let set $\partial\sigma_r/\partial t = \partial\sigma_\theta/\partial t = \partial\sigma_z/\partial t = 0$. Equations [F-15] and [F-16] can be equated to Equation [F-17], giving:

(a) Polar governing equations considering the radial flow only:

$$\frac{\partial u_a}{\partial t}+C_a\left(\frac{\partial u_w}{\partial t}\right)+c_{v_r}^a\left(\frac{\partial^2 u_a}{\partial r^2}+\frac{1}{r}\frac{\partial u_a}{\partial r}\right)=0 \quad [F\text{-}18a]$$

$$\frac{\partial u_w}{\partial t}+C_w\left(\frac{\partial u_a}{\partial t}\right)+c_{v_r}^w\left(\frac{\partial^2 u_w}{\partial r^2}+\frac{1}{r}\frac{\partial u_w}{\partial r}\right)=0 \quad [F\text{-}18b]$$

(b) Polar governing equations considering both radial and vertical flows:

$$\frac{\partial u_a}{\partial t}+C_a\left(\frac{\partial u_w}{\partial t}\right)+c_{v_r}^a\left(\frac{\partial^2 u_a}{\partial r^2}+\frac{1}{r}\frac{\partial u_a}{\partial r}\right)+c_{v_z}^a\left(\frac{\partial^2 u_a}{\partial z^2}\right)=0 \quad [F\text{-}19a]$$

$$\frac{\partial u_w}{\partial t}+C_w\left(\frac{\partial u_a}{\partial t}\right)+c_{v_r}^w\left(\frac{\partial^2 u_w}{\partial r^2}+\frac{1}{r}\frac{\partial u_w}{\partial r}\right)+c_{v_z}^w\left(\frac{\partial^2 u_w}{\partial z^2}\right)=0 \quad [F\text{-}19b]$$

Equations [F-18] and [F-19] present the governing flow equations in the axisymmetric condition. Simplified forms of these equations can be found in Equations [8-1] and [8-2]. Note that the consolidation coefficients for air (i.e. C_a, $c_{v_r}^a$ and $c_{v_z}^a$) and water (i.e. C_w, $c_{v_r}^w$ and $c_{v_z}^w$) phases are defined in Equation [8-3].

APPENDIX G – Solutions for excess pore pressure dissipation and average degree of consolidation in the axisymmetric consolidation

Example 1 - Axisymmetric consolidation with radial flow only

In this example, during the consolidation process, pore-air and pore-water dissipate in the radial direction only. Thus, initial conditions can be presented as follows:

$$u_a(r,0) = u_a^0 \qquad [G\text{-}1a]$$

$$u_w(r,0) = u_w^0 \qquad [G\text{-}1b]$$

Constant terms Ξ_a and Ξ_w ($i = 0, 1, 2 \ldots$) then become:

$$\Xi_a = \frac{2\,X^i}{\Upsilon^i\sqrt{\xi^i}}\,u_a^0 \qquad [G\text{-}2a]$$

$$\Xi_w = \frac{2\,X^i}{\Upsilon^i\sqrt{\xi^i}}\,u_w^0 \qquad [G\text{-}2b]$$

By repeating the analytical procedure in Equations [8-9] – [8-26] while discarding the permeability coefficients in the domain z (i.e. k_{a_z} and k_{w_z}) and the Fourier sine series, solutions predicting excess pore-air and pore-water pressure dissipation for Equation [8-1] can be obtained and then combined with Equation [G-2] become:

$$u_a(r,t) = \frac{X^i}{\Upsilon^i\sqrt{\xi^i}}\,D^i\left(\frac{\sqrt{\xi^i}}{r_w}r\right)\left\{\frac{\Omega_1\left[e^{\alpha_1\frac{\xi^i}{(r_w)^2}t} - e^{\alpha_2\frac{\xi^i}{(r_w)^2}t}\right] + \Psi_1\left[e^{\alpha_1\frac{\xi^i}{(r_w)^2}t} + e^{\alpha_2\frac{\xi^i}{(r_w)^2}t}\right]}{\eta}\right\} \qquad [G\text{-}3a]$$

$$u_w(r,t) = \frac{X^i}{\Upsilon^i\sqrt{\xi^i}}\,D^i\left(\frac{\sqrt{\xi^i}}{r_w}r\right)\left\{\frac{\Omega_1'\left[e^{\alpha_1\frac{\xi^i}{(r_w)^2}t} - e^{\alpha_2\frac{\xi^i}{(r_w)^2}t}\right] + \Psi_1'\left[e^{\alpha_1\frac{\xi^i}{(r_w)^2}t} + e^{\alpha_2\frac{\xi^i}{(r_w)^2}t}\right]}{\eta}\right\} \qquad [G\text{-}3b]$$

where $\eta = \left[\left(c_{v_r}^a - c_{v_r}^w\right)^2 + 4c_{v_r}^a c_{v_r}^w C_w C_a\right]^{\frac{1}{2}}$,

$\alpha_1 = \frac{1}{2}\left(\frac{c_{v_r}^a + c_{v_r}^w + \eta}{1 - C_w C_a}\right)$, $\alpha_2 = \frac{1}{2}\left(\frac{c_{v_r}^a + c_{v_r}^w - \eta}{1 - C_w C_a}\right)$,

$\Omega_1 = \left(c_{v_r}^a - c_{v_r}^w\right)u_a^0 - 2c_{v_r}^w C_a\,u_w^0$, $\Psi_1 = \eta\,u_a^0$,

$$\Omega_1' = \left(c_{v_r}^{w} - c_{v_r}^{a}\right)\, u_w^0 - 2c_{v_r}^{a} C_w\, u_a^0, \text{ and} \qquad \Psi_1' = \eta\, u_w^0. \tag{G-4}$$

In addition, the average degree of consolidation $\overline{U}$ can be presented as below:

$$\overline{U} = \left|\frac{\bar{\varepsilon}_{v_1}(t)}{\bar{\varepsilon}_{v_1}(\infty)}\right| = \frac{(m_2^s - m_1^s)\left\{\frac{2\pi\int_{r_w}^{r_e} u_a(r,t)\, rdr}{\pi[(r_e)^2-(r_w)^2]} - u_a^0\right\} - m_2^s\left\{\frac{2\pi\int_{r_w}^{r_e} u_w(r,t)\, rdr}{\pi[(r_e)^2-(r_w)^2]} - u_w^0\right\}}{(m_1^s - m_2^s)\, u_a^0 + m_2^s\, u_w^0} \tag{G-5}$$

where $\int_{r_w}^{r_e} u_a(r,t)\, rdr = \frac{(X^i)^2}{\Upsilon^i \xi^i}\left\{\frac{\Omega_1\left[e^{\alpha_1\frac{\xi^i}{(r_w)^2}t} - e^{\alpha_2\frac{\xi^i}{(r_w)^2}t}\right] + \Psi_1\left[e^{\alpha_1\frac{\xi^i}{(r_w)^2}t} + e^{\alpha_2\frac{\xi^i}{(r_w)^2}t}\right]}{\eta}\right\}$; and

$$\int_{r_w}^{r_e} u_w(r,t)\, rdr = \frac{(X^i)^2}{\Upsilon^i \xi^i}\left\{\frac{\Omega_1'\left[e^{\alpha_1\frac{\xi^i}{(r_w)^2}t} - e^{\alpha_2\frac{\xi^i}{(r_w)^2}t}\right] + \Psi_1'\left[e^{\alpha_1\frac{\xi^i}{(r_w)^2}t} + e^{\alpha_2\frac{\xi^i}{(r_w)^2}t}\right]}{\eta}\right\}. \tag{G-6}$$

Example 2 - Axisymmetric consolidation with both radial and vertical flows

(a) Uniform initial condition ($\zeta_a = \zeta_w = 0$)

When $\zeta_a = \zeta_w = 0$, the constant terms Ξ_a and Ξ_w ($i = 0, 1, 2 \ldots$; $j = 0, 1, 2 \ldots$), as presented in Equation [8-23], can be obtained as follows:

$$\Xi_a = \frac{4\, X^i}{\Upsilon^i \sqrt{\xi^i}} \frac{Z^j}{\sqrt{\mu^j}}\, u_a^0 \tag{G-7a}$$

$$\Xi_w = \frac{4\, X^i}{\Upsilon^i \sqrt{\xi^i}} \frac{Z^j}{\sqrt{\mu^j}}\, u_w^0 \tag{G-7b}$$

where $Z^j = 1$ for the PTIB boundary condition; or

$= 1 - (-1)^j$ for the PTPB boundary condition. [G-8]

Solutions predicting excess pore-air and pore-water pressure dissipation can be further expanded from Equation [8-26] while combining with Equation [G-7], resulting in:

(i) The PTIB boundary condition:

$$u_a(r,z,t) = \sum_{j=0}^{\infty} \frac{2X^i}{\Upsilon^i\sqrt{\xi^i}} \frac{1}{\sqrt{\mu^j}} D^i \left(\frac{\sqrt{\xi^i}}{r_w} r\right) \sin\left(\frac{\sqrt{\mu^j}}{H} z\right) \left[\frac{\Omega_2\left(e^{\alpha_1^{ij}t} - e^{\alpha_2^{ij}t}\right) + \Psi_2\left(e^{\alpha_1^{ij}t} + e^{\alpha_2^{ij}t}\right)}{\eta^{ij}}\right] \quad [G\text{-}9a]$$

$$u_w(r,z,t) = \sum_{j=0}^{\infty} \frac{2X^i}{\Upsilon^i\sqrt{\xi^i}} \frac{1}{\sqrt{\mu^j}} D^i \left(\frac{\sqrt{\xi^i}}{r_w} r\right) \sin\left(\frac{\sqrt{\mu^j}}{H} z\right) \left[\frac{\Omega_2'\left(e^{\alpha_1^{ij}t} - e^{\alpha_2^{ij}t}\right) + \Psi_2'\left(e^{\alpha_1^{ij}t} + e^{\alpha_2^{ij}t}\right)}{\eta^{ij}}\right] \quad [G\text{-}9b]$$

(ii) The PTPB boundary condition:

$$u_a(r,z,t) = \sum_{j=0}^{\infty} \frac{2X^i}{\Upsilon^i\sqrt{\xi^i}} \frac{[1-(-1)^j]}{\sqrt{\mu^j}} D^i \left(\frac{\sqrt{\xi^i}}{r_w} r\right) \sin\left(\frac{\sqrt{\mu^j}}{H} z\right) \left[\frac{\Omega_2\left(e^{\alpha_1^{ij}t} - e^{\alpha_2^{ij}t}\right) + \Psi_2\left(e^{\alpha_1^{ij}t} + e^{\alpha_2^{ij}t}\right)}{\eta^{ij}}\right] \quad [G\text{-}10a]$$

$$u_w(r,z,t) = \sum_{j=0}^{\infty} \frac{2X^i}{\Upsilon^i\sqrt{\xi^i}} \frac{[1-(-1)^j]}{\sqrt{\mu^j}} D^i \left(\frac{\sqrt{\xi^i}}{r_w} r\right) \sin\left(\frac{\sqrt{\mu^j}}{H} z\right) \left[\frac{\Omega_2'\left(e^{\alpha_1^{ij}t} - e^{\alpha_2^{ij}t}\right) + \Psi_2'\left(e^{\alpha_1^{ij}t} + e^{\alpha_2^{ij}t}\right)}{\eta^{ij}}\right] \quad [G\text{-}10b]$$

where $\Omega_2 = \left(c_v^a\lambda_a^{ij} - c_v^w\lambda_w^{ij}\right) u_a^0 - 2c_v^w C_a\lambda_w^{ij}\, u_w^0$, $\Psi_2 = \eta^{ij}\, u_a^0$,

$\Omega_2' = \left(c_v^w\lambda_w^{ij} - c_v^a\lambda_a^{ij}\right) u_w^0 - 2c_v^a C_w\lambda_a^{ij}\, u_a^0$, and $\Psi_2' = \eta^{ij}\, u_w^0$. [G-11]

The average degree of consolidation $\overline{U}$ capturing the uniform initial condition can be further expressed from Equation [8-30]:

$$\overline{U} = \left|\frac{\bar{\varepsilon}_{v_2}(t)}{\bar{\varepsilon}_{v_2}(\infty)}\right| = \frac{(m_2^s - m_1^s)\left\{\frac{2\pi\int_0^H\int_{r_w}^{r_e} u_a(r,z,t)\, rdrdz}{\pi[(r_e)^2-(r_w)^2]\,H} - u_a^0\right\} - m_2^s\left\{\frac{2\pi\int_0^H\int_{r_w}^{r_e} u_w(r,z,t)\, rdrdz}{\pi[(r_e)^2-(r_w)^2]\,H} - u_w^0\right\}}{(m_1^s - m_2^s)\, u_a^0 + m_2^s\, u_w^0} \quad [G\text{-}12]$$

where

(i) The PTIB boundary condition:

$$\int_0^H\int_{r_w}^{r_e} u_a(r,z,t)\, rdrdz = \sum_{j=0}^{\infty} \frac{2\left(X^i\right)^2}{\Upsilon^i\,\xi^i} \frac{H}{\mu^j} \left[\frac{\Omega_2\left(e^{\alpha_1^{ij}t} - e^{\alpha_2^{ij}t}\right) + \Psi_2\left(e^{\alpha_1^{ij}t} + e^{\alpha_2^{ij}t}\right)}{\eta^{ij}}\right] \quad [G\text{-}13a]$$

$$\int_0^H \int_{r_w}^{r_e} u_w(r,z,t)\, rdrdz = \sum_{j=0}^{\infty} \frac{2\,(X^i)^2}{\Upsilon^i\,\xi^i}\,\frac{H}{\mu^j}\left[\frac{\Omega_2'\left(e^{\alpha_1^{ij}t}-e^{\alpha_2^{ij}t}\right)+\Psi_2'\left(e^{\alpha_1^{ij}t}+e^{\alpha_2^{ij}t}\right)}{\eta^{ij}}\right] \quad \text{[G-13b]}$$

(ii) The PTPB boundary condition:

$$\int_0^H \int_{r_w}^{r_e} u_a(r,z,t)\, rdrdz =$$

$$\sum_{j=0}^{\infty} \frac{2\,(X^i)^2}{\Upsilon^i\,\xi^i}\,\frac{H\left[1-(-1)^j\right]^2}{\mu^j}\left[\frac{\Omega_2\left(e^{\alpha_1^{ij}t}-e^{\alpha_2^{ij}t}\right)+\Psi_2\left(e^{\alpha_1^{ij}t}+e^{\alpha_2^{ij}t}\right)}{\eta^{ij}}\right] \quad \text{[G-14a]}$$

$$\int_0^H \int_{r_w}^{r_e} u_w(r,z,t)\, rdrdz =$$

$$\sum_{j=0}^{\infty} \frac{2\,(X^i)^2}{\Upsilon^i\,\xi^i}\,\frac{H\left[1-(-1)^j\right]^2}{\mu^j}\left[\frac{\Omega_2'\left(e^{\alpha_1^{ij}t}-e^{\alpha_2^{ij}t}\right)+\Psi_2'\left(e^{\alpha_1^{ij}t}+e^{\alpha_2^{ij}t}\right)}{\eta^{ij}}\right] \quad \text{[G-14b]}$$

(b) Linear initial condition ($\zeta_a, \zeta_w > 0$)

When both $\zeta_a > 0$ and $\zeta_w > 0$, the constant terms Ξ_a and Ξ_w ($i = 0, 1, 2 \ldots$; $j = 0, 1, 2 \ldots$), as presented in Equation [8-23], are as follows:

(i) The PTIB boundary condition:

$$\Xi_a = \frac{4\,X^i}{\Upsilon^i\sqrt{\xi^i}}\,\frac{1}{\sqrt{\mu^j}}\,u_a^0\left[\sqrt{\mu^j}-(-1)^j\zeta_a\right] \quad \text{[G-15a]}$$

$$\Xi_w = \frac{4\,X^i}{\Upsilon^i\sqrt{\xi^i}}\,\frac{1}{\sqrt{\mu^j}}\,u_w^0\left[\sqrt{\mu^j}-(-1)^j\zeta_w\right] \quad \text{[G-15b]}$$

(ii) The PTPB boundary condition:

$$\Xi_a = \frac{4\,X^i}{\Upsilon^i\sqrt{\xi^i}}\,\frac{1}{\sqrt{\mu^j}}\,u_a^0\left[1+(-1)^j(\zeta_a-1)\right] \quad \text{[G-16a]}$$

$$\Xi_w = \frac{4\,X^i}{\Upsilon^i\sqrt{\xi^i}}\,\frac{1}{\sqrt{\mu^j}}\,u_w^0\left[1+(-1)^j(\zeta_w-1)\right] \quad \text{[G-16b]}$$

Solutions predicting excess pore-air and pore-water pressure dissipation can be expanded from Equation [8-26] while combining with Equations [G-15] and [G-16], giving:

(i) The PTIB boundary condition:

$$u_a(r,z,t) = \sum_{j=0}^{\infty} \frac{2X^i}{\Upsilon^i\sqrt{\xi^i}} \frac{1}{\mu^j} D^i \left(\frac{\sqrt{\xi^i}}{r_w} r\right) \sin\left(\frac{\sqrt{\mu^j}}{H} z\right) \left[\frac{\Omega_3\left(e^{\alpha_1^{ij}t} - e^{\alpha_2^{ij}t}\right) + \Psi_3\left(e^{\alpha_1^{ij}t} + e^{\alpha_2^{ij}t}\right)}{\eta^{ij}}\right] \quad [G\text{-}17a]$$

$$u_w(r,z,t) = \sum_{j=0}^{\infty} \frac{2X^i}{\Upsilon^i\sqrt{\xi^i}} \frac{1}{\mu^j} D^i \left(\frac{\sqrt{\xi^i}}{r_w} r\right) \sin\left(\frac{\sqrt{\mu^j}}{H} z\right) \left[\frac{\Omega_3'\left(e^{\alpha_1^{ij}t} - e^{\alpha_2^{ij}t}\right) + \Psi_3'\left(e^{\alpha_1^{ij}t} + e^{\alpha_2^{ij}t}\right)}{\eta^{ij}}\right] \quad [G\text{-}17b]$$

(ii) The PTPB boundary condition:

$$u_a(r,z,t) = \sum_{j=0}^{\infty} \frac{2X^i}{\Upsilon^i\sqrt{\xi^i}} \frac{1}{\sqrt{\mu^j}} D^i \left(\frac{\sqrt{\xi^i}}{r_w} r\right) \sin\left(\frac{\sqrt{\mu^j}}{H} z\right) \left[\frac{\Omega_4\left(e^{\alpha_1^{ij}t} - e^{\alpha_2^{ij}t}\right) + \Psi_4\left(e^{\alpha_1^{ij}t} + e^{\alpha_2^{ij}t}\right)}{\eta^{ij}}\right] \quad [G\text{-}18a]$$

$$u_w(r,z,t) = \sum_{j=0}^{\infty} \frac{2X^i}{\Upsilon^i\sqrt{\xi^i}} \frac{1}{\sqrt{\mu^j}} D^i \left(\frac{\sqrt{\xi^i}}{r_w} r\right) \sin\left(\frac{\sqrt{\mu^j}}{H} z\right) \left[\frac{\Omega_4'\left(e^{\alpha_1^{ij}t} - e^{\alpha_2^{ij}t}\right) + \Psi_4'\left(e^{\alpha_1^{ij}t} + e^{\alpha_2^{ij}t}\right)}{\eta^{ij}}\right] \quad [G\text{-}18b]$$

where $\Omega_3 = \left(c_v^a\lambda_a^{ij} - c_v^w\lambda_w^{ij}\right)\left[\sqrt{\mu^j} - (-1)^j\zeta_a\right] u_a^0 - 2c_v^w C_a\lambda_w^{ij}\left[\sqrt{\mu^j} - (-1)^j\zeta_w\right] u_w^0$;

$\Psi_3 = \eta^{ij}\left[\sqrt{\mu^j} - (-1)^j\zeta_a\right] u_a^0$;

$\Omega_3' = \left(c_v^w\lambda_w^{ij} - c_v^a\lambda_a^{ij}\right)\left[\sqrt{\mu^j} - (-1)^j\zeta_w\right] u_w^0 - 2c_v^a C_w\lambda_a^{ij}\left[\sqrt{\mu^j} - (-1)^j\zeta_a\right] u_a^0$;

$\Psi_3' = \eta^{ij}\left[\sqrt{\mu^j} - (-1)^j\zeta_w\right] u_w^0$;

$\Omega_4 = \left(c_v^a\lambda_a^{ij} - c_v^w\lambda_w^{ij}\right)\left[1 + (-1)^j(\zeta_a - 1)\right] u_a^0 - 2c_v^w C_a\lambda_w^{ij}\left[1 + (-1)^j(\zeta_w - 1)\right] u_w^0$;

$\Psi_4 = \eta^{ij}\left[1 + (-1)^j(\zeta_a - 1)\right] u_a^0$;

$\Omega_4' = \left(c_v^w\lambda_w^{ij} - c_v^a\lambda_a^{ij}\right)\left[1 + (-1)^j(\zeta_w - 1)\right] u_w^0 - 2c_v^a C_w\lambda_a^{ij}\left[1 + (-1)^j(\zeta_a - 1)\right] u_a^0$; and

$\Psi_4' = \eta^{ij}\left[1 + (-1)^j(\zeta_w - 1)\right] u_w^0$. [G-19]

The average degree of consolidation $\overline{U}$ capturing the linear initial condition is expressed as follows:

$$\overline{U} = \left|\frac{\bar{\varepsilon}_{v_3}(t)}{\bar{\varepsilon}_{v_3}(\infty)}\right| = \frac{(m_2^s - m_1^s)\left\{\frac{2\pi\int_0^H\int_{r_w}^{r_e} u_a(r,z,t)\,rdrdz}{\pi[(r_e)^2-(r_w)^2]\,H} - u_a^0\left(1-\frac{\zeta_a}{2}\right)\right\} - m_2^s\left\{\frac{2\pi\int_0^H\int_{r_w}^{r_e} u_w(r,z,t)\,rdrdz}{\pi[(r_e)^2-(r_w)^2]\,H} - u_w^0\left(1-\frac{\zeta_w}{2}\right)\right\}}{(m_1^s - m_2^s)\,u_a^0\left(1-\frac{\zeta_a}{2}\right) + m_2^s\,u_w^0\left(1-\frac{\zeta_w}{2}\right)}$$

[G-20]

where

(i) The PTIB boundary condition:

$$\int_0^H\int_{r_w}^{r_e} u_a(r,z,t)\,rdrdz = \sum_{j=0}^{\infty}\frac{2\,(X^i)^2}{\Upsilon^i\,\xi^i}\,\frac{H}{(\mu^j)^{\frac{3}{2}}}\left[\frac{\Omega_3\left(e^{\alpha_1^{ij}t}-e^{\alpha_2^{ij}t}\right)+\Psi_3\left(e^{\alpha_1^{ij}t}+e^{\alpha_2^{ij}t}\right)}{\eta^{ij}}\right]$$

[G-21a]

$$\int_0^H\int_{r_w}^{r_e} u_w(r,z,t)\,rdrdz = \sum_{j=0}^{\infty}\frac{2\,(X^i)^2}{\Upsilon^i\,\xi^i}\,\frac{H}{(\mu^j)^{\frac{3}{2}}}\left[\frac{\Omega_3'\left(e^{\alpha_1^{ij}t}-e^{\alpha_2^{ij}t}\right)+\Psi_3'\left(e^{\alpha_1^{ij}t}+e^{\alpha_2^{ij}t}\right)}{\eta^{ij}}\right]$$

[G-21b]

(ii) The PTPB boundary condition:

$$\int_0^H\int_{r_w}^{r_e} u_a(r,z,t)\,rdrdz =$$

$$\sum_{j=0}^{\infty}\frac{2\,(X^i)^2}{\Upsilon^i\,\xi^i}\,\frac{H\,[1-(-1)^j]}{\mu^j}\left[\frac{\Omega_4\left(e^{\alpha_1^{ij}t}-e^{\alpha_2^{ij}t}\right)+\Psi_4\left(e^{\alpha_1^{ij}t}+e^{\alpha_2^{ij}t}\right)}{\eta^{ij}}\right]$$

[G-22a]

$$\int_0^H\int_{r_w}^{r_e} u_w(r,z,t)\,rdrdz =$$

$$\sum_{j=0}^{\infty}\frac{2\,(X^i)^2}{\Upsilon^i\,\xi^i}\,\frac{H\,[1-(-1)^j]}{\mu^j}\left[\frac{\Omega_4'\left(e^{\alpha_1^{ij}t}-e^{\alpha_2^{ij}t}\right)+\Psi_4'\left(e^{\alpha_1^{ij}t}+e^{\alpha_2^{ij}t}\right)}{\eta^{ij}}\right]$$

[G-22b]

APPENDIX H – Initial excess pore pressures in response to constant loading in the axisymmetric consolidation

Following Fredlund et al. (2012), the 3D constitutive equation for the soil structure and air phase in the polar coordinates (r, θ, z) can be expressed considering the total stress increments $d\sigma_r$, $d\sigma_\theta$ and $d\sigma_z$ as follows:

$$\frac{dV}{V_0} = m_1^s d\left(\frac{\sigma_r+\sigma_\theta+\sigma_z}{3} - u_a\right) + m_2^s d(u_a - u_w) \quad [H\text{-}1a]$$

$$\frac{dV_a}{V_0} = m_1^a d\left(\frac{\sigma_r+\sigma_\theta+\sigma_z}{3} - u_a\right) + m_2^a d(u_a - u_w) \quad [H\text{-}1b]$$

Under an isotropic loading condition, total stress increments in the polar system would be equal (i.e., $d\sigma_r = d\sigma_\theta = d\sigma_z$), thus Equation [H-1] becomes:

$$\frac{dV}{V_0} = m_1^s d(\sigma_r - u_a) + m_2^s d(u_a - u_w) \quad [H\text{-}2a]$$

$$\frac{dV_a}{V_0} = m_1^a d(\sigma_r - u_a) + m_2^a d(u_a - u_w) \quad [H\text{-}2b]$$

The volume changes, dV and dV_a, due to pore fluid compression and air compression, respectively, can be expressed as:

$$\frac{dV}{V_0} = \frac{(1-S_r+hS_r)n}{u_a+u_{atm}} du_a + S_r n \beta_w du_w \quad [H\text{-}3a]$$

$$\frac{dV_a}{V_0} = \frac{(1-S_r+hS_r)n}{u_a+u_{atm}} du_a \quad [H\text{-}3b]$$

where h is the volumetric coefficient of solubility; and

$$\beta_w = -\frac{1}{V_w}\frac{dV_w}{du_w}, \text{ is the compressibility of water.} \quad [H\text{-}4]$$

Combining Equations [H-2a] and [H-3a] and Equations [H-2b] and [H-3b], resulting in:

$$m_1^s d(\sigma_r - u_a) + m_2^s d(u_a - u_w) = \frac{(1-S_r+hS_r)n}{u_a+u_{atm}} du_a + S_r n \beta_w du_w \quad [H\text{-}5a]$$

$$m_1^a d(\sigma_r - u_a) + m_2^a d(u_a - u_w) = \frac{(1-S_r+hS_r)n}{u_a+u_{atm}} du_a \quad [H\text{-}5b]$$

Simulataneously solving Equations [H-5a] and [H-5a] to determine the changes in excess pore-air and pore-water pressures in response to the change in total stress, thus,

$$B_a = \frac{du_a}{d\sigma_r} = \frac{R_2^s R_1^a - R_2^a}{1 - R_1^s R_1^a} \quad \text{[H-6a]}$$

$$B_w = \frac{du_w}{d\sigma_r} = \frac{R_2^s - R_1^s R_2^a}{1 - R_1^s R_1^a} \quad \text{[H-6b]}$$

where $R_1^s = \frac{m_2^s - m_1^s - \frac{(1-S_r+hS_r)n}{u_a+u_{atm}}}{m_2^s + nS_r\beta_w}$; $R_2^s = \frac{m_1^s}{m_2^s + nS_r\beta_w}$;

$R_1^a = \frac{m_2^a}{m_2^a - m_1^a - \frac{(1-S_r+hS_r)n}{u_a+u_{atm}}}$; and $R_2^a = \frac{m_1^a}{m_2^a - m_1^a - \frac{(1-S_r+hS_r)n}{u_a+u_{atm}}}$. [H-7]

The terms B_a and B_w are the pore pressure parameters with respect to the air and water phases, respectively, under the isotropic loading condition. Since terms R_1^s, R_1^a and R_2^a contain the absolute pore-air pressure, an iterative technique is required to solve for du_a and du_w. Referring to Fredlund et al. (2012), it is worth noting that suction (i.e. $u_a - u_w$) reduces with the increasing isotropic stress. As the stress increases significantly, the parameters B_a and B_w would approach 1 and subsequently suction becomes zero.

APPENDIX I – Excess pore pressure dissipation rates induced by time-dependent loadings in the axisymmetric consolidation

i. Ramped loading

By substituting Equation [9-43a] into Equation [9-38], the excess pore-air and pore-water pressures generated by an application of the ramped loading can be determined as follows:

$$u_a(r,z,t) = \sum_{j=0}^{\infty} \varpi^{ij}\, D^i \left(\frac{r\sqrt{\xi^i}}{r_w}\right) \sin\left(\frac{z\sqrt{\mu^j}}{H}\right) \left\{ \frac{\Omega\left(e^{\alpha_1^{ij}t} - e^{\alpha_2^{ij}t}\right) + \Psi\left(e^{\alpha_1^{ij}t} + e^{\alpha_2^{ij}t}\right)}{2\eta^{ij}} + X_1 \left[\frac{e^{\alpha_1^{ij}t}\left(\alpha_1^{ij} + \beta_1^{ij}\right)}{\alpha_1^{ij}\left(\alpha_1^{ij} - \alpha_2^{ij}\right)} + \frac{e^{\alpha_2^{ij}t}\left(\alpha_2^{ij} + \beta_1^{ij}\right)}{\alpha_2^{ij}\left(\alpha_2^{ij} - \alpha_1^{ij}\right)} + \frac{\beta_1^{ij}}{\alpha_1^{ij}\alpha_2^{ij}} \right] \right\} \quad \text{[I-1a]}$$

$$u_w(r,z,t) = \sum_{j=0}^{\infty} \varpi^{ij}\, D^i \left(\frac{r\sqrt{\xi^i}}{r_w}\right) \sin\left(\frac{z\sqrt{\mu^j}}{H}\right) \left\{ \frac{\Omega'\left(e^{\alpha_1^{ij}t} - e^{\alpha_2^{ij}t}\right) + \Psi'\left(e^{\alpha_1^{ij}t} + e^{\alpha_2^{ij}t}\right)}{2\eta^{ij}} + X_1' \left[\frac{e^{\alpha_1^{ij}t}\left(\alpha_1^{ij} + \beta_2^{ij}\right)}{\alpha_1^{ij}\left(\alpha_1^{ij} - \alpha_2^{ij}\right)} + \frac{e^{\alpha_2^{ij}t}\left(\alpha_2^{ij} + \beta_2^{ij}\right)}{\alpha_2^{ij}\left(\alpha_2^{ij} - \alpha_1^{ij}\right)} + \frac{\beta_2^{ij}}{\alpha_1^{ij}\alpha_2^{ij}} \right] \right\} \quad \text{[I-1b]}$$

where $X_1 = (1+2K)\frac{a(C_a c_\sigma^w - c_\sigma^a)}{C_a C_w - 1}$; $\quad X_1' = (1+2K)\frac{a(C_w c_\sigma^a - c_\sigma^w)}{C_a C_w - 1}$;

$\beta_1^{ij} = \frac{c_\sigma^a c_v^w \lambda_w^{ij}}{C_a c_\sigma^w - c_\sigma^a}$; and $\quad \beta_2^{ij} = \frac{c_\sigma^w c_v^a \lambda_a^{ij}}{C_w c_\sigma^a - c_\sigma^w}$. $\quad$ [I-2]

ii. Asymptotic loading

By substituting Equation [9-43b] into Equation [9-38], the excess pore-air and pore-water pressures induced by the asymptotic loading can be estimated as shown:

$$u_a(r,z,t) = \sum_{j=0}^{\infty} \varpi^{ij}\, D^i \left(\frac{r\sqrt{\xi^i}}{r_w}\right) \sin\left(\frac{z\sqrt{\mu^j}}{H}\right) \left\{ \frac{\Omega\left(e^{\alpha_1^{ij}t} - e^{\alpha_2^{ij}t}\right) + \Psi\left(e^{\alpha_1^{ij}t} + e^{\alpha_2^{ij}t}\right)}{2\eta^{ij}} + X_2 \left[\frac{e^{-bt}\left(\beta_1^{ij} - b\right)}{\left(b + \alpha_1^{ij}\right)\left(b + \alpha_2^{ij}\right)} + \frac{e^{\alpha_1^{ij}t}\left(\alpha_1^{ij} + \beta_1^{ij}\right)}{\left(b + \alpha_1^{ij}\right)\left(\alpha_1^{ij} - \alpha_2^{ij}\right)} + \frac{e^{\alpha_2^{ij}t}\left(\alpha_2^{ij} + \beta_1^{ij}\right)}{\left(b + \alpha_2^{ij}\right)\left(\alpha_2^{ij} - \alpha_1^{ij}\right)} \right] \right\} \quad \text{[I-3a]}$$

$$u_w(r,z,t) = \sum_{j=0}^{\infty} \varpi^{ij}\, D^i \left(\frac{r\sqrt{\xi^i}}{r_w}\right) \sin\left(\frac{z\sqrt{\mu^j}}{H}\right) \left\{ \frac{\Omega'\left(e^{\alpha_1^{ij}t} - e^{\alpha_2^{ij}t}\right) + \Psi'\left(e^{\alpha_1^{ij}t} + e^{\alpha_2^{ij}t}\right)}{2\eta^{ij}} + X_2' \left[\frac{e^{-bt}\left(\beta_2^{ij} - b\right)}{\left(b+\alpha_1^{ij}\right)\left(b+\alpha_2^{ij}\right)} + \right.\right.$$

$$\left.\left. \frac{e^{\alpha_1^{ij}t}\left(\alpha_1^{ij} + \beta_2^{ij}\right)}{\left(b+\alpha_1^{ij}\right)\left(\alpha_1^{ij} - \alpha_2^{ij}\right)} + \frac{e^{\alpha_2^{ij}t}\left(\alpha_2^{ij} + \beta_2^{ij}\right)}{\left(b+\alpha_2^{ij}\right)\left(\alpha_2^{ij} - \alpha_1^{ij}\right)} \right] \right\} \qquad \text{[I-3b]}$$

where $X_2 = (1+2K)\frac{Abq_0(C_a c_\sigma^w - c_\sigma^a)}{C_a C_w - 1}$; and $X_2' = (1+2K)\frac{Abq_0(C_w c_\sigma^a - c_\sigma^w)}{C_a C_w - 1}$. [I-4]

iii. Sinusoidal loading

By substituting Equation [9-43c] into Equation [9-38], the excess pore-air and pore-water pressures induced by the applied sinusoidal loading can be determined as shown:

$$u_a(r,z,t) =$$

$$\sum_{j=0}^{\infty} \varpi^{ij}\, D^i \left(\frac{r\sqrt{\xi^i}}{r_w}\right) \sin\left(\frac{z\sqrt{\mu^j}}{H}\right) \left\{ \frac{\Omega\left(e^{\alpha_1^{ij}t} - e^{\alpha_2^{ij}t}\right) + \Psi\left(e^{\alpha_1^{ij}t} + e^{\alpha_2^{ij}t}\right)}{2\eta^{ij}} + \right.$$

$$\left. X_3 \left\{ \frac{e^{\alpha_1^{ij}t}\alpha_1^{ij}\left(\alpha_1^{ij} + \beta_1^{ij}\right)}{\left[\left(\alpha_1^{ij}\right)^2 + \phi^2\right]\left(\alpha_1^{ij} - \alpha_2^{ij}\right)} + \frac{e^{\alpha_2^{ij}t}\alpha_2^{ij}\left(\alpha_2^{ij} + \beta_1^{ij}\right)}{\left[\left(\alpha_2^{ij}\right)^2 + \phi^2\right]\left(\alpha_2^{ij} - \alpha_1^{ij}\right)} + \frac{\zeta\cos(\phi t) + \xi\sin(\phi t)}{\left[\left(\alpha_1^{ij}\right)^2 + \phi^2\right]\left[\left(\alpha_2^{ij}\right)^2 + \phi^2\right]} \right\} \right\} \qquad \text{[I-5a]}$$

$$u_w(r,z,t) =$$

$$\sum_{j=0}^{\infty} \varpi^{ij}\, D^i \left(\frac{r\sqrt{\xi^i}}{r_w}\right) \sin\left(\frac{z\sqrt{\mu^j}}{H}\right) \left\{ \frac{\Omega'\left(e^{\alpha_1^{ij}t} - e^{\alpha_2^{ij}t}\right) + \Psi'\left(e^{\alpha_1^{ij}t} + e^{\alpha_2^{ij}t}\right)}{2\eta^{ij}} + \right.$$

$$\left. X_3' \left\{ \frac{e^{\alpha_1^{ij}t}\alpha_1^{ij}\left(\alpha_1^{ij} + \beta_2^{ij}\right)}{\left[\left(\alpha_1^{ij}\right)^2 + \phi^2\right]\left(\alpha_1^{ij} - \alpha_2^{ij}\right)} + \frac{e^{\alpha_2^{ij}t}\alpha_2^{ij}\left(\alpha_2^{ij} + \beta_2^{ij}\right)}{\left[\left(\alpha_2^{ij}\right)^2 + \phi^2\right]\left(\alpha_2^{ij} - \alpha_1^{ij}\right)} + \frac{\zeta'\cos(\phi t) + \xi'\sin(\phi t)}{\left[\left(\alpha_1^{ij}\right)^2 + \phi^2\right]\left[\left(\alpha_2^{ij}\right)^2 + \phi^2\right]} \right\} \right\} \qquad \text{[I-5b]}$$

where $X_3 = (1+2K)\frac{Bq_0\phi(C_a c_\sigma^w - c_\sigma^a)}{C_a C_w - 1}$; $X_3' = (1+2K)\frac{Bq_0\phi(C_w c_\sigma^a - c_\sigma^w)}{C_a C_w - 1}$;

$\zeta = \alpha_1^{ij}\alpha_2^{ij}\beta_1^{ij} - \left(\alpha_1^{ij} + \alpha_2^{ij} + \beta_1^{ij}\right)\phi^2$;

$\zeta' = \alpha_1^{ij}\alpha_2^{ij}\beta_2^{ij} - \left(\alpha_1^{ij} + \alpha_2^{ij} + \beta_2^{ij}\right)\phi^2$;

$\xi = \phi\left\{\phi^2 - \left[\beta_1^{ij}\left(\alpha_1^{ij} + \alpha_2^{ij}\right) + \alpha_1^{ij}\alpha_2^{ij}\right]\right\}$; and

$\xi' = \phi\left\{\phi^2 - \left[\beta_2^{ij}\left(\alpha_1^{ij} + \alpha_2^{ij}\right) + \alpha_1^{ij}\alpha_2^{ij}\right]\right\}$. [I-6]

iv. Damped sine wave loading

By substituting Equation [9-43d] into Equation [9-38], the excess pore-air and pore-water pressures generated by the damped sine wave loading can be determined as follows:

$$u_a(r,z,t) = \sum_{j=0}^{\infty} \varpi^{ij}\, D^i \left(\frac{r\sqrt{\xi^i}}{r_w}\right) \sin\left(\frac{z\sqrt{\mu^j}}{H}\right) \left\{ \frac{\Omega\left(e^{\alpha_1^{ij}t} - e^{\alpha_2^{ij}t}\right) + \Psi\left(e^{\alpha_1^{ij}t} + e^{\alpha_2^{ij}t}\right)}{2\eta^{ij}} + X_4 \left\{ \frac{e^{\alpha_1^{ij}t}\alpha_1^{ij}\left(\alpha_1^{ij}+\beta_1^{ij}\right)}{\left[\left(\alpha_1^{ij}+c\right)^2+\varphi^2\right]\left(\alpha_1^{ij}-\alpha_2^{ij}\right)} + \frac{e^{\alpha_2^{ij}t}\alpha_2^{ij}\left(\alpha_2^{ij}+\beta_1^{ij}\right)}{\left[\left(\alpha_2^{ij}+c\right)^2+\varphi^2\right]\left(\alpha_2^{ij}-\alpha_1^{ij}\right)} + \frac{e^{-ct}[\upsilon\cos(\varphi t)+\varsigma\sin(\varphi t)]}{\varphi\left[\left(\alpha_1^{ij}+c\right)^2+\varphi^2\right]\left[\left(\alpha_2^{ij}+c\right)^2+\varphi^2\right]} \right\} \right\} \quad \text{[I-7a]}$$

$$u_w(r,z,t) = \sum_{j=0}^{\infty} \varpi^{ij}\, D^i \left(\frac{r\sqrt{\xi^i}}{r_w}\right) \sin\left(\frac{z\sqrt{\mu^j}}{H}\right) \left\{ \frac{\Omega'\left(e^{\alpha_1^{ij}t} - e^{\alpha_2^{ij}t}\right) + \Psi'\left(e^{\alpha_1^{ij}t} + e^{\alpha_2^{ij}t}\right)}{2\eta^{ij}} + X_4' \left\{ \frac{e^{\alpha_1^{ij}t}\alpha_1^{ij}\left(\alpha_1^{ij}+\beta_2^{ij}\right)}{\left[\left(\alpha_1^{ij}+c\right)^2+\varphi^2\right]\left(\alpha_1^{ij}-\alpha_2^{ij}\right)} + \frac{e^{\alpha_2^{ij}t}\alpha_2^{ij}\left(\alpha_2^{ij}+\beta_2^{ij}\right)}{\left[\left(\alpha_2^{ij}+c\right)^2+\varphi^2\right]\left(\alpha_2^{ij}-\alpha_1^{ij}\right)} + \frac{e^{-ct}[\upsilon'\cos(\varphi t)+\varsigma'\sin(\varphi t)]}{\varphi\left[\left(\alpha_1^{ij}+c\right)^2+\varphi^2\right]\left[\left(\alpha_2^{ij}+c\right)^2+\varphi^2\right]} \right\} \right\} \quad \text{[I-7b]}$$

where $X_4 = (1+2K)\frac{Cq_0\varphi(C_a c_\sigma^w - c_\sigma^a)}{C_a C_w - 1}$; $\quad X_4' = (1+2K)\frac{Cq_0\varphi(C_w c_\sigma^a - c_\sigma^w)}{C_a C_w - 1}$;

$$\upsilon = \varphi\left[\alpha_1^{ij}\alpha_2^{ij}\beta_1^{ij} - 2c\alpha_1^{ij}\alpha_2^{ij} - (c^2+\varphi^2)\left(\alpha_1^{ij}+\alpha_2^{ij}+\beta_1^{ij}\right)\right];$$

$$\upsilon' = \varphi\left[\alpha_1^{ij}\alpha_2^{ij}\beta_2^{ij} - 2c\alpha_1^{ij}\alpha_2^{ij} - (c^2+\varphi^2)\left(\alpha_1^{ij}+\alpha_2^{ij}+\beta_2^{ij}\right)\right];$$

$$\varsigma = (c^2+\varphi^2)^2 + c\left(\alpha_1^{ij}+\alpha_2^{ij}-\beta_1^{ij}\right)(c^2+\varphi^2) + \left[(c^2-\varphi^2)\alpha_1^{ij}\alpha_2^{ij} - \beta_1^{ij}\left(\alpha_1^{ij}+\alpha_2^{ij}\right)(c^2+\varphi^2)\right] - c\alpha_1^{ij}\alpha_2^{ij}\beta_1^{ij}; \text{ and}$$

$$\varsigma' = (c^2+\varphi^2)^2 + c\left(\alpha_1^{ij}+\alpha_2^{ij}-\beta_2^{ij}\right)(c^2+\varphi^2) + \left[(c^2-\varphi^2)\alpha_1^{ij}\alpha_2^{ij} - \beta_2^{ij}\left(\alpha_1^{ij}+\alpha_2^{ij}\right)(c^2+\varphi^2)\right] - c\alpha_1^{ij}\alpha_2^{ij}\beta_2^{ij}. \quad \text{[I-8]}$$